RNA WORLD HYPOTHESIS AND THE ORIGIN OF LIFE: ASTROCHEMISTRY PERSPECTIVE

EDITED BY: Ashraf - Ali, André Canosa and David Leisawitz
PUBLISHED IN: Frontiers in Astronomy and Space Sciences

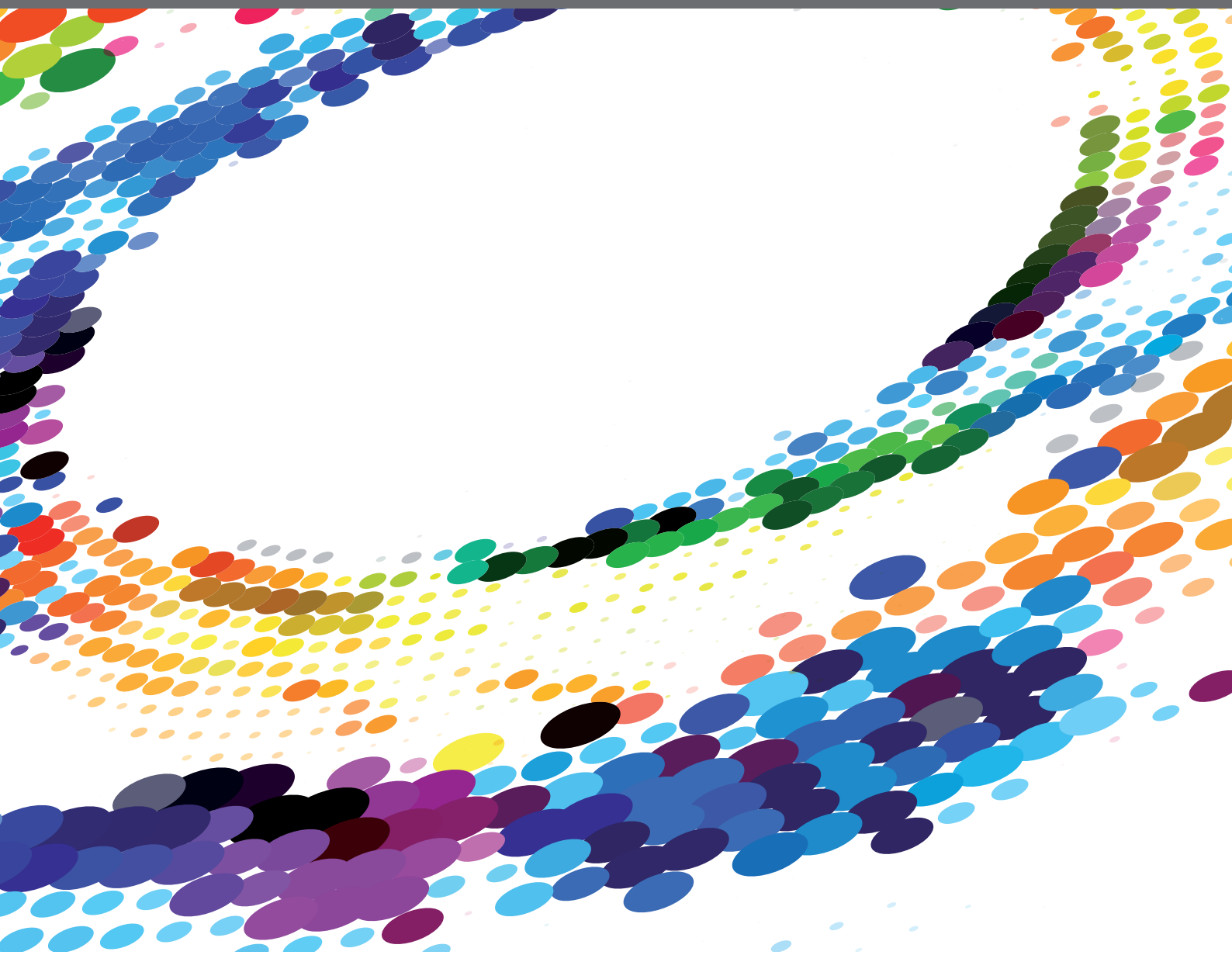

frontiers Research Topics

frontiers

ISSN 1664-8714
ISBN 978-2-83250-073-6
DOI 10.3389/978-2-83250-073-6

About Frontiers

Frontiers is more than just an open-access publisher of scholarly articles: it is a pioneering approach to the world of academia, radically improving the way scholarly research is managed. The grand vision of Frontiers is a world where all people have an equal opportunity to seek, share and generate knowledge. Frontiers provides immediate and permanent online open access to all its publications, but this alone is not enough to realize our grand goals.

Frontiers Journal Series

The Frontiers Journal Series is a multi-tier and interdisciplinary set of open-access, online journals, promising a paradigm shift from the current review, selection and dissemination processes in academic publishing. All Frontiers journals are driven by researchers for researchers; therefore, they constitute a service to the scholarly community. At the same time, the Frontiers Journal Series operates on a revolutionary invention, the tiered publishing system, initially addressing specific communities of scholars, and gradually climbing up to broader public understanding, thus serving the interests of the lay society, too.

Dedication to Quality

Each Frontiers article is a landmark of the highest quality, thanks to genuinely collaborative interactions between authors and review editors, who include some of the world's best academicians. Research must be certified by peers before entering a stream of knowledge that may eventually reach the public - and shape society; therefore, Frontiers only applies the most rigorous and unbiased reviews.
Frontiers revolutionizes research publishing by freely delivering the most outstanding research, evaluated with no bias from both the academic and social point of view. By applying the most advanced information technologies, Frontiers is catapulting scholarly publishing into a new generation.

What are Frontiers Research Topics?

Frontiers Research Topics are very popular trademarks of the Frontiers Journals Series: they are collections of at least ten articles, all centered on a particular subject. With their unique mix of varied contributions from Original Research to Review Articles, Frontiers Research Topics unify the most influential researchers, the latest key findings and historical advances in a hot research area! Find out more on how to host your own Frontiers Research Topic or contribute to one as an author by contacting the Frontiers Editorial Office: frontiersin.org/about/contact

RNA WORLD HYPOTHESIS AND THE ORIGIN OF LIFE: ASTROCHEMISTRY PERSPECTIVE

Topic Editors:
Ashraf - Ali, University of Maryland, College Park, United States
André Canosa, UMR6251 Institut de Physique de Rennes (IPR), France
David Leisawitz, National Aeronautics and Space Administration, United States

Citation: Ali, A., Canosa, A., Leisawitz, D., eds. (2022). RNA World Hypothesis and the Origin of Life: Astrochemistry Perspective. Lausanne: Frontiers Media SA. doi: 10.3389/978-2-83250-073-6

Table of Contents

frontiers | Frontiers in Astronomy and Space Sciences

TYPE Editorial
PUBLISHED 11 August 2022
DOI 10.3389/fspas.2022.989509

OPEN ACCESS

EDITED BY
Cristina Puzzarini,
University of Bologna, Italy

REVIEWED BY
Eric Herbst,
University of Virginia, United States
Malgorzata Biczysko,
Shanghai University, China

*CORRESPONDENCE
Ashraf Ali,
aali1234@umd.edu

SPECIALTY SECTION
This article was submitted to Astrochemistry, a section of the journal Frontiers in Astronomy and Space Sciences

RECEIVED 08 July 2022
ACCEPTED 15 July 2022
PUBLISHED 11 August 2022

CITATION
Ali A, Canosa A and Leisawitz D (2022), Editorial: RNA world hypothesis and the origin of life: Astrochemistry perspective. *Front. Astron. Space Sci.* 9:989509. doi: 10.3389/fspas.2022.989509

Editorial: RNA world hypothesis and the origin of life: Astrochemistry perspective

Ashraf Ali[1]*, André Canosa[2] and David Leisawitz[3]

[1]Department of Physics, University of Maryland, College Park, MD, United States, [2]CNRS, IPR (Institut de Physique de Rennes)–UMR 6251, Université de Rennes, Rennes, France, [3]Goddard Space Flight Center, National Aeronautics and Space Administration, Greenbelt, MD, United States

KEYWORDS

RNA-world, laboratory astrochemistry, radio-astronomy, sub-millimeter astronomy, ground-based observations, space-based observations, interstellar chemistry, reaction kinetics

Editorial on the Research Topic
RNA World Hypothesis and the Origin of Life: Astrochemistry Perspective

The primary goal of this Research Topic is to address the chemistry occurring in space: from interstellar prebiotic molecules to the origin of life. In the RNA-World Hypothesis, RNA is the predecessor to the first life form on Earth. This view has been largely accepted by chemists, and a general consensus has been reached that we indeed live in an RNA Universe, where self-replicating RNA plays a central role (Altman and Cech, 1989; Turk-MacLeod et al., 2013).

To study the RNA-World hypothesis and the origin of life, the first step is to understand how and where small prebiotic molecules could form and how far the molecular complexity could proceed, as interstellar clouds evolve toward star formation (see Figure 1). To try to achieve this goal, efforts are required in different directions from integrated experimental and theoretical studies of elementary reactions at low temperatures, to high-resolution molecular-spectroscopy laboratory studies supported by quantum-chemical calculations, to astronomical observations.

Then, twelve articles, summarized below, contributed to this Research Topic. Interstellar chemistry is reviewed and laboratory rotational spectroscopy is addressed as one bridge between laboratory astrochemistry and astronomical observations. Millimeter and sub-millimeter telescope features are also briefly introduced. Afterwards, several contributions focus on recent observational discoveries, projects (FAUST) or instrumental tools, among others, SKA or OASIS. Some laboratory contributions illustrating the activity in millimeter spectroscopy, gas-phase reactivity and quantum theoretical calculations conclude the present Research Topic. We expect that this research topic provides the readers with the current state of knowledge on the chemistry at different evolutionary stages of star and planet formation. This is the

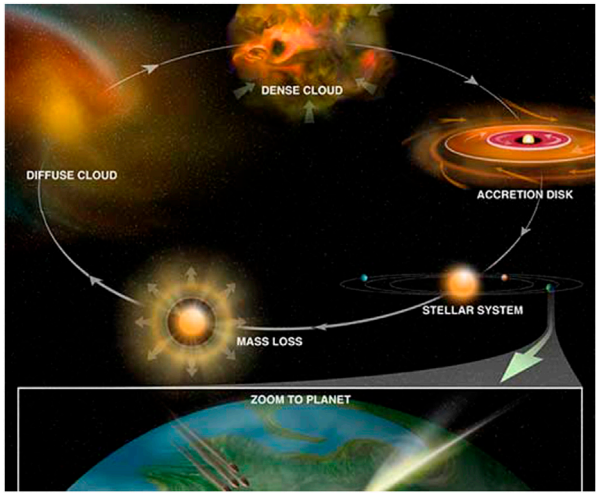

FIGURE 1
Life cycle of matter in space: from diffuse clouds to stellar and planetary formation. Credit Bill Saxton, NRAO.

chemistry at the basis of astrobiology and, in particular, of the RNA-world hypothesis for the origin of life.

In "Unusual Chemical Processes in Interstellar Chemistry: Past and Present", Herbst reviewed the historical development of the interpretation of interstellar chemistry. Both gas-phase processes and reactions on the surfaces of dust grains, the latter particularly on and in water-dominated ice mantles, in cold clouds are described. First, after an introduction on the interstellar medium (ISM), the author addresses in detail the gas-phase chemistry, with particular emphasis on radiative association. Both theoretical models and laboratory experiments are detailed. Some emphasis is put on reactions with a U-shaped rate dependence on temperature. The second part of the review, which focuses on granular chemistry, starts with a detailed review of rate equations and then introduces stochastic approaches. These are thoroughly described together with the modifications of rate equations to bring their results closer to stochastic treatments. Significant examples are provided such as the formation of methanol (CH_3OH): by revising the older literature, the mechanism currently accepted is addressed, which is CO sequential hydrogenation on grains followed by desorption of CH_3OH.

"*Gas-phase Chemistry in the Interstellar Medium: the Role of Laboratory Astrochemistry*" is the perspective contribution by Puzzarini. Here, the author provides an overview of the general problem of how molecules are formed and can further react. The role of rotational spectroscopy in guiding astronomical detections is also addressed, with emphasis placed on the interplay of quantum chemistry and experiment. The recent detection of propargylimine in the quiescent G+0.693–0.027 molecular cloud is taken as an example to outline the importance of such interplay. The author emphasizes the importance of carrying out computational studies at the state of the art in thermochemical characterization of reactive potential energy surfaces. This is illustrated by taking the reaction of methylamine (CH_3NH_2) with cyano (CN) radical as an example. A generalized system for the reaction of methanimine (CH_2NH) with a generic small radical X (e.g., OH, CN, CP, and CCH) is also presented.

Mifsud et al. contributed with a review article entitled "*The Role of Terahertz and Far-IR Spectroscopy in Understanding the Formation and Evolution of Interstellar Prebiotic Molecules*". This paper mainly consists of two sections. Section 1 describes the gas-phase ion chemistry of diffuse clouds and pre-stellar dense (dark) clouds. An overview of ongoing observational projects which include radio/sub-millimeter/Far-IR frequencies in their operational ranges is also presented there. Section 2 first addresses the spectrometer and detector technology, with particular emphasis on the THz/FIR region. In the second part of section 2, telescope facilities are summarized, while in the third part the interest is on laboratory astrochemistry using THz/FIR spectroscopy.

"*Organic Molecules in Interstellar Space: Latest Advances*" is a critical review by Guélin and Cernicharo. The authors highlight the latest astronomical observations in three different sources in interstellar space, using large sub-millimeter and radio observatories equipped with a new generation of quantum-limited and highly sensitive receivers that allowed the detection of vanishingly weak rotational transitions in molecules. The three sources are: 1) TMC-1 (a cold pre-stellar core located in the Taurus constellation); 2) an arm of a spiral galaxy at redshift z = 0.89; and 3) a young Quasar at redshift z = 2.6. TMC-1 turned out to be an amazingly rich chemical laboratory. The authors address the most exciting on-going line surveys of TMC-1 between 20 and 50 GHz: GOTHAM (GBT Observations of TMC-1: Hunting Aromatic Molecules) which uses the Green Bank Telescope facility and QUIJOTE (Q-band Ultra-sensitive Inspection Journey in the Obscure TMC-1 Environment), which takes advantage of the Yebes 40-m ground-based telescope. Both GOTHAM and QUIJOTE surveys recently reported the detection of several cyclic molecules. While GOTHAM relied on a spectral stacking technique, QUIJOTE was able to detect individual rotational lines in their surveys, owing to the sub milli-Kelvin sensitivity of the receiver. The QUIJOTE detection of indene is the first one for a double-ring species.

The authors in this review also present the detection of ten new molecules in the arm of a spiral galaxy, 6 billion light-yr distant, and twelve molecular species in a quasar at 11 billion light-yr. The chemical composition of the gas in distant galaxies seems not much different from that in the nearby interstellar clouds in the Milky Way. A profound sense of regularity in molecular composition throughout the Universe is implicated in this review article. The authors conclude that similarly to TMC-1, distant galaxies may comprise aromatic rings and complex prebiotic molecules, putative precursors of the RNA

nucleobases. However, the lines of such complex species lie below the detection limits of current investigations.

In their paper entitled "*Molecular Precursors of the RNA-world in Space: New Nitriles in the G+0.693–0.027 Molecular Cloud,*" Rivilla et al. used both the IRAM 30-m and Yebes 40-m ground-based telescopes to obtain high sensitivity spectra of the G+0.693–0.027 cloud in the 71.8–116.7 GHz, 124.8–175.5 GHz and 199.8–238.3 GHz windows. This molecular cloud, located in the Galactic Centre, raised a lot of attention quite recently with the discovery of the propargylimine molecule, which is thought to play a fundamental role in the formation of amino acids (see also Puzzarini's contribution). In the present paper, the authors focus on several nitriles including four oxygen-bearing species: namely cyanic acid (detected and quantified), cyanoformaldehyde, glycolonitrile (both only tentatively detected) and cyanoacetaldehyde (abundance upper limit provided only); and three C_4H_3N isomers: cyanoallene, propargyl cyanide and cyanopropyne. The chemistry of these molecules is also discussed and the authors point out that formation of the C_4H_3N isomers can result from gas-phase chemistry involving the CN radical and unsaturated hydrocarbons like methylacetylene or allene. Impact of the studied nitriles to prebiotic chemistry and further to the formation of building blocks of RNA is also noted with an abundant bibliography.

Codella et al. contributed a perspective article entitled "*Enlightening the Chemistry of Infalling Envelopes and Accretion Disks around Sun-like Protostars: the ALMA FAUST Project*". The primary goal of the FAUST (Fifty AU STudy) Large Program (LP) is to reveal and quantify the variety of chemical compositions found in the envelopes and disks in a sample of class 0 and I protostars at scales of 50 au, which can be considered as representative of the chemical diversity observed at larger scales. For each source, FAUST proposes a list of specific molecules that will be able to: 1) disentangle the zones of the 50–2000 au envelope/disk system; 2) characterize the organic complexity in each of them; 3) probe their ionization structure; and 4) measure their molecular deuteration. With an unprecedented sensitivity as well as spatial and spectral resolution, the FAUST project will provide a legacy dataset that will be a milestone for astrochemistry and star formation studies.

Jimenez-Serra et al. contributed with a perspective article: "*The SKA as a Prebiotic Molecule Detector*" in which they addressed the issue of possibly detecting sugars with three and four carbon atoms, such as glyceraldehyde $CHOCHOHCH_2OH$, dihydroxyacetone $CH_2OHCOCH_2OH$, and erythrulose $C_4H_8O_4$, in the ISM using the Square Kilometer Array (SKA) working in the centimeter-wave region. The SKA will be the largest radio interferometer telescope in the world operating at centimeter and meter wavelengths. The authors illustrate the possibility of detecting these large sugars and other prebiotic complex organic molecules (COMs) at rather low excitation temperatures (T_{ex}). Indeed, sources where COMs show low T_{ex} represent better targets for the search and discovery of new large prebiotic species in the ISM. It is also suggested that carrying out observations in absorption against a bright continuum background source may allow the detection of low-abundance COMs. Furthermore, it was pointed out that Giant Molecular Clouds (GMCs) located in the Galactic Center such as G+0.693–0.027 are well suited targets. Finally, the paper discusses future expansion of the SKA: The BAND 6 Receivers will increase the frequency coverage up to 50 GHz.

"*Astrochemistry with the Orbiting Astronomical Satellite for Investigating Stellar Systems*" by Bergner et al. is a research article addressing OASIS (Orbiting Astronomical Satellite for Investigating Stellar Systems): a proposed NASA mission for a space-based observatory (at THz frequencies) that will study astrochemistry of prebiotic molecules involving the CHNOPS elements. OASIS will utilize an inflatable 14-m reflector along with a heterodyne receiver to observe prestellar cores, class 0 and I protostars and their envelopes, protostellar outflows, and protoplanetary disks (evolved class II) with unprecedented sensitivity and angular resolution. OASIS covers a wide frequency range in four bands: Band-1 (455–575 GHz), Band-2 (1,100–2,200 GHz), Band-3 (2,475–2,875 GHz), and Band-4 (3,682–3,692 GHz). OASIS is expected to take the next giant step in the far-infrared spectral range, following the Herschel Space Observatory and the Stratospheric Observatory for Infrared Astronomy (SOFIA). OASIS will place constraints on abundances of light hydrides in protoplanetary disks, high-excitation organics in hot corinos and the envelopes of low-mass protostellar systems. This mission will enable the survey of line transitions of NH_3 and H_2S in protoplanetary disks specifically. It will thus provide the excitation conditions, ortho-to-para ratios, and isotopic fractionation levels of these molecules in disks. The OASIS survey of high-excitation lines in the far-infrared of organics such as acetaldehyde (CH_3CHO), dimethyl ether (CH_3OCH_3), ethanol (C_2H_5OH), and methyl formate (CH_3OCHO) in protostellar hot corinos and envelopes will play a critical role in understanding the formation and evolution of prebiotic molecules.

In "*Rotational Rest Frequencies and First Astronomical Search of Protonated Methylamine*," a research article by Schmid et al., the laboratory rest frequencies for rotational transitions of protonated methylamine, $CH_3NH_3^+$, measured in a cryogenic 22-pole ion trap machine and employing an action spectroscopy scheme, are reported for the first time. Thirteen transitions, between 80 and 240 GHz, were measured in the ground vibrational state. Since methylamine (CH_3NH_2) already has been identified in space, its protonated species is surely an interesting candidate for detection. The authors carried out a high-resolution rotational spectroscopic experiment, which was able to point out a substructure in the spectrum that was attributed to internal rotation splitting. An unsuccessful astronomical search in the star-forming objects SgrB2(N) and

SgrB2(M) using the ALMA (Atacama Large Millimeter/submillimeter Array) facility was also performed.

In "*Gas-Phase Reactivity of OH Radicals with Ammonia (NH_3) and Methylamine (CH_3NH_2) at around 22 K*," Gonzalez et al. report on the hydrogen abstraction reaction using the CRESU technique (Rowe et al., 2022). In their experimental studies, the authors observe the quantum tunneling effect, which was theoretically predicted for the hydrogen abstraction reaction by the OH radical attacking NH_3. Despite the fact that the OH + NH_3 reaction has a significant energy barrier, a non-Arrhenius behavior was experimentally confirmed. For the OH + CH_3NH_2 reaction, there are two possible exothermic channels: H-abstraction from the methyl group or from the amino group. The investigation pointed out that the reaction is much faster at 22-K than at 300-K. To conclude, the authors discuss the implication of the measured rate coefficients in modeling the abundance of interstellar NH_3 and CH_3NH_2.

A theoretical original research paper on "*Electronically Excited States of Potential Interstellar, Anionic Building Blocks for Astrobiological Nucleic Acids*" is reported by Santaloci et al. In their work, the closed-shell excited states of deprotonated anionic derivatives of benzene, naphthalene, and anthracene functionalized with either a hydroxyl or ethynyl group are quantum chemically characterized. The main focus is on the dipole-bound excited states (DBXSs) of these anion derivatives, and whether the anions are involved in the formation of nucleic acids in gas-phase astrophysical environments. The authors also discuss the possible role of functionalized polycyclic aromatic hydrocarbon (PAH) anions in the formation of nucleobases in the gas-phase.

Finally, Mathew et al., contributed with the perspective article entitled "*Methanol in the RNA world: Astrochemistry Perspective*". In this perspective article the authors anticipate that extraterrestrial methanol played a central role in the evolution of prebiotic-molecule precursors in the origin and structure of RNA world, with an extended bibliography.

Concluding remarks

The articles comprising this Research Topic provide a sample of research activities in the field of Astrochemistry, with the aim of understanding the formation of prebiotic molecules at different stages of star formation and their potential role in the origin of life. It is our opinion that synergies among observation, experiment, theory and modeling as well as among chemistry, physics and astronomy, which is peculiar to the research activities in the field of Astrochemistry are well represented in this compendium.

Author contributions

AA, AC, and DL contributed to the writing, and evaluation of the document.

Conflict of interest

The authors declare that the research was conducted in the absence of any commercial or financial relationships that could be construed as a potential conflict of interest.

Publisher's note

References

Altman, S., and Cech, T. R. (1989). *Nobel lectures*.

Rowe, B. R., Canosa, A., and Heard, D. E. (2022). *Uniform supersonic flows in chemical physics: Chemistry close to absolute zero studied using the CRESU method*. World Scientific. doi:10.1142/q0324

Turk-MacLeod, R., Gerland, U., and Chen, I. (2013). "Life: the physical underpinnings of replication," in *Astrochemistry and Astrobiology*. Editors I. W. M. Smith, C. S. Cockell, and S. Leach (Springer), 271–306.

frontiers in Astronomy and Space Sciences

REVIEW
published: 29 November 2021
doi: 10.3389/fspas.2021.757619

The Role of Terahertz and Far-IR Spectroscopy in Understanding the Formation and Evolution of Interstellar Prebiotic Molecules

Duncan V. Mifsud[1,2†], Perry A. Hailey[1†], Alejandra Traspas Muiña[3†], Olivier Auriacombe[4†], Nigel J. Mason[1†] and Sergio Ioppolo[3†]*

[1]Centre for Astrophysics and Planetary Science, School of Physical Sciences, University of Kent, Canterbury, United Kingdom, [2]Institute for Nuclear Research (Atomki), Debrecen, Hungary, [3]School of Electronic Engineering and Computer Science, Queen Mary University of London, London, United Kingdom, [4]Microwave Electronics Laboratory, Department of Microtechnology and Nanoscience, Chalmers University of Technology, Göteborg, Sweden

Stellar systems are often formed through the collapse of dense molecular clouds which, in turn, return copious amounts of atomic and molecular material to the interstellar medium. An in-depth understanding of chemical evolution during this cyclic interaction between the stars and the interstellar medium is at the heart of astrochemistry. Systematic chemical composition changes as interstellar clouds evolve from the diffuse stage to dense, quiescent molecular clouds to star-forming regions and proto-planetary disks further enrich the molecular diversity leading to the evolution of ever more complex molecules. In particular, the icy mantles formed on interstellar dust grains and their irradiation are thought to be the origin of many of the observed molecules, including those that are deemed to be "prebiotic"; that is those molecules necessary for the origin of life. This review will discuss both observational (e.g., ALMA, SOFIA, Herschel) and laboratory investigations using terahertz and far-IR (THz/F-IR) spectroscopy, as well as centimeter and millimeter spectroscopies, and the role that they play in contributing to our understanding of the formation of prebiotic molecules. Mid-IR spectroscopy has typically been the primary tool used in laboratory studies, particularly those concerned with interstellar ice analogues. However, THz/F-IR spectroscopy offers an additional and complementary approach in that it provides the ability to investigate intermolecular interactions compared to the intramolecular modes available in the mid-IR. THz/F-IR spectroscopy is still somewhat under-utilized, but with the additional capability it brings, its popularity is likely to significantly increase in the near future. This review will discuss the strengths and limitations of such methods, and will also provide some suggestions on future research areas that should be pursued in the coming decade exploiting both space-borne and laboratory facilities.

Keywords: terahertz spectroscopy, far-IR spectroscopy, astrochemistry, interstellar chemistry, prebiotic chemistry, review

OPEN ACCESS

Edited by:
Ashraf-Ali, University of Maryland, College Park, United States

Reviewed by:
Cristina Puzzarini, University of Bologna, Italy
Eric Herbst, University of Virginia, United States

****Correspondence:***
Duncan V. Mifsud
duncanvmifsud@gmail.com

†ORCID:
Duncan V. Mifsud
0000-0002-0379-354X
Perry A. Hailey
0000-0002-8121-9674
Alejandra Traspas Muiña
0000-0002-4304-2628
Olivier Auriacombe
0000-0002-5810-8650
Nigel J. Mason
0000-0002-4468-8324
Sergio Ioppolo
0000-0002-2271-1781

Specialty section:
This article was submitted to Astrochemistry, a section of the journal Frontiers in Astronomy and Space Sciences

Received: *12 August 2021*
Accepted: *08 November 2021*
Published: *29 November 2021*

Citation:
Mifsud DV, Hailey PA, Traspas Muiña A, Auriacombe O, Mason NJ and Ioppolo S (2021) The Role of Terahertz and Far-IR Spectroscopy in Understanding the Formation and Evolution of Interstellar Prebiotic Molecules. Front. Astron. Space Sci. 8:757619. doi: 10.3389/fspas.2021.757619

1 INTERSTELLAR CHEMISTRY: FROM PRINCIPLES TO PRACTICE

The idea of active chemistry occurring within interstellar space is a relatively new one. Historically, interstellar temperatures and pressures were considered to be far too low to permit atoms or ions to come into contact with each other and overcome a reaction activation energy barrier. However, since the first evidence of interstellar molecular species arose in the late 1930s, the scientific community has come to recognize that the interstellar medium is home to a plethora of structurally diverse molecules, with different environments displaying their own characteristic chemistry. A more complete description of the history of astrochemistry may be found in the work of Feldman (2001).

Matter in the interstellar medium is composed of around 99% atomic or molecular hydrogen and 1% carbonaceous or silicate dust grains. This matter is cycled through a number of phases each displaying a characteristic chemistry (**Figure 1**). The smallest over-densities result in the formation of diffuse clouds, which possess particle densities of 10^2–10^3 cm^{-3} and kinetic temperatures of a few hundred K (Smith 1992). Diffuse clouds are relatively transparent to visible light and are continuously exposed to the interstellar radiation field which results in the dissociation and ionization of molecular material. As such, these clouds are dominated by the presence of atoms and ions, particularly H and H^+, although a few molecular species do survive (Snow and Bierbaum 2008). Indeed, the first molecules to be detected in interstellar space were detected in diffuse interstellar media via optical spectroscopy (Smith 1992; Feldman 2001; Larsson et al., 2012). With the notable exception of the formation of H_2 (Wakelam et al., 2017), most of the chemistry within diffuse interstellar clouds is mediated by gas-phase reactions (Geppert and Larsson 2013).

Accumulation of gaseous material within diffuse clouds may occur as a result of random perturbations, stellar winds, or more violent phenomena such as supernovae-induced shock waves. As diffuse clouds begin to accumulate matter, the proportion of molecular material (mainly H_2) increases. This is accompanied by a diminishing of the proportion of ionized species present: for example, the dominant form of carbon changes to the atomic form from C^+ and the number of free electrons also decreases (Snow and Bierbaum 2008). Thus, the accumulation of matter results in an evolution of so-called "atomic" diffuse clouds to "molecular" diffuse clouds.

Further accumulation of material as a result of gravitational attractions results in the formation of a dense interstellar cloud (also known as a dark interstellar cloud). These clouds are, as

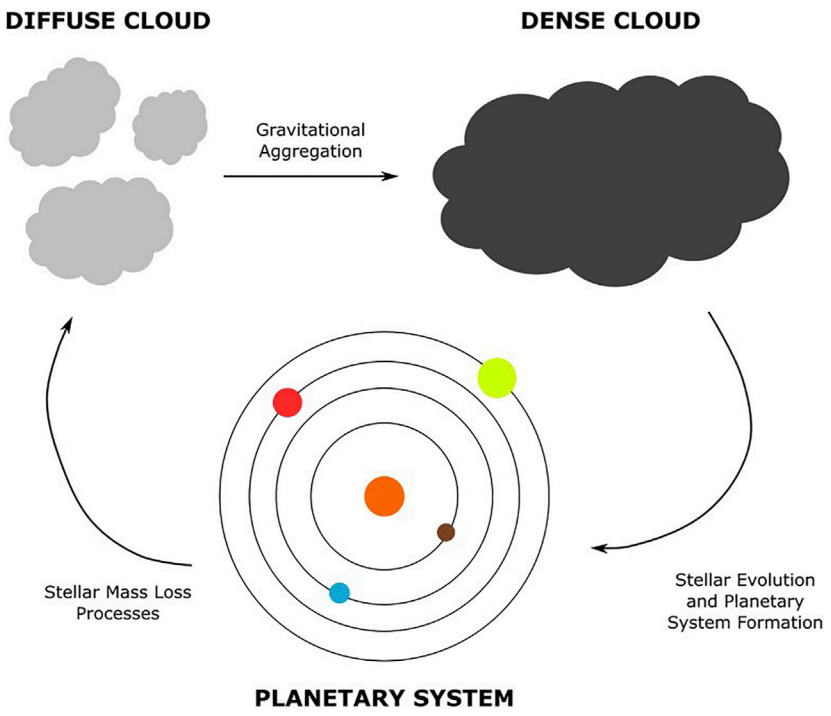

FIGURE 1 | Matter in the interstellar medium is cycled through various phases: the aggregation of matter results in optically transparent diffuse clouds evolving into dense, dark molecular clouds. These clouds are considered to be "stellar nurseries" in which localized gravitational collapse results in the formation of a proto-star, with further accretion of material occurring via magneto-hydrodynamic flows onto the growing star. Within a few million years, the stellar object evolves into a pre-main sequence star surrounded by a proto-planetary disk. Collisions within the disk result in the accretion of dust grains which slowly grow to form planetesimals, thus taking the first steps towards the formation of a planetary system. Once the star's nuclear fuel has been exhausted, it may follow one of two routes depending on the stellar mass: low-mass stars undergo several mass-loss processes in which molecular material is dispersed back into the interstellar medium leaving behind a remnant white dwarf, whereas high-mass stars instead explode as supernovae with their cores eventually becoming either neutron stars or black holes.

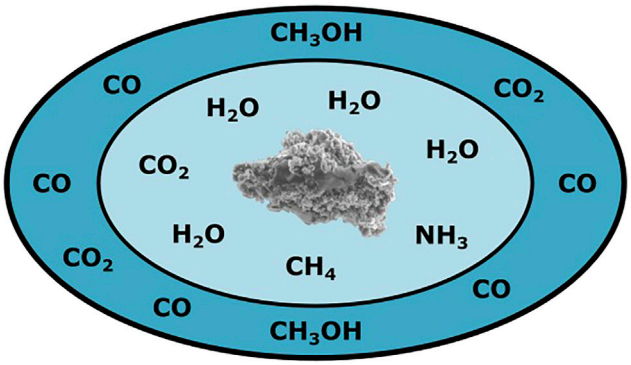

FIGURE 2 | Median structure of icy grain mantles within dense interstellar clouds. Shown in the image, a diagram (not to scale) of a typical icy mantle divided into two zones: a lower polar layer rich in H_2O molecules and hydrogenated heteroatoms, and an upper apolar layer largely consisting of CO and related molecules. More detailed information can be found in the work of Öberg (2016).

their name suggests, characterized by higher particle number densities of up to 10^6 cm^{-3} and are the primary location of stellar formation. The increase in density results in a concomitant increase in cloud opacity. As such, the far- and vacuum-UV components of the interstellar radiation field are attenuated at the edges of the cloud, resulting in an interior with a temperature of 7–20 K (Galli et al., 2002). The higher particle densities of these dark clouds enhance the efficiency of reactions in the gas phase, particularly those between ions and molecules, and contribute to the formation of several new species including complex organic molecules (Bergin and Tafalla 2007; Öberg 2016; Arumainayagam et al., 2019).

At the low temperatures encountered within the interiors of dense interstellar clouds, many species are able to freeze-out onto the surfaces of the carbonaceous and silicate dust grains, thus forming an icy mantle. This icy mantle is typically composed of two zones (**Figure 2**): a lower polar layer which results from the deposition and synthesis (via hydrogenation reactions) of polar molecules such as H_2O, NH_3, and also CH_4; and an upper apolar layer characterized by the presence of CO and related molecules such as CO_2 and CH_3OH (Larsson et al., 2012; Öberg 2016).

These molecular icy grain mantles play host to a rich chemistry mediated by several phenomena and which may result in the formation of complex molecules. For instance, galactic cosmic rays are not attenuated by the boundaries of the dense cloud, and so are able to penetrate through to the cloud core and induce chemistry within the icy layers. Interactions between these cosmic rays and gas-phase H_2 results in the emission of Lyman-α photons which may induce photochemistry. Photochemistry in icy grain mantles may also be induced by lower wavelength photons which enter the cloud via less dense regions. Thermal chemistry may also occur in ices proximal to a heat source, such as a nascent star.

In this section, we review the chemistry which occurs within diffuse and dense interstellar clouds with a particular focus on reactions involving ionic species, and those which result in the formation of complex organic molecules. We should note that, in the literature, the term "complex organic molecule" typically refers to a saturated molecule which may be conceivably formed by geological or biochemical processes. However, for the purposes of this review, we extend this definition to include the unsaturated polyatomic carbon chains which have been detected in astrophysical settings. An understanding of interstellar chemistry is an important prerequisite for a discussion of the experimental and observational techniques used in astrochemistry, and although mentions of detections via terahertz and far-IR (THz/F-IR) spectroscopy and related techniques will be made, further details on such techniques will be given in the subsequent section. Reviews on the chemistry occurring during the various other phases of the astrochemical cycle (**Figure 1**) are also available elsewhere (van Dishoeck and Blake 1998; Williams and Hartquist 1999; Larsson et al., 2012; Geppert and Larsson 2013; van Dishoeck 2014).

1.1 Diffuse Interstellar Clouds: Overview of Ion Chemistry

As mentioned previously, matter within most diffuse interstellar clouds is primarily composed of atomic and ionic material, with a significantly smaller number of molecules also being present due to the high rates of photon and cosmic ray induced dissociation and ionization processes. Consequentially, the chemistry within these clouds is dominated by gas-phase reactions including those involving or producing ions. At the edges of the diffuse cloud, where stellar UV radiation is more intense, photo-ionization of carbon atoms produces C^+, while within the diffuse cloud interior cosmic ray driven chemistry is more dominant and allows for the ionization of H and H_2 (Smith 1992). The formation of H_2^+ in particular is important, as this species is the direct precursor to H_3^+:

$$H_2 + H_2^+ \rightarrow H + H_3^+$$

For a long time, the formation and presence of H_3^+ within diffuse clouds were highly controversial due to its suspected high rate of dissociative recombination mediated by electrons emitted from the photo-ionization of carbon atoms (Larson et al., 2000; Larsson et al., 2008). However, its direct observation in diffuse clouds (McCall et al., 1998) combined with the discovery of a new method of recombination (Kokoouline and Greene 2003) confirmed its presence and role within interstellar chemistry: H_3^+ efficiently donates a proton to other atoms and molecules due to the low proton affinity of H_2. The resultant protonated species is reactive, and is thus capable of triggering various chains of ion-molecule reactions. For instance, the reaction with CO produces HCO^+, while the reaction with atomic oxygen produces OH^+:

$$H_3^+ + CO \rightarrow H_2 + HCO^+$$
$$H_3^+ + O \rightarrow H_2 + OH^+$$

OH^+ may also be formed as a result of a two-step process starting with the charge-transfer reaction between atomic oxygen and H^+ to yield O^+, which subsequently reacts with H_2 to furnish OH^+ (Yamamoto 2017). The formation of OH^+ is the first step

towards the formation of interstellar gas-phase H_2O. The reaction of OH^+ with one moiety of H_2 yields H_2O^+, and the reaction with a second moiety produces H_3O^+ (Larsson et al., 2012). The H_3O^+ molecular ion is isoelectronic with NH_3 and so is a stable species which resists further reactions with H_2 (Geppert and Larsson 2013). Instead, it undergoes dissociative recombination with electrons to yield either OH (~60% of outcomes) or H_2O (~25% of outcomes).

The detections of OH^+, H_2O^+, and H_3O^+ within diffuse interstellar environments have been made using ground- and space-based telescopes working in the THz/F-IR range, such as the Atacama Pathfinder Experiment (APEX) and the HIFI instrument aboard the Herschel Space Observatory (for more detail, refer to **Section 2**), thus confirming their contribution to chemistry in such settings (Gerin et al., 2010a; Gupta et al., 2010; Wyrowski et al., 2010; Wiesemeyer et al., 2016). A reaction scheme analogous to the formation of H_2O from OH^+ has also been invoked to explain the formation of HCl within diffuse clouds starting from Cl^+. Such a reaction scheme has been validated by the detection of the relevant intermediate species HCl^+ and H_2Cl^+ by the HIFI instrument (Lis et al., 2010; De Luca et al., 2012).

Reactions leading to the formation of carbon-bearing molecules within diffuse interstellar media are more challenging to explain compared to the oxygen and chlorine chemistry outlined above. Indeed, the formation of CH^+, one of the earliest known interstellar molecules (Douglas and Herzberg 1941), is still not completely understood and several simulations have underestimated its observed abundance within diffuse clouds (e.g., van Dishoeck and Black 1986; Pan et al., 2004; Godard et al., 2009). It is apparent that the formation of CH^+ cannot rely on the reaction between H_2 and C^+ due to the considerable endothermicity of this reaction (Myers et al., 2015; Valdivia et al., 2017; Mosely et al., 2021; Plašil et al., 2021). In light of this, alternative mechanisms have been suggested to account for its presence within the diffuse interstellar medium. For instance, it has been suggested that the radiative association of C^+ and H_2 to yield CH_2^+ with the concomitant emission of a photon is the first step towards interstellar CH^+, as the photo-dissociation of the former may lead to the latter (Yamamoto 2017). However, the rate at which radiative association occurs is fairly low (Graff et al., 1983; Barinovs and van Hemert 2006) and indeed the primary reaction pathway of CH_2^+ within diffuse interstellar media is the reaction with H_2 which furnishes CH_3^+. As such, the potential contribution of this reaction network in accounting for interstellar CH^+ abundances is probably low.

Another proposed formation route for CH^+ is the direct reaction between C^+ and H_2 if the endothermicity of the reaction is overcome by some mechanism which causes a localized warming effect which raises the temperature to a few thousand K. Initially, it was thought that this localized warming could be achieved in regions of the diffuse cloud processed by magneto-hydrodynamic shock waves (Elitzur and Watson 1980; Draine and Katz 1986). However, such processes are now thought to be an unlikely source of CH^+ as the radial velocity for this molecule and for CH have been observed to be similar. Among other ideas, gas heating caused by turbulences within the cloud has also been found to be unsatisfactory in accounting for the observed abundances of CH^+ (Godard and Cernicharo 2013), as have reactions between C^{2+} and H_2 in X-ray dominated regions of the diffuse cloud (Plašil et al., 2021). Alfvén waves have also been suggested as a potential source of CH^+ (Federman et al., 1996), however, to the best of the authors' knowledge, this has been neither corroborated nor firmly rejected. As such, the elusive source of CH^+ within diffuse interstellar media remains an unanswered question. There thus exists a strong motivation to address this problem, as the formation of CH^+ may be an important step in the synthesis of significantly more complex carbon-based molecules such as fullerenes and polycyclic aromatic hydrocarbons (PAHs), which are suspected of being the primary carriers of observed diffuse interstellar bands and which may bear relevance to the synthesis of prebiotic molecules (Taylor and Duley 1997).

With regards to molecular detections in diffuse interstellar clouds, a significant number have been made using methods and techniques which exploit the submillimeter, millimeter, and centimeter regions of the electromagnetic spectrum, including THz/F-IR spectroscopy (Snow and McCall 2006; Yamamoto 2017). Indeed, such techniques are the preferred method for detecting polyatomic molecules, as these molecules are difficult to identify using optical spectroscopy (as was done historically) due to the pre-dissociative nature of their excited states. The HIFI instrument aboard the Herschel Space Observatory in particular has proven to be invaluable to the detection and mapping of molecules in diffuse interstellar media, having provided much information on the chemistry of hydrogen-, carbon-, oxygen-, nitrogen-, sulfur-, fluorine-, and chlorine-bearing molecules within diffuse clouds (Gerin et al., 2010a, 2010b, 2012; Neufeld et al., 2010a, 2010b, 2012a; Langer et al., 2010; Persson et al., 2010; Sonnentrucker et al., 2010; Monje et al., 2011, 2013; De Luca et al., 2012; Esplugues et al., 2014; Schilke et al., 2014; Indriolo et al., 2015; Jacob et al., 2020).

Other instruments and telescopes have also aided greatly in the elucidation of the chemical complexity of the diffuse interstellar medium. For example, APEX, the Atacama Large Millimeter/Submillimeter Array (ALMA), and the GREAT instrument aboard the Stratospheric Observatory for Infrared Astronomy (SOFIA) have all been used in the detection of sulfur-bearing molecules, including isotopologues (Menten et al., 2011; Neufeld et al., 2012b, 2015; Muller et al., 2017). Perhaps the most exciting of all has been the series of recent ALMA observations of complex molecules. The work of Thiel et al. (2017), for instance, investigated the presence of prebiotic complex organic molecules within diffuse media and detected several species, including CH_3OH, CH_3CN, CH_3CHO, HC_3N, and $CHONH_2$. Such results are of immense consequence, as they imply that certain molecular precursors to life either form early on in the astrochemical cycle (**Figure 1**), or else survive a process of expansion from denser interstellar media.

1.2 Dense (Dark) Interstellar Clouds: Overview of Ion Chemistry

Condensation of diffuse clouds results in the formation of dense (dark) clouds. During this process, the dominant material is

converted from atomic and ionic species to molecular ones. For instance, H_2 becomes the dominant form of hydrogen, while the dominant form of carbon changes sequentially from C^+, to C, and finally to CO (Snow and Bierbaum 2008; Larsson et al., 2012). As such, these structures have also been appropriately dubbed molecular clouds. In their review, Arumainayagam et al. (2019) highlighted the chemical productivity of dense clouds and identified three milieux for astrochemical reactions within them. The first of these is gas-phase chemistry, which includes radical-radical, radical-neutral, and ion-neutral reactions. The second is chemistry occurring on bare carbonaceous or silicate dust grain surfaces, while the third includes all chemical reactions occurring via energetic and non-energetic processing of icy grain mantles. In this sub-section, we will largely limit ourselves to a brief overview of ion-molecule reactions which occur in the gas-phase within dense interstellar clouds.

Gas-phase ion-neutral reactions within dense interstellar clouds are favorable, barrierless chemical processes. The source of the ionic species within the cloud is somewhat dependent upon the location of the reaction within the cloud structure. Within the densest regions (surrounding the cloud core), ionization of molecules is caused almost exclusively by penetrating galactic cosmic rays. However, within the less dense regions of the clumpy cloud structure, far- and vacuum-UV components of the interstellar radiation field are the primary cause of molecular ionization via photon-induced electron loss processes. Furthermore, in the presence of OB stars, irradiation of molecular material by X-rays may also contribute to the formation of ionic species.

Cosmic ray induced ionization of H_2 leads indirectly to the formation of H_3^+ as was described for diffuse interstellar clouds. The low proton affinity of H_2 allows H_3^+ to be an efficient proton donor to other species (Larsson et al., 2012). For example, the reaction with N_2 yields N_2H^+, which is frequently used as a tracer for N_2 within interstellar space when observing with radio telescopes, since N_2 does not possess a permanent dipole moment. Ionized hydrogen, primarily in the form of H^+, readily undergoes reactions with other atoms such as nitrogen atoms. The resultant product NH^+ may undergo subsequent hydrogenation reactions with H_2 to sequentially form NH_2^+, NH_3^+, and NH_4^+ (Geppert and Larsson 2013). Finally, dissociative recombination with an incident electron efficiently affords gas-phase NH_3 (Öjekull et al., 2004).

Interestingly, the analogous reaction pathway to the formation of gas-phase CH_4 is not thought to be significant within dense clouds. This is because once CH_5^+ is formed, the dominant dissociative recombination mechanism involves the simultaneous loss of two hydrogen atoms, creating CH_3 rather than CH_4 (Semaniak et al., 1998; Viti et al., 2000). The formation of CH_4 and several other carbon-based molecules within the interstellar medium is instead likely to rely on other mechanisms, such as hydrogenation reactions at the surfaces of dust grains (Qasim et al., 2020).

A large number of carbon-based complex organic molecules are known to exist within dense clouds. Until recently, it was thought that these molecules formed within the solid phase in icy grain mantles and were released into the gas phase upon thermal or photo-desorption. However, a growing body of literature has documented the presence of such gas-phase complex organic molecules within starless and pre-stellar cores, where such desorption processes do not take place. Scibelli and Shirley (2020), for instance, have detected CH_3OH and CH_3CHO in several such environments and have suggested that the radicals and molecules responsible for the formation of these species may be formed in the ice phase. The release of energy upon their formation allows them to sublimate into the gas phase (a process termed reactive desorption) whereupon they react to form these product molecules.

Another region of dense clouds which may host a rich gas-phase chemistry leading to the formation of complex organic molecules is the edge of the cloud: the photo-dissociation region (PDR). In this region, the cloud interacts with the intense UV components of the interstellar radiation field resulting in the desorption of solid-phase molecules and an increase in the occurrence of gas-phase processes. Using the IRAM 30 m telescope, Cuadrado et al. (2017) were able to perform a millimeter line survey towards the edge of the Orion Bar PDR and successfully detected a plethora of complex molecules including carboxylic acids, aldehydes, alkenes, and sulfur-containing molecules. Soma et al. (2018) reported similar results. The production and survival of complex molecules in such an environment is significant from the perspective of astrobiology and, although their exact formation mechanisms are still not completely understood, it is likely that a non-negligible contribution comes from gas-phase reactions.

Of course, other processes leading to the formation of complex organic molecules within dense interstellar clouds are also known. Garrod et al. (2008), for instance, demonstrated that the warm up of icy grain mantles previously processed by galactic cosmic rays under cold conditions yielded various complex organic molecules in abundances which matched those documented observationally, while Balucani et al. (2015) invoked radiative association as a gas-phase process leading to their formation. An interesting mechanism which has been suggested to account for the formation of complex organic molecules is that of non-diffusive surface reactions, which have been experimentally shown to yield such species in reasonably high abundances (Fedoseev et al., 2015, 2017; Chuang et al., 2016; Ioppolo et al., 2021).

The presence and distribution of complex, potentially prebiotic molecules within the interstellar medium have been extensively probed using various ground- and space-based observatories. Perhaps the most productive of these studies, however, have been those which have made use of the ALMA for molecular detections (Belloche et al., 2016, 2019; Garrod et al., 2017; Jørgensen et al., 2018; Calcutt et al., 2019; Willis et al., 2020). The impact of ALMA observations on the detection of interstellar molecules has been massive: first detections of prebiotic molecules which were previously controversial or unconfirmed, such as urea (NH_2CONH_2), have been achieved (Belloche et al., 2019), and more information has been gleaned on

interstellar chemical processes such as deuteration (Belloche et al., 2016).

To conclude this sub-section, we provide an overview of two especially fruitful ongoing observational projects which include THz/F-IR, millimeter, and centimeter frequencies in their operational ranges: the GOTHAM and ARKHAM projects. These projects are run using the Robert C. Byrd 100 m Green Bank Telescope in the United States and have provided significant data demonstrating the presence of complex organic molecules within interstellar space, with a particular focus on aromatic species. Although operating in a similar fashion, the projects themselves have somewhat different objectives.

The GOTHAM project is primarily concerned with establishing a chemical inventory of the Taurus Molecular Cloud, one of the nearest dense clouds, by performing high-sensitivity wide-band spectral line surveys. Such work is motivated by the fact that benzonitrile (*c*-C_6H_5CN) was recently discovered in this pre-stellar source (McGuire et al., 2018a), contrasting with a working hypothesis which postulates that larger interstellar aromatic molecules are produced in the circumstellar regions of post-AGB stars and subsequently break down into smaller sub-units such as benzene (*c*-C_6H_6) under energetic processing (Tielens 2008): so-called "top-down" chemistry. However, these results suggest that reactions between smaller precursor molecules may also contribute to the formation of larger aromatics within pre-stellar regions through a "bottom-up" chemistry approach.

GOTHAM observations of the Taurus Molecular Cloud, combined with laboratory-generated spectra and computational models, have successfully identified many molecules, some of which had not yet been described in the interstellar medium. The unsaturated molecules detected within this dense cloud may play a pivotal role in the formation of larger aromatic molecules, as well as other species relevant to the origins of life. Early work from GOTHAM identified propargyl cyanide ($HCCCH_2CN$) and the cyanopolyyne $HC_{11}N$ in the Taurus Molecular Cloud (McGuire et al., 2020; Loomis et al., 2021). Cyclic molecules have also been discovered, including 1-cyanocyclopentadiene and 2-cyanocyclopentadiene (Burkhardt et al., 2021a; McCarthy et al., 2021; Lee et al., 2021a). Other cyano and isocyano species have also been detected (Xue et al., 2020; Lee et al., 2021b).

The ARKHAM project is focused on investigating whether the chemistry observed in the Taurus Molecular Cloud is also found in other pre-stellar and proto-stellar sources so as to assess whether or not the resultant molecules survive the birth and evolution of a proto-star. Results from the project have shown that benzonitrile has been detected in four additional sources: Serpens 1A, Serpens 1B, Serpens 2, and MC27/L1521F (Burkhardt et al., 2021b). Such detections illustrate that aromatic chemistry is favorable and extensive throughout the very earliest stages of star formation. Interestingly, the observed abundances of benzonitrile exceeded those predicted by models, despite these models being well-suited to other large carbon-based molecules such as cyanopolyynes. It is therefore probable that the formation mechanisms of other aromatic species in pre-stellar sources differ from those of linear molecules and are not yet well understood.

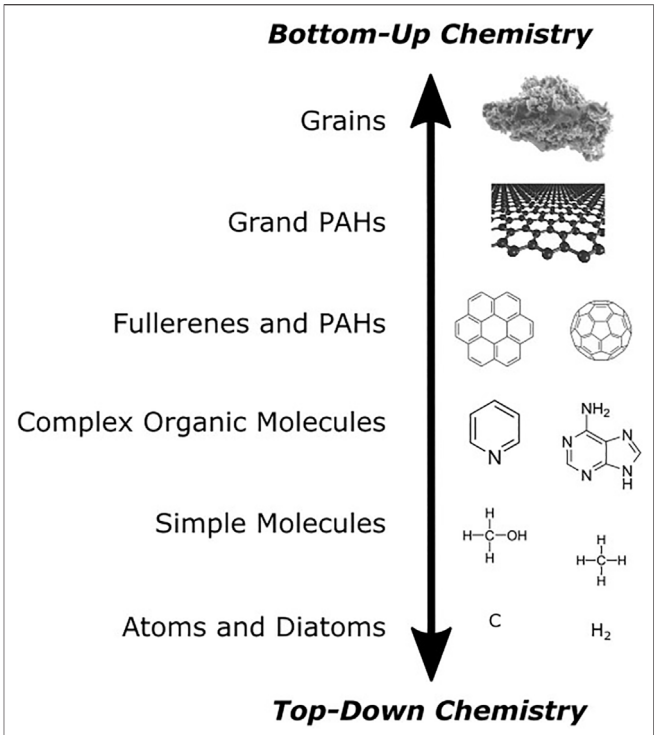

FIGURE 3 | Schematic diagram exhibiting models of "top-down" and "bottom-up" chemistry using carbon molecules as an example. In the "bottom-up" perspective, the association of atoms and simple molecules allows for the formation of larger molecules such as CH_4 and CH_3OH. Further additions to the molecular structure may result in the formation of a complex organic molecule, such as an aromatic molecule or a PAH. Two-dimensional extension of the PAH structure produces graphite, which itself may be considered the basis of (sub-)micron sized interstellar carbonaceous dust grains. The "top-down" chemical perspective is essentially the reverse of this, in which larger molecular structures are broken up as a result of energetic processing, thus yielding simpler molecules.

1.3 The Link to Prebiotic Chemistry

Joint observational and laboratory investigations are key to deciphering the exact mechanisms of formation of the various complex organic molecules observed within interstellar and circumstellar media. To date, these studies have largely relied on a "bottom-up" chemical perspective in which large complex molecules are produced from simpler starting molecules undergoing some form of processing (such as photolysis or radiolysis). However, as has been demonstrated by the GOTHAM and ARKHAM projects, the formation of certain molecules (such as aromatic species) is likely to be dependent on some combination of "bottom-up" and "top-down" chemistry (McGuire et al., 2020): that is to say that they are formed both from the joining together of smaller molecules, ions, and radicals, as well as the break-up of larger structures (**Figure 3**).

PAHs are perhaps the best class of interstellar molecules to exemplify the contributions of "top-down" and "bottom-up" astrochemistry due to the fact that they are thought to be relatively ubiquitous in interstellar media, and also because they are able to undergo many chemical transformations yielding a plethora of molecular structures with various sizes,

complexities, and arrangements of the aromatic rings, as well as different chemical characteristics such as the inclusion of heteroatoms and the addition of functional groups (such as amino or carboxylic moieties). Indeed, such chemical transformations are thought to be key to the formation of very small grains and fullerenes which result from the respective agglomeration and destruction of PAHs, as well as serving as a carbon feedstock for the production of molecules relevant to biology (Tielens 2008; Groen et al., 2012).

For instance, when mixed with H_2O and subjected to energetic processing (a scenario which is plausible within icy grain mantles in the dense interstellar medium), PAHs have been shown to incorporate oxygen into their molecular structure and display new functional groups such as alcohols, ethers, and ketones (Cook et al., 2015). The addition of a ketone moiety to the PAH is biologically significant, as this provides the base structure for the vitamin K chemical family. Incorporation of heteroatoms (such as oxygen and nitrogen) into the ring structure of the PAH as a result of the energetic processing of mixed icy grain mantles is also possible (Materese et al., 2015), and the resultant heterocyclic molecules are also of great biological significance with nitrogen-containing heterocycles such as pyrimidine and purine being the building blocks for nucleobases.

Pyrimidine has yet to be formally detected within the interstellar medium, however it possesses many similar physico-chemical characteristics to PAHs and so is expected to exist to some extent within icy grain mantles. The UV irradiation of frozen pyrimidine in the presence of H_2O, CH_3OH, NH_3, and CH_4 has been shown to yield the nucleobases uracil, cytosine, and thymine (Nuevo et al., 2009, 2012, 2014; Bera et al., 2016). Similarly, the irradiation of purine in ices containing NH_3 and H_2O leads to the formation of the nucleobases guanine and adenine (Bera et al., 2017; Materese et al., 2017, 2018). Although the idea of an extended lifetime for these nucleobases within interstellar and near-Earth environments has been called into question (Peeters et al., 2003), if there exists some plausible mechanism by which they survive the stellar evolution phases of the astrochemical cycle depicted in **Figure 1**, then it is possible that they may have been delivered to the early Earth via meteoritic or cometary impacts, thus providing the starting material for the so-called "RNA World Hypothesis".

The RNA World Hypothesis (Orgel 2004; Bernhardt 2012; Neveu et al., 2013; Higgs and Lehman 2015) hypothesizes that RNA or RNA-like molecules mediated the necessary information processing and metabolic transformations required for life to emerge from the early Earth's prebiotic environment. Systems based on RNA could act as a precursor to the significantly more complex system of RNA, DNA, and proteins on which current life is based, and it has been recognized that the ribonucleotide co-enzymes now used by many proteins may in fact be molecular fossils from an RNA-based metabolism (White 1976; Raffaelli 2011). The existence of naturally occurring ribozyme catalysts, such as self-splicing introns and the ribonuclease P catalyst (Kruger et al., 1982; Doudna and Cech 2002), along with the fact that ribosomal RNA actually catalyzes the formation of peptide bonds in the ribosome (Lang et al., 2008), has lent some weight to this hypothesis. However, much is still unknown as to the exact mechanisms by which life could arise in the RNA World, and so the hypothesis remains one among many seeking to explain the origins of biology from chemistry.

The "top-down" aspect of PAH astrochemistry has also been considered by previous studies (Merino et al., 2014; Dartois et al., 2020). For instance, Merino et al. (2014) demonstrated experimentally that hydrogen atom interaction with graphene on top of SiC at elevated temperatures triggers an erosion process which results in the ejection of PAH-like flakes. Such results offer an alternative and efficient synthetic pathway for the formation of gas-phase PAHs in the interstellar medium. In the envelopes of evolved stars, SiC condenses to form grains whereupon thermal annealing by the proximal star results in an elemental segregation and the synthesis of a carbon-rich surface (Frenklach et al., 1989; Merino et al., 2014). Exposure of this surface to hydrogen atoms is likely in this environment, and the elevated temperatures (>1000 K) permit a thermally assisted etching effect to take place, thus resulting in the desorption of PAHs.

The dissociation of PAHs themselves into smaller molecules is also a possible process, and has been invoked to explain the interstellar presence of fullerenes, particularly C_{60}. Experimental and modelling studies have shown that PAHs containing 60-66 carbon atoms may be completely dehydrogenated by UV photons to a graphene-like structure, after which the structure folds into a cage. Photon-induced shrinking of the structure then proceeds via the rate-limiting loss of C_2 units until the C_{60} fullerene structure is attained (Berné and Tielens 2012; Zhen et al., 2014; Berné et al., 2015). The need to further characterize this "top-down" chemistry, particularly as it relates to other smaller carbon-based molecular species which may be relevant to prebiotic chemistry, was highlighted by van Dishoeck (2017).

2 THE USE OF THZ/F-IR SPECTROSCOPY IN ASTROCHEMISTRY

THz/F-IR frequencies cover the region of the electromagnetic spectrum ranging between 0.3–10 THz (10-333 cm^{-1}), although the upper boundary is somewhat arbitrary and some sources consider it to be as high as 30 THz (Dhillon et al., 2017). Since, by some popular definitions, the THz/F-IR range begins at a wavelength of 1 mm and proceeds to shorter wavelengths, it is sometimes also referred to as the submillimeter band. The main advantages of performing spectroscopy at such frequencies are the possibility of resolving rotational and ro-vibrational spectral transitions of gaseous molecular species, and the potential to probe long-range interactions between molecules in the solid phase in terms of low-energy intra- and intermolecular modes (Brown and Carrington 2003; Profeta and Scandolo 2011; Townes and Schawlow 2013). Thus, THz/F-IR spectroscopy makes for a unique tool in the detection of gases and ices in interstellar clouds and circumstellar disks against the widespread dust continuum via a number of distinct absorption and emission spectral signatures.

For example, the H_2O molecule (whose energy transitions are well-defined) is an asymmetric rotor with an irregular set of energy levels characterized by the rotational quantum number J

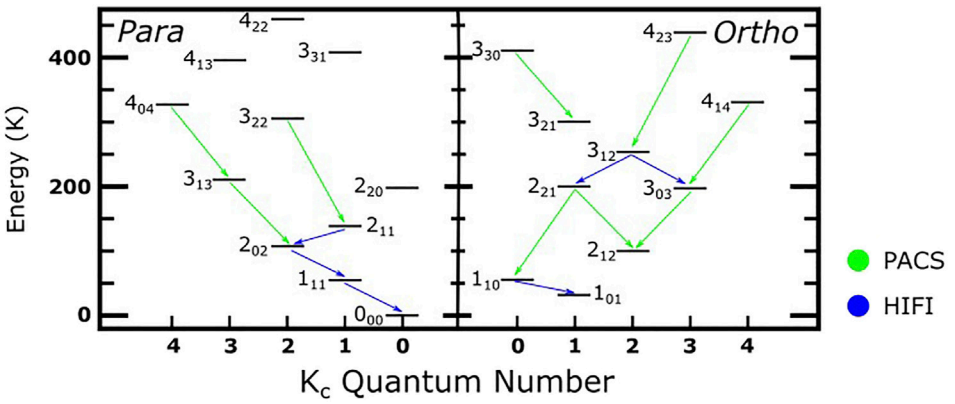

FIGURE 4 | Energy level diagram of ortho- and para-H_2O showing the transitions observed by the PACS and HIFI instruments aboard the Herschel Space Observatory. Further information may be found in the work of van Dishoeck et al. (2013).

and the pseudo-quantum numbers K_a and K_c (which replace the quantum number K used when considering symmetric rotors). These pseudo-quantum numbers represent hypothetical quantum states for the asymmetric rotor were it to assume the geometry of a prolate and oblate rotor, respectively (Cooke and Ohring 2012). Depending on the orientation of the nuclear spins of the constituent hydrogen atoms, the H_2O molecule is either ortho- (if the spins of the hydrogen atoms are parallel) or para- (if the spins are anti-parallel). Each excitation or de-excitation of electrons from one energy level to another results in the propagation of photons of a certain energy (i.e., frequency). **Figure 4** shows the energy levels of ortho- and para-H_2O in terms of their pseudo-quantum numbers as detected by the Herschel Space Observatory. In this section, we provide a detailed description of the technical fundamentals of THz/F-IR spectroscopy, as well as an overview of its current applications to astrochemistry.

2.1 Spectrometer and Detector Technology

THz/F-IR laboratory spectroscopy measurements may be acquired using several different methods: Fourier-transform IR spectroscopy (Griffiths and de Haseth 1986), spectroscopy based on photo-mixing (Preu et al., 2011) or parametric conversion (Kawase et al., 1996; Kiessling et al., 2013), backward-wave oscillator spectroscopy (Medvedev et al., 2010), chirped-pulse Fourier-transform spectroscopy (Park and Field 2016), time-domain spectroscopy (Auston, 1975; van Exter et al., 1989; Mittleman et al., 1998), and cascaded frequency multiplication (Drouin et al., 2005; Li and Yao 2010). These methods are all based on the detection of a continuous wave, broadband source, or pulsed THz/F-IR radiation illuminating gaseous or solid (i.e., ice) molecular samples of a species, and having varying frequency spectral ranges, sensitivities, and performances. For example, chirped-pulse spectrometers have a frequency bandwidth of up to 100 GHz (Park and Field 2016), while backward oscillation and time-domain spectrometers have frequency ranges of up to 2.1 THz and 7.5 THz, respectively (Komandin et al., 2013; Allodi et al., 2014).

THz/F-IR time-domain spectroscopy can combine the generation of a THz/F-IR pulse in a zinc telluride crystal via opto-electronic rectification or from plasma filamentation in air using (in both cases) a femtosecond laser with a delay line and opto-electronic detection method in order to record the time domain trace (Allodi et al., 2013). This kind of spectroscopy has been widely used for gas-phase spectral line characterization in vacuum chambers (Kilcullen et al., 2015), in the study of refractive indices (Giuliano et al., 2019), and in the study of intermolecular transitions in astrophysical ice analogues, where the THz/F-IR signal is reflected by or transmitted through the gas or ice. Although it is able to provide critical information regarding the frequency of the spectral transition and the absorption coefficient, it does have a few disadvantages including slow acquisition times and a fine-tuning requirement (Trofimov and Varentsova 2016). As such, these instruments are appropriate only for laboratory settings, and other detectors are usually found in observatories.

One form of THz/F-IR spectroscopy which has found widespread use within laboratory astrochemistry settings is that based on cascaded frequency multiplications (Drouin et al., 2005; Li and Yao 2010). This technology is based on using a sweep synthesizer as the source of radiation, which is used in a phase-locked continuous wave mode during measurements and which has a low phase-noise output. A filter (typically an yttrium iron garnet) is swept simultaneously to this synthesizer so as to suppress any frequency spurs. Frequency sextuplers allow for the production of millimeter radiation having a few milliwatts of power, which is then amplified via the use of microwave integrated circuit amplifiers to generate millimeter radiation with a few hundred milliwatts of power. Cascaded doublers or triplers then follow these amplifiers and generate the submillimeter (i.e., THz/F-IR) wavelength radiation.

Incoherent or direct detector arrays are commonly used in THz/F-IR observatories combined with multiplexer readout systems. They require a higher sensitivity than the photon background noise (such as the microwave background) and

TABLE 1 | Examples of the sensitivities achieved by selected observatories operating in the THz/F-IR range.

Observatory	Aperture (m)	Instrument	Frequency Band (GHz)	Detector Technology
IRAM Telescope	30	NIKA2	150, 260	KIDs
CSO (Caltech Submillimeter Observatory)	10.4	MUSIC	142, 212, 272	KIDs
		SHARC II	666, 857	Bolometers
		MAKO	857	KIDS
		Heterodyne Receiver	117–920	SIS
		Z-Spec	190–230	Bolometers
JCMT (James Clerk Maxwell Telescope)	15	SCUBA	353, 666	Bolometers
		SCUBA2	353, 666	TES
		HARP	325–375	SIS
		Nāmakanui	86, 215-371	SIS
ODIN	1.1	SMR	118–580	Schottky
SMA (Submillimeter Array)	6 × 6	Band 1–4	180–700	SIS
APEX (Acatama Pathfinder Experiment)	12	ArTeMis	666, 856	Bolometers
		SEPIA	157–738	SIS
		nFLASH	196–507	SIS
		CHAMP	620–850	SIS
		PI230	157–211	SIS
		LABOCA	345	Bolometers
NEOMA Interferometer	10 × 15	Band 1–4	71–371	SIS
Hershel Space Observatory	3.5	SPIRE	500–1500	Bolometers
		PACS bol.	1427–5000	Bolometers
		PACS phot.	1363–6000	Photoconductors
		HIFI	83–1000	Bolometers
SOFIA (Stratospheric Observatory for Infrared Astronomy)	2.5	HAWC+	1250–6000	TES
		FIFI-LS	1500–5880	Photoconductors
		GREAT	490–4745	HEB
LMT (Large Millimeter Telescope)	50	TolTEC	150, 220, 280	KIDs
		SEQUOIA	85–116	SIS
		AzTEC	272	Bolometers
		RSR	75–110	SIS
ALMA (Atacama Large Millimeter/Sub-millimeter Array)	54 × 12 12 × 7	Band 3–10	84–950	SIS
Millimetron	10	Band 1–2	33–116	HEMT
		Band 3–5	211–650	SIS
OST (Origins Space Telescope)	5.9–9.1	Imaging	1000–3000	-
		Spectroscopy	1000–3000	-

high pixel counts. The main technologies used are bolometers (exploiting the neutron transmutation doping process or implanted silicon), superconducting transition-edge-sensed bolometers (TESBs), and kinetic inductance detectors (KIDs) (Farrah et al., 2019). Prior to the development of TESBs and KIDs, bolometers operating at temperatures of 300 K or lower were used in observatories. Incoming radiation results in a change in the detector temperature which is read out as a change in its resistivity. Standard bolometers, however, are limited in their total pixel number which has led to the development and preferential use of other technologies, including TESBs and KIDs.

A TESB consists of a superconducting film operating near its superconducting transition temperature (Henderson et al., 2016; Thornton et al., 2016). The signal is seen as a current through a resistive film at a low temperature of around 100 mK (Suzuki et al., 2016). TESBs have high sensitivities which have allowed them to find use in many space-based instruments, as shown in **Table 1**. KIDs have a similar sensitivity to TESBs but operate below their superconducting transition temperature; below 300 mK (Griffin et al., 2016). The inductance of the detector material is increased due to broken Cooper pairs from incident photons on the superconducting film. In a resonant circuit, the shift in inductance causes a change in the resonant frequency which may be detected (Day et al., 2003).

Coherent systems used in astronomy are based on the heterodyne detection principle: the THz/F-IR high-frequency (RF) signals from molecules in space are down-converted to a lower frequency band typically of a few GHz known as the intermediate frequency (IF). The IF is easily measurable by sensitive back-ends operating at low frequency (such as power meters, spectrum analyzers, digital spectrometers, etc.). The device used for detection and down-conversion is a mixer which requires the input of a local oscillator (LO) signal at the same frequency as the studied RF signal. LO generators need to have narrow linewidths, low noise, high stability, and a broad tunability with sufficient output power to couple to the mixer. In the THz/F-IR domain, multiple chains based on Schottky diodes and quantum cascade lasers (>3 THz) are most commonly used (Valavanis et al., 2019).

There are three main types of mixers used in radio telescopes: superconductor-insulator-superconductor (SIS) diodes (Kojima et al., 2017), hot electron bolometers (HEBs) (Burke et al., 1999), and Schottky diodes (Maestrini et al., 2010). State of the art SIS diodes and HEBs offer the best system noise temperature

performances at around 5–10 times the quantum noise limit. These mixers require only a few microwatts of LO power to operate and are very common for instruments with frequency ranges higher than 1 THz and between 1–6 THz for SIS diodes and HEBs, respectively. SIS diode mixers offer wider IF bandwidths and better sensitivities than do HEBs. However, SIS diodes require cooling to 4 K thus necessitating the use of a complex cryostat. On the other hand, Schottky mixers operate at temperatures above 70 K, a frequency range of up to 3 THz, and an IF bandwidth wider than 8 GHz. Their main disadvantages are their lower sensitivity which is between 30–50 times the quantum noise limit, and their milliwatt LO power requirement (Wilson et al., 2008).

The high-resolution spectroscopy possible when using a coherent detector in telescope facilities is achieved by using a digital technique with real-time fast Fourier-transform (FFT) so as to produce high-resolution spectral data. This idea was first proposed by Weinreb (1961) and has been improved upon over the past 60 years in terms of acquisition speed, frequency bandwidth, power efficiency, cost, and size. Nowadays, three main digital systems are used in astronomy to sample the signal waveform at set time intervals: opto-acoustic spectrometers, digital autocorrelation spectrometers (Emrich 1997), and FFT spectrometers (Klein et al., 2012; Price 2016).

Opto-acoustic spectrometers are based on the diffraction of the signal on a Bragg crystal illuminated by a laser beam and detected by charge-coupled devices. This technique was used in the HIFI instrument aboard the Herschel Space Observatory (Siebertz et al., 2007). The main drawback of this spectrometer is its size, which defines its precision and spectral resolution. Digital autocorrelation spectrometers are based on the multiplication of a signal by a delayed version of the same signal using a series of delays. Spectrum measurement is achieved after the application of a Fourier transformation. Such spectrometers can have a bandwidth of a few GHz with a spectral resolution on the scale of one-hundredth of a kHz. Lastly, FFT spectrometers are based on field-programmable gate array (FPGA) chips. The FPGAs are combined with analogue-to-digital converters having a high data sampling rate of a few GHz samples per second. Their numerous spectral channels decompose the incoming RF signal into small sections giving an instantaneous FFT of a few kHz, as seen on the APEX telescope (Klein et al., 2006).

2.2 Telescope Facilities

Since the construction of the first radio telescope in 1937 (Kraus 1988), several telescopes operating in the THz/F-IR range have been successfully built and used by the astronomical community. A principal advantage of performing observations in the THz/F-IR range is the high sensitivity to low-abundance molecules within star-forming regions. Furthermore, observed emission and absorption features can be mapped for all areas within the stellar environment, such as snowlines where ice desorption processes begin to occur.

Progress in the sensitivity of detector technology over the past 50 years has permitted the investigation of interstellar molecular clouds at various wavelengths which has allowed us to improve

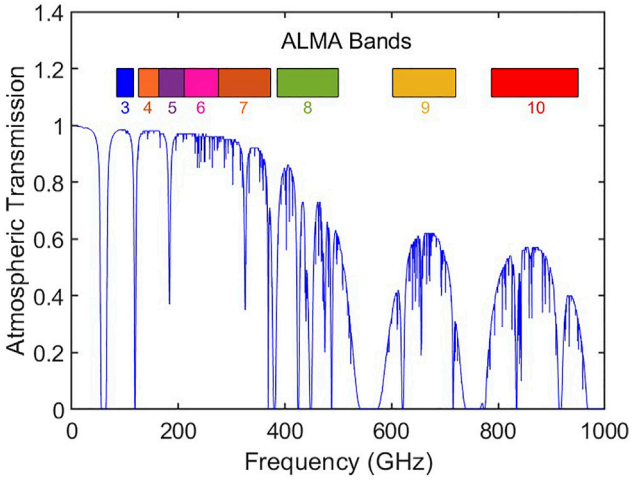

FIGURE 5 | Zenith atmospheric transmission of H_2O vapor of the ALMA telescope with precipitable H_2O vapors of 0.5 mm simulated from the *Atmospheric Transmission at Microwaves* model described by Pardo et al. (2001). Further information may be found in the work of Maiolino (2008).

our understanding of space chemistry. Powerful telescopes have been used with imaging and high spectral resolution instruments combined with large dish antennae. These telescopes have been instrumental in major scientific breakthroughs, such as the discovery of new molecules in the interstellar medium and elucidating the mechanisms for planetary system formation. A summary of the most important telescopes operating in the THz/F-IR range is given in **Table 1**.

In general, two varieties of observatory exist: ground-based (sometimes also referred to as atmosphere-based) and space-borne telescopes. Ground-based observatories are installed either on the ground at high altitudes or in airborne facilities. Atmospheric transmission has a direct impact on the sensitivity of these observatories at THz/F-IR frequencies since atmospheric molecules (especially H_2O) present strong absorption lines over these frequencies. As such, high atmospheric H_2O content limits atmospheric transmission, thus making observation heavily dependent upon weather conditions and altitude: drier sites to install ground-based telescopes are found at higher altitudes (**Figure 5**). Brief descriptions of the ground-based ALMA and space-borne Herschel Space Observatory now follow.

ALMA is a ground-based international astronomy facility built over an area of 6596 m^2 at an altitude of 5000 m located at Llano de Chajnanto in the Atacama Desert, Chile. The 66 high-precision antennae making up the facility are either 12 m (54 of them) or 7 m (12 of them) in diameter. These sizes, combined with the area of the array, give a spatial resolution of 0.2–0.004 arcseconds (1 arcsecond = 1/3,600 degrees). ALMA is composed of ten receivers using Schottky local oscillator sources and SIS diode mixers cooled to 4 K which give up to 16 GHz bandwidth with a spectral resolution of a few kHz. The covered frequency bands range from 31.3–950 GHz in ten windows (**Figure 5**) with a maximum 8 GHz IF. The lower frequency Bands 1 and 2 are not

yet operational. The number of spectral channels available is 4096 per IF. For Bands 3–8, receivers operate in single sideband detection mode acquiring both H and V polarization while Bands 9 and 10 operate in double sideband mode.

Space-based telescopes are not limited by atmospheric attenuations in the way that ground-based observatories are, but do have limitations connected with the size of their antenna aperture. The Herschel Space Observatory was commissioned by the European Space Agency and launched in 2009. The telescope was composed of a 3.5 m diameter dish which was passively cooled by liquid helium at 4 K. Overt time, the liquid helium reserves necessary for detector cooling were gradually depleted, and the end of the telescope's operations came about in April 2013.

Three scientific instruments were on board the Herschel Space Observatory: a high-spectral resolution heterodyne spectrometer called HIFI (Heterodyne Instrument for the Far-Infrared), an imaging photometer called PACS (Photodetector Camera Array), and a medium resolution grating spectrometer called SPIRE (Spectral and Photometric Imaging Receiver). THz/F-IR frequencies were covered by the HIFI instrument from 408-1908 GHz separated in 12 windows using HEB and SIS diode mixer technology. PACS was composed of a camera integral field spectrometer combined with an imaging photometer operating between 1.427-6 THz and bolometers at frequencies centered around 1.873 THz, 2.997 THz, and 4.282 THz (Rosenthal et al., 2002). Finally, the SPIRE instrument had three main photometers at 600 GHz, 856 GHz, and 119 GHz, as well as a two-band imaging Fourier-transform spectrometer with bolometers operating between 447–1550 GHz (Griffin et al., 2010).

Amongst the key scientific objectives of the Herschel Space Observatory was an investigation of the formation of stellar and planetary systems, and increasing our understanding of the physics and chemistry of the interstellar medium, our Solar System, and extra-galactic galaxies. The HIFI instrument detected more than 100,000 spectral features in a single spectrum (Bergin et al., 2010). Through the Water in Star-Forming Regions with Herschel (WISH) program, many molecules such as H_2O, CO, and O_2 were detected in various astrophysical environments (Goldsmith et al., 2011). Molecules and radicals including H_2O and OH^- were detected further our and deeper in proto-planetary disks than before from surveys of THz/F-IR spectral lines using PACS (Fedele et al., 2013). Cold water reservoirs were discovered in two extra-solar planet-forming disks (TW Hydrae) through the detection of H_2O gas produced by UV photo-desorption of the ice made by HIFI (Hogerheidje et al., 2011). H_2O vapor was also detected in a pre-stellar core at the early stage of stellar formation using HIFI observations combined with models of the UV photo-desorption processes (Casselli et al., 2012).

Ground-based and space-borne observatories operating in the THz/F-IR range, including those listed in **Table 1**, have aided astronomers in elucidating the chemistry of interstellar space by allowing them to obtain spectroscopic information of molecular species (colloquially termed "molecular fingerprints"). Indeed, the improvement of technology throughout these past decades has allowed for the definitive identification of many new molecular signatures, largely through observation of their rotational emission spectra. **Figure 6** shows the comparison of spectra acquired by ALMA Band 10 and the HIFI instrument aboard the Herschel Space Observatory while observing the NGC 6334I region (McGuire et al., 2018b). As can be seen, the number of spectral lines attributed to CO and CH_3OH which are resolved by ALMA Band 10 is significantly higher than that detected by HIFI (Zernickel et al., 2012).

Computer modelling and laboratory measurements of molecular spectra are often needed to assign observed spectral lines to particular molecular species. This is especially true in the case of complex organic molecules such as isopropyl cyanide ($(CH_3)_2CHCN$), which was the first branched carbon-chain molecule to be detected and which was found in Sgr B2 using the ALMA Band 3 (Belloche et al., 2014). Later, CH_3OCH_2OH and CH_3Cl were observed for the first time by ALMA Bands 6 and 7 in NGC 6334I, and by ALMA Band 7 in IRAS 16293-2422, respectively (Fayolle et al., 2017; McGuire et al., 2017). However, many molecules and radical species may not be observed in the gaseous phase but may play a central role in the formation of observed gaseous species as a result of their presence and reactions in solid icy grain mantles. The use of laboratory THz/F-IR measurements in astrochemical research, particularly as it pertains to solid-phase chemistry, will be elaborated on in the next sub-section.

2.3 Laboratory Astrochemistry Using THz/F-IR Spectroscopy

Over 200 molecules have been detected and spectroscopically resolved in interstellar regions within our galaxy, and more than 60 have been observed in extra-galactic molecular clouds (Müller et al., 2005), ranging in complexity from simple diatomics to the more structurally complex fullerenes and PAHs. An overarching aim of laboratory astrochemistry is to be able to understand the physico-chemical processes which occur in these astrophysical environments so as to better comprehend the chemical reactions which lead to the formation of such molecules. Such work is motivated by the knowledge that such reactions can result in the production of various molecules and minerals. For instance, interstellar biomolecules which may form in dense, quiescent molecular clouds may be subsequently incorporated into the stellar and planetary systems which evolve from these clouds and thus play a defining role in the emergence of life within these systems (Watanabe and Kouchi, 2002; Jones et al., 2011; Fedoseev et al., 2017; Chuang et al., 2020; Sandford et al., 2020; Ioppolo et al., 2021). The synthesis of smaller, volatile molecules in astrophysical environments is equally important, as such molecules may contribute to the development of planetary and lunar atmospheres or transient exospheres (Milillo et al., 2016; Teolis and Waite 2016). Additionally, condensation processes and grain alterations contribute to the formation of minerals which are significant to the geological and geochemical evolution of planets and moons, including graphite, corundum, moissanite, and forsterite (Frenklach et al., 1989; Hazen et al., 2008; Hazen and Ferry 2010).

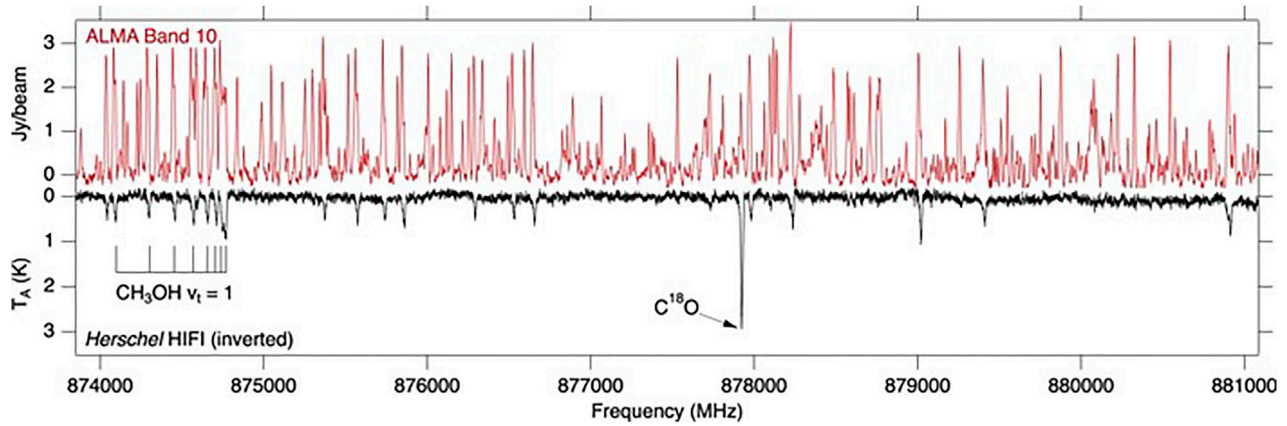

FIGURE 6 | Comparison of the spectra acquired by ALMA Band 10 and HIFI while observing the NGC 6334I region. Figure taken from McGuire et al. (2018b) and reproduced with permission from the AAS.

The unambiguous identification of such molecules by infrared and radio telescopes (including those which operate in the THz/F-IR range) relies on the availability and completeness of gas- and solid-phase spectroscopic databases at the corresponding frequencies for a great variety of molecules. Such information is obtained by performing classical laboratory measurements (Wlodarczak 1995; Smith 2011; Cataldo et al., 2013a; Allodi et al., 2013; Widicus-Weaver 2019; Mifsud et al., 2021). Presently, the two most commonly referenced catalogues are the Cologne Database for Molecular Spectroscopy (Müller et al., 2001; Endres et al., 2016) and the Jet Propulsion Laboratory (Pickett et al., 1998) catalogues, which give the frequency and amplitude of several molecular transitions. Two accessible databases listing vibrational transitions at IR wavelengths are also available: the HITRAN database (Rothman et al., 2009) and the EXOMOL line list.

Broadly speaking, laboratory astrochemistry studies are largely concerned with investigating reactions which occur in either the gas phase or the condensed (ice) phase. Experiments are typically performed using high or ultra-high vacuum chambers. For instance, a novel method of performing gas-phase spectroscopy is to make use of a heterodyne radiometer so as to observe the absorption features of various gaseous species within the chamber, thus functioning in a similar fashion to several telescope facilities. Two laboratory broadband emission THz/F-IR radiometers based on heterodyne detection methods have been developed: the first is based on Schottky-barrier technology combined with a FFT digital spectrometer operating between 80 and 110 GHz (Wehres et al., 2017), while the second is based on cryo-cooled SIS diode mixer technology operating between 270 and 290 GHz (Wehres et al., 2018). By using such instruments, the spectroscopic features of pyridine and CH_3CN have been successfully measured and matched with analytical simulations. Similarly, a Schottky-based receiver has been used in combination with a FFT digital spectrometer and vacuum chamber to observe the emission line of N_2O at 355.6 GHz (Parkes et al., 2018).

Laboratory experiments concerned with the solid phase also require the use of high or ultra-high vacuum chambers, wherein interstellar ice analogues may be synthesized on cold substrates via the direct or background deposition of dosed gases or vapors, or the effusive evaporation of refractories. The deposited ices are then processed in such a way as to simulate astrophysical conditions: atom (or free radical) additions represent non-energetic pathways towards molecule formation (Linnartz et al., 2015; Chuang et al., 2016; Potapov et al., 2017; Ioppolo et al., 2021); bombardment with energetic charged particles (i.e., electrons and ions) simulates ice interactions with galactic cosmic rays, the solar wind, or planetary magnetospheric plasmas (Baragiola et al., 1999; Dalton et al., 2013; Ding et al., 2013; Boamah et al., 2014; Boduch et al., 2015; Fulvio et al., 2018; Ioppolo et al., 2020; Garozzo et al., 2010); irradiation with photons (both ionizing and non-ionizing) simulates extra-terrestrial photochemistry (Bernstein et al., 2002; Lo et al., 2014; Öberg 2016; Mullikin et al., 2018); energetic shocks simulate collisions between interstellar or Solar System bodies (Goldman et al., 2010; Martins et al., 2013), and thermal processing simulates the chemical and structural changes induced within interstellar icy grain mantles proximal to nascent stars, or in Solar System bodies as they approach perihelion (Ehrenfreund et al., 1999; Kaňuchová et al., 2017).

The changes in the physico-chemical properties of the ice analogues induced by such processing have been traditionally monitored using mid-IR or UV-VIS spectroscopy (Mason et al., 2006; Boersma et al., 2014). This has been advantageous in that such laboratory work is complementary to observational work using space-borne telescopes working within these ranges of the electromagnetic spectrum, such as the Spitzer Space Telescope and the Hubble Space Telescope. Although not yet widely used within laboratory settings, the utility and applicability of THz/F-IR spectroscopy is being increasingly recognized due to its

ability to detect lower frequency molecular vibrations, as well as intermolecular interactions and translational vibrations within solid lattices (Bertie 1968; Bertie and Jacobs 1977; Kulesa 2011; McIntosh et al., 2012). The remainder of this sub-section will be devoted to a discussion on the application of THz/F-IR spectroscopy to laboratory studies of astrophysical ice analogues.

THz/F-IR spectra differ depending upon the structural morphology of the ice (e.g., amorphous or crystalline solid phases), as demonstrated by Moore and Hudson (1992, 1994, 1995). For instance, recent studies investigating CO_2 in H_2O and CH_3OH ice matrices at various temperatures have revealed that the measured THz/F-IR spectra are especially sensitive to the degree of segregation within the ice structure. Results have shown that CO_2 roaming during warming of the ice results in a localized accumulation, or segregation. When mixed with crystalline H_2O ice, this CO_2 segregation results in a disruption of the hydrogen bonding network between adjacent H_2O molecule layers, causing the H_2O spectral resonance features to be shifted, distorted, or attenuated (Allodi et al., 2014). On the other hand, CO_2 absorption bands were observed to become narrower and more defined when segregation from CH_3OH ice occurred as a result of warming (McGuire et al., 2016).

Such work clearly demonstrates the sensitivity of THz/F-IR spectroscopy not only to the nature of the chemical species present within the ice, but also to the physical structure of the ice. Given that the nature of the observed spectral absorption features is dependent upon the temperature, degree of crystallinity, segregation, and thermal history of the ice, THz/F-IR spectroscopy appears to be highly suitable for assessing not only the composition and temperature characteristics of astrophysical ices, but also their morphology (Ioppolo et al., 2014). To date, relatively few of the observed molecules have been investigated using THz/F-IR spectroscopy. Amorphous solid H_2O, for instance, presents a spectral line at 1 THz. CH_3OH, CH_3CHO, and $(CH_3)_2CO$ have been found to have a broad feature at around 4 THz, while in HCOOH and CH_3COOH this broad absorption feature is centered at about 7 THz (Ioppolo et al., 2014).

Laboratory THz/F-IR spectroscopy has also been used in the analysis of more complex molecular structures such as PAHs. Although these molecules are believed to be ubiquitous in interstellar and circumstellar media (Tielens 2008; Kwok and Zhang 2011), few single structures have been positively identified (McGuire et al. 2021). Systematic analysis of a series of PAHs, as well as their hydrogenated and alkylated derivatives, has revealed that the THz/F-IR spectra of these molecules display so-called "Jumping Jack" modes which correspond to the in-plane vibrations around the central molecular core (Cataldo et al., 2013b). As such, these spectra provide crucial information related to the number of fused aromatic rings present within the molecule, and are thus valuable in identifying the individual molecular carriers of PAH diffuse interstellar absorption bands. Other complex molecules, including those which may be of relevance to prebiotic chemistry, have also been studied using THz/F-IR spectroscopy (Widicus-Weaver et al., 2005; Carroll et al., 2010).

Recently, a new laboratory-based method for observing desorption mechanisms occurring within the interstellar medium and star-forming regions has been developed. Studying such desorption has been traditionally performed using mid-IR spectrophotometers and quadrupole mass spectrometers, however this has the drawback of not being able to detect ions and radicals and is difficult to relate to observations made using radio telescopes (Fraser et al., 2002; Collings et al., 2003; Fuchs et al., 2009; Muñoz-Caro et al., 2010). In principle, it is possible to desorb (either via thermal or non-thermal mechanisms) ices formed of pure or layered molecules and observe the resultant gas phase in the THz/F-IR frequency range. One way to do this is to passively observe the emission of those molecules during desorption in an astrochemical chamber equipped with a heterodyne radiometer (Auriacombe et al., 2015, 2016); another is by performing microwave absorption spectroscopy. The region in which desorbing molecules are observed may be directly above the ice, and the relevant spectral transitions may be detected with a HEB (see **Figure 2** in Yocum et al., 2019). Alternatively, a chirped-pulse Fourier-transform spectrometer can be used to observe the desorption occurring inside a waveguide (Theulé et al., 2020). These emerging techniques are capable of bringing new insights and possibilities to our understanding of the desorption processes in star-forming regions.

Although the use of THz/F-IR spectroscopy is growing within laboratory-based astrochemical research (driven by developments in the relevant technologies and an increase in the commercial availability of the necessary spectrometers), much of the current work takes place at large-scale facilities. A complete and thorough description of the research conducted using THz/F-IR radiation at such facilities would go beyond the scope of this review, and we instead direct the interested reader to other works (e.g., Neil 2014). However, it is worthwhile to take some time to briefly describe the Free Electron Lasers for Infrared Experiments (FELIX) facility located in Nijmegen, the Netherlands, where an ultrahigh-vacuum chamber has been installed as the Laboratory Ice Surface Astrophysics (LISA) end-station thus permitting the characterization of astrophysical ice analogues which have been processed as a result of THz/F-IR irradiation.

The FELIX facility is home to four free electron lasers which provide short-pulsed coherent light covering the microwave to mid-IR regions of the electromagnetic spectrum. The FELIX-1 and FELIX-2 free electron laser beamlines respectively operate over the ~65–330 cm^{-1} and ~225–3300 cm^{-1} ranges and are capable of providing bursts of micro-pulses with selective and tunable wavelengths whose duration may be readily controlled. These beamlines are therefore highly suited to providing THz/F-IR (as well as mid-IR) radiation for use in laboratory studies of astrophysical ice analogues, which are prepared in the LISA end-station.

The LISA is an ultrahigh-vacuum chamber with nominal base pressure in the region of a few 10^{-10} mbar containing an elongated rectangular gold-coated deposition substrate which may be cooled down to 15 K using a closed-cycle helium cryostat head with a cooled compressor. The gold-coated substrate is manipulated by means of a *xyz*-linear translator

allowing for the irradiation of different spots of the ice during a single experiment, as well as a rotary stage mostly employed for alignment purposes. Pure gases and gas mixtures are pre-prepared in a dosing line prior to being injected into the main chamber via an all-metal leak valve, wherein background deposition of the gases occurs to form the astrophysical ice analogues. Such background deposition of gases onto the deposition substrate allows for a more uniform ice deposition, and the resultant ice analogue may be used in systematic studies. Ices processed by mid-IR or THz/F-IR irradiation delivered by the FELIX beamlines may be monitored in two ways: mid-IR reflection-absorption spectroscopy may be used to monitor any physico-chemical effects induced as a result of the ice stimulation, and quadrupole mass spectrometry may be used to monitor species which desorb thermally from the bulk parent ice.

The FELIX-LISA facility has found regular use in effectively characterizing the physico-chemical changes induced in astrophysical ice analogues as a result of stimulation by incident irradiation. For instance, Noble et al. (2020) investigated the effect of resonant irradiation of amorphous solid H_2O using mid-IR radiation supplied by the FELIX-2 beamline. Their results indicated that irradiation with wavelengths corresponding to the mid-IR stretching, bending, and libration modes of amorphous H_2O resulted in a wide-ranging structural rearrangement of the ice into a crystalline-like form due to vibrational relaxation of the intermolecular hydrogen bonding network. Results such as these, combined with the experimental capabilities of large-scale facilities such as FELIX, make future dedicated studies looking into the irradiation of lower frequency THz/F-IR modes of astrophysical ice analogues especially attractive.

As has been demonstrated, the application of THz/F-IR spectroscopy to observational and laboratory astrochemistry has the potential to unravel much information related to the structure and reactivity of molecules in space. To date, however, THz/F-IR experiments at large-scale facilities such as FELIX tasked with investigating the chemistry of interstellar and Solar System ice analogues have not been explored to their fullest potential due to the fact that the dedicated pump-probe experiments required to study such chemistry are not available at the time of writing. The present LISA end-station configuration comprises an FTIR spectrophotometer with an extended spectral range to the far-IR. Such a system may be used to time-resolve transient events within the ice structure (such as diffusion of molecules through different ice layers and segregation events in mixed ices) at millisecond timescales.

To fully benefit from the unique capabilities of a free electron laser (i.e., a wide-range tunability, high peak power, and a controllable repetition rate), THz/F-IR time-domain spectroscopy with single-shot detection techniques should be employed to extend time resolutions to a few tens of picoseconds (Redlich et al., 2003; Perakis et al., 2013; Shalit et al., 2013; Mead et al., 2019). With such a configuration, free electron laser THz/F-IR radiation could be used to "pump" (i.e., inject energy into) inter- and intramolecular vibrations of solid species that, having been excited by the sudden excess of energy, will subsequently rearrange selectively or diffuse within the ice and possibly react with other species. Diffusion and reaction of molecules could be triggered and controlled by operating a free electron laser across its spectral range and could then be monitored by means of a THz/F-IR single-shot spectrometer in the solid phase, while desorbed species could be monitored by implementing a broadband emission THz/F-IR radiometer as described previously. The combination of a free electron laser and new advanced techniques in laboratory astrochemistry thus has the potential to reveal unprecedented details on fundamental phenomena which could play important roles in the formation of complex prebiotic molecules in space, and would thus expand our understanding of the relevant extra-terrestrial physics and chemistry.

Experimental work such as that proposed to be performed at the FELIX-LISA facility on broadband emission THz/F-IR radiometry would also contribute much to our interpretation of observational data. The importance of commissioning new space-borne observational facilities operating in the THz/F-IR was highlighted in the recently published *Pathways to Discovery in Astronomy and Astrophysics for the 2020s* roadmap (National Academies of Sciences, Engineering, and Medicine, 2021), particularly in light of the fact that the Space Infrared Telescope for Cosmology and Astrophysics (SPICA) is no longer being considered for launch. Interestingly, the far-IR is one of the spectral ranges where astronomical data with sub-arcsecond resolution is not currently available: a fact which is somewhat at odds with the potential usefulness of spectroscopic measurements in this range (Linz et al., 2021). A number of space-based observatories, such as the Far-Infrared Spectroscopic Surveyor (FIRSS) and the Terahertz Exploration and Zooming-In for Astrophysics (THEZA) telescopes have also been proposed to fill in this gap (Gurvits et al., 2021; Rigopoulou et al., 2021), and the acquisition of laboratory reference data will doubtlessly aid in further characterizing the molecular composition of the cosmos.

3 CONCLUSION AND RECOMMENDATIONS FOR FUTURE WORK

In summary, we have provided a brief overview of the chemistry occurring in both diffuse and dense (dark) interstellar clouds with a focus on ion-molecule reactions in the gas phase which are relevant to the formation of complex prebiotic molecules, as well as how THz/F-IR techniques have aided in the elucidation of these reactions and how such reactions may relate to the RNA World Hypothesis on the abiogenic origins of life. We have also provided a review on current THz/F-IR spectrometer and detector technology in both laboratory and observatory settings, as well as their present and potential future applications to laboratory solid-phase astrochemistry. We conclude by emphasizing that further progress in THz/F-IR astrochemistry has the potential to provide great insight to several fundamental astrochemical processes and should therefore be pursued.

AUTHOR CONTRIBUTIONS

DM, PH, AM, OA, and SI wrote the manuscript and all authors were responsible for corrections and improvements.

FUNDING

Our research has benefitted from support provided by the Europlanet 2024 RI, which has received funding from the European Union's Horizon 2020 Research Innovation Program under grant agreement No. 871149.

ACKNOWLEDGMENTS

DM is the grateful recipient of a University of Kent Vice-Chancellor's Research Scholarship. AM thanks Queen Mary University of London for doctoral funding. SI acknowledges the Royal Society for financial support.

REFERENCES

Allodi, M. A., Baragiola, R. A., Baratta, G. A., Barucci, M. A., Blake, G. A., Boduch, P., et al. (2013). Complementary and Emerging Techniques for Astrophysical Ices Processed in the Laboratory. *Space Sci. Rev.* 180, 101–175. doi:10.1007/s11214-013-0020-8

Allodi, M. A., Ioppolo, S., Kelley, M. J., McGuire, B. A., and Blake, G. A. (2014). The Structure and Dynamics of Carbon Dioxide and Water Containing Ices Investigated via THz and Mid-IR Spectroscopy. *Phys. Chem. Chem. Phys.* 16, 3442. doi:10.1039/c3cp53767f

Arumainayagam, C. R., Garrod, R. T., Boyer, M. C., Hay, A. K., Bao, S. T., Campbell, J. S., et al. (2019). Extraterrestrial Prebiotic Molecules: photochemistry vs. Radiation Chemistry of Interstellar Ices. *Chem. Soc. Rev.* 48, 2293–2314. doi:10.1039/c7cs00443e

Auriacombe, O., Fraser, H., Ellison, B., Ioppolo, S., and Rea, S. (2016). Terahertz Desorption Emission Spectroscopy (THz DES) – ALMA in the Lab. *Paper presented Am. Astronomical Soc. Meet.* 228, 104–203.

Auriacombe, O., Fraser, H., Ellison, B., and Rea, S. (2015). Desorption Emission Spectroscopy Using THz Radiometry (THz DES). *IET Conf. Proc.* 3, 1. doi:10.1049/ic.2015.0093

Auston, D. H. (1975). Picosecond Optoelectronic Switching and Gating in Silicon. *Appl. Phys. Lett.* 26, 101–103. doi:10.1063/1.88079

Balucani, N., Ceccarelli, C., and Taquet, V. (2015). Formation of Complex Organic Molecules in Cold Objects: The Role of Gas-phase Reactions. *Mon. Not. R. Astron. Soc.* 449, L16–L20. doi:10.1093/mnrasl/slv009

Baragiola, R. A., Atteberry, C. L., Bahr, D. A., and Jakas, M. M. (1999). Solid-state Ozone Synthesis by Energetic Ions. *Nucl. Instr. Methods Phys. Res. Section B: Beam Interactions Mater. Atoms* 157, 233–238. doi:10.1016/s0168-583x(99)00431-0

Barinovs, Ğ., and van Hemert, M. C. (2006). CH^+ Radiative Association. *ApJ* 636, 923–926. doi:10.1086/498080

Belloche, A., Garrod, R. T., Müller, H. S. P., Menten, K. M., Medvedev, I., Thomas, J., et al. (2019). Re-exploring Molecular Complexity with ALMA (ReMoCA): Interstellar Detection of Urea. *Astron. Astrophys.* 628, 10. doi:10.1051/0004-6361/201935428

Belloche, A., Garrod, R. T., Müller, H. S. P., and Menten, K. M. (2014). Detection of a Branched Alkyl Molecule in the Interstellar Medium: Iso -propyl Cyanide. *Science* 345, 1584–1587. doi:10.1126/science.1256678

Belloche, A., Müller, H. S. P., Garrod, R. T., and Menten, K. M. (2016). Exploring Molecular Complexity with ALMA (EMoCA): Deuterated Complex Organic Molecules in Sagittarius B2(N2). *Astron. Astrophys.* 587, 91. doi:10.1051/0004-6361/201527268

Bera, P. P., Nuevo, M., Materese, C. K., Sandford, S. A., and Lee, T. J. (2016). Mechanisms for the Formation of Thymine under Astrophysical Conditions and Implications for the Origin of Life. *J. Chem. Phys.* 144, 144308. doi:10.1063/1.4945745

Bera, P. P., Stein, T., Head-Gordon, M., and Lee, T. J. (2017). Mechanisms of the Formation of Adenine, Guanine, and Their Analogues in UV-Irradiated Mixed NH_3:H_2O Molecular Ices Containing Purine. *Astrobiology* 17, 771–785. doi:10.1089/ast.2016.1614

Bergin, E. A., Phillips, T. G., Comito, C., Crockett, N. R., Lis, D. C., Schilke, P., et al. (2010). Herschel observations of EXtra-ordinary Sources (HEXOS): The Present and Future of Spectral Surveys with Herschel/HIFI. *A&A* 521, L20. doi:10.1051/0004-6361/201015071

Bergin, E. A., and Tafalla, M. (2007). Cold Dark Clouds: The Initial Conditions for star Formation. *Annu. Rev. Astron. Astrophys.* 45, 339–396. doi:10.1146/annurev.astro.45.071206.100404

Berné, O., Montillaud, J., and Joblin, C. (2015). Top-down Formation of Fullerenes in the Interstellar Medium. *Astron. Astrophys.* 577, A133. doi:10.1051/0004-6361/201425338

Berné, O., and Tielens, A. G. G. M. (2012). Formation of Buckminsterfullerene (C_{60}) in Interstellar Space. *Proc. Nat. Acad. Sci. USA* 109, 401. doi:10.1073/pnas.1114207108

Bernhardt, H. S. (2012). The RNA World Hypothesis: the Worst Theory of the Early Evolution of Life (Except for All the Others). *Biol. Direct* 7, 23. doi:10.1186/1745-6150-7-23

Bernstein, M. P., Dworkin, J. P., Sandford, S. A., Cooper, G. W., and Allamandola, L. J. (2002). Racemic Amino Acids from the Ultraviolet Photolysis of Interstellar Ice Analogues. *Nature* 416, 401–403. doi:10.1038/416401a

Bertie, J. E. (1968). Far-infrared Spectra of the Ices. *Appl. Spectrosc.* 22, 638. doi:10.1366/000370268774384164

Bertie, J. E., and Jacobs, S. M. (1977). Far-infrared Absorption by Ices Ih and Ic at 4.3 °K and the Powder Diffraction Pattern of Ice Ic. *J. Chem. Phys.* 67, 2445. doi:10.1063/1.435218

Boamah, M. D., Sullivan, K. K., Shulenberger, K. E., Soe, C. M., Jacob, L. M., Yhee, F. C., et al. (2014). Low-energy Electron-Induced Chemistry of Condensed Methanol: Implications for the Interstellar Synthesis of Prebiotic Molecules. *Faraday Discuss.* 168, 249–266. doi:10.1039/c3fd00158j

Boduch, P., Dartois, E., de Barros, A. L. F., da Silveira, E. F., Domaracka, A., Lv, X.-Y., et al. (2015). Radiation Effects in Astrophysical Ices. *J. Phys. Conf. Ser.* 629, 012008. doi:10.1088/1742-6596/629/1/012008

Boersma, C., Bauschlicher, C. W., Ricca, A., Mattioda, A. L., Cami, J., Peeters, E., et al. (2014). The NASA Ames PAH IR Spectroscopic Database Version 2.00: Updated Content, Web Site, and On(off)line Tools. *ApJS* 211, 8. doi:10.1088/0067-0049/211/1/8

Brown, P. J., and Carrington, A. (2003). *Rotational Spectroscopy of Diatomic Molecules*. Cambridge: Cambridge University Press.

Burke, P. J., Schoelkopf, R. J., Prober, D. E., Skalare, A., Karasik, B. S., Gaidis, M. C., et al. (1999). Mixing and Noise in Diffusion and Phonon Cooled Superconducting Hot-Electron Bolometers. *J. Appl. Phys.* 85, 1644–1653. doi:10.1063/1.369299

Burkhardt, A. M., Lee, K. L. K., Changala, P. B., Shingledecker, C. N., Cooke, I. R., Loomis, R. A., et al. (2021a). *Discovery of the Pure Polycyclic Aromatic Hydrocarbon Indene (C-C_9h_8) with GOTHAM Observations of TMC-1*. ArXiv [Preprint]. Available at: https://arxiv.org/abs/2104.15117 (Accessed May 16, 2021).

Burkhardt, A. M., Loomis, R. A., Shingledecker, C. N., Lee, K. L. K., Remijan, A. J., McCarthy, M. C., et al. (2021b). Ubiquitous Aromatic Carbon Chemistry at the Earliest Stages of star Formation. *Nat. Astron.* 5, 181–187. doi:10.1038/s41550-020-01253-4

Calcutt, H., Willis, E. R., Jørgensen, J. K., Bjerkeli, P., Ligterink, N. F. W., Coutens, A., et al. (2019). The ALMA-PILS Survey: Propyne (CH_3CCH) in IRAS 16293-2422. *Astron. Astrophys.* 631, 137. doi:10.1051/0004-6361/201936323

Carroll, P. B., Drouin, B. J., and Widicus Weaver, S. L. (2010). The Submillimeter Spectrum of Glycolaldehyde. *ApJ* 723, 845–849. doi:10.1088/0004-637x/723/1/845

Casselli, P., Keto, E., Bergin, E. A., Tafalla, M., Aikawa, Y., Douglas, T., et al. (2012). First Detection of Water Vapor in a Pre-stellar Core. *Astrophys. J. Lett.* 759, L37.

Cataldo, F., Angelini, G., Aníbal García-Hernández, D., and Manchado, A. (2013b). Far Infrared (Terahertz) Spectroscopy of a Series of Polycyclic Aromatic

Hydrocarbons and Application to Structure Interpretation of Asphaltenes and Related Compounds. *Spectrochimica Acta A: Mol. Biomol. Spectrosc.* 111, 68–79. doi:10.1016/j.saa.2013.03.077

Cataldo, F., García-Hernández, D. A., and Manchado, A. (2013a). Far- and Mid-infrared Spectroscopy of Complex Organic Matter of Astrochemical Interest: Coal, Heavy Petroleum Fractions and Asphaltenes. *Mon. Not. R. Astron. Soc.* 429, 3025–3039. doi:10.1093/mnras/sts558

Chuang, K.-J., Fedoseev, G., Ioppolo, S., van Dishoeck, E. F., and Linnartz, H. (2016). H-atom Addition and Abstraction Reactions in Mixed CO, H^2CO and CH^3OH Ices - an Extended View on Complex Organic Molecule Formation. *Mon. Not. R. Astron. Soc.* 455, 1702–1712. doi:10.1093/mnras/stv2288

Chuang, K. J., Fedoseev, G., Qasim, D., Ioppolo, S., Jäger, C., Henning, T., et al. (2020). Formation of Complex Molecules in Translucent Clouds: Acetaldehyde, Vinyl Alcohol, Ketene, and Ethanol via 'non-Energetic' Processing of C_2H_2 Ice. *Astron. Astrophys.* 635, 199. doi:10.1051/0004-6361/201937302

Collings, M. P., Dever, J., Fraser, H., and McCoustra, M. R. S. (2003). Laboratory Studies of the Interaction of Carbon Monoxide with Water Ice. *Astrophys. Space Sci.* 285, 663. doi:10.1023/a:1026144806831

Cook, A. M., Ricca, A., Mattioda, A. L., Bouwman, J., Roser, J., Linnartz, H., et al. (2015). Photochemistry of Polycyclic Aromatic Hydrocarbons in Cosmic Water Ice: The Role of PAH Ionization and Concentration. *ApJ* 799, 14. doi:10.1088/0004-637x/799/1/14

Cooke, S. A., and Ohring, P. (2012). Decoding Pure Rotational Molecular Spectra for Asymmetric Molecules. *J. Spectrosc.* 2013, 698392.

Cuadrado, S., Goicoechea, J. R., Cernicharo, J., Fuente, A., Pety, J., and Tercero, B. (2017). Complex Organic Molecules in Strongly UV-Irradiated Gas. *Astron. Astrophys.* 603, 124. doi:10.1051/0004-6361/201730459

Dalton, J. B., Cassidy, T., Paranicas, C., Shirley, J. H., Prockter, L. M., and Kamp, L. W. (2013). Exogenic Controls on Sulfuric Acid Hydrate Production at the Surface of Europa. *Planet. Space Sci.* 77, 45–63. doi:10.1016/j.pss.2012.05.013

Dartois, E., Charon, E., Engrand, C., Pino, T., and Sandt, C. (2020). Mechanochemical Synthesis of Aromatic Infrared Band Carriers. *A&A* 637, A82. doi:10.1051/0004-6361/202037725

Day, P. K., LeDuc, H. G., Mazin, B. A., Vayonakis, A., and Zmuidzinas, J. (2003). A Broadband Superconducting Detector Suitable for Use in Large Arrays. *Nature* 425, 817–821. doi:10.1038/nature02037

De Luca, M., Gupta, H., Neufeld, D., Gerin, M., Teyssier, D., Drouin, B. J., et al. (2012). Herschel/Hifi Discovery of Hcl + in the Interstellar Medium. *ApJ* 751, L37. doi:10.1088/2041-8205/751/2/l37

Dhillon, S. S., Vitiello, M. S., Linfield, E. H., Davies, A. G., Hoffmann, M. C., Booske, J., et al. (2017). The 2017 Terahertz Science and Technology Roadmap. *J. Phys. D: Appl. Phys.* 50, 043001. doi:10.1088/1361-6463/50/4/043001

Ding, J. J., Boduch, P., Domaracka, A., Guillous, S., Langlinay, T., Lv, X. Y., et al. (2013). Implantation of Multiply Charged Sulfur Ions in Water Ice. *Icarus* 226, 860–864. doi:10.1016/j.icarus.2013.07.002

Doudna, J. A., and Cech, T. R. (2002). The Chemical Repertoire of Natural Ribozymes. *Nature* 418, 222–228. doi:10.1038/418222a

Douglas, A. E., and Herzberg, G. (1941). Note on CH{+} in Interstellar Space and in the Laboratory. *ApJ* 94, 381. doi:10.1086/144342

Draine, B. T., and Katz, N. (1986). Magnetohydrodynamic Shocks in Diffuse Clouds. II - Production of CH(+), OH, CH, and Other Species. *ApJ* 310, 392. doi:10.1086/164693

Drouin, B. J., Maiwald, F. W., and Pearson, J. C. (2005). Application of Cascaded Frequency Multiplication to Molecular Spectroscopy. *Rev. Scientific Instr.* 76, 093113. doi:10.1063/1.2042687

Ehrenfreund, P., Kerkhof, O., Schutte, W. A., Boogert, A. C. A., Gerakines, P. A., Dartois, E., et al. (1999). Laboratory Studies of Thermally Processed H_2O-CH_3OH-CO_2 Ice Mixtures and Their Astrophysical Implications. *Astron. Astrophys.* 350, 240.

Elitzur, M., and Watson, W. D. (1980). Interstellar Shocks and Molecular CH/+/in Diffuse Clouds. *ApJ* 236, 172. doi:10.1086/157730

Emrich, A. (1997). "Autocorrelation Spectrometers for Spaceborne (Sub) Millimeter Astronomy," in *The Far Infrared and Submillimeter Universe*. Editor A. Wilson (Noordwijk: NTRS), 361.

Endres, C. P., Schlemmer, S., Schilke, P., Stutzki, J., and Müller, H. S. P. (2016). The Cologne Database for Molecular Spectroscopy, CDMS, in the Virtual Atomic and Molecular Data Centre, VAMDC. *J. Mol. Spectrosc.* 327, 95–104. doi:10.1016/j.jms.2016.03.005

Esplugues, G. B., Viti, S., Goicoechea, J. R., and Cernicharo, J. (2014). Modelling the sulphur Chemistry Evolution in Orion KL. *Astron. Astrophys.* 567, 95. doi:10.1051/0004-6361/201323010

Farrah, D., Sminth, K. E., Ardila, D., Bradford, C. M., DiPirro, M. J., Ferkinhoff, C., et al. (2019). Review: Far-Infrared Instrumentation and Technological Development for the Next Decade. *J. Astron. Telesc. Instrum. Syst.* 5, 020901. doi:10.1117/1.jatis.5.2.020901

Fayolle, E. C., Öberg, K. I., Öberg, K. I., Jørgensen, J. K., Altwegg, K., Calcutt, H., et al. (2017). Protostellar and Cometary Detections of Organohalogens. *Nat. Astron.* 1, 703–708. doi:10.1038/s41550-017-0237-7

Fedele, D., Bruderer, S., van Dishoeck, E. F., Carr, J., Herczeg, G. J., Salyk, C., et al. (2013). Digit Survey of Far-Infrared Lines from Protoplanetary Disks. *Astron. Astrophys.* 559, 77. doi:10.1051/0004-6361/201321118

Federman, S. R., Rawlings, J. M. C., Taylor, S. D., and Williams, D. A. (1996). Synthesis of Interstellar CH+ without OH. *Mon. Not. R. Astron. Soc.* 279, L41–L46. doi:10.1093/mnras/279.3.l41

Fedoseev, G., Chuang, K.-J., Ioppolo, S., Qasim, D., Dishoeck, E. F. v., and Linnartz, H. (2017). Formation of Glycerol through Hydrogenation of CO Ice under Prestellar Core Conditions. *ApJ* 842, 52. doi:10.3847/1538-4357/aa74dc

Fedoseev, G., Cuppen, H. M., Ioppolo, S., Lamberts, T., and Linnartz, H. (2015). Experimental Evidence for Glycolaldehyde and Ethylene Glycol Formation by Surface Hydrogenation of CO Molecules under Dense Molecular Cloud Conditions. *Mon. Not. R. Astron. Soc.* 448, 1288–1297. doi:10.1093/mnras/stu2603

Feldman, P. A. (2001). Molecular Astronomy from a Canadian Perspective: The Early Years. *Can. J. Phys.* 79, 89–100. doi:10.1139/p01-002

Fraser, H. J., Collings, M. P., and McCoustra, M. R. S. (2002). Laboratory Surface Astrophysics experiment. *Rev. Scientific Instr.* 73, 2161–2170. doi:10.1063/1.1470232

Frenklach, M., Carmer, C. S., and Feigelson, E. D. (1989). Silicon Carbide and the Origin of Interstellar Carbon Grains. *Nature* 339, 196–198. doi:10.1038/339196a0

Fuchs, G. W., Cuppen, H. M., Ioppolo, S., Romanzin, C., Bisschop, S. E., Andersson, S., et al. (2009). Hydrogenation Reactions in Interstellar CO Ice Analogues. *A&A* 505, 629–639. doi:10.1051/0004-6361/200810784

Fulvio, D., Baratta, G. A., Sivaraman, B., Mason, N. J., da Silveira, E. F., de Barros, A. L. F., et al. (2018). Ion Irradiation of N_2O Ices and NO_2:N_2O_4 Ice Mixtures: First Steps to Understand the Evolution of Molecules with the N–O Bond in Space. *Mon. Not. R. Astron. Soc.* 483, 381. doi:10.1093/mnras/sty3081

Galli, D., Walmsley, M., and Gonçalves, J. (2002). The Structure and Stability of Molecular Cloud Cores in External Radiation fields. *A&A* 394, 275–284. doi:10.1051/0004-6361:20021125

Garozzo, M., Fulvio, D., Kaňuchová, Z., Palumbo, M. E., and Strazzulla, G. (2010). The Fate of S-Bearing Species after Ion Irradiation of Interstellar Icy Grain Mantles. *Astron. Astrophys.* 509, 67. doi:10.1051/0004-6361/200913040

Garrod, R. T., Belloche, A., Müller, H. S. P., and Menten, K. M. (2017). Exploring Molecular Complexity with ALMA (EMoCA): Simulations of Branched Carbon-Chain Chemistry in Sgr B2(N). *Astron. Astrophys.* 601, 48. doi:10.1051/0004-6361/201630254

Garrod, R. T., Weaver, S. L. W., and Herbst, E. (2008). Complex Chemistry in Star-forming Regions: An Expanded Gas-Grain Warm-up Chemical Model. *ApJ* 682, 283–302. doi:10.1086/588035

Geppert, W. D., and Larsson, M. (2013). Experimental Investigations into Astrophysically Relevant Ionic Reactions. *Chem. Rev.* 113, 8872–8905. doi:10.1021/cr400258m

Gerin, M., De Luca, M., Black, J., Goicoechea, J. R., Herbst, E., Neufeld, D. A., et al. (2010a). Interstellar OH+, H_2O^+ and H_2O^+ along the Sight-Line to G10.6-0.4. *A&A* 518, L110. doi:10.1051/0004-6361/201014576

Gerin, M., Kaźmierczak, M., Jastrzebska, M., Falgarone, E., Hily-Blant, P., Godard, B., et al. (2010b). The Tight Correlation of CCH and C-C_3h_2 in Diffuse and Translucent Clouds. *Astron. Astrophys.* 525, 116. doi:10.1051/0004-6361/201015050

Gerin, M., Levrier, F., Falgarone, E., Godard, B., Hennebelle, P., Le Petit, F., et al. (2012). Hydride Spectroscopy of the Diffuse Interstellar Medium: New Clues on the Gas Fraction in Molecular Form and Cosmic ray Ionization Rate in Relation to H 3 +. *Phil. Trans. R. Soc. A.* 370, 5174–5185. doi:10.1098/rsta.2012.0023

Giuliano, B. M., Gavdush, A. A., Müller, B., Zaytsev, K. I., Grassi, T., Ivlev, A. V., et al. (2019). Broadband Spectroscopy of Astrophysical Ice Analogues I: Direct Measurement of the Complete Refractive index of CO Ice Using Terahertz

Time-Domain Spectroscopy. *Astron. Astrophys.* 629, 112. doi:10.1051/0004-6361/201935619

Godard, B., and Cernicharo, J. (2013). A Complete Model of CH^+ Rotational Excitation Including Radiative and Chemical Pumping Processes. *Astron. Astrophys.* 550, 8. doi:10.1051/0004-6361/201220151

Godard, B., Falgarone, E., and Pineau des Forêts, G. (2009). Models of Turbulent Dissipation Regions in the Diffuse Interstellar Medium. *A&A* 495, 847–867. doi:10.1051/0004-6361:200810803

Goldman, N., Reed, E. J., Fried, L. E., William Kuo, I.-F., and Maiti, A. (2010). Synthesis of Glycine-Containing Complexes in Impacts of Comets on Early Earth. *Nat. Chem* 2, 949–954. doi:10.1038/nchem.827

Goldsmith, P. F., Liseau, R., Bell, T. A., Black, J. H., Chen, J.-H., Hollenbach, D., et al. (2011). Herschel measurements of Molecular Oxygen in Orion. *ApJ* 737, 96. doi:10.1088/0004-637x/737/2/96

Graff, M. M., Moseley, J. T., and Roueff, E. (1983). Resonant and Nonresonant Processes in the Formation of CH(+) by Radiative Association. *ApJ* 269, 796. doi:10.1086/161088

Griffin, M. J., Abergel, A., Abreu, A., Ade, P. A. R., André, P., Augueres, J.-L., et al. (2010). TheHerschel-SPIRE Instrument and its In-Flight Performance. *A&A* 518, L3. doi:10.1051/0004-6361/201014519

Griffin, M. J., Baselmans, J., Baryshev, A., Doyle, S., Grim, M., Hargrave, P., et al. (2016). "SPACEKIDS: Kinetic Inductance Detectors for Space Applications," in *Proc. SPIE 9914, Millimeter, Submillimeter, and Far-Infrared Detectors and Instrumentation for Astronomy VIII* (Springer), 991407. doi:10.1117/12.2231100

Griffiths, P., and de Haseth, J. (1986). *Fourier Transform Infrared Spectroscopy*. New York City (NY): John Wiley & Sons.

Groen, J., Deamer, D. W., Kros, A., and Ehrenfreund, P. (2012). Polycyclic Aromatic Hydrocarbons as Plausible Prebiotic Membrane Components. *Orig. Life Evol. Biosph.* 42, 295–306. doi:10.1007/s11084-012-9292-3

Gupta, H., Rimmer, P., Pearson, J. C., Yu, S., Herbst, E., Harada, N., et al. (2010). Detection of OH^+ and H_2O^+ towards Orion KL. *A&A* 521, L47. doi:10.1051/0004-6361/201015117

Gurvits, L. I., Paragi, Z., Casasola, V., Conway, J., Davelaar, J., Falcke, H., et al. (2021). THEZA: TeraHertz Exploration and Zooming-In for Astrophysics. *Exp. Astron.* 51, 559–594. doi:10.1007/s10686-021-09714-y

Hazen, R. M., and Ferry, J. M. (2010). Mineral Evolution: Mineralogy in the Fourth Dimension. *Elements* 6, 9–12. doi:10.2113/gselements.6.1.9

Hazen, R. M., Papineau, D., Bleeker, W., Downs, R. T., Ferry, J. M., McCoy, T. J., et al. (2008). Mineral Evolution. *Am. Mineral.* 93, 1693–1720. doi:10.2138/am.2008.2955

Henderson, S. W., Stevens, J. R., Amiri, M., Austermann, J., Beall, J. A., Chaudhuri, S., et al. (2016). "Readout of Two-Kilopixel Transition-Edge Sensor Arrays for Advanced ACTPol," in *Proc. SPIE 9914, Millimeter, Submillimeter, and Far-Infrared Detectors and Instrumentation for Astronomy VIII* (Springer), 9914. doi:10.1117/12.2233895

Higgs, P. G., and Lehman, N. (2015). The RNA World: Molecular Cooperation at the Origins of Life. *Nat. Rev. Genet.* 16, 7–17. doi:10.1038/nrg3841

Hogerheijde, M. R., Bergin, E. A., Brinch, C., Cleeves, L. I., Fogel, J. K., Blake, G. A., et al. (2011). Detection of the Water Reservoir in a Forming Planetary System. *Science* 334, 338–340. doi:10.1126/science.1208931

Indriolo, N., Neufeld, D. A., Gerin, M., Schilke, P., Benz, A. O., Winkel, B., et al. (2015). Herschel survey of Galactic Oh^+, H_2O^+, and H_3O^+: Probing the Molecular Hydrogen Fraction and Cosmic-ray Ionization Rate. *ApJ* 800, 40. doi:10.1088/0004-637x/800/1/40

Ioppolo, S., Fedoseev, G., Chuang, K.-J., Cuppen, H. M., Clements, A. R., Jin, M., et al. (2021). A Non-energetic Mechanism for glycine Formation in the Interstellar Medium. *Nat. Astron.* 5, 197–205. doi:10.1038/s41550-020-01249-0

Ioppolo, S., Kaňuchová, Z., James, R. L., Dawes, A., Jones, N. C., Hoffmann, S. V., et al. (2020). Vacuum Ultraviolet Photoabsorption Spectroscopy of Space-Related Ices: 1 keV Electron Irradiation of Nitrogen- and Oxygen-Rich Ices. *Astron. Astrophys.* 641, 154. doi:10.1051/0004-6361/201935477

Ioppolo, S., McGuire, B. A., Allodi, M. A., and Blake, G. A. (2014). THz and Mid-IR Spectroscopy of Interstellar Ice Analogs: Methyl and Carboxylic Acid Groups. *Faraday Discuss.* 168, 461–484. doi:10.1039/c3fd00154g

Jacob, A. M., Menten, K. M., Wyrowski, F., Winkel, B., and Neufeld, B. A. (2020). Extending the View of ArH^+ Chemistry in Diffuse Clouds. *Astron. Astrophys.* 643, 91. doi:10.1051/0004-6361/202039197

Jones, B. M., Bennett, C. J., and Kaiser, R. I. (2011). Mechanistical Studies on the Production of Formamide (H_2Ncho) within Interstellar Ice Analogs. *ApJ* 734, 78. doi:10.1088/0004-637x/734/2/78

Jørgensen, J. K., Müller, H. S. P., Calcutt, H., Coutens, A., Drozdovskaya, M. N., Öberg, K. I., et al. (2018). The ALMA-PILS Survey: Isotopic Composition of Oxygen-Containing Complex Organic Molecules toward IRAS 16293-2422B. *Astron. Astrophys.* 620, 170. doi:10.1051/0004-6361/201731667

Kaňuchová, Z., Boduch, P., Domaracka, A., Palumbo, M. E., Rothard, H., and Strazzulla, G. (2017). Thermal and Energetic Processing of Astrophysical Ice Analogues Rich in SO_2. *Astron. Astrophys.* 604, 68. doi:10.1051/0004-6361/201730711

Kawase, K., Sato, M., Taniuchi, T., and Ito, H. (1996). Coherent Tunable THz-wave Generation from LiNbO3 with Monolithic Grating Coupler. *Appl. Phys. Lett.* 68, 2483–2485. doi:10.1063/1.115828

Kelvin Lee, K. L., Changala, P. B., Loomis, R. A., Burkhardt, A. M., Xue, C., Cordiner, M. A., et al. (2021a). Interstellar Detection of 2-cyanocyclopentadiene, C5H5CN, a Second Five-Membered Ring toward TMC-1. *ApJL* 910, L2. doi:10.3847/2041-8213/abe764

Kelvin Lee, K. L., Loomis, R. A., Burkhardt, A. M., Cooke, I. R., Xue, C., Siebert, M. A., et al. (2021b). Discovery of Interstellar Trans-cyanovinylacetylene (HC ≡ CCH = CHC ≡ N) and Vinylcyanoacetylene (H_2C = CHC3N) in GOTHAM Observations of TMC-1. *ApJ* 908, L11. doi:10.3847/2041-8213/abdbb9

Kiessling, J., Breunig, I., Schunemann, P. G., Buse, K., and Vodopyanov, K. L. (2013). High Power and Spectral Purity Continuous-Wave Photonic THz Source Tunable from 1 to 4.5 THz for Nonlinear Molecular Spectroscopy. *New J. Phys.* 15, 105014. doi:10.1088/1367-2630/15/10/105014

Kilcullen, P., Hartley, I. D., Jensen, E. T., and Reid, M. (2015). Terahertz Time Domain Gas-phase Spectroscopy of Carbon Monoxide. *J. Infrared Milli. Terahz. Waves* 36, 380–389. doi:10.1007/s10762-014-0139-z

Klein, B., Hochgürtel, S., Krämer, I., Bell, A., Meyer, K., and Güsten, R. (2012). High-resolution Wide-Band Fast Fourier Transform Spectrometers. *A&A* 542, L3. doi:10.1051/0004-6361/201218864

Klein, B., Philipp, S. D., Güsten, R., Krämer, I., and Samtleben, D. (2006). A New Generation of Spectrometers for Radio Astronomy: Fast Fourier-Transform Spectrometer. *Proc. SPIE* 6275, 62751. doi:10.1117/12.670831

Kojima, T., Kroug, M., Uemizu, K., Niizeki, Y., Takahashi, H., and Uzawa, Y. (2017). Performance and Characterization of a Wide if SIS-Mixer-Preamplifier Module Employing High-J C SIS Junctions. *IEEE Trans. Thz Sci. Technol.* 7, 694–703. doi:10.1109/tthz.2017.2758260

Kokoouline, V., and Greene, C. H. (2003). Unified Theoretical Treatment of Dissociative Recombination of D_{3h} Triatomic Ions: Applications to H_3^+ and D_3^+. *Phys. Rev. A.* 68, 012703. doi:10.1103/physreva.68.012703

Komandin, G. A., Chuchupal, S. V., Lebedev, S. P., Goncharov, Y. G., Korolev, A. F., Porodinkov, O. E., et al. (2013). BWO Generators for Terahertz Dielectric Measurements. *IEEE Trans. Thz Sci. Technol.* 3, 440–444. doi:10.1109/tthz.2013.2255914

Kraus, J. D. (1988). Grote Reber – Founder of Radio Astronomy. *J. R. Astron. Soc. Can.* 82, 107.

Kruger, K., Grabowski, P. J., Zaug, A. J., Sands, J., Gottschling, D. E., and Cech, T. R. (1982). Self-splicing RNA: Autoexcision and Autocyclization of the Ribosomal RNA Intervening Sequence of tetrahymena. *Cell* 31, 147–157. doi:10.1016/0092-8674(82)90414-7

Kulesa, C. (2011). Terahertz Spectroscopy for Astronomy: From Comets to Cosmology. *IEEE Trans. Terahertz Sci. Technol.* 1, 232–240. doi:10.1109/tthz.2011.2159648

Kwok, S., and Zhang, Y. (2011). Mixed Aromatic-Aliphatic Organic Nanoparticles as Carriers of Unidentified Infrared Emission Features. *Nature* 479, 80–83. doi:10.1038/nature10542

Lang, K., Erlacher, M., Wilson, D. N., Micura, R., and Polacek, N. (2008). The Role of 23S Ribosomal RNA Residue A2451 in Peptide Bond Synthesis Revealed by Atomic Mutagenesis. *Chem. Biol.* 15, 485–492. doi:10.1016/j.chembiol.2008.03.014

Langer, W. D., Velusamy, T., Pineda, J. L., Goldsmith, P. F., Li, D., and Yorke, H. W. (2010). C^+ detection of Warm Dark Gas in Diffuse Clouds. *A&A* 521, L17. doi:10.1051/0004-6361/201015088

Larson, Å., Djurić, N., Zong, W., Greene, C. H., Orel, A. E., Al-Khalili, A., et al. (2000). Resonant Ion-Pair Formation in Electron Collisions with HD^+ and OH^+. *Phys. Rev. A.* 62, 042707. doi:10.1103/physreva.62.042707

Larsson, M., Geppert, W. D., and Nyman, G. (2012). Ion Chemistry in Space. *Rep. Prog. Phys.* 75, 066901. doi:10.1088/0034-4885/75/6/066901

Larsson, M., McCall, B. J., and Orel, A. E. (2008). The Dissociative Recombination of H_3^+ - a Saga Coming to an End? *Chem. Phys. Lett.* 462, 145–151. doi:10.1016/j.cplett.2008.06.069

Li, W., and Yao, J. (2010). Investigation of Photonically Assisted Microwave Frequency Multiplication Based on External Modulation. *IEEE Trans. Microwave Theor. Techn.* 58, 3259–3268. doi:10.1109/tmtt.2010.2075671

Linnartz, H., Ioppolo, S., and Fedoseev, G. (2015). Atom Addition Reactions in Interstellar Ice Analogues. *Int. Rev. Phys. Chem.* 34, 205–237. doi:10.1080/0144235x.2015.1046679

Linz, H., Beuther, H., Gerin, M., Goicoechea, J. R., Helmich, F., Krause, O., et al. (2021). Bringing High Spatial Resolution to the Far-Infrared. *Exp. Astron.* 51, 661–697. doi:10.1007/s10686-021-09719-7

Lis, D. C., Pearson, J. C., Neufeld, D. A., Schilke, P., Müller, H. S. P., Gupta, H., et al. (2010). Herschel/HIFI Discovery of Interstellar Chloronium (H_2Cl^+). *A&A* 521, L9. doi:10.1051/0004-6361/201014959

Lo, J.-I., Chou, S.-L., Peng, Y.-C., Lin, M.-Y., Lu, H.-C., and Cheng, B.-M. (2014). Photochemistry of Solid Interstellar Molecular Samples Exposed to Vacuum-Ultraviolet Synchrotron Radiation. *J. Electron Spectrosc. Relat. Phenomena* 196, 173–176. doi:10.1016/j.elspec.2013.12.014

Loomis, R. A., Burkhardt, A. M., Shingledecker, C. N., Charnley, S. B., Cordiner, M. A., Herbst, E., et al. (2021). An Investigation of Spectral Line Stacking Techniques and Application to the Detection of HC11N. *Nat. Astron.* 5, 188–196. doi:10.1038/s41550-020-01261-4

Maestrini, A., Thomas, B., Wang, H., Jung, C., Treuttel, J., Jin, Y., et al. (2010). Schottky Diode-Based Terahertz Frequency Multipliers and Mixers. *Comptes Rendus Physique* 11, 480–495. doi:10.1016/j.crhy.2010.05.002

Maiolino, R. (2008). Prospects for AGN Studies with ALMA. *New Astron. Rev.* 52, 339–357. doi:10.1016/j.newar.2008.06.012

Martins, Z., Price, M. C., Goldman, N., Sephton, M. A., and Burchell, M. J. (2013). Shock Synthesis of Amino Acids from Impacting Cometary and Icy Planet Surface Analogues. *Nat. Geosci* 6, 1045–1049. doi:10.1038/ngeo1930

Mason, N. J., Dawes, A., Holtom, P. D., Mukerji, R. J., Davis, M. P., Sivaraman, B., et al. (2006). VUV Spectroscopy and Photo-Processing of Astrochemical Ices: An Experimental Study. *Faraday Discuss.* 133, 311. doi:10.1039/b518088k

Materese, C. K., Nuevo, M., McDowell, B. L., Buffo, C. E., and Sandford, S. A. (2018). The Photochemistry of Purine in Ice Analogs Relevant to Dense Interstellar Clouds. *ApJ* 864, 44. doi:10.3847/1538-4357/aad328

Materese, C. K., Nuevo, M., and Sandford, S. A. (2015). N- Ando-Heterocycles Produced from the Irradiation of Benzene and Naphthalene in H_2O/NH_3-Containing Ices. *ApJ* 800, 116. doi:10.1088/0004-637x/800/2/116

Materese, C. K., Nuevo, M., and Sandford, S. A. (2017). The Formation of Nucleobases from the Ultraviolet Photoirradiation of Purine in Simple Astrophysical Ice Analogues. *Astrobiology* 17, 761–770. doi:10.1089/ast.2016.1613

McCall, B. J., Geballe, T. R., Hinkle, K. H., and Oka, T. (1998). Detection of H 3 + in the Diffuse Interstellar Medium toward Cygnus OB2 No. 12. *Science* 279, 1910–1913. doi:10.1126/science.279.5358.1910

McCarthy, M. C., Lee, K. L. K., Loomis, R. A., Burkhardt, A. M., Shingledecker, C. N., Charnley, S. B., et al. (2021). Interstellar Detection of the Highly Polar Five-Membered Ring Cyanocyclopentadiene. *Nat. Astron.* 5, 176–180. doi:10.1038/s41550-020-01213-y

McGuire, B. A., Brogan, C. L., Hunter, T. R., Remijan, A. J., Blake, G. A., Burkhardt, A. M., et al. (2018b). First Results of an ALMA Band 10 Spectral Line Survey of NGC 6334I: Detections of Glycolaldehyde ($HC(O)CH_2OH$) and a New Compact Bipolar Outflow in HDO and CS. *ApJ* 863, L35. doi:10.3847/2041-8213/aad7bb

McGuire, B. A., Burkhardt, A. M., Kalenskii, S., Shingledecker, C. N., Remijan, A. J., Herbst, E., et al. (2018a). Detection of the Aromatic Molecule Benzonitrile (C -C 6 H 5 CN) in the Interstellar Medium. *Science* 359, 202–205. doi:10.1126/science.aao4890

McGuire, B. A., Burkhardt, A. M., Loomis, R. A., Shingledecker, C. N., Kelvin Lee, K. L., Charnley, S. B., et al. (2020). Early Science from GOTHAM: Project Overview, Methods, and the Detection of Interstellar Propargyl Cyanide ($HCCCH_2CN$) in TMC-1. *ApJ* 900, L10. doi:10.3847/2041-8213/aba632

McGuire, B. A., Ioppolo, S., Allodi, M. A., and Blake, G. A. (2016). THz Time-Domain Spectroscopy of Mixed CO_2-CH_3OH Interstellar Ice Analogs. *Phys. Chem. Chem. Phys.* 18, 20199–20207. doi:10.1039/c6cp00632a

McGuire, B. A., Loomis, R. A., Burkhardt, A. M., Lee, K. L. K., Shingledecker, C. N., Charnley, S. B., et al. (2021). Detection of Two Interstellar Polycyclic Aromatic Hydrocarbons via Spectral Matched Filtering. *Science* 371, 1265–1269. doi:10.1126/science.abb7535

McGuire, B. A., Shingledecker, C. N., Willis, E. R., Burkhardt, A. M., El-Abd, S., Motiyenko, R. A., et al. (2017). ALMA Detection of Interstellar Methoxymethanol (CH_3OCH_2OH). *Astrophys. J. Lett.* 851, 2. doi:10.3847/2041-8213/aaa0c3

McIntosh, A. I., Yang, B., Goldup, S. M., Watkinson, M., and Donnan, R. S. (2012). Terahertz Spectroscopy: A Powerful New Tool for the Chemical Sciences? *Chem. Soc. Rev.* 41, 2072–2082. doi:10.1039/c1cs15277g

Mead, G., Katayama, I., Takeda, J., and Blake, G. A. (2019). An Echelon-Based Single Shot Optical and Terahertz Kerr Effect Spectrometer. *Rev. Scientific Instr.* 90, 053107. doi:10.1063/1.5088377

Medvedev, I. R., Neese, C. F., Plummer, G. M., and De Lucia, F. C. (2010). Submillimeter Spectroscopy for Chemical Analysis with Absolute Specificity. *Opt. Lett.* 35, 1533. doi:10.1364/ol.35.001533

Menten, K. M., Wyrowski, F., Belloche, A., Güsten, R., Dedes, L., and Müller, H. S. P. (2011). Submillimeter Absorption from SH^+, a New Widespread Interstellar Radical, $^{13}CH^+$ and HCl. *Astron. Astrophys.* 525, 77. doi:10.1051/0004-6361/201014363

Merino, P., Švec, M., Martinez, J. I., Jelinek, P., Lacovig, P., Dalmiglio, M., et al. (2014). Graphene Etching on SiC Grains as a Path to Interstellar Polycyclic Aromatic Hydrocarbons Formation. *Nat. Commun.* 5, 3054. doi:10.1038/ncomms4054

Mifsud, D. V., Kaňuchová, Z., Herczku, P., Ioppolo, S., Juhász, Z., Kovács, S. T. S., et al. (2021). Sulfur Ice Astrochemistry: A Review of Laboratory Studies. *Space Sci. Rev.* 217, 14. doi:10.1007/s11214-021-00792-0

Milillo, A., Plainaki, C., De Angelis, E., Mangano, V., Massetti, S., Mura, A., et al. (2016). Analytical Model of Europa's O_2 Exosphere. *Planet. Space Sci.* 130, 3–13. doi:10.1016/j.pss.2015.10.011

Mittleman, D. M., Jacobsen, R. H., Neelamani, R., Baraniuk, R. G., and Nuss, M. C. (1998). Gas Sensing Using Terahertz Time-Domain Spectroscopy. *Appl. Phys. B: Lasers Opt.* 67, 379–390. doi:10.1007/s003400050520

Monje, R. R., Emprechtinger, M., Phillips, T. G., Lis, D. C., Goldsmith, P. F., Bergin, E. A., et al. (2011). Herschel/Hifi Observations of Hydrogen Fluoride toward Sagittarius B2(M). *ApJ* 734, L23. doi:10.1088/2041-8205/734/1/l23

Monje, R. R., Lis, D. C., Roueff, E., Gerin, M., De Luca, M., Neufeld, D. A., et al. (2013). Hydrogen Chloride in Diffuse Interstellar Clouds along the Line of Sight to W31C (G10.6-0.4). *ApJ* 767, 81. doi:10.1088/0004-637x/767/1/81

Moore, M. H., and Hudson, R. L. (1994). Far-infrared Spectra of Cosmic-type Pure and Mixed Ices. *Astron. Astrophys. Suppl. Ser.* 103, 45.

Moore, M. H., and Hudson, R. L. (1995). Far-infrared Spectral Changes Accompanying Proton Irradiation of Solids of Astrochemical Interest. *Radiat. Phys. Chem.* 45, 779. doi:10.1016/0969-806X(94)00099-6

Moore, M. H., and Hudson, R. L. (1992). Far-infrared Spectral Studies of Phase Changes in Water Ice Induced by Proton Irradiation. *ApJ* 401, 353. doi:10.1086/172065

Mosely, E. R., Draine, B. T., Tomida, K., and Stone, J. M. (2021). Turbulent Dissipation, CH^+ Abundance, H_2 Line Luminosities, and Polarization in the Cold Neutral Medium. *Mon. Not. R. Astron. Soc.* 500, 3290. doi:10.1093/mnras/staa3384

Müller, H. S. P., Schlöder, F., Stutzki, J., and Winnewisser, G. (2005). The Cologne Database for Molecular Spectroscopy: A Useful Tool for Astronomers and Spectroscopists. *J. Mol. Struct.* 742, 215. doi:10.1016/j.molstruc.2005.01.027

Müller, H. S. P., Thorwith, S., Roth, D. A., and Winnewisser, G. (2001). The Cologne Database for Molecular Spectroscopy. *CDMS. Astron. Astrophys.* 370, L49. doi:10.1051/0004-6361:20010367

Muller, S., Müller, H. S. P., Black, J. H., Gerin, M., Combes, F., Curran, S., et al. (2017). Detection of CH^+, SH^+, and Their ^{13}C- and ^{34}S-Isotopologues toward PKS 1830-211. *Astron. Astrophys.* 606, 109. doi:10.1051/0004-6361/201731405

Mullikin, E., van Mulbregt, P., Perea, J., Kasule, M., Huang, J., Buffo, C., et al. (2018). Condensed-Phase Photochemistry in the Absence of Radiation Chemistry. *ACS Earth Space Chem.* 2, 863–868. doi:10.1021/acsearthspacechem.8b00027

Muñoz-Caro, G. M., Jiménez-Escobar, A., Martín-Gago, J. Á., Rogero, C., Atienza, C., Puertas, S., et al. (2010). New Results on thermal and Photodesorption of CO Ice Using the Novel InsterStellar Astrochemistry Chamber (ISAC). *Astron. Astrophys.* 522, 108. doi:10.1051/0004-6361/200912462

Myers, A. T., McKee, C. F., and Li, P. S. (2015). The CH^+ Abundance in Turbulent, Diffuse Molecular Clouds. *Mon. Not. R. Astron. Soc.* 453, 2747. doi:10.1093/mnras/stv1782

National Academies of Sciences, Engineering, and Medicine (2021). *Pathways to Discovery in Astronomy and Astrophysics for the 2020s*. Washington DC: The National Academies Press. doi:10.17226/26141

Neil, G. R. (2014). Accelerator Sources for THz Science: A Review. *J. Infrared Milli Terahz Waves* 35, 5–16. doi:10.1007/s10762-013-9999-x

Neufeld, D. A., Falgarone, E., Gerin, M., Godard, B., Herbst, E., Pineau des Forêts, G., et al. (2012b). Discovery of Interstellar Mercapto Radicals (SH) with the GREAT Instrument on SOFIA. *A&A* 542, L6. doi:10.1051/0004-6361/201218870

Neufeld, D. A., Godard, B., Gerin, M., Pineau des Forêts, G., Bernier, C., Falgarone, E., et al. (2015). Sulfur-bearing Molecules in Diffuse Molecular Clouds: New Results from SOFIA/GREAT and the IRAM 30 M Telescope. *Astron. Astrophys.* 577, 49. doi:10.1051/0004-6361/201425391

Neufeld, D. A., Goicoechea, J. R., Sonnentrucker, P., Black, J. H., Pearson, J., Yu, S., et al. (2010a). Herschel/HIFI Observations of Interstellar OH+and H_2O+towards W49N: a Probe of Diffuse Clouds with a Small Molecular Fraction. *A&A* 521, L10. doi:10.1051/0004-6361/201015077

Neufeld, D. A., Roueff, E., Snell, R. L., Lis, D., Benz, A. O., Bruderer, S., et al. (2012a). Herschel observations of Interstellar Chloronium. *ApJ* 748, 37. doi:10.1088/0004-637x/748/1/37

Neufeld, D. A., Sonnentrucker, P., Phillips, T. G., Lis, D. C., De Luca, M., Goicoechea, J. R., et al. (2010b). Strong Absorption by Interstellar Hydrogen fluoride:Herschel/HIFI Observations of the Sight-Line to G10.6-0.4 (W31C). *A&A* 518, L108. doi:10.1051/0004-6361/201014523

Neveu, M., Kim, H.-J., and Benner, S. A. (2013). The "Strong" RNA World Hypothesis: Fifty Years Old. *Astrobiology* 13, 391–403. doi:10.1089/ast.2012.0868

Noble, J. A., Cuppen, H. M., Coussan, S., Redlich, B., and Ioppolo, S. (2020). Infrared Resonant Vibrationally Induced Restructuring of Amorphous Solid Water. *J. Phys. Chem. C* 124, 20864–20873. doi:10.1021/acs.jpcc.0c04463

Nuevo, M., Materese, C. K., and Sandford, S. A. (2014). The Photochemistry of Pyrimidine in Realistic Astrophysical Ices and the Production of Nucleobases. *ApJ* 793, 125. doi:10.1088/0004-637x/793/2/125

Nuevo, M., Milam, S. N., Sandford, S. A., Elsila, J. E., and Dworkin, J. P. (2009). Formation of Uracil from the Ultraviolet Photo-Irradiation of Pyrimidine in Pure H_2O Ices. *Astrobiology* 9, 683–695. doi:10.1089/ast.2008.0324

Nuevo, M., Milam, S. N., and Sandford, S. A. (2012). Nucleobases and Prebiotic Molecules in Organic Residues Produced from the Ultraviolet Photo-Irradiation of Pyrimidine in $NH_3$and H_2O^+ NH_3Ices. *Astrobiology* 12, 295–314. doi:10.1089/ast.2011.0726

Öberg, K. I. (2016). Photochemistry and Astrochemistry: Photochemical Pathways to Interstellar Complex Organic Molecules. *Chem. Rev.* 116, 9631. doi:10.1021/acs.chemrev.5b00694

Öjekull, J., Andersson, P. U., Någård, M. B., Pettersson, J. B. C., Derkatch, A. M., Neau, A., et al. (2004). Dissociative Recombination of NH_4^+ and ND_4^+ Ions: Storage Ring Experiments and *Ab Initio* Molecular Dynamics. *J. Chem. Phys.* 120, 7391. doi:10.1063/1.1669388

Orgel, L. E. (2004). Prebiotic Chemistry and the Origin of the RNA World. *Crit. Rev. Biochem. Mol. Biol.* 39, 99–123. doi:10.1080/10409230490460765

Pan, K., Federman, S. R., Cunha, K., Smith, V. V., and Welty, D. E. (2004). Cloud Structure and Physical Conditions in Star-forming Regions from Optical Observations. I. Data and Component Structure. *Astrophys J. Suppl. S* 151, 313–343. doi:10.1086/381805

Pardo, J. R., Cernicharo, J., and Serabyn, E. (2001). Atmospheric Transmission at Microwaves (ATM): an Improved Model for Millimeter/submillimeter Applications. *IEEE Trans. Antennas Propagat.* 49, 1683–1694. doi:10.1109/8.982447

Park, G. B., and Field, R. W. (2016). Perspective: The First Ten Years of Broadband Chirped Pulse Fourier Transform Microwave Spectroscopy. *J. Chem. Phys.* 144, 200901. doi:10.1063/1.4952762

Parkes, S., Dunstan, M., Scott, P., Dillon, D., Spark, A., Ellison, B., et al. (2018). "A Wideband Spectrometer in the Microsemi RTG4 FPGA," in Paper Presented at Data Systems in Aerospace Conference, DASIA 2018 (Oxford, UK: IEEE).

Peeters, Z., Botta, O., Charnley, S. B., Ruiterkamp, R., and Ehrenfreund, P. (2003). The Astrobiology of Nucleobases. *ApJ* 593, L129–L132. doi:10.1086/378346

Perakis, F., Borek, J. A., and Hamm, P. (2013). Three-dimensional Infrared Spectroscopy of Isotope-Diluted Ice Ih. *J. Chem. Phys.* 139, 014501. doi:10.1063/1.4812216

Persson, C. M., Black, J. H., Cernicharo, J., Goicoechea, J. R., Hassel, G. E., Herbst, E., et al. (2010). Nitrogen Hydrides in Interstellar Gas. *A&A* 521, L45. doi:10.1051/0004-6361/201015105

Pickett, H. M., Poynter, R. L., Cohen, E. A., Delitsky, M. L., Pearson, J. C., and Müller, H. S. P. (1998). Submillimeter, Millimeter, and Microwave Spectral Line Catalog. *J. Quantitative Spectrosc. Radiative Transfer* 60, 883–890. doi:10.1016/s0022-4073(98)00091-0

Plašil, R., Rednyk, S., Kovalenko, A., Tran, T. D., Roučka, Š., Dohnal, P., et al. (2021). Experimental Study on the CH^+ Formation from Doubly Charged Carbon and Molecular Hydrogen. *Astrophys. J.* 910, 155. doi:10.3847/1538-4357/abe86c

Potapov, A., Jäger, C., Henning, T., Jonusas, M., and Krim, L. (2017). The Formation of Formaldehyde on Interstellar Carbonaceous Grain Analogs by O/H Atom Addition. *ApJ* 846, 131. doi:10.3847/1538-4357/aa85e8

Preu, S., Döhler, G. H., Malzer, S., Wang, L. J., and Gossard, A. C. (2011). Tunable, Continuous-Wave Terahertz Photomixer Sources and Applications. *J. Appl. Phys.* 109, 061301. doi:10.1063/1.3552291

Price, D. C. (2016). *Spectrometers and Polyphase Filterbanks in Radio Astronomy*. ArXiv [Preprint]. Available at: https://arxiv.org/abs/1607.03579 (Accessed April 24, 2021).

Profeta, G., and Scandolo, S. (2011). Far-infrared Spectrum of Ice I_h: A First-Principles Study. *Phys. Rev. B* 84, 024103. doi:10.1103/physrevb.84.024103

Qasim, D., Fedoseev, G., Chuang, K.-J., He, J., Ioppolo, S., van Dishoeck, E. F., et al. (2020). An Experimental Study of the Surface Formation of Methane in Interstellar Molecular Clouds. *Nat. Astron.* 4, 781–785. doi:10.1038/s41550-020-1054-y

Raffaelli, N. (2011). "Nicotinamide Coenzyme Synthesis: A Case of Ribonucleotide Emergence or a Byproduct of the RNA World?," in *Origins of Life: The Primal Self-Organization*. Editors R. Egel, D. H. Lankenau, and A. Y. Mulkidjanian (Heidelberg: Springer), 185–208. doi:10.1007/978-3-642-21625-1_9

Redlich, B., van der Meer, L., Zacharias, H., Meijer, G., and von Helden, G. (2003). FEL Induced Dynamics of Small Molecules on Surfaces: N2O on NaCl(100). *Nucl. Instrum. Methods Phys. Res. A.* 507, 556–560. doi:10.1016/b978-0-444-51417-2.50126-7

Rigopoulou, D., Pearson, C., Ellison, B., Wiedner, M., Okada, V. O., Tan, B. K., et al. (2021). The Far-Infrared Spectroscopic Surveyor (FIRSS). *Exp. Astron.* 51, 699–728. doi:10.1007/s10686-021-09716-w

Rosenthal, D., Beeman, J. W., Geis, N., Grözinger, U., Hönle, R., Katterloher, R. O., et al. (2002). *Stressed Ge:Ga Detector Arrays for PACS and FIFI LS. Far-IR, Sub-mm and Mm Detector Technology Workshop*. Monterey, CA: Springer.

Rothman, L. S., Gordon, I. E., Barbe, A., Benner, D. C., Bernath, P. F., Birk, M., et al. (2009). The HITRAN 2008 Molecular Spectroscopic Database. *J. Quantitative Spectrosc. Radiative Transfer* 110, 533–572. doi:10.1016/j.jqsrt.2009.02.013

Sandford, S. A., Nuevo, M., Bera, P. P., and Lee, T. J. (2020). Prebiotic Astrochemistry and the Formation of Molecules of Astrobiological Interest in Interstellar Clouds and Protostellar Disks. *Chem. Rev.* 120, 4616–4659. doi:10.1021/acs.chemrev.9b00560

Schilke, P., Neufeld, D. A., Müller, H. S. P., Comito, C., Bergin, E. A., Lis, D. C., et al. (2014). Ubiquitous Argonium (ArH^+) in the Diffuse Interstellar Medium: A Molecular Tracer of Almost Purely Atomic Gas. *Astron. Astrophys.* 566, 29. doi:10.1051/0004-6361/201423727

Scibelli, S., and Shirley, Y. (2020). Prevalence of Complex Organic Molecules in Starless and Prestellar Cores within the Taurus Molecular Cloud. *ApJ* 891, 73. doi:10.3847/1538-4357/ab7375

Semaniak, J., Larson, A., Le Padellec, A., Stromholm, C., Larsson, M., Rosen, S., et al. (1998). Dissociative recombination and excitation of CH_5^+: Absolute cross sections and branching fractions. *ApJ* 498, 886–895. doi:10.1086/305581

Shalit, A., Perakis, F., and Hamm, P. (2013). Two-dimensional Infrared Spectroscopy of Isotope-Diluted Low Density Amorphous Ice. *J. Phys. Chem. B* 117, 15512–15518. doi:10.1021/jp4053743

Siebertz, O., Schmülling, F., Gal, C., Schloeder, F., Hartogh, P., Natale, V., et al. (2007). The Wide-Band Spectrometer (WBS) for the HIFI Instrument of Herschel. *Proc. ISSTT* 135, 1.

Smith, D. (1992). The Ion Chemistry of Interstellar Clouds. *Chem. Rev.* 92, 1473–1485. doi:10.1021/cr00015a001

Smith, I. W. M. (2011). Laboratory Astrochemistry: Gas-phase Processes. *Annu. Rev. Astron. Astrophys.* 49, 29–66. doi:10.1146/annurev-astro-081710-102533

Snow, T. P., and Bierbaum, V. M. (2008). Ion Chemistry in the Interstellar Medium. *Annu. Rev. Anal. Chem.* 1, 229–259. doi:10.1146/annurev.anchem.1.031207.112907

Snow, T. P., and McCall, B. J. (2006). Diffuse Atomic and Molecular Clouds. *Annu. Rev. Astron. Astrophys.* 44, 367–414. doi:10.1146/annurev.astro.43.072103.150624

Soma, T., Sakai, N., Watanabe, Y., and Yamamoto, S. (2018). Complex Organic Molecules in Taurus Molecular Cloud-1. *ApJ* 854, 116. doi:10.3847/1538-4357/aaa70c

Sonnentrucker, P., Neufeld, D. A., Phillips, T. G., Gerin, M., Lis, D. C., De Luca, M., et al. (2010). Detection of Hydrogen Fluoride Absorption in Diffuse Molecular Clouds with Herschel/HIFI: an Ubiquitous Tracer of Molecular Gas. *A&A* 521, L12. doi:10.1051/0004-6361/201015082

Suzuki, T., Khosropanah, P., Ridder, M. L., Hijmering, R. A., Gao, J. R., Akamatsu, H., et al. (2016). Development of Ultra-low-noise TES Bolometer Arrays. *J. Low Temp. Phys.* 184, 52–59. doi:10.1007/s10909-015-1401-z

Taylor, S. D., and Duley, W. W. (1997). The Formation of Long Carbon Chains in Diffuse Clouds. *Mon. Not. R. Astron. Soc.* 286, 344–348. doi:10.1093/mnras/286.2.344

Teolis, B. D., and Waite, J. H. (2016). Dione and Rhea Seasonal Exospheres Revealed by Cassini CAPS and INMS. *Icarus* 272, 277–289. doi:10.1016/j.icarus.2016.02.031

Theulé, P., Endres, C., Hermanns, M., Bossa, J. B., and Potapov, A. (2020). High-resolution Gas-phase Spectroscopy of Molecules Desorbed from an Ice Surface: A Proof-Of-Principle Study. *ACS Earth Space Chem.* 4, 86. doi:10.1021/acsearthspacechem.9b00246

Thiel, V., Belloche, A., Menten, K. M., Garrod, R. T., and Müller, H. S. P. (2017). Complex Organic Molecules in Diffuse Clouds along the Line of Sight to Sagittarius B2. *A&A* 605, L6. doi:10.1051/0004-6361/201731495

Thornton, R. J., Ade, P. A. R., Aiola, S., Angilè, F. E., Amiri, M., Beall, J. A., et al. (2016). The Atacama Cosmology Telescope: The Polarization-Sensitive Actpol Instrument. *ApJS* 227, 21. doi:10.3847/1538-4365/227/2/21

Tielens, A. G. G. M. (2008). Interstellar Polycyclic Aromatic Hydrocarbon Molecules. *Annu. Rev. Astron. Astrophys.* 46, 289–337. doi:10.1146/annurev.astro.46.060407.145211

Townes, C., and Schawlow, A. (2013). *Microwave Spectroscopy*. Mineola (NY): Dover Publications.

Trofimov, V., and Varentsova, S. (2016). Essential Limitations of the Standard THz TDS Method for Substance Detection and Identification and a Way of Overcoming Them. *Sensors* 16, 502. doi:10.3390/s16040502

Valavanis, A., Auriacombe, O., Rawlings, T., Han, Y., Rea, S., Crook, M., et al. (2019). Waveguide-integrated THz Quantum-cascade Lasers for Atmospheric Research Satellite Payloads. *Proc. IEEE Mtt-s IWS* 1, 1. doi:10.1109/ieee-iws.2019.8803875

Valdivia, V., Godard, B., Hennebelle, P., Gerin, M., Lesaffre, P., and Le Bourlot, J. (2017). Origin of CH^+ in Diffuse Molecular Clouds. *Astron. Astrophys.* 600, 114. doi:10.1051/0004-6361/201629905

van Dishoeck, E. F. (2014). Astrochemistry of Dust, Ice and Gas: Introduction and Overview. *Faraday Discuss.* 168, 9–47. doi:10.1039/c4fd00140k

van Dishoeck, E. F. (2017). Astrochemistry: Overview and Challenges. *Proc. IAU* 13, 3–22. doi:10.1017/s1743921317011528

van Dishoeck, E. F., and Black, J. H. (1986). Comprehensive Models of Diffuse Interstellar Clouds - Physical Conditions and Molecular Abundances. *ApJS* 62, 109. doi:10.1086/191135

van Dishoeck, E. F., and Blake, G. A. (1998). Chemical Evolution of star-forming Regions. *Annu. Rev. Astron. Astrophys.* 36, 317–368. doi:10.1146/annurev.astro.36.1.317

van Dishoeck, E. F., Herbst, E., and Neufeld, D. A. (2013). Interstellar Water Chemistry: From Laboratory to Observations. *Chem. Rev.* 113, 9043–9085. doi:10.1021/cr4003177

van Exter, M., Fattinger, C., and Grischkowsky, D. (1989). High-brightness Terahertz Beams Characterized with an Ultrafast Detector. *Appl. Phys. Lett.* 55, 337–339. doi:10.1063/1.101901

Viti, S., Williams, D. A., and O'Neill, P. T. (2000). Hydrocarbons in Diffuse and Translucent Clouds. *Astron. Astrophys.* 354, 1062.

Wakelam, V., Bron, E., Cazaux, S., Dulieu, F., Gry, C., Guillard, P., et al. (2017). H 2 Formation on Interstellar Dust Grains: The Viewpoints of Theory, Experiments, Models and Observations. *Mol. Astrophysics* 9, 1–36. doi:10.1016/j.molap.2017.11.001

Watanabe, N., and Kouchi, A. (2002). Efficient Formation of Formaldehyde and Methanol by the Addition of Hydrogen Atoms to CO in H_2O-CO Ice at 10 K. *Astrophys. J.* 571, 173. doi:10.1086/341412

Wehres, N., Heyne, B., Lewen, F., Hermanns, M., Schmidt, B., Endres, C., et al. (2017). 100 GHz Room-Temperature Laboratory Emission Spectrometer. *Proc. IAU* 13, 332–345. doi:10.1017/s1743921317007803

Wehres, N., Maßen, J., Borisov, K., Schmidt, B., Lewen, F., Graf, U. U., et al. (2018). A Laboratory Heterodyne Emission Spectrometer at Submillimeter Wavelengths. *Phys. Chem. Chem. Phys.* 20, 5530–5544. doi:10.1039/c7cp06394f

Weinreb, S. (1961). Digital Radiometer. *Proc. IEEE* 49, 1099.

White, H. B. (1976). Coenzymes as Fossils of an Earlier Metabolic State. *J. Mol. Evol.* 7, 101–104. doi:10.1007/bf01732468

Widicus Weaver, S. L., Butler, R. A. H., Drouin, B. J., Petkie, D. T., Dyl, K. A., De Lucia, F. C., et al. (2005). Millimeter-Wave and Vibrational State Assignments for the Rotational Spectrum of Glycolaldehyde. *Astrophys J. Suppl. S* 158, 188–192. doi:10.1086/429292

Widicus Weaver, S. L. (2019). Millimeterwave and Submillimeterwave Laboratory Spectroscopy in Support of Observational Astronomy. *Annu. Rev. Astron. Astrophys.* 57, 79–112. doi:10.1146/annurev-astro-091918-104438

Wiesemeyer, H., Güsten, R., Heyminck, S., Hübers, H. W., Menten, K. M., Neufeld, D. A., et al. (2016). Far-infrared Study of Tracers of Oxygen Chemistry in Diffuse Clouds. *Astron. Astrophys.* 585, 76. doi:10.1051/0004-6361/201526473

Williams, D. A., and Hartquist, T. W. (1999). The Chemistry of star-forming Regions. *Acc. Chem. Res.* 32, 334–341. doi:10.1021/ar970114o

Willis, E. R., Garrod, R. T., Belloche, A., Müller, H. S. P., Barger, C. J., Bonfard, M., et al. (2020). Exploring Molecular Complexity with ALMA (EMoCA): Complex Isocyanides in Sgr B2(N). *Astron. Astrophys.* 636, 29. doi:10.1051/0004-6361/201936489

Wilson, T. L., Rohlfs, K., and Hüttemeister, S. (2008). *Tools of Radio Astronomy*. Heidelberg: Springer.

Wlodarczak, G. (1995). Rotational Spectroscopy and Astrochemistry. *J. Mol. Struct.* 347, 131–142. doi:10.1016/0022-2860(95)08541-3

Wyrowski, F., Menten, K. M., Gusten, R., and Belloche, A. (2010). First Interstellar Detection of OH^+. *Astron. Astrophys.* 518, 26. doi:10.1051/0004-6361/201014364

Xue, C., Willis, E. R., Loomis, R. A., Kelvin Lee, K. L., Burkhardt, A. M., Shingledecker, C. N., et al. (2020). Detection of Interstellar HC_4NC and an Investigation of Isocyanopolyyne Chemistry under TMC-1 Conditions. *ApJ* 900, L9. doi:10.3847/2041-8213/aba631

Yamamoto, S. (2017). *Introduction to Astrochemistry: Chemical Evolution from Interstellar Clouds to Star and Planet Formation*. Tokyo: Springer.

Yocum, K. M., Smith, H. H., Todd, E. W., Mora, L., Gerakines, P. A., Milam, S. N., et al. (2019). Millimeter/Submillimeter Spectroscopic Detection of Desorbed Ices: A New Technique in Laboratory Astrochemistry. *J. Phys. Chem. A.* 123, 8702–8708. doi:10.1021/acs.jpca.9b04587

Zernickel, A., Schilke, P., Schmiedeke, A., Lis, D. C., Brogan, C. L., Ceccarelli, C., et al. (2012). Molecular Line Survey of the High-Mass star-forming Region NGC 6334I with Herschel/HIFI and the Submillimeter Array. *Astron. Astrophys.* 546, 87. doi:10.1051/0004-6361/201219803

Zhen, J., Castellanos, P., Paardekooper, D. M., Linnartz, H., and Tielens, A. G. G. M. (2014). Laboratory Formation of Fullerenes from PAHs: Top-Down Interstellar Chemistry. *ApJ* 797, L30. doi:10.1088/2041-8205/797/2/l30

Conflict of Interest: The authors declare that the research was conducted in the absence of any commercial or financial relationships that could be construed as a potential conflict of interest.

Publisher's Note: All claims expressed in this article are solely those of the authors and do not necessarily represent those of their affiliated organizations, or those of the publisher, the editors and the reviewers. Any product that may be evaluated in this article, or claim that may be made by its manufacturer, is not guaranteed or endorsed by the publisher.

frontiers in Astronomy and Space Sciences

ORIGINAL RESEARCH
published: 30 November 2021
doi: 10.3389/fspas.2021.777107

Electronically Excited States of Potential Interstellar, Anionic Building Blocks for Astrobiological Nucleic Acids

*Taylor J. Santaloci [1], Marie E. Strauss [2] and Ryan C. Fortenberry [1]**

[1]Department of Chemistry and Biochemistry, University of Mississippi, Oxford, MS, United States, [2]Department of Chemistry, Physics, and Engineering, Biola University, La Mirada, CA, United States

Functionalizing deprotonated polycyclic aromatic hydrocarbon (PAH) anion derivatives gives rise to electronically excited states in the resulting anions. While functionalization with –OH and $-C_2H$, done presently, does not result in the richness of electronically excited states as it does with –CN done previously, the presence of dipole-bound excited states and even some valence excited states are predicted in this quantum chemical analysis. Most notably, the more electron withdrawing $-C_2H$ group leads to valence excited states once the number of rings in the molecule reaches three. Dipole-bound excited states arise when the dipole moment of the corresponding neutral radical is large enough (likely around 2.0 D), and this is most pronounced when the hydrogen atom is removed from the functional group itself regardless of whether functionalized by a hydroxyl or enthynyl group. Deprotonatation of the hydroxyl group in the PAH creates a ketone with a delocalized highest occupied molecular orbital (HOMO) unlike deprotonation of a hydrogen on the ring where a localized lone pair on one of the carbon atoms serves as the HOMO. As a result, hydroxyl functionlization and subsequent deprotonation of PAHs creates molecules that begin to exhibit structures akin to nucleic acids. However, the electron withdrawing $-C_2H$ has more excited states than the electron donating –OH functionalized PAH. This implies that the $-C_2H$ electron withdrawing group can absorb a larger energy range of photons, which signifies an increasing likelihood of being stabilized in the harsh conditions of the interstellar medium.

Keywords: dipole bound anion, dipole bound states, quantum chemistry, basis sets, PAHs

OPEN ACCESS

Edited by:
Ashraf - Ali,
University of Maryland, United States

Reviewed by:
Jack Simons,
The University of Utah, United States
Sankar Prasad Bhattacharyya,
Indian Association for the Cultivation of Science, India

****Correspondence:***
Ryan C. Fortenberry
r410@olemiss.edu

Specialty section:
This article was submitted to Astrochemistry, a section of the journal Frontiers in Astronomy and Space Sciences

Received: *14 September 2021*
Accepted: *08 November 2021*
Published: *30 November 2021*

Citation:
Santaloci TJ, Strauss ME and Fortenberry RC (2021) Electronically Excited States of Potential Interstellar, Anionic Building Blocks for Astrobiological Nucleic Acids. Front. Astron. Space Sci. 8:777107. doi: 10.3389/fspas.2021.777107

1 INTRODUCTION

The *Cassini-Huygens* mission investigated the atmospheric structure, surface morphology, composition, and meteorology of Saturn's moon Titan (Coustenis, 2007). The Cassini plasma spectrometer electron spectrometer (CAPS-ELS) detected negatively charged materials with masses large enough such that polynucleotides could be one potential explanation for these detected species. The CAPS-ELS found a large breadth of possible anion sizes in Titan's atmosphere with the least populated region of counts for atomic sizes of 10–100 amu/q.Ali et al. (2015) The most populous region reported was between 100 and 10,000 amu/q. Hence, the most abundant anions are the same size as nucleic acids, polycyclic aromatic hydrocarbons (PAHs), and polypeptides. This indicates that smaller anions react with molecules to form into larger anions. These anions may have lifetimes in

extraterrestrial environments long enough for them to engage in novel astrobiochemistry (Schild et al., 1974; Snow, 1975; Hanel et al., 1981; Kunde et al., 1981; Maguire et al., 1981; Samuelson et al., 1981; Yung et al., 1984; Yung, 1987; Lepp and Dalgarno, 1988; Bradforth et al., 1993; Kawaguchi et al., 1995; Aoki et al., 1996; Clifford et al., 1997; Moustefaoui et al., 1998; Tulej et al., 1998; Aoki, 2000; Millar et al., 2000; Terzieva and Herbst, 2000; Molina-Cuberos et al., 2002; McCarthy et al., 2006; Brünken et al., 2007; Cernicharo et al., 2007; Coates et al., 2007; Remijan et al., 2007; Cernicharo et al., 2008; Ross et al., 2008; Thaddeus et al., 2008; Agúndez et al., 2010; Cordiner et al., 2011; López-Puertas et al., 2013).

Additionally, theoretical studies show that nitrogen containing PAHs, or polycyclic nitrogenated hydrocarbons (PANHs), likely also exist in Titan's atmosphere (Kuiper, 1944; Allen et al., 1980; McKay, 1996; Clarke and Ferris, 1997; Ricca et al., 2001). The formation of PANHs starts with the addition of a cyano-containing group to a benzene ring. This has a small reaction barrier of 8 kcal/mol and forms aromatic nitriles. Additionally, these are known intermediates in the formation of purine, pyrimidine, and their derivatives (Ricca et al., 2001). Also, Titan's atmosphere produces enough energy to surpass the 8 kcal/mol barrier (Walsh, 1995). However, the interplay between neutral PAHs or PANHs and anions of the same molecular mass has yet to be established for Titan or really anywhere. While PAHs like naphthalene can capture free electrons to form anions, PANHs or functionalized PAHs with electronegative functional groups like −CN, −OH or $-C_2H$ can capture free electrons more efficiently (Theis et al., 2015a). Hence, sprinkling a few different atomic species within the PAH structure enhances the anionic chemistry significantly. As a result, the foundations of nucleic acid molecular structure, purine and pyrimidine, may enhance the growth of molecular anions in astrophysical environments like Titan's atmosphere. Additionally, nucleic acids are thought to be a first step for the creation of extraterrestrial life since they are one of the main constituents of DNA and RNA strands making such chemistry a fascinating venue for the production of biologically-relevent astromolecules.

The chemistry behind the formation of biologically-relevant molecular anions in Titans atmosphere is unknown. Puzzarini and coworkers suggestion follows suit with Olah's non-classical carbocationic chemistry in that the formation of large anionic macromolecules proceeds through a series of carbocationic reactions, which eventually results in an open shell neutral radical. The open shell neutral radical would then undergo a radiative electron attachment process (Olah et al., 2016; Puzzarini et al., 2017). The radiative electron attachment process can form anions through dipole-bound states along pathway. McCarthy and coworkers provide the strongest support for the dipole-bound formation pathway by the observation of the interstellar $C_{2n}H$ radicals and their corresponding anions. The ground state for C_4H is $^2\Sigma^+$, and the excited state is $^2\Pi$. However, for larger $C_{2n}H$ radicals, the ground state becomes $^2\Pi$. Typically, the $^2\Sigma^+$ states will have dipole moments of ≈0.8 D or smaller, and the $^2\Pi$ state will have dipole moments of ≈4.0 D or larger(Maier, 1998; Pino et al., 2002; Agúndez et al., 2008). To follow the dipole-bound formation pathway, the dipole moment must be ≈2.0 D or larger. Thus, C_4H must excite into the $^2\Pi$ excited state to undergo the dipole-bound formation pathway. Whereas, the larger $C_{2n}Hs$ will undergo the dipole-bound formation pathway at the $^2\Pi$ ground state. The latter process is the energetically favorable reaction. Furthermore, experimental interstellar observations show that C_4H^- is less abundant in space than their corresponding radical, and C_6H^- is more abundant than their corresponding radical implying that excitation must take place from the $^2\Sigma^+$ state of C_4H. As such, the focus of this present work is to study open-shell radicals and determine if there are any anionic excited states as these likely play a vital role in interstellar anion chemistry as it is currently understood (Yamamoto et al., 1987; Shen et al., 1990; McCarthy et al., 1995; Woon, 1995; Hoshina et al., 1998; Taylor et al., 1998; van Hemert and van Dishoeck, 2008; Fortenberry et al., 2010; Fortenberry, 2015).

Computational analysis on isomeric anionic complexes of uracil shows evidence of dipole-bound anion formation (Hendricks et al., 1998) In order to explore such behavior, Gutowski and co-workers (Gutowski et al., 1996) previously utilized both photoelectron spectroscopy (PES) and theoretical computations in examining a uracil-glycine anion complex. The PES spectra show a broad feature with a maximum intensity at 1.8 eV implying removal of an electron from an anion state at this energy. In support of this, the theoretical work concludes that the excess electron in the uracil-glycine complex is a π^* orbital localized on the uracil rings. Furthermore, later theoretical work by Adamowics and coworkers also predicts that uracil-glycine complexes have dipole moments of approximately 5 D. These items imply that uracil can form dipole-bound anions (Hendricks et al., 1996, 1998; Desfrancois et al., 1996; Jalbout et al., 2003).

Fermi and Teller, the first to study dipole-bound anions with the aid of quantum mechanics, found that the binding energy of an excess electron is dependent upon the corresponding neutral radical's dipole moment (Fermi and Teller, 1947). Specifically, the dipole moment should be greater than 1.63 D in order to keep a free electron bound to the positive end of the dipole moment. Dipole-bound anions of the type described by Fermi and Teller are dominated by the excess electron residing in a highly-diffuse, Rydberg-like *s* orbital with higher dipole moments required for higher angular momentum states in these hydrogen-like, diffuse orbitals. In more recent studies, the neutral radical dipole moment has been shown to require closer to or even exceeding 2.0 D for the diffuse *s* orbitals to be populated in dipole-bound anions (Compton et al., 1996; Gutowski et al., 1996; Jordan and Wang, 2003; Simons, 2008). This suggests that when the magnitude of the dipole moment becomes larger, the probability also increases that a dipole-bound state of an anion will exist underneath the electron binding energy (eBE), the energy required to remove the electron from the molecular system) giving a proportional relationship between the magnitude of the dipole moment and the eBE. However, dipole-bound states do not have to solely be ground electronic states. If the anion is valence in nature for its ground electronic state, dipole-bound excited states (DBXSs) may be accessed *via* electronic transitions (Mead et al., 1984; Lykke et al., 1987; Mullin

et al., 1992, 1993; Gutsev and Adamowicz, 1995; Fortenberry, 2015). Since Fermi and Teller's equations (Fermi and Teller, 1947) dictate that only one dipole-bound state can be present for each angular momentum value, DBXSs are rare, but uracil appears to demonstrate such behavior. Hence, the analysis of DBXSs for molecular precursors to nucleotides will require specialized tools.

As with the uracil anion complexes examined above (Hendricks et al., 1998, 1996), quantum chemistry provides a detailed means for determining the properties of dipole-bound anions and/or DBXSs. The diffuse, Rydberg-like *s* orbitals need an adequate quantum chemical basis set in order to be accurately described. One effective basis set is utilizing standard correlation consistent basis sets with large numbers of diffuse functions, such as the t-aug-cc-pVTZ (tapVTZ) set. However, such linear combinations of atomic orbitals to make molecular orbitals (LCAO-MO) approaches are too computationally expensive (Fortenberry and Crawford, 2011a). An alternate approach is to add even-tempered diffuse functions onto a dummy atom and keep the LCAO-MO approach for the valence orbital description (Mach et al., 2010; Fortenberry and Crawford, 2011b; Santaloci and Fortenberry, 2021). For the aug-cc-pVDZ basis set on the real atoms, this method lowers the number of basis functions by 48%, which, in return, lowers the computational cost significantly, without affecting the accuracy of the results (Fortenberry and Crawford, 2011b; Theis et al., 2015a; Morgan and Fortenberry, 2015).

Another important aspect of the basis set includes the placement and number of the employed diffuse functions. Past studies (Fortenberry and Crawford, 2011b; Theis et al., 2015b; Bassett and Fortenberry, 2017; Santaloci and Fortenberry, 2020, 2021) have placed the diffuse functions at either the center of charge (COC) or center of mass (COM). The COM is the mass weighted Cartesian origin, and the COC is at the positive pole of the corresponding neutral radical dipole moment computed, in this case, at the anion geometry. Placement of the diffuse functions at the COC lowers the energies of the excitations and is less likely to destabilize the occupied molecular orbitals (Santaloci and Fortenberry, 2020). Additionally, such a position is consistent with theory in that the binding of the excess, diffuse electron has its locus at the point with the most positive charge. As a result, the COC will be utilized for incorporating the additional diffuse functions.

The goal of this present work is to determine how functionalizing deprotonated PAHs will affect the anion photochemistry of such species. Previous work has shown that deprotonated anions will almost always exhibit valence ground states opening the possibility for DBXSs, if the corresponding neutral radical dipole moments are large enough (Fortenberry and Crawford, 2011a; Fortenberry and Crawford, 2011b; Hammonds et al., 2011; Fortenberry et al., 2014). Additionally, the presence of nitrogen heteroatoms promotes additional excited states of anions including DBXS (Theis et al., 2015b). Cyano-functionalization also promotes such behavior (Santaloci and Fortenberry, 2020, 2021), but other functional groups remain to be studied. Herein, the photochemical behavior of deprotonated PAH anions with hydroxyl and ethynyl functional groups are explored. Unlike –CN, the resulting molecular anions for both of these additions can be deprotonated on the functional group themselves likely shifting the behavior of the electronic structure.

Most notably, hydroxides can become ketones and vice versa in nucleobases under certain conditions. As this work will show, the most stable deprotonated anions for –OH and $-C_2H$ functionalized PAHs have the hydrogen atoms removed from these functional groups. In the case of the hydroxyl group, this actually forms a ketone and a delocalized π highest occupied molecule orbital (HOMO). Consequently, such a process could open the door for new photo physically-driven chemistry and faster kinetics for the formation of nucleic acids in astrophysical environments such as Titan's atmosphere (Bevilacqua, 2003; Vay et al., 2019). Additionally, ethynyl-functionalized molecules have now been observed in the interstellar medium (Cernicharo et al., 2021), and the triatomic radical is one of the most abundant molecules in space (Heikkilä et al., 1999) likely helping in the buildup of larger PAHs (Tielens, 2008). This work will provide the isomerization energies, transition energies, and oscillator strengths for singly-deprotonated anions of benzene, naphthalene, and anthracene functionalized with a hydroxyl or ethynyl group. The goal of this work is to analyze the absorption properties of these singly deprotonated anionic PAHs, which will assist in understanding the type of anions that could potentially arise in the building of larger PAHs-like molecules including nulceotides.

2 COMPUTATIONAL METHODS

In this work, benzene, naphthalene, and anthracene singly deprotonated and functionalized with either a hydroxyl or ethynyl group and analyzed quantum chemically. The functional groups are placed at multiple positions for naphthalene and anthracene. Similar to past studies (Santaloci and Fortenberry, 2020, 2021), the closed shell anion and neutral radical geometries are optimized with B3LYP/aug-cc-pVDZ within Gaussian09 and Gaussian16 (Dunning, 1989; Becke, 1993; Frisch et al., 2016). The optimized geometries provide the relative energies for each radical or anion isomer of each molecule/functional group combination. The optimized geometries of the anion are then utilized to compute a neutral radical dipole moment and the coordinates for the closed-shell anion excited state computations.

The electronically excited states are computed with both CFOUR (Stanton et al., 2008) and Molpro (Werner et al., 2015) using equation of motion coupled cluster theory at the singles and doubles level (EOM-CCSD) (Stanton et al., 1993; Krylov, 2008; Shavitt and Bartlett, 2009) with a double-zeta correlation consistent basis set (aug-cc-pVDZ) expanded with six s-type, six p-type, and two d-type additional, even-tempered diffuse basis functions called the aug-cc-pVDZ+6s6p2d, or more simply the apVDZ+6s6p2d, basis set. The augmented basis functions are placed at the COC, and the anion geometries are utilized to mimic absorption behavior because the closed-shell anion is being excited. A past study on cyano functionalized PAHs shows that the EOM-CCSD computations with the apVDZ+6s6p2d basis approach the Hartree-Fock Limit, but this level of theory still has an error range of roughly 1 meV when comparing between computed values for the DBXS energy and the eBE (Bassett and Fortenberry, 2017; Santaloci and Fortenberry, 2021). The eBE is the maximum amount of

TABLE 1 | The relative energies and neutral radical dipole moments of singly deprotonated phenol isomers.

	Isomer	Radical Rel.E (eV)	Anion Rel.E (eV)	Radical dipole (Debye)
Phenol	1	0.0000	0.0000	4.06
	2	1.1649	1.7016	1.07
	3	1.1446	2.1639	0.42
	4	1.1978	2.2843	1.42
	5	1.1459	2.2386	2.11
	6	1.2353	2.1164	2.26
Ethynylbenzene	1	0.5333	0.0000	6.87
	2	0.0435	1.1316	1.45
	3	0.0000	1.1308	0.84
	4	0.0115	1.1084	0.35

energy than can be absorbed by the anion before the electron leaves the system entirely. Specifically here, the eBEs are computed using EOM-CCSD under the ionization potential formalism (EOMIP) (Stanton and Gauss, 1994) with the aug-cc-pVDZ basis set. The electrons in the system are of a valence nature and do not need additional diffuse functions to accurately portray the existence of the resulting neutral radical. The experimental eBE for CH_2CN^- is 1.543 eV, for example, and the benchmark theoretical value computed in the same way as that described above (EOMIP-CCSD/aug-cc-pVDZ) is 1.524 eV, a difference of less than 0.02 eV (Lykke et al., 1987; Gutsev and Adamowicz, 1995; Cordiner and Sarre, 2007; Fortenberry and Crawford, 2011a; Morgan and Fortenberry, 2015).

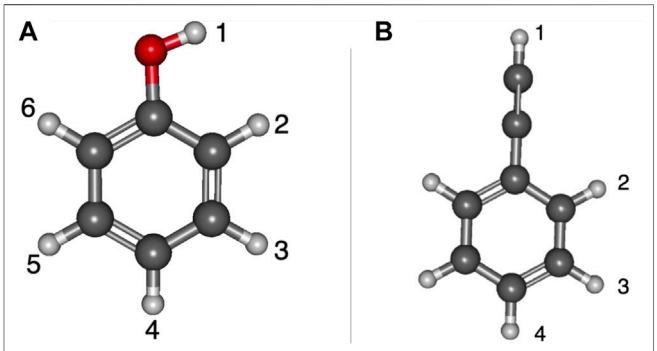

FIGURE 1 | Optimized structures of phenol and ethynylbenzene with numbered positions of deprotonation: **(A)** phenol, **(B)** ethynylbenzene.

3 RESULTS

The singly functionalized $-C_2H$ or $-OH$ PAH anions are of either C_s or C_{2v} symmetry. Correspondingly, the electronically excited state's term will either be $^1A'/^1A_1$ or $^1A''/^1B_1$. The HOMO is typically isolated to a lone pair on the carbon where the hydrogen is removed. However, the HOMO is defined by the out of plane π orbitals when deprotonation takes place either on the hydroxyl or the ethynyl group. Consistent with past work, herein the dipole-bound excitation has an electron transition from the HOMO into a large, diffuse, Rydberg *s*-type orbital, and the defined +6s6p2d, additional diffuse functions mimic the diffuseness of the Rydberg-like orbitals. The dipole moment for the neutral radical computed at the optimized geometry of the anion also must be larger than 2.0 D in order to confidently determine whether the dipole-bound state exists in this simulation absorption. Furthermore, any possible valence excitation will naturally be well below the eBE, and the neutral radical dipole moment is independent of the excitation. As a result, the valence excitation does not need a neutral radical dipole moment of greater than 2.0 D.

3.1 Benzene

3.1.1 Relative Energies and Dipole Moments

Table 1 shows the relative energies and the radical dipole moments for the deprotonated phenol and ethynylbenzene classes of molecules. Furthermore, the deprotonation sites are labeled in **Figure 1**. The deprotonation sites correspond to the first column of the tables throughout the paper. For instance, in **Table 1**, phenol radical/anion 1 is the removal of the hydrogen on the oxygen atom.

For phenol, radical/anion 1 is the most stable isomer of each respective group and has the largest radical dipole moment of 4.06 D. Furthermore, radical/anion 1 is lower in energy than the rest by more than 1 eV, which is a result of the hydroxyl group becoming a ketone functional group stabilizes the system. Radical 6 and anion 4 are the least stable of their sets, but most of the relative energies are self-similar because the electron donating nature of the hydroxyl group does not greatly affect the stability of the electrons in the HOMO. Radical 6 is 1.2353 eV higher in energy than radical 1, and anion 4 is 2.2843 eV less stable than anion 1. Additionally, anion 2 is the second most stable. This is likely due to the hydrogen on the oxygen constructively interfering with the adjacent lone pair stabilizing the anionic charge. This trend is not as clear for the radical section, but the difference between the least stable (radical 6) to radical 2 is only 0.07 eV. Besides radical 1, only radicals 5 and 6 have dipole moments large enough to have a dipole-bound excitation in their corresponding anions. At the opposite end of the spectrum, the radical 2 dipole moment is only 1.07 D.

3.1.2 Vertical Excitation Energies

Conversely for the other functional group and due to the electron withdrawing nature of ethynyl, the singly-occupied HOMO is

TABLE 2 | The singly deprotonated anion derivatives eBEs and excited state transition energies.

	Isomer	2 $^1A_1$/2 $^1A'$	1 $^1B_2$/3 $^1A'$	1 $^1B_1$/1 $^1A\ni$	1 $^1A_2$/2 $^1A\ni$	eBE (eV)
Phenol	1	2.0987	2.1280	2.0832	2.0918	2.0890
	2	2.0152	2.0190	2.0228	2.0545	2.0059
	3	1.6059	1.6099	1.6135	1.6453	1.5976
	4	1.4621	1.4655	1.4696	1.5014	1.4585
	5	1.5103	1.5134	1.5179	1.5494	1.5066
	6	1.6517	1.6547	1.6593	1.6907	1.6469
Ethynylbenzene	1	3.2130	3.2375	3.1560	3.2059	3.2055
	2	1.8194	1.8228	1.8271	1.8590	1.8181
	3	1.7454	1.7493	1.7530	1.7851	1.7389
	4	1.9110	1.9152	1.9186	1.9507	1.9105

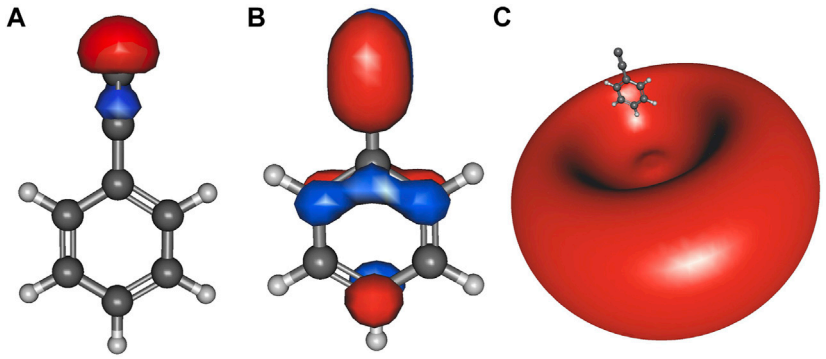

FIGURE 2 | Ethynylbenzene anion 1 a_1 HOMO-2 **(A)**; b_1 HOMO **(B)**, and the a_1 LUMO **(C)** dipole-bound orbital.

destabilized to a much greater extent in the radical form when the hydrogen removal site on the ethynyl group. Radical 3, where the singly-occupied orbital is in the *meta* position, is the most stable, but there is littler isomeric energy difference between it and radicals 2 and 4. This is similar to the previous benzonitrile anion study where the least stable radical has the largest dipole moment at 5.18 D and is also the most stable anion for the benzonitrile isomer group (Santaloci and Fortenberry, 2020, 2021). Hence, functionalization with $-C_2H$ and $-CN$ show similarities.

Table 2 lists the electronically excited state transition energies and eBEs of the phenol and ethynylbenzene anion isomers. **Figure 2** shows the orbitals involved in electronic excitations for ethynylbenzene anion 1 as an example. The HOMO, in this case, is the out-of-plane π orbital (**Figure 2B**). In the other isomers, when the deprotonation is on the ring and the symmetry of the anion becomes C_s, the HOMO looks more like **Figure 2A**. Most of the anions throughout the paper are C_s. When this C_{2v} to C_s shift occurs, the deprotonation moves to the ring, and the in-plane lone pair is the least stable orbital.

When the deprotonation occurs on the hydroxyl or ethynyl group, a valid dipole-bound excitation occurs, but such is not present for any of the other isomers where the deprotonation occurs on the ring even though phenol radicals 5 and 6 showed dipole moments of greater than 2.0 D. Regardless, the phenol anion 1 dipole-bound transition is 5.8 meV and ethynylbenzene anion 1 is 49 meV underneath their respective eBEs. Furthermore, the bound phenol absorption wavelength is

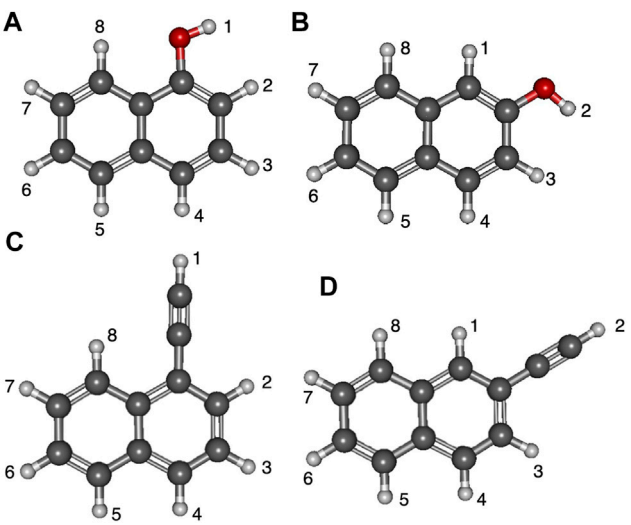

FIGURE 3 | Optimized structures of the four naphthalene derivatives with numbered positions of deprotonation: **(A)** 1-hydroxynaph, **(B)** 2-hydroxynaph, **(C)** 1-ethynylnaph, **(D)** 2-ethynylnaph.

595 nm, and the ethynylbenzene absorption wavelength is 392 nm. The phenol DBXS transition is capable of capturing much lower energy photons, whereas the ethynylbenzene absorption is approaching the violet region but barely within

TABLE 3 | The relative energies and neutral radical dipole moments of hydroxynaphthalene derivatives.

	Isomer	Radical rel. E.	Anion rel. E.	Radical dipole (D)
1-hydroxynaph	1	0.0000	0.0000	4.10
	2	1.4589	1.8347	0.72
	3	1.4868	2.3976	2.32
	4	1.5388	2.3879	1.54
	5	1.4959	2.2711	1.35
	6	1.4958	2.2830	0.41
	7	1.5017	2.2334	0.94
	8	1.3832	1.5842	2.08
	2R	1.5784	2.2930	2.47
	8R	1.4678	2.5143	1.56
2-hydroxynaph	1	1.3790	2.1488	2.30
	2	0.0000	0.0000	5.02
	3	1.3421	2.0937	1.16
	4	1.2878	2.1088	0.63
	5	1.2785	2.2776	0.80
	6	1.2905	2.3792	1.76
	7	1.2735	2.3643	2.36
	8	1.2884	2.3368	2.34
	1R	1.2924	1.7415	0.95
	3R	1.2866	1.6770	2.02

TABLE 4 | The relative energies and neutral radical dipole moments of ethynylnaphthalene derivatives.

	Isomer	Radical rel. E.	Anion rel. E.	Radical dipole (D)
1-ethynylnaph	1	0.3792	0.0000	7.53
	2	0.0388	1.1084	1.52
	3	0.0066	1.1082	1.13
	4	0.0144	1.0362	0.44
	5	0.0087	1.1324	0.27
	6	0.0036	1.2258	0.78
	7	0.0000	1.2573	1.29
	8	0.0204	1.2999	1.48
2-ethynylnaph	1	0.0465	0.9958	1.53
	2	0.4591	0.0000	8.36
	3	0.0461	1.1008	1.78
	4	0.0043	1.0366	1.03
	5	0.0057	1.0746	0.90
	6	0.0000	1.1222	0.26
	7	0.0008	1.1416	0.78
	8	0.0082	1.0692	1.41

the UV region. Lastly, both phenol and ethynyl derivatives do not exhibit any valence excited states.

3.2 Naphthalene

3.2.1 Relative Energies and Dipole Moments

Figure 3 displays the deprotonation positions of naphthalene isomers functionalized with the hydroxyl groups. The ethynyl group naphthalene isomer numbering is much the same. The two isomers of naphthalene have the functional groups placed either at position 1 or 2. Position 1 has functional groups placed on the inner portion of the ring, and position 2 is when functionalization takes place on the outer part of the naphthalene like with quinoline and isoquinoline. Additionally, the deprotonation sites are labeled to correspond with the subsequent tables.

Tables 3, **4** portray the relative energies of the radicals and anions for the 1-naphthalene isomers. 1-hydroxynaphthalene has 10 and 1-ethynylnaphthalene has 8 radical/anion isomers. The hydroxynaphthalene class has an additional two isomers because the hydrogen on the oxygen points towards either side of the naphthalene. When the hydrogen is rotated to the opposite side an "R" is added to the label. For example, 1-hydroxynaphthalene 2 has the hydrogen facing toward the deprotonated carbon and 2R has the hydrogen rotated away. All other arrangements of "R" produce insignificant changes in the electronic structure and will not be explored.

The relative energies of both ethynyl- and hydroxy-functionalization follow the same trend as the benzene section. For the hydroxynaphthalene, the radical/anion energies are the most stable when the ketone group forms. The hydroxynaphthalene isomers have a total of 9 radicals with a dipole moment above 2.0 D. Specifically, 1-hydroxynaphthalene neutral radicals 1, 2R, 3, and 8 along with 2-hydroxynaphthalene radicals 1, 2, 7, 8, and 3R have dipole moments greater than 2.0 D. 2-hydroxynaphthalene radical 2 has the largest dipole moment at 5.0 D, but the next highest is the 1-hydroxynaphthalene radical 1 at 4.1 D. Additionally, the dipole moments of 1-hydroxynaphthalene 2R and 2-hydroxynaphthalene 3R are significantly larger than their unrotated counterparts. The 1-hydroxynaphthalene radical 2 and 2-hydroxynaphthalene radical 3 both possess dipole moments below 1.2 D. This is a result of the hydrogen on the oxygen, which distorts the dipole moment and stabilizes the partial negative charge.

Likewise, the ethynylnaphthalene anion isomers are the most stable when the hydrogen is deprotonated from the ethynyl group. The ethynylnaphthalene radicals act differently than the hydroxynaphthalene isomers. The least stable ethynyl radicals are the most stable ethynylnaphthalene anions, again like with the −CN functionalization (Santaloci and Fortenberry, 2021), implying a trend for when the functional group is a strong electron withdrawing group. Furthermore, 1-ethynylnaphthalene radical 7 and 2-ethynylnaphthalene radical 6 are the most stable. Both of these have the lone pair on the opposite side of the ring from the functional group. Interestingly, the other radicals that surround the ethynyl group demonstrate relative energies within at most 0.046 eV of each other. This relatively small difference results in only two ethynylnaphthalene neutral radicals dipole moments being larger than 2.0 D. Both of these radicals are the most stable anions and have the highest corresponding neutral radical dipole moments seen so far: 7.5 D for 1-ethynylnaphthalene anion 1 and 8.4 D for 2-ethynylnaphthalene anion 2. This indicates only two anions in the ethynylnaphthalene class can bind a free electron to form a dipole-bound state.

When comparing the 1-naphthalene and 2-naphthalene classes, the most stable anions are found in the 2-naphthalene regardless of the functional group at position 2. Specifically, the 2-hydroxynaphthalene anion 2 is 0.16 eV lower in energy than the

TABLE 5 | The singly deprotonated hydroxynaphthalene anion derivatives eBEs and transition energies.

	Isomer	Excited states		eBE
		$2\,^1A'$	$1\,^1A''$	
1-hydroxynaph	1	2.1491	2.1327	2.1396
	2	1.9095	1.9172	1.8978
	3	1.7997	1.8069	1.7979
	4	1.8145	1.8221	1.8128
	5	1.9213	1.9286	1.9214
	6	1.9010	1.9075	1.9003
	7	1.9758	1.9823	1.9748
	8	2.6704	2.6821	2.6711
	2R	2.2549	2.2627	2.2554
	8R	1.6067	1.6143	1.6047
2-hydroxynaph	1	2.2954	2.3005	2.2933
	2	2.2619	2.2423	2.2532
	3	1.9967	2.0040	1.9942
	4	2.0161	2.0222	2.0089
	5	1.8239	1.8302	1.8223
	6	1.7156	1.7221	1.7133
	7	1.7404	1.7481	1.7381
	8	1.7525	1.7603	1.7509
	1R	1.9687	1.9765	1.9668
	3R	2.3925	2.3990	2.3858

TABLE 6 | The singly deprotonated ethynylnaphthalene anion derivatives eBEs and transition energies.

	Isomer	Excited states		eBE
		$2\,^1A'$	$1\,^1A''$	
1-ethynylnaph	1	3.2355	3.1859	3.2272
	2	2.0685	2.0751	2.0672
	3	1.9959	2.0019	1.9939
	4	2.1207	2.1283	2.1208
	5	1.9838	1.9899	1.9828
	6	1.8933	1.8990	1.8915
	7	1.8582	1.8646	1.8569
	8	1.7956	1.8033	1.7958
2-ethynylnaph	1	2.1537	2.1613	2.1532
	2	3.2771	3.2149	3.2702
	3	2.0386	2.0459	2.0379
	4	2.0134	2.0207	2.0127
	5	2.0039	2.0119	2.0044
	6	1.9849	1.9913	1.9838
	7	1.9483	1.9549	1.9474
	8	2.0326	2.0410	2.0333

1-hydroxynaphthalene anion 1, and the 2-ethynylnaphthalene anion 2 is 0.01 eV is lower in energy than 1-ethynylnaphthalene anion 1. This is, again, consistent with the previous work on cyanonaphthalenes (Santaloci and Fortenberry, 2021). The reason for such behavior is that the molecule is slightly enlongated in the 2 position which increases the total spatial extent for the orbitals. From a particle-in-a-box (PIB) argument, as the box becomes longer the wave function stabilizes the lower energy.

3.2.2 Vertical Excitation Energies

Table 5 shows that all of the possible valence excited state transition energies are above the eBEs for each isomer. The hydroxynaphthalene DBXS transition energies for 1-hydroxynaphthalene anion 1 and 2-hydroxynaphthalene anion 2 are clearly underneath the eBE. Specifically, 1-hydroxynaphthalene anion 1 is 6.9 meV and 2-hydroxynaphthalene anions 2 is 10.9 meV, respectively, below their eBEs. Other DBXS candidates, like 1-hydroxynaphthalene anions 8 and 2R, may exist since their excitation energies are within 1 meV of the eBE. Both of these anions are next to the oxygen when the hydrogen is facing away from it. The destabilization of the oxygen lone pair to their radical lone pair results in the dipole moment being above 2.0 D, but the excitation energies fall within the error range and can not be confidently concluded as a DBXS through the present quantum chemical analysis.

Table 6 shows the electronically excited state energies for the deprotonated ethynylnaphthalene anion isomers. Similar to ethynylbenzene, the only conclusive DBXS transition originates from the lone pair on the ethynyl group. However, there are a couple of transition energies that are below the eBE. These are 1-ethynylnaphthalene anion 4 and 8 as well as 2-ethynylnaphthalene anion 5 and 8. Since, the radicals' dipole moments are not large enough to stabilize the electron in a diffuse orbital, the dipole-bound state likely cannot be present. Analysis of the MOs does not support these being valence excited states. Future work will analyze the behavior of these possibly bound electronically excited states. Furthermore, the DBXS transition energies for 1-ethynylnaphthalene anion 1 and 2-ethynylnaphthalene anion 2 are largely underneath the eBE. Specifically, 1-ethynylnaphthalene anion 1 is 41.3 meV and 2-ethynylnaphthalene anion 2 is 55.3 meV below the eBE. This is a result of the large radical dipole moments. **Figure 4** shows the orbitals involved in the DBXS excitation of 2-ethynylnaphthalene anion 2, and the hydroxynaphthalene orbitals, not shown, appear similar. The left side of **Figure 4** is the HOMO, and the right is the diffuse *s*-type Rydberg LUMO. Similar to the benzene class of anions discussed previously, the hydroxynaphthalene excitations are between the 550–581 nm range, and the ethynylnaphthalene excitations are clearly lower between 386 and 390 nm. Again, the ethynylnaphthalene can capture UV light and hydroxynaphthalene is in the greenish-yellow region.

3.3 Anthracene

3.3.1 Relative Energies and Dipole Moments

Supplementary Figures S1, S2 represent the three derivatives of deprotonated ethynyl- and hydroxyanthracene. There are ten isomers for 1-hydroxyanthracene and six isomers for 1-ethynylanthracene. Similar to past studies, only six of the 1-ethynylanthracene isomers are unique due to the symmetry. For both hydroxyl- and ethynylanthracene, the other two derivatives have ten isomers and are Cs symmetry.

Tables 7, **8** show the relative and excitation energies for all the hydroxyanthracene derivatives. In line with phenol and hydroxynaphthalene, the most stable radical and anion isomers exist when the hydrogen is deprotonated off of the oxygen. For all three hydroxyanthracene derivative sets, the second most stable radical and anion occur when deprotonation takes place on the adjacent carbon where the hydrogen on the oxygen is facing the

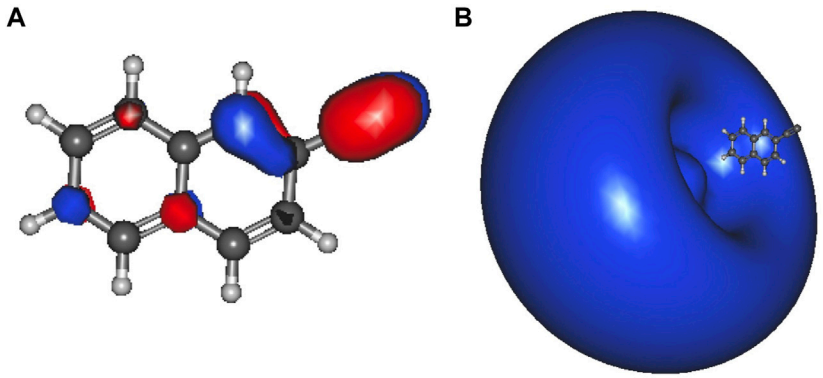

FIGURE 4 | 2-ethynylnaphthalene anion 2 a′ HOMO **(A)**;and the a′ LUMO **(B)** dipole-bound orbital.

TABLE 7 | The relative energies and neutral radical dipole moments of hydroxyanthracene derivatives.

	Isomer	Radical rel. E.	Anion rel. E.	Radical dipole (D)
1-hydroxyanthra	1	0.0000	0.0000	3.80
	2	1.7833	1.7872	5.18
	3	1.9144	2.4849	0.59
	4	1.9083	2.5435	0.33
	5	1.9060	2.5234	1.20
	6	1.9517	2.5070	1.29
	7	1.9078	2.6266	1.52
	8	1.8954	2.6850	2.27
	9	1.9050	2.7337	2.31
	10	1.9274	2.8033	1.69
2-hydroxyanthra	1	2.7200	2.3886	1.30
	2	0.0000	0.0000	4.42
	3	1.6079	1.8987	0.56
	4	1.5783	2.3630	0.42
	5	1.6275	2.4195	1.21
	6	1.5946	2.2590	1.34
	7	1.5820	2.3904	1.60
	8	1.5766	2.4422	2.24
	9	1.5809	2.4546	2.20
	10	1.5845	2.4143	1.46
3-hydroxyanthra	1	1.4595	2.2749	2.30
	2	1.5400	2.2199	2.33
	3	0.0000	0.0000	6.16
	4	1.4405	1.6997	1.23
	5	1.4468	2.1316	0.77
	6	1.4418	2.1708	0.94
	7	1.4362	2.3592	1.04
	8	1.4387	2.4393	2.04
	9	1.4302	2.4314	2.58
	10	1.4406	2.3930	2.45

TABLE 8 | The singly deprotonated hydroxyanthracene anion derivatives eBEs and transition energies.

	Isomer	Excited states		eBE
		$2\ ^1A'$	$1^1A''$	
1-hydroxyanthra	1	2.0800	2.0637	2.0743
	2	2.7775	3.0307	2.7688
	3	2.1413	2.1500	2.1420
	4	2.0630	2.0721	2.0642
	5	2.0918	2.1015	2.0932
	6	2.1515	2.1602	2.1494
	7	1.9705	2.0972	1.9699
	8	1.9325	1.9381	1.9299
	9	1.8633	1.8691	1.8610
	10	1.7755	1.7822	1.7738
2-hydroxyanthra	1	2.0051	2.0106	2.0032
	2	2.2014	2.1827	2.1925
	3	2.4241	2.4333	2.4236
	4	2.0190	2.0275	2.0195
	5	1.9475	1.9572	1.9482
	6	2.1330	2.1385	2.1305
	7	1.9696	1.9761	1.9667
	8	1.9325	1.9371	1.9285
	9	1.9087	1.9143	1.9050
	10	1.9506	1.9571	1.9481
3-hydroxyanthra	1	2.1076	2.1136	2.1052
	2	2.1479	2.1555	2.1440
	3	2.3225	2.3064	2.3134
	4	2.6255	2.6328	2.6248
	5	2.2480	2.2568	2.2489
	6	2.2311	2.2371	2.2255
	7	1.9953	2.0016	1.9932
	8	1.9106	1.9164	1.9068
	9	1.9323	1.9381	1.9268
	10	1.9541	1.9608	1.9440

resulting lone pair. The least stable radicals and anions differ for each hydroxyanthracene. However, there is no significant difference in energy between the least stable and third most stable radicals and anions for all three hydroxyanthracenes, which range from 0.01 to 0.06 eV from one another. An example is 1-hydroxyanthracene radical 6, which is the least stable compared to radical 8, which is the third most stable. These two radicals differ in relative energy by 0.06 eV.

Comparable to the hydroxynaphthalene derivatives, the most stable anion and radical isomer for the larger ring class is 1-hydroxyanthracene, and the least stable is 3-hydroxyanthracene. The radical dipole moment once more seemingly increases with radical isomeric instability; the largest radical dipole moments are

TABLE 9 | The relative energies and neutral radical dipole moments of singly deprotonated ethynylanthracene derivatives.

	Isomer	Radical rel. E.	Anion rel. E.	Radical dipole (D)
1-ethynylanthra	1	0.1330	0.0000	8.14
	2	0.0185	1.3694	1.39
	3	0.0000	1.3079	1.44
	4	0.0088	1.2781	1.07
	5	0.0124	1.1745	0.25
	6	0.0219	0.9552	0.20
2-ethynylanthra	1	0.0295	0.0414	1.38
	2	0.2801	0.0000	8.36
	3	0.0382	0.0396	1.67
	4	0.0089	0.0398	1.36
	5	0.0122	0.0366	0.59
	6	0.0216	0.0351	0.40
	7	0.0065	0.0422	0.27
	8	0.0011	0.0450	0.75
	9	0.0000	0.0452	1.26
	10	0.0099	0.0441	1.46
3-ethynylanthra	1	0.0145	0.8912	1.47
	2	0.0465	0.9726	1.65
	3	0.3726	0.0000	10.23
	4	0.0514	1.0966	2.04
	5	0.0082	1.0274	1.23
	6	0.0164	0.9238	1.07
	7	0.0089	1.0901	0.96
	8	0.0002	1.1465	0.20
	9	0.0000	1.1589	0.74
	10	0.0093	1.0761	1.41

TABLE 10 | The singly deprotonated ethynylanthracene anion derivatives eBEs and transition energies.

	Isomer	Excited states		eBE
		$2\ ^1A'$	$1\ ^1A''$	
1-ethynylanthra	1	3.1139	3.0259	3.1068
	2	1.9338	1.9490	1.9409
	3	2.0514	2.0580	2.0509
	4	2.0699	2.0763	2.0690
	5	2.1793	3.0657	2.1870
	6	2.4741	2.1783	2.4746
2-ethynylanthra	1	2.1496	2.0018	2.1444
	2	2.9398	3.1602	3.2316
	3	2.2465	1.9564	2.2424
	4	2.1671	1.7677	2.1639
	5	2.3072	2.0633	2.3045
	6	2.3516	2.1547	2.3424
	7	2.1027	1.9203	2.1004
	8	2.0268	2.0338	2.0246
	9	2.0235	2.0309	2.0213
	10	2.0393	2.0471	2.0374
3-ethynylanthra	1	2.4086	2.2191	2.4053
	2	2.3402	2.1646	2.3351
	3	2.9294	3.2251	3.2920
	4	2.1984	2.2046	2.1942
	5	2.1788	2.1851	2.1755
	6	2.3401	2.1791	2.3371
	7	2.1430	2.1526	2.1431
	8	2.1106	2.1203	2.1113
	9	2.0866	2.0961	2.0871
	10	2.1666	2.1779	2.1684

in the 3-hydroxyanthracene. Specifically, the 3-hydroxyanthracene radical 3 dipole moment is 6.2 D, 2-hydroxyanthracene radical 2 is 4.4 D, and 1-hydroxyanthracene radical 1 is 3.8 D. There are other notable radicals with dipole moments larger than 2.0 D. For 1-hydroxyanthracene, radicals 8 and 9 are 2.2 and 2.1 D. 2-hydroxyanthracene radicals 8, and 9 are 2.2, and 2.0 D. 3-hydroxyanthracene radicals 1, 2, 8, 9 and 10 are 2.3, 2.3, 2.0, 2.6 and 2.5 D. A past study on cyanoanthracene reveals that the dipole moments of the radicals become larger when the ring length becomes larger (Santaloci and Fortenberry, 2020).

Tables 9, **10** display the relative and excitations energies for the ethynylanthracene derivatives. The relative energies follow the same type of trend reported in the previous cyanoanthracene study (Santaloci and Fortenberry, 2021) The least stable anion is the most stable radical and vice versa. Unlike hydroxyanthracene, the radical and anion do not have a significant energy difference between their isomers. This is a result of no hydrogen bonding effect and no formation of a different functional group. The largest energy difference for the radicals is 2-ethynylanthracene radical 4 with relative energy of 0.0396 eV compared to the most stable isomer, radical 9. For the anions, their largest relative energy is from 1-ethynylanthracene anion 2 at 1.4 eV compared to anion 1.

The largest radical dipole for the ethynylanthracene derivatives is, once more, for the isomer resulting from deprotonation on the ethynyl group. Specifically, the 1-ethynylanthracene radical 1 has a dipole moment of 8.1 D; 2-ethynylanthracene radical 2 has a dipole moment of 8.4 D; 3-ethynylanthracene radical 3 has a dipole moment of 10.2 D. 3-ethynylanthracene is the only ethynylanthracene isomer that has more than one radical with a dipole moment larger than 2.0 D. Namely, radical 4 has a dipole moment of 2.0 D. For the ethynylanthracene class, only 4 radicals have dipole moments greater than 2.0 D.

3.3.2 Vertical Excitation Energies

Tables 8, **10** display the electronically excited states of the deprotonated hydroxyl and ethynylanthracene anions. Comparable to ethynylbenzene, the carbon on the 1-ethynylanthracene functional group and adjacent to the ethynyl group is C_{2v} symmetry with the $2\ ^1A_1$ state being likely a DBXS, and the $1\ ^1B_1$ state would be valence. Additionally, similar to phenol, the 1-hydroxyanthracene is C_{2v} symmetry when the deprotonation site is on the oxygen. Furthermore, the excitation into the $2\ ^1A_1$ state is potentially a DBXS, and $1\ ^1B_1$ would be valence. Lastly, similar to the naphthalenes, all of the remaining derivatives will be C_s symmetry, which indicates the dipole-bound states will be $2\ ^1A'$, and any possible valence states will be $1\ ^1A''$.

In the hydroxy-functionalized isomers, the dipole-bound excitation only exists when the ketone group forms upon deprotonation from the oxygen atom. For 1-hydroxyanthracene, excitations from anions 1, 4, and 5 are outside the 1 meV error range of the eBE. However, the only neutral radical dipole moment greater than 2.0 D is anion 1. 2-hydroxyanthracene has a dipole-bound excitation for anion 2. Similar to 1-hydroxyanthracene, 2-hydroxyanthracene anions 4 and 5 do not have large enough dipole moments but have excitations that are only 0.5 and 0.7 meV

underneath the eBE. Congruent to other hydroxyanthracenes, 3-hydroxyanthracene anion 5 has an excitation 0.9 meV below the eBE. These excitations may be more exotic types of excitation that go beyond the present study. Lastly, none of the hydroxyanthracene derivatives have any valence excitation characteristics.

When ethynyl functionalization on anthracene occurs, more types of excitations appear. For the ethynylanthracene class, there are both valence and dipole bound excitations. All three ethynylanthracene exhibit both dipole-bound and valence excitations. **Figure 4** shows the HOMO to valence LUMO and dipole-bound LUMO orbitals for 3-ethynylanthracene anion 3. The dipole-bound orbital is closely related for all of the valid hydroxyanthracene and ethynylanthracene dipole-bound excitations. Interestingly, there are only four neutral radical dipole moments large enough to stabilize a free electron. Three of those four isomers are deprotonated on the ethynyl group. Specifically, anion 1 of 1-ethynylanthracene is 81 meV, anion 2 of 2-ethynylanthracene is 29 meV, and anion 3 of 3-ethynylanthracene is 66 meV underneath the eBE. 3-ethynylanthracene anion 4 is the remaining isomer with a large corresponding neutral radical dipole moment, but it does not exhibit an excited state below the eBE. Also, 1-ethynylanthracene anion 6, 2-ethynylanthracene anion 1-7, and 3-ethynylanthracene anion 1, 2, 3, and 6 have valence excitations. 1-ethynylanthracene anion 2 and 5, 3-ethynylanthracene anion 8, 9, and 10 do not have corresponding neutral radicals that possess large enough dipole moments. However, these isomers have excitation energies underneath the eBE, which again alludes to a more complex type of quantum electronics.

Lastly, similar to the past classes, the hydroxyanthracene excitations are higher in energy than the ethynylanthracene. For hydroxyanthracene, the dipole bound transitions are 537–600 nm, and ethynylanthracene dipole-bound transitions are between the range of 384–409 nm. Also, ethynylanthracene has the first instance of valence excitations examined in this work, and the absorption range is 558–700 nm, which is in the same region as the hydroxyanthracene dipole-bound transitions.

4 OSCILLATOR STRENGTHS

The oscillator strengths are given in the **Supplementary Material**. Similar to past PAH and PANH studies, the oscillator strengths are on the order of 1×10^{-4} if the dipole-bound state exists (Theis et al., 2015a,b; Fortenberry et al., 2016; Santaloci and Fortenberry, 2021). Furthermore, the oscillator strengths become larger the farther away the HOMO electron density is away from the COC. Additionally, when the oscillator strength for the dipole-bound states computed here are not large but large enough to contribute to absorption spectra when found over large enough path lengths as likely takes place under interstellar conditions. Additionally, when the excited state transition energy is above the eBE, the resulting oscillator strengths tendency to be below $1 \times 10^{-}6$, which shows that those states above the eBE would not contribute to any spectra even if they could somehow be stabilized.

5 CONCLUSION

When closed shell PAH anion single deprotonation occurs on the functional group, a DBXS will exist. However, when the deprotonation site is on the ring, the type of excited state for excitation becomes obscure. To be clear, if the excitation energy is greater than 1 meV underneath the eBE and the neutral radical dipole moment is larger than 2.0 D, then such a state is most likely a DBXS. On the other hand, if the excitation energy is within 1 meV underneath the eBE and the neutral radical dipole moment is less than 2.0 D, the state likely cannot be classified as dipole-bound. This implies a possibility of a different type of anion excitation. An example is 3-ethynylanthracene anions 6–10, which have neutral radical dipole moments of less than 2.0 D, but the DBXS excitation energies are within 1 meV underneath the eBE. When the dipole moment is less than 2.0 D, some other property of the PAH must keep the electron bound to result in the excitation being underneath the eBE.

Differently, the number of valence excitations depends on whether the functional group is electron donating or electron withdrawing. The electron donating hydroxyl group stabilizes the ring structures, which produces a larger gap between the HOMO and LUMO. As a result, the hydroxyl functionalized PAHs examined herein do not have any valence excited state anions. Typically, the stronger the electron donating group the better the ring stabilization. Electron withdrawing functionalization appears to produce the opposite effect. Past studies on singly deprotonated cyano functionalized PAHs show that valence excitations begin to appear when the number of rings is two (Santaloci and Fortenberry, 2021). When the ring number is three, then every deprotonated structure has a valence excited state. Interestingly, when the electron withdrawing group is a weaker ethynyl group (compared to −CN), valence excitations only begin to appear once three rings are present. Specifically, only 11 out of 30 ethynylanthracene anions possess valence excitations. The ethynyl group destabilizes the HOMO less than the cyano group but is still a destabilizing group. The valence excited state oscillator strengths are approximately $<1 \times 10^{-4}$, which is large enough to contribute to absorption spectra, but only when there is a sufficient population of molecules.

The energy of the photon that an anion absorbs to form a possible DBXS is higher in energy than the valence states. When the functional group is an electron donating group, like hydroxyl, the excitation energies become higher when the number of rings increases. Notably, for the electron withdrawing ethynyl group, the excitation energies lower when the ring number increases, but the excited states are well below the eBE. This suggests the hydroxyl groups are able to stabilize the HOMOs of larger PAH anions better than the ethynyl group. This supports the idea that deprotonation of hydroxyl groups may be an intermediate in the formation of nucleobases in gas-phase, astrophysical environments. However, broadly speaking, deprotonated PAH anions functionalized with electron donating groups will be less likely to have electronicallly excited anions than those with electron withdrawing groups.

Hence, from a stability perspective, the hydroxyl, electron donating group produces a more stable structure, especially for deprotonation on the functional group itself (thus creating the ketone like those found in nucleotides), which will better allow these anions to persist in collision-dominated environments. In regions with a higher photon flux, however, the less stable PAHs functionalized with electron withdrawing groups will be able to absorb the incident photons much more effeciently likely producing longer lifetimes for this opposite class of molecules. As a result, if anions are involved in the formation of nucleic acids, both of these seemingly counteracting processes may be taking place at different times in their evolution in order to assist in nucleic acid formation.

DATA AVAILABILITY STATEMENT

The original contributions presented in the study are included in the article/**Supplementary Material**, further inquiries can be directed to the corresponding author.

AUTHOR CONTRIBUTIONS

TS performed the computational work. RF concieved of the idea, managed the project, and secured the funding. All three authors were involved in analyzing the results as well as writing and editing the manuscript.

FUNDING

This work is supported by NASA grant NNX17AH15G, NSF grant OIA-1757220, NSF REU grant CHE-1757888, the College of Liberal Arts at the University of Mississippi, and a graduate resesearch fellowship from the Mississippi Space Grant Consortium.

ACKNOWLEDGMENTS

The depictions of the molecules are provided by Gabedit.

SUPPLEMENTARY MATERIAL

The Supplementary Material for this article can be found online at: https://www.frontiersin.org/articles/10.3389/fspas.2021.777107/full#supplementary-material

REFERENCES

Agúndez, M., Cernicharo, J., Guélin, M., Gerin, M., McCarthy, M. C., and Thaddeus, P. (2008). Search for Anions in Molecular Sources: C4H-Detection in L1527. *A&A* 478, L19–L22. doi:10.1051/0004-6361:20078985

Agúndez, M., Cernicharo, J., Guélin, M., Kahane, C., Roueff, E., Kłos, J., et al. (2010). Astronomical Identification of CN-, the Smallest Observed Molecular Anion. *A&A* 517, L2. doi:10.1051/0004-6361/201015186

Ali, A. E. C. S., Jr., Sittler, E. C., Chornay, D., Rowe, B. R., and Puzzarini, C. (2015). Organic Chemistry in Titan's Upper Atmosphere and its Astrobiological Consequences: I. Views towards Cassini Plasma Spectrometer (CAPS) and Ion Neutral Mass Spectrometer (INMS) Experiments in Space. *Planet. Space Sci.* 109-110, 46–63. doi:10.1016/j.pss.2015.01.015

Allen, M., Yung, Y. L., and Pinto, J. P. (1980). Titan - Aerosol Photochemistry and Variations Related to the sunspot Cycle. *ApJ* 242, L125–L128. doi:10.1086/183416

Aoki, K. (2000). Candidates for U-Lines at 1377 and 1394 MHz in IRC+10216: Ab Initio Molecular Orbital Study. *Chem. Phys. Lett.* 323, 55–58. doi:10.1016/s0009-2614(00)00469-3

Aoki, K., Ikuta, S., and Murakami, A. (1996). Equilibrium Geometries and Stabilities of the C3H Radical: Ab Initio MO Study. *J. Mol. Struct. THEOCHEM* 365, 103–110. doi:10.1016/0166-1280(96)04513-7

Bassett, M. K., and Fortenberry, R. C. (2017). Symmetry Breaking and Spectral Considerations of the Surprisingly Floppyc-C3h Radical and the Related Dipole-Bound Excited State Ofc-C3h−. *J. Chem. Phys.* 146, 224303. doi:10.1063/1.4985095

Becke, A. D. (1993). Density-functional Thermochemistry. III. The Role of Exact Exchange. *J. Chem. Phys.* 98, 5648–5652. doi:10.1063/1.464913

Bevilacqua, P. C. (2003). Mechanistic Considerations for General Acid−Base Catalysis by RNA: Revisiting the Mechanism of the Hairpin Ribozyme. *Biochemistry* 42, 2259–2265. doi:10.1021/bi027273m

Bradforth, S. E., Kim, E. H., Arnold, D. W., and Neumark, D. M. (1993). Photoelectron Spectroscopy of CN−, NCO−, and NCS−. *J. Chem. Phys.* 98, 800–810. doi:10.1063/1.464244

Brünken, S., Gupta, H., Gottlieb, C. A., McCarthy, M. C., and Thaddeus, P. (2007). Detection of the Carbon Chain Negative Ion C 8 H - in TMC-1. *ApJ* 664, L43–L46. doi:10.1086/520703

Cernicharo, J., Agúndez, M., Cabezas, C., Tercero, B., Marcelino, N., Pardo, J. R., et al. (2021). Pure Hydrocarbon Cycles in Tmc-1: Discovery of Ethynyl Cyclopropenylidene, Cyclopentadiene, and Indene. *A&A* 649, L15. doi:10.1051/0004-6361/202141156

Cernicharo, J., Guélin, M., Agúndez, M., Kawaguchi, K., McCarthy, M., and Thaddeus, P. (2007). Astronomical Detection of C$\mathsf{_{4}H^-}$, the Second Interstellar Anion. *A&A* 467, L37–L40. doi:10.1051/0004-6361:20077415

Cernicharo, J., Guélin, M., Agúndez, M., McCarthy, M. C., and Thaddeus, P. (2008). Detection of C 5 N - and Vibrationally Excited C 6 H in IRC +10216. *ApJ* 688, L83–L86. doi:10.1086/595583

Clarke, D. W., and Ferris, J. P. (1997). Titan Haze: Structure and Properties of Cyanoacetylene and Cyanoacetylene-Acetylene Photopolymers. *Icarus* 127, 158–172. doi:10.1006/icar.1996.5667

Clifford, E. P., Wenthold, P. G., Lineberger, W. C., Petersson, G. A., and Ellison, G. B. (1997). Photoelectron Spectroscopy of the NCN- and HNCN- Ions. *J. Phys. Chem. A.* 101, 4338–4345. doi:10.1021/jp964067d

Coates, A. J., Crary, F. J., Lewis, G. R., Young, D. T., Waite, J. H., Jr., and Sittler, E. C., Jr. (2007). Discovery of Heavy Negative Ions in Titan's Ionosphere. *Geophys. Res. Lett.* 34. doi:10.1029/2007gl030978

Compton, R. N., Carman, H. S., Jr., Abdoul-Carime, H., Schermann, J. P., Hendricks, J. H., Lyapustina, S. A., et al. (1996). On the Binding of Electrons to Nitromethane: Dipole and Valence Bound Anions. *J. Chem. Phys.* 105, 3472–3478. doi:10.1063/1.472993

Cordiner, M. A., and Sarre, P. J. (2007). The CH$_\mathsf{2}$CN- Molecule: Carrier of the $\mathsf{\lambda}$8037 Diffuse Interstellar Band. *A&A* 472, 537–545. doi:10.1051/0004-6361:20077358

Cordiner, M., Charnley, S., Buckle, J., Walsh, C., and Millar, T. (2011). Discovery of Interstellar Anions in Cepheus and Auriga. *Astrophys. J. Lett.* 730, 1–5. doi:10.1088/2041-8205/730/2/l18

Coustenis, A. (2007). What Cassini-Huygens Has Revealed about Titan. *Astron. Geophys.* 48, 2.14–2.20. doi:10.1111/j.1468-4004.2007.48214.x

Desfrancois, C., Abdoul-Carime, H., and Schermann, J. (1996). Electron Attachment to Isolated Nucleic Acid Bases. *J. Chem. Phys.* 104, 7762. doi:10.1063/1.471484

Dunning, T. H. (1989). Gaussian Basis Sets for Use in Correlated Molecular Calculations. I. The Atoms boron through Neon and Hydrogen. *J. Chem. Phys.* 90, 1007–1023. doi:10.1063/1.456153

Fermi, E., and Teller, E. (1947). The Capture of Negative Mesotrons in Matter. *Phys. Rev.* 72, 399–408. doi:10.1103/physrev.72.399

Fortenberry, R. C., and Crawford, T. D. (2011a). Singlet Excited States of Silicon-Containing Anions Relevant to Interstellar Chemistry. *J. Phys. Chem. A.* 115, 8119–8124. doi:10.1021/jp204844j

Fortenberry, R. C., and Crawford, T. D. (2011b). Theoretical Prediction of New Dipole-Bound Singlet States for Anions of Interstellar Interest. *J. Chem. Phys.* 134, 154304. doi:10.1063/1.3576053

Fortenberry, R. C. (2015). Interstellar Anions: The Role of Quantum Chemistry. *J. Phys. Chem. A.* 119, 9941–9953. doi:10.1021/acs.jpca.5b05056

Fortenberry, R. C., King, R. A., Stanton, J. F., and Crawford, T. D. (2010). A Benchmark Study of the Vertical Electronic Spectra of the Linear Chain Radicals C2H and C4H. *J. Chem. Phys.* 132, 144303. doi:10.1063/1.3376073

Fortenberry, R. C., Moore, M. M., and Lee, T. J. (2016). Excited State Trends in Bidirectionally Expanded Closed-Shell PAH and PANH Anions. *J. Phys. Chem. A.* 120, 7327–7334. doi:10.1021/acs.jpca.6b06654

Fortenberry, R. C., Morgan, W. J., and Enyard, J. D. (2014). Predictable Valence Excited States of Anions. *J. Phys. Chem. A.* 118, 10763–10769. doi:10.1021/jp509512u

Frisch, M. J., Trucks, G. W., Schlegel, H. B., Scuseria, G. E., Robb, M. A., Cheeseman, J. R., et al. (2016). *Gaussian 16 Revision C.01*. Wallingford CT [Dataset]: Gaussian Inc.

Gutowski, M., Skurski, P., Boldyrev, A. I., Simons, J., and Jordan, K. D. (1996). Contribution of Electron Correlation to the Stability of Dipole-Bound Anionic States. *Phys. Rev. A.* 54, 1906–1909. doi:10.1103/physreva.54.1906

Gutsev, G. L., and Adamowicz, L. (1995). The Valence and Dipole-Bound States of the Cyanomethide Ion, CH2CN−. *Chem. Phys. Lett.* 246, 245–250. doi:10.1016/0009-2614(95)01097-s

Hammonds, M., Pathak, A., Candian, A., and Sarre, P. (2011). Spectroscopy of Protonated and Deprontonated PAHs. *EAS Publ. Ser.* 46, 373–379.

Hanel, R., Conrath, B., Flasar, F. M., Kunde, V., Maguire, W., Pearl, J., et al. (1981). Infrared Observations of the Saturnian System from *Voyager 1*. *Science* 212, 192–200. doi:10.1126/science.212.4491.192

Heikkilä, A., Johansson, L. E. B., and Olofsson, H. (1999). Molecular Abundance Variations in the Magellanic Clouds. *Astron. Astrophys.* 344, 817–847.

Hendricks, J. H., Lyapustina, S. A., de Clercq, H. L., Snodgrass, J. T., and Bowen, K. H. (1996). Dipole Bound, Nucleic Acid Base Anions Studied via Negative Ion Photoelectron Spectroscopy. *J. Chem. Phys.* 104, 7788–7791. doi:10.1063/1.471482

Hendricks, J., Lyapustine, A., de Clercq, H., and Bowen, K. (1998). The Dipole Bound-To-Covalent Anion Transformation in Uracil. *J. Chem. Phys.* 8, 108. doi:10.1063/1.475360

Hoshina, K., Kohguchi, H., Ohshima, Y., and Endo, Y. (1998). Laser-induced Fluorescence Spectroscopy of the C4H and C4D Radicals in a Supersonic Jet. *J. Chem. Phys.* 108, 3465–3478. doi:10.1063/1.475746

Jalbout, A. F., Pichugin, K. Y., and Adamowicz, L. (2003). An Excess Electron Connects Uracil to glycine. *Eur. Phys. J. D - At. Mol. Opt. Phys.* 26, 197–200. doi:10.1140/epjd/e2003-00224-4

Jordan, K. D., and Wang, F. (2003). Theory of Dipole-Bound Anions. *Annu. Rev. Phys. Chem.* 54, 367–396. doi:10.1146/annurev.physchem.54.011002.103851

Kawaguchi, K., Kasai, Y., Ishikawa, S., and Kaifu, N. (1995). A Spectral-Line Survey Observation of IRC+10216 between 28 and 50 GHz. *Publ. Astron. Soc.-Japan* 47, 853–876.

Krylov, A. I. (2008). Equation-of-Motion Coupled-Cluster Methods for Open-Shell and Electronically Excited Species: The Hitchhiker's Guide to Fock Space. *Annu. Rev. Phys. Chem.* 59, 433–462. doi:10.1146/annurev.physchem.59.032607.093602

Kuiper, G. P. (1944). Titan: a Satellite with an Atmosphere. *Astrophys. J.* 100. doi:10.1086/144679

Kunde, V. G., Aikin, A. C., Hanel, R. A., Jennings, D. E., Maguire, W. C., and Samuelson, R. E. (1981). C4H2, HC3N and C2N2 in Titan's Atmosphere. *Nature* 292, 686–688. doi:10.1038/292686a0

Lepp, S., and Dalgarno, A. (1988). Polycyclic Aromatic Hydrocarbons in Interstellar Chemistry. *Astrophys. J.* 324, 533. doi:10.1086/165915

López-Puertas, M., Dinelli, B. M., Adriani, A., Funke, B., García-Comas, M., Moriconi, M. L., et al. (2013). Large Abundances of Polycyclic Aromatic Hydrocarbons in Titan's Upper Atmosphere. *ApJ* 770, 132. doi:10.1088/0004-637x/770/2/132

Lykke, K. R., Neumark, D. M., Andersen, T., Trapa, V. J., and Lineberger, W. C. (1987). Autodetachment Spectroscopy and Dynamics of CH2CN− and CD2CN−. *J. Chem. Phys.* 87, 6842–6853. doi:10.1063/1.453379

Mach, T. J., King, R. A., and Crawford, T. D. (2010). A Coupled Cluster Benchmark Study of the Electronic Spectrum of the Allyl Radical†. *J. Phys. Chem. A.* 114, 8852–8857. doi:10.1021/jp102292x

Maguire, W. C., Hanel, R. A., Jennings, D. E., Kunde, V. G., and Samuelson, R. E. (1981). C3H8 and C3H4 in Titan's Atmosphere. *Nature* 292, 683–686. doi:10.1038/292683a0

Maier, J. P. (1998). Electronic Spectroscopy of Carbon Chains. *J. Phys. Chem. A.* 102, 3462–3469. doi:10.1021/jp9807219

McCarthy, M. C., Gottlieb, C. A., Gupta, H., and Thaddeus, P. (2006). Laboratory and Astronomical Identification of the Negative Molecular Ion C 6 H -. *ApJ* 652, L141–L144. doi:10.1086/510238

McCarthy, M. C., Gottlieb, C. A., Thaddeus, P., Horn, M., and Botschwina, P. (1995). Structure of the Cccn and Cccch Radicals: Isotopic Substitution and Ab Initio Theory. *J. Chem. Phys.* 103, 7820–7827. doi:10.1063/1.470198

McKay, C. P. (1996). Elemental Composition, Solubility, and Optical Properties of Titan's Organic Haze. *Planet. Space Sci.* 44, 741–747. doi:10.1016/0032-0633(96)00009-8

Mead, R. D., Lykke, K. R., Lineberger, W. C., Marks, J., and Brauman, J. I. (1984). Spectroscopy and Dynamics of the Dipole-bound State of Acetaldehyde Enolate. *J. Chem. Phys.* 81, 4883–4892. doi:10.1063/1.447515

Millar, T. J., Herbst, E., and Bettens, A. R. P. (2000). Large Molecules in the Envelope Surroundings IRC+10216. *Mon. Not. R. Astron. Soc.* 316, 195–200. doi:10.1046/j.1365-8711.2000.03560.x

Molina-Cuberos, G. J., Schwingenschuh, K., López-Moreno, J. J., Rodrigo, R., Lara, L. M., and Anicich, V. (2002). Nitriles Produced by Ion Chemistry in the Lower Ionosphere of Titan. *J. Geophys. Res. Planet.* 107, 9–11. doi:10.1029/2000je001480

Morgan, W. J., and Fortenberry, R. C. (2015). Additional Diffuse Functions in Basis Sets for Dipole-Bound Excited States of Anions. *Theor. Chem. Acc.* 134, 47. doi:10.1007/s00214-015-1647-1

Moustefaoui, T., Rebrion-Rowe, C., Le Garrec, J.-L., Rowe, R. C., and Mitchell, Brian. A. J. (1998). Low Temperature Electron Attachment to Polycyclic Aromatic Hydrocarbons. *Faraday Discuss.* 109, 71–82. doi:10.1039/a800490k

Mullin, A. S., Murray, K. K., Schulz, C. P., and Lineberger, W. C. (1993). Autodetachment Dynamics of Acetaldhyde Enolate Anion. *Ch2cho*$^-$. *J. Phys. Chem.* 97, 10281–10286. doi:10.1021/j100142a005

Mullin, A. S., Murray, K. K., Schulz, C., Szaflarski, D. M., and Lineberger, W. (1992). Autodetachment Spectroscopy of Vibrationally Excited Acetaldehyde Enolate Anion. *Ch2cho*$^-$. *Chem. Phys.* 166, 207–213. doi:10.1016/0301-0104(92)87019-6

Olah, G., Mathew, T., Prakesh, S., and Rusul, G. (2016). Chemical Aspects of Astrophysically Observed Extraterrestrial Methonal, Hydrocarbon Derivatives, and Ions. *J. Am. Chem. Soc.* 138, 1717–1722. doi:10.1021/jacs.6b00343

Pino, T., Tulej, M., Güthe, F., Pachkov, M., and Maier, J. P. (2002). Photodetachment Spectroscopy of the $C_{2n}H^-$ (N=2–4) Anions in the Vicinity of Their Electron Detachment Threshold. *J. Chem. Phys.* 116, 6126–6131. doi:10.1063/1.1451248

Puzzarini, C., Baiardi, A., Bloine, J., Barone, V., Murphy, T., Drew, D., et al. (2017). Spectroscopic Characterization of Key Aromatic and Heterocyclic Molecules: A Route toward the Origin of Life. *Astron. J.* 154, 82. doi:10.3847/1538-3881/aa7d54

Remijan, A. J., Hollis, J. M., Lovas, F. J., Cordiner, M. A., Millar, T. J., Markwick-Kemper, A. J., et al. (2007). Detection of C_8H^- and Comparison with C_8H toward IRC +10216. *Astrophys. J.* 664, L47–L50. doi:10.1086/520704

Ricca, A., Bauschlicher, C. W., and Bakes, E. L. O. (2001). A Computational Study of the Mechanisms for the Incorporation of a Nitrogen Atom into Polycyclic Aromatic Hydrocarbons in the Titanhaze. *Icarus* 154, 516–521. doi:10.1006/icar.2001.6694

Ross, T., Baker, E., Snow, T., Destree, J., and Rachford, B. (2008). The Search for H^- in Astrophysical Environments. *Astrophys. J.* 684, 358–363. doi:10.1086/590242

Samuelson, R., Hanel, R., Kunde, V., and Maguire, W. (1981). Mean Molecular Weight and Hydrogen Abundance of Titan's Atmosphere. *Nature* 292, 688–693. doi:10.1038/292688a0

Santaloci, T., and Fortenberry, R. (2021). Electronically Excited States of Closed-Shell, Cyano-Functionalized Polycyclic Aromatic Hydrocarbon Anions. *Chem* 3, 296–313. doi:10.3390/chemistry3010022

Santaloci, T. J., and Fortenberry, R. C. (2020). On the Possibilities of Electronically Excited States in Stable Amine Anions: Dicyanoamine, Cyanoethynylamine, and Diethynylamine. *M. Astrophy.* 19, 100070. doi:10.1016/j.molap.2020.100070

Schild, R., Chaffee, F., Frogel, J., and Persson, S. (1974). The Nature of Infrared Excesses in Extreme Be Stars. *Astrophys. J.* 190, 73–83. doi:10.1086/152848

Shavitt, I., and Bartlett, R. (2009). *MBPT and Coupled-Cluster Theory of Many-Body Methods in Chemistry and Physics*, 59. Cambridge: Cambridge University Press.

Shen, L. N., Doyle, T. J., and Graham, W. R. M. (1990). Fourier Transform Spectroscopy of C_4H (Butadiynyl) in Ar at 10 K C-H and C ≡C Stretching Modes. *J. Chem. Phys.* 93, 1597–1603. doi:10.1063/1.459138

Simons, J. (2008). Molecular Anions. *J. Phys. Chem. A.* 112, 6401–6511. doi:10.1021/jp711490b

Snow, T. (1975). A Search for H^- in the Shell Surrounding Chi Ophiuchi. *Astrophys. J.* 198, 361–367. doi:10.1086/153611

Stanton, J. F., and Gauss, J. (1994). Analytic Energy Derivatives for Ionized States Described by the Equation-Of-Motion Coupled Cluster Method. *J. Phys. Chem.* 101, 8938–8944. doi:10.1063/1.468022

Stanton, J. F., Gauss, J., Cheng, L., Harding, M. E., Matthews, D. A., and Szalay, P. G. (2008). CFOUR, Coupled-Cluster Techniques for Computational Chemistry, a Quantum-Chemical Program Package. With Contributions from A. *J. Chem. Phys.* 152 (21), 214108, 2008 . Watts and the integral packages MOLECULE (J. Almlöf and P.R. Taylor), PROPS (P.R. Taylor), ABACUS (T. Helgaker, H.J. Aa. Jensen, P. Jørgensen, and J. Olsen), and ECP routines by A. V. Mitin and C. vDataset. doi:10.1063/5.0004837

Stanton, J. F., and Bartlett, R. J. (1993). The Equation of Motion Coupled-Cluster Method: A Systematic Biorthogonal Approach to Molecular Excitation Energies, Transition-Probabilities, and Excited-State Properties. *J. Chem. Phys.* 98, 7029–7039. doi:10.1063/1.464746

Taylor, T. R., Xu, C., and Neumark, D. M. (1998). Photoelectron Spectra of the $C_{2n}H^-$ (N=1–4) and $C_{2n}D^-$ (N=1–3) Anions. *J. Chem. Phys.* 108, 10018–10026. doi:10.1063/1.476462

Terzieva, R., and Herbst, E. (2000). Radiative Electron Attachment to Small Linear Carbon Cluster and its Significance for the Chemistry of Diffuse Interstellar Clouds. *Int. J. Mass. Spectrom.* 201, 135–142. doi:10.1016/s1387-3806(00)00212-8

Thaddeus, P., Gottlieb, C. A., Gupta, H., Brünken, S., McCarthy, M. C., Agúndez, M., et al. (2008). Laboratory and Astronomical Detection of the Negative Molecular Ion C_3N^-. *J. Astrophys. Astron.* 677, 1132–1139. doi:10.1086/528947

Theis, M. L., Candian, A., Tielens, A. G. G. M., Lee, T. J., and Fortenberry, R. C. (2015b). Electronically Excited States of Anisotropically Extended Singly-Deprotonated PAH Anions. *J. Phys. Chem. A.* 119, 13048–13054. doi:10.1021/acs.jpca.5b10421

Theis, M. L., Candian, A., Tielens, A. G. G. M., Lee, T. J., and Fortenberry, R. (2015a). Electronically Excited States of PANH Anions. *Phys. Chem. Chem. Phys.* 17, 14761. doi:10.1039/c5cp01354b

Tielens, A. G. G. M. (2008). Interstellar Polycyclic Aromatic Hydrocarbon Molecules. *Annu. Rev. Astron. Astrophys.* 46, 289–337. doi:10.1146/annurev.astro.46.060407.145211

Tulej, M., Kirkwoods, D., Pachkov, M., and Maier, J. (1998). Gas-phase Electronic Transitions of Carbon Chain Anions Coinciding with Diffuse Interstellar Bands. *Astrophys. J. Lett.* 506, L69–L73. doi:10.1086/311637

van Hemert, M. C., and van Dishoeck, E. F. (2008). Photodissociation of Small Carbonaceous Molecules of Astrophysical Interest. *Chem. Phys.* 343, 292–302. doi:10.1016/j.chemphys.2007.08.011

Vay, K. L., Salibi, E., Song, E. Y., and Mutschler, H. (2019). Nucleic Acid Catalysis under Potential Prebiotic Conditions. *Chem-asian J.* 15, 214–230. doi:10.1002/asia.201901205

Walsh, S. P. (1995). Characterization of the Minimum Energy Paths for the Ring Closure Reactions of C_4H_3 with Acetylene. *J. Chem. Phys.* 103.

Werner, H.-J., Knowles, P. J., Knizia, G., Manby, F. R., Schütz, M., Celani, P., et al. (2015). *Molpro, Version 2015.1, a Package of* Ab Initio *Programs*. Dataset.

Woon, D. E. (1995). A Correlated Ab Initio Study of Linear Carbon-Chain Radicals C_nH (N=2-7). *Chem. Phys. Lett.* 244, 45–52. doi:10.1016/0009-2614(95)00906-k

Yamamoto, S., Saito, S., Guelin, M., Cernicharo, J., Suzuki, H., and Ohishi, M. (1987). Laboratory Microwave Spectroscopy of the Vibrational Satellites for the ν 7 and 2 ν 7 States of C_4H and Their Astronomical Identification. *Astrophys. J. Lett.* 323, L149. doi:10.1086/185076

Yung, Y. (1987). An Update of Nitrile Photochemistry on Titan. *Icarus* 72, 468–472. doi:10.1016/0019-1035(87)90186-2

Yung, Y. L., Allen, M., and Pinto, J. P. (1984). Photochemistry of the Atmosphere of Titan-Comparison between Model and Observation. *Astrophys. J. Suppl. S.* 55, 465–506. doi:10.1086/190963

Conflict of Interest: The authors declare that the research was conducted in the absence of any commercial or financial relationships that could be construed as a potential conflict of interest.

Publisher's Note: All claims expressed in this article are solely those of the authors and do not necessarily represent those of their affiliated organizations, or those of the publisher, the editors and the reviewers. Any product that may be evaluated in this article, or claim that may be made by its manufacturer, is not guaranteed or endorsed by the publisher.

frontiers in Astronomy and Space Sciences

REVIEW
published: 08 December 2021
doi: 10.3389/fspas.2021.776942

Unusual Chemical Processes in Interstellar Chemistry: Past and Present

Eric Herbst[1,2]*

[1]Department of Chemistry, University of Virginia, Charlottesville, VA, United States, [2]Department of Astronomy, University of Virginia, Charlottesville, VA, United States

The chemistry that occurs in interstellar clouds consists of both gas-phase processes and reactions on the surfaces of dust grains, the latter particularly on and in water-dominated ice mantles in cold clouds. Some of these processes, especially at low temperature, are very unusual by terrestrial standards. For example, in the gas-phase, two-body association reactions form a metastable species known as a complex, which is then stabilized by the emission of radiation under low-density conditions, especially at low temperatures. In the solid phase, it has been thought that the major process for surface reactions is diffusive in nature, occurring when two species undergoing random walks collide with each other on a surface that has both potential wells and intermediate barriers. There is experimental evidence for this process, although very few rates at low interstellar temperatures are well measured. Moreover, since dust particles are discrete, modeling has to take account that reactant pairs are on the same grain, a problem that can be treated using stochastic approaches. In addition, it has been shown more recently that surface reactions can occur more rapidly if they undergo any of a number of non-diffusive processes including so-called three-body mechanisms. There is some experimental support for this hypothesis. These and other unusual gaseous and solid-state processes will be discussed from the theoretical and experimental points of view, and their possible role in the synthesis of organic molecules in interstellar clouds explained. In addition, their historical development will be reviewed.

Keywords: interstellar medium, molecular synthesis, astrochemistry, radiative association, dust particles, diffusion, stochastic, radiolysis

OPEN ACCESS

Edited by:
André Canosa, UMR6251 Institut de Physique de Rennes, France

Reviewed by:
Valentine Wakelam, UMR5804 Laboratoire d'astrophysique de Bordeaux, France
Francois Lique, University of Rennes 1, France
Tom Millar, Queen's University Belfast, United Kingdom

***Correspondence:**
Eric Herbst
eh2ef@virginia.edu

Specialty section:
This article was submitted to Astrochemistry, a section of the journal Frontiers in Astronomy and Space Sciences

Received: *14 September 2021*
Accepted: *26 October 2021*
Published: *08 December 2021*

Citation:
Herbst E (2021) Unusual Chemical Processes in Interstellar Chemistry: Past and Present. Front. Astron. Space Sci. 8:776942. doi: 10.3389/fspas.2021.776942

INTRODUCTION

The Interstellar Medium

The interstellar medium is exceedingly diverse (Tielens, 2005). Much of it is composed of so-called interstellar clouds of gas and dust, which range from rather wispy diffuse clouds to dense clouds that are impervious to background light and so can appear black against the sky. Temperatures range from 50—100 K in diffuse clouds down to 10 K or below in cold dense clouds. Cold regions in clouds with warmer regions are often called "cold cores." Gas densities can be as low as 10 cm^{-3} in diffuse clouds to upwards of 10^5 cm^{-3} in dense regions. The larger clouds can be very heterogeneous in both temperature and density.

TABLE 1 | Classes of gaseous and icy interstellar molecules.

Simple	H_2	CO	H_2O	H_3^+ (H_2D^+)	HCN	HNC	NH_3
Carbon-chains	CCCCS	HNCCC	CCCCCCH	CCCCCCH-	$HC_{11}N$		
COMs	CH_3OH	CH_3OCH_3	$HCOOCH_3$	C_2H_5CN	CH_3NH_2	n-C_3H_7CN	i-C_3H_7CN
Inorganic	PN	MgNC	HCP	NaCN	TiO_2	NaCl	PH_3
Fullerenes	C_{60}	C_{60}^+	C_{70}				
PAH's	C_6H_5CN	$C_{10}H_7CN$	c-C_9H_8	c-C_5H_5CN	o-C_6H_4		
Ices	H_2O	CO_2	CO	CH_4	CH_3OH	NH_3	OCN-

Portions of dense interstellar clouds are also the sites of star and exoplanet formation, which occur via a long sequence of individual stages of differing physical conditions, mainly higher temperatures and densities, which depend strongly on whether low-mass stars such as our sun or high-mass stars are the final product (Draine, 2011). The production of low-mass stars arises from the collapse and warm-up of cold cores through regions known as "prestellar cores" followed by "protostellar cores," a term for stars in the act of formation, during which gas and dust collapse inwards to form so-called "hot corinos" with temperatures exceeding 100 K. During this stage, early-stage disks are formed surrounding the protostar. As the disks form, the collapsing dust particles eventually collide with each other to form larger objects, such as comets, meteors, and terminating in exo-planets, while the disks become so-called planetary disks. So-called giant clouds can have thousands of stars already formed from protostars and probably equally many in the act of formation. The evolutionary stages of high-mass stars are somewhat different than the stages for low-mass stars. Here, the term "hot core" for example refers to hot objects that occur post-massive star formation and can be linked to ultra-compact HII regions.

In most interstellar sources, molecules can be found in the gas-phase; altogether more than 250 molecules have been detected in interstellar and circumstellar clouds (see Woon, 2021 for a detailed listing). The collection of molecules in sources of differing physical conditions are different; indeed the chemical composition can help to understand these physical conditions. The dominant molecule in virtually all sources is molecular hydrogen, which is not surprising because it is the most abundant element. Rather than listing all of the interstellar molecules observed to date, we have preferred to give the reader a sense of the different types of molecules detected in the interstellar medium. Groups of selected gaseous molecules such as "carbon-chains" and "complex organic molecules" are listed in rows in **Table 1**. The chosen molecules are well-known species. Also listed in this table are some molecules detected on and in ice mantles that surround dust particles in cold regions of clouds. The dust particles themselves consist either of carbonaceous or silicate materials and range in size from several Angstroms to over a micro-meter. Most gas-phase molecules in dense clouds are detected via their rotational spectra (Townes and Schawlow, 1955); most of these molecules are organic in nature. Some are very much like terrestrial organic species whereas others are very unusual by the standards of our planet. The larger terrestrial-like molecules are semi-saturated and are known as "Complex Organic Molecules", or COMs for short, even though the criterion of complexity is applied at the rather low value of a minimum of six atoms (Herbst and van Dishoeck, 2009). The more unusual species are often referred to as "carbon chains" and are highly unsaturated linear or near-linear species. These carbon chains include radicals and ions, both positively and negatively charged. The most abundant species in granular ices is water, with other abundant species either carbonaceous in nature, such as carbon monoxide and dioxide, and other small species such as ammonia. Molecules found in granular icy mantles are detected via vibrational spectroscopy and range in size up to methanol, which is also found in the gas (Wilson et al., 1980). Vibrational spectroscopy can in general not be done easily from the ground, and space observatories such as the JWST, now planned for launch in December 2021, are needed.

Interstellar molecules are synthesized via a diverse collection of chemical processes that consist of well-known reactions and very unusual processes, an improved understanding of which has occurred because of their likely interstellar importance. These reactions are collected together in networks, such as KIDA (Kinetic Database for Astrochemistry; Wakelam et al., 2015; http://kida.astrophy.u-bordeaux.fr/) and UDFA (UMIST Database For Astrochemistry; Markwick, 2012; McElroy et al., 2013, http://udfa.ajmarkwick.net/) and used in large simulations with up to a hundred thousand chemical reactions to determine molecular abundances or synthetic spectra via solutions of kinetic equations and radiative transfer. Reactions on grain surfaces have been added to KIDA and the combined gas-grain network is known as Nautilus (Ruaud et al., 2016). Another gas-grain network, named MAGICKAL, has been built by Garrod (2013a) and, albeit complete, particularly emphasizes surface chemistry. In this review, some of the unusual gas-phase and granular processes will be discussed within a historical background. These reactions include those that can occur efficiently only in low density regions.

GAS PHASE PROCESSES

Radiative Association

Radiative association is a process in which two atoms or molecules collide to form a short-lived intermediate, which can be stabilized by emission of radiation. The process has rarely been seen in the laboratory (Gerlich and Horning, 1992; Luca et al., 2002), but is thought to be of importance in both

diffuse and dense interstellar clouds. In the early days of astrochemistry, the gas-phase chemistry in diffuse clouds was of paramount importance, because some of these clouds, with gas densities of 10^2 cm^{-3} and temperatures of 50–100 K (Black and Dalgarno, 1977) are relatively close to the earth and could be studied by absorption in the visible and ultraviolet (Federman et al., 1980; Carruthers, 1970).

Radiative association of two atoms in diffuse clouds has been investigated theoretically. If we consider two atoms colliding, the most common mechanism allows the atoms to travel along an excited electronic state, while radiating to bound levels of the ground state. This process can be treated semiclassically or fully quantum mechanically (Giusti-Suzor et al., 1976). The formation of the diatomic molecule CH^+ was originally thought to occur via the radiative association (Solomon and Klemperer, 1972; Giusti-Suzor et al., 1976).

$$C^+ + H \rightarrow CH^+ + h\nu \quad (1)$$

with a rate coefficient of approximately 10^{-17} cm^3 s^{-1}, which corresponds to 1 in 10^8 collisions. This process is not sufficiently rapid to produce the observed abundance of CH^+. Once it was known that much of the hydrogen in diffuse clouds could be molecular in nature, however, the production of both CH and CH^+ was predicted to occur via the precursor CH_2^+ produced in the radiative association (Black and Dalgarno, 1973; Herbst et al., 1977):

$$C^+ + H_2 \rightarrow CH_2^+ + h\nu, \quad (2)$$

which occurs via several excited electronic states, and was calculated to be more rapid than reaction (1) by two to three orders of magnitude. The production of CH_2^+ then leads to CH via dissociative recombination:

$$CH_2^+ + e^- \rightarrow CH + H \quad (3)$$

although there is a competitive channel in which CH_2^+ reacts with H_2 to form CH_3^+ + H. The formation of CH^+ was thought to occur via photodissociation of the species CH_2^+ and CH_3^+. Although this mechanism produces a sufficient abundance of CH in diffuse clouds, the production of CH^+ was once again insufficient to account for its abundance. A shock-wave mechanism which powers the endothermic reaction to form CH^+ (Elitzur and Watson, 1978):

$$C^+ + H_2 \rightarrow CH^+ + H, \quad (4)$$

is still under consideration. Calculated state-to-state rate constants involving the lowest two vibrational states of H_2 under the conditions of the Orion Bar photon-dominated region indicate a role for vibrational excitation to power **Equation 4** (Zanchet et al., 2013). A more recent candidate is intermittent turbulence (Falgarone and Puget, 1995; Moseley et al., 2021).

By the mid 1970s, the chemistry of so-called dense interstellar clouds began to overtake the study of diffuse clouds due to the development of radio astronomical techniques and to the abundance of organic molecules starting with H_2CO (Snyder et al., 1969), which are abundant in these regions. With gas densities of at least 10^4 cm^{-3}, and temperatures as low as 10 K, these clouds provide a better environment for chemistry than diffuse clouds (Watson, 1972a; Watson, 1972b; Herbst and Klemperer, 1973). The original thinking was that the gas-phase chemistry is dominated by barrierless ion-neutral reactions with ions produced by cosmic ray bombardment. Among the ion-neutral processes, radiative association was considered in early models of dense cloud chemistry (Herbst and Klemperer, 1973). Unlike the simple approach to radiative association of diatomic species, the basic idea is that the multidimensional potential surface from reactants to products has an intermediate deep well, known as a complex, rather than the more common transition state barrier. The complex, in its ground electronic state, can relax via emission of excited vibrational states to stable levels of the ground state. Although complexes involving neutral species are less studied theoretically, they can be important for systems with two neutral radicals (Vuitton et al., 2012). Whether we are considering an ion-molecule or a neutral-neutral system, we can write the overall radiative association as

$$A + B \rightleftarrows AB^* \rightarrow AB; C + D, \quad (5)$$

where A and B designate reactants, AB* the intermediate complex, AB, the relaxed stable association product formed via emission from the complex, and C and D competitive reaction products. These products can form from the complex and so compete directly with complex emission or they can be formed from reactants and compete indirectly by division of the total rate coefficient.

Theoretical Methods

If the complex can be stabilized by emission of radiation with some degree of efficiency, radiative association can be an important process for the growth of molecules in the cold interstellar medium at densities far too low for collisional stabilization. In most instances, however, the stabilization by radiation is less efficient than the re-dissociation of the complex into reactants. The competition between dissociation into products and radiative stabilization of the complex depends strongly on whether the C + D products are endothermic. In the simplest treatment, which assumes the complex to be at steady-state, the rate coefficient for radiative association k_{ra} (cm^3 s^{-1}) is given by the equation (Herbst, 1980a):

$$k_{ra} = k_1 k_r / \{k_{-1} + k_2 + k_r\} \quad (6)$$

where k_1 (cm^3 s^{-1}) is the rate coefficient for complex formation, k_{-1} (s^{-1}) is the complex re-dissociation rate, k_r (s^{-1}) is the radiative stabilization rate, normally assumed to consist of single photon emission in the infrared, and k_2 (s^{-1}) is the rate at which the complex dissociates into new products, a process which often possesses a barrier. Indeed, if there is no barrier in the exit channel and the process is exothermic, the complex normally produces products rapidly, perhaps even more rapidly than re-dissociation, vitiating the radiative channel, and radiative association becomes too inefficient to be of importance. In a common case, there is no rapid process for complex destruction

so that only redissociation and radiative stabilization compete, although the re-dissociation rate normally exceeds the radiative stabilization rate, k_r. With the assumption that polyatomic molecular vibrations can be treated as coupled harmonic oscillators, the rate of emission of an infra-red photon can be obtained as a linear function of overall vibrational energy in excess of the zero-point energy (Herbst, 1982) with values ranging from 10—10^3 s^{-1}.

Under the condition that $k_{-1} > k_r$, the radiative association rate coefficient reduces to the much simpler equation:

$$k_{ra} = (k_1/k_{-1})k_r. \tag{7}$$

With the assumption that the ratio k_1/k_{-1} can be treated via the principle of detailed balancing (Herbst, 1980a,b), the rate coefficient can be written in terms of canonical partition functions q, which are normalized sums over the populations of individual levels at a temperature T for the reactants and the complex (Herbst, 1980a,b):

$$k_{ra} = \frac{q_{AB*}}{q_A q_B} k_r. \tag{8}$$

Solution of **Equation 8** shows that a larger radiative association rate coefficient is associated with 1) a lower temperature, 2) a larger number of atoms in the complex, and 3) a deeper complex well. Looked at another way, the inverse temperature dependence stems from the longer period of time necessary for the complex vibrational motion to transfer sufficient energy to a mode, so that it leads to re-dissociation. In a temperature range when the rotational partition functions can be treated continuously and the vibrational partition functions discretely, the temperature dependence of the radiative association rate coefficient is given by the expression $k_{ra} \propto T^{-(ra+rb+1)/2}$ where r_a and r_b are the number of rotational degrees of freedom of the two reactants A and B. Thus, for two asymmetric tops, the inverse temperature dependence goes as $T^{-3.5}$. **Equations 7** and **8** fail if the re-dissociation rate falls below the radiative stabilization rate of the complex ($k_{-1} < k_r$), at which the radiative association rate is predicted to exceed the collisional rate of the two reactants, an unphysical result. If k_{-1} is only slightly larger than k_r, use of **Equation 6** in the absence of a competitive exothermic channel ($k_2 = 0$) leads to a much lower temperature dependence, especially at low temperatures.

The canonical expression in **Equation 8** does not deal directly with the long-range attractive potential nor with detailed angular momentum considerations. Following Bates (1979a) and (1979b), Herbst (1980b) modified the canonical expression to include the orbital angular momentum L in a quasi-diatomic centrifugal barrier term built upon the long-range Langevin potential for ion-neutral collisions. The result is a modification of the canonical approach leading to a weaker temperature dependence.

A far more complex treatment, including all assorted angular momenta, was introduced by Klots (1976), and Chesnavich and Bowers (1977), and was later utilized by Herbst (1985a) and Tennis et al. (2021). This approach, known as the phase space approach, allows the use of different long-range potentials, including those applicable to neutral-neutral systems, and is microcanonical in nature. Moreover, it is able to treat non-equilibrium systems such as shocks, as well as systems in which radiative association competes with barriers in the exit channel of non-associative channels. An example occurs for the association of $CH_3^+ + NH_3$ to form $CH_3NH_3^+$ in competition with the barriered exit channel leading to $H_4CN^+ + H_2$ (Herbst, 1985b).

With the phase space theory, the overall microcanonical rate coefficient k_{ra} for radiative association is given by the equation (Herbst, 1985a)

$$k_{ra}(J_A, J_B, E_{coll} \rightarrow J, E) = \frac{k_1(J_A, J_B, E_{coll} \rightarrow J, E)k_r}{k_{-1}(J, E) + k_r + k_2}, \tag{9}$$

where E is the total energy of the system, E_{coll} is the collision energy, J is the total angular momentum, and J_A and J_B are the angular momenta of the reactants. The rate coefficients k_i in **Equation 9** designate the rates of the same processes as those in **Equation 6**. The value of k_1 is determined by the product of the relative velocity of the reactants and the phase space capture cross section, determined by either the long-range attractive potential relevant to ion-neutral or neutral-neutral collisions. The complex re-dissociation rate k_{-1} is obtained from k_1 by microscopic reversibility (Klots, 1976). Roaming, a term designating motion between two different potentials, can also be included in the k_2 term in **Equation 8** (Sivaramakrishnan et al., 2011; Tennis et al., 2021). Thermal or non-thermal rate coefficients of k_{ra} can be obtained by suitable integrations (Chesnavich and Bowers, 1977). A recent example of a calculated radiative association rate coefficient between the radicals $CH_3 + CH_3O$ to form dimethyl ether using the phase space approach has been done by Tennis et al. (2021). With the inclusion of a competitive roaming channel in the calculations to form the exothermic products $CH_4 + H_2CO$, the radiative association rate coefficient at 10 K is approximately 3×10^{-11} cm^3 s^{-1}, or 0.1 of the collisional value. The rate coefficient is possibly large enough to account for the abundance of dimethyl ether in the low temperature source TMC-1 (Balucani et al., 2015).

Although phase space theories (and simpler approaches) can be used to study neutral-neutral radiative association, this is not as common as theories based on the re-dissociation of the complex. In a major paper, Ryzhov et al. (1996) showed that both the RRKM approach and the Variational transition state theoretical approach (VTST) can be utilized to obtain radiative association rate coefficients. Although this paper discussed these approaches with regard to an ion-neutral system, later papers have reported studies of neutral-neutral association, both radiative and collisional. An important paper in this field involves the atmosphere of Titan, the moon of Saturn with a large number of organic species (Vuitton et al., 2012). The theoretical method used in this paper involves transition state approaches in which the barrier is defined from the bottom of the complex well. Detailed balance converts complex dissociation into complex stabilization. The potential can be defined in much more detail than in the phase space approaches, which utilize long-range capture potentials only. Since there is no experimental information to the best of our knowledge for any neutral-neutral

radiative association, comparison can only be made with other theoretical treatments. Let us compare the phase space/canonical and transition state theories for similar reactions. The radical-radical reaction

$$CH_3 + CH_3 \rightarrow C_2H_6 + h\nu \quad (10)$$

has been studied from 50 to 300 K by Vuitton et al. (2012) whereas Tennis et al. (2021) have studied the similar reaction

$$CH_3 + CH_3O \rightarrow C_2H_6O + h\nu \quad (11)$$

using the phase space and canonical theories in the range 10—100 K. At 100 K, the methyl-methyl reaction is calculated to have a rate coefficient of 1.3×10^{-12} cm^3 s^{-1}, whereas the methyl-methoxy reaction has a calculated rate coefficient of 3.2×10^{-12} cm^3 s^{-1} with the phase space theory and, for completeness, a value of 3.3×10^{-11} cm^3 s^{-1} with the canonical theory. The binding energies of the complex in the two reactions are similar. Note that reaction (11) has one more heavy atom so, according to Vuitton et al. should have roughly the larger rate coefficient by 1-2 orders of magnitude if the complex species have similar binding energies. The temperature dependence of $CH_3 + CH_3$ goes as $T^{-3.23}$ where that of $CH_3 + CH_3O$ goes as roughly T^{-3}, at temperatures well above 100 K, but shows a lesser temperature dependence as the association approaches the limiting collisional value.

Radiative Association and Laboratory Experiments

Radiative association has not been studied extensively in the laboratory because it only occurs at low densities; at higher densities collisional stabilization of the complex dominates, a process often known as three-body or ternary association. At even higher densities, saturation sets in. Ion-molecule collisions leading to one type of association or another have been studied in the laboratory by a variety of techniques. As listed roughly in order of decreasing gas density, the techniques include the SIFT (Selected Ion flow drift-tube; Smith et al., 1990) and CRESU (reaction kinetics in uniform supersonic flow; Marquette et al., 1985) techniques, which operate at higher densities, and the ion-cyclotron resonance technique (Huntress and Beauchamp, 1969) as well as a variety of ion traps such as the Penning trap which can operate at low enough densities to reach a region where radiative association can be studied (Barlow et al., 1984). The CRESU technique can be used for both ion-neutral and neutral-neutral collisions and operates down to temperatures of near 10 K (Cooke and Sims, 2019).

For a wide range of densities of the bath gas M, the rate law for collisional stabilization of the complex is third-order (ternary) and increases linearly with the bath gas density:

$$\frac{d[AB]}{dt} = k_{3b}[A][B][M], \quad (12)$$

where

$$k_{3b} = k_1 k_2 / k_{-1}. \quad (13)$$

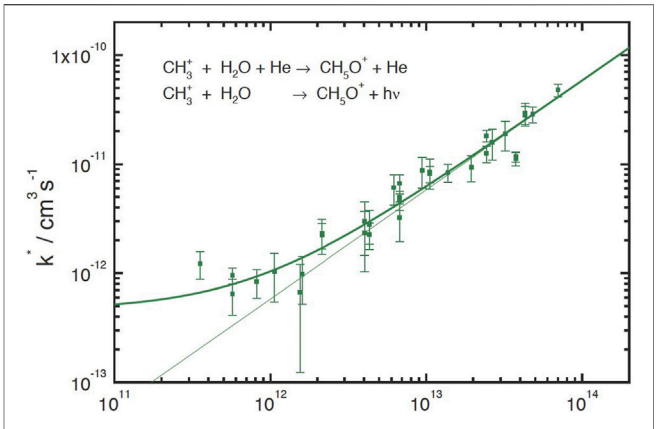

FIGURE 1 | Dependence of the effective rate coefficient for $CH_3^+ + H_2O$ association as a function of the He number density. The ion trap was operated at 20 K. The average H_2O density was 8×10^7 cm^{-3}. The measured values have been approximated by the function $k^* = k_{3b}$ [He] + k_{ra} which shows curvature above the ternary regime and leads to an approximate value for the radiative association rate coefficient of $k_{ra} = 5 \times 10^{-13}$ cm^3 s^{-1}. The thin linear line simulates the pure ternary regime. Permission requested to reproduce **Figure 3** of Luca et al. (2002) as printed originally by MATFYZPRESS (Sokolovská 49/83, 186 00 Praha 8-Karlín, Czechia) in the WDS'02 Proceedings of Contributed Papers, PART II, 294–300, 2002.

Here k_2 is the collisional stabilization rate coefficient, which is estimated to be 10^{-10} cm^3 s^{-1} for neutral complexes and 10^{-9} cm^3 s^{-1} for ionic complexes. At still higher densities, the rate law reaches saturation, where all collisions produce stable complexes. The radiative stabilization of the complex is independent of [M] at low densities and the rate of radiative association can be written as

$$\frac{d[AB]}{dt} = k_{ra}[A][B] \quad (14)$$

where

$$k_{ra} = k_1 k_r / k_{-1}, \quad (15)$$

as already discussed in **Section 2.2**. The two derivatives are equal when $k_2[M] = k_r$. Assuming the emission rate to be $\approx 10^2$ s^{-1} (Herbst, 1982), this occurs when the bath gas [M] = 10^{12} cm^{-3} for neutral reactants and an order of magnitude less for ionic-neutral reactants if the collision rate coefficient k_2 is assumed to be 10^{-10} cm^3 s^{-1} for neutral-neutral collisions and 10^{-9} cm^3 for ion-neutral collisions.

Although ternary processes are not expected to occur in the interstellar medium, they can be used indirectly in experiments to measure radiative association. If an experiment starts at higher densities and the density is gradually lowered until the two association mechanisms are equal, one should expect to see a region in which extrapolation to zero density shows a feature that gradually becomes horizontal when radiative association is dominant. **Figure 1** illustrates the experimental dependence of the rate of association between $CH_3^+ + H_2O$ in a bath gas of Helium with a 22-pole ion trap at an effective temperature of 50 ± 30 K (Luca et al., 2002). The figure shows that by a density of 10^{12} cm^{-3}, the dependence loses its linear relationship with He

and tends to flatten out, eventually reaching an extrapolated value for the radiative association rate coefficient at a density of 10^{11} cm^{-3} of approximately 5×10^{-13} cm^3 s^{-1}, or (more accurately) an upper limit of 2×10^{-12} cm^3 s^{-1}. This value at 50 K is lower than the calculated canonical value of 9×10^{-12} cm^3 s^{-1} and is closer to the centrifugal barrier value of 2×10^{-12} cm^3 s^{-1} (Herbst, 1980a; Herbst, 1980b). It should be noted that the extrapolation to low densities is dependent to some extent on the bath gas used, so that a more detailed experiment would involve the use of different bath gases. Another ion trap measurement was undertaken by Barlow et al. (1984), who used a Penning trap to study radiative association directly at low density. For the system $CH_3^+ + H_2$ at a temperature of 13 K, the rate coefficient was measured to be 1.1×10^{-13} cm^3 s^{-1}. It is likely that the Penning trap is the more reliable result, but the value at 13 K is well below the canonical theoretical value at 10 K of 6×10^{-10} cm^3 s^{-1} and the centrifugal barrier result at the same temperature of 7×10^{-11} cm^3 s^{-1}. (Herbst, 1980a,b).

A more approximate use of ternary (three-body) association in the determination of radiative association rates is to convert the measured ternary rate into the unmeasured radiative association. From **Eqs 13** and **15**, one can see that the removal of k_2 and its replacement by k_r converts a ternary rate coefficient into a radiative rate coefficient. This approach is most accurate if the ternary association is not in or near the collisionally saturated regime where complex formation occurs on every collision and **Equation 9** no longer holds. Although the SIFT apparatus is often used for the conversion, its operating density at roughly 10^{16} cm^{-3} (Adams and Smith, 1978; Smith and Adams, 1978) can put it close to the saturation limit at very low temperatures (Schiff and Bohme 1979). A detailed study of this approach with an emphasis on the CRESU apparatus has been reported by Herbst (2022).

A number of additional complications can confuse the issue when there is more than one product possibly undergoing radiative association. For example, McEwan et al. (1980), with an ion-cyclotron apparatus, studied the association reactions

$$CH_3^+ + HCN \rightarrow CH_3NCH^+; CH_3CNH^+ \qquad (16)$$

at room temperature and found, over a large density range of 3.5×10^{10} cm^{-3}—7.0×10^{12} cm^{-3}, an observed rate coefficient of 2×10^{-10} cm^{-3}, independent of density, but less than an experimental result of 2×10^{-9} cm^{-3} at the much higher density of 10^{16} cm^{-3}, which can be assumed to be the saturated collisional rate. A subsequent experimental paper by Anicich et al. (1995) confirms that radiative association does indeed occur. But theoretical calculations by Defrees et al. (1985) indicate that the radiative association can produce both CH_3CNH^+ and CH_3NCH^+ and that the use of a master equation calculation leads to an approximate abundance ratio for CH_3NC/CH_3CN between 0.1 and 0.4.

Role in Molecular Synthesis in Cold Dense Clouds

In addition to the well-studied association reaction between CH_3^+ and H_2 (Gerlich and Horning, 1992), Smith (1992), reviewing the approach of Smith and Adams (1978) which used conversion from ternary association rates, concluded that association reactions between CH_3^+ and a variety of neutral molecules (e.g. CO, CH_3OH, H_2CO, NH_3, H_2O, HCN, CH_3CN, and HC_3N) can occur as radiative association in the low densities of interstellar clouds. The product molecular ions produced react subsequently via dissociative recombination with electrons to form neutral species including some now regarded as COMs, such as CH_2CO, CH_3OH, C_2H_5OH, CH_3OCH_3, CH_3CHO, CH_3NH_2, CH_3CN, CH_3NC, C_2H_5CN, and CH_3C_3N. (See **Figure 2** as shown in Smith, 1992). In addition to these processes, Huntress and Mitchell (1979) proposed analogous association reactions involving the ions CH_3O^+, CH_3CO^+, CH_5^+, HCO^+, NO^+, and H_2CN^+ leading to the synthesis of a large number of species up to eight atoms in size.

In retrospect, although some of these suggestions for COM formation have some merit pending more detailed theory or experiment, others may be optimistic because of a number of problems. First, much of the existing information on radiative association rates has been obtained by conversion of ternary collisional processes measured in the laboratory. As discussed above, this conversion ideally requires a collisional association process far removed from saturation, or extrapolation of ternary systems to low densities to reach the radiative limit (Gerlich and Horning, 1992; Luca et al., 2002). In the absence of evidence to the contrary, the radiative association reaction coefficients can be obtained from ternary measurements at higher temperatures where it its more likely that the three-body region is reached. The proper temperature dependence is then needed to obtain radiative association rates at lower temperatures. A large number of reported radiative association rate coefficients were tabulated by Smith and Adams (1978), using this approach. The value obtained for $CH_3^+ + H_2O$ at 20 and 50 K is considerably higher than the value obtained by Luca et al. (2002). Conversion using an ion-cyclotron apparatus, which can operate at low densities, is likely to avoid the high-density problem, although reaching low temperatures is also a problem. The complex case of CRESU studies has been discussed by Herbst (2022).

The second problem concerns the products of dissociative recombination reactions. Some of the rate coefficients for these processes had been known during the early years of astrochemistry and typically range from 10^{-6}—10^{-7} cm^3 s^{-1} at room temperature with a temperature dependence of $T^{-1/2}$. The neutral products and their branching fractions, however, were almost completely undetermined, to the best of our knowledge. Much of the early literature on chemical simulations of dense clouds contained the guess that the branching fractions were dominated by a product channel with one hydrogen atom and a heavy species, or by a heavy molecule with two hydrogen atoms removed. The situation regarding product branching fractions gradually improved with experiments using both bench top experiments (Herd et al., 1990) and large-scale experiments with magnetic storage rings (Zajfman et al., 2003; Mitchell et al., 2005; Geppert and Larsson, 2013). The net result is that branching fractions in which atomic H and a larger species are formed most often constitute a minor fraction of the products; e.g., 5–10%, not the 50–100% as assumed earlier. The case of NH_4^+ is an exception. Here the NH_3 + H channel has a measured

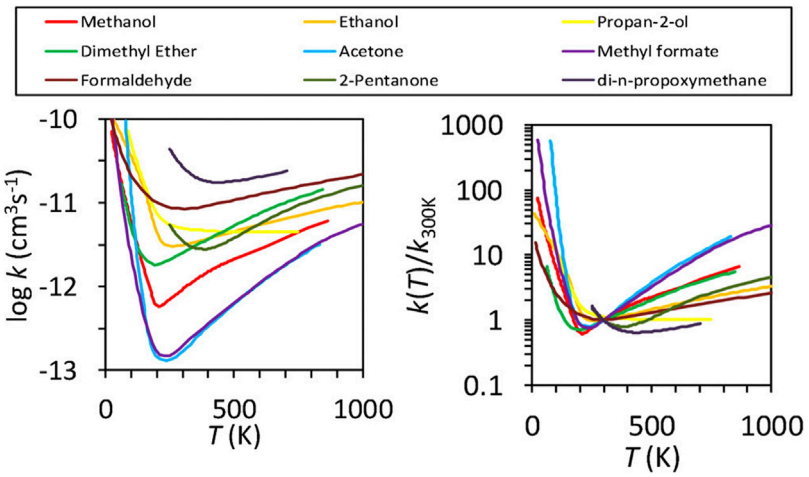

FIGURE 2 | Rate coefficients, *k* (left panel), and the ratio, *k*(T)/*k* (300 K) (right panel), as functions of temperature for reactions of OH with assorted organic molecules. The lines, which show the "U-shaped" dependence of rate on temperature, are interpolated fits to literature data. Permission requested to reproduce this figure, which originally appeared as **Figure 3** in Heard (2018).

branching fraction of 0.8—0.9, which can be partially explained by dynamic studies, which indicate that the dissociation occurs via the ground neutral potential (Öjekull et al., 2004). This process coupled with the efficient production of NH_4^+ (see below) allows the gas-phase production of ammonia to proceed efficiently at low temperatures.

If we consider the formation of methanol via the radiation association between CH_3^+ and H_2O to form $CH_3OH_2^+$ followed by the dissociative recombination to form methanol:

$$CH_3OH_2^+ + e \rightarrow CH_3OH + H, \tag{17}$$

and compare optimistic rates (Adams and Smith, 1978; Smith and Adams, 1978) with the best current estimates (Luca et al., 2002; Geppert et al., 2006), the overall rate using current estimates is the lower by 3-4 orders of magnitude. The net result is that the current explanation to explain the abundance of methanol probably does not involve the radiative association and dissociative recombination steps, but involves a totally different and much more rapid process: successive addition of atomic H to CO on grains followed by desorption into the gas:

$$CO - s \rightarrow HCO - s \rightarrow H_2CO - s \rightarrow H_3CO\,(H_2COH) - s \rightarrow CH_3OH\uparrow \tag{18}$$

where the s refers to surface species (Watanabe and Kouchi, 2002). Moreover, even if the radiative associative processes proposed by Smith and Adams (1978) and Huntress and Mitchell (1979) and reviewed by Smith (1992) are accurate, there is no guarantee that they are more important than other gas-phase and grain-surface mechanisms.

In addition to radiative association by ion-molecule systems, radiative association via two neutral species, typically radicals, has been suggested as a possible source of complex organic molecules. In particular, the radiative association between the radicals CH_3 and CH_3O to form CH_3OCH_3 (dimethyl ether) has been suggested as an important synthetic process in cold cores (Balucani et al., 2015). A phase space calculation at 10 K leads to a rate coefficient of 3×10^{-11} cm^3 s^{-1}, which is close to the collisional limit (Tennis et al., 2021). A number of other radical-radical association reactions are probably important in the upper atmosphere of Titan (Vuitton et al., 2012).

Reactions With a U-Shaped Rate Dependence on Temperature

As in radiative association, there are other bimolecular reactions in which both a collision complex and a barrier along a potential exist. The most interesting of these reactions are those in which the rate coefficient has a U-shaped temperature dependence in which the rate coefficient has a minimum at intermediate temperatures and then increases as the temperature increases and decreases from the minimum. One of the earliest studies of such a reaction concerns NH_3^+ and H_2 (Herbst et al., 1991):

$$NH_3^+ + H_2 \rightarrow NH_4^+ + H, \tag{19}$$

which has been studied both experimentally and theoretically. It was thought initially that this reaction could lead to the formation of ammonia in cold interstellar clouds (10 K) with the ammonia formed by dissociative recombination of NH_4^+. Early experimental studies, however, showed the reaction to be slow at room temperature with a rate coefficient of 5×10^{-13} cm^3 s^{-1}, and to increase in rate at higher temperatures with a fitted barrier of 2.1 kcal mol^{-1} (Smith and Adams, 1981). Such an activation energy would imply an exceedingly slow rate at low temperatures such as 10 K, leading to the need for another mechanism to produce ammonia in the cold interstellar medium. Smith and Adams (1981) then found surprisingly that although the rate coefficient decreased at temperatures down to about 100 K, it then leveled off at 80—100 K. An ion-trap study by Luine and

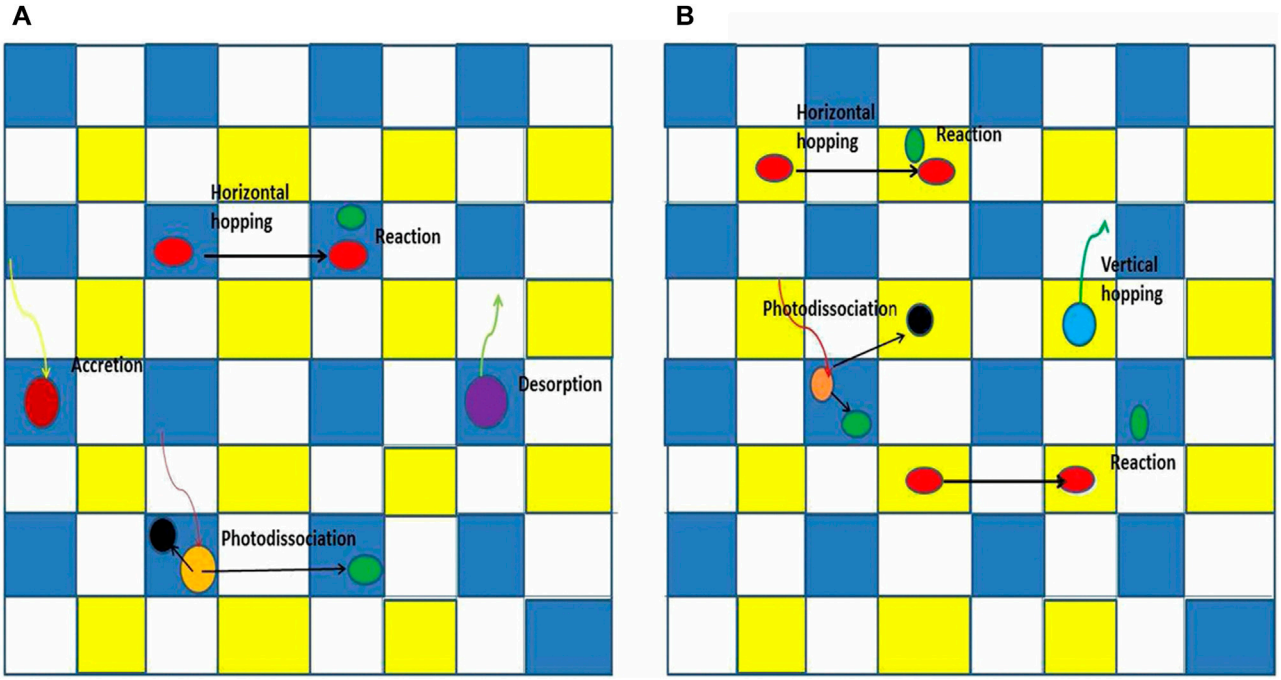

FIGURE 3 | Drawings of stochastic motions in a rectangular grid of sites in two situations. Major stochastic processes on grain surfaces in the form of a rectangular grid of sites. Blue sites are normal sites, occupied by normal species, while yellow sites are interstitial sites, normally unoccupied or occupied by weakly bound interstitial species, and white sites cannot be occupied. **(Panel A)** shows the topmost layer, while **(Panel B)** shows an inner (bulk) layer. Figure reproduced from **Figure 1** of Chang and Herbst. (2014).

Dunn (1985) and a drift-tube study by Böhringer (1985) found that the rate coefficient actually begins to increase at still lower temperatures, reaching approx.10^{-12} cm^3 s^{-1} at 10 K, a rate coefficient large enough to reinstate reaction (19) followed by dissociative recombination as a prime candidate to produce ammonia in the cold ISM. The initial suggestion for a mechanism to explain the overall temperature dependence of $NH_3^+ + H_2$ was a complex in the entrance channel followed by tunneling under a subsequent transition state barrier. (See **Figures 1**, **2** of Herbst et al., 1991). Quantum chemical and phase space calculations including tunneling led to satisfactory agreement with the experimental results (Herbst et al., 1991). An experimental study of an analogous reaction between $C_2H_2^+$ and H_2 at temperatures near 2 K also invoked a tunneling mechanism to explain the inverse temperature dependence (Hawley and Smith, 1989).

More recently, CRESU experiments have been employed to study a number of neutral-neutral reactions with the same U-shaped temperature dependence. The initial investigation was done by Shannon et al. (2013) on the system OH + CH_3OH:

$$OH + CH_3OH \rightarrow CH_3O + H_2O \qquad (20)$$

and showed a strong inverse temperature dependence at temperatures below 70 K, with the result at 63 K two orders of magnitude higher than at 200 K. See also the subsequent measurements of Ocaña et al. (2019) at temperatures from 177.5 K down to 11.7 K. Note that at lower temperatures, the dominant product is methoxy (CH_3O) rather than the lower energy form hydroxymethane (H_2COH), although transition states for both processes exist. Shannon et al. (2013) suggested the same mechanism mentioned above by Herbst et al. (1991) in which the formation of a hydrogen-bonded complex is followed by tunneling under a barrier. To support this mechanism, they utilized the MESMER code (Glowacki et al., 2012), which handles multiple potential wells, to reproduce their experimental results. A specific theoretical approach is discussed by Cooke and Sims (2019) for reactions involving CN. Here the system first enters a so-called loose transition followed by a tight transition state, which can be still lower in energy than the reactants. The results of a two-transition state model are shown in their **Figure 3**. The dominant transition state switches from loose at low temperatures to tight at higher temperatures.

Much experimental and theoretical work followed the initial work of Shannon et al. (2013). Heard (2018) plotted a large number of reactions studied with the CRESU technique involving the radical OH and a variety of organic species that have a U-shaped rate dependence on temperature. **Figure 2** reproduces the plot: one panel shows the rate coefficient vs temperature, the other the rate coefficient divided by the 300 K value vs temperature. Both show the characteristic U-shape with an increase in rate down to temperatures near 10 K. One point of contention is whether or not the process is binary or tertiary, given the high density of the CRESU experiments. Low temperature results on OH + CH_3OH show the results to be independent of total density, hence binary, but there are

theoretical (Gao et al., 2018) and experimental results to the contrary. For example, Ocaña et al. (2019) showed the process to show some pressure dependence at 120–150 K, whereas no pressure dependence was found at temperatures below 100 K. A number of other theoretical treatments, including the quasi-classical trajectory approach and the ring polymer approach have been discussed by Canosa (2019). From the point of view of astrochemistry, if the OH + CH_3OH reaction is indeed rapid and binary at 10 K, it is clearly important in the formation of CH_3O (Acharyya et al., 2015; Balucani et al., 2015). The methoxy radical can then undergo radiative association with the methyl radical (CH_3) to form dimethyl ether (Balucani et al., 2015).

GRANULAR PROCESSES

Reactions on interstellar grains play an important role in interstellar chemistry, especially for low temperature regions, where dust particles are covered by a thick layer of ices dominated by water, CO, and CO_2. Perhaps the most important process, however, is the formation of molecular hydrogen from two hydrogen atoms, which can even occur in diffuse clouds. A detailed review of this process has recently appeared (Wakelam et al., 2017). Hydrogen atoms are also important in the formation of surface methanol from carbon monoxide, where four reactions are needed, as shown in **Equation 18**. Methanol remains the most complex molecule detected on grain surfaces, although theoretical calculations show that molecules as complex as glycine can also be formed on granular surfaces (Garrod, 2013a).

Direct experiments on surface reactions (Minissale et al., 2013; He et al., 2015), and on related processes such as non-thermal reactive desorption (Minissale et al., 2016), photodesorption (Fayolle et al., 2011), radiolysis (Tomosada et al., 2012), and photodissociation followed by reaction (Dupuy et al., 2021) have also been undertaken. Experimental tests of reaction mechanisms—diffusive (Langmuir-Hinshelwood; Katz et al., 1999) and Eley-Rideal (Yuan et al., 2014)—have also been performed, although the latter occurs rarely. Measurements on diffusive surface reactions can often be fit by models of diffusion with important parameters being two types of barriers—those due to diffusion and those due to chemical activation (Herbst and Millar, 2008). Simple models for diffusion are often used in place of more complex analyses of reactions when inserted into chemical simulations. Unlike the case of gas-phase reactions though, the connection between laboratory experiments and processes in the low-density interstellar medium is a complex one, and necessitates a larger amount of theoretical discussion.

For many years, the chemistry occurring on ice mantles surrounding interstellar grains of carbon or silicates has been treated by coupled rate equations which treat reactions via random diffusive motion of weakly bound adsorbates, a process known as the Langmuir-Hinshelwood mechanism (Hasegawa, 1993). There are two main problems with this approach, although both can be ameliorated if not totally cured. The first problem, historically, has to do with the small number of reactive species that can be available for reactions on a single grain, which leads to the need for discrete treatments with uncertainties (Biham et al., 2001; Green et al., 2001). This need can be treated by a variety of stochastic methods, or, less rigorously, by a modification of the diffusive rate equations. The second, which is much less historical, has to do with the rate of diffusion at low temperatures, which can in some instances be too slow to explain the synthesis of large molecules. The solution here is to find more rapid processes, which typically involve three bodies and are at least partially non-diffusive in nature (Jin and Garrod, 2020).

Rate Equations vs Stochastic Treatments

Before we discuss stochastic treatments of the chemistry occurring on interstellar dust particles, we need to review the more standard rate equations. Rate equations in standard chemical treatments normally contain the assumption that large numbers of species are involved so that chemical concentrations can be treated as averages. This assumption is normally so common that chemists don't even have to worry about the possibility that the assumption need not hold in all instances. Although the rate equations for gas-phase processes in the interstellar medium can use this standard form, the equations for chemistry on dust particles are more complex (Hasegawa, 1993). Here the simplest approach is to compute the probability that a moving particle A, normally assumed to be weakly bound or "physisorbed" to the grain or to a lower monolayer of the ice mantle, will hop over a potential or tunnel through it and react according to the probability that a second particle B is available for reaction at the adjacent site. The probability that this adjacent site contains a reactive molecule is simply the fraction of granular minimum energy sites occupied by B. The first-order (s^{-1}) hopping rate for a species A is given by the equation:

$$k_{hop} = \nu \exp\left(-\frac{E_b}{T}\right) \tag{21}$$

where ν is the "attempt" frequency and E_b is the diffusive energy barrier, which is normally assumed to be a fraction of the desorption energy. The term "attempt frequency" stands for the pre-exponential term when it is in frequency units. For physisorbed species, it is typically 1-3 x 10^{12} s^{-1}. The tunneling rate, typically through a rectangular barrier with a width of a = 0.1–0.2 nm, is given by the expression

$$k_{tun} = \nu \exp\left[-2\left(\frac{a}{\hbar}\right)\sqrt{2\mu E_b}\right], \tag{22}$$

where μ is the reduced mass of A and B, although more realistic potentials such as the Eckart potential have been utilized. The overall rate of diffusive reaction occurring via hopping to an adjacent site in which A and B react to form AB is given by the equation

$$\frac{d[AB]}{dt} = -\left(\frac{d[A]}{dt} + \frac{d[B]}{dt}\right) = -\left(k_{\mathrm{hop,A}} + k_{\mathrm{hop,B}}\right)[A][B]/N, \tag{23}$$

where [A] and [B] are defined by the number of sites they occupy while N is the number of sites on the monolayer on which A and B diffuse, which is typically 10^6 for a grain of 0.1 μ. The formula can be extended to inner monolayers of the mantle. This

approach does not account for long-range motion in between collisions (Willis and Garrod, 2017).

If species A and B react without a chemical activation barrier, the probability of a reaction between the two species is 100% if located in the same site. If, on the other hand, there is a chemical activation energy barrier E_A, the rate of reaction is reduced. While tunneling is often assumed to occur for chemical reactions, it is often ignored for diffusive barriers. There are two ways to account for activation energy. In the simpler of the two, one multiplies the right-hand side of **Equation 23** with a Boltzmann term of the type $\kappa = \exp(-E_A/T)$ or an equivalent form for tunneling with E_A replacing E_b in **Equation 22**. The second and more accurate method, known as the competitive approach, defines κ in terms of the competition between the diffusive barrier and the activation energy barrier. Assume that the activation energy is much smaller than the diffusive barrier. Then the species A and B will have many chances to react before they move off to other sites. On the other hand, if the activation energy is much larger than the diffusive barrier, the A and B species will be much more likely to move on rather than react. If we assume that tunneling under the activation energy barrier dominates diffusive hopping, the formula for κ is given by (Herbst and Millar, 2008):

$$\kappa = \frac{k_{tun}}{k_{tun} + k_{hop,A} + k_{hop,B}}. \quad (24)$$

If the activation tunneling exceeds the diffusive hopping, κ approaches unity, so that the activation energy is essentially zero.

Although the earliest gas-grain models of interstellar chemistry assumed that diffusion occurred throughout the ice mantle, an approach known as a two-phase model, it is now more common to utilize a three-phase model, where the three phases refer to the gas, the surface of the ice mantle, and the bulk mantle ice. It is typically assumed that diffusion is slower in the bulk (Garrod, 2013a; Ruaud et al., 2015, Ruaud et al., 2016). Three-phase gas-grain models (e.g., Nautilus and Magickal) have been reasonably successful in simulating the chemistry of cold dense cores, hot cores, protoplanetary disks, and photon-dominated regions.

Stochastic Approaches

But suppose that we deal with small closed systems, such as the surfaces of tiny dust particles, in which there may be small numbers of reactive species, and suppose there are many such dust particles. One could take the standard volume average used in rate equations and get a totally wrong answer. As an extreme example, assume that on each dust grain there exists one hydrogen atom and we are interested in the rate of the formation of molecular hydrogen. The rate approach would ignore on which grains the hydrogen atoms exist, and come up with a non-zero rate of formation of H_2. But it is obvious that in reality the answer would be that zero hydrogen molecules are formed. Of course, a more common situation might be that only a few hydrogen atoms exist per grain, so that the rate of formation of H_2 over a large number of grains would be non-zero, but the uncertainties in these small numbers per grain would be quite large. So, a more accurate treatment under these conditions would include discrete numbers of species per grain with large fluctuations. Such techniques include the master equation approach, in which differential equations involving probabilities are used instead of normal rate equations. Each differential equation consists of the relationship between the time derivative of the probability that a specific discrete number of each species, say three atoms of species A, and terms involving the incoming flux of species from the gas, the desorption rate of molecules from the surface, and the recombination on the surface, all involving the probability of gain or loss of three atoms of species A.

Let us take the simple system of atomic and molecular hydrogen, as done by Biham et al. (2001), and consider the time dependence of the probability of zero hydrogen atoms $P_H(0)$ on a grain. The appropriate differential equation is given by:

$$\frac{dP_H(0)}{dt} = -F_H P_H(0) + W_H P_H(1) + 2 \times 1 \times A_H P_H(2). \quad (25)$$

Here the first term on the right concerns incoming flux (which does not occur), the second term consists of desorption, in which one atom on a grain desorbs and increases the probability that no atoms remain, while the third term increases the probability that no atoms remain by the recombination of two hydrogen atoms on a grain. The master equation consists of all of the differential equations involving the time-dependent probability of discrete numbers of H atoms and H_2 molecules. In principle, there is no limit to the number of equations, but if only one monolayer is considered the limit can be obtained from the number of adsorption sites. Assuming that the number of species of H or H_2 eventually decreases, cut-off can occur when the probability of a given number becomes arbitrarily small. From the individual probabilities, an expectation value can be obtained as well as the average of the squared probabilities, leading to a standard deviation of the concentrations of H and H_2. The results are normally tabulated in terms of a recombination efficiency, which is equal to the flux of desorbing H_2 per adsorbed H atoms. For large grains, the standard rate treatment and the master equation treatment get the same efficiency. For smaller grains, however, the standard rate approach and the master equation approach differ; the smaller the grain, the larger the difference. In particular, recombination efficiency of the standard rate approach stays constant at a given value while the master equation efficiency decreases beyond a certain size grain. The drop occurs because the average number of H atoms approaches a number smaller than 2, confirming that for small grains, there is insufficient atomic hydrogen to produce H_2.

Biham et al. (2001) also developed a somewhat more complex system, which involves both oxygen and hydrogen atoms and the molecules formed from them—H_2, OH, O_2, and H_2O– as had been studied by Caselli et al. (1998) in a study of how to improve rate equations. They also showed that to a good approximation one can use rate equations for some species and the master equation for the others. This hybrid approach is useful when extending the simulations to larger gas-grain systems (Stantcheva et al., 2002).

In addition to Biham et al. (2001), early master equation stochastic treatments include those of Charnley (2001), and Green et al. (2001). Green et al. (2001) used a similar master equation technique to study the simple system of H and H_2, as had Biham et al. (2001), but solved the system exactly rather than numerically. They also studied the hydrogen-oxygen system of Caselli et al. (1998) as well as a more complex system of these authors involving the atoms H, N, and O forming the additional molecules NH, NH_2, NH_3, N_2, and NO.

Charnley (2001) used a system of reactions involving the adsorption of H, O, CO and exothermic reactions. He calculated the surface abundances of CO, CO_2, O_2, and H_2O as a function of time. Stantcheva et al. (2002) used a somewhat larger system, which followed the reactions and products starting with H, O, and CO species in the gas, including ten reactions to produce H_2, OH, H_2O, HCO, H_2CO, H_3CO, CH_3OH, O_2 and CO_2. These surface species were divided into major and minor ones. The purpose of the division is to restrict the master equation to minor species on the surface, so simpler and fast normal rate equations can be used for major species on the surface and all species in the gas. The master equation of Stantcheva et al. (2002) included a five-fold joint probability $\frac{dP}{dt}(i_1, i_2, i_3, i_4, i_5)$ for minor species (H, O, OH HCO, H_3CO) on the surface. In a subsequent paper, Stantcheva and Herbst. (2004) reported the results of a gas-grain model, in which rate equations were used for the gas chemistry and a master equation for the surface chemistry.

Master equation solutions can be mimicked by an assortment of Monte Carlo techniques, in which random numbers are utilized to follow the motions of species. Depending upon the degree of detail, Monte Carlo calculations can be divided into macroscopic and microscopic approaches, the latter determining the position of all atoms in an ensemble such as a dust particle, whether on lattices or off them. Although interstellar clouds are composed of both gas and dust particles, the problems discussed up to now clearly involve mainly the dust chemistry.

The advantage of the master equation approach over the Monte Carlo approach is that the differential equations for the surface species—master equation or rate equation—and the gas-phase species can be solved simultaneously. When a Monte Carlo approach is utilized for the surface, rate equations cannot be used for the gas-phase species because the clocks for rate equations and for random number generation are different. One can use a macroscopic Monte Carlo approach for the gas-phase chemistry, in which the coordinates of individual molecules are not followed, while a microscopic Monte Carlo approach can be used for the more detailed trajectories of the atoms and molecules on and in the ice mantle. Although this hybrid Monte Carlo approach may be slower than the master equation approach, it is less difficult to set up, especially when dealing with large numbers of equations. The Monte Carlo procedure has two advantages over the master equation approach: it can be used for inhomogeneous surfaces, and it treats random walk correctly.

There are a number of different Monte Carlo techniques depending upon the problem to be solved.

An early approach was used by Tielens and Hagen (1982). Another approach—a purely microscopic system - has been used to study molecular hydrogen formation on various regular and irregular surfaces (Chang et al., 2005; Iqbal et al., 2012). Here we report studies that use a technique known sometimes as the continuous-time random walk approach (CTRW), formulated originally by Montroll and Weiss (1965). The CTRW technique can follow the motion of atoms between discrete surface sites, which cannot be done with other MC techniques (**Figure 3**). The basic idea is to call random numbers to determine where on a surface a given type of atom is, what process it is undergoing, and at what time it occurs (Chang et al., 2005). The physics occurs on a 2D or 3D grid of boxes, with the boxes representing sites for atoms or molecules, ranging from atop the mantle to deep within the granular structure. The output consists of the molecules in specific binding sites on the surface or a number of monolayers atop the ice mantle as a function of time. although barriers between sites can slow the process, as mentioned above. The time between successive events is known as a waiting time, and the waiting time between successive events for a given process is given by a Poisson distribution with a random number in the range (0,1). The system moves forward by choosing the process with the time in the future nearest the current time.

For a simulation in which both gaseous and granular chemistry occur, two variants of the CTRW process are needed. In macroscopic approaches, used for the gas, one starts with an initial volume V containing initial abundances of gaseous atoms and molecules (Charnley, 1998; Vasyunin et al., 2009; Chang and Herbst, 2012). The following discussion comes from Chang et al. (2005). Here, the volume is not divided into sites. The unimolecular rate (s^{-1}) for each reaction considered, designated r_i, is calculated according to the type of process: a one-body process such as photodissociation, a two-body process such as any two-body reaction, and accretion onto a grain. The time for each reaction *i* to occur—the so-called waiting time –is given by the expression $\tau_i = -\ln(Z)/r_i$, where Z is a random number in the range (0,1). For example, if Z = ½, the waiting time is equal to $0.693/r_i$, and if Z = 0.9, the waiting time is $0.105/r_i$. We then consider the absolute time for each reaction by adding the waiting time to either the time when the reaction last occurred or when the chemistry started. If the *i*th reaction occurs first, we recalculate the concentrations of reactants and species involved in this reaction. The rates of other reactions are also recalculated if the numbers of their reactants change.

The microscopic approach, used for the grain chemistry, must be coupled to the macroscopic model for the gas. The details of the coupling are discussed by Chang and Herbst (2012). Comparison between microscopic-macroscopic Monte Carlo and master equation calculations for small gas-grain systems can show reasonable agreement. For large gas-grain systems the macroscopic-microscopic system is by far the easier to use even though treatment of the gas-phase chemistry does require the macroscopic CTRW approach. The microscopic Monte Carlo approach for three-dimensional dust mantles is very time-consuming, however, and, in addition, there are problems caused by the random number generation for systems in which concentrations vary greatly. For example, the concentration of molecular hydrogen is so much larger than all other species that specific fixes are needed to avoid choosing H_2 each time a random species is picked. A few large-scale

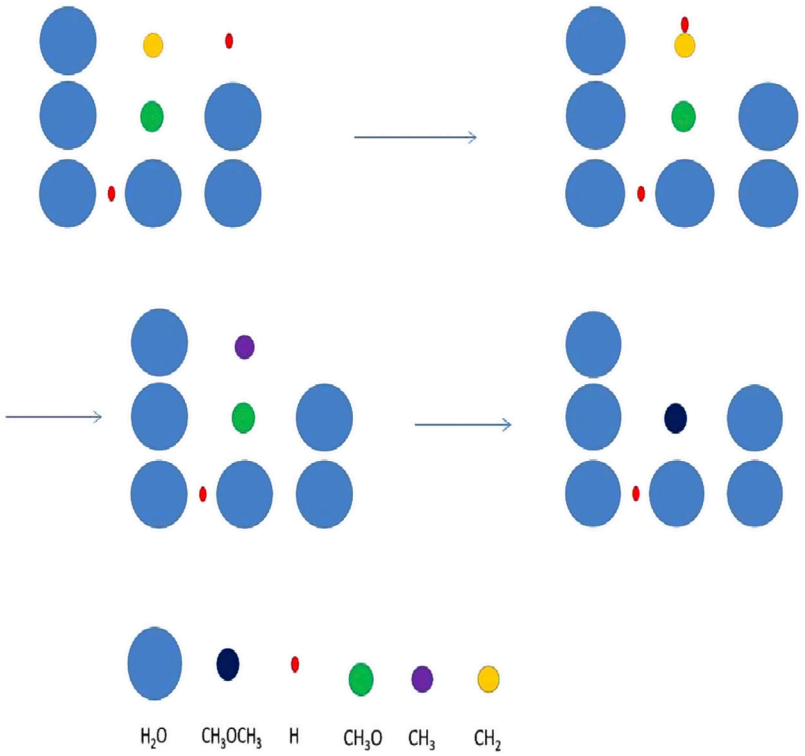

FIGURE 4 | A mechanism of stochastic surface motions leading to the formation of dimethyl ether. The mechanism is labelled three-body motion or a chain reaction, and here consists of a diffusive and a short distance nondiffusive motion. The process commences when H and CH_2 produce CH_3, mainly by diffusive motion by atomic hydrogen. The methyl radical (purple) quickly reacts with a methoxy radical (CH_3O) lying immediately beneath it in a diffusionless manner to form dimethyl ether. Figure reproduced from **Figure 1** of Chang and Herbst (2016).

simulations have been done with the microscopic-macroscopic technique (see **Figure 4**), and the chemical simulations show that stochastic methods can be used to produce complex organic molecules at low temperatures (Chang and Herbst, 2014, Chang and Herbst, 2016). A third stochastic approach, known as the hybrid moment approach, has also been formulated (Du and Parise, 2011) and found to be faster than the Monte Carlo method.

The simulations of surface, mantle, and bulk chemistry of grains can be divided into two types of methods, known as on-lattice and off-lattice approaches. The on-lattice approach equates a grid of boxes with sites in which molecules can be found, but can still mimic irregular systems. The off-lattice uses an actual potential, typically composed of sums of Lennard-Jones potentials. Motion of atoms and molecules then leads to a change in the overall potential. Off-lattice calculations are often used for the joint build-up of dust particles, determination of porosity, and the chemistry that occurs during the build-up (Garrod, 2013b; Christianson and Garrod, 2021).

Modifications of Rate Equations

Given the difficulties of carrying out chemical simulations using stochastic approaches, several investigators have attempted to modify the rate equations to bring the results closer to those of stochastic calculations. The first attempt was reported by Caselli et al. (1998), who used several simple systems at 10 K. In the first, a gas of O and H atoms accretes onto grain surfaces to form H_2, OH, and O_2, while in the second, N atoms are also added to the gas to form the additional surface molecules NH_3 and H_2O. In the third system the gas also contains H_2. Monte Carlo simulations similar to those of Tielens and Hagen (1982) were used to calculate chemical abundances, and a number of modifications to the rate equations were tested to see how well the modifications allow the rate equation approach to reproduce the results of the Monte Carlo approach. Suitable modifications involving the O, H system were found for the following diffusive rate coefficients: k_{HH}, k_{HO}, and k_{OO}, by converting them to sums of rates of evaporation and sweeping, or accretion and sweeping, depending upon whether x > 1 or x < 1 where x is defined by the division of the evaporation rate of H by the accretion rate of H ($t_{evap}^{-1}/t_{acc}^{-1}$). With these corrections and some others, it was possible to reproduce some Monte Carlo results for the simple system. The authors noted that the use of modifications for complex gas-grain systems will lead to smaller effects given the large number of alternative pathways. This outcome was tested by Shalabiea et al. (1998) using the time-dependent gas-grain model for dark interstellar clouds of Hasegawa and Herbst (1993); it was also found that the modifications were needed at only the earliest times.

An improved set of modifications was introduced by Garrod, (2008), and utilized and compared successfully with a large gas-grain simulation treated by the unified Monte Carlo method of Vasyunin et al. (2009). One important rate coefficient concerns the switch-over between deterministic and stochastic contributions. It is based on two equations, the first of which governs the rate of the probabilistic surface reaction between species A and B, $R_{\rm mod}$ (AB):

$$R_{mod}(AB) = R_{arr}(B)\cdot P(A)\cdot \eta_{AB}(A) + R_{arr}(A)\cdot P(B)\cdot \eta_{AB}(B) \quad (26)$$

where $R_{\rm arr}$ stands for arrival/formation rate of a species, P for the probability of a species being present when the other arrives, and η for the efficiency of the reaction between A and B. The efficiency takes into account competition with selected other reactions. The probability P(i = A or B) is given by the Poisson probability distribution {N(i)}, which can be obtained by use of a random number. The other major equation yields the total production rate, which includes the deterministic and modified rates for reaction A+ B:

$$R_{tot}(AB) = f_{AB}\cdot R_{mod}(AB) + (1 - f_{AB})\cdot k_{AB} \cdot < N(A) >< N(B) > \quad (27)$$

Here f is a switching function, equal to 1 when both expectation values < N(A)> and <N(B)> are less than or equal to unity, but which is much lower when either of these quantities is greater than unity. The second term is written in terms of a rate coefficient, with expectation values of A and B, as shown in **Equation 15** of Garrod (2008).

These improved modified rate equations do an excellent job of reproducing the Monte Carlo calculations of Vasyunin et al. (2009). The modified rate approach of Garrod (2008) has also been used successfully to study the effect of surface inhomogeneity on surface reaction rates (Cuppen and Garrod, 2011), where it agrees well with CTRW Monte Carlo results for a study of the surface formation of molecular hydrogen.

Diffusionless Processes

The idea of diffusionless processes on a surface was first discussed by Theulé et al. (2013) and reviewed in Theulé (2020). If we consider two species in adjacent sites, they need not undergo a long-range barriered diffusive motion, although chemical activation energy can still play a role. In this situation, the rate coefficient can be given by the simple Arrhenius Law (Theulé, 2020):

$$k(T) = A\exp\left(-\frac{E_a}{T}\right) \quad (28)$$

where A is the pre-exponential factor and $E_{\rm a}$ is the activation energy in K. In the absence of such chemical activation energy, one can imagine a process that is essentially "instantaneous,"or, more realistically, on the order of a vibrational frequency. This two-body process can be considered part of a more complex process, one example of which is a three-body surface process. As an example, consider the formation of CO_2 on an ice mantle. The

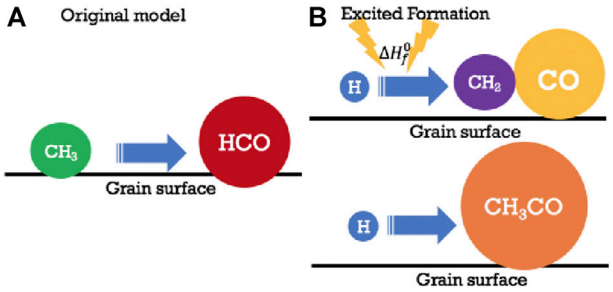

FIGURE 5 | Several other mechanisms involving diffusive and nondiffusive formation mechanisms on grains. In **(A)**, a simple diffusive reaction involving radicals CH_3 and HCO leads to acetaldehyde, albeit slowly at low temperatures. In **(B)** once again H and CH_2 produce CH_3, which in this case has sufficient energy from the exothermic process to react with a neighboring CO molecule to form CH_3CO, which can easily be hydrogenated with H atoms via diffusive reaction to form CH_3CHO. Permission given to reproduce this figure, originally appearing as **Figure 1** in Jin and Garrod. (2020), by IOP Publishing.

CO + O reaction has a significant activation barrier and also a diffusion barrier on the surface or inner ice monolayers. As a result, this process is rather slow at low temperatures. Imagine, on the other hand, two surface atoms H and O, which can diffuse rapidly even at 10 K (Katz et al., 1999; Minissale et al., 2014). If they form an OH radical, and the radical lies above a CO molecule in an inner monolayer, the OH and CO can undergo a well-known reaction to form CO_2 and H with a small activation energy in a rapid diffusionless process. So, this three-body process contains both diffusive and nondiffusive aspects (see **Figure 5**).

How does one treat the mathematics of combined diffusive and non-diffusive processes? If a CTRW stochastic treatment is used, the process occurs naturally since one follows the motion of all particles, using an on-lattice or off-lattice potential. For ordinary rate equations, a useful equation for the rate $R_{\rm AB}$ of either of these processes has been written by Jin and Garrod (2020):

$$R_{AB} = f_{act}(AB)R_{comp}(A)\left(\frac{N(B)}{N_S}\right) + f_{act}(AB)R_{comp}(B)\left(\frac{N(A)}{N_S}\right), \quad (29)$$

in which individual reactants can be treated separately. Here R_{AB} is an overall rate coefficient, $f_{\rm act}$ is the efficiency related to activation energy barriers (and κ; see **Eq. (24)**) if they exist, $R_{\rm comp}$ is a so-called "completion rate" for species A or B, and is defined by the specific process, $N(A)$ and $N(B)$ are the numbers of A and B species on the grain mantle, and N_S is the number of surface (or bulk) mantle sites. For an ordinary diffusive process with both A and B diffusing, the completion rate is related to the hopping or tunneling over a diffusive barrier, which is similar to **Equations 21** and **23**.

For a process between two species that do not undergo diffusive motion (e.g. CO + OH above), the completion rate involves the probability that A and B lie in adjacent sites and can

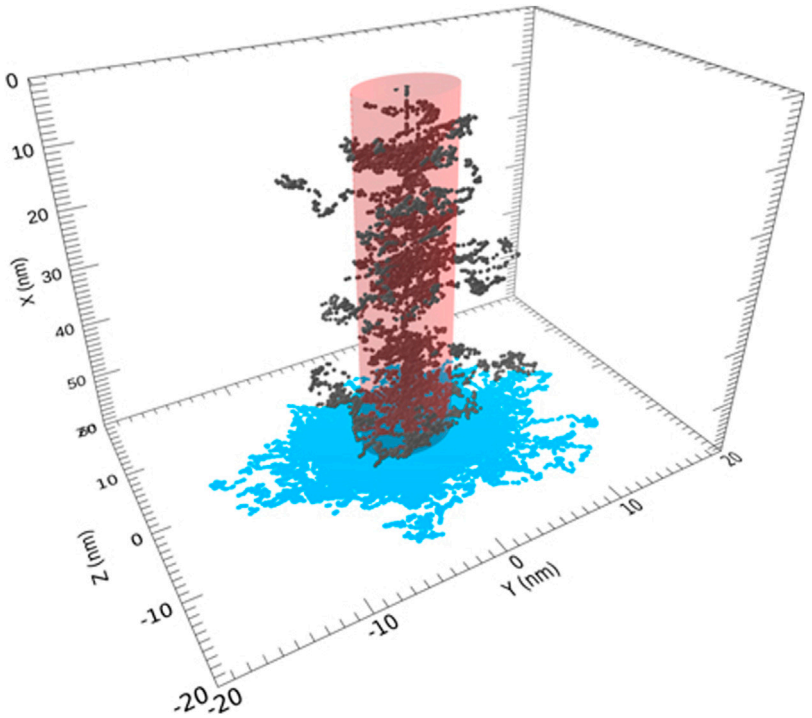

FIGURE 6 | Portion of the track for a 0.1 MeV proton and secondary electrons within the cylindrical region of amorphous ices is shown. The incident ion enters through the center of the top surface. Permission requested to reproduce this figure, originally appearing as **Figure 2** of Shingledecker et al. (2020).

undergo an "instantaneous" nondiffusive motion to lead to a product. For a diffusive process followed by a nondiffusive one (as is the case for CO_2 above), one can compute the diffusive rate via **Equation 29** to obtain the result for H + O forming OH, and multiply the result by the probability that OH lies above or adjacent to a CO molecule. Here use of **Equation 29** has a single R_{comp} for OH that does not include a Boltzmann term because the completion rate only involves the probability that a CO molecule lies in an adjacent site to OH, which is $N(CO)/N_S$. More complex approaches exist if there is activation energy for one process.

Particular values of R_{comp} are mentioned in Jin and Garrod (2020) for the following diffusionless processes: the Eley-Rideal mechanism, a number of types of three-body processes involving collisions, and photodissociation-induced reactions, in which photons produce a reactant. The Eley-Rideal mechanism involves no diffusion or horizontal motion; a species lands vertically atop an adsorbate and undergoes reaction. For example, suppose we consider the reaction between O and CO to form CO_2, a process that has an activation energy of about 1000 K. If the O atom lands upon CO at a constant rate, the value of $R_{comp}(O)$ is equal to its rapid accretion rate if there is no activation energy.

Now consider an unusual photodissociation process in which oxygen-containing species on a grain surface (e.g. O_2, H_2O) undergo photodissociation to produce a metastable state of an oxygen atom–O (^{1}D)—which lives for a long enough period to react nondiffusively with almost any other species on the grain mantle that lies in an adjacent site. There are two values of $R_{comp} = R_{photo}\ N(i)$ for each molecule i undergoing photodissociation to form O (^{1}D): one for external radiation and the other for cosmic-ray-induced radiation (Carder et al., 2021). The particular reaction with methane (CH_4) has been studied in the laboratory, and produces methanol and formaldehyde (Bergner et al., 2017). The results can be reproduced assuming that after photodissociation, the newly formed metastable oxygen instantaneously reacts with methane lying adjacent to or under the O (^{1}D) to form methanol and formaldehyde (Carder et al., 2021). Analogous reactions with larger hydrocarbons than methane can lead to larger complex organic molecules.

According to Jin and Garrod (2020), large organic molecules can be formed efficiently in cold regions with the inclusion of diffusionless processes of various types. An extension to higher temperatures can be found in Garrod et al. (2021). In addition to providing an explanation for the formation of complex organic molecules in cold interstellar clouds, the nondiffusive surface chemistry explains a number of experiments in the laboratory at low temperatures in which species such as glycolaldehyde, ethylene glycol, and methyl formate are produced starting from HCO and H_2CO (Fedoseev et al., 2015; Chuang et al., 2016). Although these experiments do not mimic interstellar conditions, they do provide additional evidence that nondiffusive chemistry does exist in interstellar clouds. Moreover, non-diffusive chemistry can often be much more efficient than diffusive chemistry at these low temperatures. In more recent work, an extension of the research of Jin and Garrod (2020) to determine the rate of formation of complex organic

molecules in regions of active star formation as temperatures rise shows a rather complex time and temperature dependence (Garrod et al., 2021).

Radiolysis

One approach in which both chemists and astronomers played a significant role is known as radiolysis. In this process, cosmic rays bombard an icy grain mantle to initiate a complex series of reactions starting with secondary electrons and neutrals and finishing up with neutral radicals, which can combine to form complex organic molecules as long as carbonaceous material, even as simple as CO or CO_2, is present in the ice. Cosmic rays are mainly highly ionized ions ranging in mass from protons to heavy nuclei. The laboratory study of radiolysis using high-energy protons or electrons but occasionally high-energy nuclei (Wakelam et al., 2021) is well advanced with many experiments in many laboratories (Bennett et al., 2005; Hudson and Moore, 2018; Christoffersen et al., 2020; Ioppolo et al., 2021) and some corresponding theory (see **Figure 6**). It was not until a few years ago that a theoretical approach to the chemistry was developed by astrochemists (Shingledecker et al., 2018), tested successfully against simple cold interstellar ices in the laboratory such as O_2 and amorphous water, and applied to interstellar icy mantles (Shingledecker and Herbst, 2018; Shingledecker et al., 2020). At the present stage, the theoretical approach has been used to study how radiolysis can form complex organic molecules such as methyl formate ($HCOOCH_3$) at low temperatures (Paulive et al., 2021).

SUMMARY

In this review, a number of unusual chemical processes thought to occur in the interstellar medium have been described. These processes include reactions in the gas phase and reactions on the surface and in the bulk of icy grain mantles. The understanding or partial understanding of these processes has aided both the fields of chemistry and astronomy. Although astrochemists can be first to suggest unusual processes that might help to solve astrochemical problems, more detailed studies—both theoretical and experimental—by chemists and chemical physicists can lead to a much greater knowledge of these unusual processes. The knowledge in turn can be used to improve chemical simulations and lead to an increase in what they can tell us about physical conditions and dynamics in the interstellar medium. Most of the unusual processes reviewed here have a history in which astrochemists played an important role, if not as exact an order as mentioned.

In the future, processes mentioned here such as radiative association, metastable reactions on icy surfaces, stochastic kinetics, and diffusionless surface reactions as well as other processes such as sputtering, negative ion formation, reactive desorption, reactive excitation, and nuclear spin astrochemistry will take a larger place in large chemical simulations and aid our understanding of the interstellar medium in general and star and planetary formation in particular.

AUTHOR CONTRIBUTIONS

EH has totally written this review manuscript.

FUNDING

This work was funded by the National Science Foundation (US) Division of Astronomical Sciences through Grant AST-19-06489.

REFERENCES

Acharyya, K., Herbst, E., Caravan, R. L., Shannon, R. J., Blitz, M. A., and Heard, D. E. (2015). The Importance of OH Radical-Neutral Low Temperature Tunnelling Reactions in Interstellar Clouds Using a New Model. *Mol. Phys.* 113, 2243–2254. doi:10.1080/00268976.2015.1021729

Adams, N. G., and Smith, D. (1978). Reactions of CH_3^+ Ions With Molecules at 300 K. *Chem. Phys. Lett.* 54, 530–534. doi:10.1016/0009-2614(78)85278-6

Anicich, V. G., Sen, A. D., Huntress, W. T., Jr., and McEwan, M. J. (1995). Association Reactions at Low Pressure. V. The CH_3^+/HCN System. A Final Word? *J. Chem. Phys.* 102, 3256–3261. doi:10.1063/1.468636

Balucani, N., Ceccarelli, C., and Taquet, V. (2015). Formation of Complex Organic Molecules in Cold Objects: the Role of Gas-phase Reactions. *MNRAS* 449, L16–L20. doi:10.1093/mnrasl/slv009

Barlow, S. E., Dunn, G. H., and Schauer, M. (1984). Radiative Association of CH_3^+ and H_2 at 13 K. *Phys. Rev. Lett.* 52, 902–905. doi:10.1103/PhysRevLett.52.902

Bates, D. R. (1979a). Ion-molecule Association. *J. Phys. B: Mol. Phys.* 12, 4135–4146. doi:10.1088/0022-3700/12/24/018

Bates, D. R. (1979b). Temperature Dependence of Ion-Molecule Association. *J. Chem. Phys.* 71, 2318–2319. doi:10.1063/1.438568

Bennett, C., Jamieson, C. S., Lebar, M. T., Osamura, Y., Mebel, A. M., and Kaiser, R. I. (2005). "A Combined Experimental and Theoretical Study on the Charged Particle Processing of Low Temperature Ices, *Astrochemistry: Recent Successes And Current Challenges*," in Proceedings of the 231st Symposium of the International Astronomical Union held in Pacific Grove, California, USA, August 29-September 2, 2005. Poster sessions., p.113.

Bergner, J. B., Öberg, K. I., and Rajappan, M. (2017). Methanol Formation via Oxygen Insertion Chemistry in Ices. *Astrophys. J.* 845, 29. doi:10.3847/1538-4357/aa7d09

Biham, O., Furman, I., Pirronello, V., and Vidali, G. (2001). Master Equation for Hydrogen Recombination on Grain Surfaces. *Astrophys. J.* 553, 595–603. doi:10.1086/320975

Black, J. H., and Dalgarno, A. (1973). The Formation of CH in Interstellar Clouds. *Astrophys. Lett.* 15, 79–82.

Black, J. H., and Dalgarno, A. (1977). Models of Interstellar Clouds. I - the Zeta Ophiuchi Cloud. *Astrophys. J. Suppl. Ser.* 34, 405–423. doi:10.1086/190455

Böhringer, H. (1985). Third-body-assisted, Binary Ion-Molecule Reactions. The Reaction $NH_3^+ + H_2 \rightarrow NH_4^+ + H$. *Chem. Phys. Lett.* 122, 185–189. doi:10.1016/0009-2614(85)80560-1

Canosa, A. (2019). Gas Phase Reaction Kinetics of Complex Organic Molecules at Temperatures of the Interstellar Medium: The OH + CH_3OH Case. *Proc. IAU* 15, 35–40. doi:10.1017/S1743921319006446

Carder, J. T., Ochs, W., and Herbst, E. (2021). Modelling the Insertion of $O(^1D)$ into Methane on the Surface of Interstellar Ice Mantles. *MNRAS* 508, 1526–1532. doi:10.1093/mnras/stab2619

Carruthers, G. R. (1970). Rocket Observation of Interstellar Molecular Hydrogen. *Astrophys. J.* 161, L81. doi:10.1086/180575

Caselli, P., Hasegawa, T. I., and Herbst, E. (1998). A Proposed Modification of the Rate Equations for Reactions on Grain Surfaces. *Astrophys. J.* 495, 309–316. doi:10.1086/305253

Chang, Q., Cuppen, H. M., and Herbst, E. (2005). Continuous-time Random-Walk Simulation of H_2 Formation on Interstellar Grains. *Astron. Astrophys.* 434, 599–611. doi:10.1051/0004-6361:20041842

Chang, Q., and Herbst, E. (2012). A Unified Microscopic-Macroscopic Monte Carlo Simulation of Gas-Grain Chemistry in Cold Dense Interstellar Clouds. *Astrophys. J.* 759, 147. doi:10.1088/0004-637X/759/2/147

Chang, Q., and Herbst, E. (2014). Interstellar Simulations Using a Unified Microscopic-Macroscopic Monte Carlo Model with a Full Gas-Grain Network Including Bulk Diffusion in Ice Mantles. *Astrophys. J.* 787, 135. doi:10.1088/0004-637X/787/2/135

Chang, Q., and Herbst, E. (2016). Unified Microscopic-Macroscopic Monte Carlo Simulations of Complex Organic Molecule Chemistry in Cold Cores. *Astrophys. J.* 819, 145. doi:10.3847/0004-637X/819/2/145

Charnley, S. B. (1998). Stochastic Astrochemical Kinetics. *Astrophys. J.* 509, L121–L124. doi:10.1086/311764

Charnley, S. B. (2001). Stochastic Theory of Molecule Formation on Dust. *Astrophys. J.* 562, L99–L102. doi:10.1086/324753

Chesnavich, W. J., and Bowers, M. T. (1977). Statistical Phase Space Theory of Polyatomic Systems: Rigorous Energy and Angular Momentum Conservation in Reactions Involving Symmetric Polyatomic Species. *J. Chem. Phys.* 66, 2306–2315. doi:10.1063/1.434292

Christianson, D. A., and Garrod, R. T. (2021). Chemical Kinetics Simulations of Ice Chemistry on Porous versus Non-porous Dust Grains. *Front. Astron. Space Sci.* 8, 21. doi:10.3389/fspas.2021.643297

Christoffersen, R., Keller, L. P., and Dukes, C. (2020). "The Role of Solar Wind Ion Processing in Space Weathering of Olivine: Unraveling the Paradox of Laboratory Irradiation Results Compared to Observations of Natural Samples," in 51st Lunar and Planetary Science Conference, The Woodlands, TX, March 16–20, 2020. LPI Contribution No. 2326, id.2147.

Chuang, K.-J., Fedoseev, G., Ioppolo, S., van Dishoeck, E. F., and Linnartz, H. (2016). H-atom Addition and Abstraction Reactions in Mixed CO, H_2CO and CH_3OH Ices - an Extended View on Complex Organic Molecule Formation. *MNRAS* 455, 1702–1712. doi:10.1093/mnras/stv2288

Cooke, I. R., and Sims, I. R. (2019). Experimental Studies of Gas-phase Reactivity in Relation to Complex Organic Molecules in Star-Forming Regions. *ACS Earth Space Chem.* 3, 1109–1134. doi:10.1021/acsearthspacechem.9b00064

Cuppen, H. M., and Garrod, R. T. (2011). Modelling of Surface Chemistry on an Inhomogeneous Interstellar Grain. *Astron. Astrophys.* 529, A151. doi:10.1051/0004-6361/201016013

Defrees, D. J., McLean, A. D., and Herbst, E. (1985). Theoretical Investigation of the Interstellar CH_3CN CH_3NC Ratio. *Astrophys. J.* 293, 236–242. doi:10.1086/163229

Draine, B. T. (2011). *Physics of the Interstellar and Intergalactic Medium*. Princeton, New Jersey: Princeton University Press.

Du, F., and Parise, B. (2011). A Hybrid Moment Equation Approach to Gas-Grain Chemical Modeling. *Astron. Astrophys.* 530, A131. doi:10.1051/0004-6361/201016262

Dupuy, R., Bertin, M., Féraud, G., Michaut, X., Marie-Jeanne, P., Jeseck, P., et al. (2021). Mechanism of Indirect Photon-Induced Desorption at the Water Ice Surface. *Phys. Rev. Lett.* 126, 15600. doi:10.1103/PhysRevLett.126.156001

Elitzur, M., and Watson, W. D. (1978). Formation of Molecular CH^+ in Interstellar Shocks. *Astrophys. J.* 222, L141–L144. doi:10.1086/182711

Falgarone, E., and Puget, J.-L. (1995). The Intermittency of Turbulence in Interstellar Clouds: Implications for the Gas Kinetic Temperature and Decoupling of Heavy Particles from the Gas Motions. *Astron. Astrophys.* 293, 840–852.

Fayolle, E. C., Bertin, M., Romanzin, C., Michaut, X., Öberg, K. I., Linnartz, H., et al. (2011). CO Ice Photodesorption: A Wavelength-dependent Study. *Astrophys. J.* 739, L36. doi:10.1088/2041-8205/739/2/L36

Federman, S. R., Glassgold, A. E., Jenkins, E. B., and Shaya, E. J. (1980). The Abundance of CO in Diffuse Interstellar Clouds - an Ultraviolet Survey. *Astrophys. J.* 242, 545–559. doi:10.1086/158489

Fedoseev, G., Cuppen, H. M., Ioppolo, S., Lamberts, T., and Linnartz, H. (2015). Experimental Evidence for Glycolaldehyde and Ethylene Glycol Formation by Surface Hydrogenation of CO Molecules under Dense Molecular Cloud Conditions. *MNRAS* 448, 1288–1297. doi:10.1093/mnras/stu2603

Gao, L. G., Zheng, J., Fernández-Ramos, A., Truhlar, D. G., and Xu, X. (2018). Kinetics of the Methanol Reaction with OH at Interstellar, Atmospheric, and Combustion Temperatures. *J. Am. Chem. Soc.* 140, 2906–2918. doi:10.1021/jacs.7b12773

Garrod, R. T. (2008). A New Modified-Rate Approach for Gas-Grain Chemical Simulations. *Astron. Astrophys.* 491, 239–251. doi:10.1051/0004-6361:200810518

Garrod, R. T. (2013a). A Three-phase Chemical Model of Hot Cores: The Formation of Glycine. *Astrophys. J.* 765, 60. doi:10.1088/0004-637X/765/1/60

Garrod, R. T., Jin, M., Matis, K. A., Jones, D., Willis, E. R., and Herbst, E. (2021). *Astrophys J. Supp. Ser.*. In press.

Garrod, R. T. (2013b). Three-dimensional, Off-Lattice Monte Carlo Kinetics Simulations of Interstellar Grain Chemistry and Ice Structure. *Astrophys. J.* 778, 158. doi:10.1088/0004-637X/778/2/158

Geppert, W. D., Hamberg, M., Thomas, R. D., Österdahl, F., Hellberg, F., Zhaunerchyk, V., et al. (2006). Dissociative Recombination of Protonated Methanol. *Faraday Discuss.* 133, 177–190. doi:10.1039/B516010C

Geppert, W. D., and Larsson, M. (2013). Experimental Investigations into Astrophysically Relevant Ionic Reactions. *Chem. Rev.* 113 (12), 8872–8905. doi:10.1021/cr400258m

Gerlich, D., and Horning, S. (1992). Experimental Investigation of Radiative Association Processes as Related to Interstellar Chemistry. *Chem. Rev.* 92, 1509–1539. doi:10.1021/cr00015a003

Giusti-Suzor, A., Roueff, E., and Regemorter, H. v. (1976). A New Calculation of the Radiative Association Rate of the CH^+ radical: Comparison between Semiclassical and Quantal Results (Interstellar Abundance). *J. Phys. B: Mol. Phys.* 9, 1021–1033. doi:10.1088/0022-3700/9/6/024

Glowacki, D. R., Liang, C.-H., Morley, C., Pilling, M. J., and Robertson, S. H. (2012). MESMER: an Open-Source Master Equation Solver for Multi-Energy Well Reactions. *J. Phys. Chem. A.* 116, 9545–9560. doi:10.1021/jp3051033

Green, N. J. B., Toniazzo, T., Pilling, M. J., Ruffle, D. P., Bell, N., and Hartquist, T. W. (2001). A Stochastic Approach to Grain Surface Chemical Kinetics. *Astron. Astrophys.* 375, 1111–1119. doi:10.1051/0004-6361:20010961

Hasegawa, T. I., Herbst, E., and Leung, C. M. (1992). Models of Gas-Grain Chemistry in Dense Interstellar Clouds with Complex Organic Molecules. *Astrophys. J. Suppl. Ser.* 82, 167–195. doi:10.1086/191713

Hasegawa, T. I., and Herbst, E. (1993). New Gas-Grain Chemical Models of Quiescent Dense Interstellar Clouds: the Effects of H_2 Tunnelling Reactions and Cosmic ray Induced Desorption. *MNRAS* 261, 83–102. doi:10.1093/mnras/261.1.83

Hawley, M., and Smith, M. A. (1992). The Gas Phase Reaction of $C_2H_2^+$ with H_2 below 3 K the Reopening of the Bimolecular $C_2H_2^+ + H_2$ Channel at Low Energy. *J. Chem. Phys.* 96, 1121–1127. doi:10.1063/1.462198

He, J., Vidali, G., Lemaire, J.-L., and Garrod, R. T. (2015). Formation of Hydroxylamine on Dust Grains via Ammonia Oxidation. *Astrophys. J.* 799, 49. doi:10.1088/0004-637X/799/1/49

Heard, D. E. (2018). Rapid Acceleration of Hydrogen Atom Abstraction Reactions of OH at Very Low Temperatures through Weakly Bound Complexes and Tunneling. *Acc. Chem. Res.* 51, 2620–2627. doi:10.1021/acs.accounts.8b00304

Herbst, E. (2022). "Cold Chemistry and beyond, Chapter 10," in *Uniform Supersonic Flows in Chemical Physics: Chemistry Close to Absolute Zero Studied Using the CRESU Method*. Editors B. R. Rowe, A. Canosa, and D. E. Heard (Singapore: World Scientific).

Herbst, E. (1985a). Radiative Association Rate Coefficients under Shocked Conditions in Interstellar Clouds - the Case of $CH_3^+ + H_2$. *Astron. Astrophys.* 153, 151–156.

Herbst, E. (1980a). A New Look at Radiative Association in Dense Interstellar Clouds. *Astrophys. J.* 237, 462–470. doi:10.1086/157889

Herbst, E. (1980b). An Additional Uncertainty in Calculated Radiative Association Rates of Molecular Formation at Low Temperatures. *Astrophys. J.* 241, 197–199. doi:10.1086/158331

Herbst, E. (1982). An Approach to the Estimation of Polyatomic Vibrational Radiative Relaxation Rates. *Chem. Phys.* 65, 185–195. doi:10.1016/0301-0104(82)85067-2

Herbst, E., DeFrees, D. J., Talbi, D., Pauzat, F., Koch, W., and McLean, A. D. (1991). Calculations on the Rate of the Ion-Molecule Reaction between NH_3^+ and H_2. *J. Chem. Phys.* 94, 7842–7849. doi:10.1063/1.460119

Herbst, E., and Klemperer, W. (1973). The Formation and Depletion of Molecules in Dense Interstellar Clouds. *Astrophys. J.* 185, 505–534. doi:10.1086/152436

Herbst, E., and Millar, T. J. (2008). "The Chemistry of Cold Interstellar Cloud Cores," in *Low Temperatures and Cold Molecules*. Editor I. W. M. Smith (London, UK: Imperial College Press), 1–54. doi:10.1142/9781848162105_0001

Herbst, E., Schubert, J. G., and Certain, P. R. (1977). The Radiative Association of CH_2^+. *Astrophys. J.* 213, 696–704. doi:10.1086/155199

Herbst, E. (1985b). The Rate of the Radiative Association Reaction between CH_3^+ and NH_3 and its Implications for Interstellar Chemistry. *Astrophys. J.* 292, 484–486. doi:10.1086/163179

Herbst, E., and van Dishoeck, E. F. (2009). Complex Organic Interstellar Molecules. *Annu. Rev. Astron. Astrophys.* 47, 427–480. doi:10.1146/annurev-astro-082708-101654

Herd, C. R., Adams, N. G., and Smith, D. (1990). OH Production in the Dissociative Recombination of H_3O^+, HCO_2^+, and N_2OH^+- Comparison with Theory and Interstellar Implications. *Astrophys. J.* 349, 388–392. doi:10.1086/168322

Hudson, R. L., and Moore, M. H. (2018). Interstellar Ices and Radiation-Induced Oxidations of Alcohols. *Astrophys. J.* 857, 89. doi:10.3847/1538-4357/aab708

Huntress, W. T., Jr., and Mitchell, G. F. (1979). The Synthesis of Complex Molecules in Interstellar Clouds. *Astrophys. J.* 231, 456–467. doi:10.1086/157207

Huntress, W. T., Jr., and Beauchamp, J. L. (1969). Application of Ion Cyclotron Resonance to the Study of Ionizing Reactions of Metastable Molecules. *Int. J. Mass Spectrom. Ion Phys.* 3, 149–152. doi:10.1016/0020-7381(69)80068-9

Ioppolo, S., Kaňuchová, Z., James, R. L., Dawes, A., Ryabov, A., Dezalay, J., et al. (2021). Vacuum Ultraviolet Photoabsorption Spectroscopy of Space-Related Ices: Formation and Destruction of Solid Carbonic Acid upon 1 keV Electron Irradiation. *Astron. Astrophys.* 646, A172. doi:10.1051/0004-6361/202039184

Iqbal, W., Acharyya, K., and Herbst, E. (2012). Kinetic Monte Carlo Studies of H_2 Formation on Grain Surfaces over a Wide Temperature Range. *Astrophys. J.* 751, 58. doi:10.1088/0004-637X/751/1/58

Jin, M., and Garrod, R. T. (2020). Formation of Complex Organic Molecules in Cold Interstellar Environments through Nondiffusive Grain-Surface and Ice-Mantle Chemistry. *Astrophys. J. Suppl. Ser.* 249, 26. doi:10.3847/1538-4365/ab9ec8

Katz, N., Furman, I., Biham, O., Pirronello, V., and Vidali, G. (1999). Molecular Hydrogen Formation on Astrophysically Relevant Surfaces. *Astrophys. J.* 522, 305–312. doi:10.1086/307642

Klots, C. E. (1976). Kinetic Energy Distributions from Unimolecular Decay: Predictions of the Langevin Model. *J. Chem. Phys.* 64, 4269–4275. doi:10.1063/1.432111

Luca, A., Voulot, D., and Gerlich, D. (2002). "Low Temperature Reactions between Stored Ions and Condensable Gases: Formation of Protonated Methanol via Radiative Association," in WDS 2002 Proceedings of Contributed Papers, Prague PART II (Praha, Czechia: MATFYZPRESS), 294–300.

Luine, J. A., and Dunn, G. H. (1985). Ion-Molecule Reaction Probabilities Near 10 K. *Astrophys. J.* 299, L67–L70. doi:10.1086/184582

Markwick, A. J. (2012). UMIST RATE12/astrochemistry.Net. Available at: http://udfa.ajmarkwick.net/.

Marquette, J. B., Rowe, B. R., Dupeyrat, G., and Roueff, E. (1985). CRESU Study of the Reaction $N^+ + H_2$ Yields $NH^+ + H$ between 8 and 70 K and Interstellar Chemistry Implications. *Astron. Astrophys.* 147, 115–120.

McElroy, D., Walsh, C., Markwick, A. J., Cordiner, M. A., Smith, K., and Millar, T. J. (2013). The UMIST Database for Astrochemistry 2012. *Astron. Astrophys.* 550, A36. doi:10.1051/0004-6361/201220465

McEwan, M. J., Anicich, V. G., Huntress, W. T., Jr., Kemperer, P. R., and Bowers, M. T. (1980). "An ICR Study of an Association Reaction at Low Pressure," in *Interstellar Molecules; Proceedings of the Symposium* (Mont Tremblant, Quebec, Canada, Dordrecht: D. Reidel Publishing), 305–306. doi:10.1007/978-94-009-9097-5_72

Minissale, M., Congiu, E., and Dulieu, F. (2016). Oxygen Diffusion and Reactivity at Low Temperature on Bare Amorphous Olivine-Type Silicate. *J. Chem. Phys.* 140 (7), 074705. doi:10.1063/1.4864657

Minissale, M., Congiu, E., and Dulieu, F. (2016). Direct Measurement of Desorption and Diffusion Energies of O and N Atoms Physisorbed on Amorphous Surfaces. *Astron. Astrophys.* 585, A146. doi:10.1051/0004-6361/201526702

Minissale, M., Congiu, E., Manicò, G., Pirronello, V., and Dulieu, F. (2013). CO_2 Formation on Interstellar Dust Grains: a Detailed Study of the Barrier of the CO + O Channel. *Astron. Astrophys.* 559, A49. doi:10.1051/0004-6361/201321453

Mitchell, J. B. A., Angelova, G., Rebrion-Rowe, C., Novotny, O., Garrec, J. L. L., Bluhme, H., et al. (2005). Branching Ratios for the Dissociative Recombination of Hydrocarbon Ions. *J. Phys. Conf. Ser.* 4, 198–204. doi:10.1088/1742-6596/4/1/028

Montroll, E. W., and Weiss, G. H. (1965). Random Walks on Lattices. II. *J. Math. Phys.* 6, 167–181. doi:10.1063/1.1704269

Moseley, E. R., Draine, B. T., Tomida, K., and Stone, J. M. (2020). Turbulent Dissipation, CH^+ Abundance, H_2 Line Luminosities, and Polarization in the Cold Neutral Medium. *MNRAS* 500, 3290–3308. doi:10.1093/mnras/staa3384

Ocaña, A. J., Blázquez, S., Potapov, A., Ballesteros, B., Canosa, A., Antiñolo, M., et al. (2019). Gas-phase Reactivity of CH_3OH toward OH at Interstellar Temperatures (11.7-177.5 K): Experimental and Theoretical Study. *Phys. Chem. Chem. Phys.* 21, 6942–6957. doi:10.1039/c9cp00439d

Öjekull, J., Andersson, P. U., Någård, M. B., Pettersson, J. B. C., Derkatch, A. M., Neau, A., et al. (2004). Dissociative Recombination of NH_4^+ and ND_4^+ Ions: Storage Ring Experiments And ab Initio Molecular Dynamics. *J. Chem. Phys.* 120, 7391–7399. doi:10.1063/1.1669388

Paulive, A., Shingledecker, C. N., and Herbst, E. (2020). The Role of Radiolysis in the Modelling of $C_2H_4O_2$ Isomers and Dimethyl Ether in Cold Dark Clouds. *MNRAS* 500, 3414–3424. doi:10.1093/mnras/staa3458

Ruaud, M., Loison, J. C., Hickson, K. M., Gratier, P., Hersant, F., and Wakelam, V. (2015). Modelling Complex Organic Molecules in Dense Regions: Eley-Rideal and Complex Induced Reaction. *MNRAS* 447, 4004–4017. doi:10.1093/mnras/stu2709

Ruaud, M., Wakelam, V., and Hersant, F. (2016). Gas and Grain Chemical Composition in Cold Cores as Predicted by the Nautilus Three-phase Model. *Mon. Not. R. Astron. Soc.* 459, 3756–3767. doi:10.1093/mnras/stw887

Ryzhov, V., Klippenstein, S. J., and Dunbar, R. C. (1996). Radiative Association of NO^+ with 3-Pentanone: Rate, Binding Energy, and Temperature Dependence. *J. Am. Chem. Soc.* 118, 5462–5468. doi:10.1021/ja953183b

Schiff, H. I., and Bohme, D. K. (1979). An Ion-Molecule Scheme for the Synthesis of Hydrocarbon-Chain and Organonitrogen Molecules in Dense Interstellar Clouds. *Astrophys. J.* 232, 740–746. doi:10.1086/157334

Shalabiea, O. M., Caselli, P., and Herbst, E. (1998). Grain Surface Chemistry: Modified Models. *Astrophys. J.* 502, 652–660. doi:10.1086/305942

Shannon, R. J., Blitz, M. A., Goddard, A., and Heard, D. E. (2013). Accelerated Chemistry in the Reaction between the Hydroxyl Radical and Methanol at Interstellar Temperatures Facilitated by Tunnelling. *Nat. Chem* 5, 745–749. doi:10.1038/nchem.1692

Shingledecker, C. N., and Herbst, E. (2018). A General Method for the Inclusion of Radiation Chemistry in Astrochemical Models. *Phys. Chem. Chem. Phys.* 20, 5359–5367. doi:10.1039/C7CP05901A

Shingledecker, C. N., Incerti, S., Ivlev, A., Emfietzoglou, D., Kyriakou, I., Vasyunin, A., et al. (2020). Cosmic-Ray Tracks in Astrophysical Ices: Modeling with the Geant4-DNA Monte Carlo Toolkit. *Astrophys. J.* 904, 189. doi:10.3847/1538-4357/abbb30

Shingledecker, C. N., Tennis, J., Gal, R. L., and Herbst, E. (2018). On Cosmic-Ray-driven Grain Chemistry in Cold Core Models. *Astrophys. J.* 861, 20. doi:10.3847/1538-4357/aac5ee

Sivaramakrishnan, R., Michael, J. V., Wagner, A. F., Dawes, R., Jasper, A. W., Harding, L. B., et al. (2011). Roaming Radicals in the thermal Decomposition of Dimethyl Ether: Experiment and Theory. *Combustion and Flame* 158, 618–632. doi:10.1016/j.combustflame.2010.12.017

Smith, D., and Adams, N. G. (1978). Molecular Synthesis in Interstellar Clouds - Radiative Association Reactions of CH_3^+ Ions. *Astrophys. J.* 220, L87–L92. doi:10.1086/182642

Smith, D., and Adams, N. G. (1981). Some Positive Ion Reactions with H_2: Interstellar Implications. *Monthly Notices R. Astronomical Soc.* 197, 377–384. doi:10.1093/mnras/197.2.377

Smith, D. (1992). The Ion Chemistry of Interstellar Clouds. *Chem. Rev.* 92, 1473–1485. doi:10.1021/cr00015a001

Smith, S. C., McEwan, M. J., Giles, K., Smith, D., and Adams, N. G. (1990). Unimolecular Decomposition of a Polyatomic Ion in a Variable-Temperature Selected-Ion-Flow-Drift Tube: Experiment and Theoretical Interpretation. *Int. J. Mass Spectrom. Ion Process.* 96, 77–96. doi:10.1016/0168-1176(90)80043-3

Snyder, L. E., Buhl, D., Zuckerman, B., and Palmer, P. (1969). Microwave Detection of Interstellar Formaldehyde. *Phys. Rev. Lett.* 22, 679–681. doi:10.1103/PhysRevLett.22.679

Solomon, P. M., and Klemperer, W. (1972). The Formation of Diatomic Molecules in Interstellar Clouds. *Astrophys. J.* 178, 389–422. doi:10.1086/151799

Stantcheva, T., Shematovich, V. I., and Herbst, E. (2002). On the Master Equation Approach to Diffusive Grain-Surface Chemistry: The H, O, CO System. *Astron. Astrophys.* 391, 1069–1080. doi:10.1051/0004-6361:20020838

Tennis, J., Loison, J.-C., and Herbst, E. (2021). Radiative Association between Neutral Radicals in the Interstellar Medium: CH_3 + CH_3O. *Submitted Astrophys. J.* [in press].

Theulé, P. (2020). "Chemical Dynamics in Interstellar Ice, Laboratory Astrophysics: from Observations to Interpretation," in *IAU Symposium 350*. Editors F. Salama and H. Linnartz. doi:10.1017/S1743921319008342

Theulé, P., Duvernay, F., Danger, G., Borget, F., Bossa, J. B., Vinogradoff, V., et al. (2013). Thermal Reactions in Interstellar Ice: A Step towards Molecular Complexity in the Interstellar Medium. *Adv. Space Res.* 52, 1567–1579. doi:10.1016/j.asr.2013.06.034

Tielens, A. G. G. M. (2005). *The Physics and Chemistry of the Interstellar Medium*. Cambridge, UK: Cambridge University Press.

Tielens, A. G. G. M., and Hagen, W. (1982). Model Calculations of the Molecular Composition of Interstellar Grain Mantles. *Astron. Astrophys.* 114, 245–260.

Tomosada, A. E., Kim, S., Osamura, Y., Yang, S. W., Chang, A. H. H., and Kaiser, R. I. (2012). First Detection of the Silylgermylene (H3SiGeH) and D4-Silylgermylene (D3SiGeD) Molecules in Low Temperature Silane-Germane Ices. *Chem. Phys.* 409, 49–60. doi:10.1016/j.chemphys.2012.10.002

Townes, C. H., and Schawlow, A. L. (1955). *Microwave Spectroscopy*. McGraw-Hill, New York: Kindle edition. Available at: https://store.doverpublications.com/0486162311.html.

Vasyunin, A. I., Semenov, D. A., Wiebe, D. S., and Henning, T. (2009). A Unified Monte Carlo Treatment of Gas-Grain Chemistry for Large Reaction Networks. I. Testing Validity of Rate Equations in Molecular Clouds. *Astrophys. J.* 691, 1459–1469. doi:10.1088/0004-637X/691/2/1459

Vuitton, V., Yelle, R. V., Lavvas, P., and Klippenstein, S. J. (2012). Rapid Association Reactions at Low Pressure: Impact on the Formation of Hydrocarbons on Titan. *Astrophys. J.* 744, 11. doi:10.1088/0004-637X/744/1/11

Wakelam, V., Bron, E., Cazaux, S., Dulieu, F., Gry, C., Guillard, P., et al. (2017). H_2 Formation on Interstellar Dust Grains: The Viewpoints of Theory, Experiments, Models and Observations. *Mol. Astrophysics* 9, 1–36. doi:10.1016/j.molap.2017.11.001

Wakelam, V., Dartois, E., Chabot, M., Spezzano, S., Navarro-Almaida, D., Loison, J.-C., et al. (2021). Efficiency of Non-thermal Desorptions in Cold-Core Conditions. *Astron. Astrophys* 652, A63. doi:10.1051/0004-6361/202039855

Wakelam, V., Loison, J.-C., Herbst, E., Pavone, B., Bergeat, A., Béroff, K., et al. (2015). The 2014 Kida Network for Interstellar Chemistry. *Astrophys. J. Suppl. Ser.* 217, 20. doi:10.1088/0067-0049/217/2/20

Watanabe, N., and Kouchi, A. (2002). Efficient Formation of Formaldehyde and Methanol by the Addition of Hydrogen Atoms to CO in H_2O-CO Ice at 10 K. *Astrophys. J.* 571, L173–L176. doi:10.1086/341412

Watson, W. D., and Salpeter, E. E. (1972a). Molecule Formation on Interstellar Grains. *Astrophys. J.* 174, 321–340. doi:10.1086/151492

Watson, W. D., and Salpeter, E. E. (1972b). On the Abundances of Interstellar Molecules. *Astrophys. J.* 175, 659–672. doi:10.1086/151587

Willis, E. R., and Garrod, R. T. (2017). Kinetic Monte Carlo Simulations of the Grain-Surface Back-Diffusion Effect. *Astrophys. J.* 840, 61. doi:10.3847/1538-4357/aa6ea7

Wilson, E. B., Jr., Decius, J. C., and Cross, P. C. (1980). *Molecular Vibrations. The Theory of Infrared and Raman Vibrational Spectra*. Mineola, NY, USA: Dover Publications.

Woon, D. E. (2021). The Astrochymist. Available at: http://www.astrochymist.org/.

Yuan, C., Cooke, I. R., and Yates, J. T., Jr (2014). A New Source of CO_2 in the Universe: a Photoactivated Eley-Rideal Surface Reaction on Water Ices. *Astrophys. J.* 791, L21. doi:10.1088/2041-8205/791/2/L21

Zajfman, D., Schwalm, D., and Wolf, A. (2003). Molecular Physics in Storage Rings: From Laboratory to Space. *Hyperfine Interactions* 146/147, 265–268. doi:10.1023/b:hype.0000004250.68609.53

Zanchet, A., Godard, B., Bulut, N., Roncero, O., Halvick, P., and Cernicharo, J. (2013). H_2(v= 0,1) + $C^+(^2P)$ ---> H + CH^+ State-To-State Rate Constants for Chemical Pumping Models in Astrophysical Media. *Astrophys. J.* 80, 766. doi:10.1088/0004-637X/766/2/80

Conflict of Interest: The author declares that the research was conducted in the absence of any commercial or financial relationships that could be construed as a potential conflict of interest.

Publisher's Note: All claims expressed in this article are solely those of the authors and do not necessarily represent those of their affiliated organizations, or those of the publisher, the editors and the reviewers. Any product that may be evaluated in this article, or claim that may be made by its manufacturer, is not guaranteed or endorsed by the publisher.

frontiers in Astronomy and Space Sciences

PERSPECTIVE
published: 23 December 2021
doi: 10.3389/fspas.2021.782006

Enlightening the Chemistry of Infalling Envelopes and Accretion Disks Around Sun-Like Protostars: The ALMA FAUST Project

C. Codella[1,2], C. Ceccarelli[2], C. Chandler[3], N. Sakai[4], S. Yamamoto[5] and The FAUST Team*

[1]INAF, Osservatorio Astrofisico di Arcetri, Firenze, Italy, [2]Univ. Grenoble Alpes, CNRS, IPAG, Saint Martin d'Hères, France, [3]National Radio Astronomy Observatory, Socorro, NM, United States, [4]RIKEN Cluster for Pioneering Research, Saitama, Japan, [5]Department of Physics, The University of Tokyo, Tokyo, Japan

The huge variety of planetary systems discovered in recent decades likely depends on the early history of their formation. In this contribution, we introduce the FAUST Large Program which focuses specifically on the early history of solar-like protostars and their chemical diversity at scales of ~ 50 au, where planets are expected to form. In particular, the goal of the project is to reveal and quantify the variety of chemical composition of the envelope/disk system at scales of 50 au in a sample of Class 0 and I protostars representative of the chemical diversity observed at larger scales. For each source, we propose a set of molecules able to (1) disentangle the components of the 50–2000 au envelope/disk system, (2) characterize the organic complexity in each of them, (3) probe their ionization structure, and (4) measure their molecular deuteration. The output will be a homogeneous database of thousands of images from different lines and species, i.e., an unprecedented source survey of the chemical diversity of solar-like protostars. FAUST will provide the community with a legacy dataset that will be a milestone for astrochemistry and star formation studies.

Keywords: astrochemistry, stars: formation, interstellar medium: molecules, interstellar medium: abundances, protostars

OPEN ACCESS

Edited by:
André Canosa, UMR6251 Institut de Physique de Rennes (IPR), France

Reviewed by:
Maryvonne Gerin, PSL research University, France
Marcelino Agundez, Spanish National Research Council (CSIC), Spain

****Correspondence:***
C. Codella
claudio.codella@inaf.it

Specialty section:
This article was submitted to Astrochemistry, a section of the journal Frontiers in Astronomy and Space Sciences

Received: *23 September 2021*
Accepted: *23 November 2021*
Published: *23 December 2021*

Citation:
Codella C, Ceccarelli C, Chandler C, Sakai N, Yamamoto S and The FAUST Team (2021) Enlightening the Chemistry of Infalling Envelopes and Accretion Disks Around Sun-Like Protostars: The ALMA FAUST Project. Front. Astron. Space Sci. 8:782006. doi: 10.3389/fspas.2021.782006

1 INTRODUCTION: THE ROOTS OF FAUST

Planets are a common product of the star formation process, and there is an incredible variety of planetary systems in the Galaxy (e.g., http://exoplanet.eu/), very different from the Solar System. The origin of such diversity, both in physics and chemistry, probably resides in the earliest history of the system formation, namely, what happens during the protostellar phases. The low-mass star formation is the complex process transforming a diffuse atomic cloud into, first, a dense molecular cloud and eventually into a Sun-like star surrounded by its planetary system. Meanwhile, the chemical composition of the gas involved in this process increases its complexity, from mostly atomic clouds to the so-called interstellar complex organic molecules (iCOMs), i.e., species with at least six atoms (e.g., methanol, CH_3OH), which can be considered as a brick to build pre-biotic chemistry (see e.g. Ceccarelli et al., 2007; Herbst and van Dishoeck, 2009; Caselli and Ceccarelli, 2012; Jørgensen et al., 2020, and references therein). Nowadays, evidence is mounting that the first steps of the process, namely, when the protostar is in the so-called Class 0 (~ 10^4 yr) and I (~ 10^5 yr) source phases (e.g., André et al., 2014, and references therein), are crucial for the future of the nascent planetary system.

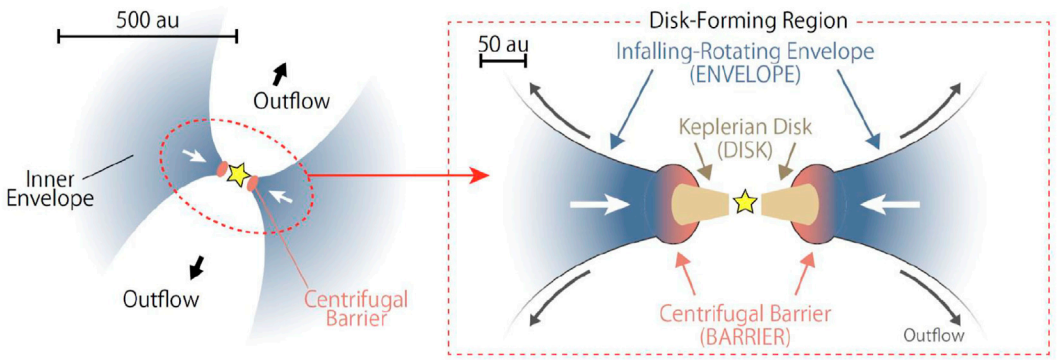

FIGURE 1 | Schematic structure of the region around solar-like Class 0 and I protostars, adapted from the study by Oya et al. (2016). Three main zones can be identified (see **Section 2**): the infalling and rotating envelope, the centrifugal barrier, and the rotating and accreting disk.

More specifically, a breakthrough result has been provided by the ALMA (Atacama Large Millimeter/submillimeter Array) interferometer, which provided images of rings and gaps (see e.g., Sheehan and Eisner, 2017; Andrews et al., 2018; Fedele et al., 2018) in the dust distribution around objects with an age less than 1 Myr. This supports that planet formation starts earlier than the classical protoplanetary stage (Class II; $\sim 10^6$ yr). These findings then support the importance of investigating the chemical complexity associated with protostars younger than 1 Myr.

In a nutshell, a Sun-like protostar is accreting its mass through a disk rotating along the equatorial plane. The disk, expected with a radius less than 100 au, is perpendicular to fast (~ 100 km s^{-1}) jets removing the angular momentum excess (see e.g., Frank et al., 2014; Lee et al., 2017a). In turn, the disk is fed by a large-scale ($\geq$ 1,000 au) rotating and infalling molecular envelope. The chemical composition of the envelopes surrounding solar-like Class 0 and I protostars on large scales (100–2000 au) can be very different. Two distinct classes have been discovered (1) the hot corinos (Ceccarelli et al., 2007) and the WCCC (warm carbon chain chemistry) sources (Sakai and Yamamoto, 2013). Hot corinos (as e.g., IRAS16293-2422) are compact ($\geq$ 100 au) and dense ($\geq 10^7$ cm^{-3}) regions, where the temperature is warm enough ($\geq$ 100 K) to thermally evaporate the frozen dust mantles. As a consequence, the gas phase is chemically enriched in iCOMs due to either direct release from dust mantles or formed in the gas phase using simpler molecules from the mantles. On the other hand, WCCC sources (as e.g., L1527) are deprived of such iCOMs and enriched with unsaturated carbon-chain species, such as $HC_{2n+1}N$, C_nH, and C_nH_2 (Higuchi et al., 2018, and references therein).

In this context, breakthrough open questions are (i) whether such diversity is also present in the inner envelope/disk system ($\sim$ 50 au) and (ii) what molecules are passed from the large-scale envelope ($\sim$ 2000 au) to the disk in which planets, comets, and asteroids form. Yet, this is crucial to know because very likely the chemical composition and fate of the future planetary systems depend on the chemical class to which the original protostar belonged. The aim of this study is to introduce the ALMA (Atacama Large Millimeter/submillimeter Array) Large Program (LP) FAUST (Fifty AU STudy of the chemistry in the disk/envelope system of Solar-like protostars; http://faust-alma.riken.jp), focused on astrochemistry of Class 0/I sources imaged at the Solar System spatial scale.

2 THE FAUST PROJECT

2.1 Context and Main Goals

The goal of FAUST is to characterize the gas chemical composition of the protostellar system, associated with several physical components at work to build a Sun-like star from a rotating and infalling envelope. FAUST builds up on previous surveys of the chemical composition of the Sun-like youngest protostars at larger spatial scales, such as ASAI (https://www.oan.es/asai/), and SOLIS (https://solis.osug.fr/), which covered the large envelopes at $\leq$ 5000 au and the transition between the large-scale envelope and the circumstellar disk at $\geq$ 5000 au and $\leq$ 100 au, respectively. The FAUST approach is to identify three zones (see **Figure 1**), as learnt from previous ALMA studies (e.g., Sakai et al., 2014a, 2017):

- ENVELOPE: Here, we mean the infalling–rotating envelope on scales of a few 100 au. The gas chemical composition evolves from that at large ($\sim$ 2000 au) scales because of the heating from the central object, which sublimates the grain mantles (Ceccarelli et al., 1996). Besides, the gas close to the outflow cavity wall might also be exposed to the UV and X-ray photons from the central object or be affected by mild transverse shocks (Stäuber et al., 2005), with a consequent chemical enrichment of the gas.
- BARRIER: The gas transits a centrifugal barrier, on scales of about 50 au, before entering the disk. The gas chemical composition may be drastically affected by the low velocity ($\sim$ 1 km s^{-1}) shock at the centrifugal barrier as grain mantles may be at least partially liberated into the gas phase and the gas heated and compressed (Sakai et al., 2014b,a; Oya et al., 2016). As a matter of fact, the IRAS 04 386 + 2557 protostar, in the L1527 Taurus core, can be considered the archetypal edge-on disk where Sakai et al. (2014b, 2017) revealed, for the first time, an increase of SO abundance at the radius of the centrifugal barrier.

TABLE 1 | List of the frequency windows and of the species covered by the selected backends, divided in four groups (see **Section 2.2**).

Setup	Frequency (GHz)	Zones	Molecular complexity	Gas Ionization	Molecular deuteration
1	214.0–219.0 229.0–234.0	c-C_3H_2, CH_3OH, SO SiO, H_2CO, $C^{18}O$	CH_3OH, NH_2CHO CH_3CHO, $HCOOCH_3$	DCO^+	N_2D^+, D_2CO
2	242.5–247.5 257.5–262.5	c-C_3H_2, CS CH_3OH, SO	CH_3OH, NH_2CHO CH_3CHO, $HCOOCH_3$ CH_3OCH_3	$H^{13}CO^+$	HDCO, CH_2DOH
3	85.0–89.0 97.0–101.0	CH_3OH, HC_3N	CH_3OH, $^{13}CH_3OH$	N_2H^+	c-C_3HD

Another enlightening case is represented by the HH212 pristine jet/disk system, located in Orion B. The disk, edge-on also in this case, shows iCOM-rich rotating rings, possibly associated with the centrifugal barrier with a radius of about 40 au (Lee et al., 2017b, 2019).

- DISK: At scales smaller than about 50 au, the gas settles in the rotationally supported disk, where the gas chemical composition is expected to be stratified (e.g., Aikawa and Herbst, 1999; Walsh et al., 2015) and affected by the dynamics and dust coagulation (e.g., Zhao et al., 2016; Ilee et al., 2017). Indeed, very recently, Podio et al., (2020) observed with ALMA the evolved Class I source IRAS 04 302 + 2247, where the bulk of the envelope has been dispersed; the molecular (CO, CS, and H_2CO) emission is vertically stratified on a scale of 50–60 au (see also van't Hoff et al., 2020). A breakthrough result would be to reveal a chemical stratification in early protostellar disks still fully embedded in the envelope. Furthermore, the observations of protostellar disks are also challenged by the presence of jets and disk winds, which are powered at similar scales (e.g., Lee et al., 2017a; Tabone et al., 2017). For a proper study of disks, it is mandatory to reveal also the fast jet flowing perpendicular to the disk equatorial plane using e.g., a standard tracer as SiO (see e.g., Codella et al., 2019). Finally, at these small scales, dust opacity increases, which strongly affects the emission spectrum from the gas (see below).

Therefore, the three zones are expected to possess distinct physical and chemical properties, likely varying from source to source and/or depending on the star-forming regions. The goal of FAUST is to disentangle the three zones with the help of their kinematic signatures and ALMA line images at 50 au spatial resolution. Our pioneering studies showing the proof of concept have already been conducted for a few sources and a few molecules (e.g., Ceccarelli et al., 2010; Oya et al., 2016; Codella et al., 2017): time is now ripe for a systematic study of many more sources and many more species, *via* an ALMA LP. In summary, the aim of FAUST is to reveal and quantify the variety of the chemical composition of the envelope/disk system of solar-like Class 0 and I protostars. Such chemical varieties will add a new dimension to the diversity of planetary systems, and we expect that it will have a substantial impact on studies of planet formation and the origin of the Solar System.

2.2 Sources and Molecular Lines

From a kinematical point of view, the envelope/disk system can be divided into three different zones. Although they could, in principle, be studied kinematically by observing CO and its isotopologue lines, but as a matter of fact, only rarer species provide a much more powerful diagnostic tool because they are differentially enhanced in the three zones, thanks to chemical composition changes (e.g., Sakai et al., 2014b, 2017; Oya et al., 2016). FAUST will simultaneously use kinematics and chemistry to fully resolve the complexity of the envelope/disk system. Four groups of species have been selected to probe different topics:

1. ZONE PROBES: c-C_3H_2, CS, CH_3OH, SO, SiO, H_2CO, $C^{18}O$, and HC_3N. We select the following species to disentangle each zone: Envelope: c-C_3H_2 and CS. These species are present in the infalling–rotating envelope, with different abundances for different sources, but their abundance significantly drops in the other two zones so that they are specific in probing the ENVELOPE zone in different sources. Barrier: CH_3OH, SO, and SiO. Their abundance is enhanced in the weak shocks at the centrifugal barrier. Narrow ($\sim 1\ km\ s^{-1}$) SiO lines could trace the release of Si from dust mantles (Guillet et al., 2011; Lesaffre et al., 2013) at the centrifugal barrier, whereas broad ($\geq 10\ km\ s^{-1}$) SiO emission is expected to trace fast jets (associated with high-velocity shocks) perpendicular to the disk. Disk: H_2CO, $C^{18}O$, and HC_3N. Given their relatively large abundance in the warm layers of the disks, lines from these species can probe the inner disk, *via* their high-velocity components.
2. MOLECULAR COMPLEXITY PROBES: CH_3OH, NH_2CHO, CH_3CHO, CH_3OCH_3, and $HCOOCH_3$. A major goal of FAUST is measuring the organic complexity in the disk/envelope system as it might be inherited at later stages by the nascent planetary system (Zhao et al., 2016). Based on previous studies, five species are particularly important to identify the organic diversity: methanol (CH_3OH), formamide (NH_2CHO), acetaldehyde (CH_3CHO), dimethyl ether (CH_3OCH_3), and methyl formate ($HCOOCH_3$). They are predicted to have a different chemical origin, with methanol a grain-surface product and formamide likely a gas-phase product (Codella et al., 2017; Skouteris et al.,

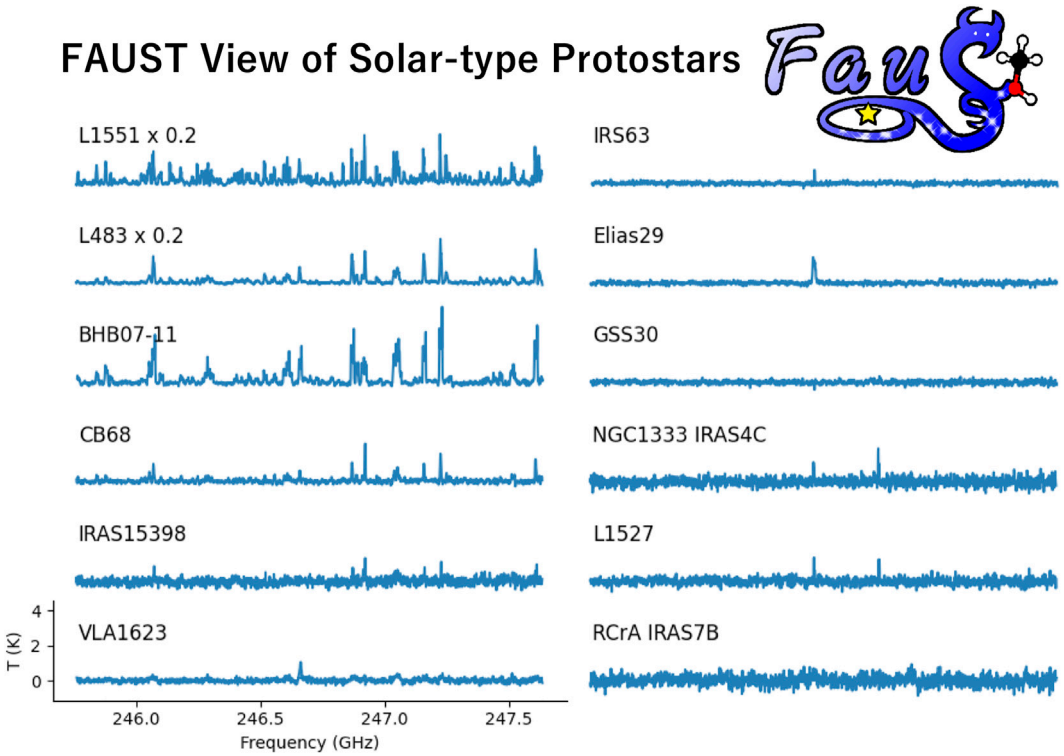

FIGURE 2 | Zoo of preliminary spectra observed towards FAUST sources (see black labels) in a portion of 2 GHz (245.7–247.7 GHz) of the frequency Setup2 (See **Table 1**). The FAUST logo is also reported. The intensity scale is in brightness temperature (K). The spectra have been obtained merging ACA data with those at high-spatial resolution. The identification of the lines is out of the focus of the present study. The goal of the sketch is to enlight the observed chemical differentiation, with some sources characterized by a rich spectra associated with iCOM emission.

2017), while for acetaldehyde, dimethyl ether, and methyl formate, the chemical synthesis route is largely debated (e.g., Garrod et al., 2008; Balucani et al., 2015).

3. GAS IONIZATION PROBES: $H^{13}CO^+$, DCO^+, and N_2H^+. The degree of ionization in the inner 100 au envelope is a very important parameter for any theory of planet formation (e.g., Balbus and Hawley, 1998). Yet, this quantity is very poorly known at these scales. Several processes can affect it, from an inner source of energetic particles and/or X-rays (Stäuber et al., 2005) to the growth of dust grains (Zhao et al., 2016). Here, we propose to use molecular ions, following a previously used methodology, to estimate the gas ionization, such as the $H^{13}CO^+/DCO^+$ and $H^{13}CO^+/N_2H^+$ abundance ratios. The first ratio measures the ionization in cold (smaller than ~ 30 K) and dense ($\geq 10^4$ cm^{-3}) gas (e.g., Caselli et al., 2008), while the second one in warm ($\geq$ 40 K) and, again, quite dense (up to ~ 10^7 cm^{-3}) gas (e.g., Ceccarelli et al., 2014b).
4. DEUTERIUM-BEARING SPECIES: c-C_3HD, N_2D^+, HDCO, D_2CO, and CH_2DOH D-bearing species are powerful diagnostic tools to study the physical conditions at present and in the past (Ceccarelli et al., 2014a). Specifically, species like c-C_3H_2 (one of the infalling–rotating envelope probe) and N_2D^+ are present-day products, whereas H_2CO and CH_3OH, being major components of the grain mantles, were mostly formed during the pre-stellar phase and introduced in the present-day gas by the presence of the accreting inner object. The respective deuterated counterparts provide, therefore, a precious tool to understand the physical conditions when these species are/were deuterated. In addition, molecular deuteration provides a sort of Ariadne's thread that links the ISM to the Solar System history (Ceccarelli et al., 2014a).

We selected a representative sample of sources that is known to exhibit a wide chemical composition diversity, based on the available large-scale observations. The following two criteria have been adopted: (1) Chemical diversity: Since, so far, the major chemical diversity is represented by WCCC and hot corino sources, we select sources that represent a continuous variation of the abundance ratio of species characteristics of these two classes. Specifically, (i) CH_3OH can be regarded as a proxy of the hot corino species because it is a crucial organic molecule, considered a parent species of larger iCOMs; (ii) small hydrocarbons such as C_2H or c-C_3H_2 are characteristics of WCCC sources. The selected sources are, therefore, associated with measured abundance ratios of these species varying by two orders of magnitude, covering the two extremes of hot corino and WCCC sources (Higuchi et al., 2018). (2) Distance and previously

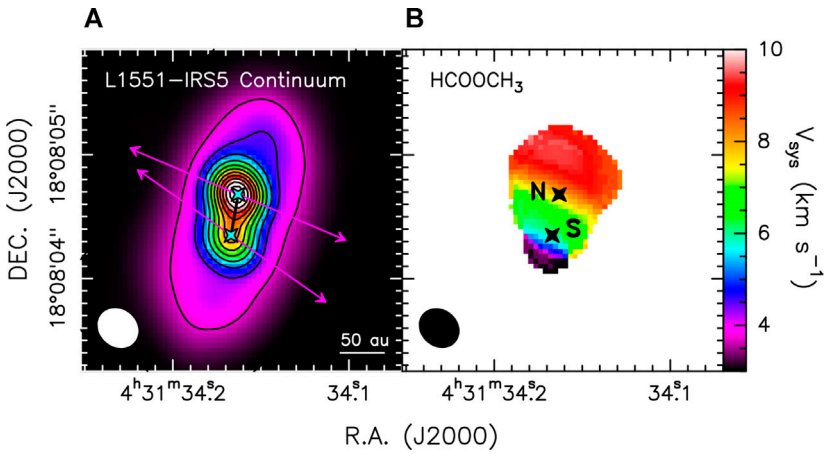

FIGURE 3 | L1551 IRS5 binary source, in Taurus. **(A)**: 1.3 mm dust continuum emission in color scale and black contours (Bianchi et al., 2020): the N and S protostars are revealed. **(B)**: Gas enriched in iCOMs around the IRS5 binary system, imaged on the 50 au scale. More specifically, the intensity-weighted velocity (also called moment 1) map of the $HCOOCH_3(18_{4,14}–17_{4,13})A$ is shown, revealing a velocity gradient perpendicular to the axes of the protostellar jets (see the arrows in the **(A)**) driven by N and S. The systemic velocities are +4.5 km s^{-1} (S object) and +7.5 km s^{-1} (N). The chemical enrichment occurs in rotating hot corinos around the protostars and/or in the rotating circumbinary disk.

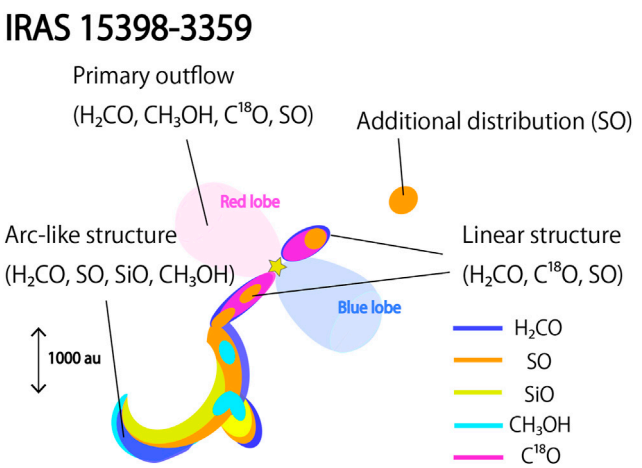

FIGURE 4 | Adapted from (Okoda et al., 2021): Schematic picture of the molecular distributions around the IRAS 15 398–3359 protostar located in the Lupus star-forming region. FAUST observations of emission lines due to different molecular species disentangle different components on large-scale associated with multiple outflows.

studied sources: We select nearby Class 0 and I sources with distance ≤ 250 pc and a bolometric luminosity ≤ 25 $L_{\odot}$.

The final list contains 13 sources located in different star-forming regions: L1527 and L1551 IRS5 (the Taurus region), IRAS 15398–3359 (Lupus), L483 (Aquila), Elias 29, VLA1623A, IRS63, and GSS30 (Ophiucus), NGC1333 IRAS4A, and IRAS4C (Perseus), BHB07-11 (Pipe), RCrA IRS17A (Cr A), and CB68 (the isolated source). We will observe the three frequency settings in **Table 1**. They target lines from the four groups of molecules described above. We require a uniform linear resolution of 50 au to identify the centrifugal barrier and to disentangle the disk from the envelope, namely, an angular resolution of 250–350 mas, depending on the distance of the source, and almost uniform brightness sensitivity. The high-angular scale of 50 au will be reached using the 12-m antenna ALMA array in different configurations. Furthermore, given the goal to also sample the molecular envelope, Atacama Compact Array (ACA/Morita Array) observations of 7-m antennas will be also performed. By combining all the visibility data obtained using both the 12-m and the 7-m antenna array, FAUST will be able to follow the physical and chemical changes from the large-scale envelope (~ 2000 au) to the inner disk/jet system. For each frequency setting, we allocate one continuum setting to measure the dust spectral energy distribution (SED) from 3 to 1 mm. The frequency resolution is set to 0.2 km s^{-1}, i.e., the sound speed at 10 K.

2.3 Data Exploitation

We will use a two-step modeling procedure to extract the information from the data, as follows: (1) Kinematics and radiative transfer models: The three zones are disentangled by comparing the velocity structure observed in the various molecular lines with kinematic models (Oya et al., 2016). The gas temperature and density structure, as well as the species column density, will be extracted from a multiline non-LTE (when possible) analysis using 1 and 3D codes (Bisbas et al., 2015; Zhao et al., 2016), taking into account the dust optical depth. The analysis of the continuum will provide the distribution of the H_2 column density. (2) Astrochemical models: The derived molecular abundances will be compared with our astrochemical models (Ceccarelli et al., 2018; Wirström and Charnley, 2018), where the physical structure will be incorporated. From this analysis, we will extract valuable constraints on the reactions involved in the formation and destruction of the observed iCOMs. FAUST members with specific expertise will contribute to the project with laboratory experiments and

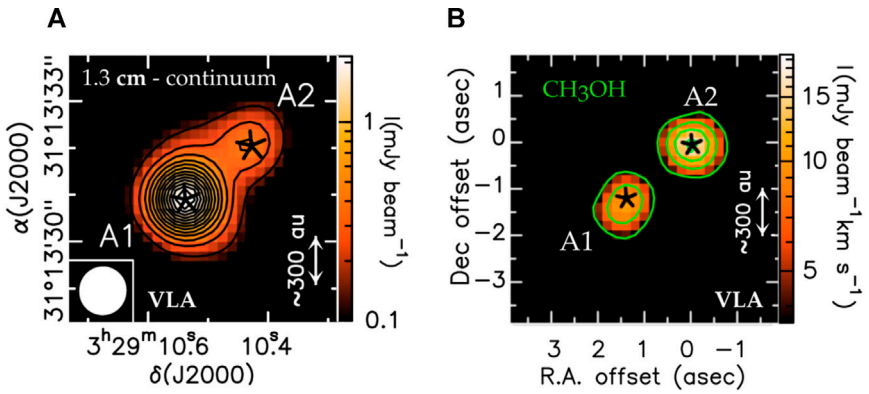

FIGURE 5 | (A): NGC1333 IRAS 4A continuum emission map at 25 GHz as imaged using VLA (Adapted from De Simone et al. (2020)). Two protostars A1 and A2 are observed. **(B)**: $CH_3OH(6_{2,4}–6_{1,5})$ velocity-integrated maps in the color scale, revealing for the first time the hot-corino associated with A1, missed by sub-millimeter surveys due to dust opacity effects.

theoretical quantum chemistry calculations (Watanabe et al., 2010; Dulieu et al., 2013; Skouteris et al., 2017). In summary, we will determine (i) the extent to which the large-scale envelope diversity is conserved in the disk/envelope system and (ii) what molecules are passed from the large-scale envelope to the disk. In this way, the goal of the FAUST project will, therefore, be achieved.

3 FIRST FAUST RESULTS AND PERSPECTIVES

The analysis of the FAUST data is in progress. However, some instructive results have been already obtained. The data were reduced by using a modified version of the ALMA calibration pipeline and an additional in-house calibration routine (Okoda et al., 2021) to correct the system temperature and spectral line data normalization. **Figure 2** reports an example of the zoo of FAUST spectra observed in a portion of the frequency Setup 2 (see **Table 1**) toward the protostellar coordinates. The spectra have been obtained merging ACA data with those at high-spatial resolution. The line identification and the discussion of the chemical content are out of focus of the present study; the goal of the spectra sketched in **Figure 2** is to enlight a chemical differentiation, indicating the source sample is not biased by some selection criterium. More precisely, four (query) sources (L1551, L483, CB68, BHB07-11, and CB68) are characterized by iCOM emission, revealing hot corino activity. The next step is a careful investigation of weaker lines and the inspection of the images obtained using each array configuration, in order to provide a complete characterization of the molecular complexity in each source.

An example of what FAUST is able to provide when studying the inner 50 au around protostars is reported by Bianchi et al. (2020), who imaged the Class I L1551-IRS5 binary system in several species, namely, methanol (including $^{13}CH_3OH$ and CH_2DOH), methyl formate ($HCOOCH_3$), and ethanol (CH_3CH_2OH). **Figure 3A** shows the dust continuum 1.3 mm emission revealing the binary components, namely, the N (northern) and S (southern) objects. The two sources are surrounded by a circumbinary disk, clearly traced by Cruz-Sáenz de Miera et al. (2019). The 50 au resolution reveals an iCOM-rich hot corino toward the N component (see the $HCOOCH_3$ map in **Figure 3B**) and, in addition, a possible second hot corino around the S object. The number of hot corinos imaged around Class I sources is, so far, limited to a handful number (e.g., De Simone et al., 2017; Yang et al., 2021). The discovery of iCOM emission in L1551-IRS5 is, thus, instructive in the effort of tracking how the chemical richness around Class 0 objects is inherited by later Class I protostars: as a matter of fact, it looks that chemistry does not dramatically change. Projects on this topic based on statistically reliable samples will be hopefully performed soon. **Figure 3B** shows the map of the velocity peak of the $HCOOCH_3(18_{4,14}–17_{4,13}A)$ line profile. A clear velocity gradient is revealed perpendicular to the axes of the protostellar jets (see the arrows in the Left panel) driven by N and S. In conclusion, the chemical enrichment occurs in rotating hot corinos around the protostars and/or in the rotating circumbinary disk.

Moving to larger spatial scales (from 50 au to 1800 au), FAUST recently published a review of the molecular emission in the Class 0 IRAS15398–3359 star-forming region in Lupus (Okoda et al., 2021). The FAUST multi-species approach (CO, $C^{18}O$, SO, H_2CO, CH_3OH, and SiO) allows Okoda et al. (2021) to well trace the dense and/or shocked material around the protostellar object. Besides the already known main outflow located along the NE-SW direction, a narrow ($\sim 1\ km\ s^{-1}$) line emission of shock tracers such as SiO and CH_3OH reveals (i) a secondary outflow with an axis normal to the main flow, and (ii) an arc-like structure related with the secondary outflow (see the schematic picture in **Figure 4**). Which is the origin of the secondary outflow? Are the outflows driven by different protostars? As a matter of fact, there is no evidence (neither in the FAUST continuum maps) of a companion of the Class 0 IRAS15398–3359 protostar. An alternative solution proposed by Okoda et al. (2021) is that the

secondary outflow is a relic of a past reorientation of the outflow launched from a single protostar and that the arc-like structure has dissipated the turbulence of the old shocked material. In principle, a dramatic change in the direction of the outflow axis could be possible if the molecular core hosting the protostar is associated with a non-uniform internal angular momentum, transferred onto the central region *via* episodic accretion.

Finally, the FAUST synergy is at work also to prepare complementary observations to those collected with the ALMA Large Program. More specifically, we started pilot projects in the cm-spectral window using the very large array (VLA) interferometer. Given the dust opacity at cm-wavelengths is negligible (e.g., Testi et al., 2014, and references therein), the main goal is to evaluate the effects of dust emission on Solar System scales, associated with both high volume and column densities (e.g., Miotello et al., 2014; Galván-Madrid et al., 2018; Galametz et al., 2019) on the collected iCOM images (and derived abundances) at (sub-) mm-wavelengths. An instructive example is provided by De Simone et al. (2020), who imaged at 1.3 cm at VLA in the FAUST context, the NGC1333-IRAS4A binary system. One of the two components 4A1 lacks iCOM emission when observed at millimeter wavelengths (see **Figure 5**), while the other component 4A2 is very rich in iCOMs. De Simone et al. (2020) found that, once imaged at 1.3 cm, methanol lines are similarly bright toward 4A1 and 4A2, proving that both are hot corinos and not only 4A2. Complementing the ALMA observations with centimeter images can be then considered the future step which the FAUST synergy will perform. The VLA-ALMA combination will allow us to perform steps ahead in the study of the protostellar environments and to understand the ultimate molecular complexity in regions with a high column density of the material and consequently high dust opacity.

DATA AVAILABILITY STATEMENT

The original contributions presented in the study are included in the article/Supplementary Materials, further inquiries can be directed to the corresponding author.

AUTHOR CONTRIBUTIONS

All authors listed have made a substantial, direct, and intellectual contribution to the work and approved it for publication.

FUNDING

This project has received funding from: 1) the European Research Council (ERC) under the European Union's Horizon 2020 research and innovation program, for the Project The Dawn of Organic Chemistry (DOC), grant agreement No 741 002; 2) the PRIN-INAF 2016 The Cradle of Life–GENESIS-SKA (General Conditions in Early Planetary Systems for the rise of life with SKA); 3) a grant-in-aid from the Japan Society for the Promotion of Science (KAKENHI: Nos. 18H05222, 19H05069, 19K14753); 4) ANR of France under the contract number ANR-16-CE31-0013; 5) the French National Research Agency in the framework of the Investissements d'Avenir program (ANR-15-IDEX-02), through the funding of the Origin of Life project of the Univ. Grenoble-Alpes, 6) the European Union's Horizon 2020 research and innovation programs under projects Astro-Chemistry Origins (ACO), Grant No 811312.

ACKNOWLEDGMENTS

This manuscript is written on behalf of the whole FAUST team (http://faust-alma.riken.jp), and it makes use of the following ALMA data: ADS/JAO.ALMA#2018.1.01205.L. ALMA is a partnership of ESO (representing its member states), NSF (United States), and NINS (Japan), together with NRC (Canada), MOST and ASIAA (Taiwan), and KASI (Republic of Korea), in cooperation with the Republic of Chile. The Joint ALMA Observatory is operated by ESO, AUI/NRAO, and NAOJ. The National Radio Astronomy Observatory is a facility of the National Science Foundation operated under cooperative agreement by Associated Universities, Inc. This is a short text to acknowledge the contributions of specific colleagues, institutions, or agencies that aided the efforts of the authors.

REFERENCES

Aikawa, Y., and Herbst, E. (1999). Molecular Evolution in Protoplanetary Disks. Two-Dimensional Distributions and Column Densities of Gaseous Molecules. *A&A* 351, 233–246.

André, P., Di Francesco, J., Ward-Thompson, D., Inutsuka, S.-I., Pudritz, R. E., and Pineda, J. (2014). From Filamentary Networks to Dense Cores in Molecular Clouds: Toward a New Paradigm for Star Formation. *Protostars and Planets* VI, 27–51. doi:10.2458/azu_uapress_9780816531240-ch002

Andrews, S. M., Huang, J., Pérez, L. M., Isella, A., Dullemond, C. P., Kurtovic, N. T., et al. (2018). The Disk Substructures at High Angular Resolution Project (DSHARP). I. Motivation, Sample, Calibration, and Overview. *ApJ* 869, L41. doi:10.3847/2041-8213/aaf741

Balbus, S. A., and Hawley, J. F. (1998). Instability, Turbulence, and Enhanced Transport in Accretion Disks. *Rev. Mod. Phys.* 70, 1–53. doi:10.1103/RevModPhys.70.1

Balucani, N., Ceccarelli, C., and Taquet, V. (2015). Formation of Complex Organic Molecules in Cold Objects: the Role of Gas-phase Reactions. *MNRAS* 449, L16–L20. doi:10.1093/mnrasl/slv009

Bianchi, E., Chandler, C. J., Ceccarelli, C., Codella, C., Sakai, N., López-Sepulcre, A., et al. (2020). FAUST I. The Hot Corino at the Heart of the Prototypical Class I Protostar L1551 IRS5. *MNRAS* 498, L87–L92. doi:10.1093/mnrasl/slaa130

Bisbas, T. G., Haworth, T. J., Barlow, M. J., Viti, S., Harries, T. J., Bell, T., et al. (2015). TORUS-3DPDR: a Self-Consistent Code Treating Three-Dimensional Photoionization and Photodissociation Regions. *Mon. Not. R. Astron. Soc.* 454, 2828–2843. doi:10.1093/mnras/stv2156

Caselli, P., and Ceccarelli, C. (2012). Our Astrochemical Heritage. *Astron. Astrophys Rev.* 20, 56. doi:10.1007/s00159-012-0056-x

Caselli, P., Vastel, C., Ceccarelli, C., van der Tak, F. F. S., Crapsi, A., and Bacmann, A. (2008). Survey of ortho-H$\mathsf{_{2}}$D$\mathsf{{+}}$ (1$\mathsf{_{1,0}}$-1$\mathsf{_{1,1}}$) in Dense Cloud Cores. *A&A* 492, 703–718. doi:10.1051/0004-6361:20079009

Ceccarelli, C., Bacmann, A., Boogert, A., Caux, E., Dominik, C., Lefloch, B., et al. (2010). Herschelspectral Surveys of star-forming Regions. *A&A* 521, L22. doi:10.1051/0004-6361/201015081

Ceccarelli, C., Caselli, P., Bockelée-Morvan, D., Mousis, O., Pizzarello, S., Robert, F., et al. (2014a). "Deuterium Fractionation: The Ariadne's Thread from the Precollapse Phase to Meteorites and Comets Today," in

Protostars and Planets VI. Editors H. Beuther, R. S. Klessen, C. P. Dullemond, and T. Henning (Springer), 859. doi:10.2458/azu_uapress_9780816531240-ch037

Ceccarelli, C., Caselli, P., Herbst, E., Tielens, A. G. G. M., and Caux, E. (2007). Extreme Deuteration and Hot Corinos: The Earliest Chemical Signatures of Low-Mass Star Formation. *Protostars and Planets* V, 47–62.

Ceccarelli, C., Dominik, C., López-Sepulcre, A., Kama, M., Padovani, M., Caux, E., et al. (2014b). Herschel Finds Evidence for Stellar Wind Particles in a Protostellar Envelope: Is This what Happened to the Young Sun? *ApJ* 790, L1. doi:10.1088/2041-8205/790/1/L1

Ceccarelli, C., Hollenbach, D. J., and Tielens, A. G. G. M. (1996). Far-Infrared Line Emission from Collapsing Protostellar Envelopes. *ApJ* 471, 400–426. doi:10.1086/177978

Ceccarelli, C., Viti, S., Balucani, N., and Taquet, V. (2018). The Evolution of Grain Mantles and Silicate Dust Growth at High Redshift. *MNRAS* 476, 1371–1383. doi:10.1093/mnras/sty313

Codella, C., Ceccarelli, C., Caselli, P., Balucani, N., Barone, V., Fontani, F., et al. (2017). Seeds of Life in Space (SOLIS). *A&A* 605, L3. doi:10.1051/0004-6361/201731249

Codella, C., Ceccarelli, C., Lee, C.-F., Bianchi, E., Balucani, N., Podio, L., et al. (2019). The HH 212 Interstellar Laboratory: Astrochemistry as a Tool to Reveal Protostellar Disks on Solar System Scales Around a Rising Sun. *ACS Earth Space Chem.* 3, 2110–2121. doi:10.1021/acsearthspacechem.9b00136

Cruz-Sáenz de Miera, F., Kóspál, Á., Ábrahám, P., Liu, H. B., and Takami, M. (2019). Resolved ALMA Continuum Image of the Circumbinary Ring and Circumstellar Disks in the L1551 IRS 5 System. *ApJ* 882, L4. doi:10.3847/2041-8213/ab39ea

De Simone, M., Ceccarelli, C., Codella, C., Svoboda, B. E., Chandler, C., Bouvier, M., et al. (2020). Hot Corinos Chemical Diversity: Myth or Reality? *ApJ* 896, L3. doi:10.3847/2041-8213/ab8d41

De Simone, M., Codella, C., Testi, L., Belloche, A., Maury, A. J., Anderl, S., et al. (2017). Glycolaldehyde in Perseus Young Solar Analogs. *A&A* 599, A121. doi:10.1051/0004-6361/201630049

Dulieu, F., Congiu, E., Noble, J., Baouche, S., Chaabouni, H., Moudens, A., et al. (2013). How Micron-Sized Dust Particles Determine the Chemistry of Our Universe. *Sci. Rep.* 3, 1338. doi:10.1038/srep01338

Fedele, D., Tazzari, M., Booth, R., Testi, L., Clarke, C. J., Pascucci, I., et al. (2018). ALMA Continuum Observations of the Protoplanetary Disk AS 209. *A&A* 610, A24. doi:10.1051/0004-6361/201731978

Frank, A., Ray, T. P., Cabrit, S., Hartigan, P., Arce, H. G., Bacciotti, F., et al. (2014). Jets and Outflows from Star to Cloud: Observations Confront Theory. *Protostars and Planets* VI, 451–474. doi:10.2458/azu_uapress_9780816531240-ch020

Galametz, M., Maury, A. J., Valdivia, V., Testi, L., Belloche, A., and André, P. (2019). Low Dust Emissivities and Radial Variations in the Envelopes of Class 0 Protostars: Possible Signature of Early Grain Growth. *A&A* 632, A5. doi:10.1051/0004-6361/201936342

Galván-Madrid, R., Liu, H. B., Izquierdo, A. F., Miotello, A., Zhao, B., Carrasco-González, C., et al. (2018). On the Effects of Self-Obscuration in the (Sub) Millimeter Spectral Indices and the Appearance of Protostellar Disks. *ApJ* 868, 39. doi:10.3847/1538-4357/aae779

Garrod, R. T., Weaver, S. L. W., and Herbst, E. (2008). Complex Chemistry in Star-forming Regions: An Expanded Gas-Grain Warm-up Chemical Model. *ApJ* 682, 283–302. doi:10.1086/588035

Guillet, V., Pineau des Forêts, G., and Jones, A. P. (2011). Shocks in Dense Clouds. *A&A* 527, A123. doi:10.1051/0004-6361/201015973

Herbst, E., and van Dishoeck, E. F. (2009). Complex Organic Interstellar Molecules. *Annu. Rev. Astron. Astrophys.* 47, 427–480. doi:10.1146/annurev-astro-082708-101654

Higuchi, A. E., Sakai, N., Watanabe, Y., López-Sepulcre, A., Yoshida, K., Oya, Y., et al. (2018). Chemical Survey toward Young Stellar Objects in the Perseus Molecular Cloud Complex. *ApJS* 236, 52. doi:10.3847/1538-4365/aabfe9

Ilee, J. D., Forgan, D. H., Evans, M. G., Hall, C., Booth, R., Clarke, C. J., et al. (2017). The Chemistry of Protoplanetary Fragments Formed via Gravitational Instabilities. *MNRAS* 472, 189–204. doi:10.1093/mnras/stx1966

Jørgensen, J. K., Belloche, A., and Garrod, R. T. (2020). Astrochemistry during the Formation of Stars. *Annu. Rev. Astron. Astrophys.* 58, 727–778. doi:10.1146/annurev-astro-032620-021927

Lee, C.-F., Codella, C., Li, Z.-Y., and Liu, S.-Y. (2019). First Abundance Measurement of Organic Molecules in the Atmosphere of HH 212 Protostellar Disk. *ApJ* 876, 63. doi:10.3847/1538-4357/ab15db

Lee, C.-F., Ho, P. T. P., Li, Z.-Y., Hirano, N., Zhang, Q., and Shang, H. (2017a). A Rotating Protostellar Jet Launched from the Innermost Disk of HH 212. *Nat. Astron.* 1, 0152. doi:10.1038/s41550-017-0152

Lee, C.-F., Li, Z.-Y., Ho, P. T. P., Hirano, N., Zhang, Q., and Shang, H. (2017b). Formation and Atmosphere of Complex Organic Molecules of the HH 212 Protostellar Disk. *ApJ* 843, 27. doi:10.3847/1538-4357/aa7757

Lesaffre, P., Pineau des Forêts, G., Godard, B., Guillard, P., Boulanger, F., and Falgarone, E. (2013). Low-velocity Shocks: Signatures of Turbulent Dissipation in Diffuse Irradiated Gas. *A&A* 550, A106. doi:10.1051/0004-6361/201219928

Miotello, A., Testi, L., Lodato, G., Ricci, L., Rosotti, G., Brooks, K., et al. (2014). Grain Growth in the Envelopes and Disks of Class I Protostars. *A&A* 567, A32. doi:10.1051/0004-6361/201322945

Okoda, Y., Oya, Y., Francis, L., Johnstone, D., Inutsuka, S.-i., Ceccarelli, C., et al. (2021). FAUST. II. Discovery of a Secondary Outflow in IRAS 15398−3359: Variability in Outflow Direction during the Earliest Stage of Star Formation? *ApJ* 910, 11. doi:10.3847/1538-4357/abddb1

Oya, Y., Sakai, N., López-Sepulcre, A., Watanabe, Y., Ceccarelli, C., Lefloch, B., et al. (2016). Infalling-Rotating Motion and Associated Chemical Change in the Envelope of IRAS 16293-2422 Source A Studied with ALMA. *ApJ* 824, 88. doi:10.3847/0004-637X/824/2/88

Podio, L., Garufi, A., Codella, C., Fedele, D., Bianchi, E., Bacciotti, F., et al. (2020). ALMA Chemical Survey of Disk-Outflow Sources in Taurus (ALMA-DOT). *A&A* 642, L7. doi:10.1051/0004-6361/202038952

Sakai, N., Oya, Y., Higuchi, A. E., Aikawa, Y., Hanawa, T., Ceccarelli, C., et al. (2017). Vertical Structure of the Transition Zone from Infalling Rotating Envelope to Disk in the Class 0 Protostar, IRAS04368+2557. *Mon. Not. R. Astron. Soc. Lett.* 467, slx002–L80. doi:10.1093/mnrasl/slx002

Sakai, N., Oya, Y., Sakai, T., Watanabe, Y., Hirota, T., Ceccarelli, C., et al. (2014a). A Chemical View of Protostellar-Disk Formation in L1527. *ApJ* 791, L38. doi:10.1088/2041-8205/791/2/L38

Sakai, N., Sakai, T., Hirota, T., Watanabe, Y., Ceccarelli, C., Kahane, C., et al. (2014b). Change in the Chemical Composition of Infalling Gas Forming a Disk Around a Protostar. *Nature* 507, 78–80. doi:10.1038/nature13000

Sakai, N., and Yamamoto, S. (2013). Warm Carbon-Chain Chemistry. *Chem. Rev.* 113, 8981–9015. doi:10.1021/cr4001308

Sheehan, P. D., and Eisner, J. A. (2017). Disk Masses for Embedded Class I Protostars in the Taurus Molecular Cloud. *ApJ* 851, 45. doi:10.3847/1538-4357/aa9990

Skouteris, D., Vazart, F., Ceccarelli, C., Balucani, N., Puzzarini, C., and Barone, V. (2017). New Quantum Chemical Computations of Formamide Deuteration Support a Gas-phase Formation of This Prebiotic Molecule. *Mon. Not. R. Astron. Soc. Lett.* 468, slx012–L5. doi:10.1093/mnrasl/slx012

Stäuber, P., Doty, S. D., van Dishoeck, E. F., and Benz, A. O. (2005). X-ray Chemistry in the Envelopes Around Young Stellar Objects. *A&A* 440, 949–966. doi:10.1051/0004-6361:20052889

Tabone, B., Cabrit, S., Bianchi, E., Ferreira, J., Pineau des Forêts, G., Codella, C., et al. (2017). ALMA Discovery of a Rotating SO/SO2 Flow in HH212. *A&A* 607, L6. doi:10.1051/0004-6361/201731691

Testi, L., Birnstiel, T., Ricci, L., Andrews, S., Blum, J., Carpenter, J., et al. (2014). "Dust Evolution in Protoplanetary Disks," in *Protostars and Planets VI*. Editors H. Beuther, R. S. Klessen, C. P. Dullemond, and T. Henning (Springer), 339. doi:10.2458/azu_uapress_9780816531240-ch015

van 't Hoff, M. L. R., Harsono, D., Tobin, J. J., Bosman, A. D., van Dishoeck, E. F., Jørgensen, J. K., et al. (2020). Temperature Structures of Embedded Disks: Young Disks in Taurus Are Warm. *ApJ* 901, 166. doi:10.3847/1538-4357/abb1a2

Walsh, C., Nomura, H., and van Dishoeck, E. (2015). The Molecular Composition of the Planet-Forming Regions of Protoplanetary Disks across the Luminosity Regime. *A&A* 582, A88. doi:10.1051/0004-6361/201526751

Watanabe, N., Kimura, Y., Kouchi, A., Chigai, T., Hama, T., and Pirronello, V. (2010). Direct Measurements of Hydrogen Atom Diffusion and the Spin Temperature of Nascent H 2 Molecule on Amorphous Solid Water. *ApJ* 714, L233–L237. doi:10.1088/2041-8205/714/2/L233

Wirström, E. S., and Charnley, S. B. (2018). Revised Models of Interstellar Nitrogen Isotopic Fractionation. *MNRAS* 474, 3720–3726. doi:10.1093/mnras/stx3030

Yang, Y.-L., Sakai, N., Zhang, Y., Murillo, N. M., Zhang, Z. E., Higuchi, A. E., et al. (2021). The Perseus ALMA Chemistry Survey (PEACHES). I. The Complex Organic Molecules in Perseus Embedded Protostars. *ApJ* 910, 20. doi:10.3847/1538-4357/abdfd6

Zhao, B., Caselli, P., Li, Z.-Y., Krasnopolsky, R., Shang, H., and Nakamura, F. (2016). Protostellar Disc Formation Enabled by Removal of Small Dust Grains. *Mon. Not. R. Astron. Soc.* 460, 2050–2076. doi:10.1093/mnras/stw1124

Conflict of Interest: The authors declare that the research was conducted in the absence of any commercial or financial relationships that could be construed as a potential conflict of interest.

frontiers in Astronomy and Space Sciences

ORIGINAL RESEARCH
published: 20 January 2022
doi: 10.3389/fspas.2021.802297

Gas-Phase Reactivity of OH Radicals With Ammonia (NH_3) and Methylamine (CH_3NH_2) at Around 22 K

Daniel González[1], *Bernabé Ballesteros*[1,2], *André Canosa*[3], *José Albaladejo*[1,2] *and Elena Jiménez*[1,2]*

[1]Departamento de Química Física, Facultad de Ciencias y Tecnologías Químicas, Universidad de Castilla-La Mancha (UCLM), Ciudad Real, Spain, [2]Instituto de Investigación en Combustión y Contaminación Atmosférica, UCLM, Ciudad Real, Spain, [3]Institut de Physique de Rennes-CNRS—UMR 6251, Université de Rennes, Rennes, France

Interstellar molecules containing N atoms, such as ammonia (NH_3) and methylamine (CH_3NH_2), could be potential precursors of amino acids like the simplest one, glycine (NH_2CH_2COOH). The gas-phase reactivity of these N-bearing species with OH radicals, ubiquitous in the interstellar medium, is not known at temperatures of cold dark molecular clouds. In this work, we present the first kinetic study of these OH-reactions at around 22 K and different gas densities [(3.4–16.7) × 10^{16} cm^{-3}] in helium. The obtained rate coefficients, with ± 2σ uncertainties, can be included in pure gas-phase or gas-grain astrochemical models to interpret the observed abundances of NH_3 and CH_3NH_2. We observed an increase of k_1 and k_2 with respect to those previously measured by others at the lowest temperatures for which rate coefficients are presently available: 230 and 299 K, respectively. This increase is about 380 times for NH_3 and 20 times for CH_3NH_2. Although the OH + NH_3 reaction is included in astrochemical kinetic databases, the recommended temperature dependence for k_1 is based on kinetic studies at temperatures above 200 K. However, the OH + CH_3NH_2 reaction is not included in astrochemical networks. The observed increase in k_1 at ca. 22 K does not significantly change the abundance of NH_3 in a typical cold dark interstellar cloud. However, the inclusion of k_2 at ca. 22 K, not considered in astrochemical networks, indicates that the contribution of this destruction route for CH_3NH_2 is not negligible, accounting for 1/3 of the assumed main depletion route (reaction with HCO^+) in this IS environment.

$$k_1\,(\mathrm{OH} + \mathrm{NH_3}) = (2.7 \pm 0.1) \times 10^{-11}\,\mathrm{cm^3 s^{-1}}$$
$$k_2\,(\mathrm{OH} + \mathrm{CH_3NH_2}) = (3.9 \pm 0.1) \times 10^{-10}\,\mathrm{cm^3 s^{-1}}$$

Keywords: ISM, prebiotic molecules, OH radicals, CRESU technique, reaction kinetics, ultralow temperatures

OPEN ACCESS

Edited by:
Majdi Hochlaf,
Université Paris Est Marne la Vallée, France

Reviewed by:
Marzio Rosi,
University of Perugia, Italy
Christian Alcaraz,
Centre National de la Recherche Scientifique (CNRS), France

***Correspondence:**
Elena Jiménez
Elena.Jimenez@uclm.es

Specialty section:
This article was submitted to Astrochemistry, a section of the journal Frontiers in Astronomy and Space Sciences

Received: *26 October 2021*
Accepted: *02 December 2021*
Published: *20 January 2022*

Citation:
González D, Ballesteros B, Canosa A, Albaladejo J and Jiménez E (2022) Gas-Phase Reactivity of OH Radicals With Ammonia (NH_3) and Methylamine (CH_3NH_2) at Around 22 K. Front. Astron. Space Sci. 8:802297. doi: 10.3389/fspas.2021.802297

INTRODUCTION

Unravelling the origin of life on the Earth has been both a challenge and a matter of debate for scientists throughout the history. However, what we can be certain about is that all ingredients essential for life are composed by a few atoms such as H, O, C, N, or S. The combination of these atoms can produce different prebiotic molecules, which are considered the precursors of life on our

planet. Principally, two main theories have been proposed for trying to explain how these molecules could have appeared on the globe (Chyba and Sagan, 1992; Bernstein, 2006). The first one states that the organic molecules that serve as the basis of life were formed in the primitive atmosphere of our planet from simpler and smaller molecules (e.g., NH_3, CH_4, H_2O, or H_2) (Miller, 1953; Bada and Lazcano, 2002; Cleaves et al., 2008). In fact, this was demonstrated experimentally by Stanley Miller in the middle of the past century when he obtained a considerable number of important compounds from the biological point of view, such as amino acids, from simple molecules like the aforementioned, after exposing them to conditions aiming at mimicking those reigning in the primitive Earth (Miller, 1953). The second one is based on the idea that the prebiotic molecules were firstly synthesized in space and then, they could have been delivered to the Earth by meteorites, comets, asteroids or even interplanetary dust particles (Ehrenfreund et al., 2002; Sandford et al., 2020). This latter hypothesis is now in trend due to the huge and unexpected discovery in the last 70 years of the chemical richness in the interstellar medium (ISM). Currently, about 250 species (including ions and neutrals) have been detected in the ISM or circumstellar shells (Woon, 2021). Interstellar molecules, which are found in ultra-cold environments (~10–100 K), such as the so-called dense or dark clouds or pre-stellar cores, range from simple diatomic molecules [e.g., CO or the hydroxyl (OH) radical] to more complex systems (e.g., fullerenes). For instance, the OH radical, firstly detected in Cassiopeia A in 1963 (Weinreb et al., 1963), is ubiquitous in the ISM. By definition, carbon-bearing species containing six atoms or more are called complex organic molecules (COMs) (Herbst and van Dishoeck, 2009). Some COMs containing C-O bonds (such as CH_3OH) and C-N bonds (such as CH_3CN) can be potential precursors of sugars and amino acids in the presence of water, respectively (Balucani, 2009), under the Earth's conditions. Although ammonia (NH_3) is not considered a COM, strictly by definition, this abundant nitrogen-bearing species is very important since it serves as temperature probe in molecular clouds like Sagittarius (Sgr) B2, where it was first detected (Cheung et al., 1968). Ammonia has also been found towards a post-star forming region, W3(OH), with an abundance relative to H_2 of 10^{-8} (Wilson et al., 1993) and in TMC-1, with a column density of $\sim 10^{15}\,cm^{-2}$ (Freeman and Millar, 1983). Another interesting N-bearing species is methylamine (CH_3NH_2), which was detected in the 1970s years for the first time towards Sgr B2 and Orion A (Fourikis et al., 1974; Kaifu et al., 1974). Abundances relative to H_2 for CH_3NH_2 have been observed to be 10^{-8} towards the hot core G10.47 + 0.33 (Ohishi et al., 2019) and 10^{-9} for Sgr B2 (Halfen et al., 2013). Both NH_3 and CH_3NH_2 have been proposed as precursors of the simplest amino acid, glycine (NH_2CH_2COOH), through H-atom abstraction reactions forming NH_2 (Sorrell, 2001; Garrod, 2013) and CH_2NH_2 radicals, (Woon, 2002; Garrod, 2013); however interstellar glycine remains undetected in the ISM so far.

Under the ISM conditions, it has been assumed since a long time (Herbst and Klemperer, 1973) that dissociative recombination of NH_4^+ is the main provider of NH_3 in the gas phase. This cation can be generated through a series of hydrogen abstraction reactions starting from $N^+ + H_2$ leading step by step to NH^+, NH_2^+, NH_3^+, and eventually NH_4^+ (Gerin et al., 2016; Rednyk et al., 2019). Alternatively, NH_2^+ can be produced by $H_3^+ + N$ (Scott et al., 1997). Although not included in interstellar chemical networks, another potential source of NH_3 was recently claimed by Gianturco et al. (2019) to be the reaction of the NH_2^- anion with H_2. Surface reactions have also been proposed as plausible mechanisms to produce ammonia via a series of atomic hydrogen additions to N-hydrides after NH has been formed through N + H → NH (Jonusas et al., 2020). Regarding CH_3NH_2, different synthetic routes have been proposed. In the gas-phase, it may be formed via the radiative association between NH_3 and the methyl radical cation (CH_3^+) followed by dissociative recombination (Herbst, 1985). But CH_3NH_2 can also be formed on grain surfaces by sequential hydrogenation of hydrogen cyanide (HCN), as experimentally observed by Theule et al. (2011). Simulations of the irradiation of CH_4 and NH_3 ices may also form CH_3NH_2 (Kim and Kaiser, 2011; Förstel et al., 2017), but also in cold and quiescent molecular clouds (Ioppolo et al., 2021). In the gas-grain chemical model by (Garrod et al., 2008), the CH_3+NH_2 reaction was also suggested as a source of CH_3NH_2 during warm-up phases.

It is also important to know how NH_3 and CH_3NH_2 are being destroyed to have a good insight of the chemical evolution of the ISM. Focusing on neutral-neutral reactions, reaction networks that astrochemical models used, such as KIDA and UDfA, include eight depletion routes for NH_3. e.g., reactions with H, CH, CN, among other radicals. Concerning CH_3NH_2, only two depleting reactions by CH and CH_3 radicals are included in KIDA database, while UDfA database does not include any. Until now, the reactivity of NH_3 with neutral radicals or atoms at ISM temperatures has been investigated experimentally in the presence of CN (Sims et al., 1994), CH (Bocherel et al., 1996), C_2H (Nizamov and Leone, 2004) and $C(^3P)$ (Bourgalais et al., 2015; Hickson et al., 2015) whereas, only the reactivity of CH_3NH_2 with CN is documented (Sleiman et al., 2018a; 2018b). Due to the important role of OH radicals as a key intermediate in multiple reactive processes in the ISM (Cazaux et al., 2010; Goicoechea et al., 2011; Acharyya et al., 2015; Linnartz et al., 2015), the kinetic database for OH-molecule reactions has been widely extended in the past years (see e.g., Taylor et al., 2008; Smith and Barnes, 2013; Ocaña et al., 2017, 2019; Potapov et al., 2017; Heard, 2018; Blázquez et al., 2019, 2020). For the OH + NH_3 reaction (**Eq. R1**), of interest in atmospheric and combustion chemistry, its gas-phase kinetics has been extensively studied both experimentally and theoretically.

$$OH + NH_3 \rightarrow H_2O + NH_2 \qquad k_1 \qquad (R1)$$

Note that other reaction channels forming $H_2NO + H_2$, HNOH + H_2, or H_2NOH + H are not thermodynamically accessible, since they are endothermic by Gibbs free energies ranging from 19.67 to 31.73 kcal/mol (Vahedpour et al., 2018). **Eq. R1** is also of astrochemical interest since it leads to the formation of NH_2 radicals, which were also observed towards the same location as ammonia (van Dishoeck et al., 1993). In the laboratory studies, the

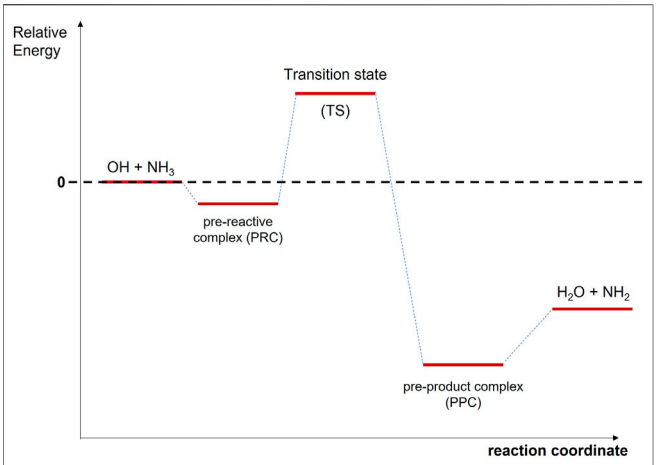

SCHEME 1 | Simplified reaction energy profile along the MEP for the OH + NH_3 reaction.

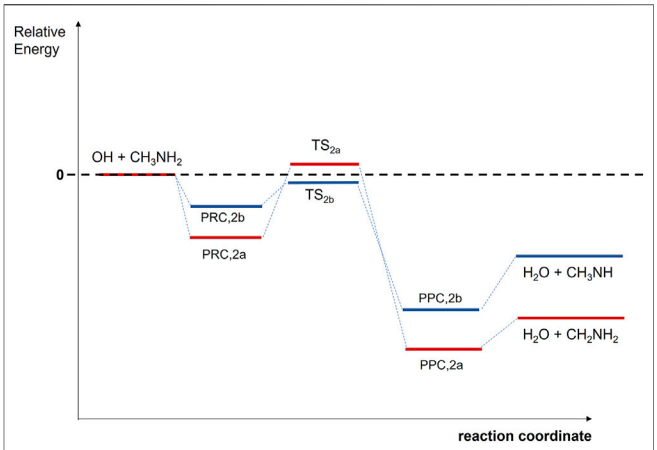

SCHEME 2 | Simplified reaction energy profile along the MEP for the OH + CH_3NH_2 reaction.

rate coefficient for R1, k_1, has been reported since the 1970's by many research groups over a wide range of temperature (230–2,360 K) and pressures (1–4,000 mbar) (Stuhl, 1973; Kurylo, 1973; Zellner and Smith, 1974; Hack et al., 1974; Perry et al., 1976; Silver and Kolb, 1980; Fujii et al., 1981, 1986; Salimian et al., 1984; Stephens, 1984; Zabielski and Seery, 1985; Jeffries and Smith, 1986; Diau et al., 1990). A summary of all previous experimental results can be found in Diau et al. (1990). The observed dependence of k_1 with temperature is positive, i.e., the rate coefficient increases when temperature increases, and the reported activation energies range from 0.5 to 9 kcal/mol in the 230–2,360 K range (Zellner and Smith, 1974; Hack et al., 1974; Perry et al., 1976; Silver and Kolb, 1980; Fujii et al., 1981, 1986; Salimian et al., 1984; Stephens, 1984; Zabielski and Seery, 1985; Jeffries and Smith, 1986; Diau et al., 1990). The computed energy barriers in the 200–4,000 K range were found to be between 2.0 and 9.05 kcal/mol (Giménez et al., 1992; Corchado et al., 1995; Bowdridge et al., 1996; Nyman, 1996; Lynch et al., 2000; Monge-Palacios et al., 2013b; Nguyen and Stanton, 2017). The reaction mechanism of R1 was also theoretically investigated (Giménez et al., 1992; Espinosa-García and Corchado, 1994; Corchado et al., 1995; Bowdridge et al., 1996; Nyman, 1996; Lynch et al., 2000; Monge-Palacios et al., 2013b; Nguyen and Stanton, 2017). The formation of a pre-reactive complex (PRC) at the entrance channel is accepted, as illustrated in **Scheme 1**, and quantum mechanical tunneling has been reported to be an important contribution to k_1, leading to the observed non-Arrhenius behavior (Espinosa-García and Corchado, 1994; Corchado et al., 1995; Bowdridge et al., 1996; Nyman, 1996; Monge-Palacios et al., 2013b; Nguyen and Stanton, 2017).

Regarding the OH + CH_3NH_2 reaction (**Eq. R2**), previous kinetic studies are restricted to temperatures higher than 295 K (Atkinson et al., 1977; Carl and Crowley, 1998; Onel et al., 2013; Butkovskaya and Setser, 2016). From the experimental point of view, Atkinson et al. (1977), Onel et al. (2013) reported the temperature dependence of reaction R2 in the 299–426 K and 298–600 K ranges, respectively. A negative temperature dependence of k_2 was observed and this rate coefficient increases when temperature decreases.

$$OH + CH_3NH_2 \rightarrow \text{products} \qquad k_2 \qquad \text{(R2)}$$

Eq. R2 may proceed by H-abstraction from methyl (–CH_3) or amino (–NH_2) groups forming CH_2NH_2 and CH_3NH radicals plus water, respectively. The formation of CH_2NH_2 radicals was measured to be the main reaction channel at room temperature (Nielsen et al., 2011, 2012; Onel et al., 2014; Butkovskaya and Setser, 2016), in agreement with theoretical predictions at 299 K and above (Galano and Alvarez-Idaboy, 2008; Tian et al., 2009). These calculations suggest a stepwise mechanism involving the formation of a PRC at the entrance channels and an energy barrier of a few kcal/mol for the H-abstraction channel from –CH_3 group, as depicted in **Scheme 2**.

As there are no kinetic data of k_1 and k_2 at temperatures of the cold dark interstellar clouds and since they are necessary to properly model the chemistry of the ISM, we present in this work the first determination of the rate coefficient for the reactions of NH_3 and CH_3NH_2, k_i (i = 1 or 2), with OH radicals at ca. 22 K using a combination of a pulsed CRESU (French acronym for Reaction Kinetics in a Uniform Supersonic Flow) reactor with laser techniques. The implications of the reported new rate coefficients will be discussed in terms of their effect on the predicted abundances of NH_3 and CH_3NH_2 in a typical cold dark interstellar cloud at 10 K.

EXPERIMENTAL METHODS

CRESU Apparatus Coupled to Pulsed Laser Photolysis-Laser Induced Fluorescence Technique

The experimental system based on the pulsed uniform supersonic expansion of a gas mixture has been already described elsewhere (Jiménez et al., 2015, 2016; Antiñolo et al., 2016; Canosa et al., 2016; Ocaña et al., 2017, 2018, 2019; Blázquez et al., 2019, 2020; Neeman et al., 2021). To carry out the kinetic experiments, three Laval nozzles (He23-HP, He23-IP, and He23-LP) were used with

TABLE 1 | Summary of the experimental conditions [total gas density (*n*), jet pressure (*p*), and reactant concentration in the jet] and corrected *pseudo*-first order rate coefficient ranges.

Reactant	Laval nozzle	$n/10^{16}$ cm^{-3}	*p*/mbar	[Reactant]/10^{13} cm^{-3}	k'-k'_0/s^{-1}	k(T) /10^{-11} cm^3 s^{-1}
NH_3	He23-HP	16.7	0.51	4.2–21.6	1932–5613	2.7 ± 0.1
	He23-IP	7.4	0.23	3.5–10.7	1177–2737	2.7 ± 0.1
	He23-LP	3.4	0.10	2.9–8.6	408–2886	2.9 ± 0.3
CH_3NH_2	He23-HP	16.7	0.51	0.3–3.1	589–11713	39.2 ± 2.0
	He23-IP	7.4	0.23	0.7–3.1	3317–11166	36.2 ± 1.4
	He23-LP	3.4	0.10	0.6–2.9	2382–12034	41.1 ± 1.5

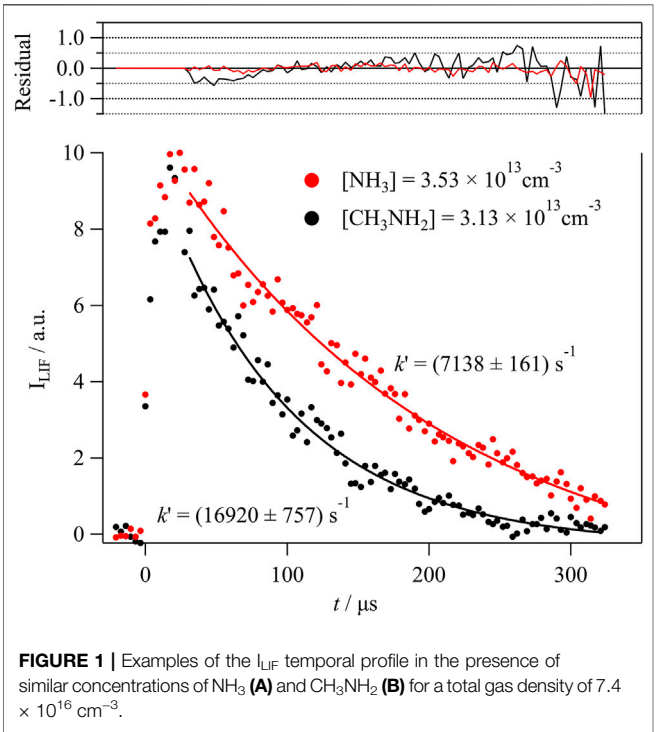

FIGURE 1 | Examples of the I_{LIF} temporal profile in the presence of similar concentrations of NH_3 **(A)** and CH_3NH_2 **(B)** for a total gas density of 7.4 × 10^{16} cm^{-3}.

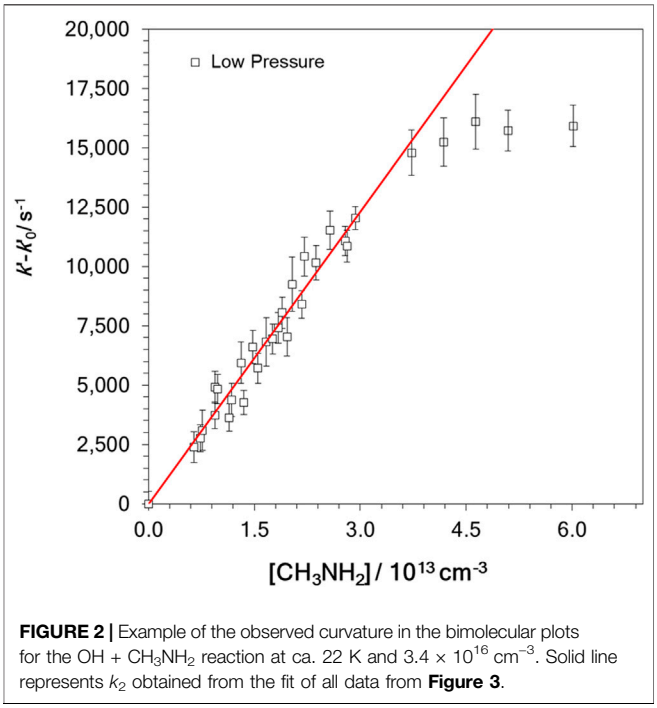

FIGURE 2 | Example of the observed curvature in the bimolecular plots for the OH + CH_3NH_2 reaction at ca. 22 K and 3.4 × 10^{16} cm^{-3}. Solid line represents k_2 obtained from the fit of all data from **Figure 3**.

helium as a carrier gas. These nozzles were designed to generate a uniform flow at around 22 K for three different jet pressures (see **Table 1**) (Jiménez et al., 2015; Canosa et al., 2016; Ocaña et al., 2017), thus allowing us to explore the influence of pressure on the reactivity at a constant temperature. Bath gas and reactants (NH_3 or CH_3NH_2) were introduced in the CRESU chamber through calibrated mass flow controllers, MFCs (Sierra Instruments, Inc., model Smart Trak, Smart-Trak 2, MicroTrak 101, and Smart-Trak 100). CH_3NH_2 was diluted in He and stored in a 20-L or 50-L bulb. Calibrated mass flow rates of these diluted mixtures ranged from 6.6 to 200 sccm (standard cubic centimeters per minute), depending on the Laval nozzle used. Dilution factor *f* ranged from 1.78 × 10^{-2} to 4.54 × 10^{-2}. In contrast, NH_3 was flown directly to the pre-expansion chamber (reservoir) from a gas cylinder through a MFC manufactured with anticorrosive materials (Sierra Instruments, Inc., model Smart-Trak 100). The flow rates of pure NH_3 ranged from 3 to 15 sccm. The OH-precursor employed was H_2O_2, since it is a clean source of OH radicals. Gaseous H_2O_2 was introduced into the reservoir by bubbling the bath gas through an aqueous solution of H_2O_2, as explained in Jiménez et al. (2005). The flow rate of He through the H_2O_2 bubbler in different experiments ranged from 35.6 to 265.8 sccm, depending on the Laval nozzle used. Within a kinetic experiment, this flow rate was kept constant to maintain invariable the contribution of the OH loss due to the OH + H_2O_2 reaction (see Kinetic *Analysis*). The gas mixture formed by He (main flow), He/H_2O_2, and the reactant was pulsed by a two holes rotary disk described in Jiménez et al. (2015).

After the gas expansion through the Laval nozzle, the jet temperature was measured by a Pitot tube to be (21.7 ± 1.4) K for the He23-HP nozzle, (22.5 ± 0.7) K for the He23-IP nozzle, and (21.1 ± 0.6) K for the He-23LP nozzle, respectively. Within the fluctuation along the flow axis (± σ), the jet temperature in all cases is ca. 22 K. The procedure to determine the jet temperature and gas density has been previously described (Jiménez et al., 2015; Canosa et al., 2016; Ocaña et al., 2017). Pulsed photolysis of H_2O_2(g) at 248 nm was achieved by the radiation coming from a KrF excimer laser (Coherent, model ExciStar XS 200) with energies at the exit of the nozzle ranging from 0.5 to 0.9 mJ/pulse at 10 Hz, depending on the nozzle used. OH radicals were monitored by collecting the laser induced fluorescence (LIF) at

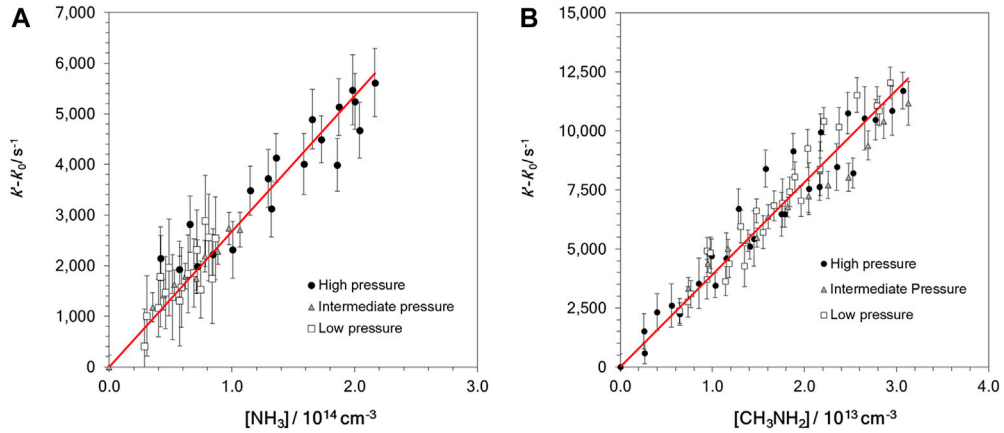

FIGURE 3 | Bimolecular plots for the OH-reactions at ca. 22 K with **(A)** NH_3 and **(B)** CH_3NH_2.

310 nm, after laser excitation at *ca.* 282 nm, as a function of the reaction time defined as the time delay between the probe laser pulse and the excimer one.

Kinetic Analysis

In **Figure 1** an example of the temporal evolution of the LIF intensity (I_{LIF}) is presented. As explained in several papers (Jiménez et al., 2015; Ocaña et al., 2018), the observed rise of the I_{LIF} signal at $t > 0$ is due to rotational relaxation of OH, coming from H_2O_2 photodissociation, that occurs in a timescale (t_0) of less than 30 μs under the conditions of the experiments, especially, at the concentration levels of the reactant, which is an effective quencher. The fit of the recorded I_{LIF} profiles to an exponential decay (solid lines in **Figure 1**) confirms that the OH loss follows a pseudo-first order kinetics.

$$\boldsymbol{I_{LIF}(t) = I_{LIF}(t_0)\, exp^{-k'(t-t_0)}} \quad \text{(E1)}$$

The pseudo-first order rate coefficient, k', includes all the OH loss processes occurring simultaneously in the cold jet.

$$\boldsymbol{k' = k'_0 + k_i[Reactant]} \quad \text{(E2)}$$

where k_i (i = 1 or 2) is the bimolecular rate coefficients for OH-reactions with NH_3 (R1) and CH_3NH_2 (R2). In the absence of reactant, k'_0 was measured, and it included the loss of OH radicals by OH-reaction with H_2O_2 and other OH losses, such as diffusion out of the detection zone. In **Table 1**, the ranges of the employed reactant concentration, [Reactant], and the determined k'–k'_0 values are summarized. According to **Eq. E2**, the slopes of the k'-k'_0 *versus* [Reactant] plots yield the bimolecular rate coefficients k_i. Nevertheless, the linear relationship between k'-k'_0 and [Reactant] is not always accomplished, as shown in the example in **Figure 2**. In this figure, a downward curvature in the plot of k'-k'_0 vs. $[CH_3NH_2]$ was observed at concentrations higher than 3×10^{13} cm^{-3}. As discussed in previous works (Ocaña et al., 2017, 2019; Blázquez et al., 2020; Neeman et al., 2021), this curvature may be the result of the dimerization of the OH-co reactant, CH_3NH_2 in this case. Considering the onset of dimerization, the red straight line in **Figure 2** represents the fit to **Eq. E2** at $[CH_3NH_2]$ below ~3×10^{13} cm^{-3}. In contrast, for reaction R1 the plot of k'-k'_0 vs. $[NH_3]$ is linear over the entire concentration range, as displayed in **Figure 3A**. Since this concentration range is much larger than the one for CH_3NH_2 and that the reactivity with OH is significantly slower for NH_3 than for CH_3NH_2, it shows that the dimerization of NH_3 is much less efficient than that of CH_3NH_2 at 22 K. In **Figure 3B**, all kinetic data obtained in the linear part of the k'-k'_0 vs. $[CH_3NH_2]$ plot are depicted. The bimolecular rate coefficient k_2 at ca. 22 K is, then, obtained from the slope of such a plot.

Reagents Gases: He (99.999%, Nippon gases), NH_3 (≥ 99.95%, Merck) and CH_3NH_2 (≥ 99.0%, Merck) were used as supplied. Aqueous solution of H_2O_2 (Sharlab, initially at 50% w/w) was pre-concentrated as explained earlier (Albaladejo et al., 2003).

RESULTS AND DISCUSSION

The OH + NH_3 Reaction

Temperature Dependence of k_1

A summary of the individual rate coefficients k_1 obtained at 22 K and different total pressures of the gas jet is presented in **Table 1**. Within the stated statistical uncertainties (± 2σ), no pressure dependence of k_1 was observed in the investigated range (0.10–0.51 mbar). For this reason, we combined all the kinetic results, as shown in **Figure 3A** The resulting rate coefficient for the OH + NH_3 reaction at ca. 22 K is:

$$\boldsymbol{k_1(\sim 22\,K) = (2.27 \pm 0.1) \times 10^{-11} cm^3 s^{-1}}$$

where the uncertainty (± 2σ) only includes statistical errors. An additional 10% uncertainty has to be added to account for the systematic errors.

As mentioned in the Introduction section, **Eq. R1** has been investigated under extensive experimental conditions of temperature (230–2,360) K and pressure (1–4,000 mbar). A summary of all previous kinetic studies can be found in the most recent investigation from Diau et al. (1990). Focusing on the works carried out as a function of temperature (Zellner and

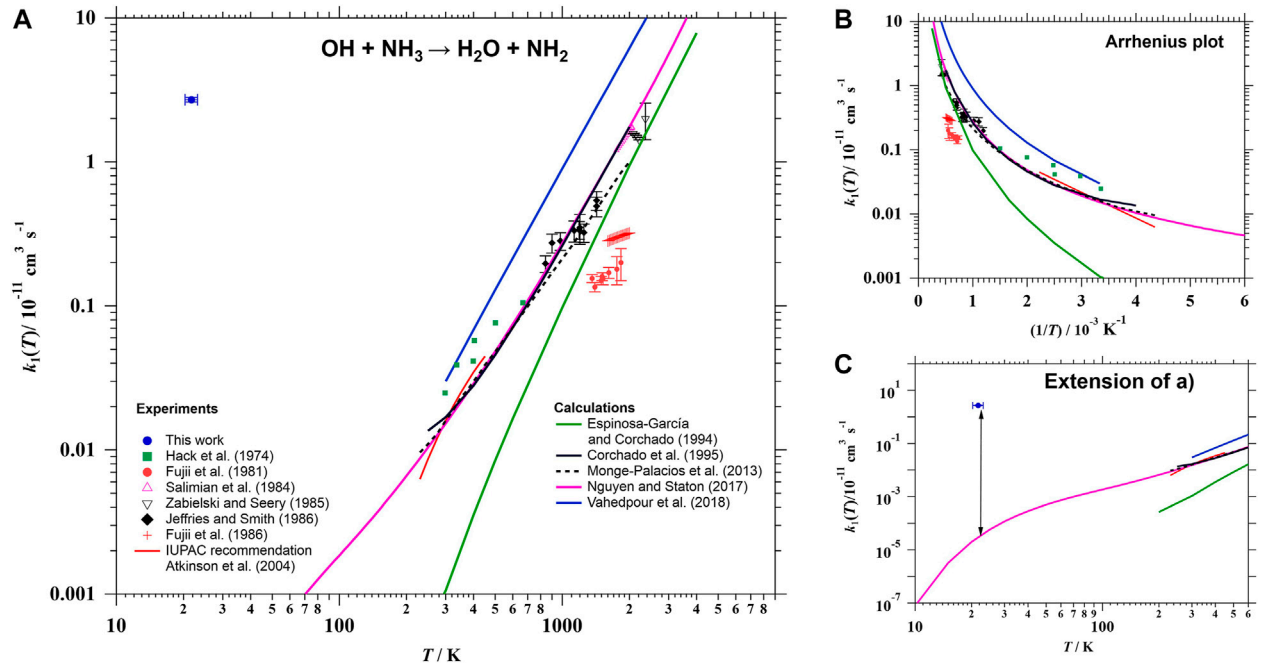

FIGURE 4 | (A) Temperature dependence of k_1 (log-log plot) in the 22–4,000 K range. Individual rate coefficients at room temperature K (Zellner and Smith, 1974; Perry et al., 1976; Silver and Kolb, 1980; Stephens, 1984; Diau et al., 1990) are not included in the figure, but they are considered in the IUPAC recommendation (red curve). **(B)** Arrhenius plot for k_1 between 170 and 4,000 K to better see the curvature (non-Arrhenius behavior). **(C)** Extension of the log-log plot shown in **(A)** to show the great enhancement of k_1 with respect to theoretical predictions at 20 K.

Smith, 1974; Hack et al., 1974; Perry et al., 1976; Silver and Kolb, 1980; Fujii et al., 1981, 1986; Salimian et al., 1984; Stephens, 1984; Zabielski and Seery, 1985; Jeffries and Smith, 1986; Diau et al., 1990), a positive temperature dependence of k_1 was observed in all cases, as shown in **Figure 4A**. For instance, IUPAC recommends a T-expression for k_1, based on previous results below 450 K (Zellner and Smith, 1974; Perry et al., 1976; Silver and Kolb, 1980; Stephens, 1984; Diau et al., 1990), with an E_a/R factor of 925 K which yields an activation energy (E_a) of 1.8 kcal/mol (Atkinson et al., 2004):

$$k_1\,(230-450\,K) = 3.5\times10^{-12}exp^{-925\ K/T}\ \ cm^3s^{-1} \qquad \text{(E3)}$$

Even so, as hydrogen atom transfer reactions usually show significant dynamical quantum effects (see Reaction mechanism), the kinetics of reaction R1 deviates from the Arrhenius behavior, showing a curvature in the plot of $ln\ k_1$ versus $1/T$. This deviation from Arrhenius behavior has been observed experimentally between 840 and 1,425 K (Jeffries and Smith, 1986) and predicted theoretically between 5 and 4,000 K (Espinosa-García and Corchado, 1994; Corchado et al., 1995; Monge-Palacios et al., 2013b; Nguyen and Stanton, 2017; Vahedpour et al., 2018). Most of the computed k_1 have been reported at temperatures higher than 200 K (Espinosa-García and Corchado, 1994; Corchado et al., 1995; Monge-Palacios et al., 2013b; Vahedpour et al., 2018). Only the calculations by Nguyen and Stanton (2017) were performed at lower temperatures and down to 5 K. For ease of presentation, kinetic data between 170 and 4,000 K are plotted in **Figure 4B** in Arrhenius form to clearly show the curvature. Down to 20 K, the predicted k_1 by Nguyen and Stanton (2017), represented by a pink line in **Figure 4C**, was 2×10^{-16} cm^3 s^{-1}. This value is around five orders of magnitude lower than the experimental result reported in this work. Certainly, further kinetic studies between 230 and 22 K (and even below) are needed and are planned in our laboratory in the future.

Reaction Mechanism

As stated in the Introduction section, the reaction mechanism of the OH + NH_3 reaction has been widely studied from a theoretical point of view. The effects of vibrational and translational energy of NH_3 and OH counter partners have been studied by quasi-classical trajectories (Nyman, 1996; Monge-Palacios and Espinosa-Garcia, 2013; Monge-Palacios et al., 2013a) and by quantum scattering calculations (Nyman, 1996). Besides these dynamical studies, *ab initio* calculations based on the transition state theory (TST) were reported. In **Scheme 1**, a simplified illustration of the relative energies to the reactants of the stationary points along the minimum energy pathway (MEP) for the OH + NH_3 system is shown. Some studies proposed that product formation in reaction R1 occurs from the transition state and reported energy barriers ranged from 2.03 kcal/mol to 8.94 kcal/mol (Giménez et al., 1992; Bowdridge et al., 1996; Lynch et al., 2000). However, other investigations proposed that reaction R1 occurs through a H-bonded PRC at the entrance channel (Corchado et al., 1995; Bowdridge et al.,

TABLE 2 | Summary of the calculated energies relative to reactants (in kcal/mol) of the stationary points in the MEP for the OH + NH_3 reaction reported in the literature (see text for more details).

PRC	TS	PPC	Products	References
−1.75	8.94	—	−10.69[a]	Giménez et al. (1992)
	9.05	−15.02	−8.98	Espinosa-García and Corchado (1994)
	3.65	−17.39	−11.96	Corchado et al. (1995)
	2.03	—	—	Bowdridge et al. (1996)
	4.4	—	−7.1	Lynch et al. (2000)
−1.8	3.3	−15.6	−10.0	Monge-Palacios et al. (2013b)
0.33	2.6	−14.47	−11.49	Nguyen and Stanton (2017)

[a]From $\Delta H^{o}_{r298\ K}$.

1996; Monge-Palacios et al., 2013b; Nguyen and Stanton, 2017). The relative energy of this PRC is positioned a few kcal/mol above the reactants (Nguyen and Stanton, 2017) or −1.8 kcal/mol (Corchado et al., 1995; Monge-Palacios et al., 2013b). In addition to the PRC, a H-bonded complex near the products (PPC, pre-product complex) (Espinosa-García and Corchado, 1994; Corchado et al., 1995; Monge-Palacios et al., 2013b; Nguyen and Stanton, 2017) is proposed at the exit channel, which is stabilized with respect to the reactants by *ca.* −15 kcal/mol. **Table 2** summarizes the relative energies of PRC, TS, and PPC from theoretical calculations reported in the literature.

Note that the reaction pathway for the OH + NH_3 system is qualitatively similar to the one calculated for the OH + CH_3OH reaction (Ocaña et al., 2019), i.e., formation of a H-bonded PRC followed by a transition state with a positive energy barrier. Following that comparison, the observed increase of k_1 can be interpreted by the formation of a long-lived PRC at very low temperatures, which surpasses the energy barrier by quantum mechanical tunnelling.

Effect of k_1 in the Abundance of Interstellar NH_3

Astrochemical networks apply modified Arrhenius expressions to estimate rate coefficients in a certain temperature interval:

$$k(T) = \alpha\left(\frac{T}{300K}\right)^{\beta} exp^{-\gamma/T} \quad \text{(E4)}$$

For example, KIDA database uses the recommended expression by Atkinson et al. (2004) (**Eq. E3**, where $\beta = 0$) and UDfA database uses the following expression:

$$k_1\,(200 - 3,000K) = 1.47 \times 10^{-13}\left(\frac{T}{300K}\right)^{2.05} exp^{-7\ K/T}\ cm^3 s^{-1} \quad \text{(E5)}$$

Note that these recommended **Eqs E3**, **E5** are valid on the stated temperature range. Using these T-expressions to extrapolate rate coefficients down to 22 K is extremely risky. One gets very low values of k_1, on the order of 10^{-27} $cm^3\ s^{-1}$ from KIDA expression **Eq. E3** and 10^{-16} $cm^3\ s^{-1}$ from UDfA **Eq. E5**, compared with the rate coefficient for the OH + NH_3 reaction determined in the present work. Using **Eqs E3** and **E5**, the rate coefficient at 230 K, k_1(230 K), and extrapolated k_1(200 K) are 6.4 and 8.3 × 10^{-14} $cm^3\ s^{-1}$, respectively. At the lowest temperature, the k_1(~22 K)/k_1(230 K) ratio is around 380. This value means that the rate of formation of NH_2 radicals from the reaction of NH_3 with OH radicals is really enhanced by more than two orders of magnitude at the typical temperature of a cold dark cloud. Using k_1, obtained in this work, and the rate coefficients from the KIDA and UDfA databases, for a typical cold dark cloud, with H_2 molecular density of 1×10^4 cm^{-3} and a temperature of 10 K (close to the one reproduced in this work) (Agúndez and Wakelam, 2013), the change in modelled abundances of NH_3 is negligible for both reaction networks. The main destruction route for NH_3 in this cold environment is the reaction with H_3O^+ cations, being the reaction of NH_3 with OH radicals around 1% of that with H_3O^+ species.

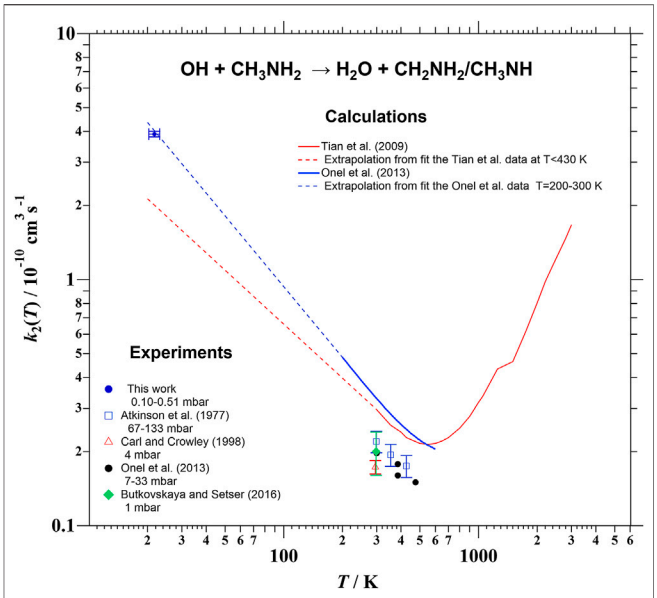

FIGURE 5 | Temperature dependence of k_2 in the 22–3,000 K range.

The OH + CH_3NH_2 Reaction

Temperature Dependence of k_2

As shown in **Table 1**, no pressure dependence of the rate coefficient for the OH + CH_3NH_2 reaction was observed in the investigated range. The resulting k_2 at ca. 22 K from the combination of all kinetic data at different gas densities (see **Figure 3B**) is:

$$k_2\,(\sim 22K) = (3.9 \pm 0.1) \times 10^{-10} cm^3 s^{-1}$$

This value together with previously reported k_2 over the 298–3,000 K temperature range (Atkinson et al., 1977; Carl and Crowley, 1998; Tian et al., 2009; Onel et al., 2013; Butkovskaya and Setser, 2016) are depicted in **Figure 5**. The temperature dependence of k_2 was first measured by Atkinson et al. (1977) at T > 299 K, who reported the following Arrhenius expression:

$$k_2\,(299 - 426\,K) = 1.02 \times 10^{-11} exp^{(455\pm300)\,cal\,mol^{-1}/RT}\ cm^3 s^{-1} \quad \text{(E6)}$$

The activation energy is slightly negative in this case, −0.45 kcal/mol; however more recently, the negative temperature dependence observed experimentally for **Eq. R2** was also reported by Onel et al. (2013) as an expression with

TABLE 3 | Summary of the calculated relative (to reactants) energies (in kcal/mol) of the stationary points in the MEP for the OH + CH_3NH_2 reaction reported in the literature (see text for more details).

Channel	PRC	TS	PPC	Products	References
R2a	—	0.36	—	−23.19	Galano and Alvarez-Idaboy (2008)
R2b	—	0.97	—	−17.00	
R2a	−0.61	−0.52	−28.48	−23.17	Tian et al. (2009)
R2b	−8.45	1.02	−23.03	−17.07	
R2a	−6.38	−1.96	−29.54	−43.52	Onel et al. (2013)
R2b	−6.38	−2.0	−24.19	−26.48	
R2a	−5.4	1.2	—	−26.0	Borduas et al. (2016)
R2b	−0.2	0.2	—	−19.0	

no activation energy and a T-dependent pre-exponential factor (black circles in **Figure 5**):

$$k_2\,(298-500K) = 1.89\times10^{-11}\left(\frac{T}{298K}\right)^{-0.56} cm^3 s^{-1} \qquad \text{(E7)}$$

Using the experimental Onel's expression, the extrapolated k_2(~22 K) is ca. 8×10^{-11} $cm^3\,s^{-1}$ (4.9 times lower than the experimental one reported here), while **Eq. E6** provides an extrapolated k_2(~22 K) of 3.4×10^{-7} $cm^3\,s^{-1}$, which is a non-realistic value for a neutral-neutral reaction. Onel et al. (2013) also computed k_2 between 200 and 500 K (blue line in **Figure 5**) to be around 60% higher than the experimental values. No experimental kinetic data have been reported at T > 500 K, however Tian et al. (2009) predicted a minimum of k_2 around 550 K and a remarkable increase of k_2 at higher temperatures, i.e., the rate coefficient for the OH + CH_3NH_2 reaction is expected to exhibit a non-Arrhenius behavior. As shown by dashed lines in **Figure 5**, the extrapolated k_2 from calculations of Onel et al. (2013) is in excellent agreement with our reported value and the value of k_2 obtained by extrapolation of Tian et al. (2009) data is only a factor of ca. 2 lower than the experimental value reported in this work. Additional kinetic studies between 298 and 22 K are clearly needed to confirm the expected trend in the T-dependence of k_2.

Reaction Mechanism

The possible exothermic reaction channels for **Eq. R2** are the H-abstraction from the methyl group (**Eq. R2a**) or from the amino group (**Eq. R2b**):

$$OH + CH_3NH_2 \rightarrow H_2O + CH_2NH_2 \qquad \text{(R2a)}$$
$$\rightarrow H_2O + CH_3NH \qquad \text{(R2b)}$$

Theoretically, the mechanism of **Eq. R2** has been investigated by several groups (Galano and Alvarez-Idaboy, 2008; Tian et al., 2009; Onel et al., 2013; Borduas et al., 2016). The calculations suggest a stepwise mechanism involving the formation of a PRC in the entrance channels (Tian et al., 2009; Onel et al., 2013; Borduas et al., 2016) and a PPC in the exit channels (Tian et al., 2009; Onel et al., 2013). On the other hand, the OH-addition to N and subsequent concerted C-C cleavage, which produces CH_3 radicals and NH_2OH, is endothermic with an energy barrier of 37.4 kcal/mol (Borduas et al., 2016). For that reason, in **Scheme 2**, the energies of the stationary points along the MEP for the OH + CH_3NH_2 reaction is only depicted for the exothermic channels R2a and R2b. The relative energies of PRC, TS, and PPC for reaction pathways R2a and R2c reported in theoretical calculations are summarized in **Table 3** (Galano and Alvarez-Idaboy, 2008; Tian et al., 2009; Onel et al., 2013); Borduas et al., 2016). In the 299–3,000 K temperature range, the dominant exothermic channel is that producing CH_2NH_2 radicals (Galano and Alvarez-Idaboy, 2008; Tian et al., 2009). The branching ratio for R2a (r) at 298 K was reported to be of 0.797 (Galano and Alvarez-Idaboy, 2008) and 0.74 (Tian et al., 2009). In contrast, Borduas et al. (2016) concluded that channels R2a and R2b are competitive, with energy barriers close to the entrance level energies of the reactants and within 1 kcal mol^{-1} of each other. Nevertheless, the dominance of R2a channel at room temperature has experimentally been confirmed by Nielsen et al. (2011, 2012), Onel et al. (2014), Butkovskaya and Setser (2016). Nielsen et al. (2011, 2012) performed experiments in EUPHORE atmospheric chamber providing a r of (0.75 ± 0.05) for channel R2a. A similar value (0.79 ± 0.15) was found by Onel et al. (2014) and by Butkovskaya and Setser (2016) (0.74 ± 0.05) No measurements or calculations were found at temperatures below room temperature. Thus, further theoretical and/or experimental studies are needed to know what the branching ratios of channels R2a (forming CH_2NH_2) and R2b (forming CH_3NH) are at interstellar temperatures.

Effect of k_2 in the Abundance of Interstellar CH_3NH_2

Neither KIDA database nor UDfA network include this OH-reaction as a potential destruction route for CH_3NH_2. However, this reaction is extremely fast at ca. 22 K as it is shown by the experimental rate coefficient for the OH + CH_3NH_2 reaction reported here. Our measured k_2(~22 K) would, then, lead to a quicker depletion of CH_3NH_2 by reaction with OH in astrochemical models. The k_2(~22 K)/k_2(298 K) ratio is around 20, indicating that the use of k_2(298 K) in modelling the ISM would underestimate the loss of CH_3NH_2 by OH by more than one order of magnitude. Using the reported k_2(~22 K) in the pure gas-phase model from Agúndez and Wakelam (2013), the destruction of CH_3NH_2 by OH radicals in a typical cold dark cloud (H_2 molecular density of 1×10^4 cm^{-3} and temperature 10 K) supposes around 1/3 of that initiated by HCO^+ (main depletion route).

CONCLUSION

The OH-reactivity of NH_3 at ca. 22 K is more than two orders of magnitude higher than that observed at the lowest temperature achieved up to now, 230 K. This confirms that the observed curvature in the Arrhenius plot reflects the increase of k_1 at low temperatures. Further studies are needed to complete the kinetic

behavior between 22 and 230 K and lower temperatures than 22 K. For CH_3NH_2, the determined rate coefficient at ca. 22 K is almost 20 times higher than the one measured at room temperature. The slightly negative temperature dependence of k_2 observed by Atkinson et al. (1977) at T > 298 K, implies that the OH-reactivity increases at temperatures lower than room temperature, as observed in this work. These new experimental data indicate that the inclusion of the rate coefficient for the OH + NH_3 reaction at 20 K in gas-phase astrochemical models does not significantly change the abundance of NH_3 in a typical cold dark cloud since the main destruction route for NH_3 is the reaction with H_3O^+. However, the inclusion of the rate coefficient for the OH + CH_3NH_2 reaction at 20 K, not considered in KIDA and UDfA networks, indicated that the contribution of this destruction route is not negligible, accounting for 1/3 of the main assumed depletion route (reaction with HCO^+) in this IS environment with temperature close to 10 K.

DATA AVAILABILITY STATEMENT

The raw data supporting the conclusion of this article will be made available by the authors, without undue reservation.

AUTHOR CONTRIBUTIONS

DG performed the experiments, analyzed the kinetic data, and wrote the draft of the article; BB and EJ contributed to the design and supervision of the experiments; AC and EJ participated in the critical revision of the article; JA and EJ got the funds for carrying out this research and managed the projects. All authors discussed the results and contributed to the final manuscript.

FUNDING

This work has been supported by the Spanish Ministry of Science and Innovation (MICINN) through the CHEMLIFE project (Ref: PID2020-113936GB-I00), the regional government of Castilla-La Mancha through CINEMOL project (Ref: SBPLY/19/180501/000052) and by the University of Castilla-La Mancha—UCLM (Ayudas para la financiación de actividades de investigación dirigidas a grupos (REF: 2020-GRIN-29016 and 2021-GRIN-31279). DG also acknowledges UCLM (Plan Propio de Investigación) for funding his contract during the performance of this investigation.

ACKNOWLEDGMENTS

The authors acknowledge Francisco J. Maigler for his technical assistance during the performance of these experiments and Dr. Marcelino Agúndez for helpful discussion on the effect of current rate coefficients on the abundance of NH_3 and CH_3NH_2 in a typical cold dark cloud.

REFERENCES

Acharyya, K., Herbst, E., Caravan, R. L., Shannon, R. J., Blitz, M. A., and Heard, D. E. (2015). The Importance of OH Radical-Neutral Low Temperature Tunnelling Reactions in Interstellar Clouds Using a New Model. *Mol. Phys.* 113, 2243–2254. doi:10.1080/00268976.2015.1021729

Agúndez, M., and Wakelam, V. (2013). Chemistry of Dark Clouds: Databases, Networks, and Models. *Chem. Rev.* 113, 8710–8737. doi:10.1021/cr4001176

Albaladejo, J., Ballesteros, B., Jiménez, E., Díaz de Mera, Y., and Martínez, E. (2003). Gas-phase OH Radical-Initiated Oxidation of the 3-halopropenes Studied by PLP-LIF in the Temperature Range 228-388 K. *Atmos. Environ.* 37, 2919–2926. doi:10.1016/S1352-2310(03)00297-8

Antiñolo, M., Agúndez, M., Jiménez, E., Ballesteros, B., Canosa, A., Dib, G. E., et al. (2016). Reactivity of OH and CH_3OH between 22 and 64 K: Modeling the Gas Phase Production of CH_3O in Barnard 1b. *ApJ* 823, 25. doi:10.3847/0004-637X/823/1/25

A. Silver, J., and E. Kolb, C. (1980). Rate Constant for the Reaction NH_3 + OH → NH_2 + H_2O over a Wide Temperature Range. *Chem. Phys. Lett.* 75, 191–195. doi:10.1016/0009-2614(80)80492-1

Atkinson, R., Baulch, D. L., Cox, R. A., Crowley, J. N., Hampson, R. F., Hynes, R. G., et al. (2004). Evaluated Kinetic and Photochemical Data for Atmospheric Chemistry: Part 1 – Gas Phase Reactions of O_x, HO_x, NO_x and SO_x Species. *Atmos. Chem. Phys.* 4, 1461–1738. doi:10.5194/acpd-3-6179-2003

Atkinson, R., Perry, R. A., and Pitts, J. N. (1977). Rate Constants for the Reaction of the OH Radical with CH_3SH and CH_3NH_2 over the Temperature Range 299-426 °K. *J. Chem. Phys.* 66, 1578–1581. doi:10.1063/1.434076

Bada, J. L., and Lazcano, A. (2002). Some like it Hot, but Not the First Biomolecules. *Science* 296, 1982–1983. doi:10.1126/science.1069487

Balucani, N. (2009). Elementary Reactions and Their Role in Gas-phase Prebiotic Chemistry. *Int. J. Mol. Sci.* 10, 2304–2335. doi:10.3390/ijms10052304

Bernstein, M. (2006). Prebiotic Materials from on and off the Early Earth. *Phil. Trans. R. Soc. B* 361, 1689–1702. doi:10.1098/rstb.2006.1913

Blázquez, S., González, D., García-Sáez, A., Antiñolo, M., Bergeat, A., Caralp, F., et al. (2019). Experimental and Theoretical Investigation on the OH + $CH_3C(O)CH_3$ Reaction at Interstellar Temperatures (T = 11.7-64.4 K). *ACS Earth Space Chem.* 3, 1873–1883. doi:10.1021/acsearthspacechem.9b00144

Blázquez, S., González, D., Neeman, E. M., Ballesteros, B., Agúndez, M., Canosa, A., et al. (2020). Gas-phase Kinetics of CH_3CHO with OH Radicals between 11.7 and 177.5 K. *Phys. Chem. Chem. Phys.* 22, 20562–20572. doi:10.1039/D0CP03203D

Bocherel, P., Herbert, L. B., Rowe, B. R., Sims, I. R., Smith, I. W. M., and Travers, D. (1996). Ultralow-Temperature Kinetics of CH($X^2\Pi$) Reactions: Rate Coefficients for Reactions with O_2 and NO (T = 13–708 K), and with NH_3 (T = 23–295 K). *J. Phys. Chem.* 100, 3063–3069. doi:10.1021/jp952628f

Borduas, N., Abbatt, J. P. D., Murphy, J. G., So, S., and Da Silva, G. (2016). Gas-Phase Mechanisms of the Reactions of Reduced Organic Nitrogen Compounds with OH Radicals. *Environ. Sci. Technol.* 50, 11723–11734. doi:10.1021/acs.est.6b03797

Bourgalais, J., Capron, M., Kailasanathan, R. K. A., Osborn, D. L., Hickson, K. M., Loison, J.-C., et al. (2015). The C(^{3}P) + NH_3 Reaction in Interstellar Chemistry. I. Investigation of the Product Formation Channels. *ApJ* 812, 106–140. doi:10.1088/0004-637X/812/2/106

Bowdridge, M., Furue, H., and Pacey, P. D. (1996). Properties of Transition Species in the Reactions of Hydroxyl with Ammonia and with Itself. *J. Phys. Chem.* 100, 1676–1681. doi:10.1021/jp9522573

Butkovskaya, N. I., and Setser, D. W. (2016). Branching Ratios and Vibrational Distributions in Water-Forming Reactions of OH and OD Radicals with Methylamines. *J. Phys. Chem. A.* 120, 6698–6711. doi:10.1021/acs.jpca.6b06411

Canosa, A., Ocaña, A. J., Antiñolo, M., Ballesteros, B., Jiménez, E., and Albaladejo, J. (2016). Design and testing of temperature tunable de Laval nozzles for applications in gas-phase reaction kinetics. *Exp. Fluids* 57. doi:10.1007/s00348-016-2238-1

Carl, S. A., and Crowley, J. N. (1998). Sequential Two (Blue) Photon Absorption by NO2 in the Presence of H2 as a Source of OH in Pulsed Photolysis Kinetic Studies: Rate Constants for Reaction of OH with CH_3NH_2, $(CH_3)_2NH$, $(CH_3)_3N$, and $C_2H_5NH_2$ at 295 K. *J. Phys. Chem. A.* 102, 8131–8141. doi:10.1021/jp9821937

Cazaux, S., Cobut, V., Marseille, M., Spaans, M., and Caselli, P. (2010). Water Formation on Bare Grains: When the Chemistry on Dust Impacts Interstellar Gas. *A&A* 522, A74. doi:10.1051/0004-6361/201014026

Cheung, A. C., Rank, D. M., Townes, C. H., Thornton, D. D., and Welch, W. J. (1968). Detection of NH3Molecules in the Interstellar Medium by Their Microwave Emission. *Phys. Rev. Lett.* 21, 1701–1705. doi:10.1103/PhysRevLett.21.1701

Chyba, C., and Sagan, C. (1992). Endogenous Production, Exogenous Delivery and Impact-Shock Synthesis of Organic Molecules: an Inventory for the Origins of Life. *Nature* 355, 125–132. doi:10.1038/355125a0

Cleaves, H. J., Chalmers, J. H., Lazcano, A., Miller, S. L., and Bada, J. L. (2008). A Reassessment of Prebiotic Organic Synthesis in Neutral Planetary Atmospheres. *Orig. Life Evol. Biosph.* 38, 105–115. doi:10.1007/s11084-007-9120-3

Corchado, J. C., Espinosa-Garcia, J., Hu, W.-P., Rossi, I., and Truhlar, D. G. (1995). Dual-Level Reaction-Path Dynamics (The ///Approach to VTST with Semiclassical Tunneling). Application to OH + NH_3 → H_3O + NH_2. *J. Phys. Chem.* 99, 687–694. doi:10.1021/j100002a037

Diau, E. W. G., Tso, T. L., and Lee, Y. P. (1990). Kinetics of the Reaction Hydroxyl + Ammonia in the Range 273-433 K. *J. Phys. Chem.* 94, 5261–5265. doi:10.1021/j100376a018

Ehrenfreund, P., Irvine, W., Becker, L., Blank, J., Brucato, J. R., Colangeli, L., et al. (2002). Astrophysical and Astrochemical Insights into the Origin of Life. *Rep. Prog. Phys.* 65, 1427–1487. doi:10.1088/0034-4885/65/10/202

Espinosa-García, J., and Corchado, J. C. (1994). Analysis of Certain Factors in the Direct Dynamics Method: Variational Rate Constant of the NH_3+OH→NH_2+H_2O Reaction. *J. Chem. Phys.* 101, 8700–8708. doi:10.1063/1.468065

Förstel, M., Bergantini, A., Maksyutenko, P., Góbi, S., and Kaiser, R. I. (2017). Formation of Methylamine and Ethylamine in Extraterrestrial Ices and Their Role as Fundamental Building Blocks of Proteinogenicα-Amino Acids. *ApJ* 845, 83. doi:10.3847/1538-4357/aa7edd

Fourikis, N., Takagi, K., and Morimoto, M. (1974). Detection of Interstellar Methylamine by its 2_{02}->1_{10} A_{a̋-}} State Transition. *ApJ* 191, L139. doi:10.1086/181570

Freeman, A., and Millar, T. J. (1983). Formation of Complex Molecules in TMC-1. *Nature* 301, 402–404. doi:10.1038/301402a0

Fujii, N., Chiba, K., Uchida, S., and Miyama, H. (1986). The Rate Constants of the Elementary Reactions of NH_3 with O and OH. *Chem. Phys. Lett.* 127, 141–144. doi:10.1016/S0009-2614(86)80243-3

Fujii, N., Miyama, H., and Asaba, T. (1981). Determination of the Rate Constant for the Reaction NH_3 + OH → NH_2 + H_2O. *Chem. Phys. Lett.* 80, 355–357. doi:10.1016/0009-2614(81)80125-X

Galano, A., and Alvarez-Idaboy, J. R. (2008). Branching Ratios of Aliphatic Amines + OH Gas-phase Reactions: A Variational Transition-State Theory Study. *J. Chem. Theor. Comput.* 4, 322–327. doi:10.1021/ct7002786

Garrod, R. T. (2013). A Three-phase Chemical Model of Hot Cores: The Formation of Glycine. *ApJ* 765, 60. doi:10.1088/0004-637X/765/1/60

Garrod, R. T., Weaver, S. L. W., and Herbst, E. (2008). Complex Chemistry in Star-forming Regions: An Expanded Gas-Grain Warm-up Chemical Model. *ApJ* 682, 283–302. doi:10.1086/588035

Gerin, M., Neufeld, D. A., and Goicoechea, J. R. (2016). Interstellar Hydrides. *Annu. Rev. Astron. Astrophys.* 54, 181–225. doi:10.1146/annurev-astro-081915-023409

Gianturco, F. A., Yurtsever, E., Satta, M., and Wester, R. (2019). Modeling Ionic Reactions at Interstellar Temperatures: The Case of NH_2- + H_2 ⇔ NH_3 + H-. *J. Phys. Chem. A.* 123, 9905–9918. doi:10.1021/acs.jpca.9b07317

Giménez, X., Moreno, M., and Lluch, J. M. (1992). Ab Initio study of the NH3 + OH Reaction. *Chem. Phys.* 165, 41–46. doi:10.1016/0301-0104(92)80041-S

Goicoechea, J. R., Joblin, C., Contursi, A., Berné, O., Cernicharo, J., Gerin, M., et al. (2011). OH Emission from Warm and Dense Gas in the Orion Bar PDR. *A&A* 530, L16. doi:10.1051/0004-6361/201116977

Hack, W., Hoyerman, K., and Wagner, H. G. (1974). Reaktionen des Hydroxylradikals mit Ammoniak und Hydrazin in der Gasphase. *Ber.Bunsenges. Phys. Chem. Chem. Phys.* 78, 386–391.

Halfen, D. T., Ilyushin, V. V., and Ziurys, L. M. (2013). Insights into Surface Hydrogenation in the Interstellar Medium: Observations of Methanimine and Methyl Amine in Sgr B2(N). *ApJ* 767, 66. doi:10.1088/0004-637X/767/1/66

Heard, D. E. (2018). Rapid Acceleration of Hydrogen Atom Abstraction Reactions of OH at Very Low Temperatures through Weakly Bound Complexes and Tunneling. *Acc. Chem. Res.* 51, 2620–2627. doi:10.1021/acs.accounts.8b00304

Herbst, E., and Klemperer, W. (1973). The Formation and Depletion of Molecules in Dense Interstellar Clouds. *ApJ* 185, 505–533. doi:10.1086/152436

Herbst, E. (1985). The Rate of the Radiative Association Reaction between CH_3(+) and NH_3 and its Implications for Interstellar Chemistry. *ApJ* 292, 484–486. doi:10.1086/163179

Herbst, E., and van Dishoeck, E. F. (2009). Complex Organic Interstellar Molecules. *Annu. Rev. Astron. Astrophys.* 47, 427–480. doi:10.1146/annurev-astro-082708-101654

Hickson, K. M., Loison, J.-C., Bourgalais, J., Capron, M., Picard, S. D. L., Goulay, F., et al. (2015). The C(^{3}P) + NH_3 Reaction in Interstellar Chemistry. Ii. Low Temperature Rate Constants and Modeling of Nh, Nh_2, and Nh_3Abundances in Dense Interstellar Clouds. *ApJ* 812, 107–125. doi:10.1088/0004-637X/812/2/107

Ioppolo, S., Fedoseev, G., Chuang, K.-J., Cuppen, H. M., Clements, A. R., Jin, M., et al. (2021). A Non-energetic Mechanism for glycine Formation in the Interstellar Medium. *Nat. Astron.* 5, 197–205. doi:10.1038/s41550-020-01249-0

Jeffries, J. B., and Smith, G. P. (1986). Kinetics of the Reaction Hydroxyl + Ammonia. *J. Phys. Chem.* 90, 487–491. doi:10.1021/j100275a027

Jiménez, E., Antiñolo, M., Ballesteros, B., Canosa, A., and Albaladejo, J. (2016). First Evidence of the Dramatic Enhancement of the Reactivity of Methyl Formate ($HC(O)OCH_3$) with OH at Temperatures of the Interstellar Medium: a Gas-phase Kinetic Study between 22 K and 64 K. *Phys. Chem. Chem. Phys.* 18, 2183–2191. doi:10.1039/C5CP06369H

Jiménez, E., Ballesteros, B., Canosa, A., Townsend, T. M., Maigler, F. J., Napal, V., et al. (2015). Development of a Pulsed Uniform Supersonic Gas Expansion System Based on an Aerodynamic Chopper for Gas Phase Reaction Kinetic Studies at Ultra-low Temperatures. *Rev. Scientific Instr.* 86, 045108. doi:10.1063/1.4918529

Jiménez, E., Lanza, B., Garzón, A., Ballesteros, B., and Albaladejo, J. (2005). Atmospheric Degradation of 2-butanol, 2-Methyl-2-Butanol, and 2,3-Dimethyl-2-Butanol: OH Kinetics and UV Absorption Cross Sections. *J. Phys. Chem. A.* 109, 10903–10909. doi:10.1021/jp054094g

Jonusas, M., Leroux, K., and Krim, L. (2020). N + H Surface Reaction under Interstellar Conditions: Does the $NH/NH_2/NH_3$ Distribution Depend on N/H Ratio? *J. Mol. Struct.* 1220, 128736. doi:10.1016/j.molstruc.2020.128736

Kaifu, N., Morimoto, M., Nagane, K., Akabane, K., Iguchi, T., and Takagi, K. (1974). Detection of Interstellar Methylamine. *ApJ* 191, L135. doi:10.1086/181569

Kim, Y. S., and Kaiser, R. I. (2011). On the Formation of Amines (RNH_2) and the Cyanide Anion (C_n^-) in Electron-Irradiated Ammonia-Hydrocarbon Interstellar Model Ices. *ApJ* 729, 68. doi:10.1088/0004-637X/729/1/68

Kurylo, M. J. (1973). Kinetics of the Reactions OH (V = O) + NH_3 →; H_2O + NH_2 and OH(v = O) + O_3 → HO_2 + O_2 at 298°K. *Chem. Phys. Lett.* 23, 467–471. doi:10.1016/0009-2614(73)89003-7

Linnartz, H., Ioppolo, S., and Fedoseev, G. (2015). Atom Addition Reactions in Interstellar Ice Analogues. *Int. Rev. Phys. Chem.* 34, 205–237. doi:10.1080/0144235X.2015.1046679

Lynch, B. J., Fast, P. L., Harris, M., and Truhlar, D. G. (2000). Adiabatic Connection for Kinetics. *J. Phys. Chem. A.* 104, 4811–4815. doi:10.1021/jp000497z

Miller, S. L. (1953). A Production of Amino Acids under Possible Primitive Earth Conditions. *Science* 117, 528–529. doi:10.1126/science.117.3046.528

Monge-Palacios, M., Corchado, J. C., and Espinosa-Garcia, J. (2013a). Dynamics Study of the OH + NH_3 Hydrogen Abstraction Reaction Using QCT Calculations Based on an Analytical Potential Energy Surface. *J. Chem. Phys.* 138, 214306–214312. doi:10.1063/1.4808109

Monge-Palacios, M., and Espinosa-Garcia, J. (2013). Role of Vibrational and Translational Energy in the OH + NH_3 Reaction: A Quasi-Classical Trajectory Study. *J. Phys. Chem. A.* 117, 5042–5051. doi:10.1021/jp403571y

Monge-Palacios, M., Rangel, C., and Espinosa-Garcia, J. (2013b). Ab Initiobased Potential Energy Surface and Kinetics Study of the OH + NH_3 hydrogen Abstraction Reaction. *J. Chem. Phys.* 138, 084305. doi:10.1063/1.4792719

Neeman, E. M., González, D., Blázquez, S., Ballesteros, B., Canosa, A., Antiñolo, M., et al. (2021). The Impact of Water Vapor on the OH Reactivity toward

CH_3CHO at Ultra-low Temperatures (21.7-135.0 K): Experiments and Theory. *J. Chem. Phys.* 155, 034306. doi:10.1063/5.0054859

Nguyen, T. L., and Stanton, J. F. (2017). High-level Theoretical Study of the Reaction between Hydroxyl and Ammonia: Accurate Rate Constants from 200 to 2500 K. *J. Chem. Phys.* 147, 152704. doi:10.1063/1.4986151

Nielsen, C., D'Anna, B., Aursnes, M., and Boreave, A. (2012). *Summary Report from Atmospheric Chemistry Studies of Amines, Nitrosamines, Nitramines and Amides; Climit Project No. 208122*. Oslo: NILU, University of Oslo.

Nielsen, C. J., D'Anna, B., Karl, M., Aursnes, M., Boreave, A., Bossi, R., et al. (2011). *Summary Report: Photo-Oxidation of Methylamine, Dimethylamine and Trimetahylamine. Climit Project No. 201604NILU 2*. Oslo: University of Oslo.

Nizamov, B., and Leone, S. R. (2004). Rate Coefficients and Kinetic Isotope Effect for the C_2H Reactions with NH_3 and ND_3 in the 104–294 K Temperature Range. *J. Phys. Chem. A.* 108, 3766–3771. doi:10.1021/jp031361e

Nyman, G. (1996). Quantum Scattering Calculations on the NH_3+OH→NH_2+H_2O Reaction. *J. Chem. Phys.* 104, 6154–6167. doi:10.1063/1.471281

Ocaña, A. J., Blázquez, S., Ballesteros, B., Canosa, A., Antiñolo, M., Albaladejo, J., et al. (2018). Gas Phase Kinetics of the OH + CH_3CH_2OH Reaction at Temperatures of the Interstellar Medium (T = 21-107 K). *Phys. Chem. Chem. Phys.* 20, 5865–5873. doi:10.1039/C7CP07868D

Ocaña, A. J., Blázquez, S., Potapov, A., Ballesteros, B., Canosa, A., Antiñolo, M., et al. (2019). Gas-phase Reactivity of CH_3OH toward OH at Interstellar Temperatures (11.7-177.5 K): Experimental and Theoretical Study. *Phys. Chem. Chem. Phys.* 21, 6942–6957. doi:10.1039/c9cp00439d

Ocaña, A. J., Jiménez, E., Ballesteros, B., Canosa, A., Antiñolo, M., Albaladejo, J., et al. (2017). Is the Gas-phase OH+H_2CO Reaction a Source of HCO in Interstellar Cold Dark Clouds? A Kinetic, Dynamic, and Modeling Study. *ApJ* 850, 28. doi:10.3847/1538-4357/aa93d9

Ohishi, M., Suzuki, T., Hirota, T., Saito, M., and Kaifu, N. (2019). Detection of a New Methylamine (CH_3NH_2) Source: Candidate for Future glycine Surveys. *Publ. Astron. Soc. Jpn.* 71, 1–11. doi:10.1093/pasj/psz068

Onel, L., Blitz, M., Dryden, M., Thonger, L., and Seakins, P. (2014). Branching Ratios in Reactions of OH Radicals with Methylamine, Dimethylamine, and Ethylamine. *Environ. Sci. Technol.* 48, 9935–9942. doi:10.1021/es502398r

Onel, L., Thonger, L., Blitz, M. A., Seakins, P. W., Bunkan, A. J. C., Solimannejad, M., et al. (2013). Gas-phase Reactions of OH with Methyl Amines in the Presence or Absence of Molecular Oxygen. An Experimental and Theoretical Study. *J. Phys. Chem. A.* 117, 10736–10745. doi:10.1021/jp406522z

Perry, R. A., Atkinson, R., and Pitts, j. N., Jr (1976). Rate Constants for the Reactions OH+H_2S→H_2O+SH and OH+NH_3→H_2O+NH_2 over the Temperature Range 297-427 °K. *J. Chem. Phys.* 64, 3237. doi:10.1063/1.432663

Potapov, A., Canosa, A., Jiménez, E., and Rowe, B. (2017). Uniform Supersonic Chemical Reactors: 30 Years of Astrochemical History and Future Challenges. *Angew. Chem. Int. Ed.* 56, 8618–8640. doi:10.1002/anie.201611240

Rednyk, S., RoučkaKovalenko, Š., Kovalenko, A., Tran, T. D., Dohnal, P., Plašil, R., et al. (2019). Reaction of NH^+, NH_2^+, and NH_3^+ Ions with H_2 at Low Temperatures. *A&A* 625, A74–A78. doi:10.1051/0004-6361/201834149

Salimian, S., Hanson, R. K., and Kruger, C. H. (1984). High Temperature Study of the Reactions of O and OH with NH_3. *Int. J. Chem. Kinet.* 16, 725–739. doi:10.1002/kin.550160609

Sandford, S. A., Nuevo, M., Bera, P. P., and Lee, T. J. (2020). Prebiotic Astrochemistry and the Formation of Molecules of Astrobiological Interest in Interstellar Clouds and Protostellar Disks. *Chem. Rev.* 120, 4616–4659. doi:10.1021/acs.chemrev.9b00560

Scott, G. B. I., Freeman, C. G., and McEwan, M. J. (1997). The Interstellar Synthesis of Ammonia. *Monthly Notices R. Astronomical Soc.* 290, 636–638. doi:10.1093/mnras/290.4.636

Sims, I. R., Queffelec, J. L., Defrance, A., Rebrion-Rowe, C., Travers, D., Bocherel, P., et al. (1994). Ultralow Temperature Kinetics of Neutral-Neutral Reactions. The Technique and Results for the Reactions CN+O_2down to 13 K and CN+NH_3down to 25 K. *J. Chem. Phys.* 100, 4229–4241. doi:10.1063/1.467227

Sleiman, C., El Dib, G., Rosi, M., Skouteris, D., Balucani, N., and Canosa, A. (2018a). Low Temperature Kinetics and Theoretical Studies of the Reaction CN + CH_3NH_2: a Potential Source of Cyanamide and Methyl Cyanamide in the Interstellar Medium. *Phys. Chem. Chem. Phys.* 20, 5478–5489. doi:10.1039/c7cp05746f

Sleiman, C., El Dib, G., Talbi, D., and Canosa, A. (2018b). Gas Phase Reactivity of the CN Radical with Methyl Amines at Low Temperatures (23-297 K): A Combined Experimental and Theoretical Investigation. *ACS Earth Space Chem.* 2, 1047–1057. doi:10.1021/acsearthspacechem.8b00098

Smith, I. W. M., and Barnes, P. W. (2013). Advances in Low Temperature Gas-phase Kinetics. *Annu. Rep. Prog. Chem. Sect. C: Phys. Chem.* 109, 140–166. doi:10.1039/c3pc90011h

Sorrell, W. H. (2001). Origin of Amino Acids and Organic Sugars in Interstellar Clouds. *Astrophys. J.* 555, L129–L132. doi:10.1086/322525

Stephens, R. D. (1984). Absolute Rate Constants for the Reaction of Hydroxyl Radicals with Ammonia from 297 to 364 K. *J. Phys. Chem.* 88, 3308–3313. doi:10.1021/j150659a034

Stuhl, F. (1973). Absolute Rate Constant for the Reaction OH+NH_3→NH_2+H_2O. *J. Chem. Phys.* 59, 635–637. doi:10.1063/1.1680069

Taylor, S. E., Goddard, A., Blitz, M. A., Cleary, P. A., and Heard, D. E. (2008). Pulsed Laval Nozzle Study of the Kinetics of OH with Unsaturated Hydrocarbons at Very Low Temperatures. *Phys. Chem. Chem. Phys.* 10, 422–437. doi:10.1039/B711411G

Theule, P., Borget, F., Mispelaer, F., Danger, G., Duvernay, F., Guillemin, J. C., et al. (2011). Hydrogenation of Solid Hydrogen Cyanide HCN and Methanimine CH_2NH at Low Temperature. *Astron. Astrophys.* 534, A64. doi:10.1051/0004-6361/201117494

Tian, W., Wang, W., Zhang, Y., and Wang, W. (2009). Direct Dynamics Study on the Mechanism and the Kinetics of the Reaction of CH_3NH_2 with OH. *Int. J. Quan. Chem.* 109, 1566–1575. doi:10.1002/qua.22000

Vahedpour, M., Douroudgari, H., Afshar, S., and Asgharzade, S. (2018). Comparison of Atmospheric Reactions of NH_3 and NH_2 with Hydroxyl Radical on the Singlet, Doublet and Triplet Potential Energy Surfaces, Kinetic and Mechanistic Study. *Chem. Phys.* 507, 51–69. doi:10.1016/j.chemphys.2018.03.022

van Dishoeck, E. F., Jansen, D. J., Schilke, P., and Phillips, T. G. (1993). Detection of the Interstellar NH_2 Radical. *Astrophys. J.* 416, L83. doi:10.1086/187076

Weinreb, S., Barret, A. H., Meeks, M. L., and Henry, J. C. (1963). Radio Observations of OH in the Interstellar Medium. *Nature* 200, 829–831. doi:10.1038/200829a0

Wilson, T. L., Gaume, R. A., and Johnston, K. J. (1993). Ammonia in the W_3(OH) Region. *Astrophys. J.* 402, 230. doi:10.1086/172126

Woon, D. E. (2021). A Continously Updated List of the Observed Molecules Is. available online: http://www.astrochymist.org.

Woon, D. E. (2002). Pathways to Glycine and Other Amino Acids in Ultraviolet-Irradiated Astrophysical Ices Determined via Quantum Chemical Modeling. *Astrophys. J.* 571, L177–L180. doi:10.1086/341227

Zabielski, M. F., and Seery, D. J. (1985). High Temperature Measurements of the Rate of the Reaction of OH with NH_3. *Int. J. Chem. Kinet.* 17, 1191–1199. doi:10.1002/kin.550171105

Zellner, R., and Smith, I. W. M. (1974). Rate Constants for the Reactions of OH with NH_3 and HNO_3. *Chem. Phys. Lett.* 26, 72–74. doi:10.1016/0009-2614(74)89086-X

Conflict of Interest: The authors declare that the research was conducted in the absence of any commercial or financial relationships that could be construed as a potential conflict of interest.

Publisher's Note: All claims expressed in this article are solely those of the authors and do not necessarily represent those of their affiliated organizations, or those of the publisher, the editors and the reviewers. Any product that may be evaluated in this article, or claim that may be made by its manufacturer, is not guaranteed or endorsed by the publisher.

frontiers in Astronomy and Space Sciences

ORIGINAL RESEARCH
published: 02 February 2022
doi: 10.3389/fspas.2021.805162

Rotational Rest Frequencies and First Astronomical Search of Protonated Methylamine

*Philipp C. Schmid[1], Sven Thorwirth[1], Christian P. Endres[2], Matthias Töpfer[1†], Álvaro Sánchez-Monge[1], Andreas Schwörer[1], Peter Schilke[1], Stephan Schlemmer[1] and Oskar Asvany[1]**

[1]I. Physikalisches Institut, Universität zu Köln, Köln, Germany, [2]Max Planck Institute for Extraterrestrial Physics, Garching bei München, Germany

We report first laboratory rest frequencies for rotational transitions of protonated methylamine, $CH_3NH_3^+$, measured in a cryogenic 22-pole ion trap machine and employing an action spectroscopy scheme. For this prolate symmetric top molecule thirteen transitions between 80 and 240 GHz were detected in the ground vibrational state, covering $J_K = 2_K - 1_K$ up to $J_K = 6_K - 5_K$ with $K = 0, 1, 2$. Some transitions exhibit noticeable structure that is attributed to internal rotation splitting. As the CN radical and several of its hydrogenated and protonated forms up to methylamine, CH_3NH_2, are well known entities in the laboratory and in space, protonated methylamine, $CH_3NH_3^+$, is a promising candidate for future radio astronomical detection.

Keywords: rotational spectroscopy, protonated methylamine, ion trap, astrochemistry, symmetric top molecule

OPEN ACCESS

Edited by:
André Canosa, UMR6251 Institut de Physique de Rennes (IPR), France

Reviewed by:
Roman Motiyenko, Université de Lille, France
Anthony Remijan, National Radio Astronomy Observatory, United States

****Correspondence:***
Oskar Asvany
asvany@ph1.uni-koeln.de

†Present Address:
Matthias Töpfer, Vinnolit GmbH & Co. KG, Hürth, Germany

Specialty section:
This article was submitted to Astrochemistry, a section of the journal Frontiers in Astronomy and Space Sciences

Received: *29 October 2021*
Accepted: *22 December 2021*
Published: *02 February 2022*

Citation:
Schmid PC, Thorwirth S, Endres CP, Töpfer M, Sánchez-Monge Á, Schwörer A, Schilke P, Schlemmer S and Asvany O (2022) Rotational Rest Frequencies and First Astronomical Search of Protonated Methylamine. Front. Astron. Space Sci. 8:805162. doi: 10.3389/fspas.2021.805162

1 INTRODUCTION

The cyano radical, CN, was one of the first molecules detected in the interstellar medium (McKellar, 1940). It is astrochemically linked to its hydrogenated and protonated forms, most of which have been detected in the interstellar medium, typically in the galactic center source Sgr B2, such as HCN (Snyder and Buhl, 1971), HNC (Snyder and Buhl, 1972; Zuckerman et al., 1972), $HCNH^+$ (Ziurys and Turner, 1986), and $H_2C = NH$ (Godfrey et al., 1973). The terminal product of this hydrogenation series is methylamine, CH_3NH_2, which has been well characterized by laboratory spectroscopy (Ohashi et al., 1987; Ilyushin and Lovas, 2007; Motiyenko et al., 2014) and was first detetcted in Sgr B2 and Orion A in 1974 by Kaifu et al. (1974) and Fourikis et al. (1974).

In interstellar environments, molecules may also occur in their protonated forms, generated by a proton transfer from a proton donor like H_3^+, e.g. $CO + H_3^+ \rightarrow HCO^+ + H_2$. Many of the simpler protonated species have been detected in the interstellar medium, such as HCO^+ (Buhl and Snyder, 1970), N_2H^+ (Turner, 1974), $HCNH^+$ (Ziurys and Turner, 1986) and $HOCO^+$ (Thaddeus et al., 1981), whereas many of the more complex ones so far are only suspected to be present. Examples are $CH_3NH_3^+$, as a product of proton transfer to methyl amine (see, e.g., the KIDA database; Wakelam et al., 2015) or from radiative association of NH_3 and CH_3^+ (Herbst, 1985), but also protonated methanol, $CH_3OH_2^+$ (Jusko et al., 2019), and protonated methane, CH_5^+ (Asvany et al., 2012; Asvany et al., 2015). In particular the latter two molecular ions have not yet been searched for in space because their laboratory microwave spectra are predicted to be quite irregular and still not known.

Following up on our recent work on the high-resolution rotational spectra of CN^+ (Thorwirth et al., 2019a) and $CH_2NH_2^+$ (Markus et al., 2019), in this study, we finally focus on the very last member of the CN hydrogenation/protonation chain, protonated methylamine, $CH_3NH_3^+$. Upon protonation,

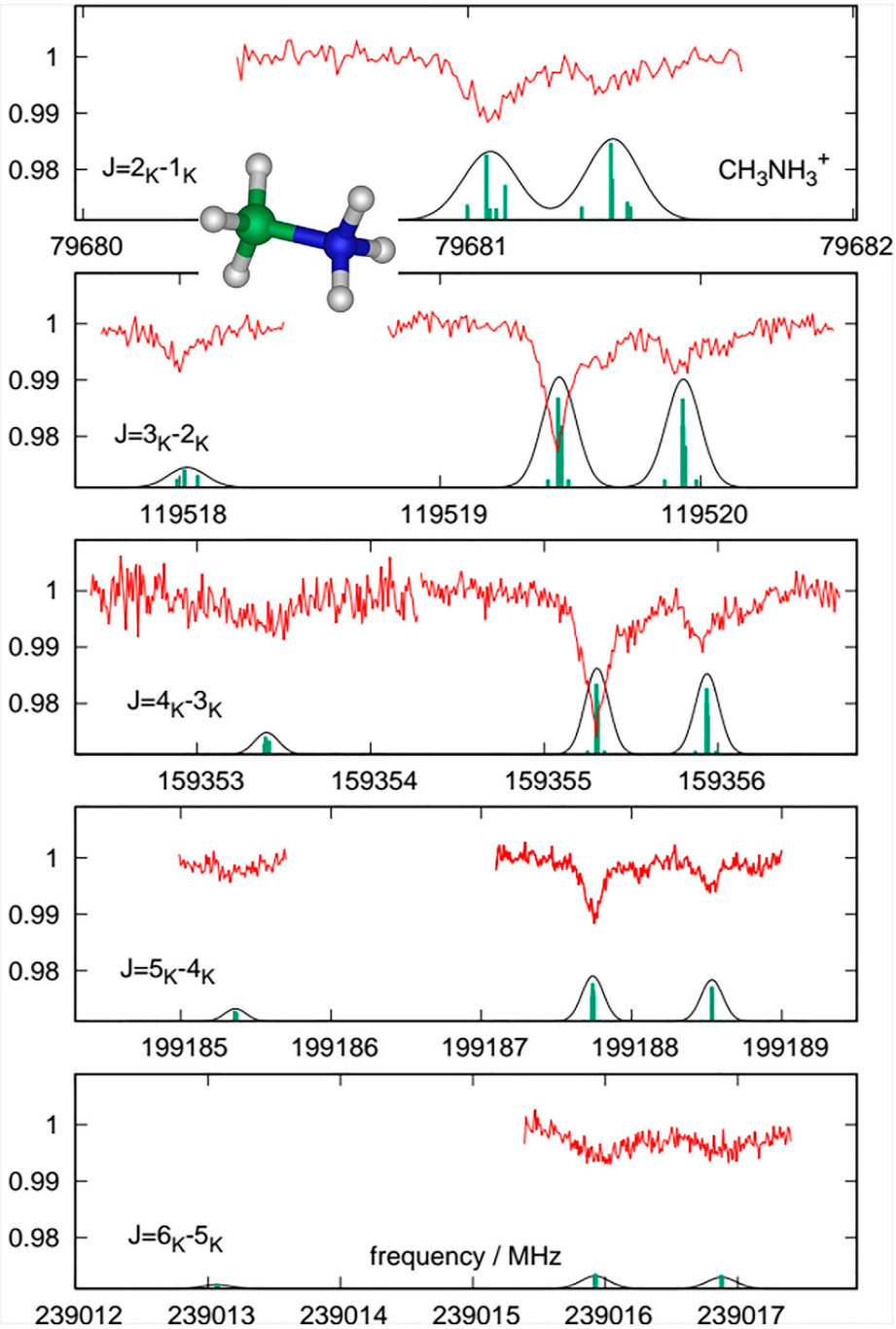

FIGURE 1 | Measurements of the $J'_K \leftarrow J''_K$ (K = 0, 1, 2) rotational transitions of $CH_3NH_3^+$ (red trace), recorded as depletion signal of the normalized $CH_3NH_3^+$–He counts. The simulations (green sticks indicate nitrogen quadrupole hyperfine structure (hfs) and their convolution is given as black traces), based on a symmetric rotor model (**Table 1**, fit I), indicate that the hyperfine splitting is not resolved and that discrepancies between the simulated and measured spectra, in particular the blue-shifted shoulders for K = 0 and 1 (red trace), are most probably due to the neglect of torsional motion in the simulation.

methylamine, CH_3NH_2, an asymmetric top molecule featuring two internal large-amplitude motions (internal rotation and inversion), is converted into a much simpler symmetric top of C_{3v} point group symmetry, in which the CH_3 and the NH_3 groups assume a staggered configuration at the global energy minimum (see inset in **Figure 1**). Literature on the spectroscopy of $CH_3NH_3^+$ is extremely sparse, with only one experimental paper presenting low-resolution infrared (IR) features of the Ar-tagged species (Michi et al., 2003), and one work reporting *ab initio* values for its IR vibrational frequencies (Zeroka and Jensen, 1998). Therefore, the spectroscopic study in the present work was complemented with new high-level quantum-chemical predictions of the

TABLE 1 | Calculated and experimental spectroscopic parameters (in MHz, unless noted otherwise) of $CH_3NH_3^+$. Two experimental fits to the measured data are presented, one (fit I) ignoring the torsional motion, and one (fit II) including torsional motion. Numbers in parentheses are one standard deviation in units of the last digit.

Parameter	C_2H_6		$CH_3NH_3^+$			
	exp.[a]	calc.[b]	calc.[b]	scaled[c]	exp. fit I	exp. fit II[d]
A_e	⋯	81 080.842	85 189.126	⋯	⋯	⋯
B_e	⋯	20 126.248	20 246.782	⋯	⋯	⋯
ΔA_0	⋯	1065.208	1222.937	⋯	⋯	⋯
ΔB_0	⋯	265.982	341.653	⋯	⋯	⋯
A_0	80 391.1(38)	81 080.842	83 966.189	83 251.9	⋯	83 251.9[e]
B_0	19 913.684(24)	19 860.266	19 905.129	19 958.7	19 920.6224(12)	19 941.65(65)
$D_J \times 10^3$	31.026(21)	30.54	34.81	35.4	35.378(27)	35.292(22)
$D_{JK} \times 10^3$	76.37(28)	77.82	84.41	82.8	79.48(38)	87.89(34)
$eQq(^{14}N)$	⋯	⋯	+0.158	⋯	⋯	⋯
μ_e/D	⋯	⋯	2.15	⋯	⋯	⋯
ρ	0.5	⋯	0.54	⋯	⋯	0.54[d]
V_3/kcal/mol	3.00	2.45	1.98	2.42	⋯	2.42[d]
$F \times 10^{-3}$	80.3911[f]	⋯	335.152 576[f]	⋯	⋯	335.152 576[f]
F_{3J}	–397.8(20)	⋯	⋯	⋯	⋯	–243.0(75)
wrms[g]	⋯	⋯	⋯	⋯	1.44	0.96

[a] *see Ozier and Moazzen-Ahmadi (2007) and Borvayeh et al. (2008).*

[b] *This study;* A_e, B_e, $eQq(^{14}N)$ *and dipole moment* μ_e *calculated at the CCSD(T)/cc-pwCVQZ, level, zero-point vibrational corrections* ΔA_0, ΔB_0 *and centrifugal distortion terms calculated at the CCSD(T)/cc-pVTZ, level. Torsional barriers* V_3 *evaluated from the CCSD(T)/cc-pwCVQZ energy difference of the staggered and eclipsed forms complemented with harmonic vibrational corrections evaluated at the CCSD(T)/cc-pVTZ level.*

[c] *Calculated* $CH_3NH_3^+$ *value further scaled with the ratio* X_{exp}/X_{calc} *of the corresponding parameter of* C_2H_6.

[d] *Fit performed using an in-house program assuming a uniform uncertainty of 15 kHz.*

[e] *Kept fixed.*

[f] C_2H_6*: Kept fixed at value of* A *rotational constant;* $CH_3NH_3^+$*: Kept fixed at the customary value of* $A/(\rho(1-\rho))$.

[g] *Weighted rms, dimensionless.*

molecular structure and force field (see **Section 3**). The ion trap experiment is briefly described in **Section 2**. The experimentally derived rotational transitions of $CH_3NH_3^+$ as well as the ground state spectroscopic parameters are summarized in **Section 4**. A first astronomical search of $CH_3NH_3^+$ towards Sgr B2(N) and Sgr B2(M) is finally presented in **Section 5**.

2 EXPERIMENTAL METHODS

The rotational transitions of $CH_3NH_3^+$ have been measured using an action spectroscopic method which exploits the rotational state dependence of the ternary attachment of He atoms to cations at low temperature (Brünken et al., 2014; Brünken et al., 2017; Doménech et al., 2017; Jusko et al., 2017; Doménech et al., 2018a; Doménech et al., 2018b; Thorwirth et al., 2019a; Asvany et al., 2021). The experiment was performed in the 4 K ion trapping machine COLTRAP described by Asvany et al. (2010, 2014). The ions were generated in a storage ion source by electron impact ionization ($E_e \approx 26$–30 eV) of the precursor gas mixture. This mixture consisted of methylamine, CH_3NH_2 (Aldrich Chem. Corporation, CAS 74-89-5, 98%), and helium (Linde 5.0) which were admitted to the ion source via two separate leakage valves. $CH_3NH_3^+$ is generated by a reaction of the type $CH_3NH_2^+ + CH_3NH_2 \rightarrow CH_3NH_3^+ + CNH_4$. A pulse of several ten thousand mass-selected parent ions ($m = 32$ u) was injected into the 22-pole ion trap filled with about 10^{14} cm^{-3} He at 4 K. At the beginning of the trapping time lasting 800 ms, $CH_3NH_3^+$-He complexes formed by three-body collisions with He. The resonant absorption of the cw millimeter-wave radiation by the trapped cold $CH_3NH_3^+$ cations is detected by observing the decrease of the number of $CH_3NH_3^+$-He complexes. A rotational line is thus recorded by repeating these trapping cycles (1 Hz) and counting the mass-selected $CH_3NH_3^+$-He complexes ($m = 36$ u) as a function of the millimeter-wave frequency. This millimeter-wave radiation was supplied by a multiplier chain source (Virginia Diodes, Inc.), covering the ranges 80–125 and 170–1100 GHz. This source was driven by a synthesizer (Rohde&Schwarz SMF100A), which was referenced to a rubidium atomic clock. The beam of the millimeter-wave source has been directed toward the ion trap via an elliptical mirror and a thin diamond vacuum window. The 160 GHz line of $CH_3NH_3^+$ was measured with a different multiplier chain (Radiometer Physics GmbH), covering the range of 110–170 GHz.

3 COMPUTATIONAL METHODS

As no previous high-resolution experimental data were available for $CH_3NH_3^+$, spectroscopic searches and analysis were based on high-level quantum-chemical calculations performed here at the CCSD(T) level of theory (Raghavachari et al., 1989). Equilibrium geometries were calculated using analytic gradient techniques (Watts et al., 1992) and Dunning's correlation-consistent basis sets as large as cc-pwCVQZ (Peterson and Dunning, 2002). Anharmonic force fields to evaluate the zero-point vibrational contributions $\frac{1}{2}\sum_i \alpha_i^{A,B,calc}$ (= ΔA_0, ΔB_0) to the equilibrium

TABLE 2 | Frequencies of pure rotational transitions (in MHz) of $CH_3NH_3^+$, obtained by fitting multiple Gaussians to the spectra in **Figure 1**. The uncertainties (1 σ) are given in parentheses in units of the last significant digits. The assignment of Model I assumes a standard symmetric top Hamiltonian whereas that of Model II assumes a symmetric top featuring torsional splitting, see text for details.

Frequency	Model I				Model II			
	J'_K	←	J''_K	*o* − *c*	J'_K, σ	←	J''_K, σ	*o* − *c*
79681.065(10)	2_1	←	1_1	0.026	2_1,0	←	1_1,0	0.019
79681.364(10)	2_0	←	1_0	0.007	2_0,0	←	1_0,0	0.010
119517.996(10)	3_2	←	2_2	−0.010	3_2,0	←	2_2,0	0.006
119519.449(10)	3_1	←	2_1	0.013	3_1,0	←	2_1,0	0.000
119519.449(10)	⋯	⋯	⋯	⋯	3_1,1	←	2_1,1	0.017
119519.621(10)	⋯	⋯	⋯	⋯	3_1, −1	←	2_1, −1	0.008
119519.908(10)	3_0	←	2_0	−0.005	3_0,0	←	2_0,0	−0.002
119520.077(10)	⋯	⋯	⋯	⋯	3_0, ±1	←	2_0, ±1	−0.006
159353.362(30)	4_2	←	3_2	−0.017	4_2,0	←	3_2,0	0.000
159355.297(10)	4_1	←	3_1	0.011	4_1,0	←	3_1,0	−0.010
159355.297(10)	⋯	⋯	⋯	⋯	4_1,1	←	3_1,1	0.012
159355.537(10)	⋯	⋯	⋯	⋯	4_1, −1	←	3_1, −1	0.011
159355.899(10)	4_0	←	3_0	−0.023	4_0,0	←	3_0,0	−0.023
159356.151(10)	⋯	⋯	⋯	⋯	4_0, ±1	←	3_0, ±1	−0.002
199185.325(30)	5_2	←	4_2	−0.031	5_2,0	←	4_2,0	−0.015
199187.748(10)	5_1	←	4_1	0.008	5_1,0	←	4_1,0	−0.024
199187.748(10)	⋯	⋯	⋯	⋯	5_1,1	←	4_1,1	0.004
199188.039(10)	⋯	⋯	⋯	⋯	5_1, −1	←	4_1, −1	−0.007
199188.518(10)	5_0	←	4_0	−0.017	5_0,0	←	4_0,0	−0.022
199188.820(10)	⋯	⋯	⋯	⋯	5_0, ±1	←	4_0, ±1	−0.009
239016.015(30)	6_1	←	5_1	0.067	6_1,0	←	5_1,0	0.019
239016.931(30)	6_0	←	5_0	0.029	6_0,0	←	5_0,0	0.013

rotational constants were calculated using analytic second-derivative techniques (Gauss and Stanton, 1997; Stanton and Gauss, 2000) followed by additional numerical differentiation to calculate the third and fourth derivatives needed for the anharmonic force field (Stanton et al., 1998; Stanton and Gauss, 2000). These calculations were carried out using the frozen core (fc) approximation in combination with the cc-pVTZ basis set (Dunning, 1989).

All calculations were performed using the CFOUR program (Matthews et al., 2020) and strategies summarized elsewhere (Puzzarini et al., 2010). The computed spectroscopic parameters are listed in **Table 1** that also provides scaled (best-estimate) parameters obtained from a comparison of experimental and calculated values of isoelectronic ethane, C_2H_6 (see, e.g., Martinez et al. (2013) for a similar procedure used in the vinyl acetylene/protonated vinyl cyanide family of isoelectronic species). Additional results from the calculations are given in the **Supplementary Material**. An estimate of the torsional barrier height was obtained using the energy difference between the staggered and the eclipsed forms of $CH_3NH_3^+$ calculated at the CCSD(T)/cc-pwCVQZ level and under consideration of harmonic zero-point vibrational contributions calculated at the CCSD(T)/cc-pVTZ level. This procedure results in a barrier of V_3 = 1.98 kcal/mol. A similar calculation of ethane, C_2H_6, yields 2.45 kcal/mol to be compared against an experimental value of 3.00 kcal/mol (Borvayeh et al., 2008). Using the ethane exp/calc-ratio of V_3 for the purpose of scaling, a best estimate value of 2.42 kcal/mol (846 cm^{-1}) for the torsional barrier in $CH_3NH_3^+$ is obtained.

4 LABORATORY RESULTS AND SPECTROSCOPIC PARAMETERS

Using frequency predictions based on the new high-level quantum-chemical calculations, the lines shown in **Figure 1** were found subsequently during targeted spectroscopic survey scans. The spectra were recorded in individual measurements in which the frequency was stepped in an up-and-down manner several times. The frequency steps were typically 2 kHz, except for the $J_K = 4_K \leftarrow 3_K$ measurement at 159 GHz, for which 10 kHz steps were applied. Such individual measurements were repeated typically ten times. In the depiction of **Figure 1**, all available spectra were accumulated and rebinned to a stepwidth of 10 kHz. This deep integration was necessary due to the comparably small signal strength (maximum depletion upon photon absorption is on the order of 2%), and due to somewhat noisy signal counts, which had its origin in ion source instabilities caused by the sticky consistency of the methylamine precursor. Also, during the measurements, care was taken to avoid power broadening. Thus, the linewidths were expected to be dominated by the Doppler broadening due to the kinetic temperature of the ions in the trap (nominal temperature T = 4 K with some residual heating to typically 8 K), and a possible contribution due to non-resolved hyperfine splitting. The line patterns detected for a given rotational transition were in line with those expected for a prolate symmetric top molecule and at first sight, no further spectroscopic complexity, as could be expected for resolved nitrogen quadrupole hyperfine structure or torsional motion between the CH_3 and NH_3 subunits, was detected in individual measurements at our experimental conditions. For all individual measurements, the detected lines were fitted to Gaussian functions, from which line centers and their uncertainties were determined, and the first results were very similar to the frequencies quoted in **Table 2** (Model I).

The measured frequencies of the pure rotational lines collected in **Table 2** (Model I) were first fit with a standard symmetric rotor Hamiltonian using the PGOPHER program (Western, 2017), yielding the set of parameters for the ground state given in **Table 1** (fit I). Since the transitions of a symmetric rotor obey the ΔK = 0 selection rule, A and D_K cannot be determined experimentally, and only B_0, D_J and D_{JK} were derived in the least-squares fitting procedure and are presented in **Table 1**. Computed parameters are also included in **Table 1** for comparison. As can be seen, the overall agreement between the calculated and scaled best-estimate values and the experimental values is very good. A simulated stick spectrum and its convolution, based on fit I of **Table 1** and accounting for the hyperfine structure due to the quadrupole moment of the ^{14}N nucleus (with spin I = 1), are included in **Figure 1**. As the computed value eQq (^{14}N) = +158 kHz is very small (see also **Table 1**), it is not surprising that the hyperfine structure is not resolved in our experiment.

Closer inspection after co-addition of all spectra revealed some noticeable blue-shifted shoulders, as discernible in the accumulation of **Figure 1**. These are particularly evident in the spectra at 119 ($J = 3_K - 2_K$) and 159 GHz ($J = 4_K - 3_K$), but are also discernible in the weaker spectrum at 199 GHz ($J = 5_K - 4_K$). In the spectrum at 119 GHz (second panel in **Figure 1** and close-up in **Figure 2**) both blue shoulders have an offset of about +170 kHz relative to the main peaks (K = 0 and 1), and this offset is found to increase for the higher

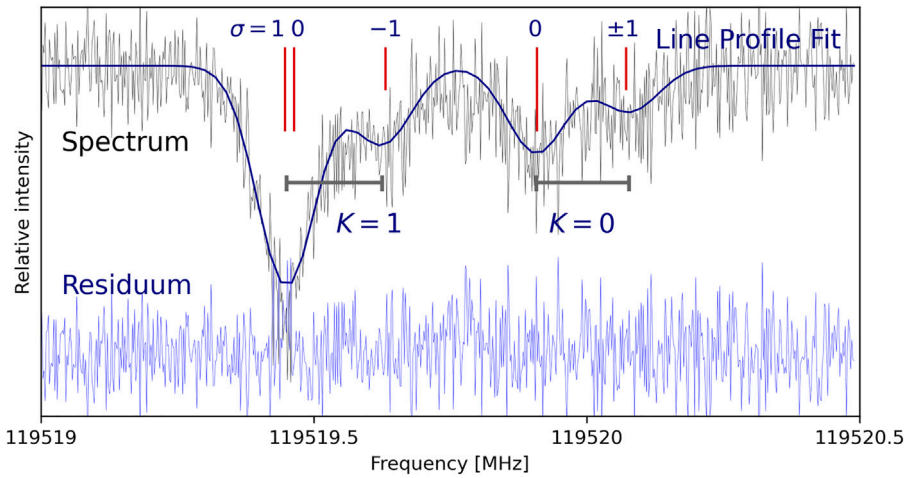

FIGURE 2 | Zoom into the transition $3_K \leftarrow 2_K$ ($K = 0, 1$) highlighting internal rotation splitting in $CH_3NH_3^+$. Four Gaussian features have been assumed in performing a line profile fit. The red vertical bars show the location of the five possible σ torsional components labeled at the top with the length of the bars indicating their contribution from spin statistical effects, see text for details. The gray horizontal markers indicate the torsional splitting of some 170 kHz observed in this particular transition (cf. transition frequencies collected in **Table 1**, Model II).

frequency transitions at 159 (≈+230 kHz) and 199 GHz (≈+290 kHz). While a detailed analysis is hampered by the overall poor signal-to-noise ratio of the spectra, a first analysis was performed here under the assumption that the spectra are affected by internal rotation, an effect that has rarely been observed previously for symmetric top molecules in their ground vibrational states (see, e.g., Ozier and Moazzen-Ahmadi, 2007, and references therein). As indicated in **Figure 2**, the structure of the $J = 3_K - 2_K$ spectrum may be decomposed into four features, two strong ones (the putative $K = 0$ and 1 components used in the first fitting procedure in **Table 1**, fit I) each of which is accompanied by a weaker satellite that is found blue-shifted relative to the main component. Similar patterns are observed for the $J = 4_K - 3_K$ and $J = 5_K - 4_K$ transitions. Ideally, a suitable model Hamiltonian should be able to reproduce both the magnitude of the torsional splitting as well as the intensities of the individual spectroscopic components. First, the magnitude of the torsional splitting to be expected in $CH_3NH_3^+$ was estimated based on the so-called *hybrid* approach described elsewhere (Wang et al., 2001) using the dominant parameters (V_3, $\rho = I_\alpha/I_c$, $F = A/(\rho \times (1 - \rho))$, F_{3J}, F_{3K}) as calculated here and complemented with parameters taken from isoelectronic ethane (Borvayeh et al., 2008). Using this approach, the splitting was predicted in very good agreement with the experimental values. In analogy to other closely related symmetric top molecules such as methyl silane, CH_3SiH_3, each rotational transition of $CH_3NH_3^+$ with $K = 1, 2$ is expected to split in up to three components ($\sigma = 0, +1, -1$) whereas transitions with $K = 0$ only split into two, $\sigma = 0, \pm1$ (Pelz et al., 1992; Ozier and Moazzen-Ahmadi, 2007). The symmetries and nuclear spin weights under consideration of torsional splitting that are needed for intensity estimates have been given, for example, in Pelz et al. (1992). From this, it is concluded that in the $CH_3NH_3^+$-spectra two strong torsional components of the $K = 1$-transitions ($\sigma = 0, 1$) are too close in frequency to be spectroscopically resolved and thus only one strong (superposition of $\sigma = 0$ and 1) and one weaker torsional component ($\sigma = -1$) are observed. The $K = 0$ splitting is also (partly) resolved and both components assigned, a stronger ($\sigma = 0$) and a weaker one ($\sigma = \pm1$), respectively. For the $K = 2$ transitions, only one component ($\sigma = 0$) can be assigned in the spectra obtained here with some confidence. Using this spectroscopic knowledge, the accumulated spectra as depicted in **Figure 1** were refitted using multiple Gaussian components, and the final frequencies and their assignments are listed in **Table 2**, Model II. With this improved spectroscopic assignment, a second fit was performed (using an in-house program and assuming a uniform frequency uncertainty of 15 kHz) leading to an alternative set of molecular parameters given in **Table 1** (fit II). In this approach, owing to the limited amount of spectroscopic information available to constrain the internal rotation problem more rigorously, several parameters required in the theoretical description were kept fixed at values calculated quantum-chemically (ρ, F, V_3). In analogy to fit I, B_0, D_J, and D_{JK} were varied in the least squares adjustment and additionally F_{3J} was released, resulting in a good fit result and agreement with the fit I and C_2H_6 parameter sets. If released also, V_3 cannot be determined statistically from the present data set and changing its value from the scaled calculated value of 2.42 kcal/mol to the unscaled value of 1.98 kcal/mol has little impact on the overall fit quality but decreases the value of F_{3J} significantly to −87(3) MHz. Based on this new set of parameters and taking into consideration the proper spin statistical effects (e.g., Pelz et al., 1992), new simulations of spectra have been obtained that are shown in **Figure 3**. The agreement between the experimental spectra and the simulations is rather compelling and hence speaking very much in favor of internal rotation as to the cause of the peculiar lineshapes and splittings observed.

5 INTERSTELLAR SEARCH

The $CH_3NH_3^+$ spectral line transitions reported in **Table 2** have frequencies > 40 GHz and constitute good targets to be searched

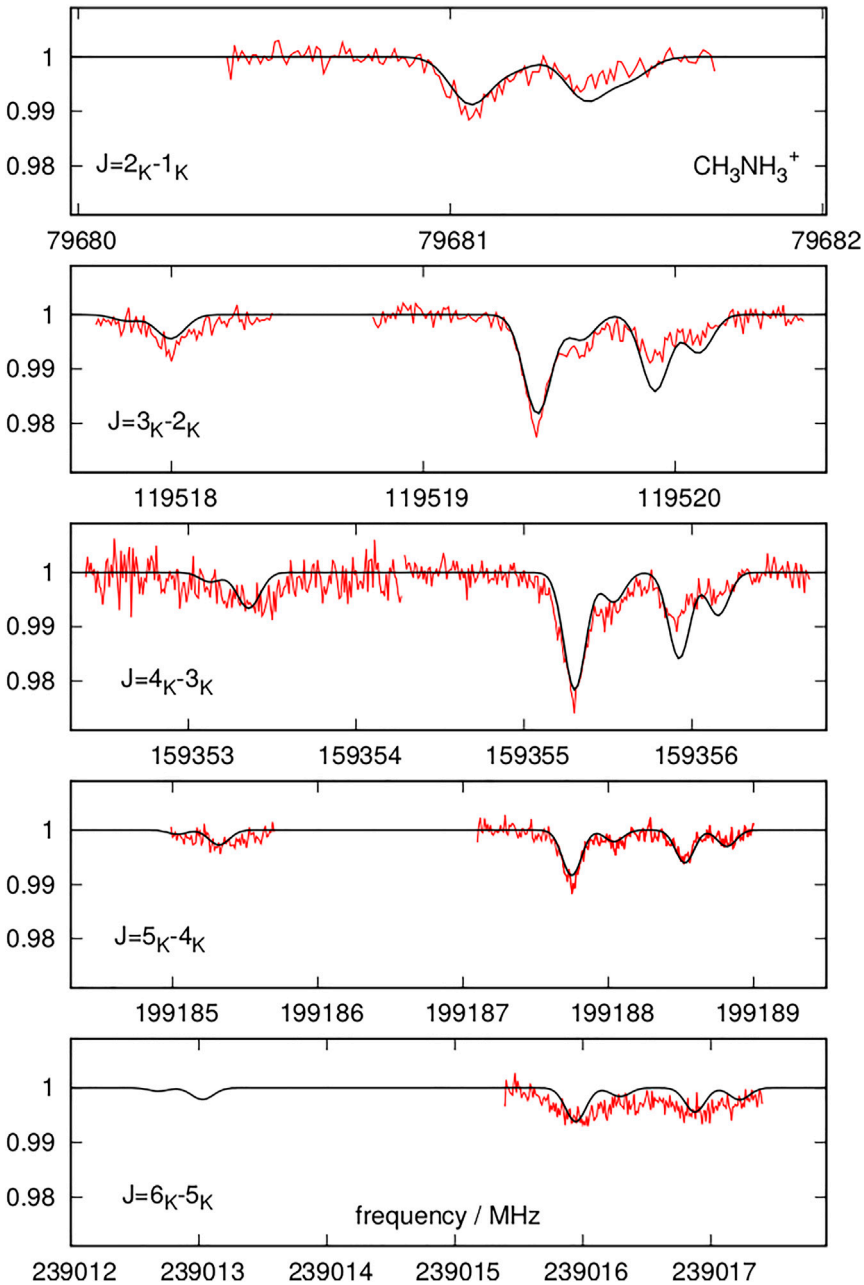

FIGURE 3 | Same as **Figure 1** but with torsional splitting included into the simulation (black line, **Table 1**, fit II). Owing to the very small magnitude of $eQq(^{14}N)$ calculated here, quadrupole hyperfine structure has not been considered in this simulation.

for with facilities like ALMA (Atacama Large Millimeter/submillimeter Array; ALMA Partnership et al., 2015). While the low-energy transitions are not covered by current ALMA bands, the $J = 4_K \rightarrow 3_K$ and $J_K = 5_K \rightarrow 4_K$ lines can be observed with the new ALMA band 5 receiver (covering a frequency range from 159 to 211 GHz), and the $J_K = 6_K \rightarrow 5_K$ transitions are observable with the commonly used band 6 receiver (211–276 GHz).

The detection of species closely related to protonated methylamine such as HCN, $HCNH^+$ or CH_3NH_2 in the star-forming region Sgr B2 (e.g., Schilke et al., 1991; Belloche et al., 2013) motivates the search for protonated methylamine in this region. We have made use of the ALMA spectral line survey published in Sánchez-Monge et al. (2017, see also Schwörer et al., 2019). The observations target the star-forming objects Sgr B2(N) and Sgr B2(M) and cover the whole ALMA band 6 with a spectral resolution of 0.7 km s^{-1} and an angular resolution of 0.″4 (corresponding to 3300 au at the distance of the source). This high angular resolution allows to resolve the regions in more than 40 different dense cores (see Sánchez-Monge et al., 2017). **Figure 4** presents the spectra extracted

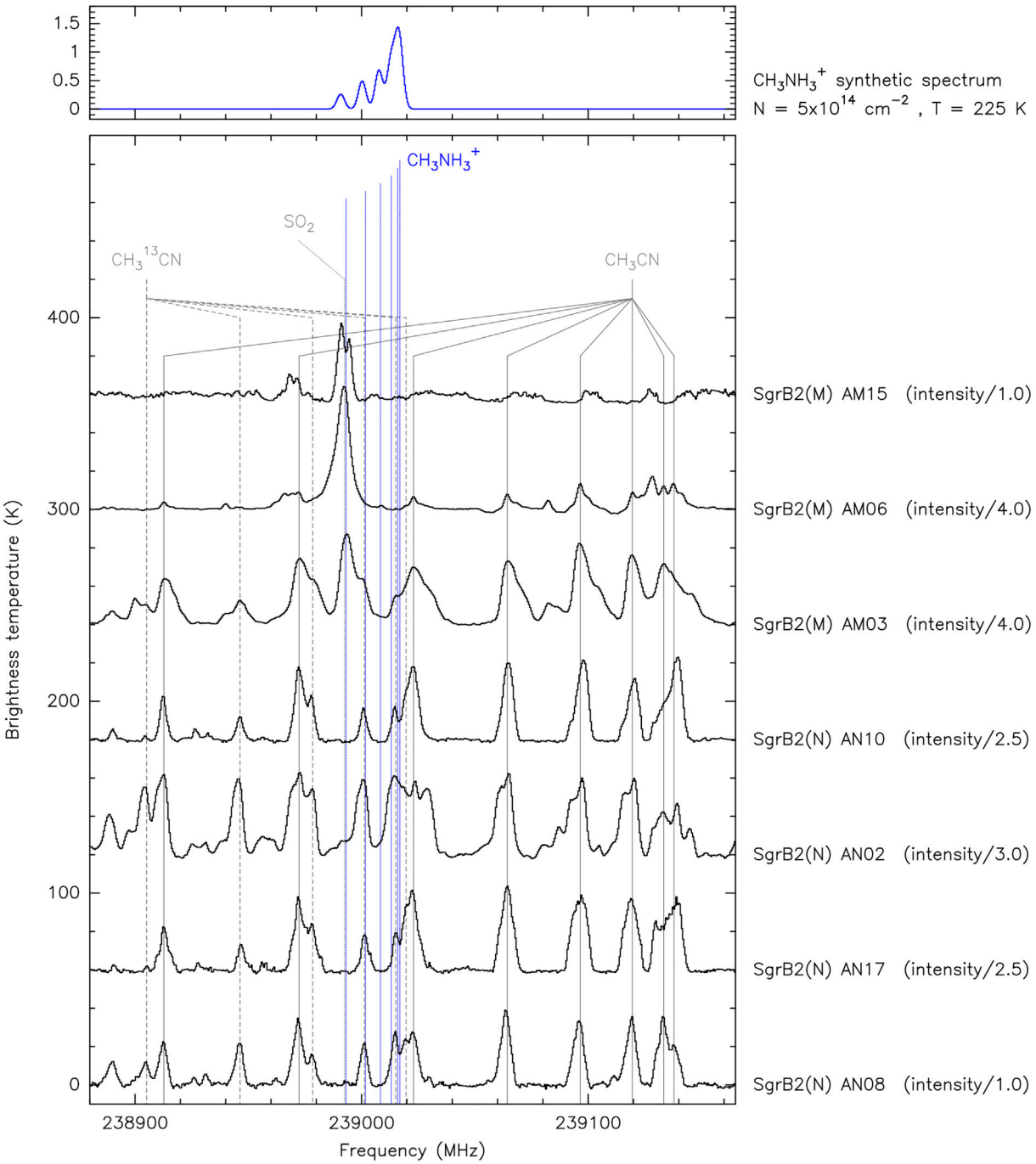

FIGURE 4 | ALMA spectra towards seven dense cores in the Sgr B2(N) and (M) regions. Data from Sánchez-Monge et al. (2017). The baseline for each spectrum corresponds to a brightness temperature of 0 K, however, the spectrum of each source has been manually shifted by 60 K (with respect to the source below) for an easier visualization of the data. The intensities of some spectra have been divided by the factor indicated to the right. Grey solid and dashed vertical lines mark the transitions of CH_3CN ($J_K = 13_K - 12_K$), $CH_3^{13}CN$ ($J_K = 13_K - 12_K$) and SO_2 ($J_{K_a,K_c} = 21_{7,15} - 22_{6,16}$). The blue vertical lines mark the $6_K \rightarrow 5_K$ transitions of $CH_3NH_3^+$. The top panel shows the expected synthetic spectrum for $CH_3NH_3^+$ as observed with ALMA at 0.″4 angular resolution and considering a column density of 5×10^{14} cm^{-2}, a temperature of 225 K, and a linewidth of 5 km s^{-1}.

towards different selected cores in both regions (see source coordinates in **Tables 1**, **2** of Sánchez-Monge et al., 2017). The spectra are obtained after averaging the emission inside the 3σ polygon that defines the source size (between 0.″5 and 0.″7). We mark with vertical lines the location of the $CH_3NH_3^+$ transitions.

We have selected objects in different evolutionary stages and with different physical properties. Cores AN02, AN17 and AM03

correspond to dense cores dominated by dust but with a rich chemistry. In particular, core AN02 has been extensively studied in the literature in the search of new chemical species (e.g., Belloche et al., 2014). We have also included objects in which an embedded HII region has been found (e.g., AN10, AM06, AM15). The presence of the UV radiation from embedded massive stars ionizing the gas and resulting in HII regions can enhance the protonation of methylamine in the photon-dominated region around the HII region. As shown in **Figure 4**, no obvious features are detected at the frequencies of the tabulated $CH_3NH_3^+$ transitions, suggesting a low abundance of protonated methylamine in Sgr B2. We have determined an upper limit of $\approx 5 \times 10^{14}$ cm^{-2} to the column density of protonated methylamine. This is estimated based on a 3-sigma noise upper limit and assuming a gas temperature of 200–300 K (as derived from other molecular species in Sgr B2, Schwörer et al., 2019). This translates into an upper limit of the fractional abundance of ~10^{-10}. The high densities of the Sgr B2 region (~ 10^5–10^8 cm^{-3}; see also Schmiedeke et al., 2016) can rapidly attenuate the radiation field and result in a low production of heavy ions like $CH_3NH_3^+$. Moreover, the $J = 6_K \rightarrow 5_K$ transitions are located close to bright CH_3CN and $CH_3^{13}CN$ ($J_K = 13_K \rightarrow 12_K$) transitions and a strong SO_2 feature which may hinder the detection of the weaker $CH_3NH_3^+$ in chemically rich, embedded objects. Observations at other frequency ranges, as well as in other astronomical sources associated with highly ionized and less dense gas, may help in the detection of this species in space.

6 CONCLUSION AND OUTLOOK

In the present study, the pure rotational spectrum of protonated methyl amine, $CH_3NH_3^+$, was observed for the first time. It is worthwhile to recall that upon protonation of CH_3NH_2, forming $CH_3NH_3^+$, the complex dynamical behaviour of the former molecular system is largely simplified, because the inversion at the NH_2 group in CH_3NH_2 is eliminated and only the torsional motion between CH_3 and NH_3 has to be potentially considered for the pure rotational spectrum of $CH_3NH_3^+$ in its ground vibrational state. In this study, a total of five pure rotational transitions from $J = 2_K - 1_K$ to $J = 6_K - 5_K$ and K up to 2 were identified. As indicated through complementary quantum-chemical calculations, explicit treatment of nuclear quadrupole hyperfine structure from the presence of the nitrogen nucleus was found to be negligible. While the strongest spectroscopic features in the spectrum can be assigned and fitted reasonably well in a straightforward fashion using a standard symmetric-top Hamiltonian, peculiar lineshapes and weak substructure identified in the spectra upon close inspection indeed required extension of the theoretical treatment to account for internal rotation. This refined model description permits very convincing reproduction of the experimental line profiles. A more comprehensive treatment of the internal rotational problem in $CH_3NH_3^+$ would certainly benefit from extension of the present work to a higher degree of rotational excitation but also from detection of vibrational satellites of $CH_3NH_3^+$ in torsionally excited states.

Future work towards the spectroscopic characterization of protonated amines offers many possibilities, not only in the millimeter-wave regime. For example, the low-resolution vibrational spectra of $CH_3NH_3^+$ and also protonated ethyl amine, $C_2H_5NH_3^+$, were observed recently in the range from 700 to 1750 cm^{-1} (Thorwirth et al., 2019b) using the FELion ion trap apparatus (Jusko et al., 2019). For the purpose of millimeter-wave radio astronomical searches of $CH_3NH_3^+$ the data presented here should already suffice. Although the column density of $CH_3NH_3^+$ in the interstellar medium may be some orders of magnitude lower than that of CH_3NH_2, the more favorable partition function of $CH_3NH_3^+$ will support radio astronomical detectability. In the search towards SgrB2 presented in this work $CH_3NH_3^+$ was unfortunately not found.

DATA AVAILABILITY STATEMENT

The raw data supporting the conclusion of this article will be made available by the authors, without undue reservation.

AUTHOR CONTRIBUTIONS

PS: measurement, manuscript writing MT: measurement ST: quantum chemical computations, data evaluation, manuscript writing CE: data evaluation, manuscript writing AS-M: data evaluation, manuscript writing AS: data evaluation, manuscript writing PS: supervision SS: supervision, manuscript writing OA: measurement, data evaluation, manuscript writing, supervision.

FUNDING

This work has been supported via Collaborative Research Centre 956, sub-projects A6 and B2, funded by the Deutsche Forschungsgemeinschaft (DFG, project ID 184 018 867), as well as DFG SCHL 341/15-1 (Gerätezentrum "Cologne Center for Terahertz Spectroscopy").

ACKNOWLEDGMENTS

The authors gratefully acknowledge the work done over the last years by the electrical and mechanical workshops of the I. Physikalisches Institut. We thank Frank Lewen for assistance using the mm-wave setup. CE is grateful for support from the Max Planck Society.

SUPPLEMENTARY MATERIAL

The Supplementary Material for this article can be found online at: https://www.frontiersin.org/articles/10.3389/fspas.2021.805162/full#supplementary-material

REFERENCES

Asvany, O., Bielau, F., Moratschke, D., Krause, J., and Schlemmer, S. (2010). Note: New Design of a Cryogenic Linear Radio Frequency Multipole Trap. *Rev. Sci. Instrum.* 81, 076102. doi:10.1063/1.3460265

Asvany, O., Brünken, S., Kluge, L., and Schlemmer, S. (2014). COLTRAP: A 22-pole Ion Trapping Machine for Spectroscopy at 4 K. *Appl. Phys. B* 114, 203–211. doi:10.1007/s00340-013-5684-y

Asvany, O., Krieg, J., and Schlemmer, S. (2012). Frequency Comb Assisted Mid-Infrared Spectroscopy of Cold Molecular Ions. *Rev. Sci. Instrum.* 83, 093110. doi:10.1063/1.4753930

Asvany, O., Markus, C. R., Roucou, A., Schlemmer, S., Thorwirth, S., and Lauzin, C. (2021). The Fundamental Rotational Transition of NO^+. *J. Mol. Spectrosc.* 378, 111447. doi:10.1016/j.jms.2021.111447

Asvany, O., Yamada, K. M. T., Brünken, S., Potapov, A., and Schlemmer, S. (2015). Experimental Ground-State Combination Differences of CH_5^+. *Science* 347, 1346–1349. doi:10.1126/science.aaa3304

Belloche, A., Garrod, R. T., Müller, H. S. P., and Menten, K. M. (2014). Detection of a Branched Alkyl Molecule in the Interstellar Medium: Iso-Propyl Cyanide. *Science* 345, 1584–1587. doi:10.1126/science.1256678

Belloche, A., Müller, H. S. P., Menten, K. M., Schilke, P., and Comito, C. (2013). Complex Organic Molecules in the Interstellar Medium: IRAM 30 m Line Survey of Sagittarius B2(N) and (M). *Astron. Astrophys.* 559, A47. doi:10.1051/0004-6361/201321096

Borvayeh, L., Moazzen-Ahmadi, N., and Horneman, V.-M. (2008). The $\nu_{12} - \nu_9$ Band of Ethane: A Global Frequency Analysis of Data from the Four Lowest Vibrational States. *J. Mol. Spectrosc.* 250, 51–56. doi:10.1016/j.jms.2008.04.009

Brünken, S., Kluge, L., Stoffels, A., Asvany, O., and Schlemmer, S. (2014). Laboratory Rotational Spectrum of l-C_3H^+ and Confirmation of its Astronomical Detection. *Astrophys. J. Lett.* 783, L4. doi:10.1088/2041-8205/783/1/l4

Brünken, S., Kluge, L., Stoffels, A., Pérez-Ríos, J., and Schlemmer, S. (2017). Rotational State-dependent Attachment of He Atoms to Cold Molecular Ions: An Action Spectroscopic Scheme for Rotational Spectroscopy. *J. Mol. Spectrosc.* 332, 67–78. doi:10.1016/j.jms.2016.10.018

Buhl, D., and Snyder, L. E. (1970). Unidentified Interstellar Microwave Line. *Nature* 228, 267–269. doi:10.1038/228267a0

Doménech, J. L., Jusko, P., Schlemmer, S., and Asvany, O. (2018a). The First Laboratory Detection of Vibration-Rotation Transitions of $^{12}CH^+$ and $^{13}CH^+$ and Improved Measurement of Their Rotational Transition Frequencies. *Astrophys. J.* 857, 61. doi:10.3847/1538-4357/aab36a

Doménech, J. L., Schlemmer, S., and Asvany, O. (2017). Accurate Frequency Determination of Vibration-Rotation and Rotational Transitions of SiH^+. *Astrophys. J.* 849, 60. doi:10.3847/1538-4357/aa8fca

Doménech, J. L., Schlemmer, S., and Asvany, O. (2018b). Accurate Rotational Rest Frequencies for Ammonium Ion Isotopologues. *Astrophys. J.* 866, 158. doi:10.3847/1538-4357/aadf83

Dunning, T. H. (1989). Gaussian Basis Sets for Use in Correlated Molecular Calculations. I. The Atoms Boron through Neon and Hydrogen. *J. Chem. Phys.* 90, 1007–1023. doi:10.1063/1.456153

ALMA PartnershipFomalont, E. B., Vlahakis, C., Corder, S., Remijan, A., Barkats, D., et al. (2015). The 2014 ALMA Long Baseline Campaign: An Overview. *Astrophys. J. Lett.* 808, L1. doi:10.1088/2041-8205/808/1/L1

Fourikis, N., Takagi, K., and Morimoto, M. (1974). Detection of Interstellar Methylamine by its $2_{02} \rightarrow 1_{10}$ A_a-State Transition. *Astrophys. J. Lett.* 191, L139. doi:10.1086/181570

Gauss, J., and Stanton, J. F. (1997). Analytic CCSD(T) Second Derivatives. *Chem. Phys. Lett.* 276, 70–77. doi:10.1016/s0009-2614(97)88036-0

Godfrey, P. D., Brown, R. D., Robinson, B. J., and Sinclair, M. W. (1973). Discovery of Interstellar Methanimine (Formaldimine). *Astrophys. Lett.* 13, 119.

Herbst, E. (1985). The Rate of the Radiative Association Reaction between CH_3^+ and NH_3 and its Implications for Interstellar Chemistry. *Astrophys. J.* 292, 484–486. doi:10.1086/163179

Ilyushin, V., and Lovas, F. J. (2007). Microwave Spectra of Molecules of Astrophysical Interest. Xxv. Methylamine. *J. Phys. Chem. Ref. Data* 36, 1141–1276. doi:10.1063/1.2769382

Jusko, P., Brünken, S., Asvany, O., Thorwirth, S., Stoffels, A., van der Meer, L., et al. (2019). The FELion Cryogenic Ion Trap Beam Line at the FELIX Free-Electron Laser Laboratory: Infrared Signatures of Primary Alcohol Cations. *Faraday Discuss.* 217, 172–202. doi:10.1039/c8fd00225h

Jusko, P., Stoffels, A., Thorwirth, S., Brünken, S., Schlemmer, S., and Asvany, O. (2017). High-resolution Vibrational and Rotational Spectroscopy of CD_2H^+ in a Cryogenic Ion Trap. *J. Mol. Spectrosc.* 332, 59–66. doi:10.1016/j.jms.2016.10.017

Kaifu, N., Morimoto, M., Nagane, K., Akabane, K., Iguchi, T., and Takagi, K. (1974). Detection of Interstellar Methylamine. *Astrophys. J. Lett.* 191, L135–L137. doi:10.1086/181569

Markus, C. R., Thorwirth, S., Asvany, O., and Schlemmer, S. (2019). High-Resolution Double Resonance Action Spectroscopy in Ion Traps: Vibrational and Rotational Fingerprints of $CH_2NH_2^+$. *Phys. Chem. Chem. Phys.* 21, 26406–26412. doi:10.1039/c9cp05487a

Martinez, O., Jr., Lattanzi, V., Thorwirth, S., and McCarthy, M. C. (2013). Detection of Protonated Vinyl Cyanide, CH_2CHCNH^+, a Prototypical Branched Nitrile Cation. *J. Chem. Phys.* 138, 094316. doi:10.1063/1.4793316

Matthews, D. A., Cheng, L., Harding, M. E., Lipparini, F., Stopkowicz, S., Jagau, T.-C., et al. (2020). Coupled-Cluster Techniques for Computational Chemistry: The CFOUR Program Package. *J. Chem. Phys.* 152, 214108. doi:10.1063/5.0004837

McKellar, A. (1940). Evidence for the Molecular Origin of Some Hitherto Unidentified Interstellar Lines. *Publ. Astron. Soc. Pac.* 52, 187. doi:10.1086/125159

Michi, T., Ohashi, K., Inokuchi, Y., Nishi, N., and Sekiya, H. (2003). Infrared Spectra and Structures of $(CH_3NH_2)_nH^+$ (n = 1-4). Binding Features of an Excess Proton. *Chem. Phys. Lett.* 371, 111–117. doi:10.1016/s0009-2614(03)00217-3

Motiyenko, R. A., Ilyushin, V. V., Drouin, B. J., Yu, S., and Margulès, L. (2014). Rotational Spectroscopy of Methylamine up to 2.6 THz. *Astron. Astrophys.* 563, A137. doi:10.1051/0004-6361/201323190

Ohashi, N., Takagi, K., Hougen, J. T., Olson, W. B., and Lafferty, W. J. (1987). Far-Infrared Spectrum and Ground State Constants of Methyl Amine. *J. Mol. Spectrosc.* 126, 443–459. doi:10.1016/0022-2852(87)90249-9

Ozier, I., and Moazzen-Ahmadi, N. (2007). "Internal Rotation in Symmetric Tops," in *Advances in Atomic, Molecular, and Optical Physics*. Editors P. R. Berman, C. C. Lin, and E. Arimondo (Amsterdam: Elsevier), 54, 423–509. doi:10.1016/s1049-250x(06)54007-8

Pelz, G., Mittler, P., Yamada, K. M. T., and Winnewisser, G. (1992). Millimeter-Wave Spectra and Revised Spectroscopic Parameters of Methylsilane. *J. Mol. Spectrosc.* 156, 390–402. doi:10.1016/0022-2852(92)90240-o

Peterson, K. A., and Dunning, T. H. (2002). Accurate Correlation Consistent Basis Sets for Molecular Core-Valence Correlation Effects: The Second Row Atoms Al-Ar, and the First Row Atoms B-Ne Revisited. *J. Chem. Phys.* 117, 10548–10560. doi:10.1063/1.1520138

Puzzarini, C., Stanton, J. F., and Gauss, J. (2010). Quantum-Chemical Calculation of Spectroscopic Parameters for Rotational Spectroscopy. *Int. Rev. Phys. Chem.* 29, 273–367. doi:10.1080/01442351003643401

Raghavachari, K., Trucks, G. W., Pople, J. A., and Head-Gordon, M. (1989). A Fifth-Order Perturbation Comparison of Electron Correlation Theories. *Chem. Phys. Lett.* 157, 479–483. doi:10.1016/s0009-2614(89)87395-6

Sánchez-Monge, Á., Schilke, P., Schmiedeke, A., Ginsburg, A., Cesaroni, R., Lis, D. C., et al. (2017). The Physical and Chemical Structure of Sagittarius B2. II. Continuum Millimeter Emission of Sgr B2(M) and Sgr B2(N) with ALMA. *Astron. Astrophys.* 604, A6. doi:10.1051/0004-6361/201730426

Schilke, P., Walmsley, C. M., Millar, T. J., and Henkel, C. (1991). Protonated HCN in Molecular Clouds. *Astron. Astrophys.* 247, 487.

Schmiedeke, A., Schilke, P., Möller, T., Sánchez-Monge, Á., Bergin, E., Comito, C., et al. (2016). The Physical and Chemical Structure of Sagittarius B2. I. Three-Dimensional Thermal Dust and Free-Free Continuum Modeling on 100 au to 45 pc Scales. *Astron. Astrophys.* 588, A143. doi:10.1051/0004-6361/201527311

Schwörer, A., Sánchez-Monge, Á., Schilke, P., Möller, T., Ginsburg, A., Meng, F., et al. (2019). The Physical and Chemical Structure of Sagittarius B2. IV. Converging Filaments in the High-Mass Cluster Forming Region Sgr B2(N). *Astron. Astrophys.* 628, A6. doi:10.1051/0004-6361/201935200

Snyder, L. E., and Buhl, D. (1972). Detection of Several New Interstellar Molecules. *Ann. N. Y. Acad. Sci.* 194, 17–24. doi:10.1111/j.1749-6632.1972.tb12687.x

Snyder, L. E., and Buhl, D. (1971). Observations of Radio Emission from Interstellar Hydrogen Cyanide. *Astrophys. J. Lett.* 163, L47. doi:10.1086/180664

Stanton, J. F., and Gauss, J. (2000). Analytic Second Derivatives in High-Order many-body Perturbation and Coupled-Cluster Theories: Computational Considerations and Applications. *Int. Rev. Phys. Chem.* 19, 61–95. doi:10.1080/014423500229864

Stanton, J. F., Lopreore, C. L., and Gauss, J. (1998). The Equilibrium Structure and Fundamental Vibrational Frequencies of Dioxirane. *J. Chem. Phys.* 108, 7190–7196. doi:10.1063/1.476136

Thaddeus, P., Guélin, M., and Linke, R. A. (1981). Three New 'nonterrestrial' Molecules. *Astrophys. J.* 246, L41–L45. doi:10.1086/183549

Thorwirth, S., Schreier, P., Salomon, T., Schlemmer, S., and Asvany, O. (2019a). Pure Rotational Spectrum of CN^+. *Astrophys. J. Lett.* 882, L6. doi:10.3847/2041-8213/ab3927

Thorwirth, S., Schmid, P. C., Töpfer, M., Brünken, S., Asvany, O., and Schlemmer, S. (2019b). "Spectroscopic Studies of Protonated Amines: $CH_3NH_3^+$ and $C_2H_5NH_3^+$," in International Symposium on Molecular Spectroscopy, 74th meeting, Champaign-Urbana, IL, U.S.A., June 17-21, Talk WF04.

Turner, B. E. (1974). U93.174 - A New Interstellar Line with Quadrupole Hyperfine Splitting. *Astrophys. J. Lett.* 193, L83. doi:10.1086/181638

Wakelam, V., Loison, J. C., Herbst, E., Pavone, B., Bergeat, A., Beroff, K., et al. (2015). The 2014 KIDA Network for Interstellar Chemistry. *Astrophys. J. Suppl. Ser.* 217, 20. doi:10.1088/0067-0049/217/2/20

Wang, S.-X., Schroderus, J., Ozier, I., Moazzen-Ahmadi, N., McKellar, A. R. W., Ilyushyn, V. V., et al. (2001). Infrared and Millimeter-Wave Study of the Four Lowest Torsional States of CH_3CF_3. *J. Mol. Spectrosc.* 205, 146–163. doi:10.1006/jmsp.2000.8235

Watts, J. D., Gauss, J., and Bartlett, R. J. (1992). Open-Shell Analytical Energy Gradients for Triple Excitation many-body, Coupled-Cluster Methods: MBPT(4), CCSD+T(CCSD), CCSD(T), and QCISD(T). *Chem. Phys. Lett.* 200, 1–7. doi:10.1016/0009-2614(92)87036-o

Western, C. M. (2017). Pgopher: A Program for Simulating Rotational, Vibrational and Electronic Spectra. *J. Quant. Spectrosc. Radiat. Transf.* 186, 221–242. doi:10.1016/j.jqsrt.2016.04.010

Zeroka, D., and Jensen, J. O. (1998). Infrared Spectra of Some Isotopomers of Methylamine and the Methylammonium Ion: A Theoretical Study. *J. Mol. Struct. THEOCHEM* 425, 181–192. doi:10.1016/s0166-1280(97)00109-7

Ziurys, L. M., and Turner, B. E. (1986). HCNH(+) - A New Interstellar Molecular Ion. *Astrophys. J.* 302, L31–L36. doi:10.1086/184631

Zuckerman, B., Morris, M., Palmer, P., and Turner, B. E. (1972). Observations of Cs, HCN, U89.2, and U90.7 in NGC 2264. *Astrophys. J. Lett.* 173, L125. doi:10.1086/180931

Conflict of Interest: The authors declare that the research was conducted in the absence of any commercial or financial relationships that could be construed as a potential conflict of interest.

Publisher's Note: All claims expressed in this article are solely those of the authors and do not necessarily represent those of their affiliated organizations, or those of the publisher, the editors and the reviewers. Any product that may be evaluated in this article, or claim that may be made by its manufacturer, is not guaranteed or endorsed by the publisher.

frontiers in Astronomy and Space Sciences

ORIGINAL RESEARCH
published: 02 February 2022
doi: 10.3389/fspas.2021.793922

Astrochemistry With the Orbiting Astronomical Satellite for Investigating Stellar Systems

Jennifer B. Bergner[1]†, Yancy L. Shirley[2], Jes K. Jørgensen[3], Brett McGuire[4,5], Susanne Aalto[6], Carrie M. Anderson[7], Gordon Chin[7], Maryvonne Gerin[8], Paul Hartogh[9], Daewook Kim[2,10], David Leisawitz[7], Joan Najita[11], Kamber R. Schwarz[12], Alexander G. G. M. Tielens[13,14], Christopher K. Walker[2], David J. Wilner[15] and Edward J. Wollack[7]*

[1]University of Chicago Department of the Geophysical Sciences, Chicago, IL, United States, [2]Department of Astronomy and Steward Observatory, University of Arizona, Tucson, AZ, United States, [3]Niels Bohr Institute, University of Copenhagen, Copenhagen, Denmark, [4]Department of Chemistry, Massachusetts Institute of Technology, Cambridge, MA, United States, [5]National Radio Astronomy Observatory, Charlottesville, VA, United States, [6]Department of Space, Earth and Environment with Onsala Space Observatory, Chalmers University of Technology, Göteborg, Sweden, [7]NASA Goddard Space Flight Center, Greenbelt, MD, United States, [8]LERMA, Observatoire de Paris, PSL Research University, CNRS, Sorbonne Université, Paris, France, [9]Max Planck Institute for Solar System Research, Goettingen, Germany, [10]Wyant College of Optical Sciences, University of Arizona, Tucson, AZ, United States, [11]NSF's NOIRLab, Tucson, AZ, United States, [12]Max-Planck-Institut für Astronomie, Heidelberg, Germany, [13]Astronomy Department, University of Maryland, College Park, MD, United States, [14]Leiden Observatory, University of Leiden, Leiden, Netherlands, [15]Center for Astrophysics, Harvard and Smithsonian, Cambridge, MA, United States

OPEN ACCESS

Edited by:
Ryan C. Fortenberry,
University of Mississippi, United States

Reviewed by:
Luca Fossati,
Austrian Academy of Sciences, Austria
Nigel John Mason,
University of Kent, United Kingdom

***Correspondence:**
Jennifer B. Bergner
jbergner@uchicago.edu

†NASA Sagan Fellow

Specialty section:
This article was submitted to Astrochemistry, a section of the journal Frontiers in Astronomy and Space Sciences

Received: 12 October 2021
Accepted: 09 December 2021
Published: 02 February 2022

Citation:
Bergner JB, Shirley YL, Jørgensen JK, McGuire B, Aalto S, Anderson CM, Chin G, Gerin M, Hartogh P, Kim D, Leisawitz D, Najita J, Schwarz KR, Tielens AGGM, Walker CK, Wilner DJ and Wollack EJ (2022) Astrochemistry With the Orbiting Astronomical Satellite for Investigating Stellar Systems. Front. Astron. Space Sci. 8:793922. doi: 10.3389/fspas.2021.793922

Chemistry along the star- and planet-formation sequence regulates how prebiotic building blocks—carriers of the elements CHNOPS—are incorporated into nascent planetesimals and planets. Spectral line observations across the electromagnetic spectrum are needed to fully characterize interstellar CHNOPS chemistry, yet to date there are only limited astrochemical constraints at THz frequencies. Here, we highlight advances to the study of CHNOPS astrochemistry that will be possible with the Orbiting Astronomical Satellite for Investigating Stellar Systems (OASIS). OASIS is a NASA mission concept for a space-based observatory that will utilize an inflatable 14-m reflector along with a heterodyne receiver system to observe at THz frequencies with unprecedented sensitivity and angular resolution. As part of a survey of H_2O and HD toward ~100 protostellar and protoplanetary disk systems, OASIS will also obtain statistical constraints on the emission of complex organics from protostellar hot corinos and envelopes as well as light hydrides including NH_3 and H_2S toward protoplanetary disks. Line surveys of high-mass hot cores, protostellar outflow shocks, and prestellar cores will also leverage the unique capabilities of OASIS to probe high-excitation organics and small hydrides, as is needed to fully understand the chemistry of these objects.

Keywords: astrochemistry, interstellar molecules, star-forming regions, far-infrared astronomy, space telescopes

1 INTRODUCTION

The elements carbon, hydrogen, nitrogen, oxygen, phosphorus, and sulfur (CHNOPS) are considered the main biogenic elements on Earth, as they are found universally in all life forms. Studying the chemistry of these elements along the star- and planet-formation sequence provides crucial insight into how they are incorporated into nascent planetesimals and planets (see review by

Öberg and Bergin, 2021). Besides regulating the bulk inventories of CHNOPS in planet-forming gas and solids, interstellar chemistry can also convert simple CHNOPS carriers into more complex organic molecules. If this chemically complex material is incorporated into icy bodies such as asteroids and comets, then it may be delivered to planetary surfaces via impact and potentially play a role in jump-starting origins-of-life chemistry (e.g., Rubin et al., 2019). Indeed, icy bodies within the Solar System appear to be composed in part of material inherited from the early stages of star formation (e.g., Alexander et al., 2017; Altwegg et al., 2017; Rubin et al., 2020) and are also implicated in the delivery of volatiles to Earth's surface (e.g., Alexander et al., 2012; Marty et al., 2017). Thus, understanding the formation and inheritance of simple and complex CHNOPS carriers along the star-formation sequence is a major aim of astrochemistry.

The Orbiting Astronomical Satellite for Investigating Stellar Systems (OASIS) observatory is a NASA Medium Explorer (MIDEX) space mission concept designed to "follow the water trail" from galaxies to oceans, by covering key rotational lines of H_2O and HD at submillimeter wavelengths with unprecedented sensitivity and angular resolution (Arenberg et al., 2021). With its broad frequency coverage and tunability between 455 and 4,745 GHz, OASIS will also cover multitudes of spectral lines from CHNOPS carriers. As much of our current understanding of astrochemical complexity is based on observations at millimeter wavelengths (McGuire, 2018), OASIS will open a new window for studying the volatile chemistry along the star- and planet-formation sequence. In particular, OASIS will transform our understanding of the astrochemistry of hydrides (e.g., NH_x, CH_x, and OH_x) and high-excitation lines of organic molecules.

In this work, our aim is to highlight knowledge gaps that OASIS will uniquely fill in our understanding of organic/prebiotic astrochemistry. For a discussion of HD and H_2O science applications, we refer the reader to Walker et al. (2021). **Section 2** presents a brief overview of the optical and technical capabilities of OASIS, how it compares to other state-of-the-art observing facilities, and the galactic star-forming regions it will observe. In **Section 3**, we describe how OASIS's unique observational capabilities will advance the study of CHNOPS astrochemistry along the star- and planet-formation sequence, from prestellar cores to protoplanetary disks. **Section 4** presents our summary and conclusions.

2 OASIS OVERVIEW

The OASIS mission concept is detailed in Walker et al. (2021). Here, we present a brief overview of the mission features most salient to the astrochemistry science use cases.

2.1 Technical Specifications

OASIS is a space-based observatory, which will be in a Sun–Earth L1 halo orbit. In the current design, OASIS utilizes an inflatable 14-m reflector, followed by aberration corrector optics achieving diffraction-limited optical performance, coupled to a state-of-the-art terahertz (THz) heterodyne receiver system (Takashima et al., 2021). This enables high sensitivity and high spectral resolving power ($> 10^6$) observations between 455 and 4,745 GHz (660 and 63 μm wavelengths). **Table 1** summarizes the key performance characteristics of the OASIS receivers. If selected, OASIS will launch by no later than December of 2028 at a total mission cost cap of $300 million, excluding launch costs.

2.2 Complementarity to Other Facilities

Figure 1 shows a comparison of the line sensitivity, spectral resolution, and angular resolution that OASIS will achieve, compared to those of other previous, existing, and future observational facilities. The spectral line sensitivity of OASIS is comparable to that of the state-of-the-art facilities ALMA and JWST and $\geq 10\times$ better than *Herschel* or SOFIA. The spectral resolving power of OASIS, particularly the high-resolution chirp transform spectrometer (CTS) mode of Band 1, is comparable to that of SOFIA, ALMA, and *Herschel*. Notably, OASIS will provide two to three orders of magnitude higher spectral resolving power than JWST's NIRSPEC and MIRI instruments, allowing for detailed kinematic studies. Last, OASIS will provide nearly an order of magnitude improvement in spatial resolution compared to previous and existing far-infrared telescopes ("cold" Spitzer, SOFIA, and *Herschel*). Also note that while ALMA is able to cover frequencies as high as 950 GHz, such observations require exceptional observing conditions and are not practical for extended surveys. As a space-based facility, OASIS will readily access these wavelengths.

OASIS also has spectral coverage overlapping with the Origins Space Telescope, a potential future facility–class mission. As proposed, Origins is a 5.9-m cryogenic telescope with three scientific instruments operating in the wavelength range 2.8–588 μm (Leisawitz et al., 2021). The Origins Survey Spectrometer (OSS) would make far-IR spectroscopic measurements with a maximum spectral resolving power R ~ 3×10^5 (Bradford et al., 2021). A fourth instrument, the Heterodyne Receiver for Origins (HERO), was also studied as a way to provide higher spectral resolving power than OSS ~10^6—10^7; (Wiedner et al., 2021). However, HERO was not included in the baseline mission concept because heterodyne detection, limited by receiver quantum noise, does not require a very cold (4.5 K) telescope such as Origins. OASIS will accomplish Origins/HERO science in a much less expensive mission.

In summary, OASIS will outperform other far-infrared facilities (*Herschel*, SOFIA) and complement near/mid-infrared (JWST) and (sub-) millimeter (ALMA) facilities as well as the future mid-/far-infrared Origins Space Telescope. These capabilities will make OASIS a powerful instrument for astrochemical studies in star- and planet-forming regions. In **Section 3**, we provide more detailed discussions of OASIS performance relative to other observatories in the context of specific science use cases.

2.3 Observations of Galactic Star-Forming Regions

As part of its aim to "follow the water trail," OASIS will observe galaxies, nearby star-forming regions, and Solar System bodies. Here, we focus on science applications in galactic star-forming

TABLE 1 | OASIS receiver overview.

—	Band 1	Band 2	Band 3	Band 4
Frequency range (GHz)	455–575	1,097–2,196	2,475–2,875	4,734–4,745
Beam size[a] (″)	10.3	3.2	2.0	1.1
Maximum IF bandwidth (GHz)	4/1[b]	3.5	3.5	3.5
Velocity resolution (km s^{-1})	3.1/0.03[b]	1.0	0.6	0.4
5σ sensitivity[c] in 1 h (Jy $beam^{-1}$ km s^{-1})	0.9	1.5	1.6	3.4

[a]*Diffraction-limited*
[b]*Two values are shown corresponding to medium or high spectral resolution modes*
[c]*Representative value within the band*

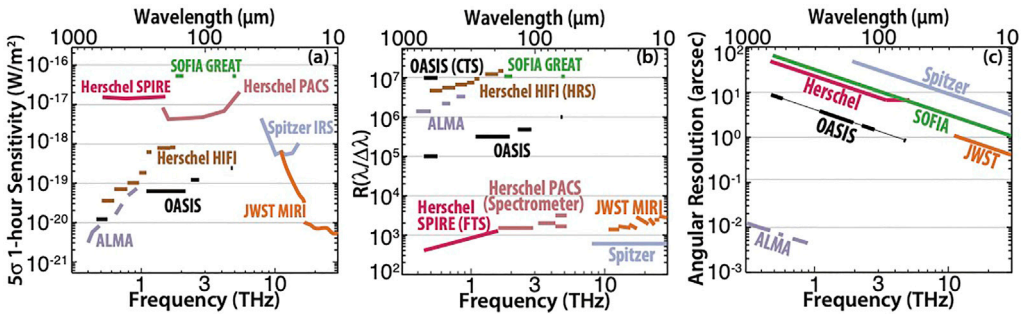

FIGURE 1 | Comparison of **(A)** spectral line sensitivity, **(B)** spectral resolving power, and **(C)** angular resolution of OASIS with other state-of-the-art telescopes.

regions. OASIS will observe various classes of objects along the star-formation sequence: prestellar cores, low- and high-mass protostars, and protoplanetary disks. In particular, disk systems will be a key focus of the OASIS mission, with the goal of measuring the H_2O content and HD-derived disk mass toward >100 sources spanning young embedded disks (Class 0/I) through evolved protoplanetary disks (Class II). Hereafter, we refer to this 100-object sample as the OASIS disk survey.

Measurements of the HD and $H_2^{18}O$ lines in OASIS Bands 3 and 4 require long integrations (12 h). Given the large simultaneous bandwidths and independent tunability of the four OASIS bands (**Table 1**), broad spectral regions in Bands 1 and 2 can be scanned at the same time. Indeed, OASIS Band 1 (455–575 GHz) can be fully covered in 12 1-h tunings to the sensitivity shown in **Figure 1A**. For Band 2 (1,100–2,200 GHz), 84 GHz of the 1.1 THz band can be covered in similar 1-h tunings. This extensive spectral coverage will contain multitudes of lines of simple and complex CHNOPS carriers.

3 CHNOPS ASTROCHEMISTRY WITH OASIS

Here, we highlight impactful astrochemical contributions that OASIS will make with Band 1 and Band 2 observations of various dense star-forming regions. We begin with objects targeted by the OASIS disk survey: Class II disks (**Section 3.1**) and Class 0/I protostars (**Section 3.2**). We next consider additional star-forming regions where line surveys with OASIS will provide novel constraints on the chemistry and physics: protostellar outflows (**Section 3.3**), high-mass hot cores (**Section 3.4**), and prestellar cores (**Section 3.5**).

3.1 Protoplanetary Disks (Class II)

Given the small angular scales and cold temperatures of mature (Class II) disks, the detection of complex molecules >6 atoms is challenging even at lower frequencies (e.g., Öberg et al., 2015; Walsh et al., 2016). Smaller molecules are, therefore, essential probes of the physics and chemistry in disks and by extension the physics and chemistry associated with planet formation. While molecules observable at millimeter wavelengths have been extensively studied in disks, there are almost no constraints on the inventories of light hydrides in disks, many of which are observable only at sub-millimeter/FIR wavelengths. Coverage of these lines with OASIS (**Figure 2**) will thus provide a novel and highly complementary avenue for exploring the volatile chemistry in disks. Here, we highlight the light hydride science that we expect to be most impactful for studies of disk chemistry.

3.1.1 NH_3 and Its Isotopologues

Of the light hydrides covered by OASIS Bands 1 and 2 (**Figure 2**), perhaps the most exciting science will be enabled by observations of NH_3. Indeed, the N budget in disks is poorly constrained given that the dominant N carrier, N_2, cannot be observed. Ice spectroscopy toward low-mass protostars, the evolutionary progenitors of disks, has revealed that NH_3 is an important N carrier in the ice, with a relative abundance of ~5% with respect to H_2O compared to <1% in nitriles, or XCN (Öberg et al., 2011a). However, while nitriles are commonly detected toward disks (e.g. Dutrey et al., 1997; Öberg et al., 2015; Guzmán et al., 2017;

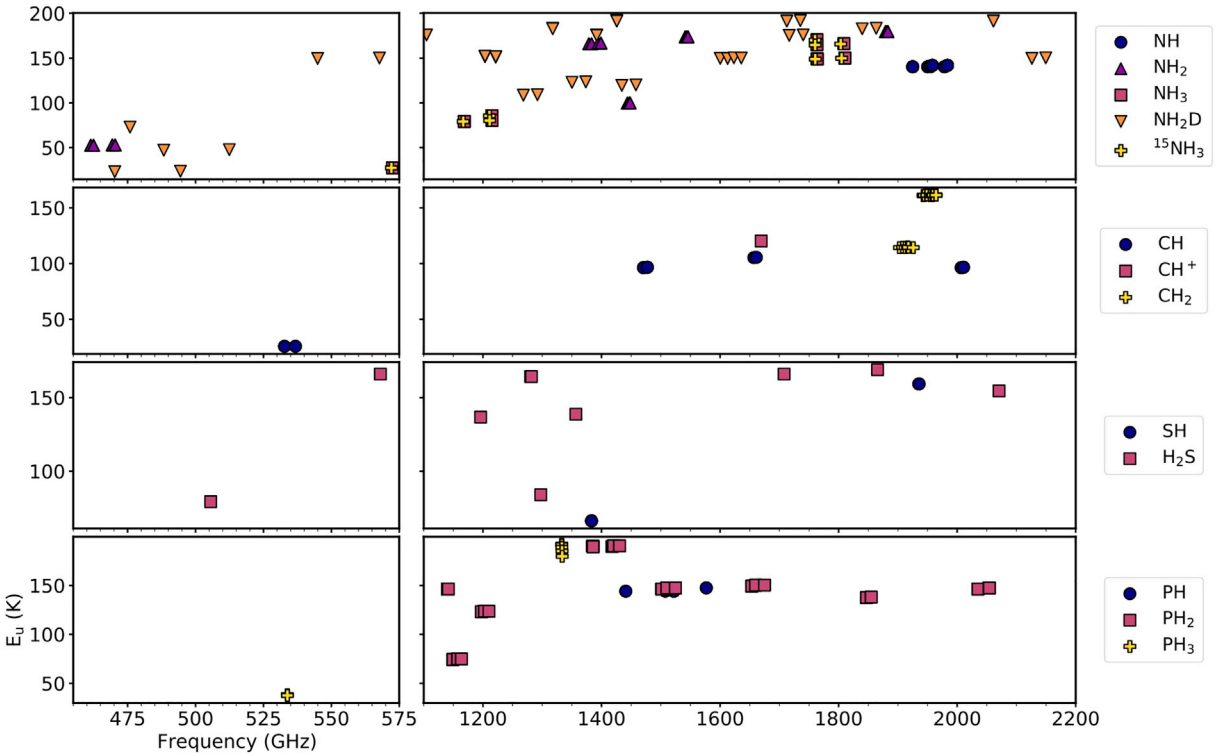

FIGURE 2 | Summary of the frequencies and upper-state energies of selected N, C, S, and P hydrides with transitions observable by OASIS Bands 1 and 2. Only lines with Einstein coefficients $>10^{-4}$ s^{-1} and upper-state energies <200 K are included.

Bergner et al., 2019b; van Terwisga et al., 2019), to date NH_3 has been detected toward just two disks. NH_3 was first detected toward the nearby TW Hya disk, via the 572 GHz transition of o-NH_3 observed by *Herschel* (Salinas et al., 2016). More recently, NH_3 was detected toward the embedded (Class I) disk GV Tau N at mid-IR wavelengths, tracing hot emission from the inner ~au (Najita et al., 2021).

Bands 1 and 2 of OASIS will cover multiple strong transitions tracing cool NH_3 (upper state energies from 27 to 170 K). While the 572 GHz NH_3 line toward TW Hya was detected with low SNR with *Herschel*, the same flux is over an order of magnitude above the OASIS 5σ detection threshold. To further assess the prospects of detecting NH_3 with OASIS, we created a toy disk model based on TW Hya. We adopt a physical structure based on the models of Cleeves et al. (2015), Zhang et al. (2017), and Huang et al. (2018). Informed by the constraints on o-NH_3 from Salinas et al. (2016), we assume a power-law abundance profile $X(r) = 8 \times 10^{-11}$ (r/100au). We assume a freeze-out temperature of 65 K (e.g., Kruczkiewicz et al., 2021), below which we attenuated the NH_3 abundance by two orders of magnitude. We use RADMC-3D (Dullemond et al., 2012) to simulate fluxes of the three o-NH_3 lines observable by OASIS and recover a comparable flux of the 572 GHz transition compared to the *Herschel* observations of TW Hya. We emphasize that this is a toy model that reproduces the observations with a reasonable physical and chemical structure, but other distributions of NH_3 in TW Hya are of course possible.

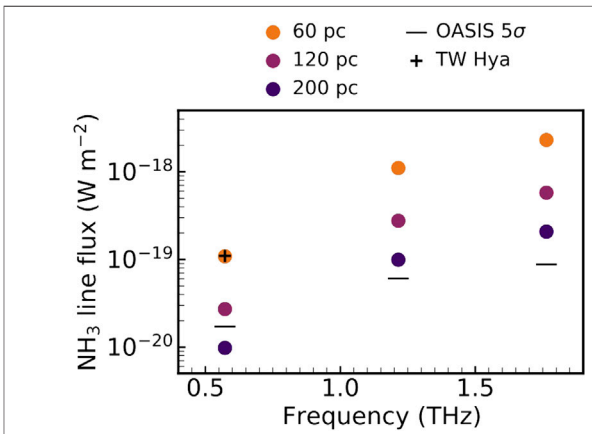

FIGURE 3 | Simulated o-NH_3 line fluxes for a TW Hya-like disk at 60, 120, and 200 pc. Horizontal bars represent the OASIS 5σ detection threshold for each line. The 572 GHz o-NH_3 flux observed by Salinas et al. (2016) is shown with a "+".

Figure 3 shows the predicted o-NH_3 fluxes for three distances representative of the source targets in the OASIS disk survey. For relatively nearby sources (<200 pc), we expect to detect all three o-NH_3 lines at high SNR. For distant sources ~200 pc, we should still detect both Band 2 transitions at moderate SNR. While some sources may have intrinsically lower fluxes than our toy model

due to, for e.g., lower gas-phase NH_3 abundances or different temperature/density structures, it is reasonable in a sample of ~100 to expect that multiple NH_3 lines will be detected toward numerous disks in the OASIS survey.

Excitingly, detection of multiple lines with OASIS will allow for the first excitation analysis of NH_3 in the outer disk. Additionally, the high spectral resolution provided by OASIS will enable a kinematic analysis of the NH_3 line profiles in sources with high SNR, providing constraints on the spatial origin of emission. Auxiliary constraints on the disk structures, provided by the OASIS observations of CO isotopologues and HD and H_2O, will permit robust NH_3 abundance retrievals. The NH_3/H_2O abundance ratio is of particular interest, as it can be directly compared with the ratio measured in comets to provide insights into how N is inherited by Solar System bodies.

While we focused our toy model on o-NH_3 for simplicity, OASIS will also cover six transitions of p-NH_3 with comparable line intensities to the modeled o-NH_3 transitions. While the statistical NH_3 ortho-to-para ratio (OPR) is 1, values <1 and >1 have been found in various interstellar environments, and are thought to correspond to the formation in the gas-phase vs. grain surface, respectively (e.g., Umemoto et al., 1999; Persson et al., 2012; Faure et al., 2013). Even for a high OPR (~2), we expect to detect multiple p-NH_3 lines toward nearby disks. Thus, OASIS will measure the OPR in NH_3, another quantity which can be directly compared to interstellar measurements to gain insight into the formation and inheritance of NH_3 in planet-forming disks. OASIS will also cover transitions of smaller nitrogen hydrides (NH and NH_2; **Figure 2**), which if detected would provide further constraints on the N budget in disks. Moreover, probing these small N hydride radicals would elucidate the role that gas-phase radical chemistry plays in incorporating N into larger species.

Numerous transitions of NH_3 isotopologues (e.g., $^{15}NH_3$ and NH_2D) are also observable by OASIS, raising the possibility of measuring isotopic fractionation levels in NH_3. The case of $^{15}NH_3$ is particularly interesting since, to date, the $^{14}N/^{15}N$ ratio in disks has only been measured via nitriles (i.e., CN and HCN; Guzmán et al., 2017; Hily-Blant et al., 2017), which form through a distinct chemistry compared to NH_3 (e.g., Visser et al., 2018). $^{15}NH_3$ transitions are close in frequency, upper-state energy, and intrinsic line strength to the analogous NH_3 transitions (**Figure 2**). Detection of these lines will likely be challenging: based on our predicted o-NH_3 line fluxes and given that the $^{14}N/^{15}N$ ratio measured in disk nitriles is $\gtrsim$100, $^{15}NH_3$ would not be detected toward TW Hya. Still, given the large number of disks in the OASIS survey, a detection of $^{15}NH_3$ is plausible and would be of high impact.

3.1.2 Other Light Hydride Science

Another promising avenue for disk science with OASIS is S hydrides. Sulfur is commonly very depleted from the gas in dense star-forming regions, though several S carriers (CS, SO, H_2S, and H_2CS) have now been detected in disks (Dutrey et al., 1997; Guilloteau et al., 2013; Phuong et al., 2018; Le Gal et al., 2019). H_2S was only recently detected in Class II disks: first toward GG Tau A (Phuong et al., 2018), followed by UY Aur (Rivière-Marichalar et al., 2021). Toward other well-known disks, deep searches for H_2S have only produced upper limits (Dutrey et al., 2011). To date, only the $1_{1,0}$–$1_{0,1}$ line (168.73 GHz) has been targeted, which is readily observable by using ground-based telescopes but also intrinsically quite weak compared to the higher frequency lines covered by OASIS. The H_2S lines at 1865.6 and 1,281.7 GHz appear particularly promising for detection in disks with OASIS, particularly if the emission originates in a somewhat warm environment. For instance, assuming a comparable source-average column density (1.3×10^{12} cm^{-2}) and emitting area (~ 3″ radius) to GG Tau A, we expect to detect these lines given a rotational temperature $\gtrsim$35 K. With warmer temperatures, closer/larger sources, or higher H_2S column densities, seven additional H_2S lines in OASIS Bands 1 and 2 (E_u 79–168 K) will also become good candidates for detection, enabling a multiline excitation analysis.

It is important to highlight that H_2S is the dominant sulfur carrier in cometary comae (Calmonte et al., 2016). The lack of constraints on H_2S abundances and distributions in protoplanetary disks has made it challenging to contextualize these measurements of cometary sulfur chemistry. By providing constraints or strong upper limits on the H_2S inventory in a physically diverse sample of ~100 disks, OASIS will greatly advance our understanding of the volatile sulfur reservoir in planet-forming disks and our own Solar System.

CH^+ was previously detected toward one disk with *Herschel* and was found to probe warm emission from the disk surface and inner rim (Thi et al., 2011). Prospects for detecting other light carbon hydrides (CH and CH_2) in disks are unclear given that there is no precedent in the literature. Similarly, the unsaturated nitrogen and sulfur hydrides (NH, NH_2, and SH) have not been previously observed toward disks. OASIS will cover numerous strong lines of each of these molecules (**Figure 2**), so it remains a possible avenue of discovery science. If detected, these lines would provide yet further constraints on the volatile C/N/S chemistry in disks. We note that phosphorus has yet to be detected in any form in a disk, and so the detection prospects for phosphorus hydrides are even less certain.

3.2 Low-Mass Protostars (Class 0/I)

3.2.1 Hot Corino Emission

A subset of low-mass protostars exhibits a rich gas-phase organic chemistry near the protostellar core and have been termed "hot corinos" in analogy to the high-mass hot cores described in **Section 3.4** (Cazaux et al., 2003; Bottinelli et al., 2004). Because this chemical richness originates from the sublimation of icy molecules, the inventory of organic molecules in the gas should reflect, at least in part, the composition of the parent ices (e.g., Garrod and Widicus Weaver, 2013).

Within the protostellar environment, a hot corino occupies a similar spatial scale as the nascent protoplanetary disk (e.g., Maury et al., 2014; Maret et al., 2020). Constraints on the organic inventories in hot corinos, therefore, provide a view of the complex organic material that is present in the ices where disk formation, and ultimately planet/planetesimal formation, is

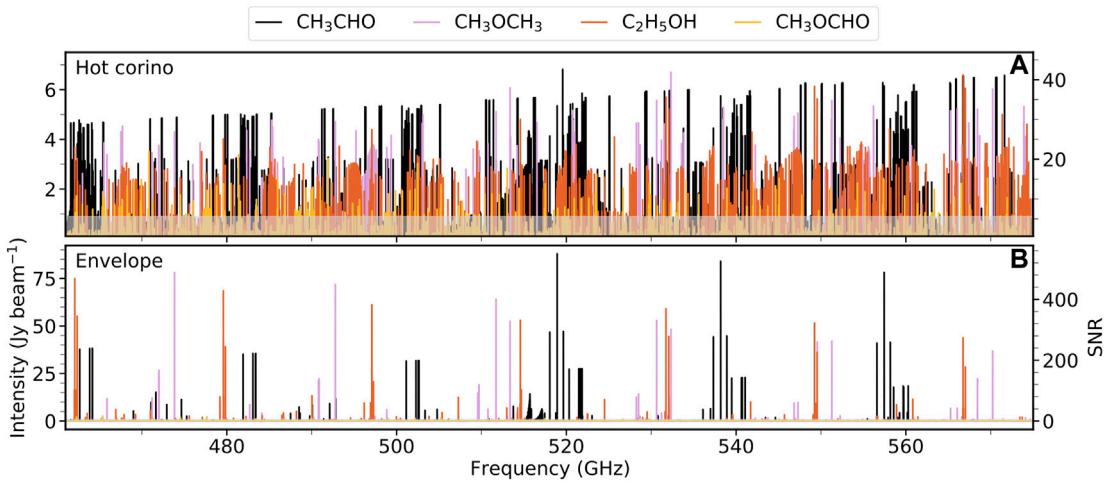

FIGURE 4 | Simulated spectra of common O-bearing organics in OASIS Band 1. Physical models are based on a hot corino **(A)** and protostellar envelope **(B)**. In both panels, the 5σ detection threshold for a 1-h integration of OASIS Band 1 is shown as a gray shaded region, assuming a 1 km s^{-1} line width.

taking place. Indeed, similarities in the organic compositions of hot corinos compared to cometary ices support the idea that comets formed at least in part from the icy material with a pre/protostellar origin (Drozdovskaya et al., 2019). Moreover, probing isotopic fractionation levels in these organics provides powerful constraints on their formation conditions (e.g., Coutens et al., 2016; Jørgensen et al., 2018). This is key to determining where along the star-formation sequence organic complexity is built up.

The archetypical hot corino source IRAS 16293–2422 (hereafter IRAS 16293) was observed as part of the *Herschel* key project CHESS (Ceccarelli et al., 2010). In the 555–636 GHz range, comparable to OASIS Band 1, numerous lines of small organics (e.g., HCN, H_2CO, and CH_3OH) were detected. However, neither rarer isotopologues of CH_3OH nor organics larger than CH_3OH were detected. With a beam size around 35″ at these frequencies and a hot corino emitting size of 0.5″, these observations suffered a beam dilution factor of nearly 5,000. Thus, previous submillimeter and THz observations of hot corinos offered virtually no constraints on the organic molecule emission.

The smaller beam size of OASIS (~ 10″ at Band 1) will provide a huge improvement in this regard. In **Figure 4A**, we show predicted spectra of four common oxygen-bearing organics toward IRAS 16293, generated using the physical and chemical model constrained by the ALMA-PILS survey (Jørgensen et al., 2016). Although the OASIS beam will still be larger than the source size, thousands of organic molecule transitions will be detected at high SNR. Coverage of numerous lines per molecule will permit a detailed analysis of their excitation conditions. Moreover, with dozens of protostellar targets, the OASIS mission will deliver demographic constraints on the complex organic inventories across hot corinos.

3.2.2 Organics in Protostellar Envelopes

Not all Class 0/I protostars are hosts to hot corino emission, yet due to non-thermal desorption mechanisms, protostellar envelopes still host detectable abundances of gas-phase emission from organic molecules (e.g., Öberg et al., 2011b; Bergner et al., 2017). **Figure 4B** shows simulated spectra assuming the same chemical model as the hot corino IRAS 16293 but adopting abundances scaled down by two orders of magnitude and a cool (30 K) gas temperature. For this simulation, we assume that the emission fills the OASIS beam, as is appropriate for a protostellar envelope. Multitudes of transitions are detectable by OASIS, with even higher SNR compared to those by hot corinos due to the larger emitting area. Interferometers are not well suited for probing this diffuse envelope emission since they are mainly sensitive to emission on smaller spatial scales and resolve out emission on larger scales. OASIS, therefore, offers a unique advantage for studying the emission of non-thermally desorbed molecules in lukewarm (~30 K) protostellar envelopes of Class 0/I sources. These constraints will provide novel insights into how organic complexity evolves during the epoch when dust and gas of the cold envelope collapse toward the central protostar and can help benchmark chemical models of such evolution (e.g., Garrod and Herbst, 2006). This avenue is also highly complementary to forthcoming JWST ice observations: ice maps constructed from observations of extincted background stars will probe similar spatial scales, enabling direct comparisons between the ice and gas compositions of the envelope (e.g., Perotti et al., 2020, 2021).

3.2.3 Deuterium Fractionation

In both hot corino and non-hot corino sources, OASIS should have sufficient sensitivity to detect deuterated isotopologues of common complex organics. **Figure 5** shows the simulated spectra for singly and doubly deuterated dimethyl ether (CH_3OCH_3) and singly deuterated ethanol (C_2H_5OH), assuming the same hot corino and envelope conditions as for **Figure 4**. For clarity, different isotopomers are combined to produce a single spectrum for each substituted molecule. While deuterated

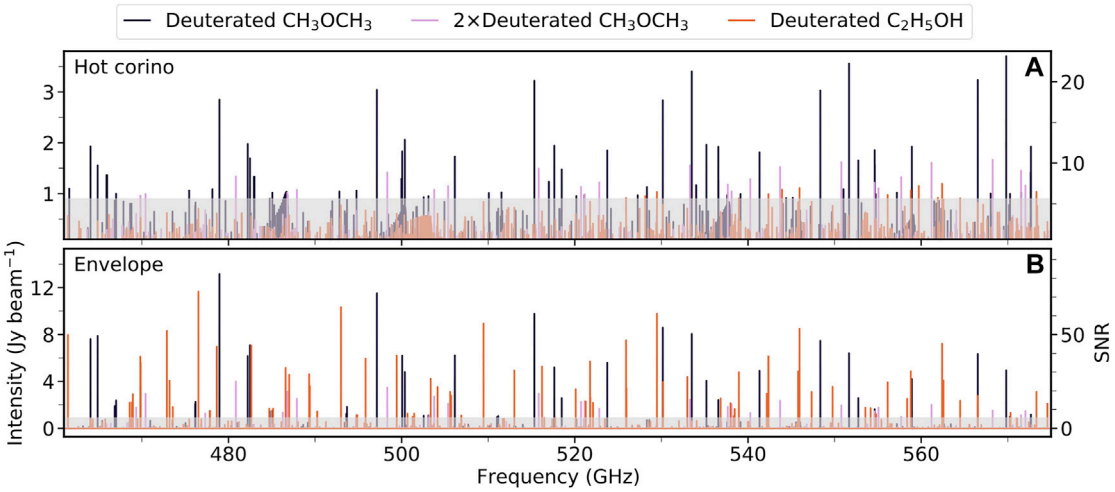

FIGURE 5 | Simulated spectra of deuterated O-bearing organics in OASIS Band 1. Physical models are based on a hot corino **(A)** and protostellar envelope **(B)**. In both panels, the 5σ detection threshold for a 1-h integration of OASIS Band 1 is shown as a gray shaded region.

ethanol lines are only slightly above the detection threshold in the hot corino simulation, both singly and doubly deuterated dimethyl ethers should be readily detectable. The envelope scenario is even more promising, with all three molecules exhibiting numerous lines well above the detection threshold.

3.2.4 Comparison to ALMA

It is important to consider how the performance of OASIS will compare to ALMA, the current state-of-the-art facility for studying complex chemistry in hot corinos. Given its sub-arcsecond spatial resolution, ALMA is better beam-matched to hot corinos than OASIS and is capable of detecting lower abundance species such as even larger molecules (e.g., glycolaldehyde; Jørgensen et al., 2016) and rarer isotopologues (Coutens et al., 2016; Jørgensen et al., 2018). Still, OASIS has several unique advantages. 1) Bandwidth: In order to obtain sufficient SNR on the HD line in Band 3, OASIS will observe many sources for ~12 h. Because Bands 1 and 2 are independently tunable, simultaneous spectral scans can cover up to 200 GHz in bandwidth assuming 1 h per scan. This spectral coverage is far beyond what is practically achievable with ALMA and will provide a detailed and unbiased picture of the inventories and excitation conditions of moderately abundant complex organics. 2) Source statistics: The OASIS mission will observe numerous Class 0/I protostars as part of its baseline mission. While surveys of organic chemistry in low-mass protostars are beginning to be undertaken with ALMA and NOEMA (e.g., Bergner et al., 2019a; Belloche et al., 2020; Yang et al., 2021), our understanding of the chemical demographics in these objects is still in its infancy. Given also that ALMA is heavily over-subscribed, OASIS will provide much-needed statistical constraints on the complex chemistry in Class 0/I protostars. 3) Maximum resolvable scale: As noted previously, due to its larger beam size, OASIS will be able to probe organic molecule emission originating in the diffuse envelope of protostars, to which ALMA observations are not sensitive. This will provide novel constraints on chemical evolution during protostellar infall. 4) Far-IR spectral coverage: While ALMA can access far-IR wavelengths with Bands 8–10, these observations require exceptional weather conditions. By contrast, there are no obstacles for observing at these wavelengths using a space telescope. Higher frequency observations generally cover lines with higher upper-state energies and are thus well suited for studying the hot emission originating close to a protostar. Additionally, for some molecules, the spectral intensity will peak in the far-IR under hot corino conditions. We highlight the case of E-C-cyanomethanamine, a HCN dimer implicated in prebiotic chemical schemes: at a temperature of 100 K, the strongest spectral lines occur around 900–1,000 GHz (Melosso et al., 2018). Thus, coverage at THz frequencies may be uniquely suited for detecting certain organics compared to lower-frequency observations.

3.3 Protostellar Outflows

The early (Class 0 and Class I) stages of low-mass protostellar evolution are often accompanied by the launching of an outflow, which promotes accretion onto the protostar by carrying away angular momentum. Encounters between the outflow and the ambient envelope material produce shocks, which can dramatically alter the local chemistry through heating and grain sputtering. In some “chemically rich” outflows, the gas-phase abundances of molecules normally associated with the ice phase (H_2CO, CH_3OH, and CH_3OCHO) are enhanced by orders of magnitude due to shock-induced ice sputtering (e.g., Garay et al., 1998; Codella and Bachiller, 1999; Requena-Torres et al., 2007; Arce et al., 2008). Thus, as for hot cores and hot corinos, chemically rich outflows offer a valuable window to probe the organic composition of interstellar ices. Moreover, studies of outflow shock physics and chemistry inform our understanding of the same processes that take place on smaller, disk-forming scales within the protostellar core.

The archetypical chemically rich outflow shock, L1157-B1, was observed as part of the *Herschel* CHESS survey (Ceccarelli et al.,

2010). The 555–636 GHz spectrum contained emission lines from high-excitation transitions of grain tracers such as NH_3, H_2CO, and CH_3OH (Codella et al., 2010). An excitation analysis of these lines revealed that they emit with temperatures ≥200 K, intermediate between the cold emission observed by longer wavelength transitions and the very hot gas traced by H_2 emission. Thus, observations of higher excitation organics toward outflow shocks can help to link these different emission regimes and disentangle how the shock chemistry and physics progresses. These insights can in turn be used to tune models of shock astrochemistry, which are needed to connect observed gas-phase abundances to the underlying grain compositions (e.g., Burkhardt et al., 2019).

Herschel observations as part of the WISH program also provided detailed constraints on the physics and chemistry toward numerous star-forming regions including protostellar outflows (van Dishoeck et al., 2011). While H_2O chemistry is not our focus, it is worth highlighting that WISH obtained extensive constraints on the abundances and origin (e.g., ice sputtering vs. gas-phase chemistry) of H_2O within outflows (van Dishoeck et al., 2021). Additionally, light hydride lines measured through the WISH program provided powerful constraints on the UV and X-ray fields around young protostars and the physics of shock propagation (Benz et al., 2016).

OASIS will offer several improvements for observations of outflows compared to *Herschel* (**Figure 1**). The improved OASIS sensitivity raises the possibility of detecting more complex species toward chemically rich shocks and characterizing their excitation in detail. With higher angular resolution, the OASIS beam will encompass a smaller range of physical environments within the outflow, leading to less spectral blending of different shock components. Last, the high-resolution mode of OASIS Band 1 has a higher spectral resolution than that of *Herschel*, allowing different velocity components within the outflow to be clearly distinguished. Thus, we expect significant improvements in the shock chemistry and physics that can be probed with OASIS compared to *Herschel*. While ALMA similarly offers improvements in sensitivity and spectral/spatial resolution compared to *Herschel*, the higher frequencies covered by OASIS are better suited for accessing the warm post-shocked material compared to ALMA.

It is also worth noting that chemically rich outflow shocks are, to date, the only low-mass star forming regions where phosphorus carriers have been detected (Yamaguchi et al., 2011; Bergner et al., 2019c). In shock chemistry models, PH_3 and smaller P hydrides are predicted to be at least as abundant as the detected P carriers PN and PO (Jiménez-Serra et al., 2018). However, PH_3 has only one strong transition observable below 500 GHz and has yet to be detected in a star-forming region. OASIS will cover multiple strong lines of P hydrides (**Figure 2**), opening the door for obtaining a more complete inventory of the volatile phosphorus carriers in star-forming regions.

3.4 High-Mass Hot Cores

The regions of hot molecular line emission within massive star-forming regions are termed hot cores. These regions are typically characterized by high temperatures (hundreds of K) and densities ($\sim 10^7$ cm^{-2}) (van der Tak et al., 2000). Originally identified based on the detection of hot NH_3 toward Orion-KL (Morris et al., 1980), hot cores were subsequently found to host an incredibly rich gas-phase organic chemistry (Blake et al., 1987). Ice mantles are the main sites of astrochemical complex organic molecule formation, and sublimation of these ices is responsible for the wealth of chemical complexity detected in hot cores (e.g., Garrod and Herbst, 2006; Herbst and van Dishoeck, 2009). The molecular line emission in hot cores provides powerful constraints on both the physical and chemical conditions in these regions (see, for e.g., Garrod and Widicus Weaver, 2013). With a rich organic chemistry, high temperatures, and large emitting areas, high-mass hot cores represent ideal targets to exploit the unique capabilities of OASIS.

Pioneering work in the submillimeter study of high-mass hot cores was performed by the *Herschel* observations of EXtra-Ordinary Sources (HEXOS) guaranteed-time program. HEXOS targeted Orion KL and Sgr B2 (N + M) with >1 THz in bandwidths from ~480–1900 GHz, with a spectral resolution around 1 MHz (Bergin et al., 2010). The HEXOS program illustrates the power of wide-bandwidth, unbiased spectral scans at THz wavelengths for probing both the physics and chemistry associated with high-mass star formation. Analyses of the submillimeter line emission and absorption generated novel constraints on the physical structure and kinematics of Orion KL and Sgr B2, including infall and stellar feedback in Sgr B2(M) (Rolffs et al., 2010), the kinematics and energetics of outflowing material in Orion KL (Phillips et al., 2010), the thermal structure and heating source in Orion KL (Wang et al., 2011), and the gas density and luminosity source within the Orion KL core (Crockett et al., 2014a).

HEXOS provided a similar wealth of insight into the chemistry of simple molecules during high-mass star formation, including constraints on H_2O deuteration levels (Bergin et al., 2010), the H_2O abundance and ortho-to-para ratio (Melnick et al., 2010), and the CO_2 abundance as traced by $HOCO^+$ (Neill et al., 2014). Additionally, many of the thousands of lines detected in the HEXOS scans correspond to complex organic molecules. Coverage of lines with a wide range in upper-state energies allowed unprecedented constraints on the column densities and excitation conditions of dozens of organic molecules toward Orion KL and Sgr B2 (Crockett et al., 2010, 2014b; Neill et al., 2014). Intriguingly, HEXOS revealed a chemical differentiation in the complex organic inventories between Orion KL and Sgr B2(N), which could arise from evolutionary differences between the high-mass hot cores (Neill et al., 2014). This underscores the potential for such surveys to probe demographics in high-mass star formation.

While *Herschel* greatly expanded our understanding of high-mass hot cores, there is an ample room for improvement with OASIS. Notably, the OASIS beam will be nearly a factor of four smaller than the *Herschel* beam at a given frequency, mitigating loss of sensitivity due to beam dilution. For instance, in OASIS Bands 1 and 2, the OASIS beam will be 10.3 and 3.2″ compared to 40.4 and 12.8″ in the corresponding *Herschel* bands, respectively. Depending on the emitting source size, this could translate to a factor of up to 16 higher line sensitivity with OASIS compared to *Herschel*.

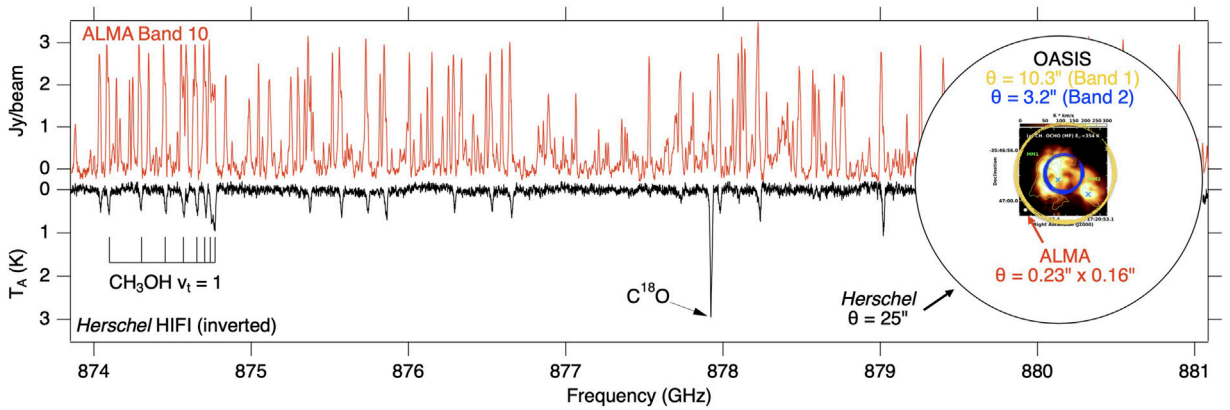

FIGURE 6 | Spectra of the high-mass star-forming region NGC 6334I as observed by ALMA (red) compared to that of *Herschel* (black, inverted). Inset shows the *Herschel*, ALMA, and OASIS Band 1 and Band 2 beam sizes overlaid on the source structure, as traced by methyl formate emission. Figure adapted from McGuire et al. (2018).

OASIS's improved line sensitivity at THz wavelengths will open a new window into studying complex organic molecules in hot cores. **Figure 6**, adapted from McGuire et al. (2018), clearly illustrates how a massive star-forming region can appear line-poor when observed by *Herschel* but harbor hundreds of spectral lines when observed with a higher sensitivity and higher resolution observatory, in this case ALMA Band 10. With OASIS, we similarly expect higher line densities of organic molecules than *Herschel*. While the increase in sensitivity will be more modest with OASIS compared to ALMA, we note that Band 9 and 10 observations with ALMA require exceptional weather conditions and also do not extend to frequencies higher than 950 GHz, whereas OASIS will provide weather-independent access to wavelengths up to 3.6 THz.

While many complex organics can be detected via lines at lower frequencies, there are several advantages to obtaining observations at far-IR wavelengths. First, the lines covered by OASIS typically probe higher upper-state energies than millimeter-wavelength lines, which can provide a powerful lever arm for constraining excitation conditions. This is especially important for high-mass hot cores, in which organics often have excitation temperatures of a few hundred K (e.g., Crockett et al., 2014b; Neill et al., 2014). Good constraints on organic molecule excitation temperatures are required to interpret the physical conditions of the emitting regions as well as the chemical relationships between different classes of molecules. Also, as noted in **Section 3.2.4**, observations at higher frequencies may enable the detection of organic molecules with intensity peaks in the far-IR.

3.5 Prestellar Cores

Prestellar cores are the gravitationally bound phase of star formation immediately prior to the formation of a protostar (Bergin and Tafalla, 2007; André et al., 2014). OASIS will provide a unique opportunity to probe transitions that are difficult or impossible to observe from the ground in prestellar cores. It is during this phase that the initial conditions are set for the chemistry of the disk and subsequent planet formation. The direct chemical inheritance from the prestellar phase to the protostellar disk has been established, for instance reflected in the D/H ratio from ALMA observations of deuterated water (Jensen et al., 2021).

The central region of a prestellar core is a cold (T_K < 10 K), dense ($n > 10^5$ cm^{-3}) environment that is well shielded from the surrounding interstellar radiation field (A_V > 10 mag). Many molecules, such as CO, deplete onto dust grains at these densities and temperatures (Willacy et al., 1998; Bacmann et al., 2002) eliminating them as probes of these regions. Deuterium fractionation of molecules via reactions with H_2D^+ becomes important (Millar et al., 1989; Roberts et al., 2003). The ground state rotational transitions of para-H_2D^+ (1.370 THz) and ortho-D_2H^+ (1.477 THz) are within OASIS Band 2; however, these lines are extremely difficult to detect toward prestellar cores due to the large energy difference between rotational energy levels (i.e., E_u/k = 65.7 K for the upper energy level of the 1.370 THz $1_{0,1}$–$0_{0,0}$ transition of para-H_2D^+). NH_2D is an excellent tracer of these coldest, densest regions of prestellar cores where deuterium fractionation enhances (NH_2D)/(NH_3) by more than four orders of magnitude above the ISM D/H ratio (Tiné et al., 2000; Ceccarelli et al., 2014; Harju et al., 2017). OASIS will observe the high critical density ($n_{crit} > 10^7$ cm^{-3}) transitions of NH_2D that probe the very centers of the cores where a disk will eventually form. In Band 1, the $1_{1,0}$–$0_{0,0}$ ground state rotation-inversion transitions of both ortho and para spin-species of NH_2D are observable at 470 and 494 GHz, respectively (**Figure 2**). These transitions may be used in combination with the 86 and 110 GHz transitions, which are observable from the ground, to constrain the physical conditions of the innermost regions. The 86/470 line ratio of ortho-NH_2D is very sensitive to the temperature in the center of the core for n (H_2) > 10^6 cm^{-3} (**Figure 7**). Observations of the 470 GHz transition are difficult from the ground because the atmospheric transmission is less than 25% with 1 mm of water vapor at a high altitude site, and subthermal energy level populations result in a low-excitation

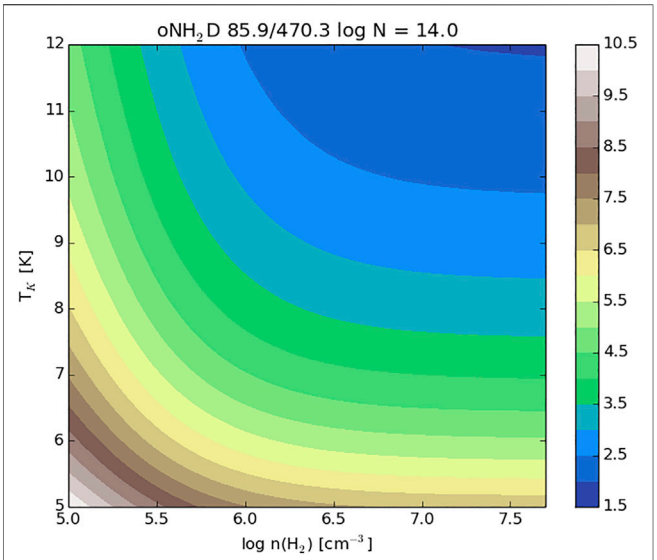

FIGURE 7 | RADEX (van der Tak et al., 2007) models of the line ratio of the 85.9 and 470.3 GHz transitions of o-NH_2D. Plotted line ratios vary from 1.5 to 10.5 for different values of the H_2 density and gas kinetic temperature. The o-NH_2D column density is assumed to be 10^{14} cm^{-3}.

temperature and therefore weak lines. The detectability of these lines from space was demonstrated with *Herschel* observations of the prestellar cores IRAS16293E and L1544 (Bacmann et al., 2012). The OASIS beam will better couple to the source emission for high critical density lines in prestellar cores than the *Herschel* beam permitting surveys of the densest prestellar cores in nearby molecular clouds.

Water observations of prestellar cores with OASIS will also play an important role in constraining the temperature profile in the outer part of the cores. Most of the water in a prestellar core is found in the solid state on the icy surfaces of dust grains (Bergin and Snell, 2002). However, photodesorption by UV photons can liberate some water molecules into the gas phase at abundances that are typically $< 10^{-9}$ with respect to H_2 (van Dishoeck et al., 2021). There are two main sources of UV photons in prestellar cores. The surrounding interstellar radiation field is the dominant heating component of dust grains in the core (Evans et al., 2001). There is also a low-intensity UV radiation field from excitation of H_2 due to collisions with electrons that come from cosmic ray ionizations of H_2 and He (Prasad and Tarafdar, 1983). The $1_{1,0}$–$1_{0,1}$ 557 GHz ground state rotational transition of ortho-H_2O can be observed in absorption against the continuum of the prestellar core (van Dishoeck et al., 2021). The line can also be seen in emission if the central density of the prestellar cores is $> 10^7$ cm^{-3}, although only a few prestellar cores are known that have this extreme central density (Caselli et al., 2012). The gas phase water in the outer part of the core at low A_V has a photodesorption rate that depends on the strength of the interstellar radiation field (G_0). A constraint on G_0 is needed to determine the dust temperature and the gas temperature profiles in the outer part of prestellar cores (Young et al., 2004). Accurate temperature profiles are crucial for radiative transfer modeling of molecular emission and absorption observed toward prestellar cores.

OASIS observations of light hydride molecules will also play an important role in constraining the kinematics of prestellar cores. The dynamical motions onto and within a prestellar core are difficult to constrain with current observational techniques. The density profile of a hydrostatic core is very similar to the density profile of a collapsing core until very late in the collapse history (Myers, 2005). Optically thick emission lines, such as HCN 1–0, can probe the internal kinematics through blue asymmetric self-absorbed emission profiles. The creation of this line profile requires very specific kinematic and molecular excitation conditions along the line of sight that are often difficult to achieve. Surveys searching for blue asymmetric line profiles generally find only a small fraction of prestellar cores with this signature (Sohn et al., 2007; Campbell et al., 2016; Seo et al., 2019). An alternative strategy is to observe red-shifted absorption lines from molecules that trace the outer portions of the core and compare to the velocities of emission lines that probe the inner regions of the core. This will be possible with OASIS observations of light hydride molecules and their deuterated isotopologues as well as with observations of H_2O. Tracers that have a wide range of critical densities probe the kinematics at different depths in the core. An example of this technique was demonstrated with *Herschel* observations of the ground state rotational transitions of ND (in emission) and NH (in absorption) toward the prestellar core IRAS 16293E (Bacmann et al., 2016).

4 SUMMARY AND CONCLUSION

The OASIS observatory is a NASA MIDEX space mission concept designed to observe at THz frequencies with unprecedented sensitivity and angular resolution. Compared to other state-of-the-art telescopes, OASIS will outperform other far-IR observatories (*Herschel* and SOFIA) and complement near/mid-IR (JWST) and (sub-) millimeter (ALMA) facilities. With its unique capacity to probe light hydrides and high-excitation organic lines, OASIS will open a new window for studying organic/prebiotic astrochemistry along the star- and planet-formation sequence. Key science use cases include:

1 OASIS will cover multiple strong transitions of NH_3 and H_2S, both of which are expected to be important volatiles in disks but are detected in only two sources to date. With ~100 source targets in the OASIS disk survey, OASIS will provide statistical constraints on the NH_3 and H_2S content in disks. It will also enable, for the first time, analyses of the excitation conditions, ortho-to-para ratios, and isotopic fractionation levels of these molecules in disks.
2. With broad spectral scans, OASIS will provide a detailed and unbiased view of the organic inventories and excitation conditions of hot corinos, lukewarm protostellar envelopes, protostellar outflows, and hot cores. Compared to ALMA, OASIS offers important advantages in its capacity to cover

wide spectral bandwidths, to obtain robust source statistics, to sample diffuse large-scale emission, and to access high-excitation lines in the far-infrared.
3. OASIS coverage of light hydrides will provide novel constraints on the physical conditions in the dense inner regions of prestellar cores, thus probing the initial conditions of protostellar and disk physics and chemistry.

Importantly, these efforts directly address high-priority science questions posed by the 2020 Decadal Survey (National Academies of Sciences, E., and Medicine, 2021), including: How are potentially habitable environments formed (E-Q3a)? And, what generates the observed chemical complexity of molecular gas (F-Q2c)?

Auxiliary laboratory efforts in THz spectroscopy will be critical for maximizing the scientific output of OASIS. Indeed, ~10% of lines in the *Herschel* spectra of Sgr B2(N) and Orion-KL were unidentified (Crockett et al., 2014b; Neill et al., 2014). The spectral line properties of many interstellar molecules are not well characterized above ~300 GHz, and some classes of molecules (e.g., isotopologues, vibrationally excited states, and unstable molecules) are particularly under-studied, though there are promising avenues for filling in these gaps (Widicus Weaver, 2019). Along with laboratory efforts, astrochemical modeling will greatly enrich the interpretation of OASIS observations. We expect OASIS to be particularly powerful for testing various mechanisms for ice-phase organic molecule production (e.g., Garrod & Herbst, 2006; Shingledecker et al., 2018; Jin & Garrod, 2020; Simons et al., 2020; Carder et al., 2021) given the detailed constraints on organic molecule inventories, abundances, and excitation conditions that will be obtained for low- and high-mass protostars and outflow shocks.

In summary, light hydrides and high-excitation organics are key players in the chemistry at various stages throughout the entire star- and planet-formation sequence. Our current understanding of these chemical regimes is limited due to the challenges of observing at THz frequencies. The OASIS mission will provide an unparalleled view of this astrochemistry, thus advancing our understanding of how and in what form the prebiotically important material is incorporated into nascent planets and planetesimals.

Software: Matplotlib (Hunter 2007), NumPy (van der Walt et al., 2011), RADEX (van der Tak et al., 2007), and RADMC-3D (Dullemond et al., 2012).

DATA AVAILABILITY STATEMENT

The raw data supporting the conclusion of this article will be made available by the authors, without undue reservation.

AUTHOR CONTRIBUTIONS

JB led the analysis and writing of the study. YS provided sections of the manuscript. JK and BM contributed figures and data. All authors contributed to manuscript editing and revision.

ACKNOWLEDGMENTS

We are grateful to the reviewers for helpful feedback on this manuscript. J.B.B. acknowledges support from NASA through the NASA Hubble Fellowship grant #HST-HF2-51 429.001-A awarded by the Space Telescope Science Institute, which is operated by the Association of Universities for Research in Astronomy, Incorporated under NASA contract NAS5-26 555. S.A. gratefully acknowledges funding from the European Research Council (ERC) under the European Union's Horizon 2020 Research and Innovation Programme (grant agreement no: 789 410).

REFERENCES

Alexander, C. M. O. D., Bowden, R., Fogel, M. L., Howard, K. T., Herd, C. D. K., and Nittler, L. R. (2012). The Provenances of Asteroids, and Their Contributions to the Volatile Inventories of the Terrestrial Planets. *Science* 337, 721–723. doi:10.1126/science.1223474

Alexander, C. M. O. D., Nittler, L. R., Davidson, J., and Ciesla, F. J. (2017). Measuring the Level of Interstellar Inheritance in the Solar Protoplanetary Disk. *Meteorit Planet. Sci.* 52, 1797–1821. doi:10.1111/maps.12891

Altwegg, K., Balsiger, H., Berthelier, J. J., Bieler, A., Calmonte, U., De Keyser, J., et al. (2017). D 2 O and HDS in the Coma of 67P/Churyumov-Gerasimenko. *Phil. Trans. R. Soc. A.* 375, 20160253. doi:10.1098/rsta.2016.0253

André, P., Di Francesco, J., Ward-Thompson, D., Inutsuka, S.-I., Pudritz, R. E., and Pineda, J. (2014). "From Filamentary Networks to Dense Cores in Molecular Clouds: Toward a New Paradigm for Star Formation," in *Protostars and Planets VI*. Editors H. Beuther, R. S. Klessen, C. P. Dullemond, and T. Henning, 27. doi:10.2458/azu_uapress_9780816531240-ch002

Arce, H. G., Santiago-García, J., Jørgensen, J. K., Tafalla, M., and Bachiller, R. (2008). Complex Molecules in the L1157 Molecular Outflow. *ApJ* 681, L21–L24. doi:10.1086/590110

Arenberg, J. W., Villareal, M. N., Yamane, J., Yu, T., Lazear, J., Pohner, J., et al. (2021). "OASIS Architecture: Key Features,". *Astronomical Optics: Design, Manufacture, and Test of Space and Ground Systems III*. Editors T. B. Hull, D. Kim, P. Hallibert, and F. Keller (International Society for Optics and Photonics SPIE), 11820, 264–283. doi:10.1117/12.2594681

Bacmann, A., Caselli, P., Ceccarelli, C., Pagani, L., and Vastel, C. (2012). "ESA Science & Technology," in *From Atoms to Pebbles: Herschel's View of Star and Planet Formation*. 15.

Bacmann, A., Daniel, F., Caselli, P., Ceccarelli, C., Lis, D., Vastel, C., et al. (2016). Stratified NH and ND Emission in the Prestellar Core 16293E in L1689N. *A&A* 587, 587A26. doi:10.1051/0004-6361/201526084

Bacmann, A., Lefloch, B., Ceccarelli, C., Castets, A., Steinacker, J., and Loinard, L. (2002). The Degree of CO Depletion in Pre-stellar Cores. *A&A* 389, 389L6–L10. doi:10.1051/0004-6361:20020652

Belloche, A., Maury, A. J., Maret, S., Anderl, S., Bacmann, A., André, P., et al. (2020). Questioning the Spatial Origin of Complex Organic Molecules in Young Protostars with the CALYPSO Survey. *A&A* 635, A198. doi:10.1051/0004-6361/201937352

Benz, A. O., Bruderer, S., van Dishoeck, E. F., Melchior, M., Wampfler, S. F., van der Tak, F., et al. (2016). Water in star-forming Regions withHerschel(WISH). *A&A* 590, 590A105. doi:10.1051/0004-6361/201525835

Bergin, E. A., Phillips, T. G., Comito, C., Crockett, N. R., Lis, D. C., Schilke, P., et al. (2010). Herschel Observations of EXtra-ordinary Sources (HEXOS): The Present and Future of Spectral Surveys with Herschel/HIFI. *A&A* 521, L20. doi:10.1051/0004-6361/201015071

Bergin, E. A., and Snell, R. L. (2002). Sensitive Limits on the Water Abundance in Cold Low-Mass Molecular Cores. *ApJL* 581, 581L105–L108. doi:10.1086/346014

Bergin, E. A., and Tafalla, M. (2007). Cold Dark Clouds: The Initial Conditions for Star Formation. *Annu. Rev. Astron. Astrophys.* 45, 339–396. doi:10.1146/annurev.astro.45.071206.100404

Bergner, J. B., Martín-Doménech, R., Öberg, K. I., Jørgensen, J. K., de la Villarmois, E. A., and Brinch, C. (2019a). Organic Complexity in Protostellar Disk Candidates. *ACS Earth Space Chem.* 3, 1564. doi:10.1021/acsearthspacechem.9b00059

Bergner, J. B., Öberg, K. I., Bergin, E. A., Loomis, R. A., Pegues, J., and Qi, C. (2019b). A Survey of C2H, HCN, and C18O in Protoplanetary Disks. *ApJ* 876, 25. doi:10.3847/1538-4357/ab141e

Bergner, J. B., Öberg, K. I., Garrod, R. T., and Graninger, D. M. (2017). Complex Organic Molecules toward Embedded Low-Mass Protostars. *ApJ* 841, 120. doi:10.3847/1538-4357/aa72f6

Bergner, J. B., Öberg, K. I., Walker, S., Guzmán, V. V., Rice, T. S., and Bergin, E. A. (2019c). Detection of Phosphorus-Bearing Molecules toward a Solar-type Protostar. *ApJ* 884, L36. doi:10.3847/2041-8213/ab48f9

Blake, G. A., Sutton, E. C., Masson, C. R., and Phillips, T. G. (1987). Molecular Abundances in OMC-1 - the Chemical Composition of Interstellar Molecular Clouds and the Influence of Massive star Formation. *ApJ* 315, 621. doi:10.1086/165165

Bottinelli, S., Ceccarelli, C., Lefloch, B., Williams, J. P., Castets, A., Caux, E., et al. (2004). Complex Molecules in the Hot Core of the Low-Mass Protostar NGC 1333 IRAS 4A. *ApJ* 615, 354–358. doi:10.1086/423952

Bradford, C. M., Cameron, B., Moore, B., Hailey-Dunsheath, S., Amatucci, E., Bradley, D., et al. (2021). Origins Survey Spectrometer: Revealing the Hearts of Distant Galaxies and Forming Planetary Systems with Far-IR Spectroscopy. *J. Astron. Telesc. Instrum. Syst.* 7, 011017. doi:10.1117/1.JATIS.7.1.011017

Burkhardt, A. M., Shingledecker, C. N., Gal, R. L., McGuire, B. A., Remijan, A. J., and Herbst, E. (2019). Modeling C-Shock Chemistry in Isolated Molecular Outflows. *ApJ* 881, 32. doi:10.3847/1538-4357/ab2be8

Calmonte, U., Altwegg, K., Balsiger, H., Berthelier, J. J., Bieler, A., Cessateur, G., et al. (2016). Sulphur-bearing Species in the Coma of Comet 67P/Churyumov-Gerasimenko. *Mon. Not. R. Astron. Soc.* 462, S253–S273. doi:10.1093/mnras/stw2601

Campbell, J. L., Friesen, R. K., Martin, P. G., Caselli, P., Kauffmann, J., and Pineda, J. E. (2016). Contraction Signatures toward Dense Cores in the Perseus Molecular Cloud. *ApJ* 819, 143. doi:10.3847/0004-637X/819/2/143

Carder, J. T., Ochs, W., and Herbst, E. (2021). Modelling the Insertion of O(1D) into Methane on the Surface of Interstellar Ice Mantles. *MNRAS* 508, 1526–1532. doi:10.1093/mnras/stab2619

Caselli, P., Keto, E., Bergin, E. A., Tafalla, M., Aikawa, Y., Douglas, T., et al. (2012). First Detection of Water Vapor in a Pre-stellar Core. *ApJ* 759, L37. doi:10.1088/2041-8205/759/2/L37

Cazaux, S., Tielens, A. G. G. M., Ceccarelli, C., Castets, A., Wakelam, V., Caux, E., et al. (2003). The Hot Core Around the Low-Mass Protostar IRAS 16293-2422: Scoundrels Rule!. *ApJ* 593, L51–L55. doi:10.1086/378038

Ceccarelli, C., Bacmann, A., Boogert, A., Caux, E., Dominik, C., Lefloch, B., et al. (2010). Herschel Spectral Surveys of star- Forming Regions Overview of the 555-636 GHz Range. *A&A* 521, L22. doi:10.1051/0004-6361/201015081

Ceccarelli, C., Caselli, P., Bockelée-Morvan, D., Mousis, O., Pizzarello, S., Robert, F., et al. (2014). "Deuterium Fractionation: The Ariadne's Thread from the Precollapse Phase to Meteorites and Comets Today," in *Protostars and Planets VI*. Editors H. Beuther, R. S. Klessen, C. P. Dullemond, and T. Henning, 859. doi:10.2458/azu_uapress_9780816531240-ch037

Cleeves, L. I., Bergin, E. A., Qi, C., Adams, F. C., and Öberg, K. I. (2015). CONSTRAINING the X-RAY and COSMIC-RAY IONIZATION CHEMISTRY of the TW Hya PROTOPLANETARY DISK: EVIDENCE for A SUB-INTERSTELLAR COSMIC-RAY RATE. *ApJ* 799, 204. doi:10.1088/0004-637X/799/2/204

Codella, C., and Bachiller, R. (1999). *A&A* 350, 659.

Codella, C., Lefloch, B., Ceccarelli, C., Cernicharo, J., Caux, E., Lorenzani, A., et al. (2010). The CHESS Spectral Survey of star Forming Regions: Peering into the Protostellar Shock L1157-B1. I. Shock Chemical Complexity. *A&A* 518, L112. doi:10.1051/0004-6361/201014582

Coutens, A., Jørgensen, J. K., van der Wiel, M. H. D., Müller, H. S. P., Lykke, J. M., Bjerkeli, P., et al. (2016). The ALMA-PILS Survey: First Detections of Deuterated Formamide and Deuterated Isocyanic Acid in the Interstellar Medium. *A&A* 590, 590L6. doi:10.1051/0004-6361/201628612

Crockett, N. R., Bergin, E. A., Neill, J. L., Black, J. H., Blake, G. A., and Kleshcheva, M. (2014a). Herschelobservations of Extra-ordinary Sources: H2S as a Probe of Dense Gas and Possibly Hidden Luminosity toward the Orion Kl Hot Core. *ApJ* 781, 114. doi:10.1088/0004-637X/781/2/114

Crockett, N. R., Bergin, E. A., Neill, J. L., Favre, C., Schilke, P., Lis, D. C., et al. (2014b). HERSCHELOBSERVATIONS OF EXTRAORDINARY SOURCES: ANALYSIS OF THE HIFI 1.2 THz WIDE SPECTRAL SURVEY TOWARD ORION KL. I. METHODS. *ApJ* 787, 112. doi:10.1088/0004-637X/787/2/112

Crockett, N. R., Bergin, E. A., Wang, S., Lis, D. C., Bell, T. A., Blake, G. A., et al. (2010). Herschel Observations of EXtra-ordinary Sources (HEXOS): The Terahertz Spectrum of Orion KL Seen at High Spectral Resolution. *A&A* 521, L21. doi:10.1051/0004-6361/201015116

Drozdovskaya, M. N., van Dishoeck, E. F., Rubin, M., Jørgensen, J. K., and Altwegg, K. (2019). Ingredients for Solar-like Systems: Protostar IRAS 16293-2422 B versus Comet 67P/Churyumov-Gerasimenko. *MNRAS* 490, 50–79. doi:10.1093/mnras/stz2430

Dullemond, C. P., Juhasz, A., Pohl, A., Sereshti, F., Shetty, R., Peters, T., et al. (2012). *RADMC-3D: A Multi-Purpose Radiative Transfer Tool*. Available at: http://ascl.net/1202.015.

Dutrey, A., Guilloteau, S., and Guelin, M. (1997). *A&A* 317, L55.

Dutrey, A., Wakelam, V., Boehler, Y., Guilloteau, S., Hersant, F., Semenov, D., et al. (2011). Chemistry in Disks. *A&A* 535, 535A104. doi:10.1051/0004-6361/201116931

Evans II, N. J., Rawlings, J. M. C., Shirley, Y. L., and Mundy, L. G. (2001). Tracing the Mass during Low-Mass Star Formation. II. Modeling the Submillimeter Emission from Preprotostellar Cores. *ApJ* 557, 193–208. doi:10.1086/321639

Faure, A., Hily-Blant, P., Le Gal, R., Rist, C., and Pineau des Forêts, G. (2013). Ortho-para Selection Rules in the Gas-phase Chemistry of Interstellar Ammonia. *ApJ* 770, 770L2. doi:10.1088/2041-8205/770/1/L2

Garay, G., Kohnenkamp, I., Bourke, T. L., Rodriguez, L. F., and Lehtinen, K. K. (1998). Molecular Abundance Enhancements in the Highly Collimated Bipolar Outflow BHR 71. *ApJ* 509, 768–784. doi:10.1086/306534

Garrod, R. T., and Herbst, E. (2006). Formation of Methyl Formate and Other Organic Species in the Warm-Up Phase of Hot Molecular Cores. *A&A* 457, 927–936. doi:10.1051/0004-6361:20065560

Garrod, R. T., and Widicus Weaver, S. L. (2013). Simulations of Hot-Core Chemistry. *Chem. Rev.* 113, 8939–8960. doi:10.1021/cr400147g

Guilloteau, S., Di Folco, E., Dutrey, A., Simon, M., Grosso, N., and Piétu, V. (2013). A Sensitive Survey for13CO, CN, H2CO, and SO in the Disks of T Tauri and Herbig Ae Stars. *A&A* 549, A92. doi:10.1051/0004-6361/201220298

Guzmán, V. V., Öberg, K. I., Huang, J., Loomis, R., and Qi, C. (2017). Nitrogen Fractionation in Protoplanetary Disks from the H13CN/HC15N Ratio. *ApJ* 836, 30. doi:10.3847/1538-4357/836/1/30

Harju, J., Daniel, F., Sipilä, O., Caselli, P., Pineda, J. E., Friesen, R. K., et al. (2017). Deuteration of Ammonia in the Starless Core Ophiuchus/H-MM1. *A&A* 600, 600A61. doi:10.1051/0004-6361/201628463

Herbst, E., and van Dishoeck, E. F. (2009). Complex Organic Interstellar Molecules. *Annu. Rev. Astron. Astrophys.* 47, 427–480. doi:10.1146/annurev-astro-082708-101654

Hily-Blant, P., Magalhaes, V., Kastner, J., Faure, A., Forveille, T., and Qi, C. (2017). Direct Evidence of Multiple Reservoirs of Volatile Nitrogen in a Protosolar Nebula Analogue. *A&A* 603, 603L6. doi:10.1051/0004-6361/201730524

Huang, J., Andrews, S. M., Cleeves, L. I., Öberg, K. I., Wilner, D. J., Bai, X., et al. (2018). CO and Dust Properties in the TW Hya Disk from High-Resolution ALMA Observations. *ApJ* 852, 122. doi:10.3847/1538-4357/aaa1e7

Hunter, J. D. (2007). Matplotlib: A 2D Graphics Environment. *Comput. Sci. Eng.* 9, 90–95. doi:10.1109/MCSE.2007.55

Jensen, S. S., Jørgensen, J. K., Kristensen, L. E., Coutens, A., van Dishoeck, E. F., Furuya, K., et al. (2021). ALMA Observations of Doubly Deuterated Water: Inheritance of Water from the Prestellar Environment. *A&A* 650, 650A172. doi:10.1051/0004-6361/202140560

Jiménez-Serra, I., Viti, S., Quénard, D., and Holdship, J. (2018). The Chemistry of Phosphorus-Bearing Molecules under Energetic Phenomena. *JApJ* 862, 128. doi:10.3847/1538-4357/aacdf2

Jin, M., and Garrod, R. T. (2020). Formation of Complex Organic Molecules in Cold Interstellar Environments through Nondiffusive Grain-Surface and Ice-Mantle Chemistry. *ApJs* 249, 26. doi:10.3847/1538-4365/ab9ec8

Jørgensen, J. K., Müller, H. S. P., Calcutt, H., Coutens, A., Drozdovskaya, M. N., Öberg, K. I., et al. (2018). The ALMA-PILS Survey: Isotopic Composition of Oxygen-Containing Complex Organic Molecules toward IRAS 16293-2422B. *A&A* 620, A170. doi:10.1051/0004-6361/201731667

Jørgensen, J. K., van der Wiel, M. H. D., Coutens, A., Lykke, J. M., Müller, H. S. P., van Dishoeck, E. F., et al. (2016). The ALMA Protostellar Interferometric Line Survey (PILS). *A&A* 595, A117. doi:10.1051/0004-6361/201628648

Kruczkiewicz, F., Vitorino, J., Congiu, E., Theulé, P., and Dulieu, F. (2021). Ammonia Snow Lines and Ammonium Salts Desorption. *A&A* 652, A29. doi:10.1051/0004-6361/202140579

Le Gal, R., Öberg, K. I., Loomis, R. A., Pegues, J., and Bergner, J. B. (2019). Sulfur Chemistry in Protoplanetary Disks: CS and H2CS. *ApJ* 876, 72. doi:10.3847/1538-4357/ab1416

Leisawitz, D., Amatucci, E., Allen, L., Arenberg, J. W., Armus, L., Battersby, C., et al. (2021). Origins Space Telescope: Baseline mission Concep. *tJournal Astronomical Telescopes, Instr. Syst.* 7, 011002. doi:10.1117/1.JATIS.7.1.011002

Maret, S., Maury, A. J., Belloche, A., Gaudel, M., André, P., Cabrit, S., et al. (2020). Searching for Kinematic Evidence of Keplerian Disks Around Class 0 Protostars with CALYPSO. *A&A* 635, 635A15. doi:10.1051/0004-6361/201936798

Marty, B., Altwegg, K., Balsiger, H., Bar-Nun, A., Bekaert, D. V., Berthelier, J-J., et al. (2017). Xenon Isotopes in 67P/Churyumov-Gerasimenko Show that Comets Contributed to Earth's Atmosphere. *Science* 356, 1069. doi:10.1126/science.aal3496

Maury, A. J., Belloche, A., André, P., Maret, S., Gueth, F., Codella, C., et al. (2014). First Results from the CALYPSO IRAM-PdBI Survey. *A&A* 563, L2. doi:10.1051/0004-6361/201323033

McGuire, B. A. (2018). 2018 Census of Interstellar, Circumstellar, Extragalactic, Protoplanetary Disk, and Exoplanetary Molecules. *ApJs* 239, 17. doi:10.3847/1538-4365/aae5d2

McGuire, B. A., Brogan, C. L., Hunter, T. R., Remijan, A. J., Blake, G. A., Burkhardt, A. M., et al. (2018). First Results of an ALMA Band 10 Spectral Line Survey of NGC 6334I: Detections of Glycolaldehyde (HC(O)CH2OH) and a New Compact Bipolar Outflow in HDO and CS. *ApJ* 863, L35. doi:10.3847/2041-8213/aad7bb

Melnick, G. J., Tolls, V., Neufeld, D. A., Phillips, T. G., Wang, S., Crockett, N. R., et al. (2010). Herschel Observations of EXtra-ordinary Sources (HEXOS): Observations of H2O and its Isotopologues towards Orion KL. *A&A* 521, L27. doi:10.1051/0004-6361/201015085

Melosso, M., Melli, A., Puzzarini, C., Codella, C., Spada, L., Dore, L., et al. (2018). Laboratory Measurements and Astronomical Search for Cyanomethanimine. *A&A* 609, A121. doi:10.1051/0004-6361/201731972

Millar, T. J., Bennett, A., and Herbst, E. (1989). Deuterium Fractionation in Dense Interstellar Clouds. *ApJ* 340, 906. doi:10.1086/167444

Morris, M., Palmer, P., and Zuckerman, B. (1980). Hot Ammonia in Orion. *ApJ* 237, 1. doi:10.1086/157837

Myers, P. C. (2005). Centrally Condensed Collapse of Starless Cores. *ApJ* 623, 280–290. doi:10.1086/428386

Najita, J. R., Carr, J. S., Brittain, S. D., Lacy, J. H., Richter, M. J., and Doppmann, G. W. (2021). High-resolution Mid-infrared Spectroscopy of GV Tau N: Surface Accretion and Detection of NH3 in a Young Protoplanetary Disk. *ApJ* 908, 171. doi:10.3847/1538-4357/abcfc6

National Academies of Sciences, E., and Medicine (2021). *Pathways to Discovery in Astronomy and Astrophysics for the 2020s*. Washington, DC: The National Academies Press. doi:10.17226/26141

Neill, J. L., Bergin, E. A., Lis, D. C., Schilke, P., Crockett, N. R., Favre, C., et al. (2014). Herschelobservations of Extraordinary Sources: Analysis of the Fullherschel/hifi Molecular Line Survey of Sagittarius B2(N). *ApJ* 789, 8. doi:10.1088/0004-637X/789/1/8

Öberg, K. I., and Bergin, E. A. (2021). Astrochemistry and Compositions of Planetary Systems. *Phys. Rep.* 893, 1–48. doi:10.1016/j.physrep.2020.09.004

Öberg, K. I., Boogert, A. C. A., Pontoppidan, K. M., van den Broek, S., van Dishoeck, E. F., Bottinelli, S., et al. (2011a). Thespitzerice Legacy: Ice Evolution from Cores to Protostars. *ApJ* 740, 109. doi:10.1088/0004-637X/740/2/109

Öberg, K. I., Guzmán, V. V., Furuya, K., Qi, C., Aikawa, Y., Andrews, S. M., et al. (2015). The Comet-like Composition of a Protoplanetary Disk as Revealed by Complex Cyanides. *Nature* 520, 198. doi:10.1038/nature14276

Perotti, G., Jørgensen, J. K., Fraser, H. J., Suutarinen, A. N., Kristensen, L. E., Rocha, W. R. M., et al. (2021). Linking Ice and Gas in the Lambda Orionis Barnard 35A Cloud. *A&A* 650, A168. doi:10.1051/0004-6361/202039669

Perotti, G., Rocha, W. R. M., Jørgensen, J. K., Kristensen, L. E., Fraser, H. J., and Pontoppidan, K. M. (2020). Linking Ice and Gas in the Serpens Low-Mass star-forming Region. *A&A* 643, A48. doi:10.1051/0004-6361/202038102

Persson, C. M., De Luca, M., Mookerjea, B., Olofsson, A. O. H., Black, J. H., Gerin, M., et al. (2012). Nitrogen Hydrides in Interstellar Gas. *A&A* 543, A145. doi:10.1051/0004-6361/201118686

Phillips, T. G., Bergin, E. A., Lis, D. C., Neufeld, D. A., Bell, T. A., Wang, S., et al. (2010). Herschel Observations of Extra-ordinary Sources (HEXOS): Detection of Hydrogen Fluoride in Absorption towards Orion KL. *A&A* 518, L109. doi:10.1051/0004-6361/201014570

Phuong, N. T., Chapillon, E., Majumdar, L., Dutrey, A., Guilloteau, S., Piétu, V., et al. (2018). First Detection of H2S in a Protoplanetary Disk. *A&A* 616, L5. doi:10.1051/0004-6361/201833766

Prasad, S. S., and Tarafdar, S. P. (1983). UV Radiation Field inside Dense Clouds - its Possible Existence and Chemical Implications. *ApJ* 267, 603. doi:10.1086/160896

Requena-Torres, M. A., Marcelino, N., Jiménez-Serra, I., Martín-Pintado, J., Martín, S., and Mauersberger, R. (2007). Organic Chemistry in the Dark Clouds L1448 and L183: A Unique Grain Mantle Composition. *ApJ* 655, L37–L40. doi:10.1086/511677

Rivière-Marichalar, P., Fuente, A., Le Gal, R., Arabhavi, A. M., Cazaux, S., Navarro-Almaida, D., et al. (2021). H2S Observations in Young Stellar Disks in Taurus. *A&A* 652, 652A46. doi:10.1051/0004-6361/202140470

Roberts, H., Herbst, E., and Millar, T. J. (2003). Enhanced Deuterium Fractionation in Dense Interstellar Cores Resulting from Multiply Deuterated H[FORMULA] [F][SUP]+[/SUP][INF]3[/INF][/F][/FORMULA]. *ApJApJL* 591, L41–L44. doi:10.1086/376962

Rolffs, R., Schilke, P., Comito, C., Bergin, E. A., van der Tak, F. F. S., Lis, D. C., et al. (2010). Reversal of Infall in SgrB2(M) Revealed by Herschel/HIFI Observations of HCN Lines at THz Frequencies. *A&A* 521, L46. doi:10.1051/0004-6361/201015106

Rubin, M., Bekaert, D. V., Broadley, M. W., Drozdovskaya, M. N., and Wampfler, S. F. (2019). Volatile Species in Comet 67P/Churyumov-Gerasimenko: Investigating the Link from the ISM to the Terrestrial Planets. *ACS Earth Space Chem.* 3, 1792–1811. doi:10.1021/acsearthspacechem.9b00096

Rubin, M., Engrand, C., Snodgrass, C., Weissman, P., Altwegg, K., Busemann, H., et al. (2020). On the Origin and Evolution of the Material in 67P/Churyumov-Gerasimenko. *Space Sci. Rev.* 216, 102. doi:10.1007/s11214-020-00718-2

Salinas, V. N., Hogerheijde, M. R., Bergin, E. A., Ilsedore Cleeves, L., Brinch, C., Blake, G. A., et al. (2016). First Detection of Gas-phase Ammonia in a Planet-Forming Disk. *A&A* 591, A122. doi:10.1051/0004-6361/201628172

Seo, Y. M., Majumdar, L., Goldsmith, P. F., Shirley, Y. L., Willacy, K., Ward-Thompson, D., et al. (2019). An Ammonia Spectral Map of the L1495-B218 Filaments in the Taurus Molecular Cloud. II. CCS and HC 7 N Chemistry and Three Modes of star Formation in the Filaments. *ApJ* 871, 134. doi:10.3847/1538-4357/aaf887

Shingledecker, C. N., Tennis, J., Gal, R. L., and Herbst, E. (2018). On Cosmic-Ray-driven Grain Chemistry in Cold Core Models. *ApJ* 861, 20. doi:10.3847/1538-4357/aac5ee

Simons, M. A. J., Lamberts, T., and Cuppen, H. M. (2020). Formation of COMs through CO Hydrogenation on Interstellar Grains. *A&A* 634, 634A52. doi:10.1051/0004-6361/201936522

Sohn, J., Lee, C. W., Park, Y. S., Lee, H. M., Myers, P. C., and Lee, Y. (2007). Probing Inward Motions in Starless Cores Using the HCN(J= 1-0) Hyperfine Transitions: A Pointing Survey toward Central Regions. *ApJ* 664, 928–941. doi:10.1086/519159

Takashima, Y., Sirsi, S., Choi, H., Arenberg, J. W., Kim, D. W., and Walker, C. K. (2021). "All Reflective THz Telescope Design with an Inflatable Primary Antenna for Orbiting Astronomical Satellite for Investigating Stellar Systems (OASIS) mission," in *Astronomical Optics: Design, Manufacture, and Test of Space and Ground Systems III*. Editors T. B. Hull, D. Kim, P. Hallibert, and F. Keller (International Society for Optics and Photonics SPIE), 11820, 233–241. doi:10.1117/12.2594610

Thi, W.-F., Ménard, F., Meeus, G., Martin-Zaïdi, C., Woitke, P., Tatulli, E., et al. (2011). Detection of CH+emission from the Disc Around HD 100546. *A&A* 530, 530L2. doi:10.1051/0004-6361/201116678

Tiné, S., Roueff, E., Falgarone, E., Gerin, M., and Pineau des Forêts, G. (2000). Detection of Doubly Deuterated Ammonia in L134N. *A&A* 354, L63–L66.

Umemoto, T., Mikami, H., Yamamoto, S., and Hirano, N. (1999). The Ortho-To-Para Ratio of Ammonia in the L1157 Outflow. *ApJL* 525, L105–L108. doi:10.1086/312337

van der Marel, N., Kristensen, L. E., van Dishoeck, E. F., and van Dishoeck, E. F. (2011b). Complex Molecules toward Low-Mass Protostars: the Serpens Core. *ApJ* 740, 14. doi:10.1088/0004-637X/740/1/14

van der Tak, F. F. S., Black, J. H., Schöier, F. L., Jansen, D. J., and van Dishoeck, E. F. (2007). A Computer Program for Fast Non-LTE Analysis of Interstellar Line Spectra. *A&A* 468, 627–635. doi:10.1051/0004-6361:20066820

van der Tak, F. F. S., van Dishoeck, E. F., Evans II, N. J., and Blake, G. A. (2000). Structure and Evolution of the Envelopes of Deeply Embedded Massive Young Stars. *ApJ* 537, 283–303. doi:10.1086/309011

van der Walt, S., Colbert, S. C., and Varoquaux, G. (2011). The NumPy Array: A Structure for Efficient Numerical Computation. *Comput. Sci. Eng.* 13, 22–30. doi:10.1109/MCSE.2011.37

van Dishoeck, E. F., Kristensen, L. E., Benz, A. O., Bergin, E. A., Caselli, P., Cernicharo, J., et al. (2011). Water in Star-forming Regions with the Herschel Space Observatory (WISH): I. Overview of Key Program and First Results. *PASP* 123, 138. doi:10.1086/658676

van Dishoeck, E. F., Kristensen, L. E., Mottram, J. C., Benz, A. O., Bergin, E. A., Caselli, P., et al. (2021). Water in star-forming Regions: Physics and Chemistry from Clouds to Disks as Probed by Herschel Spectroscopy. *A&A* 648, A24. doi:10.1051/0004-6361/202039084

van Terwisga, S. E., van Dishoeck, E. F., Cazzoletti, P., Facchini, S., Trapman, L., Williams, J. P., et al. (2019). The ALMA Lupus Protoplanetary Disk Survey: Evidence for Compact Gas Disks and Molecular Rings from CN. *A&A* 623, 623A150. doi:10.1051/0004-6361/201834257

Visser, R., Bruderer, S., Cazzoletti, P., Facchini, S., Heays, A. N., and van Dishoeck, E. F. (2018). Nitrogen Isotope Fractionation in Protoplanetary Disks. *A&A* 615, A75. doi:10.1051/0004-6361/201731898

Walker, C. K., Chin, G., and Aalto, S. (2021). "Astronomical Optics,". *Astronomical Optics: Design, Manufacture, and Test of Space and Ground Systems III*. Editors T. B. Hull, D. Kim, P. Hallibert, and F. Keller (International Society for Optics and Photonics SPIE), 11820, 181–232. doi:10.1117/12.2594847

Walsh, C., Loomis, R. A., Öberg, K. I., Kama, M., van 't Hoff, M. L. R., Millar, T. J., et al. (2016). First Detection of Gas-phase Methanol in a Protoplanetary Disk. *ApJ* 823, L10. doi:10.3847/2041-8205/823/1/L10

Wang, S., Bergin, E. A., Crockett, N. R., Goldsmith, P. F., Lis, D. C., Pearson, J. C., et al. (2011). Herschel Observations of EXtra-ordinary Sources (HEXOS): Methanol as a Probe of Physical Conditions in Orion KL. *A&A* 527, A95. doi:10.1051/0004-6361/201015079

Widicus Weaver, S. L. (2019). Millimeterwave and Submillimeterwave Laboratory Spectroscopy in Support of Observational Astronomy. *Annu. Rev. Astron. Astrophys.* 57, 79–112. doi:10.1146/annurev-astro-091918-104438

Wiedner, M. C., Aalto, S., Amatucci, E. G., Baryshev, A. M., Battersby, C., Belitsky, V. Y., et al. (2021). Heterodyne Receiver for Origins. *J. Astronomical Telescopes, Instr. Syst.* 7, 011007. doi:10.1117/1.JATIS.7.1.011007

Willacy, K., Langer, W. D., and Velusamy, T. (1998). Dust Emission and Molecular Depletion in L1498. *ApJL* 507, L171–L175. doi:10.1086/311695

Yamaguchi, T., Takano, S., Sakai, N., Sakai, T., Liu, S.-Y., Su, Y.-N., et al. (2011). Detection of Phosphorus Nitride in the Lynds 1157 B1 Shocked Region. *Publ. Astron. Soc. Jpn.* 63, L37–L41. doi:10.1093/pasj/63.5.L37

Yang, Y.-L., Sakai, N., Zhang, Y., Murillo, N. M., Zhang, Z. E., Higuchi, A. E., et al. (2021). Erratum: The Perseus ALMA Chemistry Survey (PEACHES). I: The Complex Organic Molecules in Perseus Embedded Protostars. *ApJ* 910, 20. doi:10.3847/1538-4357/abdfd6

Young, K. E., Lee, J. E., Evans II, N. J., Goldsmith, P. F., and Doty, S. D. (2004). Probing Pre-Protostellar Cores with Formaldehyde. *ApJ* 614, 252–266. doi:10.1086/423609

Zhang, K., Bergin, E. A., Blake, G. A., Cleeves, L. I., and Schwarz, K. R. (2017). Mass Inventory of the Giant-Planet Formation Zone in a Solar Nebula Analogue. *Nat. Astron.* 1, 0130. doi:10.1038/s41550-017-0130

Conflict of Interest: The authors declare that the research was conducted in the absence of any commercial or financial relationships that could be construed as a potential conflict of interest.

frontiers in Astronomy and Space Sciences

PERSPECTIVE
published: 10 February 2022
doi: 10.3389/fspas.2021.811342

Gas-phase Chemistry in the Interstellar Medium: The Role of Laboratory Astrochemistry

Cristina Puzzarini *

Rotational and Computational Spectroscopy Lab, Department of Chemistry "Giacomo Ciamician", University of Bologna, Bologna, Italy

"Who" and how? In this simple question the complexity of the interstellar chemistry is encapsulated. "Who" refers to what molecules are present in the interstellar medium (ISM) and "how" to the mechanisms that led to their formation. While the large number of molecules discovered in the ISM (~250) demonstrates the rich chemistry occurring there, a significant number of unknown species are waiting for an identification and the processes that led to the synthesis of the identified species are still hotly debated or even unknown. Gas-phase laboratory studies in the fields of rotational spectroscopy and quantum chemistry provide an important contribution to answering the question above. An overview on the role played by rotational spectroscopy and quantum chemistry in the unraveling of the gas-phase chemistry of the interstellar medium is presented.

Keywords: astrochemistry, gas-phase reactivity, rotational spectroscopy, prebiotic molecules, ISM

OPEN ACCESS

Edited by:
Ashraf—Ali,
University of Maryland, United States

Reviewed by:
Jonathan Tennyson,
University College London,
United Kingdom
Stephen Klippenstein,
Argonne National Laboratory (DOE),
United States

***Correspondence:**
Cristina Puzzarini
cristina.puzzarini@unibo.it

Specialty section:
This article was submitted to Astrochemistry, a section of the journal Frontiers in Astronomy and Space Sciences

Received: *08 November 2021*
Accepted: *20 December 2021*
Published: *10 February 2022*

Citation:
Puzzarini C (2022) Gas-phase Chemistry in the Interstellar Medium: The Role of Laboratory Astrochemistry. Front. Astron. Space Sci. 8:811342. doi: 10.3389/fspas.2021.811342

1 INTRODUCTION

The conditions of the interstellar medium (ISM) are extreme, with temperatures ranging between 10 and 10^2 K, very low number densities varying from 10^{-4}–10^8 cm^{-3}, and energetic or even ionizing radiation. Despite these extreme conditions, which severely hinder chemical reactivity, the chemistry of the ISM is a remarkably rich subject that is far from being disclosed. Nearly 50 years ago, the first polyatomic molecules, both organic and inorganic in nature, were discovered and led to the emergence of a new discipline: Astrochemistry. This is an interdisciplinary and multifaceted field, which is–in the words of A. Dalgarno (who is considered the "father of Astrochemistry")–a "blending of astronomy and chemistry in which each area enriches the other in a mutually stimulating interaction" (Dalgarno, 2008).

Astrochemical modeling has been developing in parallel with the discovery of molecular species and the derivation of their formation routes. While the fist diatomic molecules were detected in the late 1930s, polyatomic molecules were first discovered in the late 1960s and the beginning of the 1970s owing to radioastronomy. Already in the seventies, the first so-called "complex organic molecules" (COMs; Herbst and van Dishoeck (2009)), namely C-bearing molecules with at least six atoms, were observed.

In the early seventies, molecular synthesis through gas-phase ion-molecule reactions was proposed to rationalize the molecular abundances observed in interstellar clouds. Later, the importance of gas-phase neutral-neutral reactions was also recognized. However, as observational capabilities advanced over the past decade, COMs began to be detected in regions where gas-phase reactions did not contribute significantly to chemical processing. It thus became clear that chemical reactions occurring on the surface of dust grains also play a crucial role in the interstellar chemistry (Caselli et al., 2004; Cuppen et al., 2017). However, the contribution of gas-

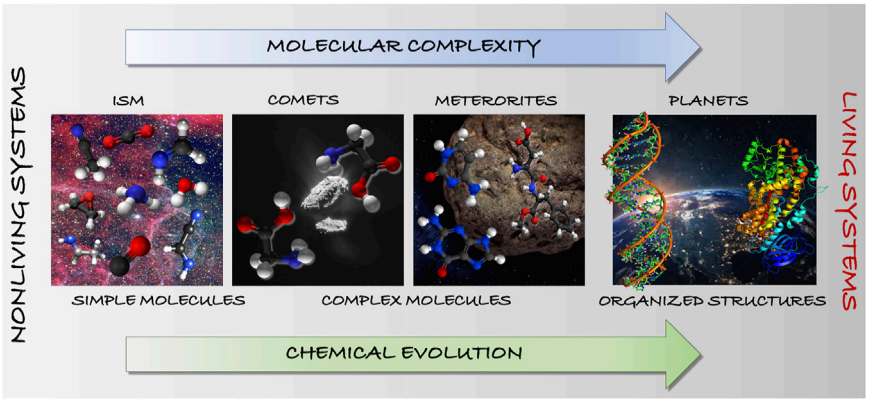

FIGURE 1 | Chemical evolution in terms of molecular and astronomical complexity: from simple to complex molecules toward pre-biological and biological systems.

phase chemistry cannot be overlooked and, indeed, a full explanation of observed molecular abundances is often obtained by accounting for both reactivity on grains and in the gas phase (Ruaud and Gorti, 2019; Laas et al., 2011; Codella et al., 2017; Baiano et al., 2020; Shingledecker et al., 2020). Despite the awareness of a rich interstellar chemistry occurring both on grains and in the gas phase, we are very far from sufficient knowledge to fully understand it: much information is still missing and only a small fraction of the elementary reactions have actually been adequately characterized. As a consequence, astrochemical networks and models still miss crucial information and species not predicted by any chemical model are detected in space.

Moving a step further, understanding how life originated on Earth is one of the greatest challenges in astrochemistry, which might be strongly related to the chemical reactivity taking place in the ISM. However, the characteristic features of the detected molecules are extremely different from the large and complex systems in the cell (see **Figure 1**). The link between these two extremes likely consists of a series of intermediate molecular species that are characterized by increasing complexity. In this sense we can identify the so-called "ingredients for life": prebiotic molecules synthesized in abiotic processes. On this ground, we can envisage the first step to gaining insight into the origin-of-life issue as the investigation of how the abiotic synthesis occurs in the ISM. This gives further importance to the investigation of surface-grain and gas-phase chemistries, and to the elucidation of their mechanisms. In this respect, a key point is the derivation of chemical models able to quantitatively account for the observed abundances. Furthermore, the comparison of the results issuing from the astrochemical models and those from astronomical observations might also allow for obtaining insights into the chemistry at work in the environment under consideration, which means–for example–understanding whether gas-phase and/or grain-surface chemistry are taking place and to what extent. To give an example, in Codella et al. (2017), a Solar-like proto-stellar shock region (L1157-B1) was considered and astronomical observations coupled with a chemical modelling analysis demonstrated that formamide could only be formed by gas-phase reactions.

Molecules can be defined as "cosmic chemical clocks" because they mark the stages of a star cycle as well as the parallelism between life development and evolution of the Universe (see **Figure 1**). To understand how life originated on Earth, a progressive hierarchy of "emergent" steps must be established, i.e. steps that add some chemical complexity to the previous system. This hierarchy is expected to lead from prebiotic molecules, to functionalized clusters of molecules (self-assembled or arrayed on a mineral surface), to self-replicating molecular systems (able to copy themselves), to encapsulation and eventually cellular life. In this hierarchical series of steps, the first one is the synthesis of the building blocks of biomolecules such as amino acids, sugars, and bases. However, these being already very complex systems for the ISM, the focus is usually shifted to small prebiotic molecules that can be precursors of the building blocks of biomolecules. Once these latter species are formed, subsequent steps then involve their assembly into macromolecules, possibly with specific functions. In this respect, it is very intriguing that nucleobases (fundamental elements of RNA and DNA) and amino acids are present in space, as demonstrated by the content of meteorites that have fallen to Earth (see, e.g., Callahan et al. (2011)) and comets (see, e.g., Hadraoui et al., 2019).

This paper is not meant to give an exhaustive contribution of the role played by laboratory astrochemistry in elucidating gas-phase chemistry. Instead, it aims at providing illustrative examples of the personal contribution of the author to the field. The manuscript is organized as follows. In the subsequent section, general considerations on the chemical reactivity in the ISM are briefly summarized. Then, we move to the specific topic of the gas-phase chemistry, therein underlining the contributions of quantum chemistry and rotational spectroscopy. Subsequently, two significant case studies are addressed: the reaction of methylamine with the cyano radical and the reaction of methanimine with small radical species. Finally, conclusions are summed up.

Types of reactions		Typical rate coefficient*
Bond formation processes		
Radiative association	$X + Y \rightarrow XY + h\nu$	$10^{-17} - 10^{-14}$
Grain-surface formation	$X + Y{:}g \rightarrow XY + g$	$\sim 10^{-17}$
Associative detachment	$X^- + Y \rightarrow XY + e$	$\sim 10^{-9}$
Bond destruction processes		
Photodissociation (÷)	$XY + h\nu \rightarrow X + Y$	$10^{-10} - 10^{-8}$
Dissociative recombination (÷)	$XY^+ + e \rightarrow X + Y$	$10^{-7} - 10^{-6}$
Collisional dissociation	$XY + M \rightarrow X + Y + M$	$\sim 10^{-26}$
Bond rearrangement processes		
Ion-molecule exchange	$X^+ + YZ \rightarrow XY^+ + Z$	$10^{-9} - 10^{-8}$
Charge-transfer	$X^+ + YZ \rightarrow X + YZ^+$	$\sim 10^{-9}$
Neutral-neutral	$X + YZ \rightarrow XY + Z$	$10^{-11} - 10^{-9}$

*Values in $cm^3\ molecule^{-1}\ s^{-1}$, except for the (÷) processes (in s^{-1})

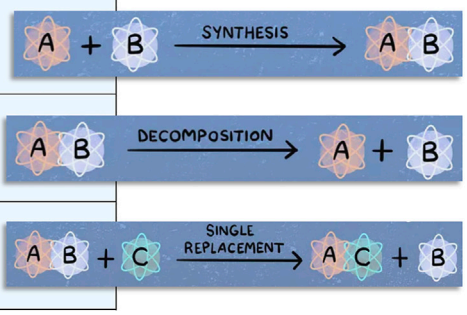

FIGURE 2 | Schematic representation of the reaction types of relevance in astrochemistry together with their typical rate coefficients.

2 MOLECULES AND REACTIVITY IN THE ISM

Figure 1 of Puzzarini (2020) summaries the steps required for the complete characterization of the chemistry occurring in an interstellar cloud. The first step is the derivation of its chemical composition, which results from a synergistic interplay of radioastronomical observations and laboratory spectroscopy (Zaleski et al., 2013; Melosso et al., 2018; McGuire, 2018; Puzzarini and Barone, 2020; Melosso et al., 2020). As explained in the following, astronomical observation of the spectroscopic features of a molecule provides unequivocal proof of its presence in the astronomical environment under consideration (Tennyson, 2005; Yamamoto, 2017; McGuire, 2018). The second step is the derivation of molecular abundances from the intensity of the observed/assigned lines (Nash, 1990; Goldsmith and Langer, 1999). In the third step, the reactivity needs to be completely characterized, which requires an investigation of all possible reactions leading to the molecules detected as well as those between the species identified. In this step, reactions in the gas phase, on grains and at their interface need to be considered. In the fourth step, the results from astronomical detections and reactivity are interpreted by suitable models (see, e.g., (Garrod et al., 2008; Holdship et al., 2017; Jiménez-Serra et al., 2018)). The simplest astrochemical models keep the physical conditions, such as the density and temperature, unchanged while the chemistry takes place. This latter is implemented in the model as a network of reactions that form and destroy all the species that have been identified in the specific environment under consideration. Therefore, astrochemical models typically contain hundreds of species and thousands of reactions. If the models are sufficiently reliable, they should be able to explain the detected molecules in the gas phase and their abundance.

The table in **Figure 2** summarizes the types of reactions occurring in the ISM together with their typical rate coefficients. Because of the low densities, only binary ion-molecule or neutral-neutral reactions can occur, with the former taking place only in the gas phase. Because of the low temperature, reactions are expected to be exothermic and to have vanishing or nearly-vanishing activation energies. While in the gas phase the reaction energy is taken away as kinetic and vibrational energy of products or through emission of photons, on grains "third-body stabilization" occurs. Given all these constraints, neutral-neutral reactions must involve at least one highly reactive molecule, i.e. a radical species. Three-body reactions only become significant at number densities above $\sim 10^{13}$ cm^{-3} such as those encountered in the atmospheres of stars and exoplanets. While the order of magnitude of rate coefficients is approximately known, this is not at all sufficient. The reliability of the results of any chemical model depends on the accuracy of the rate coefficients of the hundreds or thousands of reactions involved.

Even though–as mentioned in the Introduction–COMs were first detected decades ago, the processes that lead to their production are still a matter of debate. They can be synthesized either on grain surfaces or by means of gas-phase chemistry; however, the contribution of each type of chemistry is often unclear or even unknown. While grain chemistry is able to explain the molecules detected in hot cores surrounding protostars and young stars (Garrod et al., 2008), the formation of COMs in cold dense sources is not well understood. Analogously, the formation of COMs in diffuse or translucent material remains at least partially a mystery.

3 GAS-PHASE CHEMISTRY IN THE INTERSTELLAR MEDIUM

Detection of new molecular species in the ISM and the characterization of the interstellar chemistry are intimately related. From one side, the new identifications put constraints on the chemical network describing the astronomical object under consideration. From the other side, the investigation of possible chemical reactions might suggest new molecules to be searched for.

3.1 Laboratory Astrochemistry: Quantum Chemistry

As already mentioned, the harsh conditions of the ISM puts severe constraints on the reactivity. Indeed, molecules do not

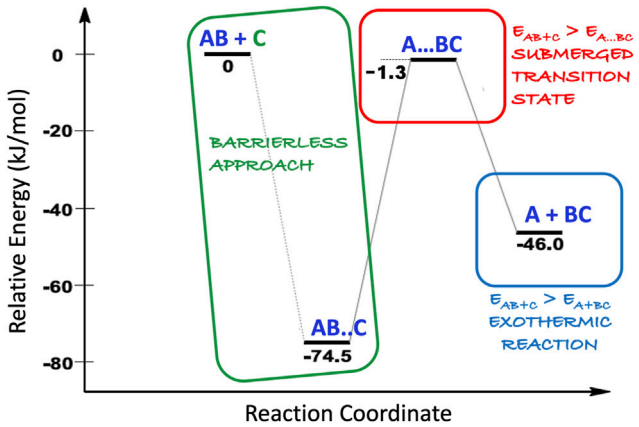

FIGURE 3 | Sketch of a simple reaction mechanism between the AB molecule and the reactive C species: all the required conditions for a reaction occurring in the ISM are highlighted. Relative energies here considered (numbers in black) are ZPE-corrected electronic energies.

have any additional thermal energy (kT, with k being the Boltzmann constant and T the absolute temperature) because of the low temperatures. The direct consequence is that only reactions that proceed with a barrierless attack and submerged barriers are allowed. This is exemplified in **Figure 3**. To fulfil this constraint, at least one of the reactants should be a reactive species such as a radical or an ion (the C species in **Figure 3**). In the gas phase, the very low densities add the additional constraint of bimolecular products: while a unimolecular species can be produced, often this is not the final product because it cannot get rid of the excess of energy through collisions, thus being unstable and either proceeding further along the reaction path or dissociatiing back to reactants. Exceptions are provided by radiative stabilization. The situation is different for grain-surface chemistry because the grain can efficiently remove the excess energy (see **Figure 2**: the "bond formation processes").

While a reaction is written emphasizing the reactants and the possible products, as evident in **Figures 5**, **6**, the reaction mechanisms are often very complicated, and several reaction paths are possible. Therefore, investigation of gas-phase reactions requires, first of all, the full characterization of reactive potential energy surfaces (PESs), as shown in **Figure 3**, from an energetic point of view (thermochemistry). While the energetic characterization is a mandatory step to understand the possible routes open in the ISM, the definitive feasibility of the reaction paths under consideration is established by the rate at which they are expected to occur, i.e. by the corresponding kinetic study.

If the reaction is investigated for the purpose of explaining the formation route of a specific product, the study starts from purposely chosen precursors among molecules already detected in the astronomical source under consideration. Alternatively, again starting from small reactive species already identified, all possible reactive pathways are worked out, with those accessible in the conditions of the ISM further detailed to "discover" new molecules. An example in this respect is offered by Vazart et al. (2016), in which the gas-phase H_2CO + NH_2 and CH_2NH + OH reactions have been investigated with an aim of understanding the formation of formamide ($CHONH_2$). Among the possible products of the CH_2NH + OH reaction, in addition to formamide, the E- and Z-methanimidic acids (CHOHNH) can be formed. These are entirely new species that deserve to be studied because a spectroscopic characterization is still missing.

Joint thermochemical-kinetic computational studies play a crucial role in astrochemistry because experiments able to reproduce the interstellar conditions are limited and, with regard to the gas phase, unable to reproduce at the same time the low temperature and the low pressure that are typical of the ISM. The preliminary investigation of the reactive PES for the identification of the reaction channels of interest can be effectively performed at a relatively low computational level, relying–for example–on models rooted in density functional theory (DFT). Among the different pathways, only those that are accessible in the typical conditions of the ISM are then further investigated at a higher level of theory. The re-investigation aims at improving the structural determination of the stationary points as well as their energetics. Since thermochemistry depends only marginally on the reference geometries, only the electronic energies are then further refined at the state of the art, usually resorting in composite schemes based on coupled-cluster theory (see, e.g., Tajti et al. (2004); Bomble et al. (2006); Harding et al. (2008); Alessandrini et al. (2020); Lupi et al. (2020b)). Indeed, the height of the energy barriers along the reaction path have a strong impact on the reaction rate. For this reason, computational methodologies able to provide energetics with a kJ/mol accuracy should be employed. The reader is referred, for example, to Lupi et al. (2020b); Tonolo et al. (2020); Puzzarini et al. (2020) for a thorough account of the methodology sketched above.

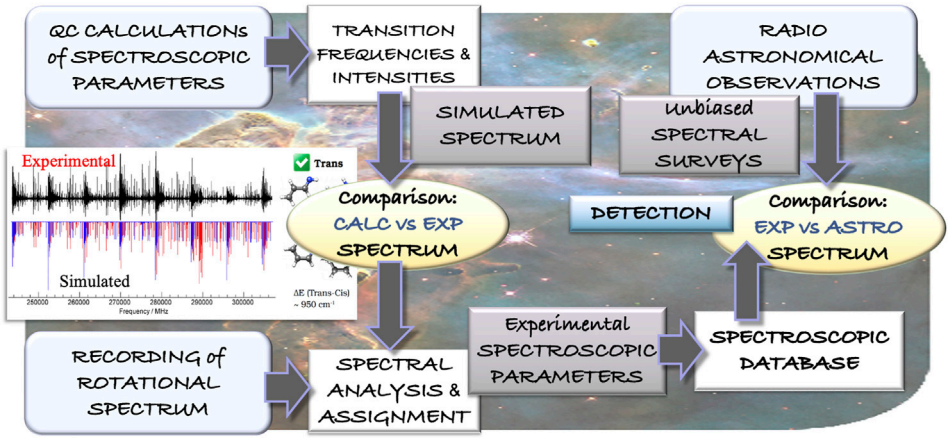

FIGURE 4 | Schematic representation of the interplay of theory and experiment in the field of rotational spectroscopy leading to the guidance of astronomical observations.

Finally, kinetic calculations are carried out in order to provide conclusive information on the feasibility of the suggested mechanisms as well as the branching ratios of the products. Noted is that the energies employed in the kinetic study should incorporate the corresponding zero-point energy (ZPE) corrections. The rate constants of elementary reactions involving a saddle point can be computed using conventional transition state theory, while the description of barrierless attack needs a specific approach. Then, the global rate constants are evaluated by employing a master equation approach.

3.2 Laboratory Astrochemistry: Rotational Spectroscopy

While the first diatomic molecules were discovered in the late 1930s, it was with the advent of radioastronomy that the hunt for molecular species started at the end of 1960s. As mentioned in the Introduction, since then, about 250 molecules have been detected. Radioastronomy relies on the collection of microwave emission from the astronomical object under study. This emission contains the so-called "molecular fingerprints", which are the rotational transitions. Indeed, the rotational features are extremely sensitive to the molecular species, and even allow for discriminating among the isotopic species of the same molecule. This is the reason why the overwhelming majority of gas-phase chemical species have been identified via their rotational signatures (McGuire, 2018). Radiotelescopes provide unbiased millimeter-/submillimeter-wave line surveys, which contain the rotational features of all molecules present in the interstellar cloud under consideration. As a consequence, their assignment requires accurate knowledge of the rotational transitions of all molecules that are expected to be present. This knowledge is obtained from rotational spectroscopy laboratory experiments. **Figure 4** exemplifies the interplay of rotational spectroscopy and radioastronomy for the identification of molecules in the ISM: starting from a computational evaluation of the spectroscopic parameters, the experimental rotational spectrum is recorded and assigned, thus leading to a spectroscopic catalog to be employed in the assignment of astronomical spectra.

As highlighted by the example mentioning the CH_2NH + OH PES, the investigation of a specific reaction can lead to the suggestion of new species to be searched for in the ISM. In this respect, another example is offered by Puzzarini et al. (2020) reporting the reaction between methylamine (CH_3NH_2) and the CN radical. While this reaction will be addressed in the next section, we here anticipate that the two main products are two radical species: CH_3NH and CH_2NH_2 (see **Figure 5**). These are new species not yet characterized even in the laboratory, and for this reason, in Puzzarini et al. (2020), an accurate computational study of their spectroscopic parameters was also carried out. For all cases analogous to the two examples above, to take a step forward, the first action item is the spectroscopic characterization of the new, potential interstellar species. This actually consists of two steps. First, a computational spectroscopy study is carried out in order to obtain a reliable and accurate prediction of the rotational parameters to guide the laboratory work (Puzzarini et al., 2010, 2019; Puzzarini and Barone, 2020; Barone et al., 2021). Because of the intrinsic high resolution of rotational spectroscopy, such an investigation should be performed at the state of the art (often employing composite schemes rooted in the coupled-cluster technique; see, e.g., Puzzarini et al. (2008); Alessandrini et al. (2018)). Second, the most promising rotational transitions are searched for and the assignment procedure of the rotational spectrum starts. This latter step is an iterative process in which the assigned transitions are fitted to an effective Hamiltonian, with the result of the fit allowing new, improved predictions and thus new assignments. The procedure is iterated until all the observed lines are properly assigned. The rotational parameters resulting from the fit can then be used to produce a line catalog to be subsequently employed in astronomical searches (Müller et al., 2005; McGuire, 2018).

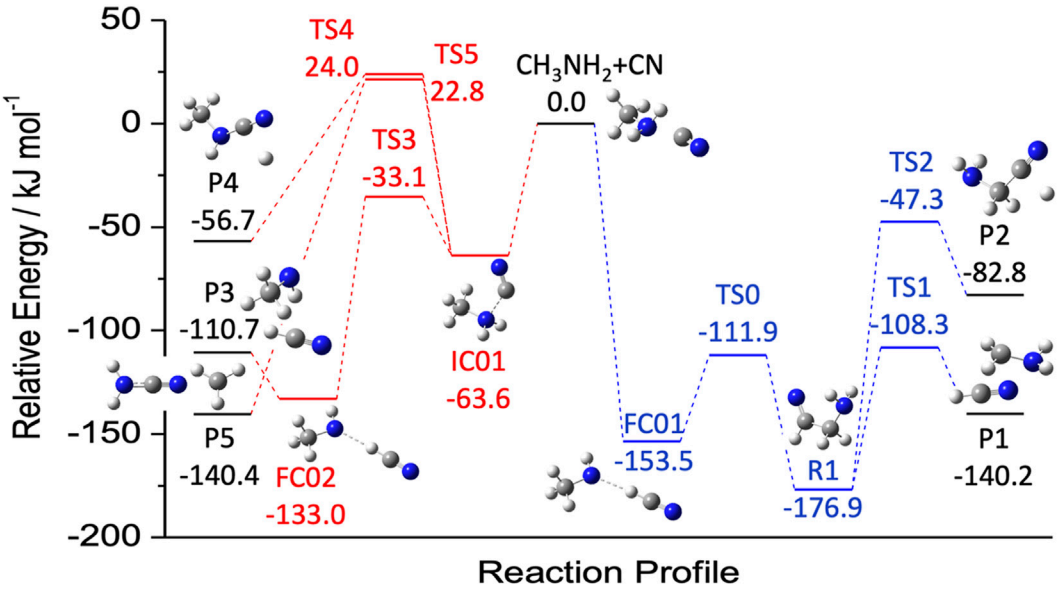

FIGURE 5 | Reaction mechanism for the attack of CN to the N (red) and C (blue) moieties of methylamine. Energies, from Puzzarini et al. (2020), were evaluated using a coupled-cluster based composite scheme (the so-called 'HEAT-like') and augmented by anharmonic zero-point energy corrections.

3.2.1 Interplay of Rotational Spectroscopy and Radioastronomy: The Detection of Propargylimine

The detection of propargylimine in the quiescent G+0.693−0.027 molecular cloud (Bizzocchi et al., 2020) is a significant example of the processes outlined above, with the interplay of computational and experimental spectroscopy with radioastronomy being graphically generalized in **Figure 4**. In Bizzocchi et al. (2020), the authors started from a high-level computational evaluation of all spectroscopic parameters required to predict the rotational spectrum (rotational constants vibrationally corrected, centrifugal-distortion constants, nuclear quadrupole-coupling constants, and electric dipole moment components), and then moved to the experimental recording of the rotational spectrum, with propargylimine being produced by pyrolizing (950°C) dipropargylamine ($(HCCCH_2)_2NH$) vapors. In such a case, the guidance of quantum chemistry in the assignment procedure of the rotational spectrum is crucial because pyrolysis leads to the formation of several byproducts. In the laboratory, the rotational spectra of both E and Z isomers of propargylimine were characterized. The spectroscopic catalogs (for E,Z species) obtained were then used to search for this imine in space, with only the most abundant (and most stable) Z isomer being detected in G+0.693−0.027.

4 METHAYLAMINE WITH THE CYANO RADICAL: THE ROLE OF THE REACTION MECHANISMS

As mentioned above, the temperature of the ISM requires that reactions do not have energy barriers toward products. Therefore, the first condition to be met is their exothermicity. This condition allows for discriminating among possible products. To address this issue, we can consider a specific example: the reaction between methaylamine (CH_3NH_2) and the cyano (CN) radical. **Figure 4** of Sleiman et al. (2018) shows that starting from these two reactants, several products can be formed, some lying above the reactants and most of them lying below. Since endothermic reactions require an external energy input, they do not proceed. In Puzzarini et al. (2020), the exothermic paths of the CH_3NH_2 + CN reaction have been further and more thoroughly investigated. This latter study is a nice example to point out that exothermicity is a necessary but not sufficient condition. Indeed, exothermic reactions can have one or more energy barriers toward the formation of products, which require an external energy input to be overcome, thus rendering them closed in the ISM.

Inspection of **Figure 5** (based on the results of Puzzarini et al. (2020)) points out that the extent of exothermicity is not a guarantee that reaction can actually occur at low temperature. Indeed, it is noted that the P5 product (NH_2CN + CH_3), which is the most exothermic, cannot be formed because the transition state TS5 is emerged, i.e., it lies above the reactants. Analogously, TS4 prevents the formation of CH_3NHCN + H (denoted as P4).

The investigation carried out in Puzzarini et al. (2020) also allowed us to stress the importance of the level of theory employed in the thermochemical characterization of a reactive PES. Indeed, because of the extreme conditions, the rate at which a reaction can occur strongly depends on the barrier heights to be overcome. It is therefore mandatory to

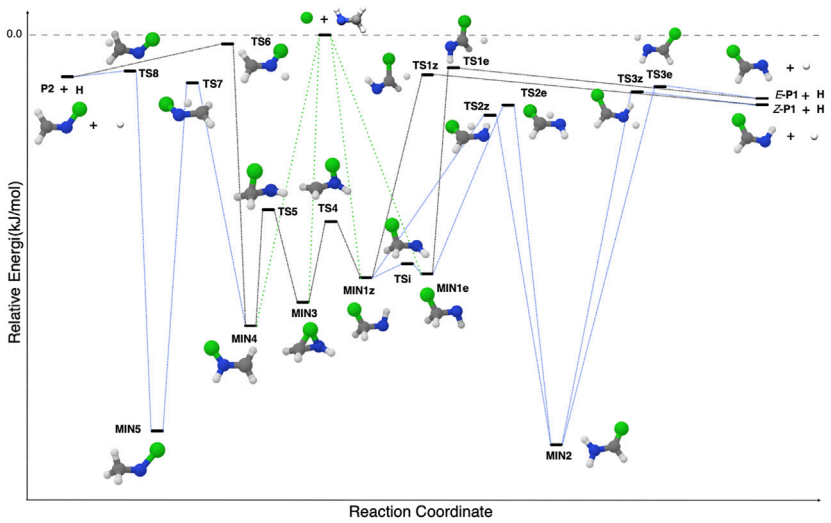

FIGURE 6 | The general mechanism for the X + CH_2NH reaction, where X (the 'green ball' in the figure) is a generic small radical.

employ computational methodologies at the state of the art, possibly providing a kJ/mol accuracy, such as the approach used in Puzzarini et al. (2020) (see, e.g., Tajti et al. (2004); Bomble et al. (2006); Harding et al. (2008); Alessandrini et al. (2020, 2021)). Actually, a low level of theory might underestimate the barrier, thus leading to a wrong conclusion. In fact, in Sleiman et al. (2018), the authors relied on DFT (the hybrid B3LYP functional in conjunction with the aug-cc-pVTZ level (Becke, 1993; Dunning Jr, 1989; Kendall et al., 1992)) and discarded instead CCSD(T)/aug-cc-pVTZ calculations (Raghavachari et al., 1989), thus erroneously concluding that the main product of the CH_3NH_2 + CN reaction is cyanamide (NH_2CN). In passing we note that, even if the CCSD(T)/aug-cc-pVTZ level of theory predicts an emerged transition state, this is only 8.3 kJ/mol above the reactants, to be compared with the value of 22.8 kJ/mol provided by the so-called 'HEAT-like' approach (Tajti et al., 2004; Lupi et al., 2020b) employed in Puzzarini et al. (2020). This suggests that even the CCSD(T) method (which is often denoted as the 'gold standard' for quantum-chemical calculations) in conjunction with a medium-sized basis set cannot be sufficiently accurate when it is used for characterizing borderline transition states.

5 METHANIMINE WITH SMALL RADICALS: A GENERAL MECHANISM

Astrochemical models are designed to simulate the interstellar chemistry, with the most complete models accounting for both gas-phase and dust-grain surface chemical processes. As already mentioned, these models use large reaction networks to link all the chemical species that are present in the interstellar object under consideration. One of the major challenges is to have a complete picture of the composition and reactivity of the interstellar object under consideration. In this respect, the derivation of general mechanisms can provide an important step forward.

In Lupi et al. (2020a), it was pointed out that the reaction of methanimine (CH_2NH) with a small radical can provide a general mechanism leading to the formation of complex imines. This general mechanism is shown in **Figure 6**. The attack on the C-end of CH_2NH leads to the formation of a C-substituted methanimine having two forms, Z and E, according to the position of the attached fragment with respect to the H (N) atom. Instead, the attack on the N-side of CH_2NH leads to a methanimine substituted at the N atom. Finally, the attack to the C-N double bond leads to an intermediate that links the C- and N-paths. This general mechanism has proven to be effective for the OH, CN, CP, and CCH radicals (Vazart et al., 2016; Lupi et al., 2020a; Alessandrini et al., 2021); however, it should be taken with caution because species like the CH_3 radical leads to a barrier in the entrance channel, likely due to its structural rearrangement (from planar to pyramidal geometry).

As mentioned above, C-substituted imines such as cyanomethanimine, ethanimine and propargylimine exist in two forms: Z and E (Melosso et al., 2018; Baiano et al., 2020; Lupi et al., 2020a). As pointed out in several works (see, e.g., Zhang et al. (2020); Shingledecker et al. (2020)), known reaction mechanisms are not able to explain the isomer abundance ratio obtained from astronomical observations. In Lupi et al. (2020a), assuming similar destruction rates for both E and Z forms of propalgylimine and cyanomethanimine, the branching ratios for the CH_2NH + CCH and, in particular, CH_2NH + CN reactions were found to semi-quantitatively predict observations. However, to obtain quantitative agreement, de la Concepción et al. (2021) pointed out the need to account for quantum tunneling effects in the E-Z

isomerization reaction to allow the system to reach the thermodynamic equilibrium. Such an outcome leads to the consequence that the origin of the E/Z ratio of imines depends exclusively on their relative stabilities. Indeed, in Puzzarini and Barone (2020), it was shown that accurate energetics (also accounting for zero-point energy corrections) are required to reproduce the kinetic temperature of cyanomethanimine assuming the observational Z/E ratio.

6 CONCLUSION

In this contribution, we have provided a flavor of the research focusing on the role of gas-phase chemistry in solving two crucial challenges: having a complete census of interstellar molecules and a clear understanding of their formation/destruction pathways. Despite all efforts, we are still far from a complete picture, but important steps have been taken and road forward is marked. This perspective was not meant to be an exhaustive account, but instead to provide an overview of the general problem. One aim was also to underline the role played by rotational spectroscopy (which can potentially even be extended to kinetic investigations (Kidwell et al., 2014; Oldham et al., 2014; Abeysekera et al., 2015; Porterfield et al., 2018)) and the importance of carrying out computational studies at the state of the art.

DATA AVAILABILITY STATEMENT

The original contributions presented in the study are included in the article, further inquiries can be directed to the corresponding author.

AUTHOR CONTRIBUTIONS

The author confirms being the sole contributor of this work and has approved it for publication.

FUNDING

The works discussed in this manuscript received the support by the Italian Space Agency (ASI; 'Life in Space' project, N. 2019-3-U.0) and University of Bologna (RFO).

ACKNOWLEDGMENTS

I would like to acknowledge all my group (https://site.unibo.it/rotational-computational-spectroscopy/en) for the continuous support and fruitful discussions.

REFERENCES

Abeysekera, C., Joalland, B., Ariyasingha, N., Zack, L. N., Sims, I. R., Field, R. W., et al. (2015). Product Branching in the Low Temperature Reaction of Cn with Propyne by Chirped-Pulse Microwave Spectroscopy in a Uniform Supersonic Flow. *J. Phys. Chem. Lett.* 6, 1599–1604. doi:10.1021/acs.jpclett.5b00519

Alessandrini, S., Barone, V., and Puzzarini, C. (2020). Extension of the "Cheap" Composite Approach to Noncovalent Interactions: The Jun-ChS Scheme. *J. Chem. Theor. Comput.* 16, 988–1006. doi:10.1021/acs.jctc.9b01037

Alessandrini, S., Gauss, J., and Puzzarini, C. (2018). Accuracy of Rotational Parameters Predicted by High-Level Quantum-Chemical Calculations: Case Study of Sulfur-Containing Molecules of Astrochemical Interest. *J. Chem. Theor. Comput.* 14, 5360–5371. doi:10.1021/acs.jctc.8b00695

Alessandrini, S., Tonolo, F., and Puzzarini, C. (2021). In Search of Phosphorus in Astronomical Environments: The Reaction between the CP Radical ($X\,^2\Sigma^+$) and Methanimine. *J. Chem. Phys.* 154, 054306. doi:10.1063/5.0038072

Baiano, C., Lupi, J., Tasinato, N., Puzzarini, C., and Barone, V. (2020). The Role of State-Of-The-Art Quantum-Chemical Calculations in Astrochemistry: Formation Route and Spectroscopy of Ethanimine as a Paradigmatic Case. *Molecules* 25, 2873. doi:10.3390/molecules25122873

Barone, V., Alessandrini, S., Biczysko, M., Cheeseman, J. R., Clary, D. C., McCoy, A. B., et al. (2021). Computational Molecular Spectroscopy. *Nat. Rev. Methods Primers* 1, 38. doi:10.1038/s43586-021-00034-1

Becke, A. D. (1993). Density-functional Thermochemistry. III. The Role of Exact Exchange. *J. Chem. Phys.* 98, 5648–5652. doi:10.1063/1.464913

Bizzocchi, L., Prudenzano, D., Rivilla, V. M., Pietropolli-Charmet, A., Giuliano, B. M., Caselli, P., et al. (2020). Propargylimine in the Laboratory and in Space: Millimetre-Wave Spectroscopy and its First Detection in the ISM. *Astron. Astrophys.* 640, A98. doi:10.1051/0004-6361/202038083

Bomble, Y. J., Vázquez, J., Kállay, M., Michauk, C., Szalay, P. G., Császár, A. G., et al. (2006). High-accuracy Extrapolated Ab Initio Thermochemistry. II. Minor Improvements to the Protocol and a Vital Simplification. *J. Chem. Phys.* 125, 064108. doi:10.1063/1.2206789

Callahan, M. P., Smith, K. E., Cleaves, H. J., Ruzicka, J., Stern, J. C., Glavin, D. P., et al. (2011). Carbonaceous Meteorites Contain a Wide Range of Extraterrestrial Nucleobases. *PNAS* 108, 13995–13998. doi:10.1073/pnas.1106493108

Caselli, P., Stantcheva, T., and Herbst, E. (2004). "Grain Surface Chemistry," in *The Dense Interstellar Medium in Galaxies*. Editors S. Pfalzner, C. Kramer, C. Straubmeier, and A. Heithausen (Berlin, Heidelberg: Springer Berlin Heidelberg), 479–486.

Codella, C., Ceccarelli, C., Caselli, P., Balucani, N., Barone, V., Fontani, F., et al. (2017). Seeds of Life in Space (SOLIS): II. Formamide in Protostellar Shocks: Evidence for Gas-phase Formation. *Astron. Astrophys* 605, L3. doi:10.1051/0004-6361/201731249

Cuppen, H., Walsh, C., Lamberts, T., Semenov, D., Garrod, R., Penteado, E., et al. (2017). Grain Surface Models and Data for Astrochemistry. *Space Sci. Rev.* 212, 1–58. doi:10.1007/s11214-016-0319-3

Dalgarno, A. (2008). A Serendipitous Journey. *Ann. Rev. Astron. Astrophys.* 46, 1–20. doi:10.1146/annurev.astro.46.060407.145216

de la Concepción, J. G., Jiménez-Serra, I., Corchado, J. C., Rivilla, V. M., and Martín-Pintado, J. (2021). The Origin of the E/Z Isomer Ratio of Imines in the Interstellar Medium. *Astrophys. J. Lett.* 912, L6. doi:10.3847/2041-8213/abf650

Dunning, T. H., Jr. (1989). Gaussian Basis Sets for Use in Correlated Molecular Calculations. I. The Atoms boron through Neon and Hydrogen. *J. Chem. Phys.* 90, 1007–1023. doi:10.1063/1.456153

Garrod, R. T., Weaver, S. L. W., and Herbst, E. (2008). Complex Chemistry in star-forming Regions: An Expanded Gas-Grain Warm-Up Chemical Model. *Astrophys. J.* 682, 283–302. doi:10.1086/588035

Goldsmith, P. F., and Langer, W. D. (1999). Population Diagram Analysis of Molecular Line Emission. *Astrophys. J.* 517, 209–225. doi:10.1086/307195

Hadraoui, K., Cottin, H., Ivanovski, S. L., Zapf, P., Altwegg, K., Benilan, Y., et al. (2019). Distributed glycine in Comet 67P/Churyumov-Gerasimenko. *Astron. Astrophys.* 630, A32. doi:10.1051/0004-6361/201935018

Harding, M. E., Vázquez, J., Ruscic, B., Wilson, A. K., Gauss, J., and Stanton, J. F. (2008). High-accuracy Extrapolated Ab Initio Thermochemistry. III. Additional Improvements and Overview. *J. Chem. Phys.* 128, 114111. doi:10.1063/1.2835612

Herbst, E., and van Dishoeck, E. F. (2009). Complex Organic Interstellar Molecules. *Ann. Rev. Astron. Astrophys.* 47, 427–480. doi:10.1146/annurev-astro-082708-101654

Holdship, J., Viti, S., Jiménez-Serra, I., Makrymallis, A., and Priestley, F. (2017). UCLCHEM: A Gas-Grain Chemical Code for Clouds, Cores, and C-Shocks. *Astron. J.* 154, 38. doi:10.3847/1538-3881/aa773f

J. Tennyson (Editor) (2005). *Astronomical Spectroscopy* (London, United Kingdom: Imperial College Press).

Jiménez-Serra, I., Viti, S., Quénard, D., and Holdship, J. (2018). The Chemistry of Phosphorus-Bearing Molecules under Energetic Phenomena. *Astrophys. J.* 862, 16. doi:10.3847/1538-4357/aacdf2

Kendall, A., Dunning, T. H., Jr., and Harrison, R. J. (1992). Electron Affinities of the First-Row Atoms Revisited. Systematic Basis Sets and Wave Functions. *J. Chem. Phys.* 96, 6796. doi:10.1063/1.462569

Kidwell, N. M., Vaquero-Vara, V., Ormond, T. K., Buckingham, G. T., Zhang, D., Mehta-Hurt, D. N., et al. (2014). Chirped-pulse Fourier Transform Microwave Spectroscopy Coupled with a Flash Pyrolysis Microreactor: Structural Determination of the Reactive Intermediate Cyclopentadienone. *J. Phys. Chem. Lett.* 5, 2201–2207. doi:10.1021/jz5010895

Laas, J. C., Garrod, R. T., Herbst, E., and Weaver, S. L. W. (2011). Contributions from Grain Surface and Gas Phase Chemistry to the Formation of Methyl Formate and its Structural Isomers. *Astrophys. J.* 728, 71. doi:10.1088/0004-637x/728/1/71

Lupi, J., Puzzarini, C., and Barone, V. (2020a). Methanimine as a Key Precursor of Imines in the Interstellar Medium: The Case of Propargylimine. *Astrophys. J. Lett.* 903, L35. doi:10.3847/2041-8213/abc25c

Lupi, J., Puzzarini, C., Cavallotti, C., and Barone, V. (2020b). State-of-the-art Quantum Chemistry Meets Variable Reaction Coordinate Transition State Theory to Solve the Puzzling Case of the H_2S + Cl System. *J. Chem. Theor. Comput.* 16, 5090–5104. doi:10.1021/acs.jctc.0c00354

McGuire, B. A. (2018). 2018 Census of Interstellar, Circumstellar, Extragalactic, Protoplanetary Disk, and Exoplanetary Molecules. *Astrophys. J. Suppl. Ser.* 239, 17. doi:10.3847/1538-4365/aae5d2

Melosso, M., Belloche, A., Martin-Drumel, M.-A., Pirali, O., Tamassia, F., Bizzocchi, L., et al. (2020). Far-infrared Laboratory Spectroscopy of Aminoacetonitrile and First Interstellar Detection of its Vibrationally Excited Transitions. *Astron. Astrophys.* 641, A160. doi:10.1051/0004-6361/202038466

Melosso, M., Melli, A., Puzzarini, C., Codella, C., Spada, L., Dore, L., et al. (2018). Laboratory Measurements and Astronomical Search for Cyanomethanimine. *Astron. Astrophys.* 609, A121. doi:10.1051/0004-6361/201731972

Müller, H. S., Schlöder, F., Stutzki, J., and Winnewisser, G. (2005). The cologne Database for Molecular Spectroscopy, CDMS: a Useful Tool for Astronomers and Spectroscopists. *J. Mol. Struct.* 742, 215–227. doi:10.1016/j.molstruc.2005.01.027

Nash, A. G. (1990). The Abundance Ratio of Formaldehyde to Ammonia in Molecular Clouds Observed toward Radio Continuum Sources. *Astrophys. J. Suppl. Ser.* 72, 303. doi:10.1086/191418

Oldham, J. M., Abeysekera, C., Joalland, B., Zack, L. N., Prozument, K., Sims, I. R., et al. (2014). A Chirped-Pulse Fourier-Transform Microwave/pulsed Uniform Flow Spectrometer. I. The Low-Temperature Flow System. *J. Chem. Phys.* 141, 154202. doi:10.1063/1.4897979

Porterfield, J. P., Eibenberger, S., Patterson, D., and McCarthy, M. C. (2018). The Ozonolysis of Isoprene in a Cryogenic Buffer Gas Cell by High Resolution Microwave Spectroscopy. *Phys. Chem. Chem. Phys.* 20, 16828–16834. doi:10.1039/c8cp02055h

Puzzarini, C., and Barone, V. (2020). The Challenging Playground of Astrochemistry: an Integrated Rotational Spectroscopy – Quantum Chemistry Strategy. *Phys. Chem. Chem. Phys.* 22, 6507–6523. doi:10.1039/d0cp00561d

Puzzarini, C., Bloino, J., Tasinato, N., and Barone, V. (2019). Accuracy and Interpretability: The Devil and the Holy Grail. New Routes across Old Boundaries in Computational Spectroscopy. *Chem. Rev.* 119, 8131–8191. doi:10.1021/acs.chemrev.9b00007

Puzzarini, C. (2020). Grand Challenges in Astrochemistry. *Front. Astron. Space Sci.* 7, 19. doi:10.3389/fspas.2020.00019

Puzzarini, C., Heckert, M., and Gauss, J. (2008). The Accuracy of Rotational Constants Predicted by High-Level Quantum-Chemical Calculations. I. Molecules Containing First-Row Atoms. *J. Chem. Phys.* 128, 194108. doi:10.1063/1.2912941

Puzzarini, C., Salta, Z., Tasinato, N., Lupi, J., Cavallotti, C., and Barone, V. (2020). A Twist on the Reaction of the CN Radical with Methylamine in the Interstellar Medium: New Hints from a State-Of-The-Art Quantum-Chemical Study. *MNRAS* 496, 4298–4310. doi:10.1093/mnras/staa1652

Puzzarini, C., Stanton, J. F., and Gauss, J. (2010). Quantum-chemical Calculation of Spectroscopic Parameters for Rotational Spectroscopy. *Int. Rev. Phys. Chem.* 29, 273–367. doi:10.1080/01442351003643401

Raghavachari, K., Trucks, G. W., Pople, J. A., and Head-Gordon, M. (1989). A Fifth-Order Perturbation Comparison of Electron Correlation Theories. *Chem. Phys. Lett.* 157, 479–483. doi:10.1016/s0009-2614(89)87395-6

Ruaud, M., and Gorti, U. (2019). A Three-phase Approach to Grain Surface Chemistry in Protoplanetary Disks: Gas, Ice Surfaces, and Ice Mantles of Dust Grains. *Astrophys. J.* 885, 146. doi:10.3847/1538-4357/ab4996

S. Yamamoto (Editor) (2017). *Introduction to Astrochemistry (Chemical Evolution from Interstellar Clouds to Star and Planet Formation* (Berlin/Heidelberg, Germany: Springer).

Shingledecker, C. N., Molpeceres, G., Rivilla, V. M., Majumdar, L., and Kästner, J. (2020). Isomers in Interstellar Environments. I. The Case of Z- and E-Cyanomethanimine. *Astrophys. J.* 897, 158. doi:10.3847/1538-4357/ab94b5

Sleiman, C., El Dib, G., Rosi, M., Skouteris, D., Balucani, N., and Canosa, A. (2018). Low Temperature Kinetics and Theoretical Studies of the Reaction CN + CH_3NH_2: a Potential Source of Cyanamide and Methyl Cyanamide in the Interstellar Medium. *Phys. Chem. Chem. Phys.* 20, 5478–5489. doi:10.1039/c7cp05746f

Tajti, A., Szalay, P. G., Császár, A. G., Kállay, M., Gauss, J., Valeev, E. F., et al. (2004). HEAT: High Accuracy Extrapolated Ab Initio Thermochemistry. *J. Chem. Phys.* 121, 11599–11613. doi:10.1063/1.1811608

Tonolo, F., Lupi, J., Puzzarini, C., and Barone, V. (2020). The Quest for a Plausible Formation Route of Formyl Cyanide in the Interstellar Medium: A State-Of-The-Art Quantum-Chemical and Kinetic Approach. *Astrophys. J.* 900, 85. doi:10.3847/1538-4357/aba628

Vazart, F., Calderini, D., Puzzarini, C., Skouteris, D., and Barone, V. (2016). State-of-the-Art Thermochemical and Kinetic Computations for Astrochemical Complex Organic Molecules: Formamide Formation in Cold Interstellar Clouds as a Case Study. *J. Chem. Theor. Comput.* 12, 5385–5397. doi:10.1021/acs.jctc.6b00379

Zaleski, D. P., Seifert, N. A., Steber, A. L., Muckle, M. T., Loomis, R. A., Corby, J. F., et al. (2013). Detection of E-Cyanomethanimine toward Sagittarius B2(N) in the Green Bank Telescope PRIMOS Survey. *ApJ* 765, L10. doi:10.1088/2041-8205/765/1/l10

Zhang, X., Quan, D., Chang, Q., Herbst, E., Esimbek, J., and Webb, M. (2020). Chemical Models of Interstellar Cyanomethanimine Isomers. *MNRAS* 497, 609–625. doi:10.1093/mnras/staa1979

Conflict of Interest: The author declares that the research was conducted in the absence of any commercial or financial relationships that could be construed as a potential conflict of interest.

Publisher's Note: All claims expressed in this article are solely those of the authors and do not necessarily represent those of their affiliated organizations, or those of the publisher, the editors, and the reviewers. Any product that may be evaluated in this article, or claim that may be made by its manufacturer, is not guaranteed or endorsed by the publisher.

frontiers in Astronomy and Space Sciences

REVIEW
published: 02 March 2022
doi: 10.3389/fspas.2022.787567

Organic Molecules in Interstellar Space: Latest Advances

Michel Guélin[1]* *and Jose Cernicharo*[2]

[1]Institut de RadioAstronomie Millimétrique, St Martin d'Hères, France, [2]Instituto de Física Fundamental, Madrid, Spain

Although first considered as too diluted for the formation of molecules *in-situ* and too harsh an environment for their survival, the interstellar medium has turned out to host a rich palette of molecular species: to date, 256 species, not counting isotopologues, have been identified. The last decade, and more particularly the last 2 years, have seen an explosion of new detections, including those of a number of complex organic species, which may be dubbed as prebiotic. Organic molecules have been discovered not just in interstellar clouds from the Solar neighbourhood, but also throughout the Milky-Way, as well as in nearby galaxies, or some of the most distant quasars. These discoveries were made possible by the completion of large sub-millimetre and radio facilities. Equipped with new generation receivers, those instruments have provided the orders of magnitude leap in sensitivity required to detect the vanishingly weak rotational lines that allowed the molecule identifications. Last 2 years, 30 prebiotic molecules have been detected in TMC-1, a dust-enshrouded gaseous cloud located at 400 light-years from the Sun in the Taurus constellation. Ten new molecular species, have been identified in the arm of a spiral galaxy seven billion light-yr distant, and 12 molecular species observed in a quasar at 11 billion light-yr. We present the latest spectral observations of this outlying quasar and discuss the implications of those detections in these 3 archetypal sources. The basic ingredients involved in the Miller-Urey experiment and related experiments (H_2, H_2O, CH_4, NH_3, CO, H_2S, ...) appeared early after the formation of the first galaxies and are widespread throughout the Universe. The chemical composition of the gas in distant galaxies seems not much different from that in the nearby interstellar clouds. It presumably comprises, like for TMC-1, aromatic rings and complex organic molecules putative precursors of the RNA nucleobases, except the lines of such complex species are too weak to be detected that far.

Keywords: interstellar matter (ISM), molecules—ISM, galaxies, astrochemistry, radio astronomy, prebiotic molecules

OPEN ACCESS

Edited by:
David Leisawitz, National Aeronautics and Space Administration, United States

Reviewed by:
Masatoshi Ohishi, National Astronomical Observatory of Japan (NINS), Japan
Pierre Cox, Institut d'astrophysique de Paris (IAP), France

***Correspondence:**
Michel Guélin
guelin@iram.fr

Specialty section:
This article was submitted to Astrochemistry, a section of the journal Frontiers in Astronomy and Space Sciences

Received: *30 September 2021*
Accepted: *11 January 2022*
Published: *02 March 2022*

Citation:
Guélin M and Cernicharo J (2022) Organic Molecules in Interstellar Space: Latest Advances. Front. Astron. Space Sci. 9:787567. doi: 10.3389/fspas.2022.787567

1 INTRODUCTION

The question of extraterrestrial life arose as soon as Earth was recognized as one amid a myriad of celestial bodies. At first, alien life was fancied as a mere mirror of the life on Earth, with living creatures possibly scaled to the size of their home planets [see *L'autre Monde* by Savinien de Cyrano de Bergerac, printed in 1657, *Cosmotheoros* by Huygens (1698), and *Micromégas* by Voltaire (1752)]. Later, advances in science let writers realize that aliens may not look so friendly (*The War of the Worlds*, H.G. Wells). Finally, it was argued that extraterrestrial life could be based on silicium or germanium, instead of carbon, and take surprising forms. The most imaginative along this line was F.

Hoyle who published, sharp 300 years after Cyrano's book, a novel that invokes an interstellar cloud as a living being: *The Black Cloud* (Hoyle, 1957). Sir Fred Hoyle, whose grand reputation stems from his elucidation of the origin of carbon and heavier elements (Burbidge et al., 1957), but also from his taste for unorthodox theories, was a defender of panspermia and a forceful opponent of Earth-based abiogenesis.

The panspermia hypothesis, first developped in the 19th century, assumes that life came from outer space in the form of microscopic organisms present on meteorites or dust particles that somehow survived their impact on the Earth. In Hoyle's view, the great advantage of panspermia was that it immensly increases the time, hence the probability, for a chance assembly of atoms into prebiotic molecules within the lifetime of a (in his view) Steady State Universe.

Subsequent discoveries have shown that such a process has occured for at least some prebiotic building blocks. The first interstellar molecules (CH, CN, CH^+) were discovered in the optical spectra of nearby stars (Swings and Rosenfeld 1937; McKellar 1940; Douglas and Herzberg 1941), but it took 30 years until more complex species (e.g., NH_3 Cheung et al., 1968) could be found in interstellar space. In echo to Hoyle's science-fiction novel, water and formaldehyde, the first organic molecule, were detected in 1969 and found ubiquitous in interstellar clouds (Cheung et al., 1969; Snyder et al., 1969). The construction of the large (36-ft diameter) radio-telescope on Kitt Peak, Arizona, and of the Bell Laboratories first Schottky barrier diode receiver fitted for millimetre-wave observations, opened the way to a surge of new discoveries: CO, the most abundant interstellar molecule after H_2 (Wilson et al., 1970), hydrogen sulfide H_2S, the first alcohol CH_3OH, ethanol, … This firework led Patrick Thaddeus, key actor on this scene, to state the Fisher's Scientific Principle: *If you can't find it at the Fisher Chemical store you will not find it in the interstellar gas* (Thaddeus, 2006). This statement, however, was soon overturned by William Klemperer and Thaddeus' own NASA team by the discovery of the first *non-terrestrial* molecular species: protonated carbon monoxyde HCO^+, protonated nitrogen N_2H^+, CCH, C_3N, and C_4H (Green et al., 1974; Herbst and Klemperer, 1974; Tucker et al., 1974; Guélin and Thaddeus, 1977; Guélin et al., 1978), all five unstable species not previoulsy observed in the laboratory.

To date, 256 molecular species, not counting isotopologues, are identified in interstellar clouds and circumstellar shells (see references hereafter). They are mostly acyclic organic molecules or radicals with C-chain backbones, as well as half a dozen rings with 5–10 C-atoms. They include aldehydes, alcohols, acids, amines and carboxamides, i.e. the main functional groups needed to initiate the formation of prebiotic molecules and RNA.

It is worth noting that no amino acid has been found to date in interstellar space, despite multiple searches for glycine (NH_2-CH_2-COOH), the simplest of them (Guélin and Cernicharo, 1989; Snyder et al., 2005; Jimenez-Serra et al., 2020). On the other hand, four putative precursors of glycine, methylamine (CH_3NH_2–Holtom et al., 2005), formamide (CH_3CHO – Rubin et al., 1971; Ferus et al., 2018), glycolonitrile ($HOCH_2CN$ –Zeng et al., 2019) and aminoacetonitrile (NH_2-CH_2-CN—Belloche et al., 2008), are detected, as is cyanomethanimine (HNCHCN—Rivilla et al., 2019) a HCN dimer and possible precursor of adenine, $H_5C_5N_5$, one of the four nucleobases of DNA.

The increasing rate of new detections mainly stems from advances in spectroscopic and astronomical instrumentation. Progress has been particularly striking in the sub-millimetre and radio domains. Those wavelenghts cover the lowest rotational lines of molecules of astrochemical interest and allow radiation to freely transit through dust-enshrouded clouds. In **Section 2**, we describe the state-of-the-art instrumentation used in current molecule searches. In **Section 3** and **Section 4**, we present recent results based on extensive spectral surveys of 3 archetypal interstellar sources: first a cold dark cloud, not unlike Hoyle's *Black Cloud*, in the Solar vicinity, then the spiral arm of a galaxy located 7 billion light-years away, finally a remote quasar at a time when the Universe was only 2.7 billion light-years old.

2 DETECTORS AND TELESCOPES AT MM/SUB-MM WAVELENGTHS

In the last decade, the field of astrochemistry has seen major advances triggered by the completion of new powerful radio telescopes, such as the Atacama Large sub-Millimetre Array (ALMA) and the Northern Extended Millimetre Array (NOEMA), coupled to impressive gains in sensitivity of receivers and in bandwidth. We here briefly review the leading facilities and their new equipment that allowed the latest progress in searching for new molecules in interstellar space.

The gains in detector sensitivity and bandwidth were linked to the development of low-noise/wide-band cryogenic amplifiers, based on HEMTs (High Electron Mobility Transistors) that operate around 15 K, and the development of mixers equipped with SIS (Superconductor-Insulator-Superconductor) junctions, based on photon-assisted electron tunneling at temperatures below 4 K. State of the art heterodyne receivers equipped with such devices now achieve noise temperatures of only few times the quantum limit ($2h\nu/k$), hence close to optimal, and ally increasingly wide tuning ranges and instantaneous bandwidths.

The heterodyne technique is based on the down-conversion of the incoming Radio Frequency (RF) signal (astronomical or from laboratory) resulting from its mixing with the narrow signal of a local oscillator. The lower frequency allows to use lower noise amplifiers and, mostly, provides a spectral resolution equal to the local oscillator line width, in practice better than 10^{-8} of the RF frequency. Whereas high sensitivity is needed for detecting the vanishingly weak rotational line emission from rare molecular species, or from very distant sources, high spectral resolution is crucial to identify with certainty the carriers of detected astronomical lines. Similarly, high spectral resolution is needed in the spectroscopic laboratory to accurately measure the rotational line pattern, hence derive the spectroscopic constants.

On the backend side, the availability of increasingly high-speed ADCs (Analog-to-Digital Converters) and powerful FPGAs (Field-programmable Gate Arrays) have allowed the

FIGURE 1 | The IRAM 30-m diameter millimeter-wave telescope operating on Pico Veleta in the Sierra Nevada, Spain, at 2,900 m altitude.

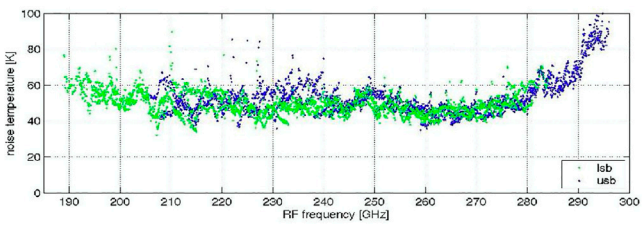

FIGURE 2 | Noise temperature in the lower (green dots) and upper (blue dots) sidebands of the 2SB SIS mixer receiver on the 30-m telescope—credit: D. Maier, IRAM.

development of digital correlators that process increasingly wide bandwidths, while keeping high spectral resolution.

The EMIR SIS junction receivers on the IRAM 30-m diameter telescope, located at an altitude of 2,900 m on Pico Veleta, near Granada, Spain (**Figure 1**), allow to simultaneously observe a 32 GHz-wide band with a spectral resolution of 200 kHz within the 73–375 GHz (λ 4 to 0.8 mm) atmospheric windows. Their intrinsic noise within this band varies between 2.5 and 5 times the quantum noise limit (**Figure 2**). The K-band HEMT receivers on the 100-m Green Bank telescope, which can observe simultaneously a band of width 6 GHz with a 66 kHz resolution, within the 26–40 GHz RF band, have a r.m.s. noise of 7 times the quantum noise limit. The new Q-band HEMT receiver on the Yebes 40-m telescope (**Figure 3**; Tercero et al., 2021) can observe simultaneously 20 GHz, within the 31–50 GHz atmospheric window, with a 38 kHz

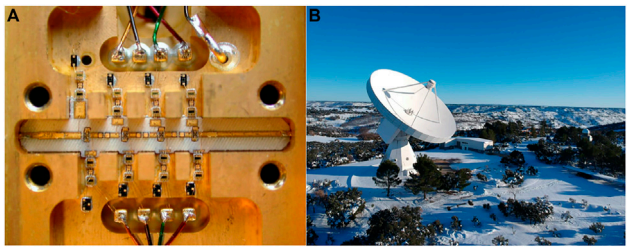

FIGURE 3 | (A) The 4-stage Q-band cryogenic amplifier on the 40-m Yebes telescope (from Tercero et al., 2021). **(B)** The 40-m Yebes telescope –credit: Pablo deVicente.

resolution and, at frequencies near 40 GHz, a r.m.s. noise around 4 times the quantum limit.

Obviously, the telescope sensitivity also depends on the antenna size, the accuracy of its reflecting surfaces (its aperture efficiency η_A) and the atmosphere transparency. Due to signal absorption by atmospheric water vapour, sensitivity is degraded at shorter radio wavelengths. This is why telescopes operating below 2 mm (i.e., above 150 GHz) are built on high altitude sites. High frequency telescopes must have more accurate surfaces to keep a high aperture efficiency[1]. Large size, high surface accuracy antennas located on high mountain sites are much more difficult to build and need to be protected against harsh weather conditions. In practice, this limits their diameter to about 30 m to operate efficiently at 1 mm wavelength or below.

In order to increase the effective area of a telescope intended to operate at wavelengths shorter than 2 mm, one chooses, rather than increasing the size of a single antenna dish, to build an array of several smaller dishes phased together, i.e., to build an interferometer. Besides cost, a decisive advantage of a phased array of mobile antennas is that its angular resolution can be much better. The latter, which scales with the instrument largest dimension D as λ/D, is a critical parameter in the radio domain.

Another advantage of interferometers vs single-dish telescopes is that they yield spectra with much flatter baselines, as they filter out intensity fluctuations caused by amplifier instabilities and by the Earth atmosphere. This is particularly valuable for the detection of the broad (broadened by Doppler effect) and very weak lines, such as those observed in remote galaxies: As shown in **Section 4.2**, this makes it possible to detect, with proper integration time, molecular lines 10^5 times weaker than the receiver noise throughout a 8 GHz-wide spectrum without removing any baseline. On a spectrum observed with a single dish, one would typically have to remove a high degree polynomial baseline, an operation that may affect the detectability of broad lines.

The interferometers used for the line surveys discussed in the next sections are ATCA, ALMA and NOEMA. ATCA is an array of 6 × 22-m diameter antennas operating down to 7-mm

[1]Aperture efficiency, η_A, according to Ruze's equation, scales with the r.m.s. surface error ϵ as $\exp(-(4\pi\epsilon/\lambda)^2)$, which means that ϵ must be $\leq 50\mu$m to achieve an efficiency $\eta_A \geq 0.5$ at a wavelength $\lambda \leq 1$ mm.

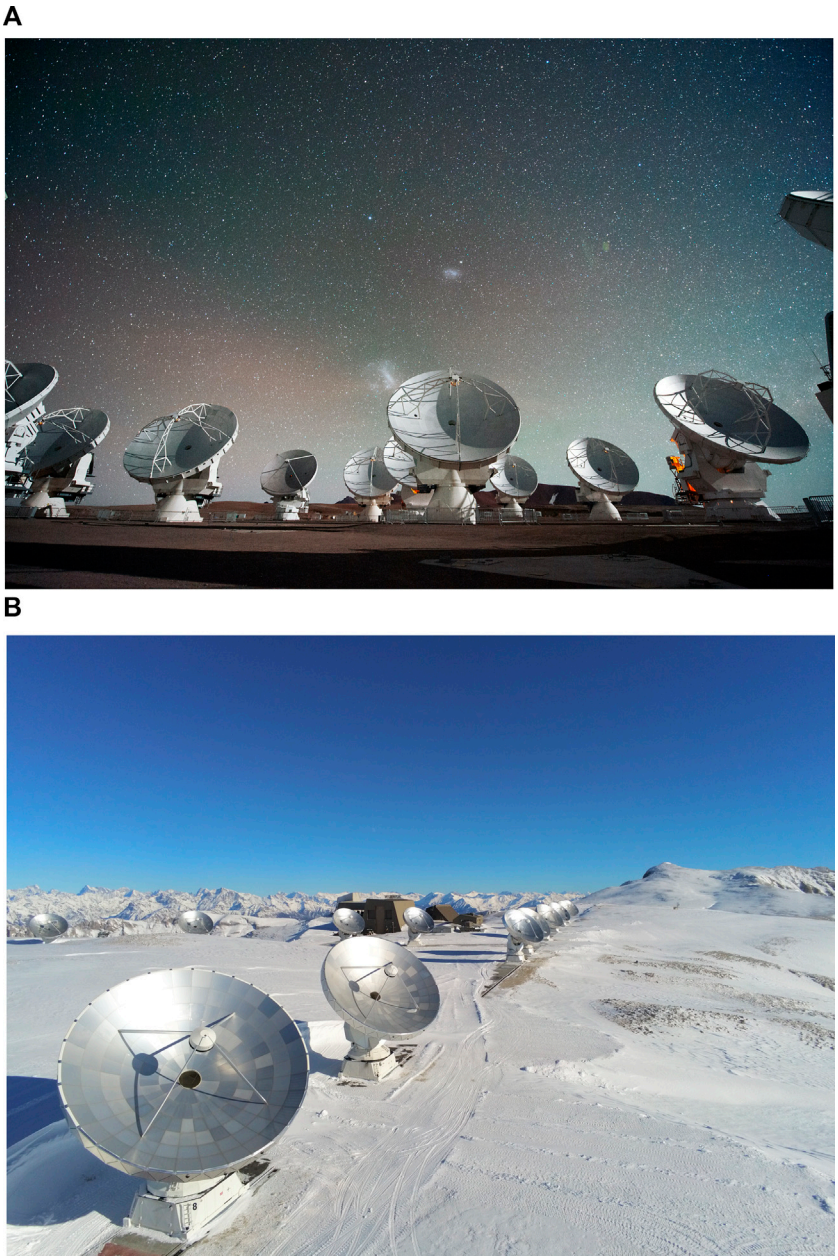

FIGURE 4 | (A) Night view of the ALMA 12-m antenna array on the Chajnantor Plateau in the Chilean Andes at 5,000 m altitude. The Magellanic Clouds appera as two white cloudlets in the night sky –credit: ESO.org. **(B)** The NOEMA interferometer, operating on the Plateau de Bure in the Alps at 2,550 m altitude. Credit: J. Boissier, IRAM.

wavelength (50 GHz) and located at 240 m altitude, −30° latitude, in New South Wales, Australia. The ALMA 12-m array consists of an array of 50 high accuracy, 12-m diameter parabolic antennas, located at 5,000 m altitude, −23° latitude, in the Atacama desert in Chile. It operates down to 0.3 mm wavelength (950 GHz) thanks to the low water vapour content of the atmosphere above the site. This 12-m array is seconded by a smaller array of twelve 7-m antennas plus four 12-m antennas, ACA, also known as the Morito-san array (**Figure 4A**). Finally, NOEMA was upgraded end of 2021 to a 12 × 15-m diameter antenna array; it is located on a 2,550 m altitude plateau in the southern Alps in France and operates down to 1 mm wavelength with 12 antennas (and currently 0.8 mm, or 375 GHz, with six antennas). NOEMA is the largest mm-wave array in the Northern Hemisphere (**Figure 4B**). Its SIS junction receivers and its wide band XF Fast Fourier Transform correlator make it particularly well suited for extragalactic spectral surveys, since it can instantaneously cover a 32 GHz-wide bandwidth with 2 MHz-wide (2.6 kms^{-1} at 230 GHz) spectral channels (see **Figure 5**).

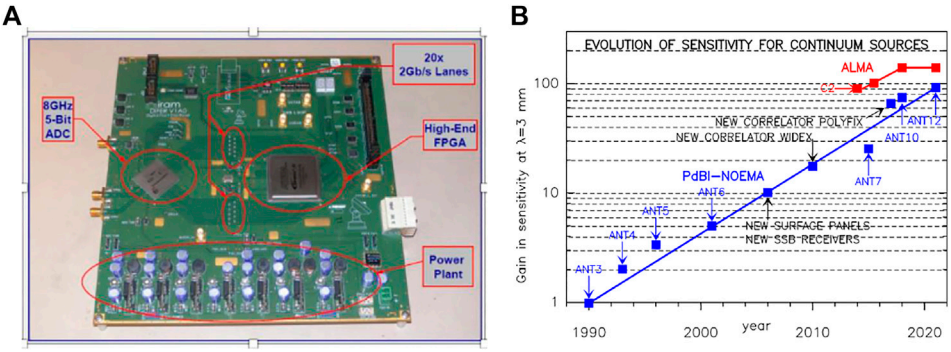

FIGURE 5 | (A) Fast sampling board of the IRAM Poyfix digital spectrometer. The board is based on a 16- Gsps, 5-bit ADC from the *e2v* company and a *Stratix-IV* FPGA employed for later filtering and signal processing. Eight such boards allow to simultaneously process the signals from a 32 GHz-wide band detected by 12 antennas (see Garcia et al., 2012). Polyfix was implemented on NOEMA in 2017. In comparison, the continuum correlator from the initial 3 antenna Plateau de Bure array was only processing 10 × 50 MHz-wide sub-bands with a 4-bit sampler. **(B)** Time evolution of the sensitivities of PdBI-NOEMA (blue squares) and ALMA (red squares) for the detection at 3-mm wavelength of continuum point sources (and for 3-mm of precipitable water vapour along the line-of-sight). Gains in sensitivity are relative to the year 1990 when the first 3 antennas of the Plateau de Bure interferometer (PdBI) were open to science observations (Guilloteau et al., 1992). The ALMA regular science observations started with Cycle 2 in 2014. Sensitivity improvements for PdBI-NOEMA (two orders of magnitude in 30 years) resulted from a) an increase in effective collecting area (addition of new antennas to the arrays and surface adjustments), b) reduction of receiver noise and c) increase in bandwidths (IF amplifiers and backend correlator). End of 2021, the r.m.s. noise figures of NOEMA (with 12 × 15-m diameter antennas) and ALMA (43 × 12-m antennas) at 3-mm, after 8 h of integration, are 7 and 3.5 μJy respectively. Adapted from R. Neri.

3 COMPLEX ORGANIC MOLECULES IN THE DARK CLOUD TMC-1

Cold dark clouds have turned up to be amazingly rich chemical laboratories, able to synthesize *in situ* a great variety of molecules. Most of the identified species are neutral molecules, although several cations, essentially protonated forms of abundant closed-shell species (Agúndez et al., 2015a, Marcelino et al., 2020, Cernicharo et al., 2020a; Cernicharo et al., 2021a; Cernicharo et al., 2021b), but also a few hydrocarbon and nitrile anions, have also been observed (Cernicharo et al., 2020b). Molecular ions have low abundances, typically below 10^{-10} relative to H_2, due to their high reactivity.

TMC-1 is a cold pre-stellar core located within Heiles' Cloud 2 in the Taurus constellation (Cernicharo and Guélin, 1987). Target of very many studies (Fuente et al., 2019, and references therein) it was early on recognized as a rich molecular source. Within the Taurus cloud complex, several dark cores present similar physical characteristics (Cernicharo et al., 1984), but TMC-1 stands out as the one where the largest amount of carbon-bearing molecular species has been detected.

TMC-1 presents an interesting carbon-rich chemistry that leads to the formation of long carbon-chains, radicals, ions and neutral closed-shell molecules such as cyanopolyynes (Cernicharo et al., 2020b; Cernicharo et al., 2020c and references therein). This cold dark core also hosts a number of nearly saturated species, such as CH_3CHCH_2, more typical of hot star-forming cores (Marcelino et al., 2007). A first polar benzenic ring, benzonitrile C_6H_5CN, has been detected in this object (McGuire et al., 2018), although benzene itself is only observed in post-AGB star envelopes. In spite of this carbon-dominated chemistry, a number of carbon chains containing oxygen have been detected in TMC-1: CCO (Ohishi et al., 1991), C_3O (Matthews et al., 1984), HC_3O^+ (Cernicharo et al., 2020a), HC_3O and C_5O (Cernicharo et al., 2021k) HC_5O, and HC_7O (Cordiner et al., 2017; McGuire et al., 2017; Cernicharo et al., 2021k). The path leading to the formation of HC_5O and HC_7O remains a mystery (Cernicharo et al., 2021k), all the more that the related chains C_4O, HC_4O, and HC_6O have not been found (HC_2O is nethertheless observed in other cold dense clouds—Agúndez et al., 2015b). Other O-bearing species, more typical of hot cores and corinos, such as CH_3OH, C_2H_3CHO, C_2H_3OH, $HCOOCH_3$ and CH_3OCH_3, have also been identified in TMC-1 mm-wave spectra (Agúndez et al., 2021a).

Since Léger and Puget's assertion (Léger and Puget, 1984; Allamandola et al., 1985) that the carriers of the unidentified infrared bands must be polycyclic aromatic hydrocarbons (PAHs), efforts have been devoted to understand how those species may form in space. Cherchneff et al. (1992) proposed that the envelopes surrounding carbon-rich AGB stars could be PAH factories. Along this line, the detection of benzene in the C-rich protoplanetary nebula CRL 618 (Cernicharo et al., 2001) suggested a bottom-up approach in which the small hydrocarbons formed during the AGB phase, such as C_2H_2 and C_2H_4, interact with the ultraviolet (UV) radiation emitted by the star when it evolves towards a white dwarf (Woods et al., 2002; Cernicharo 2004). Alternately, in a top-down approach, PAHs would result from the stripping of graphite grain surfaces chemically processed or irradiated by stellar UV (Pilleri et al., 2015; Martínez et al., 2020). Hence, it is startling to discover that a cold dark cloud, shielded from UV and devoid of internal energy sources, hosts not only very long C-chain molecules such as HC_9N, but also C-cycles and aromatic rings.

This exciting result mainly stems from two on-going line surveys of TMC-1 between 20 and 50 GHz: GOTHAM (**G**BT **O**bservations of **T**MC-1: Hunting **A**romatic **M**olecules; McGuire et al., 2018) and QUIJOTE (**Q**-band **U**ltrasensitive **I**nspection **J**ourney in the obscure **T**MC-1 **E**nvironment; Cernicharo et al.,

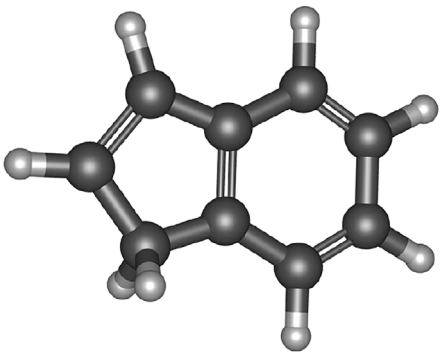

FIGURE 6 | Indene structure (from Cernicharo et al., 2021d).

2021c). Both surveys follow the pioneering work of Kaifu et al. (2004), who first surveyed the whole 8.8–50 GHz frequency spectrum in that source with the Nobeyama 45-m telescope. N. Kaifu, S. Saito and their colleagues identified in the surveyed band 414 lines pertaining to 38 molecular species. The Nobeyama survey data were subsequently used by McGuire et al. (2018) to find, through spectral stacking, a hint of the presence of benzonitrile, a presence superbly confirmed by the GOTHAM survey.

The GOTHAM and QUIJOTE surveys represent a major leap in sensitivity with respect to previous works. They use the 100-m diameter GBT and the recently completed 40-m Yebes radio telescope, that benefit from higher effective areas and, mostly, from lower noise and broader bandwidth receivers. The teams of both surveys reported the detection of several cyclic molecules. The GOTHAM team mostly used a spectral stacking technique (consisting, for a given polar molecule, in a weighted average of the very many rotational transitions covered by the survey) to achieve their detections. The QUIJOTE team, owing to the higher (sub milli-kelvin) sensitivity of its survey, was able to detect individual lines without the need to rely on blind line stacking (**Figure 7**). Among the QUIJOTE detections, we stress those of indene, the first double-cycle detected in space (**Figures 6**, **7** and Cernicharo et al., 2021c; see also Burkhardt et al., 2021), of cyclopentadiene (Cernicharo et al., 2021d), and *ortho*-benzyne (Cernicharo et al., 2021c). Detections reported by the GOTHAM and QUIJOTE teams include ethynyl and cyano derivatives of cyclopentadiene, benzene, and naphthalene (McCarthy et al., 2021; Lee et al., 2021; Cernicharo et al., 2021f; Cernicharo et al., 2021j).

It is unlikely that such complex molecules and cycles arose from a reservoir pre-existing to the formation of the TMC-1 core: they could have hardly survived in the diffuse gas transparent to UV radiation. McGuire et al. (2021) propose a reasonable chemical network starting with the phenyl radical that may explain the observed abundances of cyanonaphthalene, but the chemical routes leading to this radical and benzene itself remain unclear. An *in situ* formation mechanism for benzene must involve abundant hydrocarbons containing from 2 to 4 carbon atoms. Moreover, those hydrocarbons should react and form C-rings in a mere 2 or 3 steps to be able to form enough benzene or phenyl radicals (Joblin and Cernicharo, 2018).

The propargyl radical, CH_2CCH, has recently been found in TMC-1 by Agúndez et al. (2021b) with an abundance close to 10^{-8} relative to H_2. In addition, complex hydrocarbons such as vinyl and allenyl acetylene have also been observed with fairly large abundances (Cernicharo et al., 2021e; Cernicharo et al., 2021f). These hydrocarbons may hold the key to form the first aromatic rings, from which larger PAHs can grow. In two recent articles reporting the detections of *ortho*-benzyne and the ethynyl derivatives of cyclopentadiene (Cernicharo et al., 2021c; Cernicharo et al., 2021g), the authors reproduce reasonably well the observed abundances of C-cycles with reactions between the radicals CH, CCH, C_4H, CH_2, ... and the C-chains CH_3CCH, H_2CCCH, CH_2CHCCH, and $H_2CCCHCCH$ (see **Figure 8**). This requires, however, to reduce the abundance of oxygen to a level close to that of carbon: the presence of free oxygen atoms, which efficiently react with the hydrocarbons, would strongly reduce the yield of five or six C-atoms rings, hence impede the formation of PAHs. A similar result was reported for other species by Fuente et al. (2019).

In addition to hydrocarbons (closed shells and radicals) and their cyano and ethynyl derivatives, TMC-1 revealed itself as an efficient sulfur factory, through the identification of a number of complex sulfur-bearing species in the QUIJOTE survey: HC_3S^+, HCCS, NCS, H_2CCS, H_2CCCS, C_4S, HCSCN, and HCSCCH (Cernicharo et al., 2021h; Cernicharo et al., 2021i).

Most remarkably, in just a couple of years, The GOTHAM and QUIJOTE surveys have increased the number of known interstellar molecules from 204 to 256 and revealed the great potential of TMC-1 for further investigations.

4 MOLECULES IN THE DISTANT UNIVERSE

How much can we learn about the interstellar gas in nearby galaxies and farther out, in the remote parts of the Universe? Observing increasingly distant sources means travelling back in time. Because the Universe is expanding, the radiation emitted by distant sources (and the spectral lines it may contain, e.g., Lyα, CII and MgII lines) appears to us redshifted. Models of the Universe expansion tell us the relation between redshift and distance. Except for the 2.7 K Cosmic Background, the remotest sources we can observe are the very first quasars, the bright radio/infrared quasi-stellar sources that appeared at the center of the primordial galaxies during the epoch of reionization, some 700 million years after the Big Bang. The most distant quasar identified as of today, J0313–1806, has a redshift $z \simeq 7.64$ when the Universe was only 680 million light-years old (Wang et al., 2021).

Whereas the lines observed in optical spectra teach us about these remote quasi-stellar objects' redshift, age and elemental composition, they are far too broad to inform us on the dynamics of the emitting gas (e.g., Wildy and Czerny 2017) and, mostly, on its molecular and isotopic compositions. Those latter can only be studied at sub-millimeter and millimeter

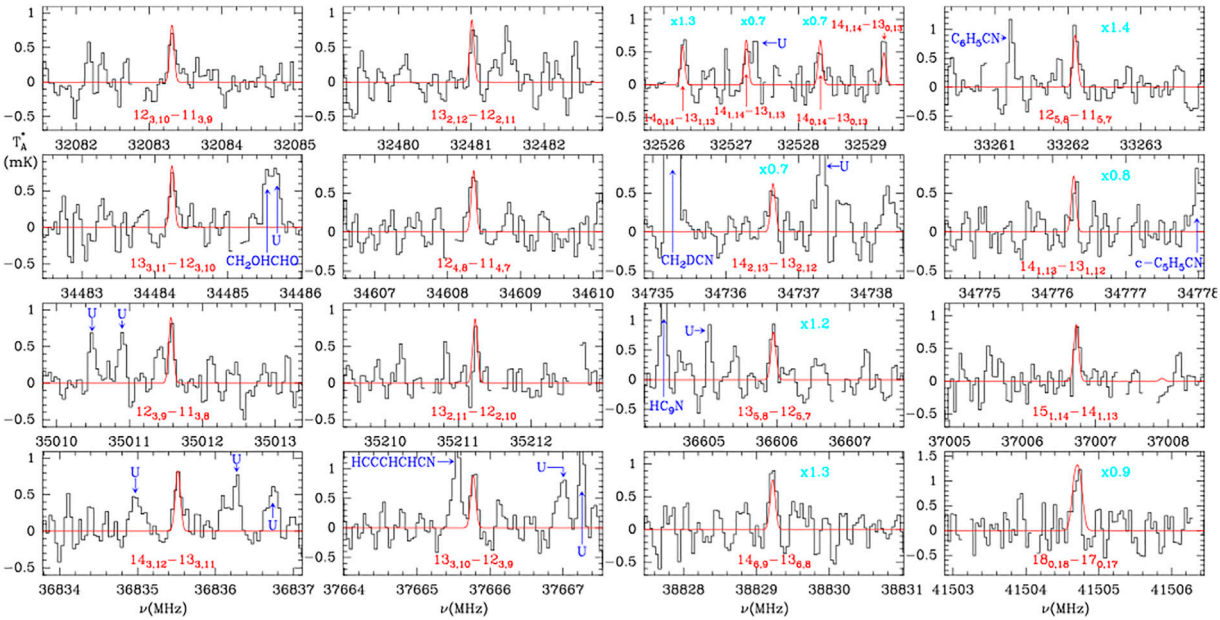

FIGURE 7 | Indene transitions observed towards TMC-1 with the Yebes 40-m radio telescope by Cernicharo et al., 2021d.

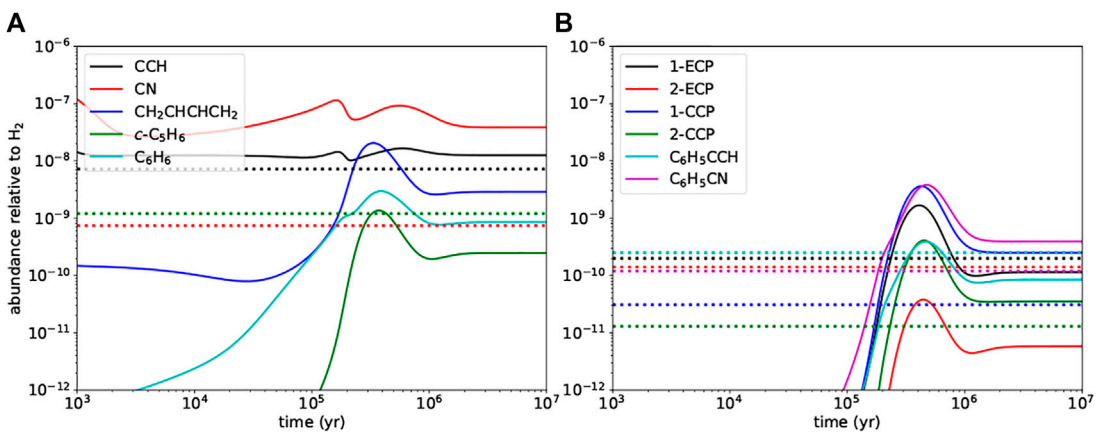

FIGURE 8 | Calculated abundances of CCH and CN derivatives of c-C_5H_6 and C_6H_6 **(B)** and of their precursors **(A)**. The horizontal dotted lines correspond to the abundances observed in TMC-1. The species 1/2-ECP correspond to two isomers of ethynyl cyclopentadiene, while the species 1/2-CCP correspond to two isomers of cyano cyclopentadiene (from Cernicharo et al., 2020g).

wavelengths, preferably in circumstances that compensate for the extreme line weakness.

The most favourable case is when the line-of-sight to the remote quasar is intercepted at halfway by a massive galaxy or a cluster of galaxies (halfway is the optimum distance for a magnification of the quasar radiation by gravitational lensing). If the quasar is radio-loud, the gas of the intervening galaxy may absorb the quasar continuum radiation, causing the rotational line pattern of the polar molecules to appear in absorption against the magnified background continuum. The gas disks of galaxies are thin, so that the absorption lines are fairly narrow and their carriers can be unambiously identified. On the same mm spectrum, but at longer wavelengths (i.e., at higher redshift), one may detect in emission, magnified by the lens, molecular lines arising in the quasar itself.

The Planck/HIFI, Hershell/HerMES, H-ATLAS and South Pole Telescope far-infrared/sub-millimetre surveys show that a fair fraction (several percent) of the high-z sub-millimetre-bright galaxies are magnified by gravitational lensing (Ade et al., 2016; Spilker et al., 2016, as well as references therein; Hodge and da Cunha, 2020). Nonetheless, and except for the relatively strong CO and H_2O lines (Yang et al., 2016; Pensabene et al., 2021), rare are the cases where the magnification is large enough to allow a clear detection of molecular lines from the intervening galaxies, or from the background quasar itself.

Besides the detections in a handful of lensed quasars (e.g., APM08279+5255) of a few lines of HCN, HNC and HCO^+ (García-Burillo et al., 2006; Guélin et al., 2007), one has essentially to rely on source stacking methods to barely detect more molecular species (Spilker et al., 2014; Reuter et al., 2020). A couple of sources, however, are lucky exceptions: a field galaxy on the line-of-sight to the bright radio-loud quasar PKS1830-211, and a strongly lensed quasi-stellar object, H1413+117, dubbed *the Cloverleaf*. We now focus on those two remarkable objects.

4.1 Molecules Inside an Arm of a Spiral Galaxy at Redshift z = 0.89

With a continuum flux of 2–3 janskys at 3-mm, the quasar PKS 1830–211 (redshift z = 2.5, Lidman et al., 1999) is the brightest lensed source at millimetre wavelengths. Its line-of-sight is intercepted by two galaxies: the nearest to us is responsible for HI absorption at redshift z = 0.19; the other, which appears on HST images as a face-on spiral galaxy, gives rise to HI and molecular line absorption at z = 0.89 (e.g., Muller et al., 2006; Combes et al., 2021). The galaxy acts as gravitational lens that splits the quasar image into two compact radio images, respectively located 0.6″ NE and 0.4″ (≃ 6 kilo light-years) SW of the galaxy center. The compact SW radio image lies just behind a spiral arm visible on the I-band HST image (**Figure 9A**).

The millimeter wave spectrum observed along both NE and SW lines-of-sight displays a dense pattern of absorption lines. The SW one is particularly rich and not unlike those observed in the arms intercepting the line-of-sight to the HII region SgrB2, close to the Milky-Way center, or those inside the central starburst of the nearby Sc spiral galaxy NGC 253 (Martin et al., 2006). A detailed analysis of the line intensities and profiles, as well as of the chemistry of their carrier molecules, allows us to estimate the physical conditions and morphology of the clouds intercepting both lines-of-sight (Muller and Guélin, 2008; Muller et al., 2014). The SW line-of-sight crosses a number of mostly cold ($\leq$ 40 K) relatively dense clouds ($n_{H_2} \geq 10^4$ H_2 molecules per cm^3), surrounded by a diffuse envelope. The NE one encounters only diffuse clouds ($n_{H_2} \leq 10^3$ cm^{-3}) transparent to stellar UV radiation.

A total of 54 molecular species (not counting isotopologues) have been identified in the parts of the spectrum surveyed to date: a 20 GHz-wide band at 7-mm wavelength with the ATCA interferometer and the Yebes 40-m telescope, a 8 GHz-wide band at 3-mm with NOEMA, and a 38 GHz-wide band between 3-mm and 0.6-mm with ALMA (Muller et al., 2011; Muller et al., 2014; Muller et al., 2016; Muller et al., 2017) and references therein (Muller et al., 2020; Tercero et al., 2020).

These species are light hydrides (HF, CH, CH^+, CH_3^+, ND, NH_2, NH_3 . . .), small hydrocarbons (CCH, C_3H, C_4H, C_3H^+, H_2CN, C_3N, . . .), sulfur-bearing species (SH^+, SO, SO_2, NS . . .) but also heavier, more complex organic molecules with up to seven atoms (see **Figure 9**): aldehydes (formaldehyde and thioformaldehyde, acetaldehyde CH_3CHO), imines (CH_2NH methanimine), amines (CH_3NH_2 methylamine), cyanides (CH_2CHCN, vinyl cyanide), amides (formamide NH_2CHO, urea $(NH_2)_2CO$), one alcohol (methanol CH_3OH), and its thioalcohol (CH_3SH, methyl mercaptan), and one organic acid (formic acid HCOOH). Their detection suggests that all the ingredients necessary for a rich prebiotic chemistry are present in the gas, although the physical conditions (density, temperature) necessary for starting such a chemistry are ways from being fulfilled even in the dense and hot prestellar cloud cores. Nevertheless, the chemical composition of the gas in this distant object is not very different from that of interstellar clouds in the Milky-Way.

The basic ingredients of Miller-Urey experiment (H_2, H_2O, CH_4 and NH_3) and of closely related experiments (CO, CO_2, H_2S, SO_2) are all present there (the nonpolar species H_2, CH_4 and CO_2 cannot be observed in the radio domain). Also present are some emblematic intermediate products of these experiments: hydrogen cyanide and isocyanide, formaldehyde, urea, acetylene, cyanoacetylene, formic acid and, mostly, formamide the key to the peptide bond. As shown by the experimental work and ab-initio calculations reported by Ferus et al. (2018), formamide is a possible source for the synthesis of amino acids and of the four RNA nucleobases (uracil, cytosine, adenine and guanine).

4.2 Molecules in a Young Quasar at Redshift z = 2.6

The Cloverleaf Quasar (H1413+117) is the archetype of gravitationally lensed quasars and one of the most luminous and best studied objects in the distant, hence young Universe. The quasar redshift (z = 2.557 86) implies a distance of 11 billion light-years from the Sun and an age of about 2 Gyr after the appearance of the very first stars, 700 million years after the Big Bang. Located at the center of a starburst galaxy, its radiation, viewed from the Earth, is magnified by a factor as large as 11 (according to models of Kneib et al., 1998; Venturini and Solomon, 2003) by 2 galaxies, with redshifts z ≃ 1 and 2, respectively, that intercept the line-of-sight and split the quasar image into 4 distinct components **Figure 10**).

The Cloverleaf quasar and its host galaxy have been studied in the X-ray, optical and radio domains, and more particularly at sub-millimetre wavelengths in the continuum and the lines of CO and HCN. The far infrared/sub-millimetre emission appears to arise from an extended (3 light-year radius) disk of gas and dust rotating around the active galactic nucleus (or AGN—Alloin et al., 1997; Barvainis et al., 1997; Solomon et al., 2003; Bradford et al., 2009).

The molecular emission is currently the object of high sensitivity line surveys using NOEMA and ALMA. Thirty four molecular lines pertaining to fourteen molecular species are identified within the (still partly) surveyed 200 GHz-wide frequency band covering the rest frequency ranges: 338–365, 526–626 and 705–786 GHz. (**Figures 11**, **12**). Some of those lines correspond to different rotational transitions of the same species, such as the J → J' = 1-0, 4-3, 6-5, 7-6, and 8-7 transitions of HCN and HCO^+, the 4-3, 6-5, 8-7 transitions of HNC, the 1-0, 3-2, 4-3, 6-5, 8-7, 9-8 transitions of ^{12}CO, the main isotopologue of CO, as well as the 5-4 and 7-6 transitions of the rare isotopologues ^{13}CO and $C^{18}O$.

The detected lines sample a wide range of energy levels and opacities for a given molecule, and different excitation conditions for molecules that are believed to be coeval. From

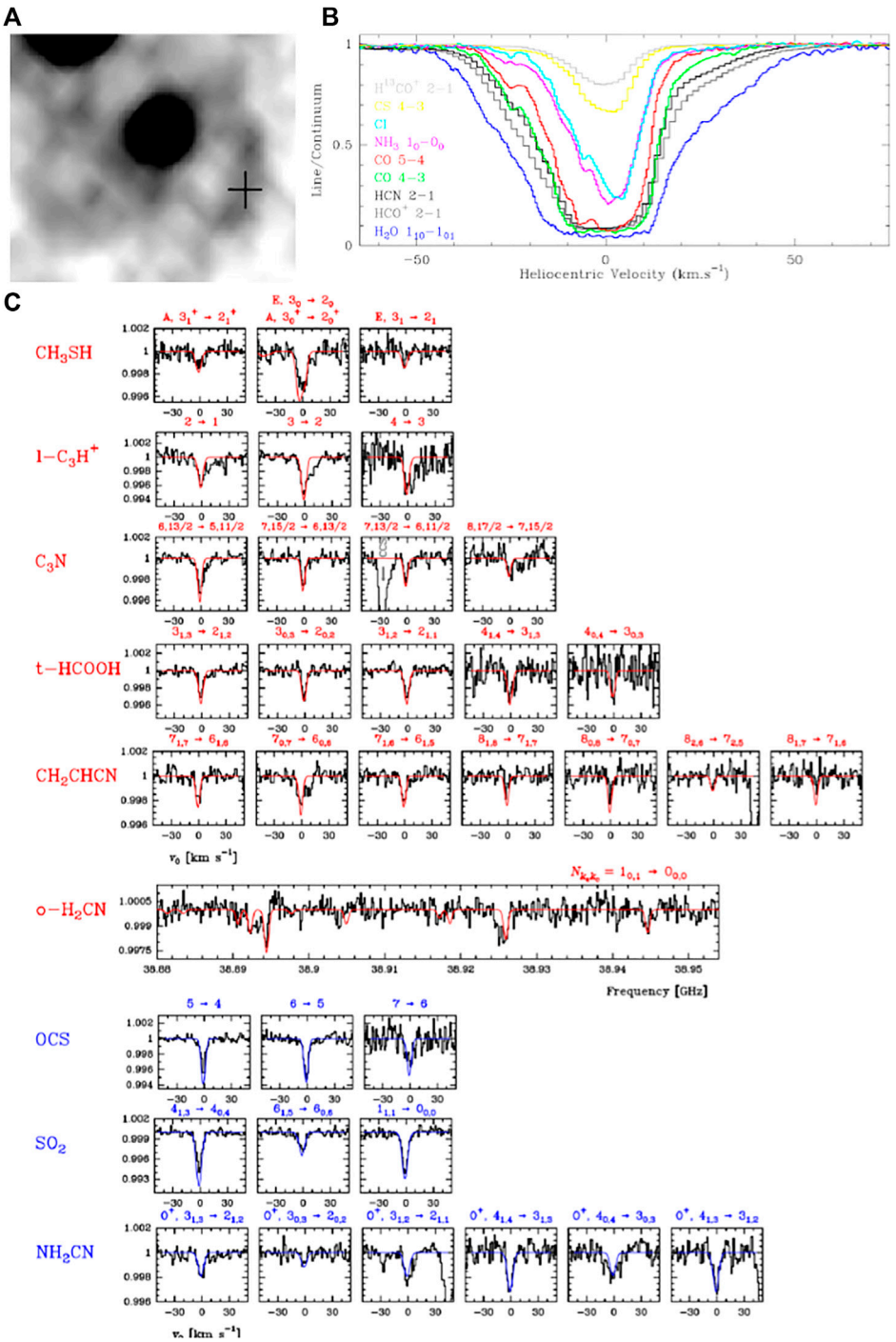

FIGURE 9 | (A): The spiral galaxy at $z = 0.89$ intercepting the line of sight to the quasar PKS 1830–211, as seen by the Hubble satellite in the I band (Winn et al., 2002). The cross shows the position where the molecular lines are observed in absorption in the SW spiral arm. **(B)**: Profiles of the strongest absorption lines observed by ALMA in the SW arm (Muller et al., 2014). Abscissa is the gas velocity in the source frame (i.e., after correction for the redshift of the source $z = 0.885\,875$). Ordinate is the line to continuum ratio, where the continuum arises from the SW image of the background quasar. **(C)**: Absorption lines observed toward the SW arm with the Yebes 40-m telescope. The species identified for the first time in an extragalactic source are highlighted in red. The molecules highlighted in blue are those that were identified for the first time in this source, but observed previously in other extragalactic sources. The *y*-axis is the normalised intensity to the total (NE + SW) continuum level (from Tercero et al., 2020).

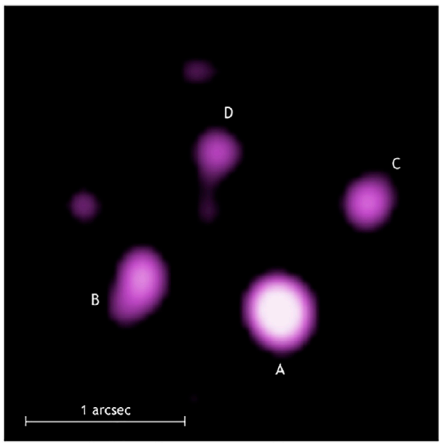

FIGURE 10 | The Cloverleaf Quasar, Chandra Xray image. Credit: NASA.

this, and from the spectral energy distribution of the quasar continuum emission, it is possible to assess the density, temperature and radiation field in the emitting region, as well as the molecular abundances. The constancy of the line width (half-power width 440 kms^{-1}) seems to imply that the molecules are distributed throughout the same rotating cloud complex.

Besides the AGN emission, the far infrared radiation field is mainly thermal emission from tiny dust grains with temperatures in the range 30–100 K, i.e., warm compared to the TMC-1 Galactic cloud, but similar to that in the HII region SgrB2 (Weiss et al., 2013). Its intensity is however far more intense than in any Galactic source, implying an exceptionally strong starburst: the mass of very dense gas is estimated to be at least 10^{10} Solar masses and the star formation rate $\dot{M} = 10^3$ Solar Masses per year (Stacey et al., 2021). This is 200 times larger than the star forming rate in the entire Milky-Way and comparable to those of the brightest ultra luminous infrared galaxies, or ULIRGs. (Solomon et al., 2003; Robintaille and Whitney, 2010).

In contrast to the absorption spectra observed toward PKS1830-211, where the line intensities primarily depend on the background quasar continuum flux, the lines detected in emission in a remote radio-quiet object like the Cloverleaf depend on its distance and are therefore very weak. No wonder that most of the molecules observed there are di- or triatomic species. Some are radicals and ions (CH, CCH, H_2O^+) characteristic of gas irradiated by stellar UV, i.e. of diffuse clouds. The others (CO, CS, HCN, HNC, HCO^+ H_2O, H_2S) are stable species belonging to UV-shielded clouds. Remarkably, these stable species are the same as the very first identified in Galactic clouds 50 years ago, when the sensitivity of mm-wave radio telescopes precluded to detect more than a dozen of molecular lines.

As much as we can tell from the line intensities in **Figures 11**, **12**, the abundances of HCN and HCO^+, relative to the abundance of CO (the best tracer of the molecular gas), are similar in the Cloverleaf Quasar ($1 - 3 \times 10^{-3}$) to those in the $z = 0.89$ spiral galaxy and in the nearby Galactic cloud TMC-1

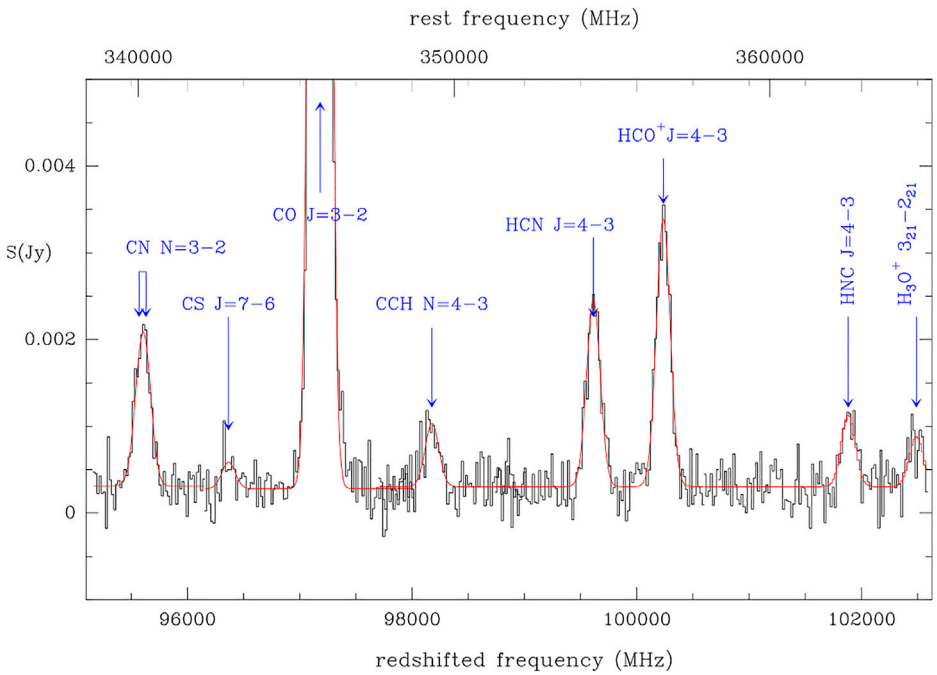

FIGURE 11 | ALMA 3-mm spectrum of the Cloverleaf Quasar covering the N/J = 3-2 lines of CN and CO, and the J = 4-3 lines of HCN and HCO^+. Ordinate scale is line flux in janskys. Abcissa is observed frequency in MHz. Upper scale is rest frequency in the quasar frame. On-source integration time is 14 h.—Guélin et al. (2022) in prep.

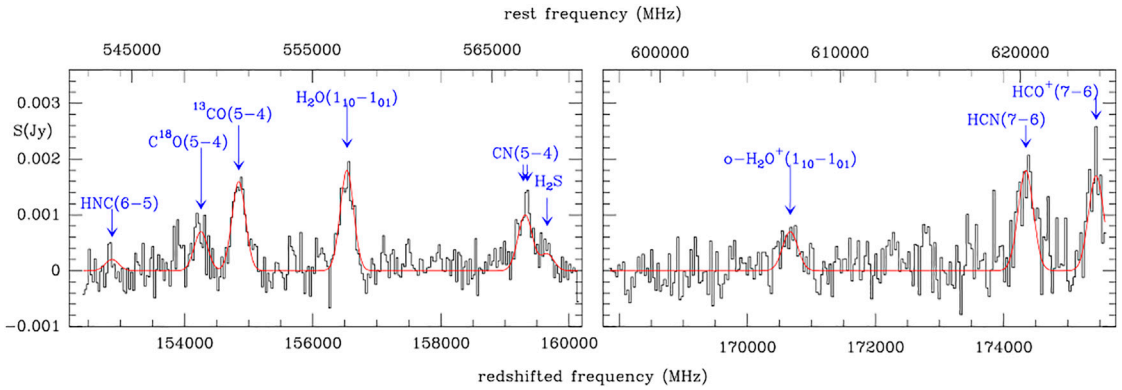

FIGURE 12 | NOEMA 2-mm spectrum of the Cloverleaf Quasar, covering lines of H_2O, H_2O^+, H_2S, CN, HCN, HNC and HCO^+, as well as of the rare isotopologues $C^{18}O$ and ^{13}CO. The 16 GHz-wide spectrum was observed with one single frequency setting in 2 polarizations. A flat (degree 0) baseline has been subtracted from each 8 GHz-wide sideband. On-source integration time is 8 h—Guélin et al. (2022) *in prep.*

(Muller et al., 2011), hence in an extremely wide range of environments and at all Cosmic ages greater than 1 Gyr. We note that the $^{13}CO/C^{18}O$ isotopic abundance ratio on **Figure 12**, 2.5, is typical of nearby star-forming galaxies and significantly larger than the values ≃ 1 reported by Zhang et al. (2018) for dust-enshrouded starbursts at similar redshift.

Water vapour is detected and fairly abundant in all those objects. It seems ubiquitous in remote quasars (Yang et al., 2016; Yang et al., 2019; Yang et al., 2020), as it is in all Milky-Way molecular sources, where it is observed in both forms, gaseous and solid. The H_2O submillimetre rotational lines, are typically the strongest after those of CO. The H_2O and CO lines have similar profiles, which seems to imply both molecular species are coeval.

5 CONCLUSION AND PROSPECTS

We do know, from the spectral analysis of stellar light and meteorites, that the elemental composition of matter is similar throughout the Universe, at least as concerns the most abundant elements: H, He, O, C, N, Ne, Si, Mg, S, P, and Fe . . . It basically follows the nuclear binding energies and, in the case of peculiar stars, depends on their mass, which governs nucleosynthesis.

Things, of course, are less straightforward as concerns the gas molecular composition, in view of the extraordinary large range of physical and enviromental conditions prevailing in IS space. It was thought, for a long time, that the harsh conditions (typically densities below few hundreds atoms per cubic cm, gas temperature of few tens of kelvin, stellar and cosmic-ray induced UV radiation) preclude the survival of any molecule, but for a few ephemeral diatomic species like the already identified CH, CH^+ and CN. That view was overturned at the end of the 1960s when it was realized that shielding by dust grains and H atoms, and self-shielding of H_2, N_2 and CO molecules, considerably reduce the photodestruction of those and very many other molecular species in IS clouds. And indeed, in the following years formaldehyde, H_2CO and CO were not only detected, but observed in about every dark or bright IS nebula. In the course of years, owing to remarkable gains in sensitivity and angular resolution of the mm-wave and far-IR telescopes, the list of molecules identified in interstellar and circumstellar clouds has steadily increased to reach 256 species [see Mc Guire (2018) for a list of molecules identified until 2018 and *The Astrochymist*[2] for a monthly update of that list.]

Most remarkably, HCN and H_2O are found to be ubiquitous in clouds shielded by dust from stellar UV radiation. As we have seen, they are observed up to the edges of the Universe. Quite sensitive to stellar UV and cosmic-ray induced photodestruction, these species cannot survive for a very long time even in the densest clouds, hence have to be renewed on relatively short timescales in a variety of environments. HCN is a prerequisite brick for the formation of polymers via peptide bonds, whereas liquid H_2O, a solvant of polar molecules, is essential in shaping up complex molecular structures. Their omnipresence in the gas or on dust grains opens the way to organic molecules: formaldehyde, formamide, methanol, ethanol, urea . . .

Along this line, the recent gains in sensitivity, allowed by the new generation radio telescopes, brought an unexpected result: the identification in the quiescent dark cloud TMC-1 of fairly complex organic compounds, linear chains or cycles, consisting of six or more C-atoms. Latest examples are benzyne (c-C_6H_4), indene (c-C_9H_8 –**Figures 6**, **7**) and cyanoethyleneallene ($H_2C_2CHC_3N$; Shingledecker et al., 2021) that were discovered this year together with a score of new hydrocarbons or cyanohydrocarbons (the attachment of a CN radical increases the polarity of hydrocarbons, easing their radio detection). Yet, TMC-1 would seem to be the last place where complex molecules would form: its relatively short age (few x 10^5 years) coupled to a vanishingly low gas density (few x 10^4 H_2 molecules per cm^3), extremely low gas temperature (T_k ≃ 10 K), and to a total lack of

[2]The Astrochymist avalaible at: http://www.astrochymist.org/.

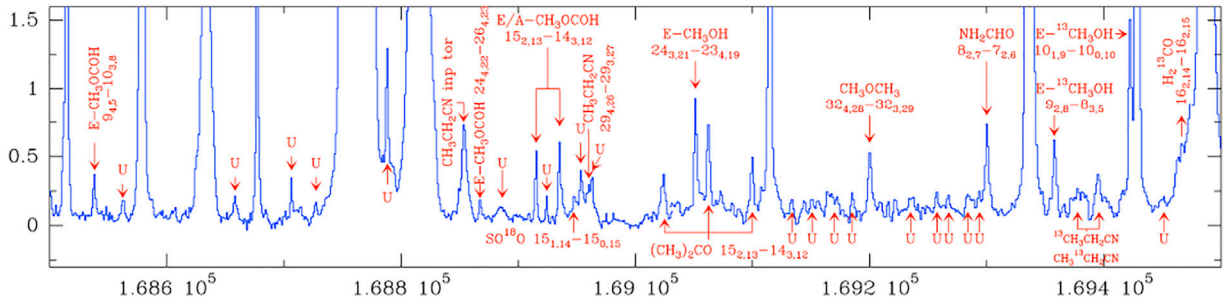

FIGURE 13 | 1 GHz-wide portion of the sub-millimeter spectrum of the Orion-KL star-forming cloud at 2 mm. The spectrum, which is part of an extended (80–281 GHz) spectral survey made with the IRAM 30-m radio telescope, is confusion-limited above 200 GHz (Tercero et al., 2010).

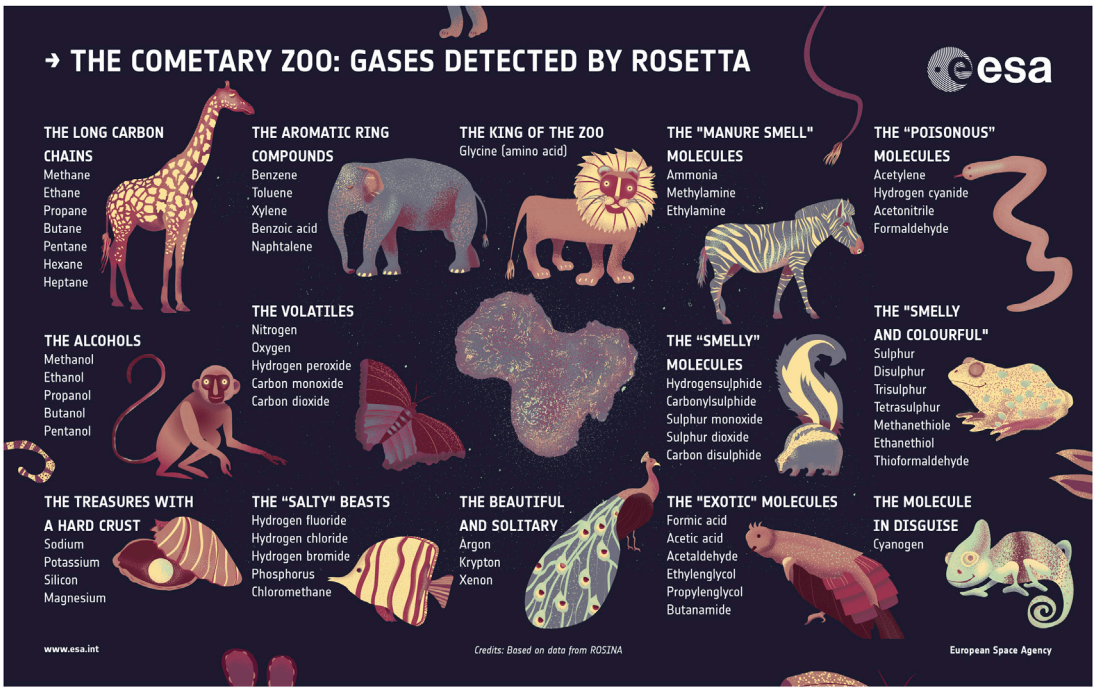

FIGURE 14 | List of gaseous atomic and molecular species detected by the Rosetta Orbiter Spectrometer (ROSINA) in the comet 67P/Churyumov-Gerasimenko (Altwegg et al., 2019) here summarised in a humorous way as a *cometary zoo* by Kathrin Altwegg, ROSINA principal investigator.

internal or nearby energy sources, should have made molecule formation a formidable challenge.

The list of molecules identified in TMC-1 has more than doubled in the last 2 years, even though, due to the very low temperature, most of the oxygen atoms are frozen on the dust grains in the form of water and dry ices, or trapped into CO molecules. For sure, many more will be discovered as low frequency searches for heavy organic molecules intensify. In warmer and denser sources, such as star-forming clouds and Giant Molecular clouds (OrionA-KL, SgrB2-N, …), not only reactions in the gas phase do proceed faster, but also the molecules formed on the grains may sublimate. Their molecular content is obviously richer than that of the cold dark clouds, especially as concerns complex organic compounds. The census of those, however, becomes more challenging, as the gas is more turbulent in such sources and the molecular lines are broader, so that the mm-wave (and far-IR) spectra reach much sooner the confusion limit (**Figure 13**). Prospects are more favourable for Protoplanetary disks, which have narrow lines. These disks, however, are very small and are barely resolved even with the largest interferometers. Their lines are very weak and, so far, only a score of molecular species have been identified there. Those species, of course, include CO, HCN, HCO^+, H_2O, NH_3, H_2S, SO (Phuong et al., 2018), but also formaldehyde, methyl cyanide, cyanoacetylene, formic acid and methanol. Many more will be detected with more sensitive searches in the near future.

The bricks essential for the construction of amino acids and the nucleobases seem therefore widespread across the Universe:

didn't Huygens prophetically write in *The Cosmotheoros: What's true in one part will hold over the whole Universe*? Does this mean they were originally accreted by the Earth from outer space? Not necessarily: it just shows those bricks form easily about everywhere and may survive in harsh environmental conditions. Most likely, they were already present in the pre-Solar nebula. They may have been destroyed by the Sun's ignition and the Earth's formation, but were quickly re-formed on the rocky/dusty surfaces of the young Earth and of a number of Solar System bodies, in particular meteorites and comets. The "Cometary Zoo" (**Figure 14**) observed on Comet Churyumov-Gerasimenko by the Rosetta space mission, seems to corroborate this view.

AUTHOR CONTRIBUTIONS

All authors listed have made a substantial, direct, and intellectual contribution to the work and approved it for publication.

ACKNOWLEDGMENTS

The authors thank the referees for their constructive suggestions and comments. J. Cernicharo thanks ERC for funding support through grant ERC-2013-Syg-610 256-NANOCOSMOS, and the Ministerio de Ciencia e Innovación of Spain (MICIU) for funding support through projects PID2019-106110GB-I00, PID2019-107115GB-C21/AEI/10.130 39/501 100 011 033, and PID2019-106235GB-I00. This paper makes use of ALMA data from project 2017.1.01 232.S, of IRAM NOEMA interferometer data from projects V03E, W19DA and S20BY, and of Yebes 40-m telescope data from projects 19A003, 20A014, 20A017, 20D023, and 21A011. ALMA is a partnership of ESO (representing its member states), NSF (United States) and NINS (Japan), together with NRC (Canada), MOST and ASIAA (Taiwan), and KASI (Republic of Korea), in cooperation with the Republic of Chile. IRAM is supported by INSU/CNRS (France), MPG (Germany) and IGN (Spain). The Yebes 40-m telescope belongs to Instituto Geografico Nacional (Spain).

REFERENCES

Ade, P. A. R., Aghanim, N., Arnaud, M., Baccigalupi, C., Banday, A. J., Barreiro, R. B., et al. (2016). The Planck List of High-Redshift Source Candidates. *Astron. Astrophys.* 596, A100. doi:10.1051/0004-6361/201527206

Agúndez, M., Cernicharo, J., and Guélin, M. (2015a). Discovery of Interstellar Ketenyl (HCCO), a Surprisingly Abundant Radical. *Astron. Astrophys.* 577, L5. doi:10.1051/0004-6361/201526317

Agúndez, M., Cernicharo, J., de Vicente, P., Marcelino, N., Roueff, E., Fuente, A., et al. (2015b). Probing Non-polar Interstellar Molecules through Their Protonated Form: Detection of Protonated Cyanogen (NCCNH+). *Astron. Astrophys.* 579, L10. doi:10.1051/0004-6361/201526650

Agúndez, M., Marcelino, N., Tercero, B., Cabezas, C., de Vicente, P., and Cernicharo, J. (2021a). O-bearing Complex Organic Molecules at the Cyanopolyyne Peak of TMC-1: Detection of C2H3CHO, C2H3OH, HCOOCH3, and CH3OCH3. *Astron. Astrophys.* 649, L4. doi:10.1051/0004-6361/202140978

Agúndez, M., Cabezas, C., Tercero, B., Marcelino, N., Gallego, J. D., de Vicente, P., et al. (2021b). Discovery of the Propargyl Radical (CH2CCH) in TMC-1: One of the Most Abundant Radicals Ever Found and a Key Species for Cyclization to Benzene in Cold Dark Clouds. *Astron. Astrophys.* 647, L10. doi:10.1051/0004-6361/202140553

Allamandola, L. J., Tielens, A. G. G. M., and Barker, J. R. (1985). Polycyclic Aromatic Hydrocarbons and the Unidentified Infrared Emission Bands - Auto Exhaust along the Milky Way. *ApJ* 290, L25. doi:10.1086/184435

Alloin, D., Guilloteau, S., Barvainis, R., Antonucci, R., and Tacconi, L. (1997). The Gravitational Lensing Nature of the Cloverleaf Unveiled in CO (7-6) Line Emission. *Astron. Astrophys.* 321, 24.

Altwegg, K., Balsiger, H., and Fuselier, S. A. (2019). Cometary Chemistry and the Origin of Icy Solar System Bodies: The View after Rosetta. *Annu. Rev. Astron. Astrophys.* 57, 113–155. doi:10.1146/annurev-astro-091918-104409

Bañados, E., Mazzucchelli, C., Momjian, E., Eilers, A.-C., Wang, F., Schindler, J.-T., et al. (2021). The Discovery of a Highly Accreting, Radio-Loud Quasar at Z = 6.82. *ApJ* 909, 80. doi:10.3847/1538-4357/abe239

Barvainis, R., Maloney, P., Antonucci, R., and Alloin, D. (1997). Multiple CO Transitions, CI, and HCN from the Cloverleaf Quasar. *ApJ* 484, 69.

Belloche, A., Menten, K. M., Comito, C., Müller, H. S. P., Schilke, P., Ott, J., et al. (2008). Detection of Amino Acetonitrile in Sgr B2(N). *Astron. Astrophys.* 482, 179–196. doi:10.1051/0004-6361:20079203

Bradford, C. M., Aguirre, J. E., Aikin, R., Bock, J. J., Earle, L., Glenn, J., et al. (2009). The Warm Molecular Gas Around the Cloverleaf Quasar. *ApJ* 705, 112–122. doi:10.1088/0004-637x/705/1/112

Burbidge, E. M., Burbidge, G. R., Fowler, W. A., and Hoyle, F. (1957). Synthesis of the Elements in Stars. *Rev. Mod. Phys.* 29, 547–650. doi:10.1103/revmodphys.29.547

Burkhardt, A. M., Long Kelvin Lee, K., Bryan Changala, P., Shingledecker, C. N., Cooke, I. R., Loomis, R. A., et al. (2021). Discovery of the Pure Polycyclic Aromatic Hydrocarbon Indene (C-C9h8) with GOTHAM Observations of TMC-1. *Astrophys. J. Lett.* 913, L18. doi:10.3847/2041-8213/abfd3a

Cernicharo, J., and Guélin, M. (1987). The Physical and Chemical State of HCL2. *Astron. Astrophys.* 176, 299.

Cernicharo, J., Guélin, M., and Askne, J. (1984). TMC 1-like Cloudlets in HCL 2. *Astron. Astrophys.* 138, 371.

Cernicharo, J., Heras, A. M., Tielens, A. G. G. M., Pardo, J. R., Herpin, F., Guélin, M., et al. (2001). [ITAL]Infrared Space Observatory's[/ITAL] Discovery of C [TINF]4[/TINF]H[TINF]2[/TINF], C[TINF]6[/TINF]H[TINF]2[/TINF], and Benzene in CRL 618. *ApJ* 546, L123–L126. doi:10.1086/318871

Cernicharo, J., Marcelino, N., Agúndez, M., Endo, Y., Cabezas, C., Bermúdez, C., et al. (2020a). Discovery of HC3O+ in Space: The Chemistry of O-Bearing Species in TMC-1. *Astron. Astrophys.* 642, L17. doi:10.1051/0004-6361/202039351

Cernicharo, J., Marcelino, N., Pardo, J. R., Agúndez, M., Tercero, B., de Vicente, P., et al. (2020b). Interstellar Nitrile Anions: Detection of C3N− and C5N− in TMC-1. *Astron. Astrophys.* 641, L9. doi:10.1051/0004-6361/202039231

Cernicharo, J., Marcelino, N., Agúndez, M., Bermúdez, C., Cabezas, C., Tercero, B., et al. (2020c). Discovery of HC4NC in TMC-1: A Study of the Isomers of HC3N, HC5N, and HC7N. *Astron. Astrophys.* 642, L8. doi:10.1051/0004-6361/202039274

Cernicharo, J., Cabezas, C., Endo, Y., Marcelino, N., Agúndez, M., Tercero, B., et al. (2021a). Space and Laboratory Discovery of HC3S+. *Astron. Astrophys.* 646, L3. doi:10.1051/0004-6361/202040013

Cernicharo, J., Cabezas, C., Bailleux, S., Margulès, L., Motiyenko, R., Zou, L., et al. (2021b). Discovery of the Acetyl Cation, CH3CO+, in Space and in the Laboratory. *Astron. Astrophys.* 646, L7. doi:10.1051/0004-6361/202040076

Cernicharo, J., Agúndez, M., Kaiser, R. I., Cabezas, C., Tercero, B., Marcelino, N., et al. (2021c). Discovery of Benzyne, O-C6h4, in TMC-1 with the QUIJOTE Line Survey. *Astron. Astrophys.* 652, L9. doi:10.1051/0004-6361/202141660

Cernicharo, J., Agúndez, M., Cabezas, C., Tercero, B., Marcelino, N., Pardo, J. R., et al. (2021d). Pure Hydrocarbon Cycles in TMC-1: Discovery of Ethynyl

Cyclopropenylidene, Cyclopentadiene, and Indene. *Astron. Astrophys.* 649, L15. doi:10.1051/0004-6361/202141156

Cernicharo, J., Agúndez, M., Cabezas, C., Marcelino, N., Tercero, B., Pardo, J. R., et al. (2021e). Discovery of CH2CHCCH and Detection of HCCN, HC4N, CH3CH2CN, and, Tentatively, CH3CH2CCH in TMC-1. *Astron. Astrophys.* 647, L2. doi:10.1051/0004-6361/202140434

Cernicharo, J., Cabezas, C., Agúndez, M., Tercero, B., Marcelino, N., Pardo, J. R., et al. (2021f). Discovery of Allenyl Acetylene, H2CCCHCCH, in TMC-1. *Astron. Astrophys.* 647, L3. doi:10.1051/0004-6361/202140482

Cernicharo, J., Agúndez, M., Kaiser, R. I., Cabezas, C., Tercero, B., Marcelino, N., et al. (2021g). Discovery of Two Isomers of Ethynyl Cyclopentadiene in TMC-1. *Astron. Astrophys.* 655, L1.

Cernicharo, J., Cabezas, C., Agúndez, M., Tercero, B., PardoMarcelino, J. R. N., Marcelino, N., et al. (2021h). TMC-1, the Starless Core Sulfur Factory: Discovery of NCS, HCCS, H2CCS, H2CCCS, and C4S and Detection of C5S. *Astron. Astrophys*. 648, L3. doi:10.1051/0004-6361/202140642

Cernicharo, J., Cabezas, C., Endo, Y., Agúndez, M., Tercero, B., Pardo, J. R., et al. (2021i). The sulphur Saga in TMC-1: Discovery of HCSCN and HCSCCH. *Astron. Astrophys.* 650, L14. doi:10.1051/0004-6361/202141297

Cernicharo, J., Agúndez, M., Kaiser, R. I., Cabezas, C., Tercero, B., Marcelino, N., et al. (2021j). Discovery of Two Isomers of Ethynyl Cyclopentadiene in TMC-1: Abundances of CCH and CN Derivatives of Hydrocarbon Cycles. *Astron. Astrophys.* 655, L1. doi:10.1051/0004-6361/202142226

Cernicharo, J., Agúndez, M., Cabezas, C., Tercero, B., Marcelino, N., Fuentetaja, R., et al. (2021k). Discovery of HCCCO and C5O in TMC-1 with the QUIJOTE Line Survey. *Astron. Astrophys.*. 656, L21. doi:10.1051/0004-6361/202142634

Cernicharo, J. (2004). The Polymerization of Acetylene, Hydrogen Cyanide, and Carbon Chains in the Neutral Layers of Carbon-Rich Proto-Planetary Nebulae. *ApJ* 608, L41–L44. doi:10.1086/422170

Cherchneff, I., Barker, J. R., and Tielens, A. G. G. M. (1992). Polycyclic Aromatic Hydrocarbon Formation in Carbon-Rich Stellar Envelopes. *ApJ* 401, 269. doi:10.1086/172059

Cheung, A. C., Rank, D. M., Townes, C. H., Thornton, D. D., and Welch, W. J. (1968). Detection of NH3 Molecules in the Interstellar Medium by Their Microwave Emission. *Phys. Rev. Lett.* 21, 1701–1705. doi:10.1103/physrevlett.21.1701

Cheung, A. C., Rank, D. M., Townes, C. H., Thornton, D. D., and Welch, W. J. (1969). Detection of Water in Interstellar Regions by its Microwave Radiation. *Nature* 221, 626.

Combes, F., Gupta, N., Muller, S., Balashev, S., Józsa, G. I. G., Srianand, R., et al. (2021). PKS1830-211: OH and Hi at Z = 0:89 and the First MeerKAT UHF Spectrum. *Astron. Astrophys*. 648, 116. doi:10.1051/0004-6361/202040167

Cordiner, M. A., Charnley, S. B., Kisiel, Z., McGuire, B. A., and Kuan, Y.-J. (2017). Deep K-Band Observations of TMC-1 with the Green Bank Telescope: Detection of HC7O, Nondetection of HC11N, and a Search for New Organic Molecules. *ApJ* 850, 187. doi:10.3847/1538-4357/aa970c

Douglas, A. E., and Herzberg, G. (1941). Note on CH^+ in Interstellar Space and in the Laboratory. *ApJ* 94, 3. doi:10.1086/144342

Ferus, M., Laitl, V., Knizek, A., Kubelík, P., Sponer, J., and Kára, J. (2018). HNCO-based Synthesis of Formamide in Planetary Atmospheres. *Astron. Astrophys.* 616, 150. doi:10.1051/0004-6361/201833003

Fuente, A., Navarro, D. G., Caselli, P., Gerin, M., Kramer, C., Roueff, E., et al. (2019). Gas Phase Elemental Abundances in Molecular cloudS (GEMS). *Astron. Astrophys.* 624, A105. doi:10.1051/0004-6361/201834654

García, R. G., Gentaz, O., Baldino, M., and Torres, M. (2012). "An 8 GHz Digital Spectrometer for Millimeter-Wave Astronomy," in Proceedings of the SPIE: Millimeter, Submillimeter, and Far-Infrared Detectors and Instrumentation for Astronomy VI, Amstrdam, September 24, 2012, 8452.

Garcia, R. G., Gentaz, O., Baldino, M., and Torres, M. (2012). An 8 GHz Digital Spectrometer for Millimeter-Wave Astronomy. *SPIE* 8452E, 2TG.

García-Burillo, S., Graciá-Carpio, J., Guélin, M., Neri, R., Cox, P., Planesas, P., et al. (2006). A New Probe of Dense Gas at High Redshift: Detection of HCO + (5-4) Line Emission in APM 08279+5255. *ApJ* 645, L17–L20. doi:10.1086/506204

Green, S., Montgomery, J. A. J., and Thaddeus, P. (1974). Tentative Identification of U93.174 as the Molecular Ion N2H/+/. *ApJ* 193, L89. doi:10.1086/181639

Guélin, M., and Cernicharo, J. (1989). "Molecular Abundances in the Dense Interstellar and Circumstellar Clouds," in The Physics and Chemistry of Interstellar Molecular Clouds, Proceedings of the Symposium. Zermatt, Switzerland. Sept 22-25, 1988. Editors G. Winnewisser and J. T. Armstrong (Berlin: Springer-Verlag), Vol. 331, 337. Lecture Notes in Physics.

Guélin, M., Salomé, P., Neri, R., García-Burillo, S., Graciá-Carpio, J., Cernicharo, J., et al. (2007). Detection of HNC and Tentative Detection of CN at Z = 3.9. *Astron. Astrophys.* 462, L45–L48. doi:10.1051/0004-6361:20066555

Guélin, M., and Thaddeus, P. (1977). Tentative Detection of the C3N Radical. *ApJ* 212, L81. doi:10.1086/182380

Guélin, M., Green, S., and Thaddeus, P. (1978). Detection of the C4H Radical toward IRC +10216. *ApJ* 224, L27. doi:10.1086/182751

Guélin, M., Omont, A., Kramer, C., Cernicharo, J., Tercero, B., Yang, C., et al. (2022). in preparation. *Astron. Astrophys.*

Guilloteau, S., Delannoy, J., Downes, D., Greve, A., Guélin, M., Lucas, R., et al. (1992). The IRAM interferometer on Plateau de Bure. *Astron. Astrophys.* 262, 6.

Herbst, E., and Klemperer, W. (1974). Is X-Ogen HCO+? *ApJ* 188, 255. doi:10.1086/152712

Hodge, J. A., and da Cunha, E. (2020). *High-redshift star Formation in the ALMA Era*. arXiv:2004.00934, 7 (12). Royal Society Open Science.

Holtom, P. D., Bennett, C. J., Osamura, Y., Mason, N. J., and Kaiser, R. I. (2005). A Combined Experimental and Theoretical Study on the Formation of the Amino Acid Glycine (NH2CH2COOH) and its Isomer (CH3NHCOOH) in Extraterrestrial Ices. *ApJ.* 626, 940–952. doi:10.1086/430106

Hoyle, F. (1957). *The Black Cloud*. London: William Heinemann Ltd.

Huygens, C. (1698). *Cosmotheoros, Book I Adriaan Moetjens*. The Hague.

Jiménez-Serra, I., Martín-Pintado, J., Rivilla, V. M., Rodríguez-Almeida, L., Alonso Alonso, E. R., Zeng, S., et al. (2020). Toward the RNA-World in the Interstellar Medium-Detection of Urea and Search of 2-Amino-Oxazole and Simple Sugars. *Astrobiology* 20, 1048–1066. doi:10.1089/ast.2019.2125

Joblin, C., and Cernicharo, J. (2018). Detecting the Building Blocks of Aromatics. *Science* 359, 156–157. doi:10.1126/science.aar4541

Kaifu, N., Ohishi, M., Kawaguchi, K., Saito, S., Yamamoto, S., Miyaji, T., et al. (2004). A 8.8-50 GHz Complete Spectral Line Survey toward TMC-1 I. Survey Data. *Publ. Astron. Soc. Jpn.* 56, 69–173. doi:10.1093/pasj/56.1.69

Kneib, J. P., Alloin, D., and Pello, R. (1998). Unveiling the Nature of the Cloverleaf Lens-System: HST/NICMOS-2 Observations. *Astron. Astrophys.* 339, L65.

Léger, A., and Puget, J. L. (1984). Identification of the "unidentified" IR Emission Features of Interstellar Dust? *Astron. Astrophys.* 137, L5.

Kelvin Lee, K. L., Changala, P. B., Loomis, R. A., Burkhardt, A. M., Xue, C., Cordiner, M. A., et al. (2021). Interstellar Detection of 2-cyanocyclopentadiene, C5H5CN, a Second Five-Membered Ring toward TMC-1. *Astrophys. J. Lett.* 910, L2. doi:10.3847/2041-8213/abe764

Lidman, C., Courbin, F., Meylan, G., Broadhurst, T., Frye, B., and Welch, W. J. W. (1999). The Redshift of the Gravitationally Lensed Radio Source PKS 1830−211. *ApJ* 514, L57–L60. doi:10.1086/311949

Marcelino, N., Cernicharo, J., Agúndez, M., Roueff, E., Gerin, M., Martín-Pintado, J., et al. (2007). Discovery of Interstellar Propylene (CH 2 CHCH 3): Missing Links in Interstellar Gas-phase Chemistry. *ApJ* 665, L127–L130. doi:10.1086/521398

Marcelino, N., Agúndez, M., Tercero, B., Cabezas, C., Bermúdez, C., Gallego, J. D., et al. (2020). Tentative Detection of HC5NH+ in TMC-1. *Astron. Astrophys.* 643, L6. doi:10.1051/0004-6361/202039251

Martínez, L., Santoro, G., Merino, P., Accolla, M., Lauwaet, K., Sobrado, J., et al. (2020). Prevalence of Non-aromatic Carbonaceous Molecules in the Inner Regions of Circumstellar Envelopes. *Nat. Astron.* 4, 97–105. doi:10.1038/s41550-019-0899-4

Martin, S., Mauersberger, R., Martin-Pintado, J., Henkel, C., and Garcia-Burillo, S. (2006). A 2 Millimeter Spectral Line Survey of the Starburst Galaxy NGC 253. *Astrophys J. Suppl. S* 164, 450–476. doi:10.1086/503297

Matthews, H. E., Irvine, W. M., Friberg, P., Brown, R. D., and Godfrey, P. D. (1984). A New Interstellar Molecule: Triearbon Monoxide. *Nature* 310, 125–126. doi:10.1038/310125a0

McCarthy, M. C., Lee, K. L. K., Loomis, R. A., Burkhardt, A. M., Shingledecker, C. N., Charnley, S. B., et al. (2021). Interstellar Detection of the Highly Polar Five-Membered Ring Cyanocyclopentadiene. *Nat. Astron.* 5, 176–180. doi:10.1038/s41550-020-01213-y

McGuire, B. A., Burkhardt, A. M., Shingledecker, C. N., Kalenskii, S. V., Herbst, E., Remijan, A. J., et al. (2017). Detection of Interstellar HC 5 O in TMC-1 with the Green Bank Telescope. *ApJ* 843, L28. doi:10.3847/2041-8213/aa7ca3

McGuire, B. A., Burkhardt, A. M., Kalenskii, S., Shingledecker, C. N., Remijan, A. J., Herbst, E., et al. (2018). Detection of the Aromatic Molecule Benzonitrile (C -C 6 H 5 CN) in the Interstellar Medium. *Science* 359, 202–205. doi:10.1126/science.aao4890

McGuire, B. A., Loomis, R. A., Burkhardt, A. M., Lee, K. L. K., Shingledecker, C. N., Charnley, S. B., et al. (2021). Detection of Two Interstellar Polycyclic Aromatic Hydrocarbons via Spectral Matched Filtering. *Science* 371, 1265–1269. doi:10.1126/science.abb7535

McGuire, B. A. (2018). Census of Interstellar, Circumstellar, Extragalactic, Protoplanetary Disk, and Exoplanetary Molecules. *ApJS* 239, 1. doi:10.3847/1538-4365/aae5d2

McKellar, A. (1940). Evidence for the Molecular Origin of Some Hitherto Unidentified Interstellar Lines. *PASP* 52, 187. doi:10.1086/125159

Muller, S., and Guélin, M. (2008). Drastic Changes in the Molecular Absorption at Redshift Z = 0.89 toward the Quasar PKS 1830-211. *Astron. Astrophys.* 491, 739–746. doi:10.1051/0004-6361:200810392

Muller, S., Guélin, M., Dumke, M., Lucas, R., and Combes, F. (2006). Probing Isotopic Ratios Atz= 0.89: Molecular Line Absorption in Front of the Quasar PKS 1830-211. *Astron. Astrophys.* 458, 417–426. doi:10.1051/0004-6361:20065187

Muller, S., Beelen, A., Guélin, M., Aalto, S., Black, J. H., Combes, F., et al. (2011). Molecules at Z = 0.89: A 4-Mm-Rest-Frame Absorption-Line Survey toward PKS 1830-211. *Astron. Astrophys.* 535, 32. doi:10.1051/0004-6361/201117096

Muller, S., Combes, F., Guélin, M., Gérin, M., Aalto, S., Beelen, A., et al. (2014). An ALMA Early Science Survey of Molecular Absorption Lines toward PKS 1830-211. Analysis of the Absorption Profiles. *Astron. Astrophys.* 566, 21. doi:10.1051/0004-6361/201423646

Muller, S., Müller, H. S. P., Black, J. H., Beelen, A., Combes, F., Curran, S., et al. (2016). OH^+ and H_2O^+ Absorption towards PKS 1830-211. *Astron. Astrophys.* 595, A128. doi:10.1051/0004-6361/201629073

Muller, S., Müller, H. S. P., Black, J. H., Gérin, M., Combes, F., and Curran, S. (2017). Detection of CH+, SH+, and Their 13C- and 34S-Isotopologues toward PKS 1830-211. *Astron. Astrophys.* 606, 109. doi:10.1051/0004-6361/201731405

Muller, S., Roueff, E., Black, J. H., Gérin, M., Guélin, M., Menten, K., et al. (2020). Detection of Deuterated Molecules, but Not of Lithium Hydride, in the Z = 0.89 Absorber toward PKS 1830-211. *Astron. Astrophys.* 637, A7. doi:10.1051/0004-6361/202037628

Ohishi, M., Ishikawa, S.-I., Yamada, C., Kanamori, H., Irvine, W. M., Brown, R. D., et al. (1991). Detection of a New Carbon-Chain Molecule, CCO. *ApJ* 380, L39. doi:10.1086/186168

Pensabene, A., Decarli, R., Bañados, E., Venemans, B., Walter, F., and Bertoldi, F. (2021). An ALMA Multi-Line Survey of the ISM in Two Quasar Host–Companion Galaxy Pairs at z > 6. *Astron. Astrophys.* 652, A66.

Phuong, N. T., Chapillon, E., Majumdar, L., Dutrey, A., Guilloteau, S., Piétu, V., et al. (2018). First Detection of H2S in a Protoplanetary Disk. *Astron. Astrophys.* 616, L5. doi:10.1051/0004-6361/201833766

Pilleri, P., Joblin, C., Boulanger, F., and Onaka, T. (2015). Mixed Aliphatic and Aromatic Composition of Evaporating Very Small Grains in NGC 7023 Revealed by the 3.4/3.3μm Ratio. *Astron. Astrophys.* 577, A16. doi:10.1051/0004-6361/201425590

Reuter, C., Vieira, J. D., Spilker, J. S., Weiss, A., Aravena, M., Archipley, M., et al. (2020). The Complete Redshift Distribution of Dusty Star-forming Galaxies from the SPT-SZ Survey. *ApJ* 902, 78. doi:10.3847/1538-4357/abb599

Rivilla, V. M., Martín-Pintado, J., Jiménez-Serra, I., Zeng, S., Martín, S., Armijos-Abendaño, J., et al. (2019). Abundant Z-Cyanomethanimine in the Interstellar Medium: Paving the Way to the Synthesis of Adenine. *MNRAS* 483, 114. doi:10.1093/mnrasl/sly228

Robintaille, T. P., and Whitney, B. A. (2010). The Present-Day star Formation Rate of the Milky-Way Determined from Spitzer Detected Young Stellar Objects. *ApJ* 710, L11. doi:10.1088/2041-8205/710/1/L11

Rubin, R. H., Swenson, G. W. J., Jr., Benson, R. C., Tigelaar, H. L., and Flygare, W. H. (1971). Microwave Detection of Interstellar Formamide. *ApJ* 169, L39. doi:10.1086/180810

Shingledecker, C. N., Lee, K. L. K., Wandishin, J. T., Balucani, N., Burkhardt, A. M., Charnley, S. B., et al. (2021). Detection of Interstellar H2CCCHC3N. *Astron. Astrophys.* 652, L12. doi:10.1051/0004-6361/202140698

Snyder, L. E., Buhl, D., Zuckerman, B., and Palmer, D. (1969). Microwave Detection of Interstellar Formaldehyde. *Phys. Rev. L.* 22, 679.

Snyder, L. E., Lovas, F. J., Hollis, J. M., Friedel, D. N., Jewell, P. R., Remijan, A., et al. (2005). A Rigorous Attempt to Verify Interstellar Glycine. *ApJS* 108, 301. doi:10.1086/426677

Solomon, P., Vanden Bout, P., Carilli, C., and Guélin, M. (2003). The Essential Signature of a Massive Starburst in a Distant Quasar. *Nature* 426, 636. doi:10.1038/nature02149

Spilker, J. S., Marrone, D. P., Aguirre, J. E., Aravena, M., Ashby, M. L. N., Béthermin, M., et al. (2014). The Rest-Frame Submillimeter Spectrum of High-Redshift, Dusty, Star-forming Galaxies. *ApJ* 785, 149. doi:10.1088/0004-637x/785/2/149

Spilker, J. S., Marrone, D. P., Aravena, M., Béthermin, M., Bothwell, M. S., Carlstrom, J. E., et al. (2016). ALMA Imaging and Gravitational Lens Models of South Pole Telescope –Selected Dusty, Sta-Forming Galaxies at High Redshifts. *ApJ* 826, 112. doi:10.3847/0004-637x/826/2/112

Stacey, H. R., McKean, J. P., Powell, D. M., Vegetti, S., Rizzo, F., and Spingola, C. (2021). The Rocky Road to Quiescence: Compaction and Quenching of Quasar Host Galaxies. *MNRAS* 500, 3667. doi:10.1093/mnras/staa3433

Swings, P., and Rosenfeld, L. (1937). Considerations Regarding Interstellar Molecules. *ApJ* 86, 4. doi:10.1086/143880

Tercero, B., Cernicharo, J., Pardo, J. R., and Goicoechea, J. (2010). A Line Confusion Limited Millimeter Survey of Orion KL. I. Sulfur Carbon Chains. *Astron. Astrophys.* 517, A96. doi:10.1051/0004-6361/200913501

Tercero, B., Cernicharo, J., Cuadrado, S., de Vicente, P., and Guélin, M. (2020). New Molecular Species at Redshift Z = 0.89. *Astron. Astrophys.* 636, L7. doi:10.1051/0004-6361/202037837

Tercero, F., López-Pérez, J. A., Gallego, J. D., Beltrán, F., García, O., Patino-Esteban, M., et al. (2021). Yebes 40 M Radio Telescope and the Broad Band Nanocosmos Receivers at 7 Mm and 3 Mm for Line Surveys. *Astron. Astrophys.* 645, 37. doi:10.1051/0004-6361/202038701

Thaddeus, P. (2006). The Prebiotic Molecules Observed in the Interstellar Gas. *Phil. Trans. R. Soc. B* 361, 1681. doi:10.1098/rstb.2006.1897

Tucker, K. D., Kutner, M. L., and Thaddeus, P. (1974). The Ethynyl Radical C2H-A New Interstellar Molecule. *ApJ* 193, L115. doi:10.1086/181646

Venturini, S., and Solomon, P. L. (2003). The Molecular Disk in the Cloverleaf Quasar. *ApJ* 590, 740. doi:10.1086/375050

Voltaire (1752). *Micromegas Les Editions de Londres*.

Wang, F., Yang, J., Fan, X., Hennawi, J. F., Barth, A. J., Banados, E., et al. (2021). A Luminous Quasar at Redshift 7.642. *ApJ* 907, L1. doi:10.3847/2041-8213/abd8c6

Weiss, A., De Breuck, C., Marrone, D. P., Vieira, J. D., Aguirre, J. E., Aird, K. A., et al. (2013). ALMA Redshifts of Millimeter-Selected Galaxies from the SPT Survey: The Redshift Distribution of Dusty Star-forming Galaxies. *ApJ* 767, 88. doi:10.1088/0004-637X/767/1/88

Wildy, C., and Czerny, B. (2017). The Relationship between Mg II Broad Emission and Quasar Inclination Angle. *FASS* 4, 43. doi:10.3389/fspas.2017.00043

Wilson, R. W., Jefferts, K. B., and Penzias, A. A. (1970). Carbon Monoxide in the Orion Nebula. *ApJ* 161, L43. doi:10.1086/180567

Winn, J., Kochanek, C., McLeod, B., Falco, E., Impey, C. D., and Rix, H. W. (2002). PKS 1830-211: A Face-On Spiral Galaxy Lens. *ApJ* 575, 103. doi:10.1086/341265

Woods, P. M., Millar, T. J., Zijlstra, A. A., and Herbst, E. (2002). The Synthesis of Benzene in the Proto-Planetary Nebula CRL 618. *ApJ* 574, L167. doi:10.1086/342503

Yang, C., Omont, A., Beelen, A., González-Alfonso, E., Neri, R., Gao, Y., et al. (2016). H_2O and H_2O^+ Emission in Lensed Hy/ULIRGs at Z=2-4. *Astron. Astrophys.* 595, A8. doi:10.1051/0004-6361/201628160

Yang, C., Gavazzi, A., and Beelen, A. (2019). CO, H_2O, H_2O^+ Line and Dust Emission in a z=3.63 Strongly Lensed Starburst Merger at Sun-Kiloparsec Scales. *Astron. Astrophys.* 624, 138. doi:10.1051/0004-6361/201833876

Yang, C., González-Alfonso, E., Omont, A., Pereira-Santaella, M., Fischer, J., Beelen, A., et al. (2020). First Detection of the 448 GHz Ortho-H_2O Line at High Redshift. *Astron. Astrophys.* 634, L3. doi:10.1051/0004-6361/201937319

Zeng, S., Quénard, D., Jiménez-Serra, I., Martín-Pintado, J., Rivilla, V. M., Testi, L., et al. (2019). First Detection of the Pre-biotic Molecule Glycolonitrile ($HOCH_2CN$) in the Interstellar Medium. *MNRAS* 484, L43. doi:10.1093/mnrasl/slz002

Zhang, Z. Y., Romano, D., Ivinson, R. J., Papadopoulos, P. P., and Matteucci, F. (2018). Stellar Populations Dominated by Massive Stars in Dusty Starburst Galaxies across Cosmic Time. *Nature* 558, 260. doi:10.1038/s41586-018-0196-x

Conflict of Interest: The authors declare that the research was conducted in the absence of any commercial or financial relationships that could be construed as a potential conflict of interest.

Publisher's Note: All claims expressed in this article are solely those of the authors and do not necessarily represent those of their affiliated organizations, or those of the publisher, the editors and the reviewers. Any product that may be evaluated in this article, or claim that may be made by its manufacturer, is not guaranteed or endorsed by the publisher.

frontiers in Astronomy and Space Sciences

PERSPECTIVE
published: 15 March 2022
doi: 10.3389/fspas.2022.843766

The SKA as a Prebiotic Molecule Detector

Izaskun Jiménez-Serra[1]*, *Jesús Martín-Pintado*[1], *Aran Insausti*[2,3], *Elena R. Alonso*[2,3], *Emilio J. Cocinero*[2,3] *and Tyler L. Bourke*[4]

[1]Department of Astrophysics, Centro de Astrobiología (CSIC/INTA), Torrejón de Ardoz, Spain, [2]Departamento de Química Física, Facultad de Ciencia y Tecnología, Universidad del País Vasco, (UPV-EHU), Bilbao, Spain, [3]Biofisika Institute (CSIC, UPV/EHU), Leioa, Spain, [4]SKA Observatory, Jodrell Bank, Macclesfield, United Kingdom

One of the theories for the origin of life proposes that a significant fraction of prebiotic material could have arrived to Earth from outer space between 4.1 and 3.8 billion years ago. This suggests that those prebiotic compounds could have originated in interstellar space, to be later on incorporated to small Solar-system bodies and planetesimals. The recent discovery of prebiotic molecules such as hydroxylamine and ethanolamine in the interstellar medium, strongly supports this hypothesis. However, some species such as sugars, key for the synthesis of ribonucleotides and for metabolic processes, remain to be discovered in space. The unmatched sensitivity of the Square Kilometre Array (SKA) at centimeter wavelengths will be able to detect even more complex and heavier prebiotic molecules than existing instrumentation. In this contribution, we illustrate the potential of the SKA to detect simple sugars with three and four carbon atoms, using a moderate investment of observing time.

Keywords: square kilometre array, complex organic molecules, prebiotic chemistry, interstellar medium, astrochemistry

OPEN ACCESS

Edited by:
Ashraf - Ali,
University of Maryland, College Park, United States

Reviewed by:
Eric Herbst,
University of Virginia, United States

***Correspondence:**
Izaskun Jiménez-Serra
ijimenez@cab.inta-csic.es

Specialty section:
This article was submitted to Astrochemistry, a section of the journal Frontiers in Astronomy and Space Sciences

Received: *26 December 2021*
Accepted: *08 February 2022*
Published: *15 March 2022*

Citation:
Jiménez-Serra I, Martín-Pintado J, Insausti A, Alonso ER, Cocinero EJ and Bourke TL (2022) The SKA as a Prebiotic Molecule Detector. Front. Astron. Space Sci. 9:843766. doi: 10.3389/fspas.2022.843766

1 INTRODUCTION

The question of the origin of life has attracted the interest of researchers for centuries. Two main lines of thought have been proposed: i) Life may have emerged endogenously so that the building blocks of life could have formed *"in situ"* on Earth; or ii) Life could have originated somewhere else in the Universe and been transported to Earth in small Solar-system bodies. Alternatively, an intermediate theory contemplates the possibility that a fraction of the prebiotic material essential for the origin of life could have originated exogenously and been transferred to a young Earth *via* planetesimal impact on its surface (Anders, 1989; Chyba and Sagan, 1992). Prebiotic molecules such as amino acids, nucleobases and sugars have indeed been detected in meteorites (Cooper et al., 2001; Pizzarello et al., 2006; Callahan et al., 2011; Furukawa et al., 2019; Glavin et al., 2020) and in comets (Altwegg et al., 2016), which supports the latter hypothesis.

In the past decade, it has become clear that the interstellar medium (ISM) is an extraordinary chemical factory. About 250 molecules, including ringed-molecules (see e.g., Cernicharo et al., 2021; McGuire et al., 2021), have so far been reported in the ISM. In addition, the pace at which new molecules are detected not only seems steady but accelerating (McGuire, 2021). In particular, the so-called complex organic molecules (or COMs)[1] have attracted great interest in recent years since a

[1]COMs are defined as carbon-based molecules with ≥6 atoms in their structure (as e.g., methanol or CH_3OH; see Herbst and van Dishoeck, 2009).

subset of them could have been involved in the first biochemical reactions leading to the origin of life. This sub-set of COMs are typically called *prebiotic*. Some examples of prebiotic COMs include urea and hydroxylamine (Belloche et al., 2019; Jiménez-Serra et al., 2020; Rivilla et al., 2020) since they are possible precursors of ribonucleotides (see e.g., Becker et al., 2019; Menor Salvan et al., 2020); ethanolamine and n-propanol because they could have triggered the formation of phospholipids (Jiménez-Serra et al., 2022; Rivilla et al., 2021); or amino acetonitrile, vynil amine and ethyl amine since they are considered precursors of amino acids (Belloche et al., 2008; Zeng et al., 2021).

One of the most extended theories about the origin of life is the primordial RNA world. In this scenario, early forms of life relied solely on RNA to store genetic information and to catalyze chemical reactions. The basic units of RNA are ribonucleotides, which are composed of a phosphate group, a nitrogenous base, and a ribose sugar (a C_5 sugar with five carbon atoms). Interestingly, only small precursors of sugars such as glycolonitrile ($HOCH_2CN$; see Patel et al., 2015) or the simplest C_2 sugar molecule, glycolaldehyde (CH_2OHCHO), have been reported in the ISM (Hollis et al., 2000; Beltrán et al., 2009; Jørgensen et al., 2012; Zeng et al., 2019). Indeed, searches of C_3 sugars such as glyceraldehyde ($CHOCHOHCH_2OH$) or dihydroxyacetone (DHA, with the chemical formula $CH_2OHCOCH_2OH$), have not yielded any robust detection (Hollis et al., 2004; Widicus Weaver and Blake, 2005; Apponi et al., 2006; Jiménez-Serra et al., 2020). In contrast, larger sugar-like species such as C_3 sugars and ribose have been found in meteorites (de Marcellus et al., 2015; Furukawa et al., 2019), which opens the possibility that these species form in interstellar space.

The search of sugars in the ISM has partly been hindered by the lack of spectroscopic rotational data since these species are thermolabile and hygroscopic. This has triggered the development of new sample preparation techniques as well as the use of ultrafast laser vaporization sources to avoid their decomposition (Cocinero et al., 2012; Calabrese et al., 2020). Recently, the rotational spectroscopy of C_4 and C_5 sugars such as erythrulose and ribose has been obtained in the laboratory (Cocinero et al., 2012; Insausti et al., 2021), which enables their search in interstellar space.

2 SEARCHING FOR SUGARS IN SOURCES WITH LOW EXCITATION TEMPERATURES (T_{EX})

The first searches in the ISM of glyceraldehyde and dihydroxyacetone (DHA) targeted the massive star-forming region SgrB2 N-LMH. While an upper limit to the abundance of glyceraldehyde of $\leq(2.4–5.7) \times 10^{-11}$ was obtained by Hollis et al. (2004), Widicus Weaver and Blake (2005) reported a tentative detection of DHA toward this source with an abundance of 1.2×10^{-9}. The latter detection, however, was never confirmed (Apponi et al., 2006). For low-mass star-forming regions, Jiménez-Serra et al. (2020) also reported upper limits to the abundance of both species in the range $\leq(0.6–4)\times10^{-10}$ toward the low-mass hot corino IRAS16293-2422 B.

Massive hot cores and low-mass hot corinos are among the most chemically rich sources in the Galaxy and, traditionally, they have been the selected targets for searches of new prebiotic COMs in the ISM (see e.g., Jørgensen et al., 2012; Belloche et al., 2014; Jørgensen et al., 2016; Belloche et al., 2019). Their disadvantage, however, lies in the fact that their observed rotational spectra present hundreds (even thousands) of different molecular rotational transitions as a result of the high excitation temperatures (of T_{ex} = 100–300 K). These high temperatures populate a wide number of energy levels of a COM since its partition function is large. In addition, at temperatures of 100–300 K COM rotational spectra present their peak emission shifted towards millimeter and sub-millimeter wavelengths, which are heavily contaminated by the emission from smaller and lighter species such as CO. Consequently, the COM spectra observed in massive hot cores and low-mass hot corinos not only largely suffer from line blending and line confusion but also present weak lines due to the large partition functions expected at high excitation temperatures.

Alternatively, sources where COMs show low excitation temperatures (T_{ex}) represent better targets for the search and discovery of new large prebiotic species in the ISM (Jiménez-Serra et al., 2014)[2]. As a result of the low T_{ex}, the emission peak of the COM observed spectra is shifted towards lower frequencies, which are cleaner from the contribution from lighter molecules. In addition, the line intensities increase since only the lowest energy levels of the COMs can be populated at such low T_{ex} and so, the number of rotational transitions present in the measured spectra is significantly smaller than in hotter sources. The frequency span for the transitions between the lowest energy levels is also much larger than for those between the higher energy levels, which helps reducing significantly line blending and line confusion in the observed spectra (Jiménez-Serra et al., 2014).

Giant Molecular Clouds (GMCs) located in the Galactic Center such as the molecular cloud G+0.693-0.027 (hereafter G+0.693) have proven to be not only efficient chemical factories for the formation of complex organics (Requena-Torres et al., 2006; Requena-Torres et al., 2008; Zeng et al., 2018), but also excellent targets for the discovery of new prebiotic species (see e.g., Jiménez-Serra et al., 2020; Rivilla et al., 2020; Rivilla et al., 2021; Zeng et al., 2021). These clouds show low H_2 gas densities of $\sim10^4$ cm^{-3} and their gas and dust temperatures are decoupled (while $T_{dust} \leq$ 20K, T_{gas} ~70–150 K; see Rodríguez-Fernández et al., 2000; Zeng et al., 2018). The low H_2 gas densities also imply that for high-dipole moment molecules (such as COMs), and despite the high gas kinetic temperatures and broad linewidths of their emission (of ~ 20 km s^{-1}), their T_{ex} is low (between 5 and 20 K) and thus their observed spectra will be less affected by line blending and line confusion. Recent searches of prebiotic molecules toward the Galactic Center molecular cloud

[2]In massive hot cores and hot corinos, $T_{ex} \sim T_{kin}$ because of the high H_2 gas densities ($\geq10^6$ cm^{-3}) found in these star-forming regions

G+0.693 have yielded the discovery of several of these species for the first time in the ISM such as hydroxylamine (NH_2OH; Rivilla et al., 2020), ethanolamine ($NH_2CH_2CH_2OH$; Rivilla et al., 2021), thioformic acid (HC(O)SH; Rodríguez-Almeida et al., 2021) or *n*-propanol (n-C_3H_7OH; Jiménez-Serra et al., 2022). As a result, Galactic Center GMCs are prime targets for the search and discovery of large C_3 and C_4 sugars in the ISM.

3 THE POTENTIAL OF THE SKA TO DETECT NEW PREBIOTIC SPECIES IN THE ISM: THE CASE OF SUGARS

The Square Kilometre Array (SKA) will be the largest radio telescope in the world operating at centimeter and meter wavelengths. The Phase 1 of this observatory will consist of two radio interferometers located at two different sites: SKA1 LOW in Western Australia and SKA1 MID in South Africa (Braun et al., 2019). SKA1 LOW will have 512 stations of 256 log periodic dipole antennas each operating within the frequency range between 50 and 350 MHz, while SKA1 MID will have a total of 197 antennas (that include the 64 antennas of the MeerKAT array) operating at frequencies between 350 MHz and 15 GHz (Braun et al., 2019). Given the frequency coverage and how dramatically the strength of the rotational transitions of high-dipole molecules drops for frequencies $\leq$ 5GHz, SKA1 MID, and in particular its Band 5 receivers covering the frequency range between 4.8 and 15.3 GHz, are well suited for searches of prebiotic molecules in the ISM. On top of the advantages of observing at centimeter wavelengths noted in **Section 2**, it is important to stress that radio interferometers such as the SKA1 filter out any extended emission in the line of sight of the targeted source, significantly decreasing the linewidths of the observed molecular line emission and reducing the level of line blending and line confusion. In **Section 3.1**, we evaluate the feasibility of detecting large sugar-like species such as glyceraldehyde, dihydroxyacetone and erythrulose in the ISM using the Band 5 receivers of SKA1 MID.

3.1 SKA1 Simulations for C_3 and C_4 Sugars in Galactic Center GMCs: Glyceraldehyde, Dihydroxyacetone and Erythrulose

The emission from COMs in the Galactic Center GMCs is known to be extended (Martín-Pintado et al., 2001; Li et al., 2017; Li et al., 2020). This is particularly interesting for absorption studies in which COMs can be searched for against a bright continuum background source. This technique may allow the detection of low-abundance COMs whose emission spectra is expected to be very weak. Indeed, in the presence of a bright background continuum source, the predicted absorption line intensity (T_L) is given by (see e.g., Martín et al., 2019):

$$T_L = \left(T_{ex} - T_c - T_{bg}\right) \times \left[1 - exp\left(-\tau_\nu\right)\right] \quad (1)$$

where T_c is the temperature of a continuum source and T_{bg} is the temperature of the comic microwave background radiation (T_{bg} = 2.73 K). If $T_c \gg T_{ex}$, this will largely enhance the observed absorption line intensity over the emission for the T_{ex} expected to be close to T_{bg}.

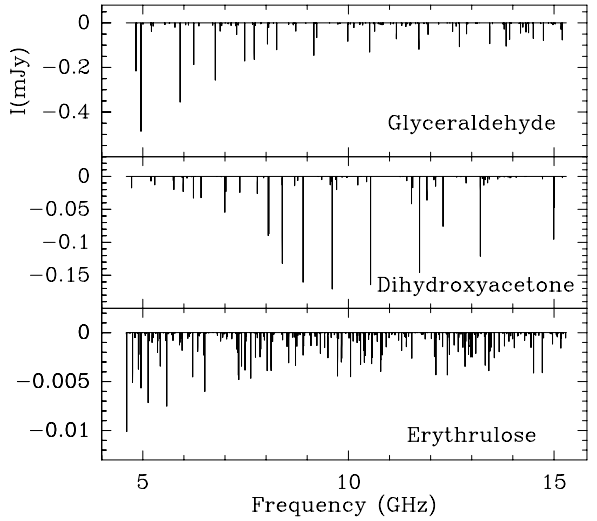

FIGURE 1 | Predicted absorption spectra of the C_3 and C_4 sugars glyceraldehyde, dihydroxyacetone and erythrulose obtained with the SLIM tool of the MADCUBA package considering the physical conditions of the G+0.693 molecular cloud (T_{ex} = 10K, linewidths of Δ_v = 20 km s^{-1} and extended emission across the beam) and a background source similar to the L source in the SgrB2 N molecular complex (measured flux of ~300 mJy within a beam of 1″ at 10 GHz). The assumed column densities for glyceraldehyde and dihydroxyacetone are 10^{13} cm^{-2} and 6.8× 10^{12} cm^{-2}, respectively, while for erythrulose we assume a column density one order of magnitude lower than that of glyceraldehyde (of 10^{12} cm^{-2}; see **Section 3.1**).

Therefore, we simulate the case of absorption spectra of glyceraldehyde, dihydroxyacetone and erythrulose ($C_4H_8O_4$) using the SLIM tool within the MADCUBA software package[3] (see Martín et al., 2019). We focus our simulations on C_3 and C_4 sugars because, as discussed in **Section 3.2**, C_5 sugars such as ribose are not expected to be abundant enough to be detected with SKA1 in a reasonable amount of observing time. We assume the physical conditions of the G+0.693 molecular cloud with a typical T_{ex} of $\leq$10K, linewidths of Δ_v = 20 km s^{-1} and extended morphology across the SKA1 beam for the COMs emission (Zeng et al., 2020). As background source, we consider the L source located in the SgrB2 N complex, which is a bright HII region found nearby the emission peak of G+0.693, and whose measured flux at 23 GHz is ~ 300 mJy within a beam of ~ 1" (de Pree et al., 1995). We have assumed that the emission from the HII region is optically thin and thus, that it shows an almost flat spectral energy distribution between 23 and 10 GHz. The simulations have been obtained considering a beam of 1", which will easily be reached by the SKA1 at the frequencies of the Band 5 receivers of SKA1 MID (see Braun et al., 2019). The spectroscopic data for glyceraldehyde have been extracted from

[3]MADCUBA, or MAdrid Data CUBe Analysis, is a software developed at the Center of Astrobiology in Madrid: https://cab.inta-csic.es/madcuba/index.html

TABLE 1 | List of transitions of glyceraldehyde, dihydroxyacetone and erythrulose that present the deepest features in the simulated spectra.

Molecule	Formula	Frequency (MHz)	Transition	Log [Int(300K)]	E_l (cm^{-1})	I_{depth} (mJy)
Glyceraldehyde	$CHOCHOHCH_2OH$	4,955.499 8	$6_{2,5} \rightarrow 6_{1,5}$	−7.700 2	3.845 8	−0.488
		5,907.255 6	$5_{2,4} \rightarrow 5_{1,4}$	−7.671 5	2.780 5	−0.360
		6,762.410 3	$4_{2,3} \rightarrow 4_{1,3}$	−7.693 1	1.888 8	−0.260
		4,835.648 0	$12_{3,10} \rightarrow 12_{2,10}$	−7.449 5	14.253 8	−0.223
		6,240.130 2	$11_{3,9} \rightarrow 11_{2,9}$	−7.312 7	12.128 5	−0.186
Dihydroxyacetone	$CH_2OHCOCH_2OH$	9,605.934 2	$4_{1,3} \rightarrow 4_{0,4}$	−7.686 9	1.258 4	−0.172
		10 540.639 1	$5_{1,4} \rightarrow 5_{0,5}$	−7.544 6	1.883 7	−0.166
		8,898.373 3	$3_{1,2} \rightarrow 3_{0,3}$	−7.842 7	0.756 3	−0.161
		11 731.758 5	$6_{1,5} \rightarrow 6_{0,6}$	−7.410 4	2.630 8	−0.147
		8,391.965 5	$2_{1,1} \rightarrow 2_{0,2}$	−8.025 3	0.378 6	−0.132
Erythrulose	$C_4H_8O_4$	4,609.671 9	$10_{3,8} \rightarrow 10_{2,8}$	−8.320 5	5.159 2	−0.010
		5,583.487 0	$9_{3,7} \rightarrow 9_{2,7}$	−8.244 2	4.262 4	−0.007 5
		5,131.326 5	$2_{2,1} \rightarrow 2_{1,1}$	−9.051 3	0.332 9	−0.0071[a]
		5,131.411 5	$2_{0,2} \rightarrow 1_{0,1}$	−8.806 1	0.086 1	−0.0071[a]
		6,508.324 0	$8_{3,6} \rightarrow 8_{2,6}$	−8.199	3.452 2	−0.006 1

[a]*Intensity of the feature resulting from the blending of the two indicated transitions.*

the CDMS catalogue (entry 090501; Endres et al., 2016), while the data for dihydroxyacetone is available in the JPL molecular catalogue (entry 90002; Pickett et al., 1998). The spectroscopic information for erythrulose can be found in Insausti et al. (2021).

As column densities, we have assumed that glyceraldehyde and dihydroxyacetone have column densities of 10^{13} cm^{-2} and 6.8×10^{12} cm^{-2}, respectively. These column densities correspond to the upper limits obtained toward G+0.693 in previous spectral surveys (see Table2 in Jiménez-Serra et al., 2020). For erythrulose, we consider that this C_4 sugar is a factor of 10 less abundant than the C_3 sugar glyceraldehyde, with an assumed column density of 10^{12} cm^{-2} for erythrulose. We note that this decrease by one order of magnitude in the column density of molecules from the same family when one carbon atom is added to the molecular structure, has been reported for alcohols (Jiménez-Serra et al., 2022) and thiols (Rodríguez-Almeida et al., 2021). The assumed spectral resolution considered in our simulations is 79.3 kHz (equivalent to a velocity resolution between ~1.6 and 5.0 km s^{-1}) across the full Band 5 frequency coverage.

Figure 1 presents the predicted absorption spectra of glyceraldehyde, dihydroxyacetone and erythrulose obtained for the extended GMC G+0.693 against the background source L. Depending on the structure of the molecule, the transitions that show the larger absorption depths lie in the range between 4.8 and 7.0 GHz for glyceraldehyde and erythrulose, and 8–14 GHz for dihydroxyacetone. The maximum bandwidth that will be covered simultaneously by the Band 5 receivers of SKA1 MID in its Phase 1 is 4 GHz at frequencies between 4.6 and 8.5 GHz, and 5 GHz for frequencies between 8.3 and 15.3 GHz. Given that the deepest absorption lines appear clustered within frequency ranges of ≤ 4-5 GHz-width, future detection experiments of these lines with SKA1 MID could be carried out in just two observing runs: one to simultaneously cover all the deepest features of glyceraldehyde and erythrulose, and a second one to simultaneously cover all the transitions of dihydroxyacetone. We stress that **Figure 1** includes all possible transitions of these C_3 and C_4 sugars available within the frequency range covered by the Band 5 receivers of SKA1 MID. The intensities of the deepest absorption features in our simulated spectra reach values of −0.47 mJy for glyceraldehyde, of −0.17 mJy for dihydroxyacetone, and −0.01 mJy for erythrulose. **Table1** lists the spectroscopic information of the deepest features found in our predicted spectra for each molecule. In **Section 3.2**, we evaluate the observing time required to perform these detection experiments with SKA1 MID during its Phase 1 of operations, which will have only 133 antennas equipped with Band 5 receivers.

3.2 Time Estimates and Key Science Projects

As seen from **Table1**, the predicted intensities for the deepest absorption features lie in the range between −0.19 and −0.5 mJy for glyceraldehyde, −0.13 and −0.2 mJy for dihydroxyacetone, and −0.006 and −0.01 mJy for erythrulose. According to Braun et al. (2019), a line sensitivity of 90 μJy will be achieved in 1 hour of observing time with the Band 5 receivers of SKA1 MID at frequencies of 4.6–8.5 GHz, and of 85 μJy at frequencies of 8.5–15.3 GHz, for a velocity resolution of ~ 30km s^{-1}.

Taking these numbers into account, the deepest absorption line of glyceraldehyde at 4955 MHz could be detected with a S/N ≥ 5 in just 8.5 h assuming a velocity resolution of 3 km s^{-1}. The weakest transitions of glyceraldehyde at 4835 MHz and at 6240 MHz, however, would require about 50 h of observing time for a similar velocity resolution and S/N. This is also the case of dihydroxyacetone, for which a total of ≥ 100hrs of integration time on-source would be needed to detect its weakest transitions at 8391 and 11 731 MHz with a S/N ≥ 5 and a velocity resolution of 3 km s^{-1}. A more time-consuming experiment would have to be performed for the discovery of the deepest absorption features of erythrulose. In order to detect the erythrulose transition at 4609 MHz with a S/N ≥ 3, and considering a velocity resolution of 20 km s^{-1} (i.e., the linewidth of the molecular emission in G+0.693; see Zeng et al., 2018), a total of ≥ 1100hrs of observing time on-source would be required.

The time estimates to perform the detection experiments of glyceraldehyde, dihydroxyacetone and erythrulose proposed above, may seem excessive. However, we note that these long

integration times are contemplated within the future Key Science Projects (KSPs) scheme that will be carried out by the SKA1. The KSPs are major surveys targeting ground-breaking transformational science in Astrophysics and Astrobiology that require considerable amount of time. Therefore, the expected integration time requests for these projects are typically of a few thousands of hours, which guarantees the detection of at least C_3 sugars such as glyceraldehyde and dihydroxyacetone, if present in the ISM. As discussed in **Section 4**, the discovery of C_4 sugars such as erythrulose may require the development of future instrumentation for SKA1 MID such as the high-frequency Band 6 receivers.

We note that, when performing deep integrations as proposed here, it is expected that the level of line confusion increases even at the low frequencies covered by the SKA1 as a consequence of weak features of low-abundance molecules becoming bright in the spectra. However, this potential problem is likely not an issue for the discovery of intermediate-sized species such as C_3 and C_4 sugars. As recently found by Jiménez-Serra et al. (2022) and by Rodríguez-Almeida et al. (2021), the addition of a $-CH_2$ group to the structure of alcohols, thiols, isocyanates, and carboxylic acids implies a decrease in their abundance by at least one order of magnitude (see also **Section 3.1**). This decrease in the abundance would imply an increase in the required SKA1 observing time by a factor of 100 and thus, for a reasonable integration time within the context of SKA1 Key Science Projects, the only sugars for which absorption features could be detected with SKA1 are the C_3 and the C_4 sugars together with their lowest-energy conformers. Indeed, for the case of *n*-propanol, only the *Ga* and *Aa* conformers with relative energies of E = 0 K and E = 40 K, have been found toward G+0.693 (the rest of conformers with energies > 50K do not show any detected features; see Jiménez-Serra et al., 2022). Therefore, although the conformers of C_3 and C_4 sugars as well as even larger sugars may be present in Galactic Center Giant Molecular Clouds such as G+0.693, these species likely do not confuse much the observed SKA1 spectrum because either their abundance is too low (as for C_5 sugars such as ribose) or their low-energy levels are not populated at the low excitation temperatures measured in these clouds (as for high-energy conformers).

4 FUTURE EXPANSION OF THE SKA: THE BAND 6 RECEIVERS

From **Section 3.2**, it is clear that, while relatively small molecules such as glyceraldehyde or dihydroxyacetone could be detected with a moderate investment of SKA1 MID observing time, larger prebiotic COMs such as erythrulose would still be well below the limit of what the SKA1 will be able to detect in its Phase 1. For this reason, one possible future expansion of SKA1 MID contemplates the development of higher-frequency receiver(s), the Band 6 receivers, which will increase the frequency coverage of SKA1 MID to higher frequencies from 15.3 up to 50 GHz. As reported in Memo 20-01 of SKA1 titled "SKA1 Beyond 15 GHz: The Science case for Band 6" (see Conway et al., 2021), high-dipole moment molecules such as COMs present rotational transitions at frequencies $\geq$20GHz that can be factors $\geq$10 brighter than those found at frequencies $\leq$15GHz (see Section 3.3.1 in this Memo). This is due to the fact that the Einstein A_{ul} coefficients increase as ν^3 with ν being the frequency, making them one order of magnitude higher at 36 GHz than at 12 GHz. This implies that observing times about ~100 times shorter would be needed to detect the C_4 sugar erythrulose in the ISM, reducing the total observing time needed for the discovery of this species from $\geq$1100hrs to a few tens of hours (or at most, to a few hundreds of hours). Therefore, if these receivers were finally included in the development program of the SKA1, they would make this observatory an unbeateable machine for the discovery of large prebiotic compounds in space.

5 CONCLUSION

In this contribution, we evaluate the feasibility of detecting small sugars in the ISM using the Band 5 receivers of SKA1 in its Phase 1. Our simulations show that Galactic Center Giant Molecular Clouds such as G+0.693 represent prime targets for future searches of these key prebiotic species in space. As shown in **Section 3.1**, the detection of small sugars could be achieved by carrying out broad spectroscopic surveys between 5 and 14 GHz in absorption against a bright continuum background source. By taking as template the L HII region source located in the SgrB2 N molecular complex, we estimate that the detection of C_3 sugars could be achieved in a few hundreds of hours. Larger C_4 sugars such as erythrulose would require thousands of hours of observing time. Future developments of the SKA such as the Band 6 receivers (which will increase the frequency coverage of SKA1 MID up to, at least, 24 GHz), will enable the search of these large sugars and other prebiotic COMs in just a few hundreds of hours.

DATA AVAILABILITY STATEMENT

The original contributions presented in the study are included in the article/supplementary material, further inquiries can be directed to the corresponding author.

AUTHOR CONTRIBUTIONS

IJ-S has written the first version of the manuscript. IJ-S and JM-P have produced the MADCUBA-SLIM simulations of the spectra of glyceraldehyde, dihydroxyacetone and erythrulose reported in **Section 3.1**. All authors have contributed to the discussion of the results and have provided comments on the text.

FUNDING

IJ-S and JM-P acknowledge partial support from the Spanish State Research Agency (AEI) through project numbers PID 2019-105552RB-C41 and MDM-2017-0737 Unidad de Excelencia María de Maeztu-Centro de Astrobiología (CSIC-INTA). EC

thanks the support received from the MINECO (PID 2020-117892RB-I00), the Basque Government (IT1162-19 and PIBA 2018-11), the UPV/EHU (PPG17/10, GIU18/207), and CSIC (PIC 2018, LINKA20249). Computational resources and laser facilities of the UPV/EHU (SGIker) and CESGA were used in this work.

ACKNOWLEDGMENTS

We would like to thank an anonymous referee for his/her positive and constructive comments on an earlier version of the manuscript.

REFERENCES

Altwegg, K., Balsiger, H., Bar-Nun, A., Berthelier, J.-J., Bieler, A., Bochsler, P., et al. (2016). Prebiotic Chemicals-Amino Acid and Phosphorus-In the Coma of Comet 67P/Churyumov-Gerasimenko. *Sci. Adv.* 2, e16002855. doi:10.1126/sciadv.1600285

Anders, E. (1989). Pre-biotic Organic Matter from Comets and Asteroids. *Nature* 342, 255–257. doi:10.1038/342255a0

Apponi, A. J., Halfen, D. T., Ziurys, L. M., Hollis, J. M., Remijan, A. J., and Lovas, F. J. (2006). Investigating the Limits of Chemical Complexity in Sagittarius B2(N): A Rigorous Attempt to Confirm 1,3-Dihydroxyacetone. *ApJ* 643, L29–L32. doi:10.1086/504979

Becker, S., Feldmann, J., Wiedemann, S., Okamura, H., Schneider, C., Iwan, K., et al. (2019). Unified Prebiotically Plausible Synthesis of Pyrimidine and Purine Rna Ribonucleotides. *Science* 366, 76–82. doi:10.1126/science.aax2747

Belloche, A., Garrod, R. T., Müller, H. S. P., and Menten, K. M. (2014). Detection of a Branched Alkyl Molecule in the Interstellar Medium: Iso -propyl Cyanide. *Science* 345, 1584–1587. doi:10.1126/science.1256678

Belloche, A., Garrod, R. T., Müller, H. S. P., Menten, K. M., Medvedev, I., Thomas, J., et al. (2019). Re-exploring Molecular Complexity with ALMA (ReMoCA): Interstellar Detection of Urea. *A&A* 628, A10. doi:10.1051/0004-6361/201935428

Belloche, A., Menten, K. M., Comito, C., Müller, H. S. P., Schilke, P., Ott, J., et al. (2008). Detection of Amino Acetonitrile in Sgr B2(N). *A&A* 482, 179–196. doi:10.1051/0004-6361:20079203

Beltrán, M. T., Codella, C., Viti, S., Neri, R., and Cesaroni, R. (2009). First Detection of Glycolaldehyde outside the Galactic Center. *ApJ* 690, L93–L96. doi:10.1088/0004-637X/690/2/L93

Braun, R., Bonaldi, A., Bourke, T., Keane, E., and Wagg, J. (2019). *Anticipated Performance of the Square Kilometre Array - Phase 1 (SKA1). arXiv e-prints*arXiv:1912.12699.

Calabrese, C., Uriarte, I., Insausti, A., Vallejo-López, M., Basterretxea, F. J., Cochrane, S. A., et al. (2020). Observation of the Unbiased Conformers of Putative Dna-Scaffold Ribosugars. *ACS Cent. Sci.* 6, 293–303. doi:10.1021/acscentsci.9b01277PMID: 32123748

Callahan, M. P., Smith, K. E., Cleaves, H. J., Ruzicka, J., Stern, J. C., Glavin, D. P., et al. (2011). Carbonaceous Meteorites Contain a Wide Range of Extraterrestrial Nucleobases. *Proc. Natl. Acad. Sci.* 108, 13995–13998. doi:10.1073/pnas.1106493108

Cernicharo, J., Agúndez, M., Cabezas, C., Tercero, B., Marcelino, N., Pardo, J. R., et al. (2021). Pure Hydrocarbon Cycles in TMC-1: Discovery of Ethynyl Cyclopropenylidene, Cyclopentadiene, and Indene. *A&A* 649, L15. doi:10.1051/0004-6361/202141156

Chyba, C., and Sagan, C. (1992). Endogenous Production, Exogenous Delivery and Impact-Shock Synthesis of Organic Molecules: an Inventory for the Origins of Life. *Nature* 355, 125–132. doi:10.1038/355125a0

Cocinero, E. J., Lesarri, A., Écija, P., Basterretxea, F. J., Grabow, J.-U., Fernández, J. A., et al. (2012). Ribose Found in the Gas Phase. *Angew. Chem. Int. Ed.* 51, 3119–3124. doi:10.1002/anie.201107973

Conway, J., Beswick, R., Bourke, T., Coriat, M., Ferrari, C., Jimenez-Serra, I., et al. (2021). *Memo 20-01, SKA1 beyond 15GHz: The Science Case for Band 6 (Square Kilometre Array).*

Cooper, G., Kimmich, N., Belisle, W., Sarinana, J., Brabham, K., and Garrel, L. (2001). Carbonaceous Meteorites as a Source of Sugar-Related Organic Compounds for the Early Earth. *Nature* 414, 879–883. doi:10.1038/414879a

de Marcellus, P., Meinert, C., Myrgorodska, I., Nahon, L., Buhse, T., d'Hendecourt, L. L. S., et al. (2015). Aldehydes and Sugars from Evolved Precometary Ice Analogs: Importance of Ices in Astrochemical and Prebiotic Evolution. *Proc. Natl. Acad. Sci. USA* 112, 965–970. doi:10.1073/pnas.1418602112

de Pree, C. G., Gaume, R. A., Goss, W. M., and Claussen, M. J. (1995). The Sagittarius B2 Star-forming Region. II. High-Resolution H66 Alpha Observations of Sagittarius B2 North. *ApJ* 451, 284. doi:10.1086/176218

Endres, C. P., Schlemmer, S., Schilke, P., Stutzki, J., and Müller, H. S. P. (2016). The Cologne Database for Molecular Spectroscopy, CDMS, in the Virtual Atomic and Molecular Data Centre, VAMDC. *J. Mol. Spectrosc.* 327, 95–104. doi:10.1016/j.jms.2016.03.005

Furukawa, Y., Chikaraishi, Y., Ohkouchi, N., Ogawa, N. O., Glavin, D. P., Dworkin, J. P., et al. (2019). Extraterrestrial Ribose and Other Sugars in Primitive Meteorites. *Proc. Natl. Acad. Sci. USA* 116, 24440–24445. doi:10.1073/pnas.1907169116

Glavin, D. P., McLain, H. L., Dworkin, J. P., Parker, E. T., Elsila, J. E., Aponte, J. C., et al. (2020). Abundant Extraterrestrial Amino Acids in the Primitive Cm Carbonaceous Chondrite Asuka 12236. *Meteorit Planet. Sci.* 55, 1979–2006. doi:10.1111/maps.13560

Herbst, E., and van Dishoeck, E. F. (2009). Complex Organic Interstellar Molecules. *Annu. Rev. Astron. Astrophys.* 47, 427–480. doi:10.1146/annurev-astro-082708-101654doi:10.1146/annurev-astro-082708-101654

Hollis, J. M., Jewell, P. R., Lovas, F. J., and Remijan, A. (2004). Green Bank Telescope Observations of Interstellar Glycolaldehyde: Low-Temperature Sugar. *ApJ* 613, L45–L48. doi:10.1086/424927

Hollis, J. M., Lovas, F. J., and Jewell, P. R. (2000). Interstellar Glycolaldehyde: The First Sugar. *Astrophysical J.* 540, L107–L110. doi:10.1086/312881

Insausti, A., Alonso, E. R., Tercero, B., Santos, J. I., Calabrese, C., Vogt, N., et al. (2021). Laboratory Observation of, Astrochemical Search for, and Structure of Elusive Erythrulose in the Interstellar Medium. *J. Phys. Chem. Lett.* 12, 1352–1359. doi:10.1021/acs.jpclett.0c03050

Jiménez-Serra, I., Martín-Pintado, J., Rivilla, V. M., Rodríguez-Almeida, L., Alonso Alonso, E. R., Zeng, S., et al. (2020). Toward the RNA-World in the Interstellar Medium-Detection of Urea and Search of 2-Amino-Oxazole and Simple Sugars. *Astrobiology* 20, 1048–1066. doi:10.1089/ast.2019.2125

Jiménez-Serra, I., Rodríguez-Almeida, L. F., Martín-Pintado, J., Rivilla, V. M., Melosso, M., Zeng, S., et al. (2022). *Precursors of Fatty Alcohols in the ISM: Discovery of N-Propanol.*

Jiménez-Serra, I., Testi, L., Caselli, P., and Viti, S. (2014). Detectability of Glycine in Solar-type System Precursors. *ApJ* 787, L33. doi:10.1088/2041-8205/787/2/L33

Jørgensen, J. K., Favre, C., Bisschop, S. E., Bourke, T. L., van Dishoeck, E. F., and Schmalzl, M. (2012). Detection of the Simplest Sugar, Glycolaldehyde, in a Solar-type Protostar with ALMA. *ApJ* 757, L4. doi:10.1088/2041-8205/757/1/L4

Jørgensen, J. K., van der Wiel, M. H. D., Coutens, A., Lykke, J. M., Müller, H. S. P., van Dishoeck, E. F., et al. (2016). The ALMA Protostellar Interferometric Line Survey (PILS). *A&A* 595, A117. doi:10.1051/0004-6361/201628648

Li, J., Shen, Z., Wang, J., Chen, X., Li, D., Wu, Y., et al. (2017). Widespread Presence of Glycolaldehyde and Ethylene Glycol Around Sagittarius B2. *ApJ* 849, 115. doi:10.3847/1538-4357/aa9069

Li, J., Wang, J., Qiao, H., Quan, D., Fang, M., Du, F., et al. (2020). Mapping Observations of Complex Organic Molecules Around Sagittarius B2 with the ARO 12 M Telescope. *Monthly Notices R. Astronomical Soc.* 492, 556–565. doi:10.1093/mnras/stz3337

Martín, S., Martín-Pintado, J., Blanco-Sánchez, C., Rivilla, V. M., Rodríguez-Franco, A., and Rico-Villas, F. (2019). Spectral Line Identification and Modelling (SLIM) in the MAdrid Data CUBe Analysis (MADCUBA) Package. *A&A* 631, A159. doi:10.1051/0004-6361/201936144

Martín-Pintado, J., Rizzo, J. R., de Vicente, P., Rodríguez-Fernández, N. J., and Fuente, A. (2001). Large-Scale Grain Mantle Disruption in the Galactic Center. *Astrophysical J.* 548, L65–L68. doi:10.1086/318937

McGuire, B. A. (2021). *2021 Census of Interstellar, Circumstellar, Extragalactic, Protoplanetary Disk, and Exoplanetary Molecules. arXiv e-prints*arXiv:2109.13848.

McGuire, B. A., Loomis, R. A., Burkhardt, A. M., Lee, K. L. K., Shingledecker, C. N., Charnley, S. B., et al. (2021). Detection of Two Interstellar Polycyclic Aromatic

Hydrocarbons *via* Spectral Matched Filtering. *Science* 371, 1265–1269. doi:10.1126/science.abb7535

Menor Salván, C., Bouza, M., Fialho, D. M., Burcar, B. T., Fernández, F. M., and Hud, N. V. (2020). Prebiotic Origin of Pre-RNA Building Blocks in a Urea "Warm Little Pond" Scenario. *ChemBioChem* 21, 3504–3510. doi:10.1002/cbic.202000510

Patel, B. H., Percivalle, C., Ritson, D. J., Duffy, C. D., and Sutherland, J. D. (2015). Common Origins of RNA, Protein and Lipid Precursors in a Cyanosulfidic Protometabolism. *Nat. Chem* 7, 301–307. doi:10.1038/nchem.2202

Pickett, H. M., Poynter, R. L., Cohen, E. A., Delitsky, M. L., Pearson, J. C., and Müller, H. S. P. (1998). Submillimeter, Millimeter, and Microwave Spectral Line Catalog. *J. Quantitative Spectrosc. Radiative Transfer* 60, 883–890. doi:10.1016/S0022-4073(98)00091-0

Pizzarello, S., Cooper, G. W., and Flynn, G. J. (2006). *The Nature and Distribution of the Organic Material in Carbonaceous Chondrites and Interplanetary Dust Particles*, 625–652. doi:10.2307/j.ctv1v7zdmm.36

Requena-Torres, M. A., Martin-Pintado, J., Martín, S., and Morris, M. R. (2008). The Galactic Center: The Largest Oxygen-bearing Organic Molecule Repository. *ApJ* 672, 352–360. doi:10.1086/523627

Requena-Torres, M. A., Martín-Pintado, J., Rodríguez-Franco, A., Martín, S., Rodríguez-Fernández, N. J., and de Vicente, P. (2006). Organic Molecules in the Galactic center. *A&A* 455, 971–985. doi:10.1051/0004-6361:20065190

Rivilla, V. M., Jiménez-Serra, I., Martín-Pintado, J., Briones, C., Rodríguez-Almeida, L. F., Rico-Villas, F., et al. (2021). Discovery in Space of Ethanolamine, the Simplest Phospholipid Head Group. *Proc. Natl. Acad. Sci. USA* 118, e2101314118. doi:10.1073/pnas.2101314118

Rivilla, V. M., Martín-Pintado, J., Jiménez-Serra, I., Martín, S., Rodríguez-Almeida, L. F., Requena-Torres, M. A., et al. (2020). Prebiotic Precursors of the Primordial RNA World in Space: Detection of NH2OH. *ApJ* 899, L28. doi:10.3847/2041-8213/abac55

Rodríguez-Almeida, L. F., Jiménez-Serra, I., Rivilla, V. M., Martín-Pintado, J., Zeng, S., Tercero, B., et al. (2021). Thiols in the Interstellar Medium: First Detection of HC(O)SH and Confirmation of C2H5SH. *ApJL* 912, L11. doi:10.3847/2041-8213/abf7cb

Rodríguez-Fernández, N. J., Martín-Pintado, J., de Vicente, P., Fuente, A., Hüttemeister, S., Wilson, T. L., et al. (2000). Non-equilibrium H_2 Ortho-To-Para Ratio in Two Molecular Clouds of the Galactic Center. *Giant Mol. Clouds Galaxy* 356, 695–704.

Widicus Weaver, S. L., and Blake, G. A. (2005). 1,3-Dihydroxyacetone in Sagittarius B2(N-LMH): The First Interstellar Ketose. *ApJThe First Interstellar Ketose* 624, L33–L36. doi:10.1086/430407

Zeng, S., Jiménez-Serra, I., Rivilla, V. M., Martín, S., Martín-Pintado, J., Requena-Torres, M. A., et al. (2018). Complex Organic Molecules in the Galactic Centre: the N-Bearing Family. *Monthly Notices R. Astronomical Soc.* 478, 2962–2975. doi:10.1093/mnras/sty1174

Zeng, S., Jiménez-Serra, I., Rivilla, V. M., Martín-Pintado, J., Rodríguez-Almeida, L. F., Tercero, B., et al. (2021). Probing the Chemical Complexity of Amines in the ISM: Detection of Vinylamine (C2H3NH2) and Tentative Detection of Ethylamine (C2H5NH2). *ApJL* 920, L27. doi:10.3847/2041-8213/ac2c7e

Zeng, S., Quénard, D., Jiménez-Serra, I., Martín-Pintado, J., Rivilla, V. M., Testi, L., et al. (2019). First Detection of the Pre-biotic Molecule Glycolonitrile (HOCH2CN) in the Interstellar Medium. *Monthly Notices R. Astronomical Soc. Lett.* 484, L43–L48. doi:10.1093/mnrasl/slz002

Zeng, S., Zhang, Q., Jiménez-Serra, I., Tercero, B., Lu, X., Martín-Pintado, J., et al. (2020). Cloud-cloud Collision as Drivers of the Chemical Complexity in Galactic Centre Molecular Clouds. *Galactic Centre Mol. clouds* 497, 4896–4909. doi:10.1093/mnras/staa2187

Conflict of Interest: The authors declare that the research was conducted in the absence of any commercial or financial relationships that could be construed as a potential conflict of interest.

Publisher's Note: All claims expressed in this article are solely those of the authors and do not necessarily represent those of their affiliated organizations, or those of the publisher, the editors, and the reviewers. Any product that may be evaluated in this article, or claim that may be made by its manufacturer, is not guaranteed or endorsed by the publisher.

frontiers | Frontiers in Astronomy and Space Sciences

ORIGINAL RESEARCH
published: 08 July 2022
doi: 10.3389/fspas.2022.876870

Molecular Precursors of the RNA-World in Space: New Nitriles in the G+0.693–0.027 Molecular Cloud

Víctor M. Rivilla[1], Izaskun Jiménez-Serra[1], Jesús Martín-Pintado[1], Laura Colzi[1], Belén Tercero[2], Pablo de Vicente[3], Shaoshan Zeng[4], Sergio Martín[5,6], Juan García de la Concepción[1], Luca Bizzocchi[7], Mattia Melosso[7,8], Fernando Rico-Villas[1] and Miguel A. Requena-Torres[9,10]*

[1]Centro de Astrobiología (CSIC-INTA), Madrid, Spain, [2]Observatorio Astronómico Nacional (OAN-IGN), Madrid, Spain, [3]Observatorio de Yebes (OY-IGN), Guadalajara, Spain, [4]Star and Planet Formation Laboratory, Cluster for Pioneering Research, RIKEN, Saitama, Japan, [5]European Southern Observatory, ALMA Department of Science, Santiago, Chile, [6]Joint ALMA Observatory, Department of Science Operations, Santiago, Chile, [7]Department of Chemistry "Giacomo Ciamician", University of Bologna, Bologna, Italy, [8]Scuola Superiore Meridionale, Università di Napoli Federico II, Naples, Italy, [9]Department of Astronomy, University of Maryland, College Park, ND, United States, [10]Department of Physics, Astronomy and Geosciences, Towson University, Towson, MD, United States

OPEN ACCESS

Edited by:
André Canosa, UMR6251 Institut de Physique de Rennes (IPR), France

Reviewed by:
Audrey Coutens, UMR5277 Institut de recherche en astrophysique et planétologie (IRAP), France
Donghui Quan, Eastern Kentucky University, United States

***Correspondence:**
Víctor M. Rivilla
vrivilla@cab.inta-csic.es

Specialty section:
This article was submitted to Astrochemistry, a section of the journal Frontiers in Astronomy and Space Sciences

Received: *15 February 2022*
Accepted: *02 June 2022*
Published: *08 July 2022*

Citation:
Rivilla VM, Jiménez-Serra I, Martín-Pintado J, Colzi L, Tercero B, de Vicente P, Zeng S, Martín S, García de la Concepción J, Bizzocchi L, Melosso M, Rico-Villas F and Requena-Torres MA (2022) Molecular Precursors of the RNA-World in Space: New Nitriles in the G+0.693–0.027 Molecular Cloud. Front. Astron. Space Sci. 9:876870. doi: 10.3389/fspas.2022.876870

Nitriles play a key role as molecular precursors in prebiotic experiments based on the RNA-world scenario for the origin of life. These chemical compounds could have been partially delivered to the young Earth from extraterrestrial objects, stressing the importance of establishing the reservoir of nitriles in the interstellar medium. We report here the detection towards the molecular cloud G+0.693–0.027 of several nitriles, including cyanic acid (HOCN), and three C_4H_3N isomers (cyanoallene, CH_2CCHCN; propargyl cyanide, $HCCCH_2CN$; and cyanopropyne (CH_3CCCN), and the tentative detections of cyanoformaldehyde (HCOCN), and glycolonitrile ($HOCH_2CN$). We have also performed the first interstellar search of cyanoacetaldehyde ($HCOCH_2CN$), which was not detected. Based on the derived molecular abundances of the different nitriles in G+0.693–0.027 and other interstellar sources, we have discussed their formation mechanisms in the ISM. We propose that the observed HOCN abundance in G+0.693–0.027 is mainly due to surface chemistry and subsequent shock-induced desorption, while HCOCN might be mainly formed through gas-phase chemistry. In the case of $HOCH_2CN$, several grain-surface routes from abundant precursors could produce it. The derived abundances of the three C_4H_3N isomers in G+0.693–0.027 are very similar, and also similar to those previously reported in the dark cold cloud TMC-1. This suggests that the three isomers are likely formed through gas-phase chemistry from common precursors, possibly unsaturated hydrocarbons (CH_3CCH and CH_2CCH_2) that react with the cyanide radical (CN). The rich nitrile feedstock found towards G+0.693–0.027 confirms that interstellar chemistry is able to synthesize in space molecular species that could drive the prebiotic chemistry of the RNA-world.

Keywords: astrochemistry, RNA-world, prebiotic chemisitry, molecules-ISM, molecular clouds

1 INTRODUCTION

Life on Earth appeared about 3.8 billion years ago, around 700 Myr after the formation of the planet (Pearce et al., 2018), but we still do not know the mechanisms that made it possible. One of the most supported hypotheses for the origin of life is known as the RNA world (Gilbert 1986), in which RNA could have performed both metabolic and genetic roles. The process by which inert matter generated first the building blocks of RNA, ribonucleotides, and ultimately RNA itself, remains a mystery. Recent laboratory experiments mimicking prebiotic conditions have shown that ribonucleotides could be synthesized starting from simple molecules (e.g. Powner et al., 2009; Patel et al., 2015; Becker et al., 2019). A plausible origin of this prebiotic material is extraterrestrial delivery (Oró 1961; Chyba and Sagan 1992; Cooper et al., 2001) during the heavy bombardment of meteorites and comets that occurred around 3.9 billions ago (Marchi et al., 2014). These basic molecular precursors may have been already formed prior to the formation of the Solar System, in its parental molecular cloud, through the chemistry that takes place in the interstellar medium (ISM). Therefore, the study of the molecular complexity of the ISM can provide us an illustrative view of the chemical reservoir that could have contributed to feed the prebiotic chemistry on the primitive Earth, and could potentially develop similar processes in other places in the Galaxy under favourable Earth-like planetary environments.

In the last decades, and especially in the last years, astrochemistry has shown that interstellar chemistry is able to synthesize building blocks of key biomolecules. Several of the precursors of ribonucleotides spotted by the prebiotic experiments in the laboratory have been detected in the ISM, like cyanoacetylene (HC_3N, Turner 1971), cyanamide (NH_2CN, Turner et al., 1975), glycolaldehyde (CH_2OHCHO, Hollis et al. 2004, urea (NH_2CONH_2, Belloche et al. 2019), hydroxylamine (NH_2OH, Rivilla et al. 2020), and 1,2-ethenediol ($(CHOH)_2$; Rivilla et al. 2022a). Among the key simple molecular precursors required for the RNA world, numerous works have stressed the dominant role of a particular family of compounds, nitriles, which are molecules with the $C^{+}N$ moiety. This simple but highly versatile functional group offers a unique potential to build-up molecular complexity and activate efficiently the formation of ribonucleotides (Powner et al. 2009; Powner and Sutherland 2010; Patel et al. 2015; Mariani et al. 2018; Becker et al. 2019; Menor Salván et al. 2020), and also other key biomolecules such as peptides or nucleobases (Menor-Salván and Marín-Yaseli 2012; Canavelli et al. 2019; Foden et al. 2020).

With the aim of extending our knowledge on the chemistry of nitriles in the ISM, in this work we have searched for more nitriles towards the molecular cloud G+0.693-0.027 (hereafter G+0.693), including some with increasing complexity that have been proposed as important precursors of prebiotic chemistry. This cloud, located in the Sgr B2 region of the center of our Galaxy, is one of the most chemically rich sources in the ISM. Numerous nitrogen-bearing species, including nitriles, have been detected (see Zeng et al., 2018; Rivilla et al., 2019b, 2021b): cyanoacetylene (HC_3N), acetonitrile (CH_3CN), cyanamide (NH_2CN), the cyanomethyl radical (H_2CCN), cyanomethanimine (HNCHCN), and the cyanomidyl radical (HNCN). In this work we report the detection of cyanic acid (HOCN), the tentative detections of glycolonitrile ($HOCH_2CN$) and cyanoformaldehyde (HCOCN), and the first interstellar search of cyanoacetaldeyde ($HCOCH_2CN$) in the ISM, for which we provide an abundance upper limit. We have also searched for three unsaturated carbon-chain nitriles, the C_4H_3N isomers. We report the detection of cyanopropyne (CH_3CCCN), and the second detections in the ISM of cyanoallene (CH_2CCHCN) and propargyl cyanide ($HCCCH_2CN$), detected previously only towards the TMC-1 dark cloud (Lovas et al. 2006; McGuire et al. 2020; Marcelino et al. 2021). In **Section 2** we present the data of the observational survey, in **Section 3** we describe the line identification and analysis, and present the results of the line fitting, and in **Section 4** we discuss about the interstellar chemistry of the different species and their possible roles in prebiotic chemistry.

2 OBSERVATIONS

A high sensitivity spectral survey was carried out towards G+0.693. We used both IRAM 30 m telescope (Granada, Spain) and Yebes 40 m telescope (Guadalajara, Spain). The observations were centred at α(J2000.0) = $17^h47^m22^s$, and δ(J2000.0) = − 28°21′27″. The position switching mode was used in all the observations with the off position located at $\Delta\alpha$ = − 885″, $\Delta\delta$ = 290” from the source position. During the IRAM 30m observations the dual polarisation receiver EMIR was connected to the fast Fourier transform spectrometers (FFTS), which provided a channel width of 200 kHz. In this work we have used data covering the spectral windows from 71.8 to 116.7 GHz, 124.8–175.5 GHz, and 199.8 – 238.3 GHz. The spectra were smoothed to velocity resolutions of 1.0 – 2.6 km s^{-1}, depending on the frequency. The observations with the Yebes 40 m radiotelescope used the Nanocosmos Q-band (7 mm) HEMT receiver (Tercero et al., 2021). The receiver was connected to 16 FFTS providing a channel width of 38 kHz and a bandwidth of 18.5 GHz per polarisation, covering the frequency range between 31.3 and 50.6 GHz. The spectra were smoothed to a resolution of 251 kHz, corresponding to velocity resolutions of 1.5 – 2.4 km s^{-1}. The noise of the spectra depends on the frequency range, with values in antenna temperature (T_A^*) as low as 1.0 mK, while in some intervals it increases up to 4.0 – 5.0 mK, for the Yebes data, and 1.3 to 2.8 mK (71 – 90 GHz), 1.5 to 5.8 mK (90 – 115 GHz), ~10 mK (115 – 116 GHz), 3.1 to 6.8 mK (124 – 175 GHz), and 4.5 to 10.6 mK (199 – 238 GHz), for the IRAM 30m data. The line intensity of the spectra was measured in units of T_A^* as the molecular emission toward G+0.693 is extended over the beam (Requena-Torres et al., 2006, 2008; Zeng et al., 2018, 2020).

3 ANALYSIS AND RESULTS

Figure 1 shows the nitriles analysed in this work, which include four oxygen-bearing nitriles: cyanic acid (HOCN), cyanoformaldehyde (or formyl cyanide, HCOCN), glycolonitrile (or 2-

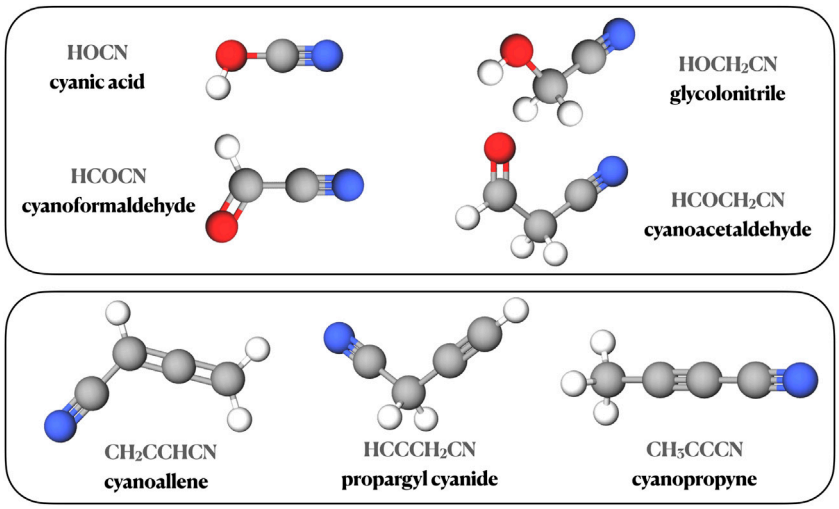

FIGURE 1 | Three-dimensional representation of the oxygen-bearing nitriles (upper panel) and the three C_4H_3N isomers (lower panel) analysed in this work. White, gray, red, and blue corresponds to hydrogen, carbon, oxygen and nitrogen atoms, respectively.

TABLE 1 | Spectroscopy of the molecules analysed in this work.

Molecule	Catalog	Entry	Date	Line List ref	Dipole Moment ref
HOCN	CDMS	43510	May 2009	Brünken et al. (2009)	Brünken et al. (2009)
HCOCN	CDMS	55501	June 2006	Bogey et al. (1995)	Császár (1989)
$HOCH_2CN$	CDMS	57512	March 2017	Margulès et al. (2017)	Margulès et al. (2017)
$HCOCH_2CN$	MADCUBA	–	January 2022	Møllendal et al. (2012)	Møllendal et al. (2012)
$HCCCH_2CN$	CDMS	65514	September 2020	Demaison et al. (1985) McGuire et al. (2020)	Demaison et al. (1985)
CH_2CCHCN	CDMS	65506	March 2006	Bouchy et al. (1973) Schwahn et al. (1986)	Bouchy et al. (1973)
CH_3CCCN	CDMS	65503	April 2004	Moïses et al. (1982) Bester et al. (1983)	Bester et al. (1984)

The molecular catalog, number and date of the entry, and the references for the line lists and dipole moments are listed.

hydroxyacetonitrile, $HCOCH_2CN$), cyanoacetaldehyde (or 3-oxopropanenitrile, $HCOCH_2CN$); and three C_4H_3N isomers: cyanoallene (or 2,3-butadienenitrile, CH_2CCHCN), propargyl cyanide (or 3-butynenitrile, $HCCCH_2CN$), and cyanopropyne (or 2-butynenitrile, CH_3CCCN). The identification and fitting of the molecular lines were performed using the SLIM (Spectral Line Identification and Modeling) tool within the MADCUBA package[1] (version 09/11/2021; Martín et al., 2019). SLIM generates synthetic spectra under the assumption of Local Thermodynamic Equilibrium (LTE), using the spectroscopy provided by laboratory experiments assisted by theoretical calculations. **Table 1** lists the spectroscopic references of all the molecules analysed. We have used entries from the Cologne Database for Molecular Spectroscopy (CDMS, Endres et al. 2016), which are based on the laboratory works and theoretical calculations indicated in **Table 1**. Moreover, we implemented into MADCUBA the spectroscopy of $HCOCH_2CN$ from Møllendal et al. (2012).

To evaluate if the molecular transitions of interest are blended with emission from other species, we have also considered the LTE model that includes the total contribution of all the species that have been identified so far towards G+0.693 (e.g., Requena-Torres et al., 2008; Zeng et al., 2018; Rivilla et al., 2019a, 2020; Jiménez-Serra et al., 2020; Rivilla et al., 2021a,b; Zeng et al., 2021; Rodríguez-Almeida et al., 2021a,b; Rivilla et al., 2022a,b). To derive the physical parameters of the molecular emission, we used the AUTOFIT tool of SLIM, which finds the best agreement between the observed spectra and the predicted LTE model, and provides the best solution for the parameters, and their associated uncertainties (see

[1]Madrid Data Cube Analysis on ImageJ is a software developed at the Center of Astrobiology (CAB) in Madrid; https://cab.inta-csic.es/madcuba/.

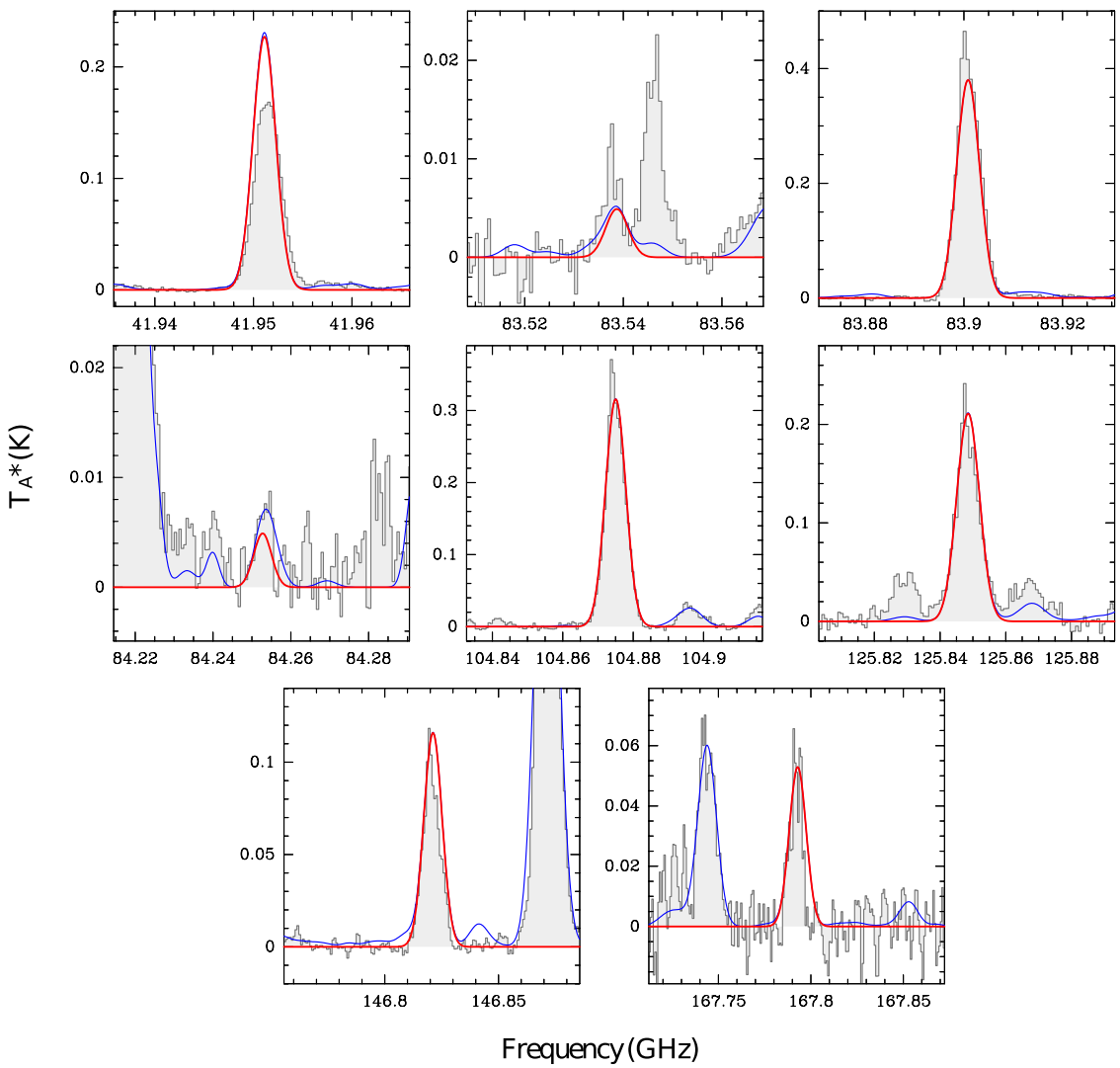

FIGURE 2 | Selected cyanic acid (HOCN) transitions (see **Table 2**) detected towards the G+0.693 molecular cloud. The best LTE fit derived with MADCUBA for the HOCN emission is shown with a red curve, while the blue curve shows the total emission considering all the species identified towards this molecular cloud. The y-axis shows the line intensity in antenna temperature scale (T_A^*) in Kelvin, and the x-axis shows the frequency in GHz.

details of the formalism used in Martín et al., 2019). The free parameters of the model are: molecular column density (N), excitation temperature (T_{ex}), linewidth (or full width at half maximum, FWHM), and velocity (v_{LSR}). We have left these four parameters free whenever possible, providing their associated uncertainties. For the cases in which the algorithm used by AUTOFIT does not converge, we have fixed some of them to allow the algorithm to converge. In the following, we present the analysis of the different molecules studied. For each species, we have applied AUTOFIT using unblended transitions and transitions that, while partially blended with other species already identified in G+0.693, properly reproduces the observed spectra. We note that for all molecules the transitions that are not shown are consistent with the observed spectra, but they are heavily blended with lines from other molecular species or they are too weak to be detected, according to the line intensities predicted by the LTE model.

3.1 Oxygen-Bearing Nitriles

3.1.1 Cyanic Acid (HOCN) and Cyanoformaldehyde (HCOCN)

HOCN was already reported towards G+0.693 by Brünken et al. (2010) (their source Sgr B2 (20,100)[2]), and also by Zeng et al. (2018) using in both cases less sensitive observations. We provide here a new analysis using deeper observations. We have detected six transitions of this species that are completely unblended, which

[2]The position of this source is offset in (α, δ) by (20″, 100″) with respect to that of Sgr B2(M), see Brünken et al. (2010).

TABLE 2 | List of detected transitions of the oxygen-bearing nitriles analysed in this work. We indicate the frequency, quantum numbers, logarithm of the Einstein coefficient (A_{ul}), energy of the upper levels of each transition (E_u), and information about the possible blending by other identified or unidentified (U) species towards G +0.693.

Molecule	Frequency (GHz)	Transition J_{K_a,K_c}	logA_{ul} (s^{-1})	E_u (K)	Blending
HOCN	41.9508371	$2_{0,2} - 1_{0,1}$	−5.3239	3.0	unblended
HOCN	83.5383960	$4_{1,4} - 3_{1,3}$	−4.4087	42.2	blended with U
HOCN	83.9005702[a]	$4_{0,4} - 3_{0,3}$	−4.3750	10.1	unblended
HOCN	84.2524547	$4_{1,3} - 3_{1,2}$	−4.3976	42.3	blended with $HCCCH_2CN$
HOCN	104.8746777[a]	$5_{0,5} - 4_{0,4}$	−4.0746	15.1	unblended
HOCN	125.8480951	$6_{0,6} - 5_{0,5}$	−3.8304	21.1	unblended
HOCN	146.8206846[a]	$7_{0,7} - 6_{0,6}$	−3.6248	28.1	unblended
HOCN	167.7923140[b]	$8_{0,8} - 7_{0,7}$	−3.4472	36.2	unblended
HCOCN	72.1192555	$1_{1,1} - 0_{0,0}$	−5.0767	3.5	blended
HCOCN	81.433113	$2_{1,2} - 1_{0,1}$	−4.9642	4.4	blended with $NH_2CH_2CH_2OH$
HCOCN	90.5710141	$3_{1,3} - 2_{0,2}$	−4.8461	5.7	unblended
HCOCN	99.5348108	$4_{1,4} - 3_{0,3}$	−4.7342	7.6	unblended
HCOCN	108.3274964	$5_{1,5} - 4_{0,4}$	−4.6301	9.8	part. blended with HCCO and U
HCOCN	207.3132961	$2_{2,0} - 1_{1,1}$	−3.7478	13.4	blended with U
$HOCH_2CN$	35.934379	$4_{1,4} - 3_{1,3}$	−5.8654	5.7	unblended
$HOCH_2CN$	37.781601	$4_{1,3} - 3_{1,2}$	−5.8001	5.9	blended with c-C_2H_4O and U
$HOCH_2CN$	44.907438	$5_{1,5} - 4_{1,4}$	−5.5549	7.9	blended with *t* – HCOOH
$HOCH_2CN$	45.975528	$5_{0,5} - 4_{0,4}$	−5.5069	6.6	unblended
$HOCH_2CN$	75.463333	$8_{1,7} - 7_{1,6}$	−4.8528	17.7	blended with *s*-C_2H_5CHO

[a]*Transition detected in Zeng et al. (2018).*
[b]*Transition tentatively detected in Zeng et al. (2018).*

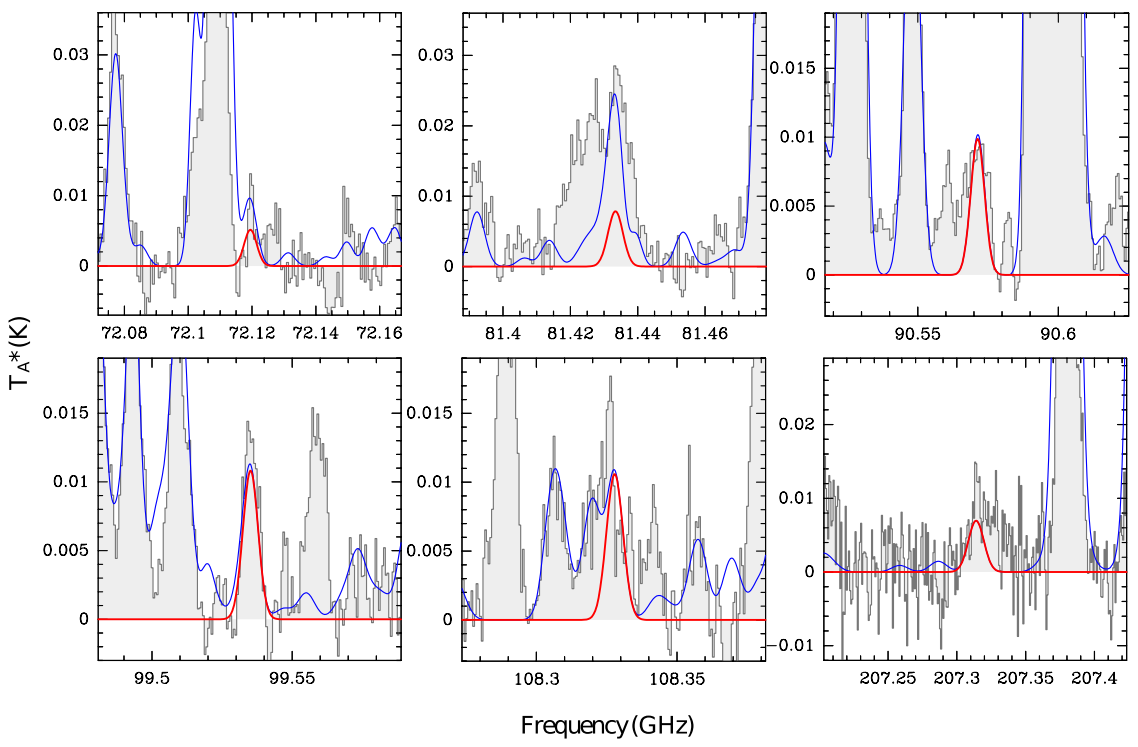

FIGURE 3 | Selected cyanoformaldehyde (HCOCN) transitions (see **Table 2**) detected towards the G+0.693 molecular cloud. The best LTE fit derived with MADCUBA for the HCOCN emission is shown with a red curve, while the blue curve shows the total emission considering all the species identified towards this molecular cloud. The y-axis shows the line intensity in antenna temperature scale (T_A^*) in Kelvin, and the x-axis shows the frequency in GHz.

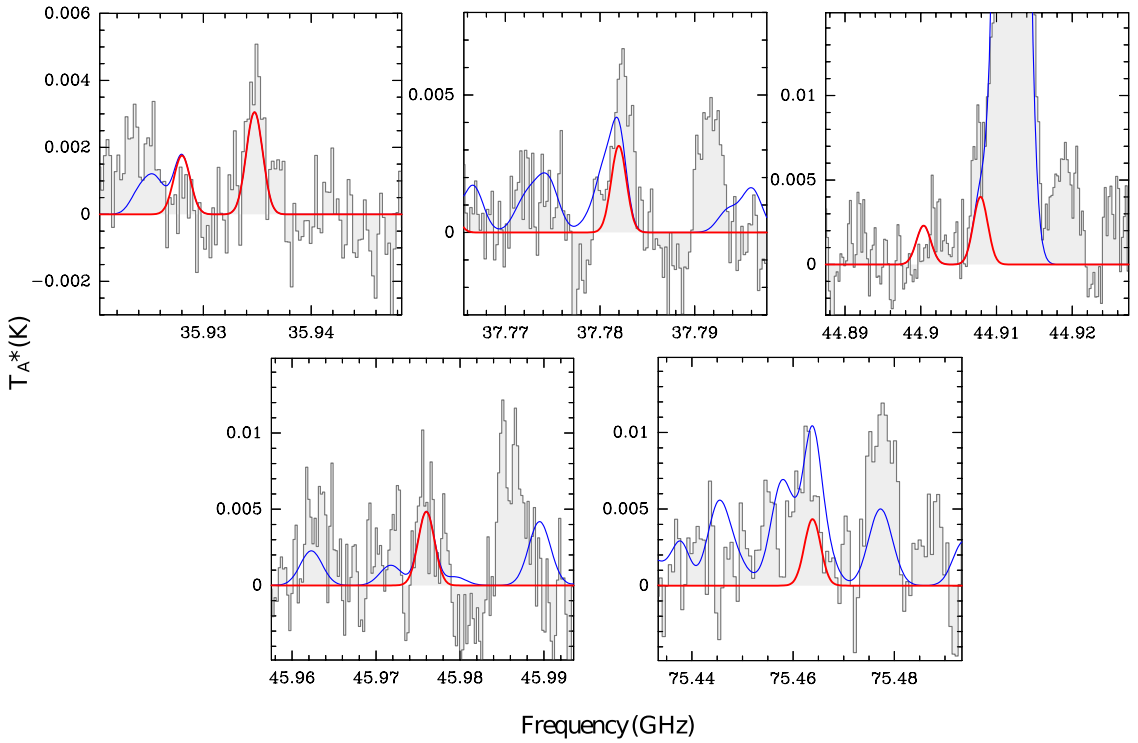

FIGURE 4 | Selected transitions of glycolonitrile ($HOCH_2CN$; see **Table 2**) detected towards the G+0.693 molecular cloud. The best LTE fit derived with MADCUBA for the $HOCH_2CN$ emission is shown with a red curve, while the blue curve shows the total emission considering all the species identified towards this molecular cloud. The y-axis shows the line intensity in antenna temperature scale (T_A^*) in Kelvin, and the x-axis shows the frequency in GHz.

are shown in **Figure 2**, and listed in **Table 2**. These transitions include the three transitions identified by Zeng et al. (2018), the confirmation of the $8_{0,8} - 7_{0,7}$ transition tentatively detected in that work (see their Figure B15), and two new transitions (**Table 2**). The best LTE fit derived by MADCUBA, where all parameters were left free, is shown in **Figure 2**, and the derived physical parameters are presented in **Table 4**. We obtained a column density of $(2.13\pm 0.04) \times 10^{13}$ cm^{-2} (**Table 4**), which translates into a molecular abundance with respect to molecular hydrogen of 1.6×10^{-10}, using $N(H_2) = 1.35 \times 10^{23}$ cm^{-2} from Martín et al. (2008). The results are consistent, within the uncertainties, with those derived by Zeng et al. (2018).

We also report here the first tentative detection of HCOCN towards G+0.693. **Figure 3** shows that the $3_{1,3} - 2_{0,2}$ (90.5710141 GHz) and $4_{1,4} - 3_{0,3}$ (99.5348108 GHz) transitions are unblended, while other transitions are partially blended with other species (**Table 2**). To perform the fit, we fixed T_{ex}, FWHM, and v_{LSR} to the ones derived from HOCN. We obtained a column density of $(0.76\pm 0.11) \times 10^{13}$ cm^{-2}, almost one order of magnitude lower than the upper limit reported by Zeng et al. (2018) of $< 6 \times 10^{13}$ cm^{-2} towards G+0.693. The derived molecular abundance is 6×10^{-11}, which is very similar to that found in the TMC-1 dark cloud by Cernicharo et al. (2021). The HOCN/HCOCN ratio is ~2.8.

3.1.2 Glycolonitrile ($HOCH_2CN$)

This species is also tentatively detected towards G+0.693. We show in **Figure 4** two molecular transitions of $HOCH_2CN$ that are unblended (**Table 2**), and those partially blended with other species already identified in this cloud. To perform the fit, we fixed T_{ex} and FWHM to the ones derived for HOCN, and used $v_{LSR} = 67$ km s^{-1}, which best reproduces the velocity of the two unblended transitions. We obtained a column density of $(0.8\pm 0.2) \times 10^{13}$ cm^{-2} (**Table 4**), and a molecular abundance of 6×10^{-11}, very similar to that of HOCN.

3.1.3 Cyanoacetaldehyde ($HCOCH_2CN$)

This molecule is not currently included in any of the commonly used molecular databases such as CDMS or the Jet Propulsion Laboratory catalog (JPL; Pickett et al., 1998). The conformational energy landscape of $HCOCH_2CN$ and the effects of the large amplitude motions on its rotational spectrum have been described in detail by Møllendal et al. (2012). We have used the spectroscopic information provided in this work to implement it into MADCUBA. The most stable rotamer (referred to as species I in the cited reference) possesses two equivalent positions in the electronic energy potential function for rotation about its C_1–C_2 bond (see **Figure 1** of Møllendal et al., 2012). They are separated by a barrier of 0.84 kJ mol^{-1} (computed at MP2 level) at the exact antiperiplanar conformation. Large amplitude vibrations and tunneling for the torsion about the C_1–C_2 bond leads to the existence of two closely spaced energy levels for the ground state labelled with a plus sign (+) for the lowest-energy level and with a minus sign (−) for the higher-energy level. These two states are separated

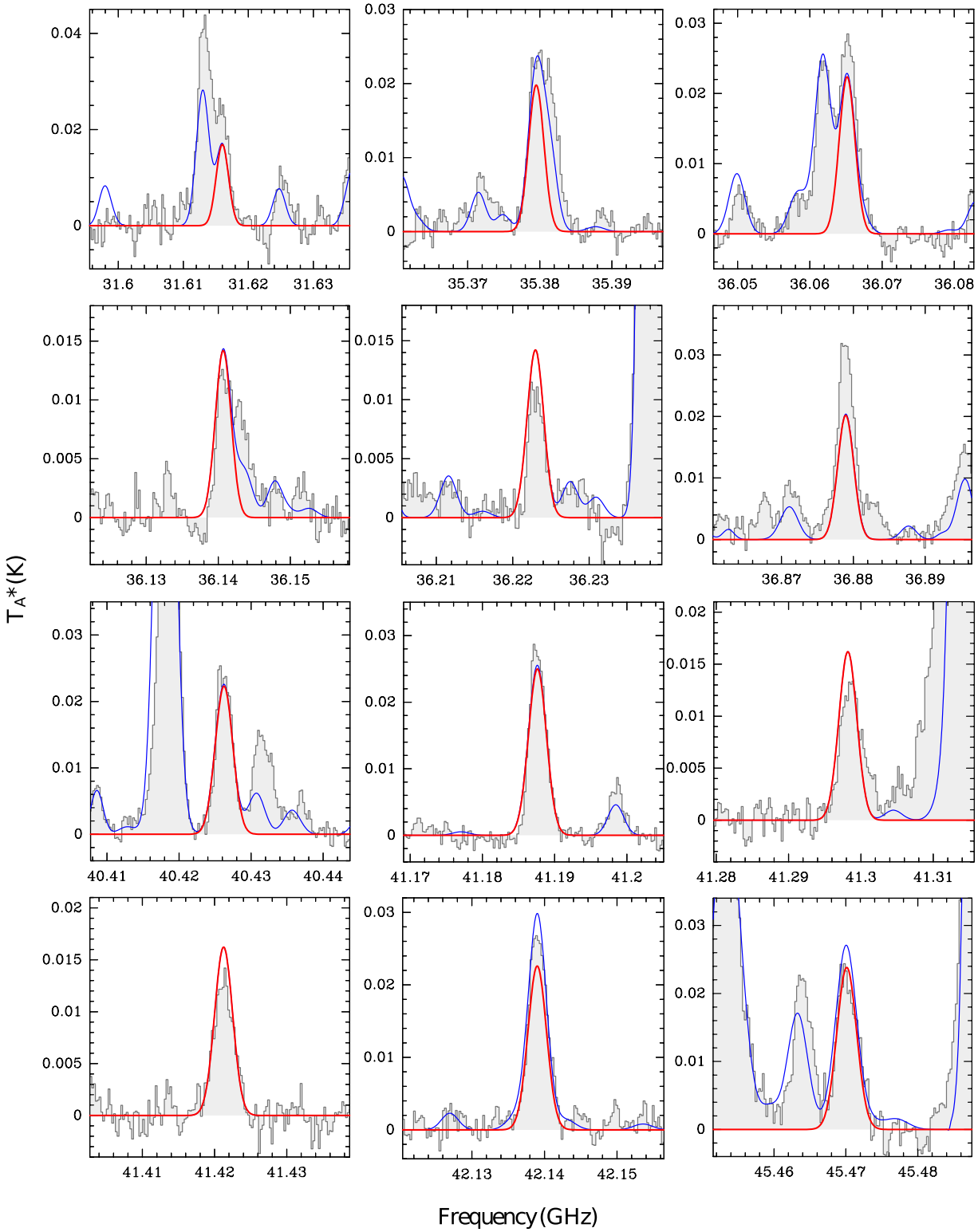

FIGURE 5 | (continued).

by an energy difference $\Delta E/h$ of ~58.8 GHz. For the present spectral calculation we have reanalysed the rotational transitions reported by Møllendal et al. (2012) using the same set of spectroscopic parameters employed in their fit 1 (see their

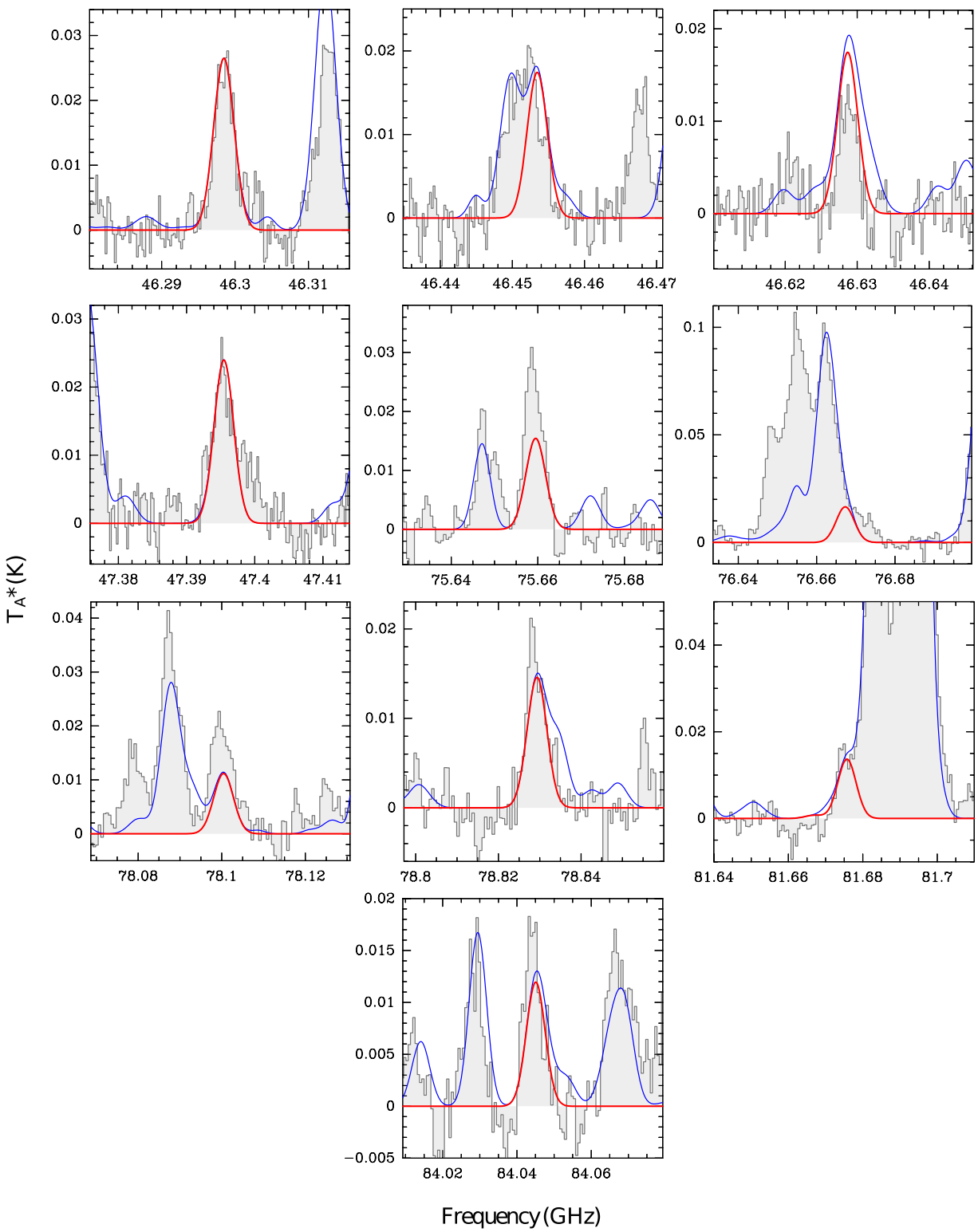

FIGURE 5 | Selected transitions of cyanoallene (CH_2CCHCN; see **Table 3**) detected towards the G+0.693 molecular cloud. The best LTE fit derived with MADCUBA for the CH_2CCHCN emission is shown with a red curve, while the blue curve shows the total emission considering all the species identified towards this molecular cloud. The y-axis shows the line intensity in antenna temperature scale (T_A^*) in Kelvin, and the x-axis shows the frequency in GHz.

TABLE 3 | List of observed transitions of the C_4H_3N isomers analysed in this work. We indicate the frequency, quantum numbers, Einstein coefficient (A_{ul}), energy of the upper levels of each transition (E_u), and information about the possible blending by other identified or unidentified (U) species towards G +0.693.

Molecule	Frequency (GHz)	Transition[a]	logA_{ul} (s^{-1})	E_u (K)	Blending
CH_2CCHCN	31.6156000	$6_{1,5} - 5_{1,4}$	−5.5633	6.4	blended with *aGg′*-$(CH_2OH)_2$
CH_2CCHCN	35.3790500	$7_{1,7} - 6_{1,6}$	−5.4086	7.9	blended with CH_3COCH_3
CH_2CCHCN	36.0646889	$7_{0,7} - 6_{0,6}$	−5.3748	6.9	unblended
CH_2CCHCN	36.1402200	$7_{2,6} - 6_{2,5}$	−5.4089	11.4	unblended
CH_2CCHCN	36.2225000	$7_{2,5} - 6_{2,4}$	−5.4059	11.4	unblended
CH_2CCHCN	36.8784700	$7_{1,6} - 6_{1,5}$	−5.3546	8.2	blended with U
CH_2CCHCN	40.4257132	$8_{1,8} - 7_{1,7}$	−5.2292	9.9	unblended
CH_2CCHCN	41.1870836	$8_{0,8} - 7_{0,7}$	−5.1981	8.9	unblended
CH_2CCHCN	41.2976561	$8_{2,7} - 7_{2,6}$	−5.2225	13.4	unblended
CH_2CCHCN	41.4207138	$8_{2,6} - 7_{2,5}$	−5.2187	13.4	unblended
CH_2CCHCN	42.1384521	$8_{1,7} - 7_{1,6}$	−5.1751	10.2	blended with c-C_3H_2
CH_2CCHCN	45.4695206	$9_{1,9} - 8_{1,8}$	−5.0716	12.0	blended with CH_3NHCHO
CH_2CCHCN	46.2978836	$9_{0,9} - 8_{0,8}$	−5.0429	11.1	unblended
CH_2CCHCN	46.4528399	$9_{2,8} - 8_{2,7}$	−5.0603	15.6	blended with CH_3CONH_2
CH_2CCHCN	46.6280696	$9_{2,7} - 8_{2,6}$	−5.0555	15.7	blended with HC_2CHO
CH_2CCHCN	47.3948488	$9_{1,8} - 8_{1,7}$	−5.0176	12.5	unblended
CH_2CCHCN	75.6463060	$7_{3,4} - 8_{2,7}$	−6.2551	17.0	blended with U
CH_2CCHCN	75.6587572	$15_{1,15} - 14_{1,14}$	−4.3956	30.2	blended with U
CH_2CCHCN	76.6665519	$15_{0,15} - 14_{0,14}$	−4.3767	29.6	blended with C_2H_5OH
CH_2CCHCN	78.0996741	$15_{2,13} - 14_{2,12}$	−4.3600	34.4	blended with U
CH_2CCHCN	78.8285795	$15_{1,14} - 14_{1,13}$	−4.3421	31.4	blended with CH_3COOH
CH_2CCHCN	81.674936	$16_{0,16} - 15_{0,15}$	−4.2935	33.5	blended with C_2H_5OH
CH_2CCHCN	84.0442448	$16_{1,15} - 15_{1,14}$	−4.2576	35.5	unblended
$HCCCH_2CN$	31.8489874	$6_{1,6} - 5_{1,5}$	−5.2773	6.2	unblended
$HCCCH_2CN$	33.8637212	$6_{1,5} - 5_{1,4}$	−5.1974	6.5	unblended
$HCCCH_2CN$	37.1392132	$7_{1,7} - 6_{1,6}$	−5.0691	8.0	unblended
$HCCCH_2CN$	38.1027037	$7_{0,7} - 6_{0,6}$	−5.0271	7.3	unblended
$HCCCH_2CN$	38.3423461	$7_{2,6} - 6_{2,5}$	−5.0555	10.6	unblended
$HCCCH_2CN$	38.6167091	$7_{2,5} - 6_{2,4}$	−5.0461	10.7	unblended
$HCCCH_2CN$	39.4865865	$7_{1,6} - 6_{1,5}$	−4.9892	8.4	unblended
$HCCCH_2CN$	42.0111351	$5_{1,5} - 4_{0,4}$	−5.4001	4.6	blended with n-C_3H_7CN
$HCCCH_2CN$	42.4217854	$8_{1,8} - 7_{1,7}$	−4.8900	10.0	unblended
$HCCCH_2CN$	43.8024266	$8_{2,7} - 7_{2,6}$	−4.8695	12.7	blended with HNCO
$HCCCH_2CN$	44.2102030	$8_{2,6} - 7_{2,5}$	−4.8574	12.8	unblended
$HCCCH_2CN$	45.0990808	$8_{1,7} - 7_{1,6}$	−4.8103	10.6	unblended
CH_3C_3N	33.0513004	$8_1 - 7_1$	−5.3573	14.6	unblended
CH_3C_3N	33.0516190	$8_0 - 7_0$	−5.3505	7.1	
CH_3C_3N	37.1826557	$9_1 - 8_1$	−5.1995	16.4	blended with CH_3OCHO
CH_3C_3N	37.1830142	$9_0 - 8_0$	−5.1942	8.9	
CH_3C_3N	41.3139909	$10_1 - 9_1$	−5.0590	18.4	blended with *aGg′*-$(CH_2OH)_2$
CH_3C_3N	41.3143891	$10_0 - 9_0$	−5.0546	10.9	
CH_3C_3N	45.4453036	$11_1 - 10_1$	−4.9321	20.6	unblended
CH_3C_3N	45.4457416	$11_0 - 10_0$	−4.9286	13.1	
CH_3C_3N	49.5765916	$12_1 - 11_1$	−4.8166	23.0	unblended
CH_3C_3N	49.5770694	$12_0 - 11_0$	−4.8136	15.5	
CH_3C_3N	74.3636580	$18_1 - 17_1$	−4.2809	41.4	unblended
CH_3C_3N	74.3643850	$18_0 - 17_0$	−4.2795	33.9	
CH_3C_3N	82.6257600	$20_1 - 19_1$	−4.1422	49.1	blended with *s*-C_2H_5CHO
CH_3C_3N	82.6265180	$20_0 - 19_0$	−4.1411	41.6	
CH_3C_3N	86.756698	$21_1 - 20_1$	−4.0780	53.3	blended with $H^{13}CO^+$
CH_3C_3N	86.757524	$21_0 - 20_0$	−4.0770	45.8	
CH_3C_3N	90.8876208	$22_1 - 21_1$	−4.0169	57.7	blended with CH_3COCH_3
CH_3C_3N	90.8884956	$22_0 - 21_0$	−4.0159	50.2	
CH_3C_3N	95.0184892	$23_1 - 22_1$	−3.9584	62.2	unblended
CH_3C_3N	95.0194037	$23_0 - 22_0$	−3.9576	54.7	
CH_3C_3N	99.1493060	$24_1 - 23_1$	−3.9026	67.0	unblended
CH_3C_3N	99.1502601	$24_0 - 23_0$	−3.9017	59.5	
CH_3C_3N	103.280069	$25_1 - 24_1$	−3.8490	71.9	unblended
CH_3C_3N	103.2810626	$25_0 - 24_0$	−3.8482	64.4	
CH_3C_3N	107.4107758	$26_1 - 25_1$	−3.7975	77.1	blended with CH_3CONH_2
CH_3C_3N	107.4118089	$26_0 - 25_0$	−3.7968	69.6	

[a]*The format of the quantum numbers is J_{K_a,K_c} for $HCCCH_2CN$ and CH_2CCHCN (asymmetric rotors), and J_K for CH_3C_3N (symmetric top molecule).*

TABLE 4 | Derived physical parameters of the nitriles towards G+0.693 analysed in this work using MADCUBA, along with their associated uncertainties. The fixed parameters used in the fit are shown without associated uncertainties (see text).

Molecule	N^a (× 10^{13} cm^{-2})	T_{ex} (K)	v_{LSR} (km s^{-1})	FWHM (km s^{-1})	Abundance^b (×10^{-10})
HOCN	2.13±0.04	7.4±0.2	68.0±0.2	19.2±0.3	1.6
HCOCN	0.76±0.11	7.4	68	19.2	0.6
$HOCH_2CN$	0.8±0.2	7.4	67	19.2	0.6
$HCOCH_2CN$	< 3.6	7.4	67	19.2	< 2.7
CH_2CCHCN	2.34±0.06	12.1±0.5	66.1±0.3	21.3±0.7	1.7
$HCCCH_2CN$	1.77±0.08	12.1	67.0±0.6	21.3	1.3
CH_3CCCN	1.35±0.03	18.6±1.0	68	21.3	1.0

[a]*The uncertainties of the column densities are derived by the AUTOFIT algorithm implemented in MADCUBA (see Martín et al., 2019 for details), and do not contain calibrations errors, which are expected to be ~ 10%.*
[b]*We adopted N(H_2) = 1.35 × 10^{23} cm^{-2}, from Martín et al. (2008).*

Table 4). The rest-frequencies have then been computed in the J = 0–70 interval with $K_{a\ max}$ = 50. Theoretical values of dipole moments μ_a = 0.932 D, μ_b = 1.574 D, and μ_c = 1.274 D, computed at CCSD level (Møllendal et al., 2012) have been employed. All the calculations have been performed with the CALPGM suite of programs Pickett (1991).

This species is not detected towards G+0.693. We have derived an upper limit for its abundance using the brightest transition according to the LTE model that are unblended, namely the $6_{2,5}$–$5_{1,4}$ transition at 101.598576 GHz. MADCUBA calculates the upper limit of the column density using the 3σ value of the integrated intensity (see details in Martín et al., 2019). We have used the same T_{ex}, FWHM, and v_{LSR} used for $HOCH_2CN$. We obtained an upper limit of the $HCOCH_2CN$ abundance of $< 2.7 \times 10^{-10}$ (**Table 4**).

3.2 C_4H_3N Isomers

We report in this section the first detection towards G+0.693 of cyanoallene (CH_2CCHCN), propargyl cyanide ($HCCCH_2CN$), and cyanopropyne (CH_3CCCN).

3.2.1 Cyanoallene (CH_2CCHCN)

Figure 5 shows the molecular transitions of CH_2CCHCN that are unblended, or only slightly blended with other species already identified in this source, whose spectroscopic information is presented in **Table 3**. The G+0.693 cloud is the second interstellar source where CH_2CCHCN has been detected, after the cold cloud TMC-1 (Lovas et al., 2006; Marcelino et al., 2021). We left N, T_{ex}, FWHM, and v_{LSR} as free parameters, and obtained a column density of (2.34± 0.06) × 10^{13} cm^{-2}, and a molecular abundance of 1.7 × 10^{-10} (**Table 4**).

3.2.2 Propargyl Cyanide ($HCCCH_2CN$)

Figure 6 shows the molecular transitions of $HCCCH_2CN$ that are unblended, or only slightly blended with other species already identified in this cloud, whose spectroscopic information is presented in **Table 3**. As in the case of its isomer CH_2CCHCN, G+0.693 is the second interstellar source where $HCCCH_2CN$ has been detected, after the cold cloud TMC-1 (McGuire et al., 2020; Marcelino et al., 2021). We fixed T_{ex} and FWHM to the values obtained for CH_2CCHCN, and left N and v_{LSR} free. We obtained a column density of (1.77± 0.08) × 10^{13} cm^{-2}, and a molecular abundance of 1.3 × 10^{-10}. The $CH_2CCHCN/HCCCH_2CN$ ratio is ~ 1.3.

3.2.3 Cyanopropyne (CH_3CCCN)

Figure 7 shows the spectra of multiple unblended or slightly blended transitions of CH_3CCCN (listed in **Table 3**). Unlike its isomers, which are asymmetric molecules, CH_3CCCN is a symmetric top molecule. For the analysis, we have used the lowest energy K = 0 and K = 1 transitions (see **Table 3**), which are the ones that dominate the line emission in a source with low T_{ex} like G+0.693 (5 – 20 K; see e.g. Zeng et al., 2018). We fixed the FWHM and v_{LSR} to the values derived for CH_2CCHCN, leaving N and T_{ex} as free parameters. We obtained a column density of (1.35± 0.03) × 10^{13} cm^{-2} (**Table 4**), and a molecular abundance of 1.0 × 10^{-10}. The isomeric ratios of CH_2CCHCN/CH_3CCCN and $HCCCH_2CN/CH_3CCCN$ are ~1.8 and ~1.3, respectively.

4 DISCUSSION

4.1 Interstellar Chemistry

4.1.1 Oxygen-Bearing Nitriles

We show in **Figure 8** the molecular abundances of the O-bearing nitriles detected towards G+0.693 studied in this work. The relative ratio of the detected species HOCN:HCOCN: $HOCH_2CN$ is 2.8:1:1. By extrapolating the hydroxy/aldehyde (OH/HCO) ratio of HOCN/HCOCN to $HOCH_2CN$/ $HCOCH_2CN$, one should expect an abundance of 0.15 × 10^{-10} for $HCOCH_2CN$, more than one order of magnitude lower than the upper limit derived from current observations (< 2.7 × 10^{-10}, see **Table 4**). This suggests that deeper observations reaching higher sensitivity will be needed to address the detection of this species.

In the following, we discuss possible formation routes of the different O-bearing nitriles, combining the results obtained in G+0.693 and in other interstellar sources with theoretical and experimental works:

- HOCN: besides G+0.693, this species was detected previously towards several other positions of the Sgr B2 region in the Galactic Center (Brünken et al., 2009; Brünken et al., 2010),

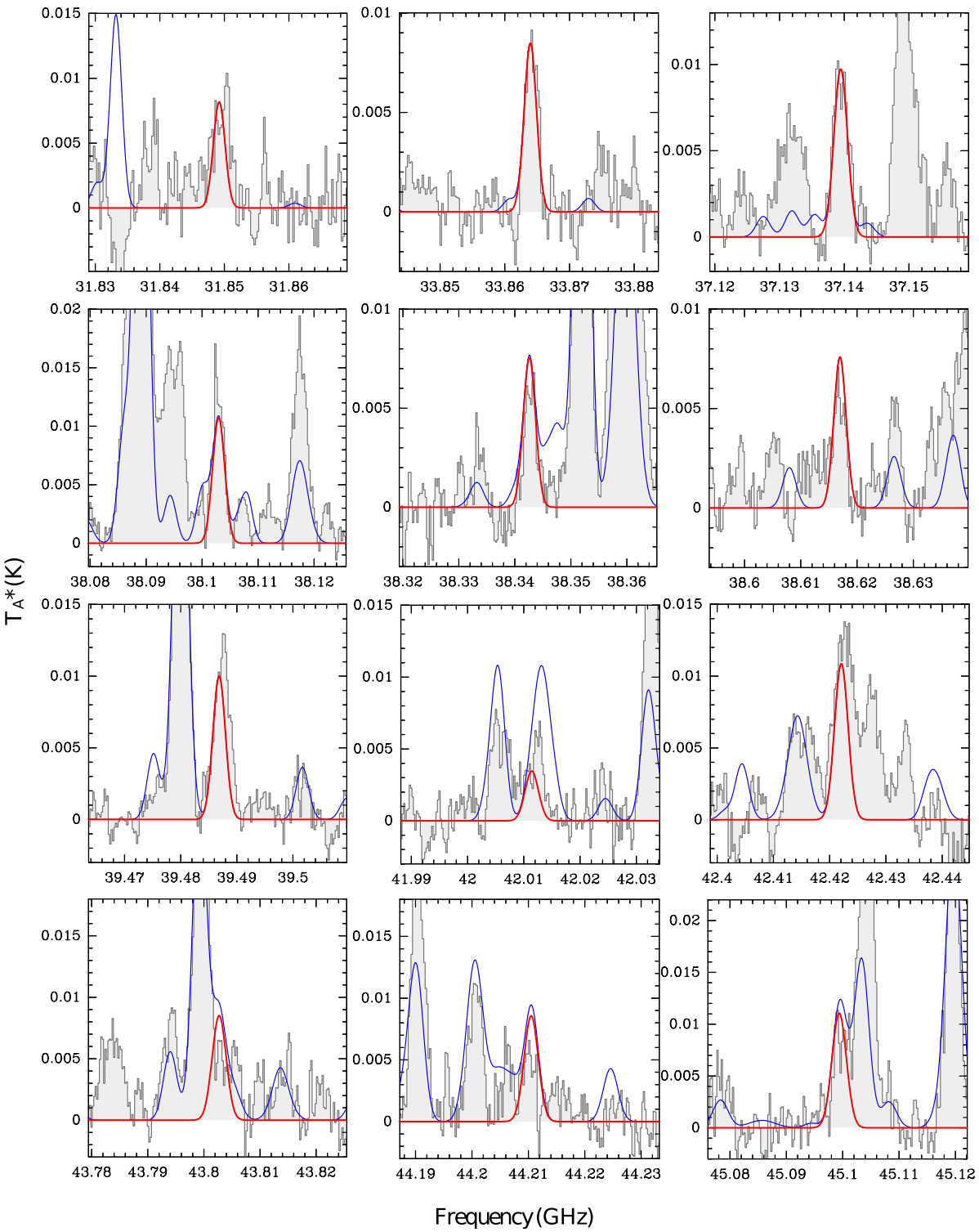

FIGURE 6 | Selected transitions of propargyl cyanide ($HCCCH_2CN$; see **Table 3**) detected towards the G+0.693 molecular cloud. The best LTE fit derived with MADCUBA for the $HCCCH_2CN$ emission is shown with a red curve, while the blue curve shows the total emission considering all the species identified towards this molecular cloud. The y-axis shows the line intensity in antenna temperature scale (T_A^*) in Kelvin, and the x-axis shows the frequency in GHz.

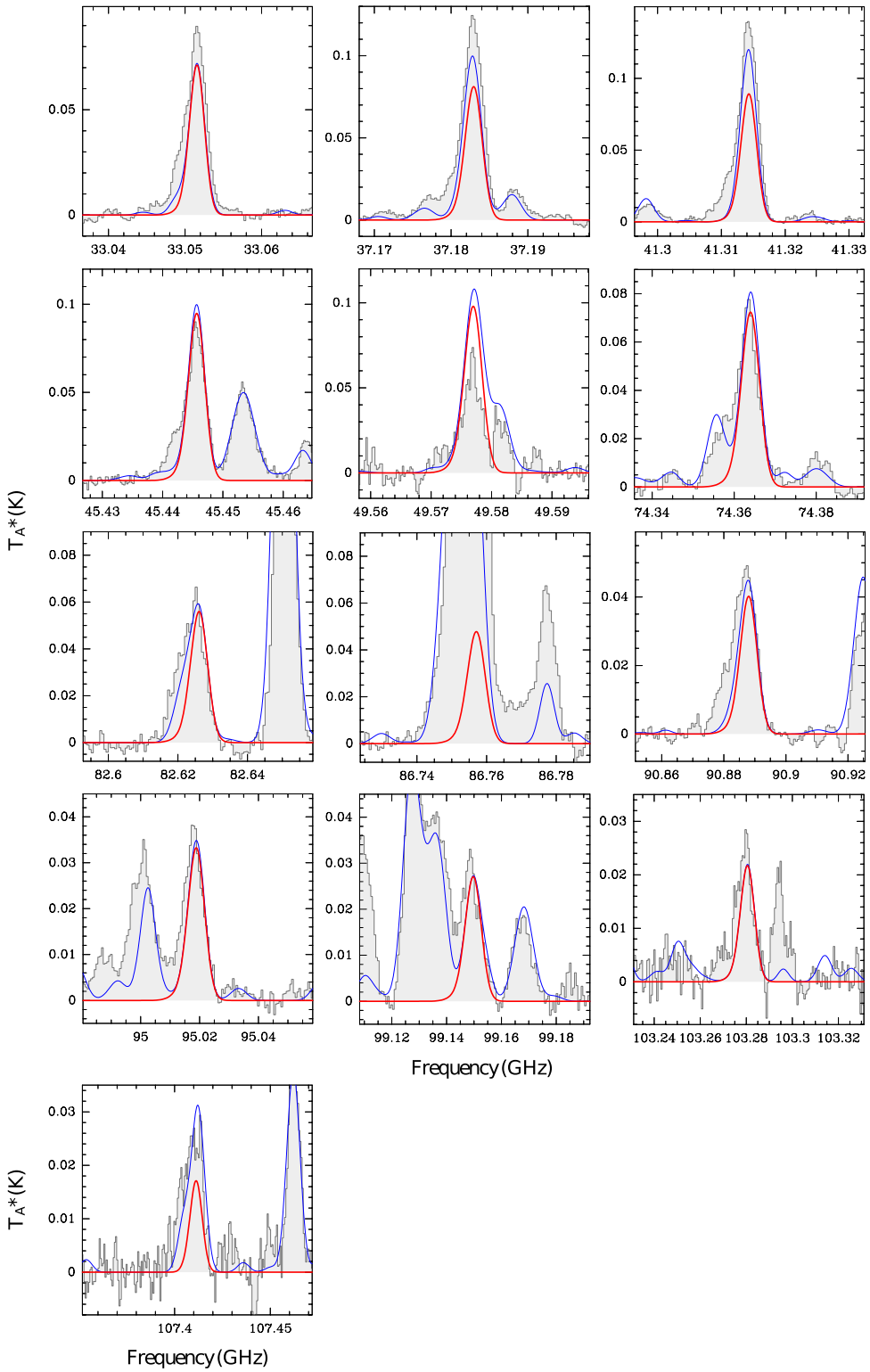

FIGURE 7 | Selected transitions of cyanopropyne (CH_3CCCN; see **Table 3**) detected towards the G+0.693 molecular cloud. The best LTE fit derived with MADCUBA for the CH_3CCCN emission is shown with a red curve, while the blue curve shows the total emission considering all the species identified towards this molecular cloud. The y-axis shows the line intensity in antenna temperature scale (T_A^*) in Kelvin, and the x-axis shows the frequency in GHz.

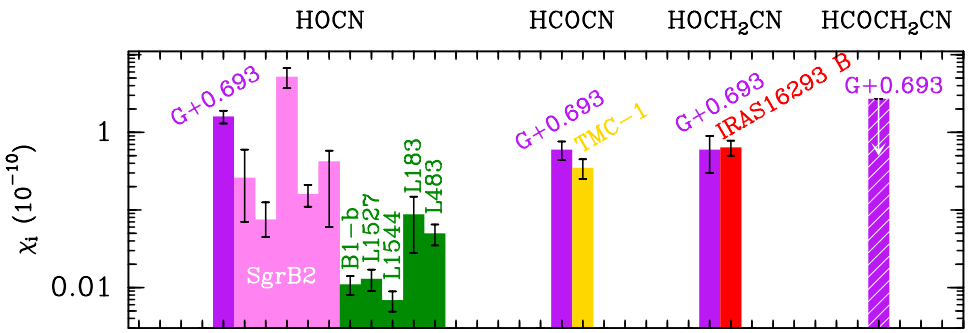

FIGURE 8 | Molecular abundances with respect to H_2 of the oxygen-bearing nitriles studied in this work derived in different interstellar sources. Purple bars correspond to G+0.693 (this work; see **Table 4**), with the $HCOCH_2CN$ value indicating an upper limit. We compare with other sources: several positions also in the Sgr B2 region (magenta; Brünken et al., 2010, see also Marcelino et al., 2010); several dense cores (B1-b, L1544, L183, and L483) and the lukewarm corino L1527 (green: Marcelino et al., 2010; Marcelino et al., 2018); the dark cloud TMC-1 (yellow; Cernicharo et al., 2021); and the IRAS 16293–2422 B hot corino (red, Zeng et al., 2019). To derive the uncertainties of the molecular abundances we have considered the uncertainties of the molecular column densities reported in the different works, or a 15% of the value of *N* if the uncertainty is not provided, and we assumed an uncertainty for the $N(H_2)$ column densities of 15%.

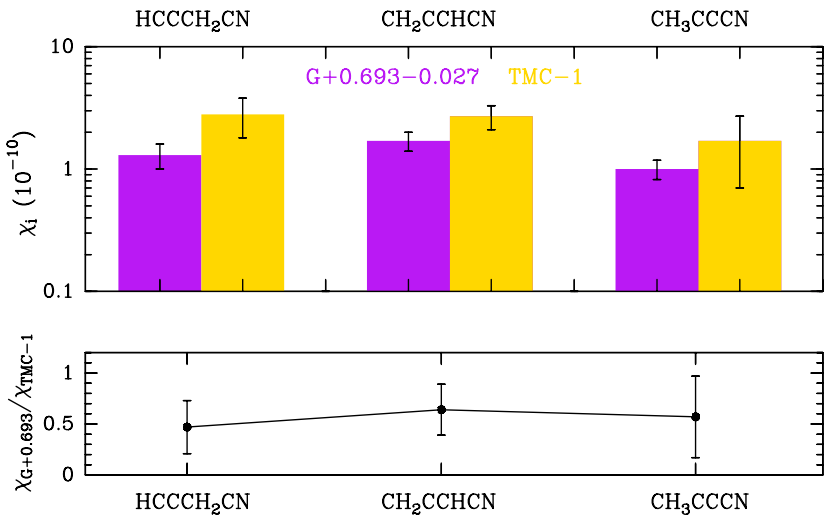

FIGURE 9 | Upper panel: Abundances with respect to H_2 of the C_3H_4N isomers detected towards G+0.693 (purple; this work) and TMC-1 (yellow, Marcelino et al., 2021). To derive the uncertainties of the molecular abundances we have considered the uncertainties of the molecular column densities of the C_3H_4N isomers reported in this work (**Table 4**) and in Marcelino et al. 2021, and we assumed an uncertainty for the $N(H_2)$ column density of 15%. Lower panel: Molecular ratios between the abundances of the C_3H_4N isomers in G+0.693 and TMC-1.

and towards several dense cores (B1-b, L1544, L183, and L483) as well as the lukewarm corino L1527 (Marcelino et al., 2010; Marcelino et al., 2018). **Figure 8** shows that the HOCN abundance derived in G+0.693 is of the same order of magnitude of those detected in other Sgr B2 positions ($\sim 10^{-11} - 10^{-10}$; Brünken et al., 2010), and higher than those derived in the dense cores and L1527 (Marcelino et al., 2018). This suggests that the role of surface-chemistry and the presence of shocks enhance the HOCN abundance, similarly to its isomer HNCO (Hasegawa and Herbst 1993; Garrod et al., 2008; Martín et al., 2008; Rodríguez-Fernández et al., 2010; Quénard et al., 2018). The chemistry of the molecular clouds of the Galactic Center, and that of G+0.693 in particular, is dominated by large-scale shocks (Martín-Pintado et al., 2001; Martín et al., 2008), which are responsible for the sputtering of dust grains, releasing many molecules formed on the grain surfaces into the gas phase (see Caselli et al., 1997; Jiménez-Serra et al., 2008). This can increase the abundance of the species by orders of magnitude. Similarly to isomer HNCO, which is efficiently formed on grain surfaces by hydrogenation of accreted OCN (Hasegawa and Herbst 1993; Garrod et al., 2008), HOCN can also be formed on grain mantles if the oxygen atom is hydrogenated:

$$OCN + H \rightarrow HOCN, \quad (1)$$

and then subsequently released by shocks (Brünken et al., 2010). An alternative surface route might be the reaction of two highly abundant species:

$$CN + OH \rightarrow HOCN \quad (2)$$

• HCOCN: this species has been detected previously in the massive hot core SgrB2 (N) (Remijan et al., 2008), and in the dark cloud TMC-1 (Cernicharo et al., 2021). The HCOCN abundances found in G+0.693 and TMC-1 are very similar, in the range of $(3.5–5) \times 10^{-11}$, as shown in **Figure 8**. These two regions have very different physical conditions, which imprint their chemistry. While in the case of the dark and cold TMC-1 cloud gas-phase chemistry is thought to be dominant, since thermal or shock-induced desorptions are highly unlikely, the chemistry of G+0.693 is strongly affected by shocks, and thus surface chemistry also plays an important role. Therefore, the similar HCOCN abundances in G+0.693 and TMC-1 points towards a predominant gas-phase chemistry origin. Indeed, the quantum chemical calculations by Tonolo et al. (2020) have shown that HCOCN species can be efficiently formed through the gas-phase reaction between formaldehyde (H_2CO) and the cyanide radical (CN), which are highly abundant species in the ISM, in which the CN radical attacks the unsaturated carbon of H_2CO and substitutes one of the H atoms:

$$H_2CO + CN \rightarrow HCOCN + H, \quad (3)$$

• $HOCH_2CN$: this species was first detected in the ISM towards the hot corino IRAS 16293–2422 B (Zeng et al., 2019), and more recently towards the SMM1 hot corino in Serpens (Ligterink et al., 2021). The abundance derived in G+0.693 is 4.3×10^{-10}, very similar to that derived in the hot component of IRAS 16293–2422 B (**Figure 8**). The chemical model by Zeng et al. (2019) considered the surface formation route proposed by the laboratory experiments of Danger et al. (2012); Danger et al. (2013):

$$H_2CO + HCN \rightarrow HOCH_2CN \quad (4)$$

and ion-neutral destruction reactions with H_3^+, HCO^+, and H_3O^+, and concluded that more chemical pathways are needed to explain the abundance observed in the hot corino IRAS 16293–2422 B. More recently, the quantum chemical cluster calculations performed by Woon (2021) have proposed new surface reactions between C^+, which is distributed throughout the whole Galactic Center (Harris et al., 2021), and two very abundant species, HCN and HNC (e.g. Colzi et al. 2022), embedded in H_2O icy grain mantles. The C^+ ion reacts with HCN and HNC forming intermediate species that attacks neighboring H_2O molecules of the ices, resulting into the radicals HOCHNC and HOCHCN. These species can be easily hydrogenated on the grain surfaces to form $HOCH_2CN$. The inclusion of these alternative surface routes in the chemical models might help to explain the $HOCH_2CN$ abundances detected in G+0.693 and hot corinos, where the molecules can be injected to the gas phase through shocks and thermal effects, respectively.

• $HCOCH_2CN$: the theoretical calculations performed by Horn et al. (2008) proposed that this species might be formed from two abundant precursors in the ISM:

$$HC_3N + H_2O \rightarrow HCOCH_2CN \quad (5)$$

However, while this reaction might occur in aqueous solution, its activation energy, 216 kJ mol^{-1} (25,980 K), is too high to occur in the ISM. Recently, Alessandrini and Melosso (2021) have studied the reaction between oxirane (or ethylene oxide, c – C_2H_4O) – also detected towards G+0.693 (Requena-Torres et al., 2008) – and the CN radical. Although the main pathway is the H abstraction from oxirane, forming the oxiranyl radical, the formation of $HCOCH_2CN$ + H is also possible with a rate of ~ 10^{-12} cm^3 $molec^{-1}$ s^{-1}. New theoretical and/or experimental works of this species are needed to determine if it can be efficiently formed in the ISM, opening the possibility for its interstellar detection.

4.1.2 C_4H_3N Isomers

The unsaturated C_4H_3N isomers towards G+0.693 have very similar abundances within a factor of 2, spanning a range of $(1.0–1.7) \times 10^{-10}$ (**Table 4**), as also previously observed in the dark cloud TMC-1 by Marcelino et al. (2021). Moreover, **Figure 9** shows that the abundances in these two molecular clouds, which have very different physical conditions, as mentioned above, are very similar. This suggests that these molecules are predominantly formed through gas-phase chemistry (see previous discussion about HCOCN). Furthermore, since the three isomers are almost equally abundant, their respective formation might be linked to common precursors. Indeed, Balucani et al. (2000) proposed that these unsaturated nitriles can be formed efficiently by reactions in which the cyanide radical (CN) attacks an unsaturated carbon of the hydrocarbons methylacetylene (CH_3CCH) and allene (CH_2CCH_2):

$$CH_3CCH + CN \xrightarrow{0.22/0.50} CH_3CCCN + H, \quad (6)$$

$$\xrightarrow{0.0/0.50} CH_2CCHCN + H\,, \quad (7)$$

$$CH_2CCH_2 + CN \xrightarrow{0.90} CH_2CCHCN + H, \quad (8)$$

$$\xrightarrow{0.10} HCCCH_2CN + H; \quad (9)$$

in which the branching ratios for each reaction are indicated above each arrow (normalized to 1). These ratios were derived using the experiments and quantum chemical calculations by Abeysekera et al. (2015)/Balucani et al. (2000) in the first two reactions, and from Balucani et al. (2002) in the latter two reactions. These radical-neutral reactions show no entrance barriers, they have exit barriers well below the energy of the reactant molecules, and are exothermic. The proposed precursors CN and CH_3CCH are abundant molecules in the ISM. In particular, they were detected towards G+0.693 with molecular abundances of 1.5×10^{-8} and 1.3×10^{-8}, respectively (Rivilla et al., 2019a; Bizzocchi et al., 2020), so they are viable precursors. Allene (CH_2CCH_2) has zero dipole moment, so its detection through rotational spectroscopy is not possible, and thus its abundance is unknown. However, the similar abundances of the three isomers suggest that it can be as abundant as CH_3CCH in the ISM.

Regardless of the actual abundance of CH_2CCH_2, which is unknown, the proposed branching ratios seem to be in conflict with the observational findings in G+0.693 and TMC-1, since they are not able to produce equal abundance for the three isomers. As already noted by Marcelino et al. (2021), it would be interesting to study the branching ratios of the CH_2CHCH_2 +

CN reaction using the chirped-pulse uniform flow experiment used by Abeysekera et al. (2015) for the CH_2CCH + CN reaction, and compare them with the values derived from quantum chemical calculations by Balucani et al. (2002), to reconcile the experimental/theoretical works with the findings of the observations.

5 CONCLUSION: IMPLICATIONS FOR THE RNA-WORLD

Compounds of the nitrile family, under early Earth conditions, offer a rich chemistry due to the large number of reactions that they can trigger. Nitriles could be transformed into amides, carboxylic acids and esters via hydrolysis and alcoholysis respectively. Autocondensation of nitriles in a basic environment could yield to cyanoketones and cyanoenamines, a high reactive intermediate in the synthesis of complex five- and six-member heterocycles (Erian 1993). The high amounts of ammonia of the reducing atmosphere of the primitive Earth is a favorable scenario to obtain amidines from nitriles (Shriner and Neumann 1944). Moreover, the NCN backbone of amidines offer an unique structure to yield complex N-containing heterocycles like purine and pyrimidine nucleobases. Furthermore, nitriles can activate the formation of the building blocks of RNA, ribonucleotides (e.g. Powner et al., 2009; Powner and Sutherland 2010; Patel et al., 2015). Two of the nitriles studied in this work, i.e. glycolonitrile and cyanoacetaldehyde, have been proposed as activation agents for the formation of more complex molecules with prebiotic relevance. The latter ($HCOCH_2CN$) is a precursor of cytosine (Robertson and Miller 1995; Nelson et al., 2001; Menor-Salván et al., 2009). The former ($HOCH_2CN$) is not only a fundamental precursor to ribonucleotides and lipids (Ritson and Sutherland 2012, 2013; Patel et al. 2015; Liu et al. 2018; Ritson et al. 2018), but also of other biologically-important molecules such as the simplest amino acid glycine (NH_2CH_2COOH; Rodriguez et al., 2019), and of the nucleobase adenine through rapid HCN oligomerisation (Schwartz and Goverde 1982; Menor-Salván and Marín-Yaseli 2012). Unsaturated carbon-chain nitriles like the C_4H_3N isomers studied in this work are also especially interesting for prebiotic chemistry because the presence of unsaturated bonds allows further chemical evolution that can produce biomolecules (Rosi et al. 2018).

This work extends the repertoire of nitriles detected in the G+0.693 molecular cloud, a region that exhibits one of the richest chemical content in the ISM, and hence it is a well suited testbed to census the molecular species present in the ISM. Besides HOCN, already reported by Brünken et al. (2010) and Zeng et al. (2018), we have provided the tentative detections towards this source of HCOCN and $HOCH_2CN$ (third detection in the ISM), and the detection of the three unsaturated C_4H_3N isomers (being the second source after TMC-1 in which all three isomers are identified). These detections confirm the rich reservoir of nitriles in space, and complete the list of prebiotic molecular precursors detected previously, including species directly involved in the synthesis of ribonucleotides such as glycolaldehyde ($HCOCH_2OH$; Hollis et al., 2004; Requena-Torres et al., 2006; Beltrán et al., 2009; Jørgensen et al., 2012), urea (Belloche et al., 2019; Jiménez-Serra et al., 2020), hydroxylamine NH_2OH (Rivilla et al., 2020), and 1,2-ethenediol (Rivilla et al. 2022a); of amino acids, such as amino acetonitrile (NH_2CH_2CN; Belloche et al., 2008; Melosso et al., 2020); and of lipids, such as ethanolamine ($NH_2CH_2CH_2OH$; Rivilla et al., 2021a), and propanol ($CH_3CH_2CH_2OH$; Jimenez-Serra et al. 2022; Belloche et al. 2022).

In star- and planet-forming regions, this chemical feedstock can be processed through circumstellar disks, and subsequently incorporated into planetesimals and objects like comets and asteroids. We know that our planet suffered a heavy bombardment of extraterrestrial bodies ~500 Myr after its formation (e.g. Marchi et al., 2014). Laboratory impact experiments have shown that a significant fraction of the molecules contained in comets and meteorites could have been delivered intact to the early Earth (Pierazzo and Chyba 1999; Bertrand et al., 2009; McCaffrey et al., 2014; Todd and Öberg 2020; Zellner et al., 2020). Once on the planetary surface, under the appropriate physical/chemical conditions, these molecules could have allowed the development of the prebiotic processes that led to the dawn of life on Earth.

DATA AVAILABILITY STATEMENT

The raw data supporting the conclusion of this article will be made available by the authors, without undue reservation.

AUTHOR CONTRIBUTIONS

VR initiated and led the project. VR, JM-P, FR-V, BT, and PdV performed the observations. VR, IJ-S, and JM-P performed the data reduction. VR, LC, SZ, and IJ-S contributed to the data analysis. LB and MM performed the calculations of the cyanoacetaldehyde spectroscopy. VR wrote an initial draft of the article. All the authors, including JG, SM and MR-T, participated in data interpretation and discussion.

FUNDING

VR has received support from the Comunidad de Madrid through the Atracción de Talento Investigador Modalidad 1 (Doctores con experiencia) Grant (COOL:Cosmic Origins of Life; 2019-T1/TIC-5379), and the Ayuda RYC2020-029387-I funded by MCIN/AEI /10.13039/501100011033. IJS, JMP, and LC have received partial support from the Spanish project numbers PID2019-105552RB-C41 and MDM-2017-0737 (Unidad de Excelencia María de Maeztu-Centro de Astrobiología, INTA-CSIC). JG acknowledges the Spanish State Research Agency (AEI) through project number MDM-2017-0737 Unidad de Excelencia "María de Maeztu"—Centro de Astrobiología and the Spanish State Research Agency (AEI) for partial financial support through Project No. PID 2019-105552RB-C41. PdV and BT thank the support from the

European Research Council (ERC Grant 610256: NANOCOSMOS) and from the Spanish Ministerio de Ciencia e Innovación (MICIU) through project PID 2019-107115GBC21. BT also acknowledges the Spanish MICIU for funding support from grant PID 2019-106235GB-I00.

ACKNOWLEDGMENTS

We thank the two reviewers for providing very constructive and useful comments and suggestions, which contributed to improve our work. We also thank Dr. Rougal Ritson for interesting discussions about the relevance of nitriles in prebiotic chemistry. We are very grateful to the IRAM 30 m and Yebes 40 m telecope staff for their precious help during the different observing runs. IRAM is supported by the National Institute for Universe Sciences and Astronomy/National Center for Scientific Research (France), Max Planck Society for the Advancement of Science (Germany), and the National Geographic Institute (IGN) (Spain). The 40 m radio telescope at Yebes Observatory is operated by the IGN, Ministerio de Transportes, Movilidad y Agenda Urbana.

REFERENCES

Abeysekera, C., Joalland, B., Ariyasingha, N., Zack, L. N., Sims, I. R., Field, R. W., et al. (2015). Product Branching in the Low Temperature Reaction of Cn with Propyne by Chirped-Pulse Microwave Spectroscopy in a Uniform Supersonic Flow. *J. Phys. Chem. Lett.* 6, 1599–1604. doi:10.1021/acs.jpclett.5b00519

Alessandrini, S., and Melosso, M. (2021). Fate of the Gas-phase Reaction between Oxirane and the Cn Radical in Interstellar Conditions. *Front. Astron. Space Sci.* 8. doi:10.3389/fspas.2021.754977

Balucani, N., Asvany, O., Huang, L. C. L., Lee, Y. T., Kaiser, R. I., Osamura, Y., et al. (2000). Formation of Nitriles in the Interstellar Medium via Reactions of Cyano Radicals, CN(X 2Σ+), with Unsaturated Hydrocarbons. *Astrophysical J.* 545, 892–906. doi:10.1086/317848

Balucani, N., Asvany, O., Kaiser, R.-I., and Osamura, Y. (2002). Formation of Three C4H3N Isomers from the Reaction of CN (X2Σ+) with Allene, H2CCCH2 (XA1), and Methylacetylene, CH3CCH (X1A1): A Combined Crossed Beam and Ab Initio Study. *J. Phys. Chem. A* 106, 4301–4311. doi:10.1021/jp0116104

Becker, S., Feldmann, J., Wiedemann, S., Okamura, H., Schneider, C., Iwan, K., et al. (2019). Unified Prebiotically Plausible Synthesis of Pyrimidine and Purine Rna Ribonucleotides. *Science* 366, 76–82. doi:10.1126/science.aax2747

Belloche, A., Garrod, R. T., Müller, H. S. P., Menten, K. M., Medvedev, I., Thomas, J., et al. (2019). Re-exploring Molecular Complexity with ALMA (ReMoCA): Interstellar Detection of Urea. *Astronomy Astrophysics* 628, A10. doi:10.1051/0004-6361/201935428

Belloche, A., Garrod, R. T., Zingsheim, O., Müller, H. S. P., and Menten, K. M. (2022). Interstellar Detection and Chemical Modeling of Iso-Propanol and its Normal Isomer. *arXiv e-prints.* arXiv:2204.09912. doi:10.1051/0004-6361/202243575

Belloche, A., Menten, K. M., Comito, C., Müller, H. S. P., Schilke, P., Ott, J., et al. (2008). Detection of Amino Acetonitrile in Sgr B2(N). *Astronomy Astrophysics* 482, 179–196. doi:10.1051/0004-6361:20079203

Beltrán, M. T., Codella, C., Viti, S., Neri, R., and Cesaroni, R. (2009). First Detection of Glycolaldehyde outside the Galactic Center. *Astrophysical J.* 690, L93–L96. doi:10.1088/0004-637X/690/2/L93

Bertrand, M., van der Gaast, S., Vilas, F., Hörz, F., Haynes, G., Chabin, A., et al. (2009). The Fate of Amino Acids during Simulated Meteoritic Impact. *Astrobiology* 9, 943–951. doi:10.1089/ast.2008.0327

Bester, M., Tanimoto, M., Vowinkel, B., Winnewisser, G., and Yamada, K. (1983). Rotational Spectrum of Methylcyanoacetylene a New Millimeter Wave Spectrometer. *Z. für Naturforsch. A* 38, 64–67. doi:10.1515/zna-1983-0112

Bester, M., Yamada, K., Winnewisser, G., Joentgen, W., Altenbach, H.-J., and Vogel, E. (1984). Millimeter Wave Spectrum of Methyldiacetylene, Ch3c4h. *Astronomy Astrophysics* 137, L20–L22.

Bizzocchi, L., Prudenzano, D., Rivilla, V. M., Pietropolli-Charmet, A., Giuliano, B. M., Caselli, P., et al. (2020). Propargylimine in the Laboratory and in Space: Millimetre-Wave Spectroscopy and its First Detection in the ISM. *Astronomy Astrophysics* 640, A98. doi:10.1051/0004-6361/202038083

Bogey, M., Demuynck, C., Destombes, J. L., and Vallee, Y. (1995). Millimeter-wave Spectrum of Formyl Cyanide, Hcocn: Centrifugal Distortion and Hyperfine Structure Analysis. *J. Mol. Spectrosc.* 172, 344–351. doi:10.1006/jmsp.1995.1183

Bouchy, A., Demaison, J., Roussy, G., and Barriol, J. (1973). Microwave Spectrum of Cyanoallene. *J. Mol. Struct.* 18, 211–217. doi:10.1016/0022-2860(73)85223-8

Brünken, S., Belloche, A., Martín, S., Verheyen, L., and Menten, K. M. (2010). Interstellar HOCN in the Galactic Center Region. *Astronomy Astrophysics* 516, A109. doi:10.1051/0004-6361/200912456

Brünken, S., Gottlieb, C. A., McCarthy, M. C., and Thaddeus, P. (2009). Laboratory Detection of Hocn and Tentative Identification in Sgr B2. *Astrophysical J.* 697, 880–885. doi:10.1088/0004-637x/697/1/880

Canavelli, P., Islam, S., and Powner, M. W. (2019). Peptide Ligation by Chemoselective Aminonitrile Coupling in Water. *Nature* 571, 546–549. doi:10.1038/s41586-019-1371-4

Caselli, P., Hartquist, T. W., and Havnes, O. (1997). Grain-grain Collisions and Sputtering in Oblique C-type Shocks. *Astronomy Astrophysics* 322, 296–301.

Cernicharo, J., Cabezas, C., Agúndez, M., Tercero, B., Pardo, J. R., Marcelino, N., et al. (2021). TMC-1, the Starless Core Sulfur Factory: Discovery of NCS, HCCS, H2CCS, H2CCCS, and C4S and Detection of C5S. *Astronomy Astrophysics* 648, L3. doi:10.1051/0004-6361/202140642

Chyba, C., and Sagan, C. (1992). Endogenous Production, Exogenous Delivery and Impact-Shock Synthesis of Organic Molecules: An Inventory for the Origins of Life. *Nature* 355, 125–132. doi:10.1038/355125a0

Colzi, L., Martín-Pintado, J., Rivilla, V. M., Jiménez-Serra, I., Zeng, S., Rodríguez-Almeida, L. F., et al. (2022). Deuterium Fractionation as a Multiphase Component Tracer in the Galactic Center. *Astrophysical JournalL* 926, L22. doi:10.3847/2041-8213/ac52ac

Cooper, G., Kimmich, N., Belisle, W., Sarinana, J., Brabham, K., and Garrel, L. (2001). Carbonaceous Meteorites as a Source of Sugar-Related Organic Compounds for the Early Earth. *Nature* 414, 879–883. doi:10.1038/414879a

Császár, A. G. (1989). Theoretical Prediction of Vibrational and Rotational Spectra. Formyl Cyanide, Hcocn, and Thioformyl Cyanide, Hcscn. *Chem. Phys. Lett.* 162, 361–368. doi:10.1016/0009-2614(89)87059-9

Danger, G., Duvernay, F., Theulé, P., Borget, F., and Chiavassa, T. (2012). Hydroxyacetonitrile ($HOCH_2CN$) Formation in Astrophysical Conditions. Competition with the Aminomethanol, a Glycine Precursor. *Astrophysical J.* 756, 11. doi:10.1088/0004-637X/756/1/11

Danger, G., Duvernay, F., Theulé, P., Borget, F., Guillemin, J.-C., and Chiavassa, T. (2013). Hydroxyacetonitrile (HOCH2cn) as a Precursor for Formylcyanide (CHOCN), Ketenimine (CH2cnh), and Cyanogen (NCCN) in Astrophysical Conditions. *Astronomy Astrophysics* 549, A93. doi:10.1051/0004-6361/201219779

Demaison, J., Pohl, I., and Rudolph, H. D. (1985). Millimeter-wave Spectrum of 3-butynenitrile: Dipole Moment and Centrifugal Distortion Constants. *J. Mol. Spectrosc.* 114, 210–218. doi:10.1016/0022-2852(85)90349-2

Endres, C. P., Schlemmer, S., Schilke, P., Stutzki, J., and Müller, H. S. P. (2016). The Cologne Database for Molecular Spectroscopy, CDMS, in the Virtual Atomic and Molecular Data Centre, VAMDC. *J. Mol. Spectrosc.* 327, 95–104. doi:10.1016/j.jms.2016.03.005

Erian, A. W. (1993). The Chemistry of .beta.-enaminonitriles as Versatile Reagents in Heterocyclic Synthesis. *Chem. Rev.* 93, 1991–2005. doi:10.1021/cr00022a002

Foden, C. S., Islam, S., Fernández-García, C., Maugeri, L., Sheppard, T. D., and Powner, M. W. (2020). Prebiotic Synthesis of Cysteine Peptides that Catalyze Peptide Ligation in Neutral Water. *Science* 370, 865–869. doi:10.1126/science.abd5680

Garrod, R. T., Weaver, S. L. W., and Herbst, E. (2008). Complex Chemistry in Star-forming Regions: An Expanded Gas-Grain Warm-up Chemical Model. *Astrophysical J.* 682, 283–302. doi:10.1086/588035

Gilbert, W. (1986). Origin of Life: The RNA World. *Nature* 319, 618. doi:10.1038/319618a0

Harris, A. I., Güsten, R., Requena-Torres, M. A., Riquelme, D., Morris, M. R., Stacey, G. J., et al. (2021). SOFIA-upGREAT Imaging Spectroscopy of the [C Ii] 158 μm Fine-structure Line of the Sgr B Region in the Galactic Center. *Astrophysical J.* 921, 33. doi:10.3847/1538-4357/ac1863

Hasegawa, T. I., and Herbst, E. (1993). New Gas-Grain Chemical Models of Quiescent Dense Interstellar Clouds: the Effects of H2 Tunnelling Reactions and Cosmic Ray Induced Desorption. *Mon. Notices R. Astronomical Soc.* 261, 83–102. doi:10.1093/mnras/261.1.83

Hollis, J. M., Jewell, P. R., Lovas, F. J., and Remijan, A. (2004). Green Bank Telescope Observations of Interstellar Glycolaldehyde: Low-Temperature Sugar. *Astrophysical J.* 613, L45–L48. doi:10.1086/424927

Horn, A., Møllendal, H., and Guillemin, J.-C. (2008). A Quantum Chemical Study of the Generation of a Potential Prebiotic Compound, Cyanoacetaldehyde, and Related Sulfur Containing Species. *J. Phys. Chem. A* 112, 11009–11016. doi:10.1021/jp805357w

Jiménez-Serra, I., Caselli, P., Martín-Pintado, J., and Hartquist, T. W. (2008). Parametrization of C-Shocks. Evolution of the Sputtering of Grains. *Astronomy Astrophysics* 482, 549–559. doi:10.1051/0004-6361:20078054

Jiménez-Serra, I., Martín-Pintado, J., Rivilla, V. M., Rodríguez-Almeida, L., Alonso Alonso, E. R., Zeng, S., et al. (2020). Toward the RNA-World in the Interstellar Medium-Detection of Urea and Search of 2-Amino-Oxazole and Simple Sugars. *Astrobiology* 20, 1048–1066. doi:10.1089/ast.2019.2125

Jimenez-Serra, I., Rodriguez-Almeida, L. F., Martin-Pintado, J., Rivilla, V. M., Melosso, M., Zeng, S., et al. (2022). Precursors of Fatty Alcohols in the ISM: Discovery of N-Propanol. *arXiv e-prints*. arXiv:2204.08267. doi:10.1051/0004-6361/202142699

Jørgensen, J. K., Favre, C., Bisschop, S. E., Bourke, T. L., van Dishoeck, E. F., and Schmalzl, M. (2012). Detection of the Simplest Sugar, Glycolaldehyde, in a Solar-type Protostar with ALMA. *Astrophysical J.* 757, L4. doi:10.1088/2041-8205/757/1/L4

Ligterink, N. F. W., Ahmadi, A., Coutens, A., Tychoniec, Ł., Calcutt, H., van Dishoeck, E. F., et al. (2021). The Prebiotic Molecular Inventory of Serpens SMM1. *Astronomy Astrophysics* 647, A87. doi:10.1051/0004-6361/202039619

Liu, Z., Mariani, A., Wu, L., Ritson, D., Folli, A., Murphy, D., et al. (2018). Tuning the Reactivity of Nitriles Using Cu(ii) Catalysis - Potentially Prebiotic Activation of Nucleotides. *Chem. Sci.* 9, 7053–7057. doi:10.1039/c8sc02513d

Lovas, F. J., Remijan, A. J., Hollis, J. M., Jewell, P. R., and Snyder, L. E. (2006). Hyperfine Structure Identification of Interstellar Cyanoallene toward Tmc-1. *Astrophysical J.* 637, L37–L40. doi:10.1086/500431

Marcelino, N., Agúndez, M., Cernicharo, J., Roueff, E., and Tafalla, M. (2018). Discovery of the Elusive Radical NCO and Confirmation of H2NCO+ in Space. *Astronomy Astrophysics* 612, L10. doi:10.1051/0004-6361/201833074

Marcelino, N., Brünken, S., Cernicharo, J., Quan, D., Roueff, E., Herbst, E., et al. (2010). The Puzzling Behavior of HNCO Isomers in Molecular Clouds. *Astronomy Astrophysics* 516, A105. doi:10.1051/0004-6361/200913806

Marcelino, N., Tercero, B., Agúndez, M., and Cernicharo, J. (2021). A Study of C4H3N Isomers in TMC-1: Line by Line Detection of HCCCH2CN. *Astronomy Astrophysics* 646, L9. doi:10.1051/0004-6361/202040177

Marchi, S., Bottke, W. F., Elkins-Tanton, L. T., Bierhaus, M., Wuennemann, K., Morbidelli, A., et al. (2014). Widespread Mixing and Burial of Earth's Hadean Crust by Asteroid Impacts. *Nature* 511, 578–582. doi:10.1038/nature13539

Margulès, L., McGuire, B. A., Senent, M. L., Motiyenko, R. A., Remijan, A., and Guillemin, J. C. (2017). Submillimeter Spectra of 2-hydroxyacetonitrile (Glycolonitrile; HOCH2cn) and its Searches in GBT PRIMOS Observations of Sgr B2(N). *Astronomy Astrophysics* 601, A50. doi:10.1051/0004-6361/201628551

Mariani, A., Russell, D. A., Javelle, T., and Sutherland, J. D. (2018). A Light-Releasable Potentially Prebiotic Nucleotide Activating Agent. *J. Am. Chem. Soc.* 140, 8657–8661. doi:10.1021/jacs.8b05189

Martín, S., Martín-Pintado, J., Blanco-Sánchez, C., Rivilla, V. M., Rodríguez-Franco, A., and Rico-Villas, F. (2019). Spectral Line Identification and Modelling (SLIM) in the MAdrid Data CUBe Analysis (MADCUBA) Package. *Astronomy Astrophysics* 631, A159. doi:10.1051/0004-6361/201936144

Martín, S., Requena-Torres, M. A., Martín-Pintado, J., and Mauersberger, R. (2008). Tracing Shocks and Photodissociation in the Galactic Center Region1. *Astrophysical J.* 678, 245–254. doi:10.1086/533409

Martín-Pintado, J., Rizzo, J. R., de Vicente, P., Rodríguez-Fernández, N. J., and Fuente, A. (2001). Large-Scale Grain Mantle Disruption in the Galactic Center. *Astrophysical JournalL* 548, L65–L68. doi:10.1086/318937

McCaffrey, V. P., Zellner, N. E. B., Waun, C. M., Bennett, E. R., and Earl, E. K. (2014). Reactivity and Survivability of Glycolaldehyde in Simulated Meteorite Impact Experiments. *Orig. Life Evol. Biosph.* 44, 29–42. doi:10.1007/s11084-014-9358-5

McGuire, B. A., Burkhardt, A. M., Loomis, R. A., Shingledecker, C. N., Kelvin Lee, K. L., Charnley, S. B., et al. (2020). Early Science from Gotham: Project Overview, Methods, and the Detection of Interstellar Propargyl Cyanide (Hccch2cn) in Tmc-1. *Astrophysical J.* 900, L10. doi:10.3847/2041-8213/aba632

Melosso, M., Belloche, A., Martin-Drumel, M.-A., Pirali, O., Tamassia, F., Bizzocchi, L., et al. (2020). Far-infrared Laboratory Spectroscopy of Aminoacetonitrile and First Interstellar Detection of its Vibrationally Excited Transitions. *Astronomy Astrophysics* 641, A160. doi:10.1051/0004-6361/202038466

Menor Salván, C., Bouza, M., Fialho, D. M., Burcar, B. T., Fernández, F. M., and Hud, N. V. (2020). Prebiotic Origin of Pre-RNA Building Blocks in a Urea "Warm Little Pond" Scenario. *ChemBioChem* 21, 3504–3510. doi:10.1002/cbic.202000510

Menor-Salván, C., and Marín-Yaseli, M. R. (2012). Prebiotic Chemistry in Eutectic Solutions at the Water-Ice Matrix. *Chem. Soc. Rev.* 41, 5404–5415. doi:10.1039/c2cs35060b

Menor-Salván, C., Ruiz-Bermejo, D. M., Guzmán, M. I., Osuna-Esteban, S., and Veintemillas-Verdaguer, S. (2009). Synthesis of Pyrimidines and Triazines in Ice: Implications for the Prebiotic Chemistry of Nucleobases. *Chem. Eur. J.* 15, 4411–4418. doi:10.1002/chem.200802656

Moïses, A., Boucher, D., Burie, J., Demaison, J., and Dubrulle, A. (1982). Millimeter-wave Spectrum of Methylcyanoacetylene. *J. Mol. Spectrosc.* 92, 497–498. doi:10.1016/0022-2852(82)90118-7

Møllendal, H., Margulès, L., Motiyenko, R. A., Larsen, N. W., and Guillemin, J.-C. (2012). Rotational Spectrum and Conformational Composition of Cyanoacetaldehyde, a Compound of Potential Prebiotic and Astrochemical Interest. *J. Phys. Chem. A* 116, 4047–4056. doi:10.1021/jp212306z

Nelson, K. E., Robertson, M. P., Levy, M., and Miller, S. L. (2001). Concentration by Evaporation and the Prebiotic Synthesis of Cytosine. *Orig. Life Evol. Biosphere* 31, 221–229. doi:10.1023/a:1010652418557

Oró, J. (1961). Mechanism of Synthesis of Adenine from Hydrogen Cyanide under Possible Primitive Earth Conditions. *Nature* 191, 1193–1194. doi:10.1038/1911193a0

Patel, B. H., Percivalle, C., Ritson, D. J., Duffy, C. D., and Sutherland, J. D. (2015). Common Origins of RNA, Protein and Lipid Precursors in a Cyanosulfidic Protometabolism. *Nat. Chem.* 7, 301–307. doi:10.1038/nchem.2202

Pearce, B. K. D., Tupper, A. S., Pudritz, R. E., and Higgs, P. G. (2018). Constraining the Time Interval for the Origin of Life on Earth. *Astrobiology* 18, 343–364. doi:10.1089/ast.2017.1674

Pickett, H. M., Poynter, R. L., Cohen, E. A., Delitsky, M. L., Pearson, J. C., and Müller, H. S. P. (1998). Submillimeter, Millimeter, and Microwave Spectral Line Catalog. *J. Quantitative Spectrosc. Radiat. Transf.* 60, 883–890. doi:10.1016/S0022-4073(98)00091-0

Pickett, H. M. (1991). The Fitting and Prediction of Vibration-Rotation Spectra with Spin Interactions. *J. Mol. Spectrosc.* 148, 371–377. doi:10.1016/0022-2852(91)90393-O

Pierazzo, E., and Chyba, C. F. (1999). Amino Acid Survival in Large Cometary Impacts. *Meteorit. Planet. Sci.* 34, 909–918. doi:10.1111/j.1945-5100.1999.tb01409.x

Powner, M. W., Gerland, B., and Sutherland, J. D. (2009). Synthesis of Activated Pyrimidine Ribonucleotides in Prebiotically Plausible Conditions. *Nature* 459, 239–242. doi:10.1038/nature08013

Powner, M. W., and Sutherland, J. D. (2010). Phosphate-mediated Interconversion of Ribo- and Arabino-Configured Prebiotic Nucleotide Intermediates. *Angew. Chem. Int. Ed.* 49, 4641–4643. doi:10.1002/anie.201001662

Quénard, D., Jiménez-Serra, I., Viti, S., Holdship, J., and Coutens, A. (2018). Chemical Modelling of Complex Organic Molecules with Peptide-like Bonds in Star-Forming Regions. *Mon. Notices R. Astronomical Soc.* 474, 2796–2812. doi:10.1093/mnras/stx2960

Remijan, A. J., Hollis, J. M., Lovas, F. J., Stork, W. D., Jewell, P. R., and Meier, D. S. (2008). Detection of Interstellar Cyanoformaldehyde (CNCHO). *Astrophysical J.* 675, L85–L88. doi:10.1086/533529

Requena-Torres, M. A., Martín-Pintado, J., Martín, S., and Morris, M. R. (2008). The Largest Oxigen Bearing Organic Molecule Repository. *Astrophysical J.* 672, 352–360. doi:10.1086/523627

Requena-Torres, M. A., Martín-Pintado, J., Rodríguez-Franco, A., Martín, S., Rodríguez-Fernández, N. J., and de Vicente, P. (2006). Organic Molecules in the Galactic Center. *Astronomy Astrophysics* 455, 971–985. doi:10.1051/0004-6361:20065190

Ritson, D. J., Battilocchio, C., Ley, S. V., and Sutherland, J. D. (2018). Mimicking the Surface and Prebiotic Chemistry of Early Earth Using Flow Chemistry. *Nat. Commun.* 9, 1821. doi:10.1038/s41467-018-04147-2

Ritson, D. J., and Sutherland, J. D. (2013). Synthesis of Aldehydic Ribonucleotide and Amino Acid Precursors by Photoredox Chemistry. *Angew. Chem. Int. Ed.* 52, 5845–5847. doi:10.1002/anie.201300321

Ritson, D., and Sutherland, J. D. (2012). Prebiotic Synthesis of Simple Sugars by Photoredox Systems Chemistry. *Nat. Chem.* 4, 895–899. doi:10.1038/nchem.1467

Rivilla, V. M., Beltrán, M. T., Vasyunin, A., Caselli, P., Viti, S., Fontani, F., et al. (2019a). First ALMA Maps of HCO, an Important Precursor of Complex Organic Molecules, towards IRAS 16293-2422. *MNRAS* 483, 806–823. doi:10.1093/mnras/sty3078

Rivilla, V. M., Colzi, L., Jiménez-Serra, I., Martín-Pintado, J., Megías, A., Melosso, M., et al. (2022a). Precursors of the RNA World in Space: Detection of (Z)-1,2-ethenediol in the Interstellar Medium, a Key Intermediate in Sugar Formation. *Astrophysical JournalL* 929, L11. doi:10.3847/2041-8213/ac6186

Rivilla, V. M., García De La Concepción, J., Jiménez-Serra, I., Martín-Pintado, J., Colzi, L., Tercero, B., et al. (2022b). Ionize Hard: Interstellar PO+ Detection. *Front. Astron. Space Sci.* 9, 829288. doi:10.3389/fspas.2022.829288

Rivilla, V. M., Jiménez-Serra, I., García de la Concepción, J., Martín-Pintado, J., Colzi, L., Rodríguez-Almeida, L. F., et al. (2021b). Detection of the Cyanomidyl Radical (HNCN): a New Interstellar Species with the NCN Backbone. *MNRAS* 506, L79–L84. doi:10.1093/mnrasl/slab074

Rivilla, V. M., Jiménez-Serra, I., Martín-Pintado, J., Briones, C., Rodríguez-Almeida, L. F., Rico-Villas, F., et al. (2021a). Discovery in Space of Ethanolamine, the Simplest Phospholipid Head Group. *Proc. Natl. Acad. Sci. U.S.A.* 118, e2101314118. doi:10.1073/pnas.2101314118

Rivilla, V. M., Martín-Pintado, J., Jiménez-Serra, I., Martín, S., Rodríguez-Almeida, L. F., Requena-Torres, M. A., et al. (2020). Prebiotic Precursors of the Primordial RNA World in Space: Detection of NH2OH. *Astrophysical J.* 899, L28. doi:10.3847/2041-8213/abac55

Rivilla, V. M., Martín-Pintado, J., Jiménez-Serra, I., Zeng, S., Martín, S., Armijos-Abendaño, J., et al. (2019b). Abundant Z-Cyanomethanimine in the Interstellar Medium: Paving the Way to the Synthesis of Adenine. *MNRAS* 483, L114–L119. doi:10.1093/mnrasl/sly228

Robertson, M. P., and Miller, S. L. (1995). An Efficient Prebiotic Synthesis of Cytosine and Uracil. *Nature* 375, 772–774. doi:10.1038/375772a0

Rodriguez, L. E., House, C. H., Smith, K. E., Roberts, M. R., and Callahan, M. P. (2019). Nitrogen Heterocycles Form Peptide Nucleic Acid Precursors in Complex Prebiotic Mixtures. *Sci. Rep.* 9, 9281. doi:10.1038/s41598-019-45310-z

Rodríguez-Almeida, L. F., Jiménez-Serra, I., Rivilla, V. M., Martín-Pintado, J., Zeng, S., Tercero, B., et al. (2021a). Thiols in the Interstellar Medium: First Detection of HC(O)SH and Confirmation of C2H5SH. *Astrophysical JournalL* 912, L11. doi:10.3847/2041-8213/abf7cb

Rodríguez-Almeida, L. F., Rivilla, V. M., Jiménez-Serra, I., Melosso, M., Colzi, L., Zeng, S., et al. (2021b). First Detection of C2H5NCO in the ISM and Search of Other Isocyanates towards the G+0.693-0.027 Molecular Cloud. *Astronomy Astrophysics* 654, L1. doi:10.1051/0004-6361/202141989

Rodríguez-Fernández, N. J., Tafalla, M., Gueth, F., and Bachiller, R. (2010). HNCO Enhancement by Shocks in the L1157 Molecular Outflow. *Astronomy Astrophysics* 516, A98. doi:10.1051/0004-6361/201013997

Rosi, M., Skouteris, D., Casavecchia, P., Falcinelli, S., Ceccarelli, C., and Balucani, N. (2018). "Formation of Nitrogen-Bearing Organic Molecules in the Reaction NH + C2H5: A Theoretical Investigation and Main Implications for Prebiotic Chemistry in Space," in International conference on computational science and its applications (Berlin, Germany: Springer), 773–782. doi:10.1007/978-3-319-95165-2_54

Schwahn, G., Schieder, R., Bester, M., and Winnewisser, G. (1986). The Millimeter Wave Spectrum of Cyanoallene, CH2 · C · CH · CN, Using a New Digital Lock-In Technique. *J. Mol. Spectrosc.* 116, 263–270. doi:10.1016/0022-2852(86)90126-8

Schwartz, A. W., and Goverde, M. (1982). Acceleration of Hcn Oligomerization by Formaldehyde and Related Compounds: Implications for Prebiotic Syntheses. *J. Mol. Evol.* 18, 351–353. doi:10.1007/bf01733902

Shriner, R. L., and Neumann, F. W. (1944). The Chemistry of the Amidines. *Chem. Rev.* 35, 351–425. doi:10.1021/cr60112a002

Tercero, F., López-Pérez, J. A., Gallego, J. D., Beltrán, F., García, O., Patino-Esteban, M., et al. (2021). Yebes 40 M Radio Telescope and the Broad Band Nanocosmos Receivers at 7 Mm and 3 Mm for Line Surveys. *Astronomy Astrophysics* 645, A37. doi:10.1051/0004-6361/202038701

Todd, Z. R., and Öberg, K. I. (2020). Cometary Delivery of Hydrogen Cyanide to the Early Earth. *Astrobiology* 20, 1109–1120. doi:10.1089/ast.2019.2187

Tonolo, F., Lupi, J., Puzzarini, C., and Barone, V. (2020). The Quest for a Plausible Formation Route of Formyl Cyanide in the Interstellar Medium: a State-Of-The-Art Quantum-Chemical and Kinetic Approach. *Astrophysical J.* 900, 85. doi:10.3847/1538-4357/aba628

Turner, B. E. (1971). Detection of Interstellar Cyanoacetylene. *Astrophysical J.* 163, L35. doi:10.1086/180662

Turner, B. E., Liszt, H. S., Kaifu, N., and Kisliakov, A. G. (1975). Microwave Detection of Interstellar Cyanamide. *Astrophysical J.* 201, L149–L152. doi:10.1086/181963

Woon, D. E. (2021). The Formation of Glycolonitrile (HOCH2CN) from Reactions of C+ with HCN and HNC on Icy Grain Mantles. *Astrophysical J.* 906, 20. doi:10.3847/1538-4357/abc691

Zellner, N. E. B., McCaffrey, V. P., and Butler, J. H. E. (2020). Cometary Glycolaldehyde as a Source of Pre-rna Molecules. *Astrobiology* 20, 1377–1388. doi:10.1089/ast.2020.2216

Zeng, S., Jiménez-Serra, I., Rivilla, V. M., Martín, S., Martín-Pintado, J., Requena-Torres, M. A., et al. (2018). Complex Organic Molecules in the Galactic Centre: the N-Bearing Family. *Mon. Notices R. Astronomical Soc.* 478, 2962–2975. doi:10.1093/mnras/sty1174

Zeng, S., Jiménez-Serra, I., Rivilla, V. M., Martín-Pintado, J., Rodríguez-Almeida, L. F., Tercero, B., et al. (2021). Probing the Chemical Complexity of Amines in the ISM: Detection of Vinylamine (C2H3NH2) and Tentative Detection of Ethylamine (C2H5NH2). *Astrophysical JournalL* 920, L27. doi:10.3847/2041-8213/ac2c7e

Zeng, S., Quénard, D., Jiménez-Serra, I., Martín-Pintado, J., Rivilla, V. M., Testi, L., et al. (2019). First Detection of the Pre-biotic Molecule Glycolonitrile (HOCH2CN) in the Interstellar Medium. *MNRAS* 484, L43–L48. doi:10.1093/mnrasl/slz002

Zeng, S., Zhang, Q., Jiménez-Serra, I., Tercero, B., Lu, X., Martín-Pintado, J., et al. (2020). Cloud-cloud Collision as Drivers of the Chemical Complexity in Galactic Centre Molecular Clouds. *MNRAS* 497, 4896–4909. doi:10.1093/mnras/staa2187

Conflict of Interest: The authors declare that the research was conducted in the absence of any commercial or financial relationships that could be construed as a potential conflict of interest.

frontiers | Frontiers in Astronomy and Space Sciences

TYPE Perspective
PUBLISHED 10 August 2022
DOI 10.3389/fspas.2022.809928

OPEN ACCESS

EDITED BY
Ashraf-Ali,
University of Maryland, College Park,
United States

REVIEWED BY
David Van Vranken,
University of California, Irvine,
United States
Ranajit Talukdar,
University of Colorado Boulder,
United States

*CORRESPONDENCE
Thomas Mathew,
tmathew@usc.edu
G. K. Surya Prakash,
gprakash@usc.edu

SPECIALTY SECTION
This article was submitted to Astrochemistry, a section of the journal Frontiers in Astronomy and Space Sciences

RECEIVED 05 November 2021
ACCEPTED 05 July 2022
PUBLISHED 10 August 2022

CITATION
Mathew T, Esteves PM and Prakash GKS (2022), Methanol in the RNA world: An astrochemical perspective. *Front. Astron. Space Sci.* 9:809928. doi: 10.3389/fspas.2022.809928

Methanol in the RNA world: An astrochemical perspective

Thomas Mathew[1]*, Pierre Mothé Esteves[2] and G. K. Surya Prakash[1]*

[1]Loker Hydrocarbon Research Institute and Department of Chemistry, University of Southern California, Los Angeles, CA, United States, [2]Department of Organic Chemistry, Instituto de Química, Universidade Federal do Rio de Janeiro, Rio de Janeiro, Brazil

The role and relevance of methanol in the origin and structure of the RNA world is discussed. Methanol is a pivotal, renewable, and regenerable source from which almost all chemical materials, simple or complex, can be accessed. Olefins and carbonyl compounds, amines and amino acids, peptides and polypeptides, and the molecular building blocks in the initial stages of the biological evolution to life's origin are obtained through methanol as a source material by its chemical transformation. The formation of methanol, whether in stellar and interstellar media, in deep sea-bottom hot hydrothermal vents or from geothermal sources, results from CO_2 hydrogenation. It is the basic reaction, setting the stage for the formation of fundamental "organic" building blocks for the formation of simple prebiotic cells to subsequent biological evolution to cells. The important observation of many organics– hydrocarbons and ions including the large expanse of methane and methanol in the interstellar medium and stellar peripheries is a clear indication of "stellar reductive processes" and ensuing reactions shedding light on the probable significant role of extraterrestrial methanol as the basic source material toward a multi-step transformation into complex life molecules such as RNA.

KEYWORDS

interstellar medium (ISM), complex organic molecules (COMs), astro methanol-to-olefin (AMTO) synthesis, carbonaceous meteorites, quantum mechanical tunneling, the Methanol Economy

1 Introduction

In this perspective, the relevance and significance of C1 molecules, especially the key role of methanol in the formation of simple to complex organic molecules, in the interstellar medium (ISM) is discussed. Since the presence of many of these molecules in ISM and their role as leading sources to signature chemical units for life's architecture such as amino acids, proteins, nucleic bases, and nucleic acids in the terrestrial world are well-known, the probability of a similar scenario in the astrochemical world is discussed. Following the introduction (Section 1), a brief discussion of extraterrestrial molecules and molecular ions, especially relevant C1 units (Section 2) is presented. In Section 3, the formation of methanol in the stellar and interstellar media as well as the proposed routes/constraints for its formation (Section 3.1), transformation of methanol to hydrocarbons

(MTHC) and its relevance in terrestrial and astrochemical world (Section 3.2), and the significance of methanol as a key synthon to access complex organic molecules and eventually to RNA and DNA (Section 3.3) is presented. The concluding Section 4 emphasizes the intermediacy of methanol as a reactive C_1 building block and its key role in protocols that would lead to the formation of fundamental building blocks for the entry to the RNA world and its subsequent biological evolution to primitive cells.

Chemistry plays a central role in every feature of human life, its environment, and its multi-faceted society (Shaik, 2003; Bertozzi, 2015; Roth, 2015; Mahaffy et al., 2019). Behind life and its processes, along with hydrogen and oxygen, the most important element which plays the biggest role is carbon. Miller & Urey (1959) pioneering studies in search of primordial chemistry in the mid-20th century rejuvenated serious discussions about the scientific understanding of nature and the source of origin of life and life molecules. Their classic experiment (Miller, 1953) was conducted using a mixture of simple precursor molecules—hydrogen, ammonia, methane, and water—under electric discharge or conditions thought to be similar to those of the primordial soup (Oparin, 1924; Haldane, 1929; Oparin, 1952) which showed the formation of varied amino acids, the building blocks to polypeptides and eventually proteins, essential to the formation of living systems. Recent observations indicate that the Earth's original atmosphere and its chemical composition might have been different from Miller's conditions. However, the results from his studies provide a significant insight into the primordial molecular interaction and chemical aspects of the evolutionary process toward further terrestrial life.

In Miller's spark experiment, the gas mixture containing the reactive product molecules HCN, aldehydes, or ketones was subsequently allowed to disperse into the aqueous phase where they underwent Strecker synthesis to yield amino acids such as glycine and other compounds. Later, further simulation studies with the permutation combination of similar experimental conditions showed even the possibility of extraterrestrial formation of many other building blocks such as sugars and nucleotides, besides amino acids (Horst et al., 2012). In the following decades, with the discovery of the structure of nucleic acids and the development of modern biology sparked by the revolutionary achievement of Watson & Crick (1953), there has been a giant leap in our understanding of biological systems and our quest to unravel the essential and historical question of ages—origin and evolution of life from inanimate precursor molecules.

In our search for the carbon source of these precursor molecules, the possible role of the simplest C1 molecules such as carbon dioxide (CO_2), methane (CH_4), or its oxygenate methanol (CH_3OH) and their derivatives has been a theme of serious discussion in the last few decades. It is now quite clear that under suitable conditions as in the liquid water lakes or in the depth of the oceans of our Earth, seeding the simplest inanimate precursor molecules such as methane, methanol, and ammonia can lead to fundamental building blocks of life such as amino acids, proteins, and sugars, as revealed by Miller's pioneering studies (Miller, 1953; Miller & Urey, 1959). The relevance and significance of C1 molecules, especially methanol as the source material for many higher organic and biological molecules including the unique multifunctional biopolymer, the RNA, will be discussed in the ensuing sections.

2 Extraterrestrial molecules and molecular ions

Nucleosynthesis of carbon and its transformations in stellar and interstellar media (ISM) is well known. The formation and transformation of molecules and molecular ions play an important role in the constitution and vitality of the interstellar medium. Interstellar medium is rich in C1 compounds and ions such as CH_4, its protonated ion CH_5^+ and its oxygenated CH_3OH, HCHO, CO, CO_2, etc. Astronomers have already identified over 250 molecular species as interstellar molecules (Yamamoto, 2017; McCarthy & McGuire, 2021; Woon, 2021; Guélin and Cernicharo, 2022). In the ISM, the carbon atom remains in its ionized form C^+, its dominant form in the gas phase (Williams, 2005; Liszt, 2011). As expected, this species and its hydrogenated and oxygenated forms contribute to a subsequent chemical evolution to rich C1 chemistry. White et al. (1999), Oka (2015) studied the presence and spectral characteristics of CH_5^+, the parent C_1 carbonium ion, with reference to related studies by Olah et al. (2009) in the development of non-classical carbonium ion chemistry through his pioneering efforts in identifying this fundamental species and its related ions along with a wide array of classical carbocations (carbenium ions) under terrestrial conditions in the condensed-state in super acid media.

Contrary to earlier thoughts that an interstellar medium poses an unsafe atmosphere for the formation of organic species and their survival, many molecules and ions (over 200), cyclic as well as open chain hydrocarbons and their derivatives have been discovered since the last five decades (Herbst & van Dishoeck 2009; Tielens, 2013; McGuire, 2022). Well established by now, both methane and its mono oxygenate methanol are among the most abundant molecular species in interstellar clouds and stellar peripheries in the observable galaxies spanning many billions of miles (Harvey-Smith & Cohen, 2006; Heward, 2006; Whittet et al., 2011). In fact, it was found that in high-mass protostellar object W33A, the abundance of methanol (CH_3OH) is significant, exceeding that of both CO and CO_2 (Gibb et al., 2000). Detection of various carbocations and their terrestrial analogs starting from CH_5^+ (methanium ion) in Titan's upper atmosphere through Cassini–Huygens mission using the ion neutral mass spectrometer (INMS) and the Cassini plasma spectrometer (CAPS) instruments on board (Ali et al., 2013; Puzzarini

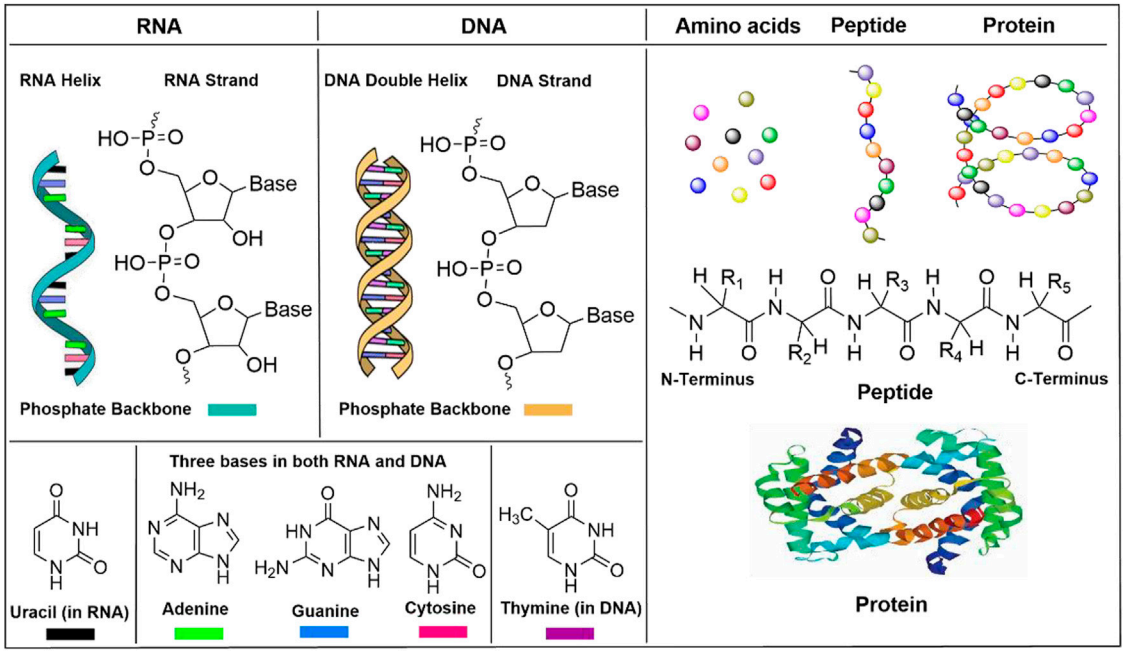

FIGURE 1
Chemistry of RNA, DNA, and protein- fundamentals of the property of life.

et al., 2014; Ali et al., 2015) not only sheds light on the ongoing abiotic organic synthesis in an extraterrestrial world—in the ISM and on the surface of other planets and stars, but also its remarkable relationship to non-classical carbonium ion chemistry similar to that observed in the terrestrial world. Studies of the aerosol contents in Titan's thermosphere–ionosphere by negative ion measurements by the CAPS′ Electron Spectrometer (ELS) showed the formation of unsaturated anion carbon chains and positive ion measurements using the ion neutral mass spectrometer (INMS) indicate cation formations of many aromatic hydrocarbons (Sittler et al., 2020).

The discovery of many polyaromatic entities such as $C_7H_{11}^+$, $C_{11}H_9^+$, $C_{15}H_{11}^+$, etc., on the surface of Titan discussed by Ali et al. (2013, 2015) and their formation as vital intermediates toward more complex systems starting with simple molecular entities such as CH_5^+ formed outside the terrestrial perimeter emphasizes the role and the scope of astrosynthesis, which leads to a molecular evolution from simple systems to complex systems (Puzzarini, 2017). The relevance of an RNA–world hypothesis to the origin of life is further supported by the current understanding of the basic elements for life architecture such as proteins (of which amino acids are the simple precursors) and nucleic acids (both DNA and RNA, of which, the phosphate backbone with ribose and nucleic bases are properly integrated) (Figure 1) as well as the presence of their source chemical entities in terrestrial, stellar, and interstellar media.

Apart from the Earth, in the other three so-called terrestrial planets- Mercury, Venus, and Mars, presence of organics has been reported. For example, a surface reflectance study with the mercury laser altimeter (MLA) on board the MESSENGER spacecraft on permanently shadowed areas near Mercury's north pole indicated the presence of surface water-ice in the optically bright regions (bright deposits) and a surface layer of complex organic material in the dark regions (dark deposits), which might have originated from impacts of comets or volatile-rich asteroids (Newmann et al., 2013). A recent re-analysis of the data from a large probe neutral mass spectrometer (LNMS) on board the Pioneer Venus Multiprobe (Pioneer 13) during its mission in 1978 showed the presence of traces of several chemical species related to anaerobic phosphorus metabolism (phosphine), anoxygenic photosynthesis (nitrite), and the nitrogen cycle in Venus' clouds (Mogul et al., 2021). Reports from the SAM (Sample Analysis at Mars) data showed conclusive evidence for the presence of organic compounds, both aliphatic and aromatic including thiophene in samples drilled out from Mars' Gale Crater (Lyons et al., 2005; Kite et al., 2017; Eigenbrode et al., 2018; ten Kate, 2018). Despite the fact that no conclusive evidence for extraterrestrial biology has been obtained so far, all these findings underscore our statement in one of our previous reports (Olah et al., 2016a) as noted by Puzzarini (Puzzarini et al., 2017), "*Of particular interest to us is the remarkable detection of varied carbocations and their similarity with their terrestrial analogs. The proven similarity with our terrestrial studied*

$$CO_2 + 4H_2 \longrightarrow CH_4 + 2H_2O \qquad \Delta H_{298K} = -39.4 \text{ kcal/mol} \quad (1)$$

$$CO_2 + H_2 \longrightarrow CO + H_2O \qquad \Delta H_{298K} = +9.8 \text{ kcal/mol} \quad (2)$$

$$CO_2 + H_2 \longrightarrow HCOOH \qquad \Delta H_{298K} = +3.6 \text{ kcal/mol} \quad (3)$$

$$CO + H_2 \longrightarrow HCHO \qquad \Delta H_{298K} = -25.5 \text{ kcal/mol} \quad (4)$$

$$CO_2 + 3H_2 \longrightarrow CH_3OH + H_2O \qquad \Delta H_{298K} = -11.8 \text{ kcal/mol} \quad (5)$$

$$CO + 3H_2 \longrightarrow CH_4 + H_2O \qquad \Delta H_{298K} = -49.2 \text{ kcal/mol} \quad (6)$$

SCHEME 1
Different possible steps in CO_2 Hydrogenation.

chemistry provides the first scientific evidence that our Earth is not a unique celestial body for producing the chemical building blocks." All these observations suggest that these ions and molecules define the future of chemical and biological complexity and activity in the interstellar medium.

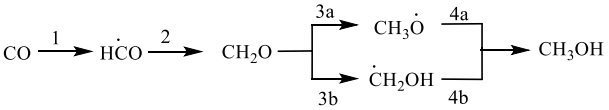

SCHEME 2
Formation of methanol by successive CO hydrogenation.

3 Relevance and significance of methanol in stellar and interstellar media

Methanol is one of the most significant, highly versatile chemicals with innumerable applications—as a synthetic feedstock for various commodity chemicals, as fuel, and as a source material in fuel cells and pharmaceuticals. Its terrestrial and extraterrestrial presence suggests its adept role in the tellural and the astrochemical world. Parent C_1 hydrocarbon methane, the major ingredient of Earth's natural gas and the terrestrial hydrogenation product of CO_2 (Sabatier's methanation reaction) (Sabatier et al., 1902; Fujita et al., 1993; Wang et al., 2011Fechete, 2016) is also present in Mars' atmosphere in conspicuous amounts with seasonal variation (Webster et al., 2018). The partially hydrogenated intermediates formic acid, formaldehyde, and methanol are key synthons in many organic synthetic reactions. The indisputable role of these signature substances, especially methanol in the molecular evolution to cells' building blocks such as sugars, nucleic bases, and proteins following known synthetic pathways is manifested by many studies in recent years. This motivates us for further exploration of astrochemical evolution in the stellar and interstellar territory.

3.1 Formation of methanol in stellar and interstellar media

Though homogeneous and heterogeneous reductions of CO_2 to methanol are already established under terrestrial conditions, the exact extraterrestrial conditions (and the suggested pathways) for the formation of vast methanol clouds in stellar and interstellar regions are yet to be revealed. The overall reduction process (methanation) is exothermic (ΔH_{298K} = −39.4 kcal/mol, Scheme 1, Eq. 1) but the initiation of the process needs optimal conditions such as high pressure, high temperature, and a suitable catalyst to overcome the kinetic barrier. At the initial stage, the reduction process can proceed through deoxygenation to CO (reverse water gas shift reaction, Scheme 1, Eq. 2) (Porosoff et al., 2016) or even direct hydrogenation to formic acid (HCOOH) if it meets the appropriate conditions. Both of these initiation steps (Scheme 1, Eqs 2, 3) are endothermic processes. However, after the initiation at the region of high temperature and pressure in the interstellar medium and the dispersal to the interstellar medium with drastic reduction in concentration and temperature, the probability for the controlled reduction process in a thin layer of interstellar CO_2 dust grains to methanol by a diffused thin layer of hydrogen (similar to terrestrial RWGS reaction) is worth considering. Various possible steps during CO_2 hydrogenation are shown in Scheme 1. The first organic acid detected in the interstellar medium was formic acid. A dense cloud of formic acid (HCOOH) was located not only in the dark cloud (e.g., L 134 N) (Irvine et al., 1988; Irvine et al., 1990) but also inside the hot cores (hot star-forming cores) in molecular clouds, namely, Sagittarius B2, Orion KL, and W51 ((Liu et al., 2001; Remijan et al., 2004; Tercero et al., 2018; Li et al., 2020). Detection of compounds such as methylenimine (H_2C=NH), intermediate

hydrogenation products from HCN in the interstellar atmosphere in cogent amounts also reveals the hydrogenation process prevalent there (Dickens et al., 1997). Individual hydrogenation experiment with both solid HCN and CH_2NH leads to the formation of methylamine suggesting the possibility of CH_2NH being the active intermediate during HCN hydrogenation to CH_3NH_2. This shows the significance of the incessant hydrogenation process occurring in ISM (Theule et al., 2011).

The major route for the formation of methanol would be the successive hydrogenation of CO on the surfaces of interstellar dust grains. (Tielens & Whittet, 1997; Watanabe et al., 2004; Hidaka et al., 2009). Using a cold (30 K) atomic hydrogen beam, Watanabe et al. (2004) investigated the hydrogenation of CO on pure solid CO and CO–H_2O mixed ice at temperatures below 20 K and noticed that it proceeds efficiently producing methanol in both cases. Upon exposure to cold H atoms, CO is consumed with successive hydrogenation first to HCHO and subsequently CH_3OH, leading to a mixture of both HCHO and CH_3OH below 12 K. $H^{\cdot}$ has good mobility which favor the formation of reduction products HCHO and CH_3OH (Bredehöft, 2020). Simulation studies also show that molecules such as CH_3OH, H_3O, and CO_2 can be formed in the solid state in the ISM without the need for energetic processing such as thermal, UV/cosmic ray processing (i.e., through H-atom addition) (Ioppolo et al., 2011). The transition of CO_2 from a solid form (dry ice, below 194.5 K) to a gaseous form at and below the ambient pressure suggests a much longer lifetime as solid and reactive interaction period for CO_2 with associated molecules in the interstellar ice grains during various events at varying temperatures compared to those for CO, which has a much lower freezing point (81.5 K, ambient pressure) but a greater reactivity once it is formed.

For a successive hydrogen addition on CO to occur at very low temperatures, quantum mechanical tunneling through the activation barrier is suggested and the formation of methanol occurs at the warm-up period and is then released when the dust is warmed by radiation from the newly formed star. Garrod et al. (2006) studied a gas-phase model that included the simulation of the surface formation of methanol on ice grains similar to the formation of molecular hydrogen. They also utilized a gas–grain code suggesting a mechanism for desorption of methanol following the warming-up due to exothermic chemical reactions. This can be a viable route for the emulation of the observed abundance of the gas-phase methanol as well as many gas-phase species in the dark and cold molecular clouds such as the well-known Taurus TMC1-CP (Soma et al., 2015). Since the calculated activation barriers for step 1 and step 3 (Scheme 2) are high, they are proposed to occur by quantum mechanical tunneling reactions (Woon, 2002). Though the formation of $\cdot CH_2OH$ in the third step (3b) is energetically viable and more exothermic than that of $CH_3O\cdot$ (3a), its probability is lower as it has a higher activation barrier (Tielens & Whittet, 1997; Woon, 2002; Osamura et al., 2005). However, it is possible that favorable reaction conditions, which can reduce the activation barrier, may also arise as a result of many astrophysical events in the interstellar medium.

Methane absorbed on the surface of interstellar space ice/dust grains, can facilitate methanol formation in an otherwise extreme dilution of space as it can also act as a reductant at appropriate temperature–pressure conditions developing over time during stellar events as observed in our extensively studied single step bi-reforming/oxidative bi-reforming reactions, under terrestrial conditions though such a comparison needs to be justified by further experimental studies (Olah et al., 2013; Olah et al., 2015; Olah and Mathew, 2015). Carbon oxides synthesized by the interaction of carbon and oxygen already formed in the interiors of stars are ejected to ISM and undergo subsequent hydrogenation on the surface of space ice/dust grains to give methanol as observed in telluric chemistry. Recently, we achieved direct glycol-assisted CO_2 hydrogenation to methanol using heterogeneous $Cu/ZnO/Al_2O_3$ with high efficacy, further underscoring the relevance of our direct CO_2-methanol concept (Sen et al., 2021) in telluric chemistry. It emphasizes the significance of the hypothesis of similar possibilities in the interstellar medium.

A spectral survey of the star forming region W51 e1/e2, mainly in the hot cores showed the signs of about 105 molecules and their isotopic species (Kalenskii and Johansson, 2010). These include CO, CS, HCN, CH_3OCH_3, CH_3COCH_3, CH_3OCHO, C_2H_5OH, CH_3CN, CH_3OH, H_2O, and SO_2 along with various molecular ions such as N_2H^+, HCO^+, and HCS^+. However, in the condensed phase of interstellar dust grains, CO, CO_2, and H_2O are the most abundant molecules. CO_2 has been identified in many interstellar sites such as dense ISM clouds, YSOs (young stellar objects) (Ehrenfreund & Charnley, 2000), and comets (Irvine et al., 2000; Bibring et al., 2015). Interestingly, the widely accepted route for CO_2 formation is the energetic processing of carbon monoxide with water acting as the oxygen donor on dust grain surfaces (Bredehöft, 2020). It reveals the interstellar water gas shift reaction (WGSR) prevalent in the stellar/interstellar medium. Therefore, it is quite reasonable to suggest that the stellar equivalent of WGSR occurs at stellar peripheries and reverse water gas shift (RWGS) reactions occur on dust grain surfaces in the interstellar medium. Other products observed during energetic processing studies {UV light (Milligan & Jacox, 1971; Allamandola et al., 1988; Watanabe & Kouchi, 2002; Watanabe et al., 2007), slow and fast electron beams (Yamamoto et al., 2004; Bennett et al., 2011; Petrik et al., 2014a; Petrik et al., 2014b; Schmidt et al., 2019); X-ray (Laffon et al., 2010)}, mimicking processes under radiative conditions (such as cosmic radiations) in the interstellar medium include formaldehyde, formic acid, and methanol. As early as over half a century ago, many researchers were able to detect ammonia (Cheung et al., 1968), methanol (Ball et al., 1970), formic acid (Zuckerman et al., 1971), and formaldehyde (Snyder et al., 1969) in the interstellar space where high energy radiation is imminent,

hence the formation of amino acids in interstellar space is well explicable. Wollin and Ericson (Wollin & Ericson, 1971) were able to isolate a series of amino acids by mixing ammonia, methanol, and formic acid/formaldehyde (all in gaseous form, detected in interstellar medium) at 115°C and subjecting the resulting product mixture to UV irradiation (275 W) at 35°C in a trial to identify the products in an astrochemical context, though the conditions and atmospheres do not hold an exact similarity.

Oxygen insertion into methane has been manifested to be an alternate pathway for the formation of methanol as well as complex organic molecules (COMs) on stellar/interstellar ice dust particles (Bergner et al., 2017). In condensed systems, oxygen insertion into CH_4 has been demonstrated by the photolysis of oxygenating compounds at very low temperatures (9–25 K) under appropriate conditions such as HOF in a CH_4 matrix under high vacuum of ~10^{-7} Torr (Appleman et al., 1989), N_2O or O_3 in to CH_4 in an Ar matrix (Parnis et al., 1993; Lugez et al., 1994), etc. UV–visible irradiation (broad-band) of argon matrices containing 2% N_2O and 10% of methane resulted in the formation of CH_3OH as the dominant photoproduct from the reaction of methane with the first excited atomic oxygen, $O(^1D)$ (Parnis et al., 1993). Similarly, oxygen insertion in the C-H bond with $O(^1D)$ generated by ozone during photolysis of CH_4/O_3 in a low-temperature argon matrix gave CH_3OH (Lugez et al., 1994) as the major product as noted in the case of silane (SiH_4) and ozone (Withnall & Andrews, 1988). It is quite intriguing to note that the vibrational spectrum of the product mixture obtained by the irradiation of a mixture of CH_3OH (0.1% in Ar) and ozone (0.5% in Ar) at 11 K, showed the formation of CO, CH_2O, H_2O, and H_2O_2 revealing further probable oxidation and oxidative dissociation pathways under ISM-like conditions (Scheme 3). Methanol oxygenation can occur either by oxygen insertion into the C-H bond or O-H bond, C-H insertion leads to dihydroxy methane or methyl hydroperoxide, which decomposes to formaldehyde and water.

Knowing the significance of methane, mono-oxygenate methanol and its role as a key synthon toward many pivotal substrates for their molecular evolution to complex biological molecules; it is worthwhile to discuss a few prominent reactions, which are suggested as fundamental routes and a practical approach to their access.

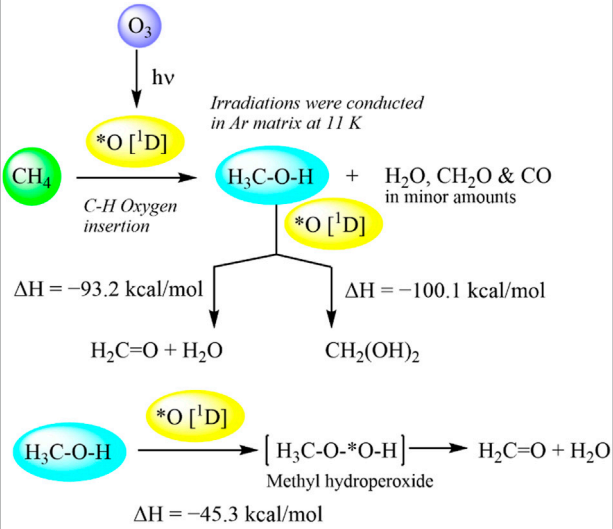

SCHEME 3
Oxygenation of methane and methanol under ISM-like conditions.

3.2 Methanol-to-hydrocarbon process

Methanol-to-hydrocarbon (MTHC) process can be considered as fundamental in the transformation of methanol to complex organic molecules (COMs). Methanol is spotted in many regions of the interstellar medium (vide supra). Vast areas of the methanol cloud spread into billions of square miles in the interstellar medium similar to the one as a cloudy bridge of methanol, which surrounds Sagittarius B2, is 288 billion miles wide in the milky way Galaxy itself (Harvey-Smith & Cohen, 2006; Heward, 2006; Whittet et al., 2011). Therefore, it is quite rational in viewing its astrochemical role as a prominent molecular synthon in the formation of COMs in the interstellar medium. In our terrestrial (telluric) hydrocarbon chemistry, methanol-to-hydrocarbon (MTHC) transformations over acidic zeolites (HZSM-5) by the Mobil research team (Miesel et al., 1976; Chang & Lang, 1977; Rollmann, 1982) as well as via a bifunctional acid–base catalysis by Olah (1983); Olah et al. (1984); Olah & Prakash (2009) have been established in the 1970s, 1980s, and later (Scheme 4). Gasoline shortage in the 1970s led to pioneering efforts by many research groups to develop a methodology for synthetic fuels (synfuels). The simple and convenient commercially developed catalytic process for the conversion of methanol to hydrocarbons (gasoline with high octane numbers, 90–95) using shape-selective zeolite catalysts was first announced by Mobil Chemicals in 1976 (Miesel et al., 1976). Gasoline of superior quality has been produced in much higher yield by this method compared to the nature of the product obtained by Fischer–Tropsch (FT) chemistry. These studies showed that not only methanol, but many hetero-organic compounds could also lead to hydrocarbons with high efficacy (Chang & Silvestri, 1977; Chang & Silvestri, 1987). Further studies (Liang et al., 1990) showed that SAPO catalysts drive this reaction with high conversion and yield. In general, methanol-to-hydrocarbon (MTHC) processes (Scheme 3) include methanol-to-olefin (MTO), methanol-to-gasoline (MTG), and methanol-to-aromatics (MTA) processes.

As more and more secrets of interstellar space and prevailing molecular composition thereof unfold, it is no wonder that

T= 298.15 K

$CH_3OH_2^+ \xrightarrow[\text{(energetic radiations as in ISM)}]{h\nu} {}^1CH_2 + H_3O^+$ (methylene (singlet))	(1)	$\Delta H_{298.15K}$ = +107.4 kcal/mol $\Delta S_{298.15K}$ = +33 cal/mol K $\Delta G_{298.15K}$ = +97.3 kcal/mol
$2\ {}^1CH_2 \longrightarrow CH_2{=}CH_2$	(2)	$\Delta H_{298.15K}$ = -188.7 kcal/mol $\Delta S_{298.15K}$ = -38 cal/mol K $\Delta G_{298.15K}$ = -177.4 kcal/mol
$CH_3OH_2^+ + CH_2{=}CH_2 \longrightarrow CH_3{-}CH_2{=}CH_2 + H_3O^+$	(3)	$\Delta H_{298.15K}$ = -1.2 kcal/mol $\Delta S_{298.15K}$ = -1 cal/mol K $\Delta G_{298.15K}$ = -0.8 kcal/mol
$CH_3OH_2^+ + H_3^+ \longrightarrow CH_5^+ + H_3O^+$	(4)	$\Delta H_{298.15K}$ = -40.3 kcal/mol $\Delta S_{298.15K}$ = +5 cal/mol K $\Delta G_{298.15K}$ = -41.8 kcal/mol
$CH_5^+ \longrightarrow {}^1CH_2$ (methylene (singlet)) $+ H_3^+$	(5)	$\Delta H_{298.15K}$ = +147.3 kcal/mol $\Delta S_{298.15K}$ = +28 cal/mol K $\Delta G_{298.15K}$ = +139.1 kcal/mol

T= 10 K

$CH_3OH_2^+ \xrightarrow[\text{(energetic radiations as in ISM)}]{h\nu} {}^1CH_2 + H_3O^+$ (methylene (singlet))	(1)	ΔH_{10K} = +105.2 kcal/mol ΔS_{10K} = +8 cal/mol K ΔG_{10K} = +105.1 kcal/mol
$2\ {}^1CH_2 \longrightarrow CH_2{=}CH_2$	(2)	ΔH_{10K} = -186.6 kcal/mol ΔS_{10K} = -12 cal/mol K ΔG_{10K} = -186.5 kcal/mol
$CH_3OH_2^+ + CH_2{=}CH_2 \longrightarrow CH_3{-}CH_2{=}CH_2 + H_3O^+$	(3)	ΔH_{10K} = -1.4 kcal/mol ΔS_{10K} = -3 cal/mol K ΔG_{10K} = -1.4 kcal/mol
$CH_3OH_2^+ + H_3^+ \longrightarrow CH_5^+ + H_3O^+$	(4)	ΔH_{10K} = -40.2 kcal/mol ΔS_{10K} = +5 cal/mol K ΔG_{10K} = -40.3 kcal/mol
$CH_5^+ \longrightarrow {}^1CH_2$ (methylene (singlet)) $+ H_3^+$	(5)	ΔH_{10K} = +145.4 kcal/mol ΔS_{10K} = +3 cal/mol K ΔG_{10K} = +145.4 kcal/mol

FIGURE 2
Probable pathways involved in the formation of ethylene and propylene by the "Astrochemical methanol to olefins (AMTO)" process in the ISM, the comparison of thermodynamic parameters at 298.15 and 10 K.

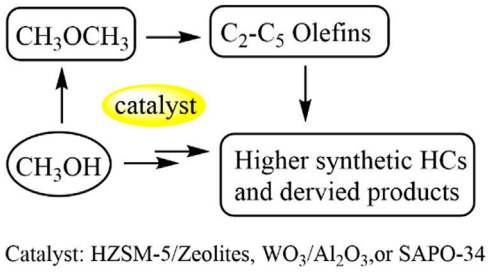

SCHEME 4
MTHC Process: From C_1-oxygenate methanol to higher hydrocarbons.

processes such as AMTO (astro methanol to olefin process similar to the terrestrial methanol to olefin process) can also occur. Computational studies showed that the conversion of methanol to ethylene can occur through the protolytic cracking of $CH_3OH_2^+$ in the presence of H_3^+ to give CH_5^+, a dominant astrochemical species in ISM (Olah et al., 1969; White and Tang, 1999; Oka, 2015), followed by a radiation-induced cleavage to CH_2 singlet and exergonic dimerization to ethylene. The reaction of H_3^+, also a dominant species in ISM (Oka, 2013; Oka, 2019), with $CH_3OH_2^+$ to form CH_5^+ is shown to be exothermic by 40.3 kcal/mol (Figure 2, Eq 4; ΔH = −41.7 kcal/mol by our earlier calculation-Olah et al., 2016b), suggesting that the AMTO route for the formation of ethylene from methanol is overall

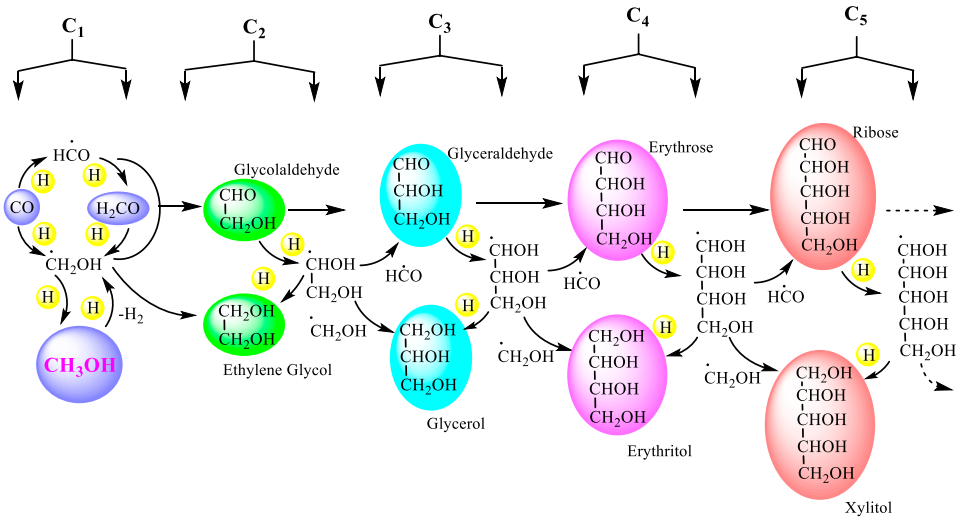

SCHEME 5
Astrohydrogenation of CO on interstellar dust grain surface, formation of methanol (wood alcohol), and the buildup of higher sugar alcohols and sugars in the interstellar medium (Fedoseev et al., 2017; Fedoseev et al., 2017).

thermodynamically favorable. Similar to the observed CH_5^+, protonation of CH_3OH to $CH_3OH_2^+$ also helps with stabilization against radiative dissociation to some extent. In our computational studies of the various steps shown with good probability for their involvement in the AMTO process, thermodynamic analysis at temperatures 298.15 and 10 K considering both the terrestrial and ISM thermal environments showed that for the conversion of methanol to ethylene, the pathway involving astrochemical protolytic cleavage of $CH_3OH_2^+$ promoted by interaction of H_3^+ to give CH_5^+-methanium ion, the simplest carbonium ion (Sefcik et al., 1974; Schreiner et al., 1993; Müller et al., 1997) can also be feasible. This pathway (Figure 2; Eq. 4) seems less probable due to charge–charge repulsion than the direct conversion of methanol to singlet methylene.

It should be pointed out that the laboratory microwave spectra for protonated methanol, $CH_3OH_2^+$, and protonated methane, CH_5^+ could not be obtained due to their irregularity from the effect of "fluxional" long-amplitude quantum motions over multiple minima on the potential energy surface. Therefore, search of these ions by rotational spectroscopy in the interstellar medium is still challenging (Puzzarini, 2017). However, it lays out a feasible connection of the chemistry of fluxonial methanium ion with methanol conversions and future studies can shed more light on the probability of these steps.

One can argue that, under extraterrestrial conditions such as varying temperatures (extremely low to high) and high-energy radiation, the feasibility of these reactions fluctuates considerably, however, optimal circumstances leading to favorable conditions may also arise intermittently. Although the radiative decomposition of the neutral form as well as the formation of protonated and clustered forms is an unavoidable process, the recurring formation of methanol can help to maintain its concentration without much depreciation. In fact, laboratory experiments approximating the composition of such systems show that the imperfection in dust grains are active sites promoting the association of $CH_3OH_2^+$ with neutral CH_3OH or even H_2 and CH_4 (association of CH_3OH with H_3^+ or CH_5^+ is also another probable course) via weak bonding interactions.

Results from the gas-phase ion cyclotron and vibrational spectroscopic studies of such clusters underscore the possibility of cluster formation (Kebarle et al., 1967; Kebarle et al., 1972; Hiraoka & Kebarle, 1975; Lau et al., 1982; Masamura, 2001; Witt et al., 2008). This shows that under suitable extraterrestrial conditions, a single carbon-containing building block can produce a large variety of hydrocarbons and their heteroatom derivatives. Therefore, as mentioned earlier, radiation induced monomolecular dehydration of methanol or "astrochemical methanol to olefins (AMTO)" process under the influence of highly energetic cosmic rays on suitable associated methanol dust or ice particles prevalent in the interstellar medium (ISM) through methyloxonium ion intermediate ($CH_3OH_2^+$) can be envisaged as a viable route to ethylene and propylene (Figure 2).

At both the terrestrial and ISM thermal conditions, the cleavage of $CH_3OH_2^+$ to give singlet methylene is an endothermic process (Figure 2; Eq. 1, equivalent to Eqs 4,5; $\Delta H_{298.15\ K}$ = +107.4 kcal/mol and $\Delta H_{10\ K}$ = +105.2 kcal/mol), while its dimerization to form ethylene is spontaneous, a highly exothermic process (Figure 2; Eq. 2; $\Delta H_{298.15\ K}$ = −188.7 kcal/mol and $\Delta H_{10\ K}$ = −186.6 kcal/mol). The structures, energies, and zero-point vibrational energies (ZPEs) of the structures were computed at the CCSD(T)/aug-cc-pVTZ level.

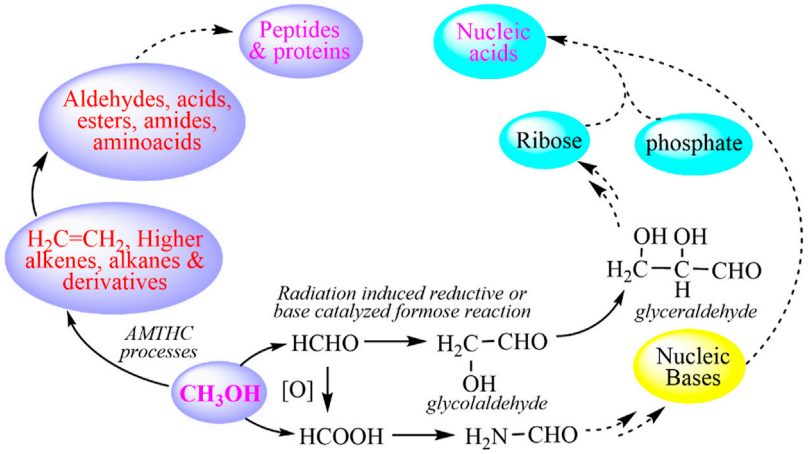

SCHEME 6
Methanol, the reactive intermediate, and viable key synthon toward prebiotic molecules.

3.3 Methanol, a key synthon toward complex organic molecules

Among the discoveries of an astrochemical recipe for the formation of various molecular forms identified in space, the formation of formaldehyde, methanol, glycolaldehyde, and glycerol, are crucial precursors and molecular backbones for the chemical evolution to form complex biological molecules, under prestellar core conditions has been achieved in recent years. Complex organic molecules (COMs) are formed in the interstellar medium by the interaction of interstellar ice grains with the ionizing radiations from galactic cosmic rays and the internal UV photon field in the cold molecular clouds containing the stellar nurseries/star-forming regions and planetary systems (Abplanalp & Kaiser, 2019). The interstellar ice mantles are comprised of molecules mainly H_2O, CO_2, CO, and CH_3OH with smaller amounts of HCHO, CH_4, NH_3, and HCOOH, of which, CH_3OH is present comparatively in significant amounts as methanol clouds (Gibb et al., 2004). Also, catalytic metal oxides/minerals (Duley, 1976; Goumans et al., 2007) and silicate grains (Jones, 2007) present in the ice dust can act as suitable catalysts for many astrochemical transformations. Therefore, our proposal of the possibility of an astrochemical MTHC reaction in the interstellar medium is based on these facts, though it needs to be further substantiated with results from more experimental studies.

Though smaller molecules such as carbon monoxide is very volatile and concentration in space is significantly low, at very low temperatures in ISM (10–25 K) they remain frozen on dust grains and accumulate creating a dense molecular cloud and seeding the formation of bigger molecules by cryogenic hydrogenation occurring in ISM. The veracity of this process has been demonstrated by mimicking hydrogenation of carbon monoxide by cryogenic hydrogen bombardment in the laboratory that resulted in the formation of formaldehyde, methanol, glycolaldehyde, and glycerol among others (Fuchs et al., 2009; Fedoseev et al., 2015; Fedoseev et al., 2017). This creates the roadmap to extraterrestrial, biologically relevant sugar molecules such as ribose and others as detected recently in carbonaceous chondrites, which include some of the most primitive meteorites (Furukawa et al., 2019). Recent studies by Kurokawa et al. (2022) have shown that surface materials of asteroids having 3.1 μm absorption features (indicative of ammoniated phyllosilicates) and carbonaceous chondrites (CCs) can originate from different regions of the same source, a single water–rock-differentiated parent body. Now, it is a generally accepted concept based on the results from numerous laboratory studies by astrochemical simulations, which imply that similar surface reactions by accumulation or coalescence of smaller species under the impact of cosmic rays, vacuum ultraviolet (VUV) photons, and thermal events prevailing in stellar and prestellar core conditions lead to the evolution of complex molecules (Charnley & Rodgers, 2008; Garrod et al., 2008; Herbst & van Dishoeck, 2009; Vasyunin, & Herbst, 2013; Walsh et al., 2014a; Walsh et al., 2014b; Linnartz et al., 2015; Öberg, 2016; Sewilo et al., 2019).

As mentioned earlier, experiments have shown that quantum mechanical tunneling can process many surface reactions, seemingly non-viable under ordinary conditions due to a high-activation barrier (Hama & Watanabe, 2013). Interaction of the H atom with CH_3OH leading to the formation of $\cdot CH_2OH$ and H_2 assisted by quantum mechanical tunneling can also be considered (Goumans & Kästner, 2010; Cuppen et al., 2017; Simonciõ et al., 2020). Radiolysis of methanol leads to $\cdot CH_2OH$, which on dimerization yields ethylene glycol (Harris et al., 1995; Bergantini et al., 2018). Formation of glycolaldehyde can be considered as the result of recombination of $\cdot CH_2OH$ and ·HCO (Butscher et al., 2015).

The aforementioned results from the studies of Fedoseev et al. (2017) suggest that under an atmosphere which allow the reaction to

continue, there is a great probability for the formation of higher sugar alcohols, sugar molecules including stream of ribose, and more complex molecules, which helps to provide answers to the questions on chemical evolution of complex biogenic molecules from cosmic origins (Scheme 5). Chemical ingredients for RNA and DNA, the basic structural motifs in the phenomenon of life—the amino acids, nucleobases, phosphates, and nucleosides are found in meteorites (Saladino et al., 2015; Saladino et al., 2016). Initial dimerization of formaldehyde to glycoladehyde through a free radical process though slow can occur under high energy radiations in the ISM. The reaction then turns autocatalytic and continues as glycoladehyde in trace quantities can catalyze the next aldol reaction to form glyceraldehyde from formaldehyde and glycoladehyde (Socha et al., 1980). With isomerization of glyceraldehyde to dihydroxy acetone and further aldol reaction, the chain grows to aldotetroses and then to ribose, the key building block of ribonucleic acid. Researchers proposed the formation of molecules of the (OH^-) type on interstellar oxide grains (Duley et al., 1978). Interstellar oxide grains which might include basic oxides such as CaO or MgO (Duley et al., 1978); corresponding hydroxides with ice particles in dust grains) can promote the base catalyzed formose reaction (Breslow, 1959) as generally studied (Scheme 6). While the formation of COMs through the recombination of reactive carbonaceous radicals during the CO to CH_3OH hydrogenation route is highly likely, we also suggested earlier that methanol itself, being very reactive C_1 oxygenate, can undergo the AMTO process forming olefins, which can provide aldehydes, amides, amino acids, etc., by known chemical transformations under varying conditions. The interstellar medium also provides varying conditions which may match up with the required parameters to drive these reactions. Formaldehyde can undergo the Cannizzaro reaction, the redox disproportionation to form methanol (and formic acid) and stepwise formose reaction (Orgel, 2000) to form sugars and Strecker reaction to form amino acids under appropriate conditions. The interstellar medium with a molecular mixture of heterosubstituted molecules such as HCN, NH_3, HCHO, $HCONH_2$, and CH_3OH (highly reactive intermediate) among interstellar ice dust particles with mineral granules can act as a continuous functional laboratory consisting of high temperature "ovens" and cryogenic "dewars" based on various galactic phenomena occurring in different regions. Therefore, astro MTO (methanol to olefin), MTHC (methanol to hydrocarbons), FTT (Fischer–Tropsch type), Cannizzaro and formose reactions, as well as the transformation of formamide to nucleobases are all probable under appropriate varying conditions of ISM developing intermittently and contribute to the cosmic origin of complex biogenic molecules (Olah et al., 2017). Identification of organic molecules such as acetaldehyde (CH_3CHO), formamide (NH_2CHO), and methyl formate ($HCOOCH_3$) achieved by remote observations at radio wavelengths also underscore the prevalent chemical processes in the ISM (Biver & Bockelée-Morvan, 2019).

Radiolysis studies of frozen methanol using heavy cosmic rays and energetic solar particle analogs show dissociation of CH_3OH to molecular species H_2CO, CH_2OH, CH_4, CO, CO_2, HCO, and $HCOOCH_3$ (de Barros et al., 2011). From HCHO (H_2CO) by radiation-induced reductive or base-catalyzed transformation, the formation of aldoses and polyalcohols from methanol can be envisaged. By the pioneering efforts of many astronomers, over 240 organic molecular species (McGuire, 2022) in neutral, ionic, and radical forms, simple (as water and ammonia) and complex were so far observed in the extraterrestrial world with the help of various onboard analytical instruments of spacecrafts such as the Cassini–Huygens spacecraft from the surface of Titan (the Moon of Saturn) and the Philae Lander that landed on comet 67P/Churyumov–Gerasimenko (Ali et al., 2015; Bibring et al., 2015) in the course of their visits. Also, albeit their presence in low concentration, at low-temperature regions, we suggest the possibility that many species in the molecular clouds (the densest interstellar clouds by ISM standards) remain in associated forms which would undergo the desired reactions as right conditions emerge. Indeed, the formation of COMs in ISM must be a slow and long process, not stipulated to a definite time period.

The interstellar medium witnesses many astrophysical events including meteorite impacts with celestial bodies. Studies showed that a significant portion of soluble organic matter observed in carbonaceous meteorites can indeed originate from organic ices, derived from dense molecular clouds (Danger et al., 2021). For example, laboratory impact experiments showed that glycolaldehyde found in the ISM, as well as glycolaldehyde mixed with montmorillonite clay, when subjected to reverberated shocks (~5 to >25 GPa), resulted in the formation of a mixture of important biologically significant molecules such as ethylene glycol, threose, and erythrose (McCaffrey et al., 2014). Meteorite impact with planetary bodies is proposed as a possible route to their delivery as the course of their origin on Earth and other planets. Recently, it has been shown that the catalytic synthesis of polyribonucleic acids from ribonucleoside triphosphates is possible on prebiotic rock glasses, which resemble the rock on Hadean Earth surface formed by volcanic activities and impacts (Jerome et al., 2022). It is probable that such rock materials, silicates, and minerals in dust grains in the interstellar medium can catalyze similar chemical transformations resulting in molecular evolution to complex systems such as RNA from simple systems.

The vast expanse of methanol observed on interstellar clouds or protoplanetary space dust shows the efficacy of the continuous formation of methanol in space by both methane oxygen insertion as well as CO_2/CO hydrogenation (Schemes 1, 2, 3, 5). Similar to water transport by comets and meteorites to the Earth while it was still young, the transportation of methanol and these astrochemicals and their transformation to more complex prebiotic molecules and protocells would have occurred under Earth's favorable (Goldilocks) conditions over a long period (Chyba & Sagan, 1997; Pizzarello & Shock, 2010; Ehrenfreund et al., 2011). The close resemblance of these molecular species and their chemistry with terrestrial chemistry supports the transport–transformation process also and help to unveil the pathways involved in various

astrochemical transformations. It is important to consider the possibility that the simplest inanimate precursor molecules such as methane, the reactive monooxygenate methanol, CO_2, ammonia etc., under favorable catalytic conditions, can react and seed into fundamental life building blocks such as amino acids, sugars, proteins, nucleic acids. and bases over a long geological time span. The chemical transformation of simple substrates with active functional groups to complex systems without catalysts and at elevated temperatures is well studied. Studies have confirmed the gas-phase formation of formamide, a key source material in the formation of nucleobases, in the star-forming region in interstellar clouds (Codella et al., 2017). Results from emission studies in the Protostellar shock regions L1157-B1 and L1157-B2 suggest them as significant sources of HNCO and NH_2CHO (Mendoza et al., 2014). For example, thermal decomposition of formamide in vacuum leads to a mixture of nucleic bases purine, cytosine, adenine, as well as hypoxanthine, pterin, urea, urocanic acid, glycine, alanine, and norvaline (Enchev et al., 2021). The formation of the nucleic bases, uracil and thymine, was observed on heating formamide at 160°C for a day (Petera et al., 2021); similar events though varying kinetically, are envisaged in galactic chimneys.

Though many prebiotic precursors are observed in the ISM, it does not prove any sign of extraterrestrial life. However, their presence manifests the prevailing abiotic astrochemical protocols leading to their formation. For example, the CO_2–H_2 hydrogenation, the most significant among the events occurring in deep sea alkaline hydrothermal vents as observed in the "Lost City" exposed through the pioneering studies by Martin et al. (2008); Martin et al. (2014); Lane (2015); Jordan et al. (2019) shed light on probable initial stages of the molecular evolution that can instigate stepwise biological evolution to primitive cells. Experiments mimicking hydrothermal vents showed that the minerals such as olivine, serpentinite, Ni or Co containing pyrite and zeolite sediments present in the vents possess catalytic properties similar to those of enzymes and therefore can serve as potential catalysts for CO_2–H_2 to methanol (CH_3OH), the reactive intermediate and a key synthon toward molecular evolution (Barge et al., 2015; Roldan et al., 2015). Presence of similar catalytic sites though in minute quantities is a possible scenario in dust grains in the ISM too which triggers similar chemical transformations as mentioned previously. Therefore, the relevance and significance of methanol as a key synthetic motif (*methanol economy concept*- Olah et al., 2014; Olah & Mathew, 2015; Olah et al., 2018) in astrochemical organic synthesis cannot be ignored, especially in light of detection of the large expanse of extraterrestrial methanol.

4 Conclusion

In this brief perspective, based on the detection of methanol, the reactive C1 oxygenate in various regions of the interstellar medium, we summarized the possible routes for its continuous formation and key role as a source material for molecular evolution to multi-carbon complex organic and biogenic molecules, including proteins, nucleic bases, and nucleic acids, thus its significance in the RNA world. The close analogy of extra-terrestrially observed molecules and ions with terrestrial hydrocarbon ions and molecules suggests not only resemblance in plausible pathways for their formations, but also can help us to answer many unanswered questions on the molecular evolution in extraterrestrial world- interstellar medium, stars, planets, moons, and their atmospheres. Though the constituents of these atmospheres vary, the existence of these molecular and ionic species must have originated by the interaction of high energy cosmic rays and radiations on elements and subsequent chemical transformations taking place on the surface of space dust (ice) and in celestial bodies as well as the transport–transformation process via comets and meteorites. The CO_2/CO hydrogenation for the formation of methanol can be viewed as the probable basic step, which lays out subsequent protocols for the formation of fundamental building blocks toward the entry to the RNA world and subsequent biological evolution to primitive cells. Therefore, it is quite rational to propose that whether under suitable extraterrestrial conditions or deep sea thermal vent conditions, formation of all signature intermediates such as amino acids, sugars, nucleic bases etc., involves the intermediacy of methanol as the reactive C_1 building block. We anticipate that the key role of methanol in the evolution of prebiotic molecules and in the RNA world will be more manifested from the results of ongoing and future studies in the area.

Data availability statement

The original contributions presented in the study are included in the article/Supplementary Material; further inquiries can be directed to the corresponding authors.

Author contributions

All authors listed have made a substantial, direct, and intellectual contribution to the work and approved it for publication.

Acknowledgments

Support of our work by the Loker Hydrocarbon Research Institute is gratefully acknowledged.

Conflict of interest

The authors declare that the research was conducted in the absence of any commercial or financial relationships that could be construed as a potential conflict of interest.

Publisher's note

References

Abplanalp, M. J., and Kaiser, R. I. (2019). On the formation of complex organic molecules in the interstellar medium: Untangling the chemical complexity of carbon monoxide–hydrocarbon containing ice analogues exposed to ionizing radiation via a combined infrared and reflectron time-of-flight analysis. *Phys. Chem. Chem. Phys.* 21, 16949–16980. doi:10.1039/c9cp01793c

Ali, A., Sittler, E. C., Jr., Chornay, D., Rowe, B. R., and Puzzarini, C. (2013). Cyclopropenyl cation – The simplest huckel's aromatic molecule – And its cyclic methyl derivatives in Titan's upper atmosphere. *Planet. Space Sci.* 87, 96–105. doi:10.1016/j.pss.2013.07.007

Ali, A., Sittler, E. C., Jr., Chornay, D., Rowe, B. R., and Puzzarini, C. (2015). Organic chemistry in Titan's upper atmosphere and its astrobiological consequences: I. Views towards Cassini plasma spectrometer (CAPS) and ion neutral mass spectrometer (INMS) experiments in space. *Plan. Space Sci.* 109–110, 46–63. doi:10.1016/j.pss.2015.01.015

Allamandola, L. J., Sandford, S. A., and Valero, G. J. (1988). Photochemical and thermal evolution of interstellar/precometary ice analogs. *Icarus* 76, 225–252. doi:10.1016/0019-1035(88)90070-x

Appleman, E. H., Downs, A. J., and Gardner, C. J. (1989). Matrix photochemistry of hypofluorous acid, HOF: Oxygen atom transfer and other reactions. *J. Phys. Chem.* 93, 598–608. doi:10.1021/j100339a021

Ball, J. H., Gottlieb, C. A., Lilley, A. E., and Radford, H. E. (1970). Detection of methyl alcohol in Sagittarius. *Astrophys. J.* 162, L203. doi:10.1086/180654

Barge, L. M., Abedian, Y., Russell, M. J., Doloboff, I. J., Cartwright, J. H. E., Kidd, R. D., et al. (2015). From chemical gardens to fuel cells: Generation of electrical potential and current across self-assembling iron mineral membranes. *Angew. Chem. Int. Ed.* 54, 8184–8187. doi:10.1002/anie.201501663

Bennett, C. J., Hama, T., Kim, Y. S., Kawasaki, M., and Kaiser, R. I. (2011). Laboratory studies on the formation of formic acid (HCOOH) in interstellar and cometary ices. *Astrophys. J.* 727, 27. doi:10.1088/0004-637x/727/1/27

Bergantini, A., Góbi, S., Abplanalp, M. J., and Kaiser, R. I. (2018). A mechanistical study on the formation of dimethyl ether (CH_3OCH_3) and ethanol (CH_3CH_2OH) in methanol-containing ices and implications for the chemistry of star-forming regions. *Astrophys. J.* 852, 70. doi:10.3847/1538-4357/aa9ce2

Bergner, J. B., Oberg, K. L., and Rajappan, M. (2017). methanol formation via oxygen insertion chemistry in ices. *Astrophys. J.* 845, 29. doi:10.3847/1538-4357/aa7d09

Bertozzi, C. R. (2015). The centrality of chemistry. *ACS Cent. Sci.* 1, 1–2. doi:10.1021/acscentsci.5b00090

Bibring, J.-P., Taylor, M. G. G. T., Alexander, C., Auster, U., Biele, J., Finzi, A. E., et al. (2015). Philae's first days on the comet. *Science* 349, 493. doi:10.1126/science.aac5116

Biver, N., and Bockelée-Morvan, D. (2019). Complex organic molecules in comets from remote-sensing observations at millimeter wavelengths. *ACS Earth Space Chem.* 3, 1550–1555. doi:10.1021/acsearthspacechem.9b00130

Bredehöft, J. H. (2020). CO_2: A small ubiquitous molecule with a lot of astrochemical debate attached. *Front. Astron. Space Sci.* 7, 33. doi:10.3389/fspas.2020.00033

Breslow, R. (1959). On the mechanism of the formose reaction. *Tetrahedron Lett.* 1, 22–26. doi:10.1016/s0040-4039(01)99487-0

Butscher, T., Duvernay, F., Theule, P., Danger, G., Carissan, Y., Hagebaum-Reignier, D., et al. (2015). Formation mechanism of glycolaldehyde and ethylene glycol in astrophysical ices from HCO· and ·CH_2OH recombination: An experimental study. *Mon. Not. R. Astron. Soc.* 453, 1587–1596. doi:10.1093/mnras/stv1706

Chang, C. D., and Lang, W. H. (1977). Process for manufacturing olefins. *U.S. Pat.* 4 (025), 575.

Chang, C. D., and Silvestri, A. J. (1987). MTG. Origin, evolution, operation. *CHEMTECH* 17, 624–631.

Chang, C. D., and Silvestri, A. J. (1977). The conversion of methanol and other *O*-compounds to hydrocarbons over zeolite catalysts. *J. Catal.* 47, 249–259. doi:10.1016/0021-9517(77)90172-5

Charnley, S. B., and Rodgers, S. D. (2008). Interstellar reservoirs of cometary matter. *Space Sci. Rev.* 138, 59–73. doi:10.1007/s11214-008-9331-6

Cheung, A. C., Rank, D. M., Townes, C. H., Thornton, D. D., and Welch, W. (1968). Detection of NH3Molecules in the interstellar medium by their microwave emission. *Phys. Rev. Lett.* 21, 1701–1705. doi:10.1103/physrevlett.21.1701

Chyba, C. F., and Sagan, C. (1997). in *Comets and the origin and evolution of life; thomas* (New York: Springer), 147–173.

Codella, C., Ceccarelli, C., Caselli, P., Balucani, N., Barone, V., Fontani, F., et al. (2017). Seeds of Life in Space (SOLIS) II. Formamide in protostellar shocks: Evidence for gas-phase formation. *Astron. Astrophys.* 605, L3. doi:10.1051/0004-6361/201731249

Cuppen, H. M., Walsh, C., Lamberts, T., Semenov, D., Garrod, R. T., Penteado, S., et al. (2017). Grain surface models and data for Astrochemistry. *Space Sci. Rev.* 212, 1–58. doi:10.1007/s11214-016-0319-3

Danger, G., Vinogradoff, V., Matzka, M., Viennet, J-C., Remusat, L., Bernard, S., et al. (2021). Exploring the link between molecular cloud ices and chondritic organic matter in laboratory. *Nat. Commun.* 12, 3538. doi:10.1038/s41467-021-23895-2

de Barros, A. L. F., Domaracka, A., Andrade, D. P. P., Boduch, P., Rothard, H., da Silveira, E. F., et al. (2011). Radiolysis of frozen methanol by heavy cosmic ray and energetic solar particle analogues. *Mon. Not. R. Astron. Soc.* 418, 1363–1374. doi:10.1111/j.1365-2966.2011.19587.x

Dickens, J. E., Irvine, W. M., DeVries, C. H., and Ohishi, M. (1997). Hydrogenation of interstellar molecules: A survey for methylenimine (CH_2NH). *Astrophys. J.* 479, 307–312. doi:10.1086/303884

Duley, W. W., Millar, T. J., and Williams, D. A. (1978). Molecule production on interstellar oxide grains. *Mon. Not. R. Astron. Soc.* 185, 915–926. doi:10.1093/mnras/185.4.915

Duley, W. W. (1976). Origin of the diffuse interstellar absorption bands. II: Evidence for MgO and CaO solids in the interstellar medium. *Astrophys. Space Sci.* 45, 253–259. doi:10.1007/bf00642662

Ehrenfreund, P., and Charnley, S. B. (2000). Organic molecules in the interstellar medium, comets, and meteorites: A voyage from dark clouds to the early earth. *Annu. Rev. Astron. Astrophys.* 38, 427–483. doi:10.1146/annurev.astro.38.1.427

Ehrenfreund, P., Spaans, M., and Holm, N. G. (2011). The evolution of organic matter in space. *Phil. Trans. R. Soc. A* 369, 538–554. doi:10.1098/rsta.2010.0231

Eigenbrode, J. L., Summons, R. E., Steele, A., Freissinet, C., Millan, M., Navarro-González, R., et al. (2018). Organic matter preserved in 3-billion-year-old mudstones at Gale crater, Mars. *Science* 360, 1096–1101. doi:10.1126/science.aas9185

Enchev, V., Angelov, I., Dincheva, I., Stoyanova, N., Slavova, S., Rangelov, M., et al. (2021). Chemical evolution: From formamide to nucleobases and amino acids without the presence of catalyst. *J. Biomol. Struct. Dyn.* 39, 5563–5578. doi:10.1080/07391102.2020.1792986

Fechete, I. (2016). Paul Sabatier – the father of the chemical theory of catalysis. *C. R. Chim.* 19, 1374–1381. doi:10.1016/j.crci.2016.08.006

Fedoseev, G., Chuang, K.-J., Ioppolo, S., Qasim, D., van Dishoeck, E. F., Linnartz, H., et al. (2017). formation of glycerol through hydrogenation of CO ice under prestellar core conditions. *Astrophys. J.* 842, 52. doi:10.3847/1538-4357/aa74dc

Fedoseev, G., Cuppen, H. M., Ioppolo, S., Lamberts, T., and Linnartz, H. (2015). Experimental evidence for glycolaldehyde and ethylene glycol formation by surface hydrogenation of CO molecules under dense molecular cloud conditions. *Mon. Not. R. Astron. Soc.* 448, 1288–1297.

Fuchs, G. W., Cuppen, H. M., Ioppolo, S., Romanzin, C., Bisschop, S. E., Andersson, S., et al. (2009). Hydrogenation reactions in interstellar CO ice analogues- A combined experimental/theoretical approach. *Astron. Astrophys.* 505, 629–639. doi:10.1051/0004-6361/200810784

Fujita, S., Nakamura, M., Doi, T., and Takezawa, N. (1993). Mechanisms of methanation of carbon dioxide and carbon monoxide over nickel/alumina catalysts. *Appl. Catal. A General* 104, 87–100. doi:10.1016/0926-860x(93)80212-9

Furukawa, Y., Chikaraishi, Y., Ohkouchi, N., Ogawa, N. O., Glavin, D. P., Dworkin, J. P., et al. (2019). Extraterrestrial ribose and other sugars in primitive meteorites. *Proc. Natl. Acad. Sci. U. S. A.* 116, 24440–24445. doi:10.1073/pnas.1907169116

Garrod, R., Park, I. H., Casellic, P., and Herbst, E. (2006). Are gas-phase models of interstellar chemistry tenable? The case of methanol. *Faraday Discuss.* 133, 51. doi:10.1039/b516202e

Garrod, R. T., Weaver, S. L. W., and Herbst, E. (2008). Complex chemistry in star-forming regions-an expanded gas-grain warm-up chemical model. *Astrophys. J.* 682, 283–302. doi:10.1086/588035

Gibb, E. L., Whittet, D. C. B., Boogert, A. C. A., and Tielens, A. G. G. M. (2004). Interstellar ice: The *infrared space observatory* legacy. *Astrophys. J. Suppl. Ser.* 151, 35–73. doi:10.1086/381182

Gibb, E. L., Whittet, D. C. B., Schutte, W. A., Boogert, A. C. A., Chiar, J. E., Ehrenfreund, P., et al. (2000). An inventory of interstellar ices toward the embedded protostar W33A. *Astrophys. J.* 536, 347–356. doi:10.1086/308940

Goumans, T. P. M., and Kästner, J. (2010). Hydrogen-atom tunneling could contribute to H_2 formation in space. *Angew. Chem. Int. Ed.* 49, 7350–7352. doi:10.1002/anie.201001311

Goumans, T. P. M., Wander, A., Catlow, C. R. A., and Brown, W. A. (2007). Silica grain catalysis of methanol formation. *Mon. Not. R. Astron. Soc.* 382, 1829–1832. doi:10.1111/j.1365-2966.2007.12491.x

Guélin, M., and Cernicharo, J. (2022). Organic molecules in interstellar space: Latest advances. *Front. Astron. Space Sci.* 9, 787567. doi:10.3389/fspas.2022.787567

Haldane, J. B. S. (1929). The origin of life. *Rationalist Ann.*, 148, 3–10.

Hama, T., and Watanabe, N. (2013). Surface processes on interstellar amorphous solid water: Adsorption, diffusion, tunneling reactions, and nuclear-spin conversion. *Chem. Rev.* 113, 8783–8839. doi:10.1021/cr4000978

Harris, T. D., Lee, D. H., Blumberg, M. Q., and Arumainayagam, C. R. (1995). Electron-induced reactions in methanol ultrathin films studied by temperature-programmed desorption: A useful method to study radiation chemistry. *J. Phys. Chem.* 99, 9530–9535. doi:10.1021/j100023a035

Harvey-Smith, L., and Cohen, R. J. (2006). Discovery of large-scale methanol and hydroxyl maser filaments in W3(OH). *Mon. Not. R. Astron. Soc.* 371, 1550–1558. doi:10.1111/j.1365-2966.2006.10806.x

Herbst, E., and van Dishoeck, E. F. (2009). Complex organic interstellar molecules. *Ann. Rev. Astron. Astrophys.* 47, 427–480. doi:10.1146/annurev-astro-082708-101654

Heward, A. (2006). *Upgraded MERLIN spies cloud of alcohol spanning 288 billion miles. PN 06/14 (NAM7)*. London, United Kingdom: Royal Astronomical Society.

Hidaka, H., Watanabe, M., Kouchi, A., and Watanabe, N. (2009). Reaction routines in the CO–H_2CO-*dn*–CH_3OH-*dm* system clarified from H(D) exposure of solid formaldehyde at low temperatures. *Astrophys. J.* 702, 291–300. doi:10.1088/0004-637x/702/1/291

Hiraoka, K., and Kebarle, P. (1975). Energetics, stabilities, and possible structures of $CH_5^+(CH_4)_n$ clusters from gas phase study of equilibriums $CH_5^+(CH_4)_{n-1}$ + CH_4 = $CH_5^+(CH_4)_n$ for n = 1-5. *J. Am. Chem. Soc.* 97, 4179–4183. doi:10.1021/ja00848a005

Hörst, S. M., Yelle, R. V., Buch, A., Carrasco, N., Cernogora, G., Dutuit, O., et al. (2012). formation of amino acids and nucleotide bases in a titan atmosphere simulation experiment. *Astrobiology* 12, 809–817. doi:10.1089/ast.2011.0623

Ioppolo, S., Cuppen, H. M., and Linnartz, H. (2011). surface formation routes of interstellar molecules: Hydrogenation reactions in simple ices. *Rend. Fis. Acc. Lincei* 22, 211. doi:10.1007/s12210-011-0135-3

Irvine, W. M., Avery, L. W., Friberg, P., Matthews, H. E., and Ziurys, L. M. (1988). Newly detected molecules in dense interstellar clouds. *Astrophys. Lett. Commun.* 26, 167–180.

Irvine, W. M., Friberg, P., Kaifu, N., Matthews, H. E., Minh, Y. C., Ohishi, M., et al. (1990). Detection of formic acid in the cold, dark cloud L 134N. *Astron. Astrophys.* 229, L9–L12.

Irvine, W. M., Schloerb, F. P., Crovisier, J., Fegley, B., Jr., and Mumma, M. J. (2000). "Comets: A link between interstellar and nebular chemistry," in *Protostars and planets IV*. Editors V. Mannings, A. P. Boss, and S. S. Russell (Tucson, AZ: University of Arizona Press), 1159–1200.

Jerome, C. A., Kim, H-J., Mojzsis, S. J., Benner, S. A., and Blondi, E. (2022). Catalytic synthesis of polyribonucleic acid on prebiotic rock glasses. *Astrobiology* 22, 629–636. doi:10.1089/ast.2022.0027

Jones, A. P. (2007). The mineralogy of cosmic dust: Astromineralogy. *Eur. J. Mineral.* 19, 771–782. doi:10.1127/0935-1221/2007/0019-1766

Jordan, S. F., Rammu, H., Zheludev, I. N., Hartley, A. M., Maréchal, A., Lane, N., et al. (2019). Promotion of protocell self-assembly from mixed amphiphiles at the origin of life. *Nat. Ecol. Evol.* 3, 1705–1714. doi:10.1038/s41559-019-1015-y

Kalenskii, S. V., and Johansson, L. E. B. (2010). Spectral Survey of the Star-Forming Region W51 e1/e2 at 3 mm. *Astron. Rep.* 54, 1084–1104. doi:10.1134/s1063772910120036

Kebarle, P., and Franklin, J. L. (1972). "Higher order reactions – ion clusters and ion solvation," in *Ion–Molecule reactions* (New York: Springer), Vol. 1.

Kebarle, P., Haynes, R. N., and Collins, J. G. (1967). *Competitive Solvation of the Hydrogen Ion by Water and Methanol Molecules Studied in the Gas Phase*, 89, 5753–5757.*J. Am. Chem. Soc.*

Kite, E. S., Gao, P., Goldblatt, C., Mischna, M. A., Mayer, D. P., Yung, Y. L., et al. (2017). Methane bursts as a trigger for intermittent lake-forming climates on post-Noachian Mars. *Nat. Geosci.* 10, 737–740. doi:10.1038/ngeo3033

Kurokawa, H., Shibuya, T., Sekine, Y., Ehlmann, B. L., Usui, F., Kikuchi, S., et al. (2022). Distant formation and differentiation of outer main belt asteroids and carbonaceous chondrite parent bodies. *AGU Adv.* 3, e2021AV000568. doi:10.1029/2021AV000568

Laffon, C., Lasne, J., Bournel, F., Schulte, K., Lacombe, S., Parent, P., et al. (2010). Photochemistry of carbon monoxide and methanol in water and nitric acid hydrate ices: A nexafs study. *Phys. Chem. Chem. Phys.* 12, 10865. doi:10.1039/c0cp00229a

Lane, N. (2015). *The vital question*. London: Profile Books Ltd.

Lau, Y. K., Ikuta, S., and Kebarle, P. (1982). Thermodynamics and kinetics of the gas-phase reactions H3O+(H2O)n-1 + water = H3O+(H2O)n. *J. Am. Chem. Soc.* 104, 1462–1469. doi:10.1021/ja00370a002

Li, J., Wang, J., Qiao, H., Quan, D., Fang, M., Du, F., et al. (2020). Mapping observations of complex organic molecules around Sagittarius B2 with the ARO 12 m telescope. *Mon. Not. R. Astron. Soc.* 492, 556–565. doi:10.1093/mnras/stz3337

Liang, J., Li, H., Zhao, S., Guo, W., Wang, R., Yang, M., et al. (1990). Characteristics and performance of SAPO-34 catalyst for methanol-to-olefin conversion. *Appl. Catal.* 64, 31–40. doi:10.1016/s0166-9834(00)81551-1

Linnartz, H., Ioppolo, S., and Fedoseev, G. (2015). Atom addition reactions in interstellar ice analogues. *Int. Rev. Phys. Chem.* 34, 205–237. doi:10.1080/0144235x.2015.1046679

Liszt, H. S. (2011). How does C+ recombine in diffuse molecular gas? *Astron. Astrophys.* 527, A45. doi:10.1051/0004-6361/201015824

Liu, S-Y., Mehringer, D. M., and Snyder, L. E. (2001). Observations of formic acid in hot molecular cores. *Astrophys. J.* 552, 654–663. doi:10.1086/320563

Lugez, C., Schriver, A., Levant, R., and Schriver-Mazzouli, L. A. (1994). A matrix-isolation infrared spectroscopic study of the reactions of methane and methanol with ozone. *Chem. Phys.* 181, 129–146. doi:10.1016/0301-0104(94)85021-6

Lyons, J. R., Manning, C., and Nimmo, F. (2005). Formation of methane on Mars by fluid–rock interaction in the crust. *Geophys. Res. Lett.* 32, L13201. doi:10.1029/2004gl022161

Mahaffy, P. G., Ho, F. M., Haack, J. A., and Brush, E. J. (2019). Can chemistry Be a central science without systems thinking? *J. Chem. Educ.* 96, 2679–2681. doi:10.1021/acs.jchemed.9b00991

Martin, M., Baross, J., Kelley, D., and Russell, M. J. (2008). Hydrothermal vents and the origin of life. *Nat. Rev. Microbiol.* 6, 805–814. doi:10.1038/nrmicro1991

Martin, W. F., Sousa, F. L., and Lane, N. (2014). Energy at life's origin. *Science* 344, 1092–1093. doi:10.1126/science.1251653

Masamura, M. (2001). *Ab initio* molecular orbital study on the structures and energetics of $CH_3OH(H_2O)$n and CH_3SH $(H_2O)_n$ in the gas phase. *J. Comput. Chem.* 22, 125–131. doi:10.1002/1096-987x(20010115)22:1<125::aid-jcc12>3.0.co;2-0

McCaffrey, V. P., Zellner, N. E. B., Waun, C. M., Bennett, E. R., and Earl, E. K. (2014). Reactivity and survivability of glycolaldehyde in simulated meteorite impact experiments. *Orig. Life Evol. Biosph.* 44, 29–42. doi:10.1007/s11084-014-9358-5

McCarthy, M. C., and McGuire, B. A. (2021). Aromatics and cyclic molecules in molecular clouds: A new dimension of interstellar organic chemistry. *J. Phys. Chem. A* 125, 3231–3243. doi:10.1021/acs.jpca.1c00129

McGuire, B. A. (2022). Census of interstellar, circumstellar, extragalactic, protoplanetary disk, and exoplanetary molecules. *Astrophys. J. Suppl. Ser.* 259 (30), 1–51. doi:10.3847/1538-4365/ac2a48

Meisel, S. L., McCullough, J. P., Lechthaler, C. H., and Weisz, P. B. (1976). Gasoline from methanol in one step. *Chemtech* 6, 86–89.

Mendoza, E., Lefloch, B., Lopez-Sepulcre, A., Ceccarelli, C., Codella, C., Boechat-Roberty, H. M., et al. (2014). Molecules with a peptide link in protostellar shocks: A comprehensive study of L1157. *Mon. Not. R. Astron. Soc.* 445, 151–161. doi:10.1093/mnras/stu1718

Miller, S. L. (1953). A production of amino acids under possible primitive earth conditions. *Science* 117, 528–529. doi:10.1126/science.117.3046.528

Miller, S. L., and Urey, H. C. (1959). Organic Compound Synthesis on the Primitive Earth: Several questions about the origin of life have been answered, but much remains to be studied. *Science* 130, 245–251. doi:10.1126/science.130.3370.245

Milligan, D. E., and Jacox, M. E. (1971). Infrared spectrum and structure of intermediates in the reaction of OH with CO. *J. Chem. Phys.* 54, 927–942. doi:10.1063/1.1675022

Mogul, R., Limaye, S. S., Way, M. J., and Cordova, J. A. (2021). Venus' mass spectra show signs of disequilibria in the middle clouds. *Geophys. Res. Lett.* 48, e2020GL091327. doi:10.1029/2020gl091327

Müller, H., Kutzelnigg, W., Noga, J., and Klopper, W. (1997). CH_5^+: The story goes on. An explicitly correlated coupled-cluster study. *J. Chem. Phys.* 106, 1863–1869. doi:10.1063/1.473340

Newmann, G. A., Cavanaugh, J. F., Sun, X., Mozarico, E. M., Smith, D. E., Zuber, M. T., et al. (2013). Bright and dark polar deposits on Mercury: Evidence for surface volatiles. *Science* 339, 296–300. doi:10.1126/science.1229764

Öberg, K. I. (2016). Photochemistry and Astrochemistry: Photochemical pathways to interstellar complex organic molecules. *Chem. Rev.* 116, 9631–9663. doi:10.1021/acs.chemrev.5b00694

Oka, T. (2019). H_3^+, the ideal probe for *in situ* measurement of the Galactic cosmic rays. *Phil. Trans. R. Soc. A* 377, 20180402. doi:10.1098/rsta.2018.0402

Oka, T. (2013). Interstellar H_3^+. *Interstellar H_3^+. Chem. Rev.* 113, 8738–8761. doi:10.1021/cr400266w

Oka, T. (2015). Taming CH_5^+, the "enfant terrible" of chemical structures. *Science* 347, 1313–1314. doi:10.1126/science.aaa6935

Olah, G. A. (1983). Bifunctional acid-base catalyzed conversion of hetero-substituted methanes into olefins. WO 1983000483 A1. *U.S. Pat.* 4, 373–109.

Olah, G. A., Doggweiler, H., Felberg, J. D., Frohlich, S., Grdina, M. J., Karpeles, R., et al. (1984). Onium Ylide chemistry. 1. Bifunctional acid-base-catalyzed conversion of heterosubstituted methanes into ethylene and derived hydrocarbons. The onium ylide mechanism of the C1 .fwdarw. C2 conversion. *J. Am. Chem. Soc.* 106, 2143–2149. doi:10.1021/ja00319a039

Olah, G. A., Goeppert, A., Czaun, M., Mathew, T., May, R. B., Prakash, G. K. S., et al. (2015). Single step Bi-reforming and oxidative Bi-reforming of methane (natural gas) with steam and carbon dioxide to metgas ($CO\text{-}2H_2$) for methanol synthesis: Self-sufficient effective and exclusive oxygenation of methane to methanol with oxygen. *J. Am. Chem. Soc.* 137, 8720–8729. doi:10.1021/jacs.5b02029

Olah, G. A., Goeppert, A., and Prakash, G. K. S. (2018). *Beyond oil and gas: The methanol economy*, 3rd updated and enlarged ed.; Wiley VCH: Weinheim, Germany.

Olah, G. A., Klopman, G., and Schlosberg, R. H. (1969). Chemistry in super acids. III." protonation of alkanes and the intermediacy of alkanonium ions, pentacoordinated carbon cations of the CH_5^+ type. Hydrogen exchange, protolytic cleavage, hydrogen abstraction, and polycondensation of methane, ethane, 2, 2-dimethylpropane (neopentane), and 2, 2, 3, 3-tetramethylbutane in FSO_3H-SbF_5 ("Magic acid") solution. *J. Am. Chem. Soc.* 91, 3261–3268. doi:10.1021/ja01040a029

Olah, G. A., and Mathew, T. (2015). *A life of magic chemistry: Autobiographical reflections including post-nobel prize years and the methanol economy*, 2nd updated ed.; John Wiley & Sons, New York, Chapters 13–15.

Olah, G. A., Mathew, T., and Prakash, G. K. S. (2017). Chemical formation of methanol and hydrocarbon ("Organic") derivatives from CO_2 and H_2 – carbon sources for subsequent biological cell evolution and life's origin. *J. Am. Chem. Soc.* 139, 566–570. doi:10.1021/jacs.6b10230

Olah, G. A., Mathew, T., and Prakash, G. K. S. (2016b). Relevance and significance of extraterrestrial abiological hydrocarbon chemistry. *J. Am. Chem. Soc.* 138, 6905–6911. doi:10.1021/jacs.6b03136

Olah, G. A., Mathew, T., Rasul, G., and Prakash, G. K. S. (2016a). Chemical aspects of astrophysically observed extraterrestrial methanol, hydrocarbon derivatives, and ions. *J. Am. Chem. Soc.* 138, 1717–1722. doi:10.1021/jacs.6b00343

Olah, G. A., and Prakash, G. K. S. (2009). Efficient and selective conversion of CO_2 to methanol, dimethyl ether and derived products. *U.S. Pat.* 7, 293–B2.

Olah, G. A., Prakash, G. K. S., Goeppert, A., Czaun, M., and Mathew, T. (2013). Self-sufficient and exclusive oxygenation of methane and its source materials with oxygen to methanol via metgas using oxidative Bi-reforming. *J. Am. Chem. Soc.* 135, 10030–10031. doi:10.1021/ja405439c

Olah, G. A., Prakash, G. K. S., and Mathew, T. (2014). "Anthropogenic carbon cycle and the methanol economy (Part XXX)," in *Across conventional lines–the sixth decade and the methanol economy* (Singapore: World Scientific), 3.

Olah, G. A., Prakash, G. K. S., Molnar, Á., and Sommer, J. (2009). *Superacid chemistry*, 2nd ed.; John Wiley & Sons: Hoboken, New Jersey.

Oparin, A. I. (1952).*The origin of life*, 2nd ed.; Dover Publications: New York.

Oparin, A. I. (1924).*The origin of life*. Moscow: Moscow Worker Publisher.

Orgel, L. E. (2000). Self-organizing biochemical cycles. *Proc. Natl. Acad. Sci. U. S. A.* 97, 12503–12507. doi:10.1073/pnas.220406697

Osamura, Y., Roberts, H., and Herbst, E. (2005). The gas-phase deuterium fractionation of formaldehyde. *Astrophys. J.* 621, 348–358. doi:10.1086/427474

Parnis, J. M., Hoover, L. E., Fridgen, T. D., and Lafleur, R. D. (1993). Stabilization of the primary products of O (^{1}D) reactions with CO, CO_2, CH_4, and other hydrocarbons in cryogenic matrices. *J. Phys. Chem.* 97, 10708–10711. doi:10.1021/j100143a030

Petera, L., Mrazikova, K., Nejdl, L., Zemankova, K., Vaculovicova, M., Pastorek, A., et al. (2021). Prebiotic route to thymine from formamide—a combined experimental–theoretical study. *Molecules* 26, 2248. doi:10.3390/molecules26082248

Petrik, N. G., Monckton, R. J., Koehler, S. P. K., and Kimmel, G. A. (2014b). Distance-dependent radiation chemistry: Oxidation versus hydrogenation of CO in electron-irradiated H_2O/CO/H_2O ices. *J. Phys. Chem. C* 118, 27483–27492. doi:10.1021/jp509785d

Petrik, N. G., Monckton, R. J., Koehler, S. P. K., and Kimmel, G. A. (2014a). Electron-stimulated reactions in layered CO/H_2O films: Hydrogen atom diffusion and the sequential hydrogenation of CO to methanol. *J. Chem. Phys.* 140, 204710. doi:10.1063/1.4878658

Pizzarello, S., and Shock, E. (2010). The organic composition of carbonaceous meteorites: The evolutionary story ahead of biochemistry. *Cold Spring Harb. Perspect. Biol.* 2, a002105. doi:10.1101/cshperspect.a002105

Porosoff, M. D., Yan, B., and Chen, J. G. (2016). Catalytic reduction of CO_2 by H_2 for synthesis of CO, methanol and hydrocarbons: Challenges and opportunities. *Energy Environ. Sci.* 9, 62–73. doi:10.1039/c5ee02657a

Puzzarini, C., Ali, A., Biczysko, M., and Barone, V. (2014). Accurate spectroscopic characterization of protonated oxirane: A potential prebiotic species in Titan's atmosphere. *Astrophys. J.* 792, 118. doi:10.1088/0004-637x/792/2/118

Puzzarini, C. (2017). Astronomical complex organic molecules: Quantum chemistry meets rotational spectroscopy. *Int. J. Quantum Chem.* 117, 129–138. doi:10.1002/qua.25284

Puzzarini, C., Baiardi, A., Bloino, J., Barone, V., Murphy, T. E., Drew, H. D., et al. (2017). Spectroscopic characterization of key aromatic and heterocyclic molecules: A route toward the origin of life. *Astron. J.* 154, 82. doi:10.3847/1538-3881/aa7d54

Remijan, A., Shiao, Y.-S., Friedel, D. N., Meier, D. S., and Snyder, L. E. (2004). A survey of large molecules of biological interest toward selected high-mass star-forming regions. *Astrophys. J.* 617, 384–398. doi:10.1086/425266

Roldan, A., Hollingsworth, N., Roffey, A., Islam, H.-U., Goodall, J. B. M., Catlow, C. R. A., et al. (2015). Bio-inspired CO_2conversion by iron sulfide catalysts under sustainable conditions. *Chem. Commun.* 51, 7501–7504. doi:10.1039/c5cc02078f

Rollmann, L. D. (1982). Selective production of olefins. *U.S. Pat.* 4 (359), 595.

Roth, D. L. (2015). Several centuries of centrality. *ACS Cent. Sci.* 1, 103–105. doi:10.1021/acscentsci.5b00198

Sabatier, P., Senderens, J. B., and Hebd, C. R. (1902). Direct hydrogenation of oxides of carbon in presence of various finely divided metals. *Séances Acad. Sci. Paris* 134, 689–691.

Saladino, R., Carota, E., Botta, G., Kapralov, M., Timoshenko, G. N., Rozanov, A., et al. (2016). First evidence on the role of heavy ion irradiation of meteorites and formamide in the origin of biomolecules. *Orig. Life Evol. Biosph.* 46, 515–521. doi:10.1007/s11084-016-9495-0

Saladino, R., Carota, E., Botta, G., Kapralov, M., Timoshenko, G. N., Rozanov, A. Y., et al. (2015). Meteorite-catalyzed syntheses of nucleosides and of other prebiotic compounds from formamide under proton irradiation. *Proc. Natl. Acad. Sci. U. S. A.* 112, E2746–E2755. doi:10.1073/pnas.1422225112

Schmidt, F., Swiderek, P., and Bredehöft, J. H. (20191974–1986). Formation of formic acid, formaldehyde, and carbon dioxide by electron-induced chemistry in ices of water and carbon monoxide. *ACS Earth Space Chem.* 3, 1974–1986. doi:10.1021/acsearthspacechem.9b00168

Schreiner, P. R., Kim, S.-J., Schaefer, H. F., and Schleyer, P. v. R. (1993). CH_5^+: The never-ending story or the final word? *J. Chem. Phys.* 99, 3716–3720. doi:10.1063/1.466147

Sefcik, M. D., Henis, J. M. S., and Gaspar, P. P. (1974). The methanium ion, CH_5^+. Evidence for the structure of a nonclassical ion from reaction studies by ion cyclotron resonance spectroscopy. *J. Chem. Phys.* 61, 4321–4328. doi:10.1063/1.1681738

Sen, R., Koch, C. J., Galvan, V., Entesari, N., Goeppert, A., Prakash, G. K. S., et al. (2021). Glycol assisted efficient conversion of CO_2 captured from air to methanol with a heterogeneous Cu/ZnO/Al_2O_3 catalyst. *J. CO_2 Util.* 54, 101762. doi:10.1016/j.jcou.2021.101762

Sewiło, M., Charnley, S. B., Schilke, P., Taquet, V., Oliveira, J. M., Shimonishi, T., et al. (2019). Complex organic molecules in star-forming regions of the magellanic clouds. *ACS Earth Space Chem.* 3, 2088–2109. doi:10.1021/acsearthspacechem.9b00065

Shaik, S. (2003). Chemistry—a central pillar of human culture. *Angew. Chem. Int. Ed.* 42, 3208–3215. doi:10.1002/anie.200330038

Simonciō cō, M. D., Krasnokutski, S. S., Henning, Th., and Jäger, C. (2020). Sensitivity of gas-grain chemical models to surface reaction barriers, Effect from a key carbon-insertion reaction, C + H_2 → CH_2. *Astron. Astrophys.* 637, A72.

Sittler, E. C., Jr., Cooper, J. F., Sturner, S. J., and Ali, A. (2020). Titan's ionospheric chemistry, fullerenes, oxygen, galactic cosmic rays and the formation of exobiological molecules on and within its surfaces and lakes. *Icarus* 344, 113246. doi:10.1016/j.icarus.2019.03.023

Snyder, L. E., Buhl, D., Zuckerman, B., and Palmer, P. (1969). Microwave detection of interstellar formaldehyde. *Phys. Rev. Lett.* 22, 679–681. doi:10.1103/physrevlett.22.679

Socha, R. F., Weiss, A. H., and Sakharov, M. M. (1980). Autocatalysis in the formose reaction. *React. Kinet. Catal. Lett.* 14 (2), 119–128. doi:10.1007/bf02061275

Soma, T., Sakai, N., Watanabe, Y., and Yamamoto, S. (2015). Methanol in the starless core, Taurus molecular cloud-1. *Astrophys. J.* 802, 74. doi:10.1088/0004-637X/802/2/74

ten Kate, I. L. (2018). Organic molecules on Mars. *Science* 360, 1068–1069. doi:10.1126/science.aat2662

Tercero, B., Cuadrado, S., López, A., Brouillet, N., Despois, D., Cernicharo, J., et al. (2018). Chemical segregation of complex organic O-bearing species in Orion KL. *Astron. Astrophys.* 620, L6. doi:10.1051/0004-6361/201834417

Theule, P., Borget, F., Mispelaer, F., Danger, G., Duvernay, F., Guillemin, J. C., et al. (2011). Hydrogenation of solid hydrogen cyanide HCN and methanimine CH_2NH at low temperature. *Astron. Astrophys.* 534, A64. doi:10.1051/0004-6361/201117494

Tielens, A. G. G. M. (2013). The molecular Universe. *Rev. Mod. Phys.* 85, 1021–1081. doi:10.1103/RevModPhys.85.1021

Tielens, A. G. G. M., and Whittet, D. C. B. (1997). in *Molecules in astrophysics: Probes & processes*. Editor E. F. van Dishoeck (Dordrecht: Kluwer), 45.

Vasyunin, A. I., and Herbst, E. (2013). Reactive desorption and radiative association as possible drivers of complex molecule formation in the cold interstellar medium. *Astrophys. J.* 769, 34. doi:10.1088/0004-637x/769/1/34

Walsh, C., Herbst, E., Nomura, H., Millar, T. J., and Weaver, S. W. (2014a). Complex organic molecules along the accretion flow in isolated and externally irradiated protoplanetary disks. *Faraday Discuss.* 168, 389–421. doi:10.1039/c3fd00135k

Walsh, C., Millar, T. J., Nomura, H., Herbst, E., Weaver, S. W., Aikawa, Y., et al. (2014b). Complex organic molecules in protoplanetary disks. *Astron. Astrophys.* 563, A33. doi:10.1051/0004-6361/201322446

Wang, W., Wang, S., Ma, X., and Gong, J. (2011). Recent advances in catalytic hydrogenation of carbon dioxide. *Chem. Soc. Rev.* 40, 3703. doi:10.1039/c1cs15008a

Watanabe, N., and Kouchi, A. (2002). Measurements of conversion rates of CO to CO_2 in ultraviolet-induced reaction of $D_2O(H_2O)$/CO amorphous ice. *Astrophys. J.* 567, 651–655. doi:10.1086/338491

Watanabe, N., Mouri, O., Nagaoka, A., Chigai, T., Kouchi, A., Pirronello, V., et al. (2007). Laboratory simulation of competition between hydrogenation and photolysis in the chemical evolution of H_2O-CO ice mixtures. *ApJ.* 668, 1001–1011. doi:10.1086/521421

Watanabe, N., Nagaoka, A., Shiraki, T., and Kouchi, A. (2004). Hydrogenation of CO on pure solid CO on and CO-H_2O mixed ice. *Astrophys. J.* 616, 638–642. doi:10.1086/424815

Watson, J. D., and Crick, F. H. C. (1953). Molecular structure of nucleic acids: A structure for deoxyribose nucleic acid. *Nature* 171, 737–738. doi:10.1038/171737a0

Webster, C. R., Mahaffy, P. R., Atreya, S. K., Moores, J. E., Flesch, G. J., Malespin, C., et al. (2018). Background levels of methane in Mars' atmosphere show strong seasonal variations. *Science* 360, 1093–1096. doi:10.1126/science.aaq0131

White, E. T., Tang, J., and Oka, T. C. H5+ (1999). CH_5^+: The infrared spectrum observed. *Science* 284, 135–137. doi:10.1126/science.284.5411.135

Whittet, D. C. B., Cook, A. M., Herbst, E., Chiar, J. E., and Shenoy, S. S. (2011). Observational constraints on methanol production in interstellar and preplanetary ices. *Astrophys. J.* 742, 28. doi:10.1088/0004-637x/742/1/28

Williams, D. A. (2005). Gas and dust in the interstellar medium. *J. Phys. Conf. Ser.* 6, 1–17. doi:10.1088/1742-6596/6/1/001

Withnall, R., and Andrews, L. (1988). Matrix reactions of methylsilanes and oxygen atoms. *J. Phys. Chem.* 92, 594–602. doi:10.1021/j100314a006

Witt, A., Ivanov, S. D., Forbert, H., and Marx, D. (2008). Microsolvation of protonated methane: Structures and energetics of $CH_5^+(H_2)_n$. *J. Phys. Chem. A* 112, 12510–12517. doi:10.1021/jp8054069

Wollin, G., and Ericson, D. B. (1971). Amino-acid synthesis from gases detected in interstellar space. *Nature* 233, 615–616. doi:10.1038/233615a0

Woon, D. E. (2002). Modeling gas-grain chemistry with quantum chemical cluster calculations. 1. Heterogeneous hydrogenation of CO and H_2CO on icy grain mantles. *Astrophys. J.* 569, 541–548. doi:10.1086/339279

Woon, D. E. (2021). The astrochymist. Available at: http://www.astrochymist.org/

Yamamoto, S., Beniya, A., Mukai, K., Yamashita, Y., and Yoshinobu, J. (2004). Low-energy electron-stimulated chemical reactions of CO in water ice. *Chem. Phys. Lett.* 388, 384–388. doi:10.1016/j.cplett.2004.03.030

Yamamoto, S. (2017). *Introduction to Astrochemistry, Astronomy and astrophysics*. Tokyo, Japan: Springer.

Zuckerman, B., Ball, J. H., and Gottlieb, C. A. (1971). Microwave detection of interstellar formic acid. *Astrophys. J.* 163, L41. doi:10.1086/180663

Advantages of publishing in Frontiers

OPEN ACCESS
Articles are free to read for greatest visibility and readership

FAST PUBLICATION
Around 90 days from submission to decision

HIGH QUALITY PEER-REVIEW
Rigorous, collaborative, and constructive peer-review

TRANSPARENT PEER-REVIEW
Editors and reviewers acknowledged by name on published articles

Frontiers
Avenue du Tribunal-Fédéral 34
1005 Lausanne | Switzerland

Visit us: www.frontiersin.org
Contact us: frontiersin.org/about/contact

REPRODUCIBILITY OF RESEARCH
Support open data and methods to enhance research reproducibility

DIGITAL PUBLISHING
Articles designed for optimal readership across devices

FOLLOW US
@frontiersin

IMPACT METRICS
Advanced article metrics track visibility across digital media

EXTENSIVE PROMOTION
Marketing and promotion of impactful research

LOOP RESEARCH NETWORK
Our network increases your article's readership